PROGRESSES IN THE DRUG TREATMENT OF CHRONIC CARDIOPULMONARY DISEASES

EDITED BY: Xiaohui Li, Djuro Kosanovic, Xiao-Jian Wang and Yunshan Cao
PUBLISHED IN: Frontiers in Pharmacology

frontiers Research Topics

ISSN 1664-8714
ISBN 978-2-88976-327-6
DOI 10.3389/978-2-88976-327-6

About Frontiers

Frontiers is more than just an open-access publisher of scholarly articles: it is a pioneering approach to the world of academia, radically improving the way scholarly research is managed. The grand vision of Frontiers is a world where all people have an equal opportunity to seek, share and generate knowledge. Frontiers provides immediate and permanent online open access to all its publications, but this alone is not enough to realize our grand goals.

Frontiers Journal Series

The Frontiers Journal Series is a multi-tier and interdisciplinary set of open-access, online journals, promising a paradigm shift from the current review, selection and dissemination processes in academic publishing. All Frontiers journals are driven by researchers for researchers; therefore, they constitute a service to the scholarly community. At the same time, the Frontiers Journal Series operates on a revolutionary invention, the tiered publishing system, initially addressing specific communities of scholars, and gradually climbing up to broader public understanding, thus serving the interests of the lay society, too.

Dedication to Quality

Each Frontiers article is a landmark of the highest quality, thanks to genuinely collaborative interactions between authors and review editors, who include some of the world's best academicians. Research must be certified by peers before entering a stream of knowledge that may eventually reach the public - and shape society; therefore, Frontiers only applies the most rigorous and unbiased reviews.
Frontiers revolutionizes research publishing by freely delivering the most outstanding research, evaluated with no bias from both the academic and social point of view. By applying the most advanced information technologies, Frontiers is catapulting scholarly publishing into a new generation.

What are Frontiers Research Topics?

Frontiers Research Topics are very popular trademarks of the Frontiers Journals Series: they are collections of at least ten articles, all centered on a particular subject. With their unique mix of varied contributions from Original Research to Review Articles, Frontiers Research Topics unify the most influential researchers, the latest key findings and historical advances in a hot research area! Find out more on how to host your own Frontiers Research Topic or contribute to one as an author by contacting the Frontiers Editorial Office: frontiersin.org/about/contact

PROGRESSES IN THE DRUG TREATMENT OF CHRONIC CARDIOPULMONARY DISEASES

Topic Editors:
Xiaohui Li, Central South University, China
Djuro Kosanovic, I.M. Sechenov First Moscow State Medical University, Russia
Xiao-Jian Wang, Fuwai Hospital, Chinese Academy of Medical Sciences and Peking Union Medical College, China
Yunshan Cao, Gansu Provincial Hospital, China

Citation: Li, X., Kosanovic, D., Wang, X.-J., Cao, Y., eds. (2022). Progresses in the Drug Treatment of Chronic Cardiopulmonary Diseases.
Lausanne: Frontiers Media SA. doi: 10.3389/978-2-88976-327-6

Table of Contents

frontiers | Frontiers in Pharmacology

EDITORIAL
published: 19 May 2022
doi: 10.3389/fphar.2022.910212

Editorial: Progresses in the Drug Treatment of Chronic Cardiopulmonary Diseases

Xiaohui Li[1]*, *Djuro Kosanovic*[2], *Xiao-Jian Wang*[3] and *Yunshan Cao*[4]

[1]Department of Pharmacology, Xiangya School of Pharmaceutical Science, Central South University, Changsha, China, [2]Department of Pulmonology, I.M. Sechenov First Moscow State Medical University (Sechenov University), Moscow, Russia, [3]Key Laboratory of Pulmonary Vascular Medicine, State Key Laboratory of Cardiovascular Disease, Fuwai Hospital, National Center for Cardiovascular Diseases, Chinese Academy Medical Sciences and Peking Union Medical College, Beijing, China, [4]Department of Cardiology, Gansu Provincial Hospital, Lanzhou, China

Keywords: chronic cardiopulmonary diseases, pulmonary embolism, pulmonary fibrosis, pulmonary hypertension, drug development

Editorial on the Research Topic

Progresses in the Drug Treatment of Chronic Cardiopulmonary Diseases

We are delighted to announce the publication of the special issue with the topic "Progresses in the Drug Treatment of Chronic Cardiopulmonary Diseases". One hundred and thirty two authors made their contributions to this issue and the editors finally assembled 18 full-length articles. The scale of accepted papers is wide covering from basic research to translational medicine and clinical studies. The content includes molecular mechanisms, meta-analysis, candidate compounds, metabolomics and bioinformatics. In our opinion these studies show advanced and useful information in this field, provide new insights into understanding of pathological mechanisms or identification of new therapeutical targets in Chronic Cardiopulmonary Diseases (CCD).

The authors paid attention to the pathophysiological mechanisms and biomarkers in challenging diseases including idiopathic pulmonary fibrosis (IPF), pulmonary hypertension (PH) and pulmonary embolism (PE). For example, it is reported that Sirtuin (Sirt2) may participate in the development of IPF *via* regulating the drosophila mothers against decapentaplegic2/3 (Smad2/3) pathway (Gong et al.). Interferon regulatory factor 9 (IRF9) facilitates pulmonary artery smooth muscle cells proliferation by regulating prohibitin1 (PHB1) expression and protein kinase B (AKT) signaling pathway to affect mitochondrial function during the development of PH (Chen et al.). MicroRNAs with pleiotropic effects have great potential as biomarkers and therapeutic targets for CCD (Condorelli et al., 2014; Saha et al., 2019; Agbu and Carthew, 2021). Luo et al. summarized the literature on miRNA functions in PE, suggesting that miRNA combined with traditional biomarkers or miRNA signatures generated from microchips may be a good predictive tool for PE occurrence and prognosis (Luo et al.).

There are three articles summarizing the advances in PH, pulmonary thromboembolism (PTE) and chronic obstructive pulmonary disease (COPD) and obstructive sleep apnea (OSAS) overlap syndrome (OS). The nitric oxide (NO) pathway is one of the key pathways underlying the pathophysiology of PH (Lau et al., 2017; Galiè et al., 2019; Gorenflo and Ziesenitz, 2021), Tettey et al. suggested that several new substances targeting on NO pathway show a promising potential to represent future alternatives. The current knowledge indicates that COPD and OSAS patients may be at higher risk to develop the cardiovascular diseases. Collection and analysis of clinical data demonstrated that patients with OS possessed deteriorating baseline characteristics and an increased prevalence of cardiovascular diseases, among them the heart failure and PH, compared to the patients with COPD or OSAS alone (Tang et al.). This is a clear reminder for

OPEN ACCESS

Edited and reviewed by:
Paolo Montuschi,
Catholic University of the Sacred Heart, Italy

***Correspondence:**
Xiaohui Li
xiaohuili@csu.edu.cn

Received: *01 April 2022*
Accepted: *19 April 2022*
Published: *19 May 2022*

Citation:
Li X, Kosanovic D, Wang X-J and Cao Y (2022) Editorial: Progresses in the Drug Treatment of Chronic Cardiopulmonary Diseases. Front. Pharmacol. 13:910212. doi: 10.3389/fphar.2022.910212

clinicians to be alerted that OS patients have elevated risk of cardiovascular diseases and that early detection and adequate treatment are crucial for these individuals. Furthermore, it is known that PTE is an important cause of death in the context of cardiovascular diseases (Duffett et al., 2020; Papamatheakis et al., 2020; Piazza, 2020). Following this line, Cao et al. emphasized an overlooked condition, *in situ* pulmonary artery thrombosis and compared the risk factors, the common and specific pathogenic mechanisms underlying PTE, *in situ* pulmonary artery thrombosis, and chronic thromboembolic pulmonary hypertension (CTEPH), coining a new concept of pulmonary artery thrombotic disease and facilitating our understanding of pathogenesis, differential diagnosis, and personalised therapeutics of the three pulmonary artery thrombotic diseases (Cao et al.).

Metabolomics and bioinformatics are increasingly used approaches to identify the differential features between the states of health and disease (Meikle et al., 2014; Ussher et al., 2016; Meyer and Calfee, 2017; Wishart, 2019; Schiano et al., 2020). Scientists from China, Netherlands, Switzerland and Germany together identified a metabolic profile that distinguished pulmonary artery smooth muscle cells from hypoxia-treated and control groups. This project discovered six hypoxia-induced metabolism associated hub genes in response to hypoxia (He et al.), which would lead to the better understanding of the profound molecular mechanisms in hypoxic PH and provide valuable clues to researchers who would follow these emerging genes in the future. Connective tissue disease-associated pulmonary arterial hypertension (CTD-PAH) related gene sets were obtained through text mining by Tan et al. Furthermore, the intersection of gene sets was analyzed for functional enrichment through the DAVID and the STRING was used for the determination of the protein-protein interaction network of the overlapping genes and the significant gene modules. As the outcome, the enriched candidate genes were finally analyzed by Drug Gene Interaction database to find 13 drugs targeting six genes which may potentially result in beneficial therapeutic effects against the severe disease, such as CTD-PAH (Tan et al.).

Meta-analysis is still popular approach with regard to the clinical research of CCD, especially for assessment of the therapeutical effects or adverse events (Schiattarella et al., 2017). Articles discuss the role of inhaled corticosteroids (ICSs) and anti-interleukin-5 (IL-5) therapies in COPD (Chen et al.; Zhang et al.). In addition, clinical practice of sodium-glucose cotransporter 2 inhibitors (SGLT2is) is summarized with regard to the prevention of cardiovascular and respiratory dysfunctions (Yin et al.; Bhatia et al., 2021). Some articles discuss compounds derived from plant extracts or medicinal chemistry research as novel potential treatments for CCD. For example, magnolol isolated from Magnolia Officinalis, Luteolin, Naringin usually extracted from tomatoes and citrus fruits and Sanguinarine, a benzophenanthridine alkaloid obtained primarily from the bloodroot plant were investigated in several pre-clinical experimental models of PH and right ventricle hypertrophy (Fu et al.; Zuo et al.; Wu et al.; Fan et al.). Results of these studies strongly suggested the promising pharmacological effects and revealed the underlying mechanisms of above mentioned natural compounds. One study also indicated the new clinical application of Xuezhikang, an extract of cholestin, which consists of lovastatin, phytosterols and isoflavones and it was previously used to reduce the serum lipid concentrations. Results showed the potential therapeutic effect of Xuezhikang on PH patients with low serum high-density lipoprotein cholesterol (HDL-C) levels (Cao et al.). In the past, we became aware of the existence of significant limitations with regard to the monotherapy, and subsequently the clinical drug combinations were continuously investigated (Lajoie et al., 2016; Savale et al., 2020; Hoeper et al., 2004). Following this paradigm, Shi et al. found that therapy with rapamycin and low dose imatinib together achieved more beneficial effects as compared to the respective monotherapies in order to prevent the PH development. Importantly, new compound and novel therapeutical strategy were developed by Li et al., this compound is HLQ2g which was designed to share the structure of Riociguat and also harbor the anti-fibrosis unit. Basically, it consists of pyrazolpyridine ring (anti-fibrosis functional group) and pyrimidine ring (stimulating soluble guanylate cyclase (sGC) functional group) (Hu et al., 2022). Bifunctional HLQ2g might represent a new pharmacological strategy for PH.

In conclusion, it is clear that despite intensive research efforts to identify and develop new therapies over the past two decades, CCD remain a group of diseases characterized with high morbidity and mortality. The urgent clinical needs are still not properly addressed. Research in this field has become a hot and key venue, waiting for exciting new findings emerging from basic and clinical investigations into the pathophysiology and precise molecular pathobiology of CCD. We strongly call for more attention to CCD and the use of more cutting-edge technology to develop better treatment options.

AUTHOR CONTRIBUTIONS

XL drafted the editorial and all authors give critial correction and suggestion. All authors approved the final version.

REFERENCES

Agbu, P., and Carthew, R. W. (2021). MicroRNA-mediated Regulation of Glucose and Lipid Metabolism. *Nat. Rev. Mol. Cell Biol.* 22, 425–438. doi:10.1038/s41580-021-00354-w

Bhatia, K., Jain, V., Gupta, K., Bansal, A., Fox, A., Qamar, A., et al. (2021). Prevention of Heart Failure Events with Sodium-Glucose Co-transporter 2 Inhibitors across a Spectrum of Cardio-Renal-Metabolic Risk. *Eur. J. Heart Fail* 23, 1002–1008. doi:10.1002/ejhf.2135

Condorelli, G., Latronico, M. V., and Cavarretta, E. (2014). microRNAs in Cardiovascular Diseases: Current Knowledge and the Road Ahead. *J. Am. Coll. Cardiol.* 63, 2177–2187. doi:10.1016/j.jacc.2014.01.050

Duffett, L., Castellucci, L. A., and Forgie, M. A. (2020). Pulmonary Embolism: Update on Management and Controversies. *BMJ* 370, m2177. doi:10.1136/bmj.m2177

Galiè, N., Channick, R. N., Frantz, R. P., Grünig, E., Jing, Z. C., Moiseeva, O., et al. (2019). Risk Stratification and Medical Therapy of Pulmonary Arterial Hypertension. *Eur. Respir. J.* 53. doi:10.1183/13993003.01889-2018

Gorenflo, M., and Ziesenitz, V. (2021). Treatment of Pulmonary Arterial Hypertension in Children. *Cardiovasc. Diagnosis Ther.*, 11. doi:10.21037/cdt-20-912

Hoeper, M. M., Oudiz, R. J., Peacock, A., Tapson, V. F., Haworth, S. G., Frost, A. E., et al. (2004). End Points and Clinical Trial Designs in Pulmonary Arterial Hypertension: Clinical and Regulatory Perspectives. *J. Am. Coll. Cardiol.* 43, 48S–55S. doi:10.1016/j.jacc.2004.02.010

Hu, L., Zhao, C., Chen, Z., Hu, G., Li, X., Li, Q., et al. (2022). An Emerging Strategy for Targeted Therapy of Pulmonary Arterial Hypertension: Vasodilation Plus Vascular Remodeling Inhibition. *Drug Discov. today* 29. doi:10.1016/j.drudis.2022.01.011

Lajoie, A. C., Lauzière, G., Lega, J. C., Lacasse, Y., Martin, S., Simard, S., et al. (2016). Combination Therapy versus Monotherapy for Pulmonary Arterial Hypertension: a Meta-Analysis. *Lancet Respir. Med.* 4, 291–305. doi:10.1016/S2213-2600(16)00027-8

Lau, E. M. T., Giannoulatou, E., Celermajer, D. S., and Humbert, M. (2017). Epidemiology and Treatment of Pulmonary Arterial Hypertension. *Nat. Rev. Cardiol.* 14, 603–614. doi:10.1038/nrcardio.2017.84

Meikle, P. J., Wong, G., Barlow, C. K., and Kingwell, B. A. (2014). Lipidomics: Potential Role in Risk Prediction and Therapeutic Monitoring for Diabetes and Cardiovascular Disease. *Pharmacol. Ther.* 143, 12–23. doi:10.1016/j.pharmthera.2014.02.001

Meyer, N. J., and Calfee, C. S. (2017). Novel Translational Approaches to the Search for Precision Therapies for Acute Respiratory Distress Syndrome. *Lancet Respir. Med.* 5, 512–523. doi:10.1016/S2213-2600(17)30187-X

Papamatheakis, D. G., Poch, D. S., Fernandes, T. M., Kerr, K. M., Kim, N. H., and Fedullo, P. F. (2020). Chronic Thromboembolic Pulmonary Hypertension: JACC Focus Seminar. *J. Am. Coll. Cardiol.* 76, 2155–2169. doi:10.1016/j.jacc.2020.08.074

Piazza, G. (2020). Advanced Management of Intermediate- and High-Risk Pulmonary Embolism: JACC Focus Seminar. *J. Am. Coll. Cardiol.* 76, 2117–2127. doi:10.1016/j.jacc.2020.05.028

Saha, P., Sharma, S., Korutla, L., Datla, S. R., Shoja-Taheri, F., Mishra, R., et al. (2019). Circulating Exosomes Derived from Transplanted Progenitor Cells Aid the Functional Recovery of Ischemic Myocardium. *Sci. Transl. Med.* 11. doi:10.1126/scitranslmed.aau1168

Savale, L., Guimas, M., Ebstein, N., Fertin, M., Jevnikar, M., Renard, S., et al. (2020). Portopulmonary Hypertension in the Current Era of Pulmonary Hypertension Management. *J. Hepatol.* 73, 130–139. doi:10.1016/j.jhep.2020.02.021

Schiano, C., Benincasa, G., Franzese, M., Della Mura, N., Pane, K., Salvatore, M., et al. (2020). Epigenetic-sensitive Pathways in Personalized Therapy of Major Cardiovascular Diseases. *Pharmacol. Ther.* 210, 107514. doi:10.1016/j.pharmthera.2020.107514

Schiattarella, G. G., Sannino, A., Toscano, E., Giugliano, G., Gargiulo, G., Franzone, A., et al. Gut Microbe-Generated Metabolite Trimethylamine-N-Oxide as Cardiovascular Risk Biomarker: a Systematic Review and Dose-Response Meta-Analysis. *Eur. Heart J.* 2017; 38:2948, 2956-+.doi:10.1093/eurheartj/ehx342

Ussher, J. R., Elmariah, S., Gerszten, R. E., and Dyck, J. R. (2016). The Emerging Role of Metabolomics in the Diagnosis and Prognosis of Cardiovascular Disease. *J. Am. Coll. Cardiol.* 68, 2850–2870. doi:10.1016/j.jacc.2016.09.972

Wishart, D. S. (2019). Metabolomics for Investigating Physiological and Pathophysiological Processes. *Physiol. Rev.* 99, 1819–1875. doi:10.1152/physrev.00035.2018

Conflict of Interest: The authors declare that the research was conducted in the absence of any commercial or financial relationships that could be construed as a potential conflict of interest.

Publisher's Note: All claims expressed in this article are solely those of the authors and do not necessarily represent those of their affiliated organizations, or those of the publisher, the editors and the reviewers. Any product that may be evaluated in this article, or claim that may be made by its manufacturer, is not guaranteed or endorsed by the publisher.

frontiers in Pharmacology

ORIGINAL RESEARCH
published: 15 April 2021
doi: 10.3389/fphar.2021.663551

Luteolin Ameliorates Experimental Pulmonary Arterial Hypertension via Suppressing Hippo-YAP/PI3K/AKT Signaling Pathway

Wanyun Zuo[1†], Na Liu[1†], Yunhong Zeng[2], Zhenghui Xiao[2], Keke Wu[1], Fan Yang[1], Biao Li[1], Qingqing Song[1], Yunbin Xiao[2] and Qiming Liu[1]**

[1]Department of Cardiovascular Medicine, The Second Xiangya Hospital of Central South University, Hunan, China, [2]Department of Cardiology, Hunan Children's Hospital, Hunan, China

Luteolin is a flavonoid compound with a variety of pharmacological effects. In this study, we explored the effects of luteolin on monocrotaline (MCT) induced rat pulmonary arterial hypertension (PAH) and underlying mechanisms. A rat PAH model was generated through MCT injection. In this model, luteolin improved pulmonary vascular remodeling and right ventricular hypertrophy, meanwhile, luteolin could inhibit the proliferation and migration of pulmonary artery smooth muscle cells induced by platelet-derived growth factor-BB (PDGF-BB) in a dose-dependent manner. Moreover, our results showed that luteolin could downregulate the expression of LATS1 and YAP, decrease YAP nuclear localization, reduce the expression of PI3K, and thereby restrain the phosphorylation of AKT induced by PDGF-BB. In conclusion, luteolin ameliorated experimental PAH, which was at least partly mediated through suppressing HIPPO-YAP/PI3K/AKT signaling pathway. Therefore, luteolin might become a promising candidate for treatment of PAH.

Keywords: luteolin, Pulmonary arterial hypertension, hippo-yap, PI3K, akt

OPEN ACCESS

Edited by:
Xiaohui Li,
Central South University, China

Reviewed by:
Xinming Xie,
Xi'an Jiaotong University, China
Steven S. An,
Rutgers Institute for Translational Medicine and Science, United States

****Correspondence:***
Yunbin Xiao
xiaoyunbinrui@126.com
Qiming Liu
qimingliu@csu.edu.cn

[†]These authors have contributed equally to this work

Specialty section:
This article was submitted to Respiratory Pharmacology, a section of the journal Frontiers in Pharmacology

Received: *03 February 2021*
Accepted: *23 March 2021*
Published: *15 April 2021*

Citation:
Zuo W, Liu N, Zeng Y, Xiao Z, Wu K, Yang F, Li B, Song Q, Xiao Y and Liu Q (2021) Luteolin Ameliorates Experimental Pulmonary Arterial Hypertension via Suppressing Hippo-YAP/PI3K/AKT Signaling Pathway. Front. Pharmacol. 12:663551. doi: 10.3389/fphar.2021.663551

INTRODUCTION

Pulmonary arterial hypertension (PAH) is a chronic, progressive, extremely malignant disease with high mortality (Edda et al., 2019), which is characterized by continuously increased pulmonary vascular pressure and pulmonary vascular resistance, ultimately leading to right heart failure and sudden death (John et al., 2012). The diagnosis and treatment of PAH has made considerable progress in recent years. The 1, three and 5-years survival rates of patients with high-risk PAH are only 70, 25 and 6% (Kylhammar et al., 2018). However, it is still difficult to reverse the outcome and reduce the high mortality rate of PAH (Lau et al., 2017; Gamou et al., 2018; Kylhammar et al., 2018). The pathogenesis of PAH is related to abnormal pulmonary artery contraction, endothelial dysfunction, vascular remodeling, and *in situ* thrombosis (Thenappan et al., 2018). Among them, the remodeling of small blood vessels caused by the abnormal proliferation and migration of pulmonary arterial smooth muscle cells (PASMCs) plays a critical role (Quatredeniers et al., 2019). Therefore, investigating the underlying mechanism of development of PAH and new molecular targets that prevent pulmonary vascular remodeling is of great importance for treatment of PAH.

The Hippo/YAP signaling pathway plays a key role in regulation of cell migration and proliferation and tissue homeostasis (Johnson and Halder, 2014), and the main factors of the Hippo/YAP signaling pathway are upstream kinase large tumor suppressor 1/2 (LATS1/2) and

downstream transcriptional activation cofactor Yes-associated protein (YAP) (Yu et al., 2015). When the Hippo/YAP signaling pathway is activated, LATS1/2, which is phosphorylated by upstream kinases, promotes the phosphorylation of serine 127 (Ser-127) of YAP, then phosphorylated YAP remains in the cytoplasm by binding to 14-3-3 phosphopeptide and is finally degraded by the proteasome. Conversely, inhibiting the activity of LATS1/2 can lead to dephosphorylation of YAP protein, which promotes its entry into the nucleus, binding to transcription factors and inducing the expression of target genes such as connective tissue growth factor (CTGF), MYC, Cysteine-rich angiogenic inducer 61 (CYR61), Cyclin D1, etc., finally promoting cell proliferation, migration and survival (Zhao et al., 2007; Johnson and Halder, 2014; He et al., 2018). It has been reported that LATS1 is inactivated and higher YAP has been detected in small remodeled pulmonary arteries from idiopathic PAH patients (Kudryashova et al., 2016). Moreover, YAP protein activation is involved in the migration and proliferation of PASMCs and the regulation of pulmonary vascular remodeling (Kudryashova et al., 2016), and studies have shown that YAP directly promotes the transcription of *Pik3cb,* which encodes catalytic subunit p110β of PI3K, through transcription enhancement association domain (TEAD), subsequently activating the PI3K/AKT pathway to promote cardiomyocyte proliferation and survival (Lin et al., 2015). Furthermore, PI3K/AKT pathway plays an important role in pulmonary vascular remodeling. Inhibition of AKT phosphorylation could impede the proliferation of PASMCs and attenuate pulmonary vascular remodeling (Teng et al., 2003; Gary-Bobo et al., 2010; Huang et al., 2017; Zhang et al., 2018).

Luteolin is one of natural flavonoid compounds with multiple pharmacological activities, including anti-inflammatory, anti-allergic, anti-tumor, anti-bacterial, anti-viral, etc.. Studies have shown that luteolin can arrest cell cycle, inhibit the proliferation of tumor cells, and reduce tumor cell migration (Imran et al., 2019; Kang et al., 2019; Feng et al., 2020; Iida et al., 2020). In addition, luteolin can also inhibit the proliferation and migration of vascular smooth muscle cells (Lang et al., 2012; Wu et al., 2018). Recently, it has been reported that luteolin can increase the degradation of YAP protein, thereby inhibiting epithelial mesenchymal transition and breast cancer cell migration (Cao et al., 2020), of which are implicated that luteolin may ameliorates pulmonary arterial hypertension via suppressing Hippo-YAP/PI3K/AKT signaling pathway. This experiment reported the protective ability of luteolin in experimental PAH, and explored its effect on the proliferation of rat primary PASMCs induced by platelet-derived growth factor-BB (PDGF-BB) via inhibiting HIPPO-YAP/PI3K/AKT signaling pathway.

MATERIALS AND METHODS

Animals

This study was performed in strict accordance with the recommendations in Guide for the Care and Use of Laboratory Animals of the National Institutes of Health. The protocol was approved by the Animal Experiment Ethics Committee of the Second Xiangya Hospital of Central South University. Animals Male Sprague–Dawley rats (180–220g, 6–8 weeks old, specific pathogen-free) were supplied by Hunan Slake Jingda Laboratory Animal Co., Ltd. All rats were housed under 12 h light/12 h dark cycle at 22 ± 3 °C and given free access to water and food.

Cell Culture

Male Sprague-Dawley rats aged 6 weeks were euthanized with pentobarbital sodium (100 mg/kg i. p.). The main pulmonary artery, the left and right pulmonary artery were quickly stripped and transferred to the ultra-clean workbench. Then carefully separate the middle layer of pulmonary artery, and the PASMCs were extracted by tissue adhesion. Primary PASMCs were cultured in DMEM/F12 supplemented by 1% streptomycin, 1% penicillin, and 15% fetal bovine serum (BOVOGEN, Cat NO. SFBS) in 5% CO_2 incubator. Cell medium was refreshed every 2–3 days and subcultured when they reached 70–80% confluence. Morphologic appearance by phase-contrast microscopy and immunofluorescence with an anti-α-smooth muscle cell (α-SMA) antibody was used to identify PASMCs (**Supplementary Figure S1**). PASMCs between Passages three and five from different isolations were used to perform independent replicate experiments and were synchronized by serum starvation before intervention.

Reagents

Luteolin with purity of greater than 98% revealed by HPLC analysis was purchased from Aladdin (Shanghai, China, Cat NO. L107329) for animals. Luteolin was provided from MedChemExpress (Monmouth Junction, NJ, United States, Cat NO. 491-70-3) for cell treatment. Carboxymethyl cellulose sodium was purchased from Aladdin (Shanghai, China, Cat NO. 9004-32-4). Monocrotaline (MCT) was provided by Sigma (United States, Cat NO. C2401). The Cell counting kit 8 (CCK-8) and cell cycle detection kit was purchased from DOJINDO (Shanghai, China, Cat NO. CK04 and C543). The EdU Cell Proliferation Kit with Alexa Fluor 555 was provided by Beyotime Biotechnology (Shanghai, China, Cat NO. C0075S). Nuclear and Cytoplasmic Protein Extraction Kit was provided by Beyotime Biotechnology (Shanghai, China, Cat NO. P0027). Bicin-choninic Acid (BCA) Protein Assay Kit was purchased from Cwbio Technology (Beijing, China, CW0014). *α*-SMA antibody was purchased from Servicebio (Wuhan, China, Cat NO. GB11044). *β*-Actin (4D3) monoclonal antibody was provided by Bioworld Technology (United States, Cat NO. BS6007M). PCNA and phospho-YAP (Ser127), total AKT and Phospho-Akt (Ser473) antibodies were provided by Cell Signaling Technology (United States, Cat NO. 14074, 13008, 4691 and 4060). LATS1 and YAP1 antibody was purchased from Proteintech (Wuhan, China, Cat NO. 17049-1-AP and 66900-1-Ig). Phospho-LATS1 (Thr1079) and PIK3CB antibodies were purchased from Affinity Biosciences (Cincinnati, OH, United States, Cat NO. AF7169 and DF6164). HRP-conjugated Affinipure Goat Anti-Mouse IgG (H + L) and HRP-conjugated Affinipure Goat Anti-Rabbit IgG (H + L) was purchased from

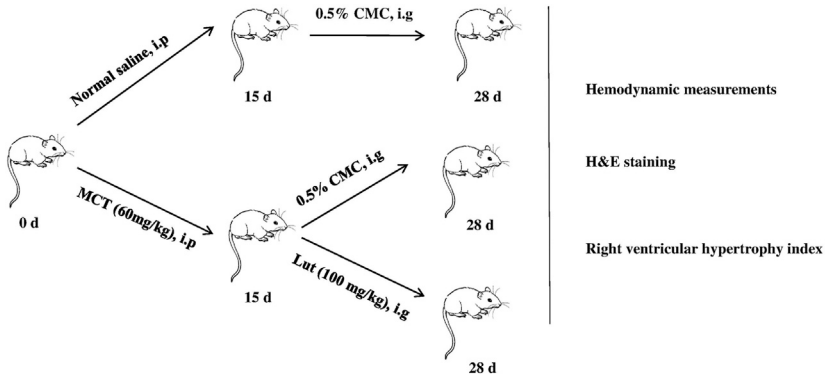

FIGURE 1 | Experimental design. PAH rat models are established by single abdominal subcutaneous injection of MCT (60 mg/kg) on day 0. Subsequently, these rats of luteolin group were also was intragastrically given luteolin at 100 mg/kg/day, suspended in 0.5% carboxymethyl cellulose sodium from days 15–28. The same volume of 0.5% carboxymethyl cellulose sodium was given to the control and MCT-exposed groups from days 15–28. At the end, various experimental methods were used to evaluated the effects of luteolin. MCT, monocrotaline.

Proteintech (Wuhan, China, Cat NO. SA00001-1 and SA00001-2). Cy3 conjugated Goat Anti-mouse IgG (H + L) and FITC conjugated Goat Anti-rabbit IgG (H + L) were provided by Servicebio (Wuhan, China, Cat NO. GB21301 and GB22303).

Experimental Design

24 male rats were randomly assigned to three groups: control group (normal control, $n = 8$), model group (MCT exposure, $n = 8$), and luteolin group (MCT + luteolin, 100 mg/kg/day, $n = 8$). MCT (60 mg/kg) was administered to induce PAH by single abdominal subcutaneous injection on day 0. The control group simultaneously received normal saline on day 0. Subsequently, these rats of luteolin group were also was intragastrically given luteolin at 100 mg/kg/day, suspended in 0.5% carboxymethyl cellulose sodium from days 15–28. The same volume of 0.5% carboxymethyl cellulose sodium was given to the control and MCT-exposed groups from days 15–28. **Figure 1** illustrates the animal experiment design and subsequent analysis. PASMCs were divided into four group: control group, DMSO group (as luteolin was dissolved in DMSO), model group (20 ng/ml PDGF-BB with DMSO) and luteolin group (different concentrations of luteolin).

Hemodynamic Measurements

For right ventricular systolic pressure (RVSP) measurement, the experimental rats were anesthetized with 1% sodium pentobarbital (130 mg/kg i. p.), RVSP was measured via putting the Millar® catheter (AD Instruments Inc. Colorado Springs, CO) into the right ventricle along the right internal jugular vein.

Evaluation of Right Ventricular Hypertrophy

Following the pressure measurements, the experimental rats were euthanized, and the lungs and hearts were harvested. The hearts were divided into the right ventricle (RV) and left ventricle (LV) plus the inter-ventricular septum (S). And the right ventricular hypertrophy index (RVHI) (RVHI = weight $_{RV}$/weight $_{LV+S}$) were calculated.

Histomorphometric Analysis

The rat lung tissues were fixed with 4% paraformaldehyde for 24 h for histomorphometric analysis, then embedded into paraffin, sliced into 5-μm-thick sections and subjected to hematoxylin and eosin (H.E.) staining. Randomly select 10–20 small pulmonary blood vessels with a diameter of 50–150 μm from each slice and analyze them at a magnification of 4. The two indicators that reflect pulmonary artery remodeling are calculated as follows: 1) pulmonary artery wall thickness ratio (wt%) = (outer diameter − inner diameter)/outer diameter and 2) pulmonary artery wall area ratio (WA%) = (transection area of the walls − lumen area)/transection area of the walls.

Measurement of Cell Proliferation

CCK-8 was used to determine the effect of different luteolin doses (5–80 μM) in PASMCs proliferation. When PASMCs grown to 70–80% confluence, cells were starved for 24 h with serum free DMEM/F12 medium. After starvation, cells were pretreated with luteolin for 1 h, treated with PDGF-BB (20 ng/ml) for 24 h and incubated with CCK-8 for the last 2 h. Cell proliferation was determined by measuring the absorbance at 450 nm.

Measurement of Cell DNA Synthesis

DNA synthesis as a measurement of cellular proliferation was obtained by EdU kit. Appropriate number of PASMCs were cultured in glass bottom dishes (Thermo Fisher Scientific, Waltham, MA, United States). After 24 h of serum-deprivation, cells were treated with luteolin (40 μM) and PDGF-BB (20 ng/ml) for 24 h. EdU incorporation was carried out according to the manufacturer's specifications and then quantification was performed by laser confocal microscopy to randomly shoot five fields (200 cells) and count the positive rate of EdU.

Migration Assays

PASMCs were plated into the six-well plate with five horizontal mark lines at the bottom, then cells were starved for 12 h when growing to 90% confluence. Three straight scratch was made

vertically in the center of the well by 1 ml pipette tip and was photographed, then the cells were incubated with the luteolin (20 μM) and PDGF-BB (20 ng/ml). After 24 h, the scratch was photographed for comparison with the previous images. The scratch area was calculated by using ImageJ software and cell migration ratio was analyzed by (scratch area 0 h − scratch area 24 h)/scratch area 0 h.

Western Blot

RIPA lysis buffer supplemented with complete protease and phosphatase inhibitor cocktail (100:1) was used for total protein extraction. Nuclear and Cytoplasmic Protein Extraction Kit was used for extraction of nuclear protein and cytoplasmic protein. The protein content was determined by BCA assay. Each sample was subjected to SDS-PAGE (8, 10 and 12.5%) and immunoblotted with PCNA antibody (diluted 1: 1,000), LATS1 (diluted 1:2000), p-LATS1 (diluted 1:500), YAP1 (diluted 1: 2000), p-YAP (diluted 1: 1,000), PIK3CB (diluted 1: 1,000), AKT (diluted 1:1,000), p-AKT (diluted 1:2000) and β-actin (diluted 1:5,000) overnight at 4°C. IgG-HRP secondary antibody was incubated (diluted 1: 5,000) for 1 h at room temperature. Antibody binding signal visualization used ECL chemiluminescence kit. Finally, ImageJ software was used to attribute densitometry values to quantify the results.

RT-qPCR

To investigate the expression of target genes, total RNA was extracted and isolated from PASMCs according to the Trizol kit instructions (Invitrogen, CA, United States). Next, the isolated RNA was reverse transcribed into cDNA using a reverse transcription kit (Thermo Fisher Scientific, MA, United States). Quantitative real-time RT-PCR was performed using the Power SYBR Green PCR Master Mix (Bio-Rad, United States). Gene expression was quantified using β-actin as an internal control. The PCR primers as following: LATS1: forward 5′-AGCTCACTCTCTGGTTGGGA−3′ and reverse 5′-CTTGGCTTGAGGTGGGATGT−3′; YAP1: forward 5′-CGT GCCCATGAGGCTTCGCA-3′ and reverse 5′-TCGGTACTG GCCTGTCGCGA-3′; β-actin: forward 5′-CACCCGCGAGTA CAAC-CTTC-3′ and reverse 5′-CCCATACCCACCATCACA CC-3′.

Immunofluorescence

Cells were fixed with 4% paraformaldehyde for 30 min at room temperature, permeabilized with 0.1% triton X-100 for 20 min, and blocked with 5% BSA at room temperature for 30 min. Cell immunofluorescence staining was performed by incubation with primary antibodies (α-SMA, diluted 1:100; YAP, diluted 1:200) overnight, and cells were subsequently washed and incubated with fluorescent secondary antibodies at room temperature for 1 h, and finally mounted by fluorescent mounting medium with DAPI. Take pictures with laser confocal microscope.

Statistical Analysis

All data were presented as mean ± standard deviation (SD) and performed using SPSS 24.0 Statistical Software. All *in vitro* experiments were repeated at least three times. Data were examined through one way ANOVA to determine differences between control and experimental groups. For all the statistical tests, $p < 0.05$ was considered as statistically significant.

RESULTS

Luteolin Effectively Improves Monocrotaline-Induced Pulmonary Arterial Hypertension and Pulmonary Vascular Remodeling

Compared to control group, 4 weeks after MCT injection, the rats showed a significant increase in RVSP and luteolin could effectively reverse the increase in RVSP induced by MCT (**Figures 2A,B**). HE staining was consistent with hemodynamic results. MCT caused manifest vascular remodeling, and luteolin significantly alleviated the thickening of the pulmonary artery wall induced by MCT (**Figures 2C–E**). Consistent results were observed for right ventricular hypertrophy index (RV/LV + S). As shown in **Figure 2F**, RV/LV ± S in the MCT group was much higher than that in the control group and luteolin could reduce the increase of RV/LV ± S caused by MCT. The above results indicated that luteolin effectively relieved MCT-induced PAH and pulmonary vascular remodeling.

Luteolin Inhibits the Proliferation of Platelet-Derived Growth Factor-BB Induced Rat Pulmonary Arterial Smooth Muscle Cells

Firstly, we used CCK-8 to detect the effect of luteolin on PDGF-BB induced PASMCs proliferation. Experimental results showed that PDGF-BB could effectively promote the proliferation of PASMCs, while luteolin inhibited PDGF-BB induced proliferation in a dose-dependent manner (**Figure 3A**). Then we used EdU incorporation experiments to evaluate the effect of luteolin on the DNA synthesis of PASMCs. The results showed that luteolin could significantly inhibit the PDGF-BB induced DNA synthesis of PASMCs (**Figures 3B,C**). Moreover, Western blot results showed that PDGF-BB exposure resulted in increased expression of proliferation protein PCNA, while luteolin inhibits the expression of PCNA induced by PDGF-BB in a concentration-dependent manner (**Figures 3D,E**). The above results indicated that luteolin inhibited PDGF-BB induced PASMCs proliferation.

Luteolin Inhibits the Migration of Platelet-Derived Growth Factor-BB Induced Rat Pulmonary Arterial Smooth Muscle Cells

The abnormal migration of PASMCs also plays a key role in pulmonary vascular remodeling. *In vitro*, scratch healing experiment was used to evaluate the effect of luteolin on

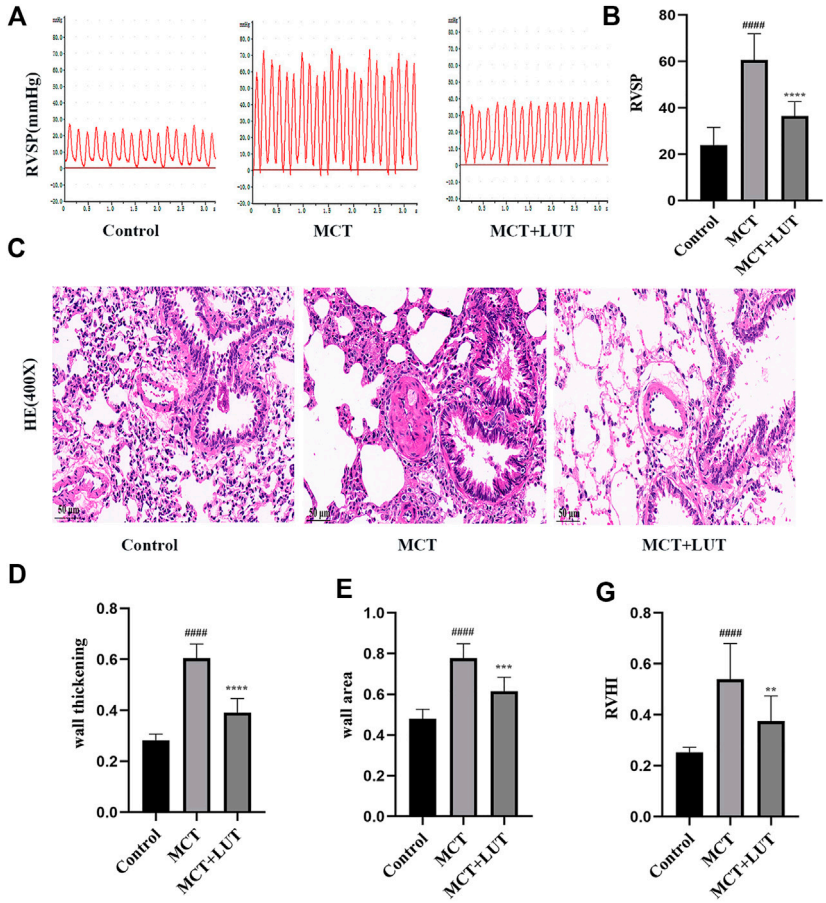

FIGURE 2 | Luteolin effectively relieves MCT-induced PAH and pulmonary vascular remodeling. **(A)** Representative images of RVSP waveform ($n = 6$). **(B)** Statistical graph of RVSP ($n = 6$). **(C)** H. E. staining of pulmonary arterioles from control rats, MCT rats and MCT + LUT rats (400X) ($n = 8$) **(D)** Statistical graph of pulmonary vessel wall thickening ($n = 8$). **(E)** Statistical graph of pulmonary vessel wall area ($n = 8$). **(F)** Statistical graph of RVHI ($n = 8$). Scale: 50 μm, bars represent means ± SD, #control group *vs* MCT group, #$p < 0.05$, ##$p < 0.01$, *MCT group *vs* LUT group, *$p < 0.05$, **$p < 0.01$, ***$p < 0.001$, ****$p < 0.0001$. LUT, luteolin; MCT, monocrotaline; PAH, RVHI, right ventricular hypertrophy index; RVSP, right ventricular systolic pressure.

PDGF-BB induced migration of PASMCs. PDGF-BB exposure resulted in an increase in PASMCs migration, which was restrained by Luteolin (**Figures 4A,B**). Notably, luteolin significantly reversed the increase in MMP9 expression induced by PDGF-BB with a dose-dependent manner (**Figures 4C,D**).

Luteolin Inhibits the Increase of Transcription and Protein Expression of Key Molecules in Hippo/Yes-Associated Protein Signaling Pathway Induced by Platelet-Derived Growth Factor-BB

After PDGF-BB stimulation, the mRNA and protein level of LATS1 and YAP were significantly increased, which could be inhibited by luteolin (**Figures 5A–F**). Furthermore, we explored the expression of phosphorylated LATS1 and YAP under PDGF-BB stimulation and luteolin treatment. The experimental results showed that phosphorylated LATS1 and YAP and total LATS1 and YAP had a similar trend, but the degree of change was not as obvious as that of total LATS1 and YAP and luteolin increased the ratio of p-YAP/YAP but not p-LATS1/LATS1 (**Figures 5C–F**).

Luteolin Decreases Yes-Associated Protein Nuclear Localization Induced by Platelet-Derived Growth Factor-BB

As a transcriptional co-activator, YAP regulates cell proliferation and migration mainly through its localization in the nucleus. Therefore, immunofluorescence and Western blot were used to explored the effect of luteolin on YAP nuclear localization. In the present study, PDGF-BB caused an increase in YAP nuclear localization, which were inhibited by luteolin (**Figures 6A–C**).

Luteolin Inhibits PI3K/AKT Signal Pathway

Hippo/YAP signaling pathway had extensive interaction with other proliferation-related signaling pathways, among which AKT is the most important candidate pathway (Kudryashova

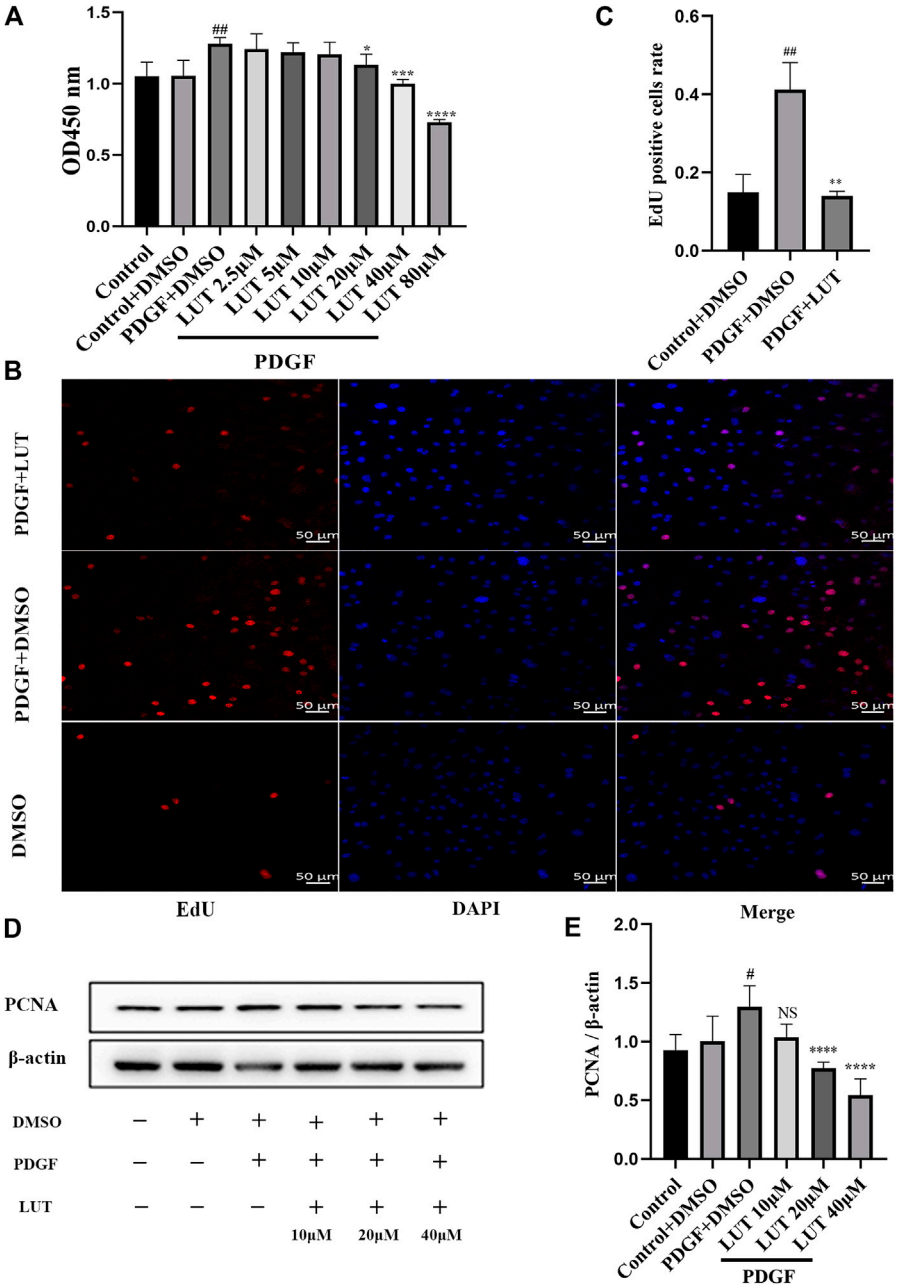

FIGURE 3 | Luteolin inhibits the proliferation of rat PASMCs induced by PDGF-BB. PASMCs were cultured in 1% serum medium for 24 h, then treated with different concentrations of luteolin for 1 h before the stimulation with PDGF-BB (20 ng/ml). **(A)** Cell proliferation was examined using the Cell Counting kit eight test ($n = 4$); **(B)** and **(C)** DNA synthesis was examined using EdU, luteolin significantly inhibited the PDGF-BB induced DNA synthesis of PASMCs ($n = 3$). **(D)** and **(E)** the expression of protein level of PCNA was determined by western blot ($n = 5$). Scale: 50 μm, Bars represent means ± SD, #DMSO group *vs* PDGF + DMSO group, #$p < 0.05$, ##$p < 0.01$, *PDGF + DMSO group *vs* PDGF + LUT group, *$p < 0.05$, **$p < 0.01$, ***$p < 0.001$, ****$p < 0.0001$. DAPI, 4,6-diamino-2-phenylindole; EdU, 5-ethynyl-2′-deoxyuridine; LUT, luteolin; PASMCs, pulmonary arterial smooth muscle cells; PCNA, proliferating cell nuclear antigen; PDGF-BB, platelet-derived growth factor-BB.

et al., 2016). Thus, we determined whether PI3K/AKT signaling pathway was also inhibited by luteolin. As anticipated, the change of PIK3CB induced by PDGF-BB was weakened by luteolin (**Figures 7A,B**). Luteolin significantly reduced the expression of phosphorylated AKT and the ratio of p-AKT/AKT induced by PDGF-BB (**Figures 7C,D**).

DISCUSSION

This study demonstrated that luteolin could significantly attenuate pulmonary vascular remodeling induced by MCT in rats. Simultaneously, luteolin could inhibit PDGF-BB-induced PASMCs proliferation and migration. Furthermore, this study

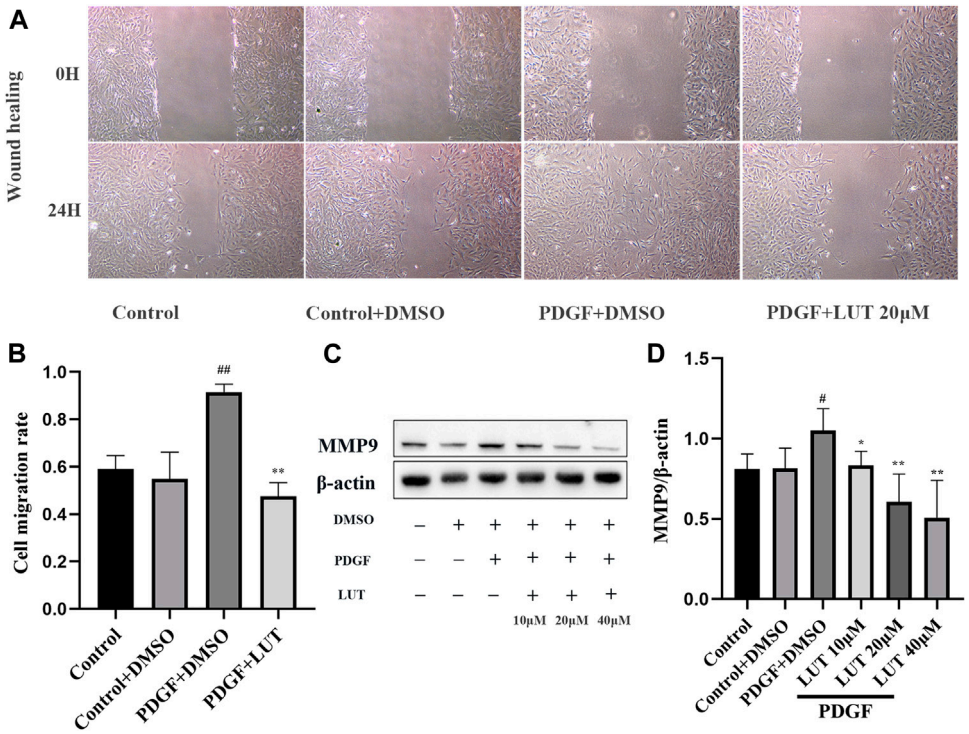

FIGURE 4 | Luteolin inhibits the migration of rat PASMCs induced by PDGF-BB. PASMCs were starved for 24 h in 1% serum medium, then treated with different concentrations of luteolin for 1 h before the stimulation with PDGF-BB (20 ng/ml). **(A)** Representative images from the wound healing assay of PASMCs (40X) ($n = 3$). **(B)** Statistical graph of wound healing experiment ($n = 3$). **(C)** and **(D)** the expression of protein level of MMP9 ($n = 3$). Bars represent means ± SD, #DMSO group *vs* PDGF + DMSO group, #$p < 0.05$, ##$p < 0.01$, *PDGF + DMSO group *vs* PDGF + LUT group, *$p < 0.05$, **$p < 0.01$, ***$p < 0.001$. MMP9, matrix metallopeptidase 9; LUT, luteolin; PASMCs, pulmonary arterial smooth muscle cells; PDGF-BB, platelet-derived growth factor-BB.

demonstrated the protective effect of luteolin was to inhibit the expression and nuclear localization of YAP and downstream PI3K/AKT signaling pathway. This study explained the mechanism of luteolin in relieving PAH, and scientifically revealed that it may become a potential drug for the treatment of PAH.

MCT is an alkaloid from the seed crotalaria spectabilis plant, which is transformed into toxicity metabolite dehydromonocrotaline (MCTP) (Wilson et al., 1992). MCTP deposits on pulmonary capillaries and pulmonary arterioles, leading to vascular endothelial cell apoptosis, PASMCs proliferation and inhibition of PASMCs apoptosis (Nogueira-Ferreira et al., 2015). PDGF-BB is the most effective mitogenic factor in vascular smooth muscle cells, which can be excessively released by stimuli such as hypoxia, inflammation and endothelial damage. Studies have shown that PDGF-BB can stimulate the activation of downstream signal molecules by binding to its corresponding receptors PDGFR α and β, thereby triggering the proliferation and migration of vascular smooth muscle (Garat et al., 2010; Perez et al., 2010; Antoniu, 2012; Xiao et al., 2017). The expressions of PDGF and PDGFR in the lung tissues of PAH patients and animal models are significantly up-regulated, and the up-regulated PDGF and PDGFR are mainly located in pulmonary arteriole smooth muscle cells (Barst, 2005; Perros et al., 2008). These studies indicate that PDGF-BB play an important role in the proliferation of PASMCs. Therefore, this study intends to use PDGF-BB-induced PASMCs proliferation model to explore whether luteolin can improve PAH by regulating the abnormal proliferation of PASMCs.

Luteolin is a low-toxicity natural flavonoid compound that exists in many natural plants, which have been proved to have a protective effect on a variety of cardiovascular diseases, such as atherosclerosis (Ding et al., 2019), ischemia-reperfusion (Wei et al., 2018; Xiao et al., 2019), heart failure (Hu et al., 2017), and hypertension (Oyagbemi et al., 2018). Moreover, a number of studies have shown that luteolin can inhibit cell proliferation (Imran et al., 2019; Kang et al., 2019; Feng et al., 2020; Iida et al., 2020), which arouses our attention to the protective effect of luteolin on PAH. In this study, we established PAH models by injection MCT and PASMCs proliferation models by PDGF-BB treatment to study the mechanism of luteolin in improving PAH. Hemodynamic detection and histological analysis showed that luteolin could significantly reduce MCT-induced increasing in RVSP, improve pulmonary vascular remodeling and relieve right ventricular hypertrophy. Moreover, PDGF-BB induced proliferation of PASMCs could be inhibited by luteolin in CCK-8 and EdU experiments. Increased migration of PASMCs

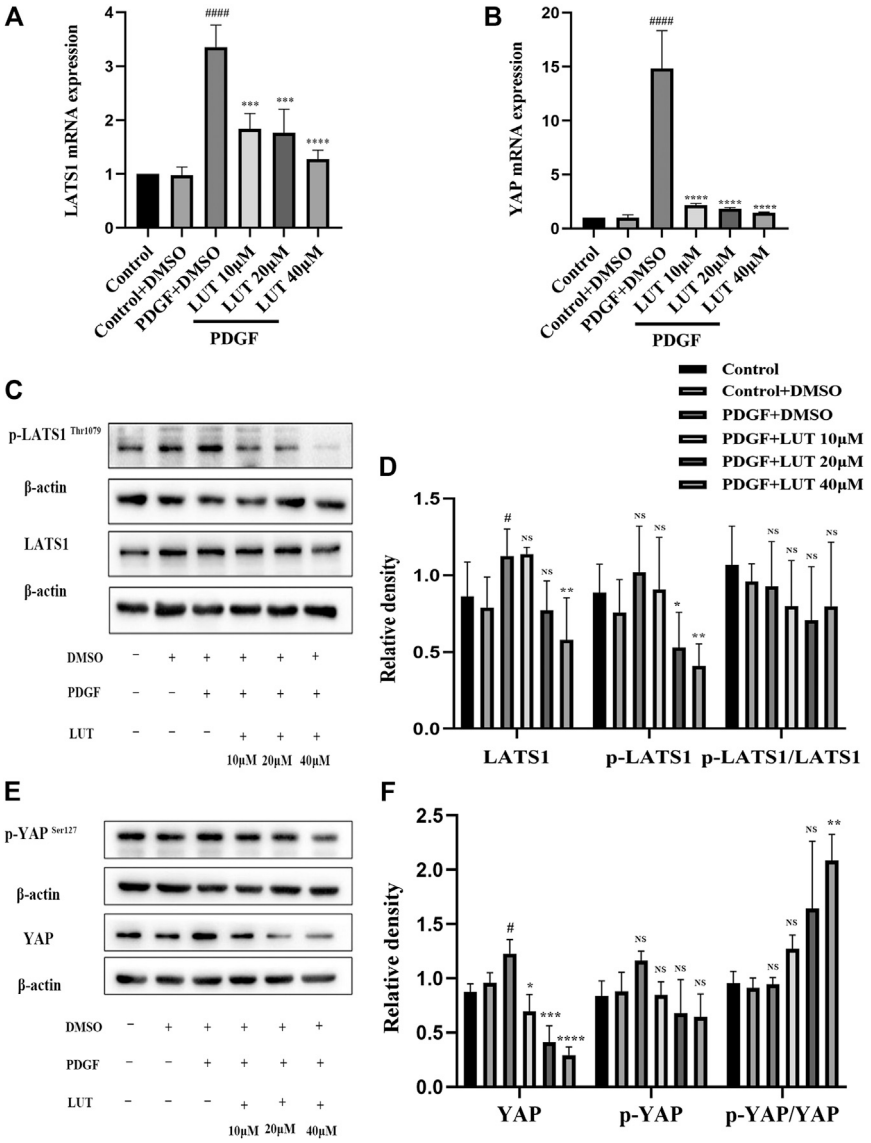

FIGURE 5 | Luteolin inhibits the increase of mRNA and protein expression of key molecules in Hippo/YAP signaling pathway induced by PDGF-BB. PASMCs were cultured in 1% serum medium for 24 h, then treated with different concentrations of luteolin for 1 h before the stimulation with PDGF-BB (20 ng/ml). **(A)** mRNA level of LATS1 ($n = 3$). **(B)** mRNA level of YAP ($n = 3$). **(C)** and **(D)** the expression of protein level of LATS1 and phosphorylated LATS1 ($n = 5$). **(E)** and **(F)** the expression of protein level of YAP and phosphorylated YAP ($n = 3$). Bars represent means ± SD of $n = 3$–6, #DMSO group *vs* PDGF + DMSO group, #$p < 0.05$, ##$p < 0.01$, ###$p < 0.0001$, ###$p < 0.0001$, ####$p < 0.00001$, *PDGF + DMSO group *vs* PDGF + LUT group, *$p < 0.05$, **$p < 0.01$, ***$p < 0.001$, ****$p < 0.0001$, NS indicates no significance. LATS1, large tumor suppressor one; LUT, luteolin; PASMCs, pulmonary arterial smooth muscle cells; PDGF-BB, platelet-derived growth factor-BB; YAP, yes-association protein.

is another important cause of pulmonary vascular remodeling, which means that inhibiting the migration of PAMSCs is also important for reversing pulmonary vascular remodeling. In this study, wound healing experiments proved that luteolin significantly inhibited the migration of PASMCs induced by PDGF-BB, which suggested luteolin improved pulmonary vascular remodeling via inhibiting migration of PASMCs. Cell migration and invasion are inseparable from the protein degradation of extracellular matrix and vascular basement membrane. MMP is a zinc-dependent proteolytic enzyme of extracellular matrix, which plays a key role in the process of cell migration and invasion (Newby et al., 1994). In pulmonary arterial hypertension, the activity and expression of MMPs increase, and reducing the activity of MMPs can increase the apoptosis of pulmonary artery endothelial cells and smooth muscle cells, and improve pulmonary vascular remodeling (Lepetit et al., 2005; Okada et al., 2009). As an important member of MMPs, MMP-9 can degrade a variety of extracellular matrix and is involved in the initial proliferation of smooth muscle cells (Southgate et al., 1992). Our

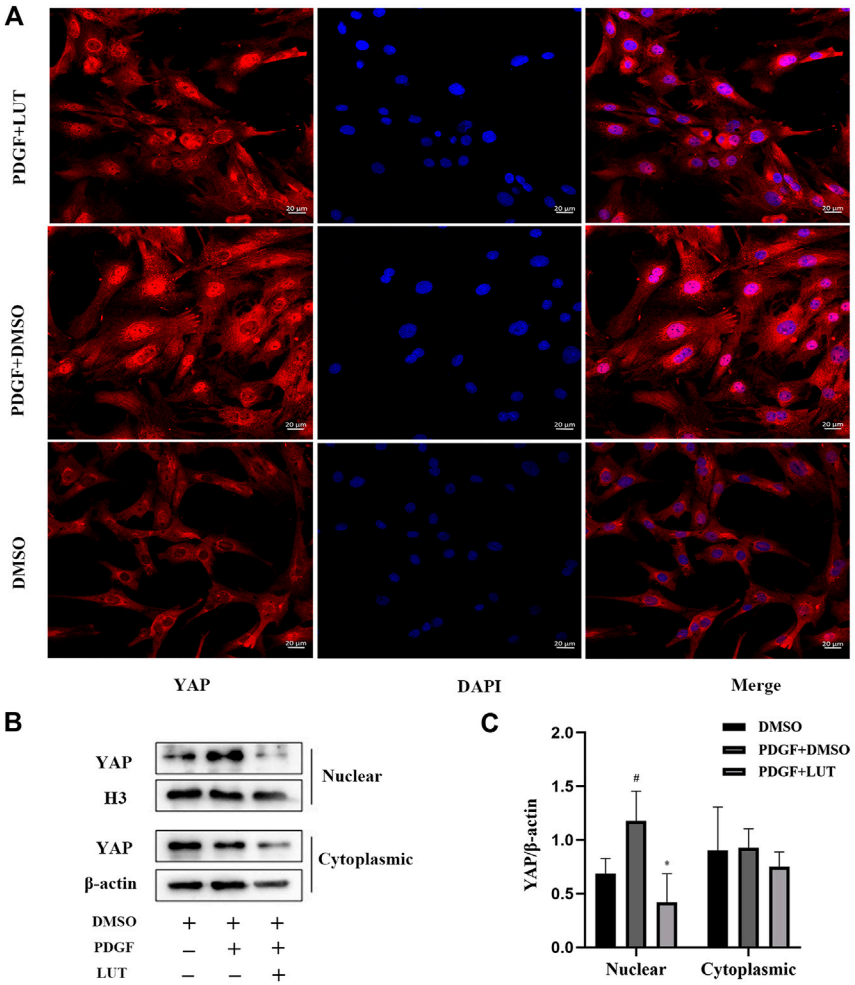

FIGURE 6 | Luteolin decreases YAP nuclear localization induced by PDGF-BB. PASMCs were cultured in 1% serum medium for 24 h, then treated with luteolin (40 μM)for 1 h before the stimulation with PDGF-BB (20 ng/ml). The nuclear and cytoplasmic proteins are extracted separately and were measured by western blot analysis (A) Representative confocal microscopy images of immunofluorescence staining of YAP (red), luteolin decreased YAP nuclear localization induced by PDGF-BB (B) and (C) YAP levels in nuclear and cytoplasmic (n = 5). Scale: 20 μm, bars represent means ± SD, #DMSO group *vs* PDGF + DMSO group, #$p < 0.05$, *PDGF + DMSO group *vs* PDGF + LUT group, *$p < 0.05$. DAPI, 4,6-diamino-2-phenylindole; LUT, luteolin; PASMCs, pulmonary arterial smooth muscle cells; PDGF-BB, platelet-derived growth factor-BB; YAP, yes-association protein.

experimental results showed that luteolin reduced the expression of MMP-9 indued by PDGF-BB, which indicated luteolin inhibited migration of pulmonary vascular remodeling via reducing MMP-9 expression.

Pulmonary vessel remodeling caused by abnormal proliferation and migration of PAMSCs is an important pathological change of PAH (Thenappan et al., 2018), and the abnormal activation of YAP plays an important role in pulmonary vessel remodeling (Kudryashova et al., 2016). The core component of the Hippo/YAP signaling pathway is composed of a kinase chain, including Ste20-like protein kinases (MST)1/2, LATS1/2, and the downstream transcriptional coactivator YAP (Yu et al., 2015). After phosphorylation of LATS1 promotes the phosphorylation of YAP. The phosphorylated YAP is retained in the cytoplasm and is degraded by the proteasome. In contrast, dephosphorylated YAP is located in the nucleus and interacts with TEAD family transcription factors to promote target gene expression (Zhao et al., 2007; Johnson and Halder, 2014; He et al., 2018). Therefore, Hippo/YAP signal pathway is a potential target for PAH therapy. Although studies have found some YAP inhibitors, there are currently no YAP/TAZ inhibitors available clinically (Liu-Chittenden et al., 2012; Oku et al., 2015). Research by Cao et al. suggested that luteolin was a new type of YAP inhibitor (Cao et al., 2020). Our experiment results showed that luteolin could inhibit the increase in LATS1 and YAP transcription and protein expression caused by PDGF-BB. However, p-LATS1 and p-YAP had consistent changes with LATS1 and YAP, although the decrease of p-YAP had no statistical significance, p-YAP/YAP ratio increased after 40 μM luteolin treatment, which suggested that luteolin actually

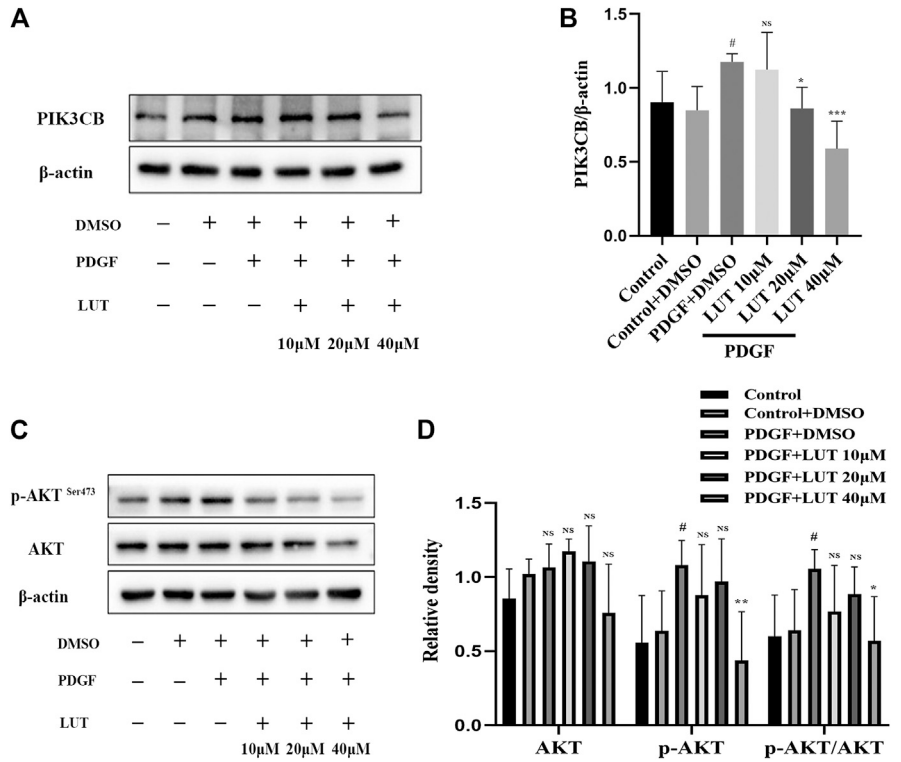

FIGURE 7 | Luteolin inhibits PI3K/AKT signal pathway. PASMCs were cultured in 1% serum medium for 24 h, then treated with different concentrations of luteolin for 1 h before the stimulation with PDGF-BB (20 ng/ml). **(A)** and **(B)** The expression of protein level of PIK3CB was determined by western blot, luteolin reduced the expression of PIK3CB induced by PDGF-BB ($n = 4$). **(C)** and **(D)** The expression of protein level of total AKT and phosphorylated AKT and the ratio of p-AKT/AKT, luteolin significantly reduced the expression of phosphorylated AKT and the ratio of p-AKT/AKT induced by PDGF-BB ($n = 5$). Bars represent means ± SD of, #DMSO group *vs* PDGF + DMSO group, #$p < 0.05$, *PDGF + DMSO group *vs* PDGF + LUT group, *$p < 0.05$, NS indicates no significance. AKT, protein kinase B; LUT, luteolin; PASMCs, pulmonary arterial smooth muscle cells; PDGF-BB, platelet-derived growth factor-BB; PIK3CB, phosphatidylinositol 3-kinase catalytic beta polypeptide.

increased the phosphorylation efficiency of YAP. The function of YAP was determined by its localization in the nucleus or cytoplasm (Mesrouze et al., 2017), further immunofluorescence and western blot analysis showed luteolin could obviously reduce nuclear localization of YAP induced by PDGF-BB, therefore, all these finding indicated that luteolin could inhibit the activation of Hippo/YAP signal pathway by reducing nuclear localization of YAP.

Furthermore, as a transcriptional co-activator in the Hippo signaling pathway, YAP interacts with related molecules in many proliferation-related signal pathways such as PI3K/AKT, Wnt/β-catenin, NOTCH, which makes the Hippo/YAP pathway and other proliferation regulation-related signal pathways form a complex signal pathway network to regulate cell growth and proliferation. Among them, AKT is the most probable candidate (Kudryashova et al., 2016). YAP can directly activate the expression of Pik3cb through TEAD, promoting the transcription of PI3K and then activating AKT (Lin et al., 2015; Shen et al., 2020). PI3K/AKT signal plays an important role in regulation of cell migration, proliferation and survival (Yu & Cui, 2016). Consistent with these studies, we also observed the inhibitory effect of luteolin on the PI3K/AKT pathway activation induced by PDGF-BB stimulation.

A large number of literatures prove that luteolin is a classic flavonoid drug that inhibits the AKT pathway. And luteolin inhibits the proliferation and migration of a variety of tumor cells and vascular smooth muscle cells via inhibiting the AKT pathway (Lang et al., 2012; Ding et al., 2014; Lim et al., 2016; Yao et al., 2019; Wu et al., 2021). The latest research also has proved that luteolin is a new type of YAP inhibitor (Cao et al., 2020). At the same time, YAP promotes cell proliferation by activating the AKT pathway (Lin et al., 2015; Shen et al., 2020). YAP and PI3K/AKT signaling pathways play an important role in regulating the proliferation and migration of PASMCs (Teng et al., 2003; Kudryashova et al., 2016; Huang et al., 2017; Zhang et al., 2018). Therefore, this study chose the Hippo-YAP/I3K/AKT signaling pathway as the target pathway for luteolin to inhibit the proliferation of PASMCs. However, luteolin also has a variety of biological activities and can inhibit the activation of multiple proliferation-related pathways. Luteolin inhibits the mitogen-activated protein kinase (MAPK) signaling pathway of the downstream signaling pathway of epidermal growth factor, thereby inhibiting the proliferation of glioblastoma (Anson et al., 2018). Luteolin restrained the proliferation and

migration of gastric cancer cells by inhibiting Notch signal transduction (Zang et al., 2017). In addition, Inflammation is also involved in the occurrence and development of PAH. Inflammatory factors such as interleukin 6, interleukin 21, interleukin 1β can also promote the proliferation and migration of PASMCs (Hashimoto-Kataoka et al., 2015; Prins et al., 2018; Zhang et al., 2020; Tang et al., 2021). luteolin exert anti-inflammatory effects though inhibiting the expression and secretion of a variety of inflammatory factors (Seelinger et al., 2008; Nabavi et al., 2015). Similarly, PDGF-BB can also promote cell proliferation and migration through a variety of other ways. The study of Xiao et al. proved that PDGF-BB enhanced the Warburg effect and promoted the proliferation of PASMCs through the PI3K/AKT/mTOR/HIF-1α pathway (Xiao et al., 2017). Zhang et al. proved that PDGF-BB activated the Ras homolog gene/a Rho-associated coiled coil-forming protein kinase (Rho/ROCK) pathway of PASMCs (Zhang et al., 2019). PDGF-BB activates MAPK pathway to induce the migration of retinal pigment epithelial cells (Chan et al., 2013) and the proliferation of PASMCs (Cui et al., 2016). Our research proved that luteolin restrained the proliferation of PASMCs and improved PAH at least partly through inhibiting Hippo-YAP/PI3K/AKT pathway, but whether luteolin inhibits the proliferation of PASMCs through signal pathways remains to be further studied.

CONCLUSION

In summary, luteolin ameliorates experimental pulmonary arterial hypertension, and which exerts protective effects partly by reducing YAP nuclear localization and inhibiting the activation of the downstream PI3K/AKT pathway. Therefore, luteolin might be a promising candidate for PAH target medicine.

DATA AVAILABILITY STATEMENT

The raw data supporting the conclusions of this article will be made available by the authors, without undue reservation.

ETHICS

The animal study was reviewed and approved by Animal Experiment Ethics Committee of the Second Xiangya Hospital of Central South University.

AUTHOR CONTRIBUTIONS

WZ was responsible for the design. WZ and NL performed execution and data curation of the project. QL and YX conducted project administration, reviewing and editing. YZ, ZX, QS carried through supervision. KW, Fan Yang, BL processed writing-original draft. All authors commented on and approved the final manuscript.

FUNDING

This project was supported by grants from the National Natural Science Foundation of China (No. 81770337), Hunan Province Traditional Chinese Medicine Research Program Project (No. 201914), Hunan Provincial Natural Science Youth Foundation of China (No. 2019JJ50881), and Hunan Provincial Key Platform Project (2018TP1028).

SUPPLEMENTARY MATERIAL

The Supplementary Material for this article can be found online at: https://www.frontiersin.org/articles/10.3389/fphar.2021.663551/full#supplementary-material.

REFERENCES

Anson, D. M., Wilcox, R. M., Huseman, E. D., Stump, T. A., Paris, R. L., Darkwah, B. O., et al. (2018). Luteolin decreases epidermal growth factor receptor-mediated cell proliferation and induces apoptosis in glioblastoma cell lines. *Basic Clin. Pharmacol. Toxicol.* 123, 678–686. doi:10.1111/bcpt.13077

Antoniu, S. A. (2012). Targeting PDGF pathway in pulmonary arterial hypertension. *Expert Opin. Ther. Targets* 16, 1055–1063. doi:10.1517/14728222.2012.719500

Barst, R. J. (2005). PDGF signaling in pulmonary arterial hypertension. *J. Clin. Invest.* 115, 2691–2694. doi:10.1172/JCI26593

Cao, D., Zhu, G.-Y., Lu, Y., Yang, A., Chen, D., Huang, H.-J., et al. (2020). Luteolin suppresses epithelial-mesenchymal transition and migration of triple-negative breast cancer cells by inhibiting YAP/TAZ activity. *Biomed. Pharmacother.* 129, 110462. doi:10.1016/j.biopha.2020.110462

Chan, C.-M., Chang, H.-H., Wang, V.-C., Huang, C.-L., and Hung, C.-F. (2013). Inhibitory effects of resveratrol on PDGF-BB-induced retinal pigment epithelial cell migration via PDGFRβ, PI3K/akt and MAPK pathways. *PLoS One* 8, e56819, doi:10.1371/journal.pone.0056819

Cui, C., Zhang, H., Guo, L.-N., Zhang, X., Meng, L., Pan, X., et al. (2016). Inhibitory effect of NBL1 on PDGF-BB-induced human PASMC proliferation through blockade of PDGFβ-p38MAPK pathway. *Biosci. Rep.* 36. doi:10.1042/BSR20160199

Ding, H., Li, D., Zhang, Y., Zhang, T., Zhu, H., Xu, T., et al. (2014). Luteolin inhibits smooth muscle cell migration and proliferation by attenuating the production of Nox4, p-Akt and VEGF in endothelial cells. *Cpb* 14, 1009–1015. doi:10.2174/1389201015666140113113843

Ding, X., Zheng, L., Yang, B., Wang, X., and Ying, Y. (2019). Luteolin attenuates atherosclerosis via modulating signal transducer and activator of transcription 3-mediated inflammatory response. *Dddt* 13, 3899–3911. doi:10.2147/DDDT.S207185

Edda, S., Sm, K., and Va, d. J. P. (2019). New and emerging therapies for pulmonary arterial hypertension. *Annu. Rev. medicin* 70, 45–59. doi:10.1146/annurev-med-041717-085955

Feng, J., Zheng, T., Hou, Z., Lv, C., Xue, A., Han, T., et al. (2020). Luteolin, an aryl hydrocarbon receptor ligand, suppresses tumor metastasis in vitro and in vivo. *Oncol. Rep.* 44, 2231–2240. doi:10.3892/or.2020.7781

Gamou, S., Kataoka, M., Aimi, Y., Chiba, T., Momose, Y., Isobe, S., et al. (2018). Genetics in pulmonary arterial hypertension in a large homogeneous Japanese population. *Clin. Genet.* 94, 70–80. doi:10.1111/cge.13154

Garat, C. V., Crossno, J. T., Jr., Sullivan, T. M., Reusch, J. E. B., and Klemm, D. J. (2010). Thiazolidinediones prevent PDGF-BB-induced CREB depletion in pulmonary artery smooth muscle cells by preventing upregulation of casein kinase 2 α′ catalytic subunit. *J. Cardiovasc. Pharmacol.* 55, 469–480. doi:10.1097/FJC.0b013e3181d64dbe

Gary-Bobo, G., Houssaini, A., Amsellem, V., Rideau, D., Pacaud, P., Perrin, A., et al. (2010). Effects of HIV protease inhibitors on progression of monocrotaline- and hypoxia-induced pulmonary hypertension in rats. *Circulation* 122, 1937–1947. doi:10.1161/CIRCULATIONAHA.110.973750

Hashimoto-Kataoka, T., Hosen, N., Sonobe, T., Arita, Y., Yasui, T., Masaki, T., et al. (2015). Interleukin-6/interleukin-21 signaling axis is critical in the pathogenesis of pulmonary arterial hypertension. *Proc. Natl. Acad. Sci. USA* 112, E2677–E2686. doi:10.1073/pnas.1424774112

He, J., Bao, Q., Yan, M., Liang, J., Zhu, Y., Wang, C., et al. (2018). The role of Hippo/yes-associated protein signalling in vascular remodelling associated with cardiovascular disease. *Br. J. Pharmacol.* 175, 1354–1361. doi:10.1111/bph.13806

Hu, W., Xu, T., Wu, P., Pan, D., Chen, J., Chen, J., et al. (2017). Luteolin improves cardiac dysfunction in heart failure rats by regulating sarcoplasmic reticulum Ca2+-ATPase 2a. *Sci. Rep.* 7, 41017. doi:10.1038/srep41017

Huang, X., Wu, P., Huang, F., Xu, M., Chen, M., Huang, K., et al. (2017). Baicalin attenuates chronic hypoxia-induced pulmonary hypertension via adenosine A2A receptor-induced SDF-1/CXCR4/PI3K/AKT signaling. *J. Biomed. Sci.* 24, 52. doi:10.1186/s12929-017-0359-3

Iida, K., Naiki, T., Naiki-Ito, A., Suzuki, S., Kato, H., Nozaki, S., et al. (2020). Luteolin suppresses bladder cancer growth via regulation of mechanistic target of rapamycin pathway. *Cancer Sci.* 111, 1165–1179. doi:10.1111/cas.14334

Imran, M., Rauf, A., Abu-Izneid, T., Nadeem, M., Shariati, M. A., Khan, I. A., et al. (2019). Luteolin, a flavonoid, as an anticancer agent: a review. *Biomed. Pharmacother.* 112, 108612. doi:10.1016/j.biopha.2019.108612

John, R. M., Tedrow, U. B., Koplan, B. A., Albert, C. M., Epstein, L. M., Sweeney, M. O., et al. (2012). Ventricular arrhythmias and sudden cardiac death. *The Lancet* 380, 1520–1529. doi:10.1016/S0140-6736(12)61413-5

Johnson, R., and Halder, G. (2014). The two faces of Hippo: targeting the Hippo pathway for regenerative medicine and cancer treatment. *Nat. Rev. Drug Discov.* 13, 63–79. doi:10.1038/nrd4161

Kang, K. A., Piao, M. J., Hyun, Y. J., Zhen, A. X., Cho, S. J., Ahn, M. J., et al. (2019). Luteolin promotes apoptotic cell death via upregulation of Nrf2 expression by DNA demethylase and the interaction of Nrf2 with p53 in human colon cancer cells. *Exp. Mol. Med.* 51, 1–14. doi:10.1038/s12276-019-0238-y

Kudryashova, T. V., Goncharov, D. A., Pena, A., Kelly, N., Vanderpool, R., Baust, J., et al. (2016). HIPPO-Integrin-linked kinase cross-talk controls self-sustaining proliferation and survival in pulmonary hypertension. *Am. J. Respir. Crit. Care Med.* 194, 866–877. doi:10.1164/rccm.201510-2003OC

Kylhammar, D., Kjellström, B., Hjalmarsson, C., Jansson, K., Nisell, M., Söderberg, S., et al. (2018). A comprehensive risk stratification at early follow-up determines prognosis in pulmonary arterial hypertension. *Eur. Heart J.* 39, 4175–4181. doi:10.1093/eurheartj/ehx257

Lang, Y., Chen, D., Li, D., Zhu, M., Xu, T., Zhang, T., et al. (2012). Luteolin inhibited hydrogen peroxide-induced vascular smooth muscle cells proliferation and migration by suppressing the Src and Akt signalling pathways. *J. Pharm. Pharmacol.* 64, 597–603. doi:10.1111/j.2042-7158.2011.01438.x

Lau, E. M. T., Giannoulatou, E., Celermajer, D. S., and Humbert, M. (2017). Epidemiology and treatment of pulmonary arterial hypertension. *Nat. Rev. Cardiol.* 14, 603–614. doi:10.1038/nrcardio.2017.84

Lepetit, H., Eddahibi, S., Fadel, E., Frisdal, E., Munaut, C., Noel, A., et al. (2005). Smooth muscle cell matrix metalloproteinases in idiopathic pulmonary arterial hypertension. *Eur. Respir. J.* 25, 834–842. doi:10.1183/09031936.05.00072504

Lim, W., Yang, C., Bazer, F. W., and Song, G. (2016). Luteolin inhibits proliferation and induces apoptosis of human placental choriocarcinoma cells by blocking the PI3K/AKT pathway and regulating sterol regulatory element binding protein activity. *Biol. Reprod.* 95, 82. doi:10.1095/biolreprod.116.141556

Lin, Z., Zhou, P., von Gise, A., Gu, F., Ma, Q., Chen, J., et al. (2015). Pi3kcbLinks hippo-YAP and PI3K-AKT signaling pathways to promote cardiomyocyte proliferation and survival. *Circ. Res.* 116, 35–45. doi:10.1161/CIRCRESAHA.115.304457

Liu-Chittenden, Y., Huang, B., Shim, J. S., Chen, Q., Lee, S.-J., Anders, R. A., et al. (2012). Genetic and pharmacological disruption of the TEAD-YAP complex suppresses the oncogenic activity of YAP. *Genes Dev.* 26, 1300–1305. doi:10.1101/gad.192856.112

Mesrouze, Y., Bokhovchuk, F., Meyerhofer, M., Fontana, P., Zimmermann, C., Martin, T., et al. (2017). Dissection of the interaction between the intrinsically disordered YAP protein and the transcription factor TEAD. *Elife* 6. doi:10.7554/eLife.25068

Nabavi, S. F., Braidy, N., Gortzi, O., Sobarzo-Sanchez, E., Daglia, M., Skalicka-Woźniak, K., et al. (2015). Luteolin as an anti-inflammatory and neuroprotective agent: a brief review. *Brain Res. Bull.* 119, 1–11. doi:10.1016/j.brainresbull.2015.09.002

Newby, A. C., Southgate, K. M., and Davies, M. (1994). Extracellular matrix degrading metalloproteinases in the pathogenesis of arteriosclerosis. *Basic Res. Cardiol.* 89 (Suppl. 1), 59–70. doi:10.1007/978-3-642-85660-0_6

Nogueira-Ferreira, R., Vitorino, R., Ferreira, R., and Henriques-Coelho, T. (2015). Exploring the monocrotaline animal model for the study of pulmonary arterial hypertension: a network approach. *Pulm. Pharmacol. Ther.* 35, 8–16. doi:10.1016/j.pupt.2015.09.007

Okada, M., Harada, T., Kikuzuki, R., Yamawaki, H., and Hara, Y. (2009). Effects of telmisartan on right ventricular remodeling induced by monocrotaline in rats. *J. Pharmacol. Sci.* 111, 193–200. doi:10.1254/jphs.09112fp

Oku, Y., Nishiya, N., Shito, T., Yamamoto, R., Yamamoto, Y., Oyama, C., et al. (2015). Small molecules inhibiting the nuclear localization of YAP/TAZ for chemotherapeutics and chemosensitizers against breast cancers. *FEBS Open Bio.* 5, 542–549. doi:10.1016/j.fob.2015.06.007

Oyagbemi, A. A., Omobowale, T. O., Ola-Davies, O. E., Asenuga, E. R., Ajibade, T. O., Adejumobi, O. A., et al. (2018). Luteolin-mediated Kim-1/NF-kB/Nrf2 signaling pathways protects sodium fluoride-induced hypertension and cardiovascular complications. *Biofactors* 44, 518–531. doi:10.1002/biof.1449

Perez, J., Hill, B. G., Benavides, G. A., Dranka, B. P., and Darley-Usmar, V. M. (2010). Role of cellular bioenergetics in smooth muscle cell proliferation induced by platelet-derived growth factor. *Biochem. J.* 428, 255–267. doi:10.1042/BJ20100090

Perros, F., Montani, D., Dorfmüller, P., Durand-Gasselin, I., Tcherakian, C., Le Pavec, J., et al. (2008). Platelet-derived growth factor expression and function in idiopathic pulmonary arterial hypertension. *Am. J. Respir. Crit. Care Med.* 178, 81–88. doi:10.1164/rccm.200707-1037OC

Prins, K. W., Archer, S. L., Pritzker, M., Rose, L., Weir, E. K., Sharma, A., et al. (2018). Interleukin-6 is independently associated with right ventricular function in pulmonary arterial hypertension. *J. Heart Lung Transplant.* 37, 376–384. doi:10.1016/j.healun.2017.08.011

Quatredeniers, M., Nakhleh, M. K., Dumas, S. J., Courboulin, A., Vinhas, M. C., Antigny, F., et al. (2019). Functional interaction between PDGFβ and GluN2B-containing NMDA receptors in smooth muscle cell proliferation and migration in pulmonary arterial hypertension. *Am. J. Physiology-Lung Cell Mol. Physiol.* 316, L445–L455. doi:10.1152/ajplung.00537.2017

Seelinger, G., Merfort, I., and Schempp, C. (2008). Anti-oxidant, anti-inflammatory and anti-allergic activities of luteolin. *Planta Med.* 74, 1667–1677. doi:10.1055/s-0028-1088314

Shen, X., Xu, X., Xie, C., Liu, H., Yang, D., Zhang, J., et al. (2020). YAP promotes the proliferation of neuroblastoma cells through decreasing the nuclear location of p27 Kip1 mediated by Akt. *Cell Prolif.* 53, e12734. doi:10.1111/cpr.12734

Southgate, K. M., Davies, M., Booth, R. F. G., and Newby, A. C. (1992). Involvement of extracellular-matrix-degrading metalloproteinases in rabbit aortic smooth-muscle cell proliferation. *Biochem. J.* 288 (Pt 1), 93–99. doi:10.1042/bj2880093

Tang, C., Luo, Y., Li, S., Huang, B., Xu, S., and Li, L. (2021). Characteristics of inflammation process in monocrotaline-induced pulmonary arterial hypertension in rats. *Biomed. Pharmacother.* 133, 111081. doi:10.1016/j.biopha.2020.111081

Teng, X., Li, D., Champion, H. C., and Johns, R. A. (2003). FIZZ1/RELMα, a novel hypoxia-induced mitogenic factor in lung with vasoconstrictive and angiogenic properties. *Circ. Res.* 92, 1065–1067. doi:10.1161/01.RES.0000073999.07698.33

Thenappan, T., Ormiston, M. L., Ryan, J. J., and Archer, S. L. (2018). Pulmonary arterial hypertension: pathogenesis and clinical management. *BMJ* 360, j5492. doi:10.1136/bmj.j5492

Wei, B., Lin, Q., Ji, Y.-G., Zhao, Y.-C., Ding, L.-N., Zhou, W.-J., et al. (2018). Luteolin ameliorates rat myocardial ischaemia-reperfusion injury through activation of peroxiredoxin II. *Br. J. Pharmacol.* 175, 3315–3332. doi:10.1111/bph.14367

Wilson, D. W., Segall, H. J., Pan, L. C., Lamé, M. W., Estep, J. E., and Morin, D. (1992). Mechanisms and pathology of monocrotaline pulmonary toxicity. *Crit. Rev. Toxicol.* 22, 307–325. doi:10.3109/10408449209146311

Wu, H.-T., Lin, J., Liu, Y.-E., Chen, H.-F., Hsu, K.-W., Lin, S.-H., et al. (2021). Luteolin suppresses androgen receptor-positive triple-negative breast cancer cell proliferation and metastasis by epigenetic regulation of MMP9 expression via the AKT/mTOR signaling pathway. *Phytomedicine* 81, 153437. doi:10.1016/j.phymed.2020.153437

Wu, Y.-T., Chen, L., Tan, Z.-B., Fan, H.-J., Xie, L.-P., Zhang, W.-T., et al. (2018). Luteolin inhibits vascular smooth muscle cell proliferation and migration by inhibiting TGFBR1 signaling. *Front. Pharmacol.* 9, 1059. doi:10.3389/fphar.2018.01059

Xiao, C., Xia, M.-L., Wang, J., Zhou, X.-R., Lou, Y.-Y., Tang, L.-H., et al. (2019). Luteolin attenuates cardiac ischemia/reperfusion injury in diabetic rats by modulating Nrf2 antioxidative function. *Oxid. Med. Cell Longev.* 2019, 1. doi:10.1155/2019/2719252

Xiao, Y., Peng, H., Hong, C., Chen, Z., Deng, X., Wang, A., et al. (2017). PDGF promotes the Warburg effect in pulmonary arterial smooth muscle cells via activation of the PI3K/AKT/mTOR/HIF-1α signaling pathway. *Cell Physiol. Biochem.* 42, 1603–1613. doi:10.1159/000479401

Yao, X., Jiang, W., Yu, D., and Yan, Z. (2019). Luteolin inhibits proliferation and induces apoptosis of human melanoma cells *in vivo* and *in vitro* by suppressing MMP-2 and MMP-9 through the PI3K/AKT pathway. *Food Funct.* 10, 703–712. doi:10.1039/c8fo02013b

Yu, F.-X., Zhao, B., and Guan, K.-L. (2015). Hippo pathway in organ size control, tissue homeostasis, and cancer. *Cell* 163, 811–828. doi:10.1016/j.cell.2015.10.044

Yu, J. S. L., and Cui, W. (2016). Proliferation, survival and metabolism: the role of PI3K/AKT/mTOR signalling in pluripotency and cell fate determination. *Dev.* 143, 3050–3060. doi:10.1242/dev.137075

Zang, M.-d., Hu, L., Fan, Z.-y., Wang, H.-x., Zhu, Z.-l., Cao, S., et al. (2017). Luteolin suppresses gastric cancer progression by reversing epithelial-mesenchymal transition via suppression of the Notch signaling pathway. *J. Transl Med.* 15, 52. doi:10.1186/s12967-017-1151-6

Zhang, M., Chang, Z., Zhang, P., Jing, Z., Yan, L., Feng, J., et al. (2019). Protective effects of 18β-glycyrrhetinic acid on pulmonary arterial hypertension via regulation of Rho A/Rho kinsase pathway. *Chem. Biol. Interact.* 311, 108749. doi:10.1016/j.cbi.2019.108749

Zhang, Q., Cao, Y., Luo, Q., Wang, P., Shi, P., Song, C., et al. (2018). The transient receptor potential vanilloid-3 regulates hypoxia-mediated pulmonary artery smooth muscle cells proliferation via PI3K/AKT signaling pathway. *Cel Prolif.* 51, e12436, doi:10.1111/cpr.12436

Zhang, Y., Yuan, R. X., and Bao, D. (2020). TGF-β1 promotes pulmonary arterial hypertension in rats via activating RhoA/ROCK signaling pathway. *Eur. Rev. Med. Pharmacol. Sci.* 24, 4988–4996. doi:10.26355/eurrev_202005_21190

Zhao, B., Wei, X., Li, W., Udan, R. S., Yang, Q., Kim, J., et al. (2007). Inactivation of YAP oncoprotein by the Hippo pathway is involved in cell contact inhibition and tissue growth control. *Genes Dev.* 21, 2747–2761. doi:10.1101/gad.1602907

Conflict of Interest: The authors declare that the research was conducted in the absence of any commercial or financial relationships that could be construed as a potential conflict of interest.

frontiers in Pharmacology

REVIEW
published: 29 June 2021
doi: 10.3389/fphar.2021.691621

Inhaled Corticosteroids and the Pneumonia Risk in Patients With Chronic Obstructive Pulmonary Disease: A Meta-analysis of Randomized Controlled Trials

Hong Chen[1], *Jian Sun*[2], *Qiang Huang*[1], *Yongqi Liu*[1], *Mengxin Yuan*[1], *Chunlan Ma*[2] *and Hao Yan*[1]*

[1]*Department of Respiratory and Critical Care Medicine, Chengdu Second People's Hospital, Chengdu, China,* [2]*Department of Respiratory, The First Affiliated Hospital of Chengdu Medical College, Chengdu, China*

OPEN ACCESS

Edited by:
Djuro Kosanovic, I.M. Sechenov First Moscow State Medical University, Russia

Reviewed by:
Srikanth Karnati, Julius Maximilian University of Würzburg, Germany
Kay Tetzlaff, University Hospital of Tübingen, Germany

***Correspondence:**
Hao Yan
eyyrespiratorymedi@163.com

Specialty section:
This article was submitted to Respiratory Pharmacology, a section of the journal Frontiers in Pharmacology

Received: *06 April 2021*
Accepted: *14 June 2021*
Published: *29 June 2021*

Citation:
Chen H, Sun J, Huang Q, Liu Y, Yuan M, Ma C and Yan H (2021) Inhaled Corticosteroids and the Pneumonia Risk in Patients With Chronic Obstructive Pulmonary Disease: A Meta-analysis of Randomized Controlled Trials. Front. Pharmacol. 12:691621. doi: 10.3389/fphar.2021.691621

Background: Whether all types of inhaled corticosteroids (ICSs) would increase the pneumonia risk in patients with chronic obstructive pulmonary disease (COPD) remains controversial. We aimed to assess the association between ICSs treatment and pneumonia risk in COPD patients, and the impact of medication details and baseline characteristics of patients on the association.

Methods: Four databases (PubMed, Embase, Cochrane Library, and Clinical Trials.gov) were searched to identify eligible randomized controlled trials (RCTs) comparing ICSs treatment with non-ICSs treatment on the pneumonia risk in COPD patients. Pooled results were calculated using Peto odds ratios (Peto ORs) with corresponding 95% confidence intervals (CIs).

Results: A total of 59 RCTs enrolling 103,477 patients were analyzed. All types of ICSs significantly increased the pneumonia risk (Peto OR, 1.43; 95% CI, 1.34–1.53). Subgroup analysis showed that there was a dose-response relationship between ICSs treatment and pneumonia risk (low-dose: Peto OR, 1.33; 95% CI, 1.22–1.45; medium-dose: Peto OR, 1.50; 95% CI, 1.28–1.76; and high-dose: Peto OR, 1.64; 95% CI, 1.45–1.85). Subgroup analyses based on treatment durations and baseline characteristics (severity, age, and body mass index) of patients were consistant with the above results. Subgroup analysis based on severity of pneumonia showed that fluticasone (Peto OR, 1.75; 95% CI, 1.44–2.14) increased the risk of serious pneumonia, while budesonide and beclomethasone did not.

Conclusions: ICSs treatment significantly increased the risk of pneumonia in COPD patients. There was a dose-response relationship between ICSs treatment and pneumonia risk. The pneumonia risk was related with COPD severity.

Keywords: inhaled corticosteroids, chronic obstructive pulmonary disease, adverse event, pneumonia, meta-analysis

INTRODUCTION

Chronic obstructive pulmonary disease (COPD) is currently the third leading cause of death in the world, and acute exacerbations contribute substantially to this (GBD 2015 Chronic Respiratory Disease Collaborators, 2017; Viniol and Vogelmeier, 2018; López-Campos et al., 2019). Treatment and prevention of repeated exacerbations have been identified as a priority by the Global Initiative for Chronic Obstructive Lung Disease (GOLD). Currently, the management of patients with stable COPD mainly relies on inhaled agents such as inhaled corticosteroids (ICSs), long-acting muscarinic antagonist (LAMA), long-acting β-agonist (LABA), etc. Among them, ICSs have been recommended by GOLD as first-line maintenance treatment in patients with repeated exacerbations to relieve the frequency and severity of acute exacerbations of COPD, and improve their quality of life (Yang et al., 2017).

Some recent studies have raised concerns about increased pneumonia risk associated with long-term use of ICSs (Dong et al., 2014; Kew and Seniukovich, 2014; Morjaria et al., 2017; Janson et al., 2018; Yang et al., 2019; Zhang et al., 2020). However, the association between various types of ICSs and the pneumonia risk remains controversial, as the conclusions of the previous published meta-analyses are different (Sin et al., 2009; Singh et al., 2009; Kew and Seniukovich, 2014; Festic et al., 2016; Yang et al., 2019). However, the reliability and generalizability of these studies might be weakened by their small sample size, since a large number of important randomized controlled trials (RCTs) after 2017 were not included in these meta-analyses (Bhatt et al., 2017; Papi et al., 2017; Siler et al., 2017; Vestbo et al., 2017; Betsuyaku et al., 2018; Chapman et al., 2018; Ferguson et al., 2018a, Ferguson et al., 2018b; Frith et al., 2018; Lipson et al., 2018; Papi et al., 2018; Ichinose et al., 2019; Kerwin et al., 2019; Rabe et al., 2020). Moreover, none of these studies assessed the difference in the pneumonia risk in COPD patients with different demographic characteristics (including severity of airflow limitation, age, body mass index [BMI], etc.).

The aim of this meta-analysis was to objectively reappraise the pneumonia risk and serious pneumonia associated with various types of ICSs in COPD patients through all available RCTs. We also aimed to assess the impact of medication details (including dosage level and treatment duration) and demographic characteristics (severity, age, and body mass index) of patients on this association.

METHODS

Protocol and Guidance

This meta-analysis was carried out according to the Preferred Reporting Items for Systematic review and Meta-Analysis (Moher et al., 2009). Ethics committee approval is not applicable for this meta-analysis. The study was registered with PROSPERO prospectively (#CRD42020213586).

Search Strategy

Two reviewers (Hong Chen and Jian Sun) independently searched the databases of PubMed, Embase, Cochrane Library, and Clinical Trials.gov from inception until February 2021, using the following terms: ("chronic obstructive pulmonary disease" OR "COPD" OR "pulmonary disease, chronic obstructive" or "chronic obstructive airway disease" OR "airflow obstruction, chronic" OR "chronic airflow obstruction" OR "chronic obstructive lung disease" OR "emphysema" OR "Bronchitis") AND ("inhaled corticosteroids" OR "ICS" OR "budesonide" OR "fluticasone" OR "mometasone" OR "beclomethasone" OR "triamcinolone" OR "ciclesonide"). Articles in English were included. Disagreements regarding eligibility were resolved by discussion by two investigators and, if necessary, consultation with a third investigator (Hao Yan).

Eligibility Criteria

We included eligible studies based on the PICOS (Participants [P], Interventions [I], Comparators [C], Outcomes [O], and Study design [S]) criteria (Shamseer et al., 2015): *1*) Participants: patients aged 40 yr or over, with stable, moderate (GOLD stage II) to very severe (GOLD stage IV) COPD. Patients with other respiratory diseases, such as asthma, bronchiectasis were excluded. *2*) Interventions: various types and doses of ICSs as the intervention treatment. *3*) Comparisons: non-ICSs treatment as a control treatment. *4*) Outcome: Pneumonia for this meta-analysis was defined as an adverse event based on the Medical Dictionary for Regulatory Activities (MedDRA, version 10.0) pneumonia-related preferred terms, including "pneumonia," "lobar pneumonia," "bronchopneumonia," "pneumonia pneumococcal," or "pneumonia staphylococcal" (Rennard et al., 2009; Sin et al., 2009). One or more of the above MedDRA terms reported in the adverse events list or the safety profiles by the RCTs would be identified as pneumonia data, and included in our analysis. Serious pneumonia was defined as a pneumonia leading to mechanical ventilation or death, or requiring hospital admission (Aaron et al., 2007; Pascoe et al., 2015). *5*) Study design: only RCTs were included. Non-RCTs, such as retrospective studies, reviews, case reports and case-control studie, were excluded.

Data Extraction and Quality Assessment

Two reviewers (Qiang Huang and Yongqi Liu) independently identified references and extracted data from eligible RCTs. Any disagreements would be resolved by discussion to reach a consensus, and consulted a third reviewer if necessary. The risk of bias of the included RCTs was assessed by two independent reviewers (Hong Chen and Mengxin Yuan) using the Cochrane risk of bias tool (Higgins et al., 2011). Any disagreements would be resolved by discussion and consultation (Hao Yan).

Subgroup Analyses

Subgroup analyses were conducted based on: *1*) types of ICSs (fluticasone, budesonide, mometasone furoate and beclomethasone); *2*) doses of ICSs (low-dose [defined as 100–250 μg/d of fluticasone propionate or equivalent], medium-dose [defined as >250–500 μg/d of fluticasone propionate or equivalent], and high-dose [defined as

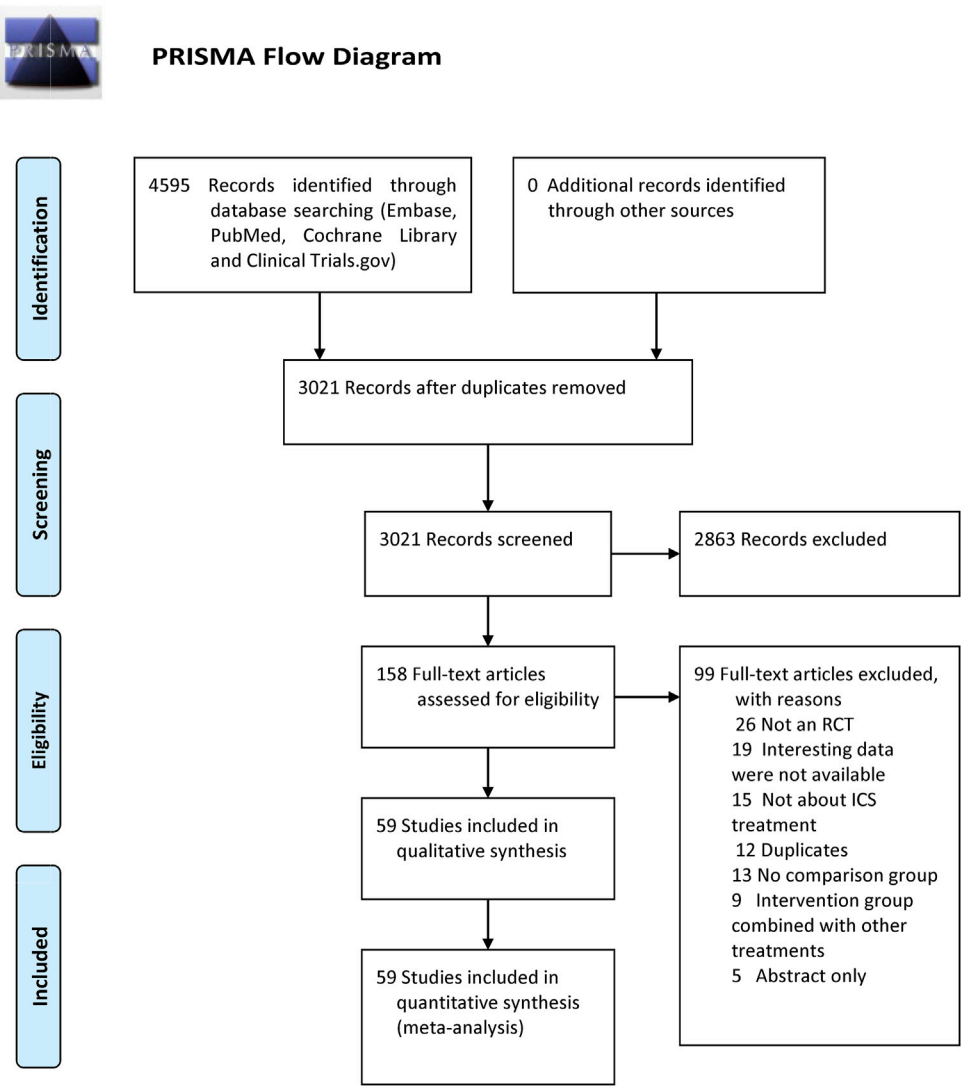

FIGURE 1 | Literature search and screening process.

>500 μg/d of fluticasone propionate or equivalent]); *4*) treatment durations (short-term ICSs treatment [defined as ≤6 mo] and long-term ICSs treatment [defined as >6 mo]); *5*) severity (moderate COPD [GOLD stage II], severe COPD [GOLD stage III] and very severe COPD [GOLD stage IV]); *6*) age of patients (<65 yr old and ≥65 yr old); *7*) body mass index (BMI) of patients (≥25 and <25).

Statistical Analysis

The Review Manager 5.3 software was used to calculate the pooled results. Considering Peto odds ratio (Peto OR) could provide the best confidence interval (CI) when events are rare (Bradburn et al., 2007), the pooled results for the comparison of ICSs treatment vs non-ICSs treatment were calculated using Peto ORs. Sensitivity analysis was performed after excluding those studies with high risk of bias. Subgroup analyes based on the baseline demographic characteristics (severity, age, and body mass index) of the patients were conducted using the individual patient level data, which was extracted from the baseline data of the included RCTs (mean or median for lung function, age and BMI). This method of analyzing the individual patient level data was used by Sobieraj et al. (Sobieraj et al., 2018) previously. A two tailed p-value <0.05 was considered to be statistically significant. Statistical heterogeneity was further measured using the I^2 test, and I^2 ≥50% indicated a substantial heterogeneity (Higgins et al., 2003).

RESULTS

Eligible Trials and Study Descriptions

Our search identified 4,595 citations. After evaluating these citations, we included 59 RCTs (Vestbo et al., 1999; Burge

TABLE 1 | Detailed characteristics of the included randomized controlled trials.

Study	Mean Age, y	Male, %	Postbron-chodilator FEV_1 (% predicted)	Tobacco use, Pack-years	BMI	Duration, months	Interventions, μg	Pneumonia incidence	Serious pneumonia incidence
								Events/ Patients	Events/ Patients
Vestbo et al. (1999)	ICS: 59 CP: 59.1	ICS: 58.6 CP: 62.1	ICS: 86·2 CP: 86·9	NR	NR	36	ICS: BUD 400 bid CP: P	ICS: 16/145 CP: 24/145	NR
Burge et al. (2000)	ICS: 63.8 CP: 63.7	ICS: 75.4 CP: 75	ICS: 50 CP: 50.3	44	ICS: 24.5 CP: 24.9	36	ICS: FP 500 bid CP: P	ICS: 20/376 CP: 9/375	ICS: 16/370 CP: 8/368
Calverley et al. (2003)	ICS: ≥40	ICS: 76	36	ICS: 39	NR	12	ICS: BUD/FM 320/9 bid; BUD 400 bid	ICS: 13/511	NR
	CP: ≥40	CP: 75		CP: 38.5			CP: FM 9 bid; P	CP: 9/511	
Szafranski et al. (2003)	ICS: 64 CP: 65	ICS: 78 CP: 79.5	ICS: 36.5 CP: 36	ICS: 44 CP: 45	NR	12	ICS: BUD 160/4.5 bid CP: FM 4.5 bid; P	ICS: 6/208 CP: 9/205	NR
Aaron et al. (2007)	ICS: 67.8 CP: 67.9	ICS: 57.9 CP: 56.6	ICS: 42.2 CP: 41.6	ICS: 50.3 CP: 50.3	ICS: 27.8 CP: 27.4	12	ICS: SFC 250/25 bid CP: S	ICS: 1/145 CP: 1/304	ICS: 1/145 CP: 1/304
Calverley et al. (2007)	ICS: 65	ICS: 75	ICS: 44.2	ICS: 48.1	ICS: 25.4	36	ICS: SFC 500/50 bid; FP 500 bid	ICS: 217/ 3098	NR
	CP: 65.1	CP: 76	CP: 43.9	CP: 49	CP: 25.4		CP: S 50 bid; P	CP: 124/ 3086	
Kardos et al. (2007)	ICS: 63.8 CP: 64	ICS: 74 CP: 77.6	ICS: 40.4 CP: 40.3	ICS: 36.8 CP: 37	NR	10	ICS: SFC 500/50 bid CP: S 50 bid	ICS: 23/507 CP: 7/487	NR
Calverley et al. (2008)	ICS: 65 CP: 65	ICS: 68 CP: 69	ICS: 46.5 CP: 47	NR	ICS: 26.4 CP: 27.1	12	ICS: MF 800 qd CP: P	ICS: 25/616 CP: 6/295	NR
Ferguson et al. (2008)	ICS: 64.9 CP: 65.0	ICS: 58 CP: 52	ICS: 39.8 CP: 40.6	ICS: 58.5 CP: 54.4	ICS: 27.3 CP: 27.7	12	ICS: SFC 250/25 bid CP: S 25 bid	ICS: 29/394 CP:15/388	ICS: 19/394 CP: 10/388
Tashkin et al. (2008)	ICS: 63.3	ICS: 68.6	ICS: 39.4	ICS: 40.8	NR	6	ICS: BUD/FM 320/9 bid; BUD 160/9 bid	ICS: 8/1120	ICS: 8/1120
	CP: 63.4	CP: 67.3	CP: 40.4	CP: 40			CP: FM 9 bid; P	CP: 2/584	CP: 2/584
Wedzicha et al. (2008)	ICS: 64 CP: 65	ICS: 81 CP: 84	ICS: 39.1 CP: 39.4	ICS: 41.3 CP: 39.5	ICS: 20–29 CP: 20–29	24	ICS: SFC 500/50 bid CP: Tio 18 qd	ICS: 50/658 CP: 24/665	ICS: 41/658 CP: 19/665
Anzueto et al. (2009)	ICS: 65.4 CP: 65.3	ICS: 51 CP: 57	ICS: 41.2 CP: 40	ICS: 57.8 CP: 56.5	ICS: 27.6 CP: 27.3	12	ICS: SFC 250/25 bid CP: S 25 bid	ICS: 26/394 CP: 10/403	NR
Rennard et al. (2009)	ICS: 63.4	ICS: 62.6	ICS: 39.1	40	NR	12	ICS: BUD/FM 320/9 bid; BUD/FM 160/9 bid	ICS:30/988	NR
	CP: 62.9	CP: 65.3	CP: 40				CP: FM 9 bid; P	CP: 40/976	
Welte et al. (2009)	ICS: 62.5	ICS: 76	ICS: 38.1	ICS: 36	ICS: 26.4	3	ICS: BUD/FM 320/9 bid + Tio 18 qd	ICS: 3/331	NR
	CP: 62.4	CP: 74	CP: 37.7	CP: 38	CP: 26.3		CP: Tio 18 qd + P	CP: 3/329	
Calverley et al. (2010)	ICS: 63.5	ICS: 80.4	NR	ICS: 37.6 CP: 39.7	NR	11	ICS: BDP/FM 200/24 bid; BUD/FM 400/ 24 bid	ICS: 5/232; 7/238	NR
	CP: 63.7	CP: 81.1					CP: FM	CP: 1/233	
Dransfield et al. (2011)	ICS: 63.6 CP: 63.5	ICS: 55 CP: 59	ICS: 56 CP: 55	ICS: 55.8 CP: 54.1	ICS: 26.7 CP: 26.6	3	ICS: SFC 250/50 bid CP: P	ICS: 3/123 CP: 0/126	NR
Doherty et al. (2012)	ICS: 60.3	ICS: 75.3	ICS: 39	ICS: 45.4	NR	12	ICS: MF/FM 400/10 bid; MF/F 200/10 bid; MF 400 bid	ICS:16/717	NR
	CP: 59.2	CP: 75	CP: 38.1	CP: 44.7			CP: FM 10 bid; P	CP: 6/479	
Hanania et al. (2012)	ICS: 61.3	ICS: 50	ICS: 56	ICS: 55.4	ICS: 27	6	ICS: SFC250/50 bid + Tio 18 qd	ICS: 2/173	NR
	CP: 61	CP: 43	CP: 57.4	CP: 54.7	CP: 27.6		CP: Tio 18 qd	CP: 0/169	
Jung et al. (2012)	ICS: 67	ICS: 97.3	ICS: 47.4	NR	ICS: 22.2	6	ICS: SFC250/50 bid + Tio 18 qd	ICS: 2/223	NR
	CP: 67.8	CP: 98.7	CP: 47.5		CP: 21.8		CP: Tio 18 qd	CP: 2/232	
Sharafkhaneh et al., 2012	ICS: ≥40	ICS: 64.6	ICS: 37.8	ICS: 45	NR	12	ICS: BUD/FM 320/9 bid; BUD/FM 160/9 bid	ICS: 45/815	NR
	CP: ≥40	CP: 56.8	CP: 37.5	CP: 43			CP: FM	CP: 11/403	
Tashkin et al. (2012a)	ICS: 60.2	ICS: 76.7	ICS: 39.2	ICS: 43	NR	12	ICS: MF/F 400/10 bid; MF/F 200/10 bid; MF 400 bid	ICS: 19/1351	NR
	CP: 59.3	CP: 77	CP: 38.8	CP: 42.4			CP: FM 10 bid; P	CP: 9/900	
Tashkin et al. (2012b)	ICS: 60.1	ICS: 78.3	≥25 and ≤60	ICS: 40.5	NR	12	ICS: MF/F 400/10 bid; MF/F 200/10 bid; MF 400 bid	ICS: 3/634	NR

(Continued on following page)

TABLE 1 | (*Continued*) Detailed characteristics of the included randomized controlled trials.

Study	Mean Age, y	Male, %	Postbron-chodilator FEV_1 (% predicted)	Tobacco use, Pack-years	BMI	Duration, months	Interventions, μg	Pneumonia incidence	Serious pneumonia incidence
								Events/ Patients	Events/ Patients
	CP: 59.7	CP: 76.5		CP: 40.3			CP: FM 10 bid; P	CP: 3/421	
Dransfield et al. (2013)	ICS: 63.6	ICS: 57	ICS: 45.6	NR	NR	12	ICS: FF/VI 200/25 qd; FF/VI 100/25 qd; FF/VI 50/25 qd	ICS: 154/ 2437	ICS: 71/2378
	CP: 63.8	CP: 57	CP: 45.2				CP: VI 25 qd	CP: 27/818	CP: 8/799
Fukuchi et al. (2013)	ICS: 64.5	ICS: 87.6	ICS: 40.9	ICS: 44.4	NR	3	ICS: BUD/FM 160/ 4.5 bid	ICS: 8/636	NR
	CP: 65.6	CP: 90.3	CP: 40.8	CP: 44.7			CP: FM 4.5 bid	CP: 7/657	
Kerwin et al. (2013)	ICS: 62.6	ICS: 65.7	ICS: 47.7	ICS: 45.7	NR	6	ICS: FF/VI 100/25qd; FF/VI 50/25 qd	ICS: 12/618	NR
	CP: 62.8	CP: 68	CP: 49.2	CP: 46.6			CP: VI 25 qd; P	CP: 8/412	
Martinez et al. (2013)	ICS: 61.7	ICS: 71.5	ICS: 47.7	ICS: 41.9	NR	6	ICS: FF/VI 200/25 qd; FF/VI 100/25 qd	ICS: 10/816	NR
	CP: 61.7	CP: 74	CP: 48.4	CP: 43.9			CP: VI 25 qd; P	CP: 2/408	
Vogelmeier et al. (2013)	ICS: 63.2	ICS: 71.6	ICS: 60.5	NR	NR	6	ICS: SFC 500/50 bid	ICS: 4/264	ICS: 2/264
	CP: 63.4	CP: 70.2	CP: 60				CP: IND/GLY 110/50 qd	CP: 0/258	CP: 0/258
Magnussen et al. (2014)	ICS: 63.6	ICS: 81.5	<50	NR	NR	12	ICS: SFC 500/50 bid + Tio 18 qd	ICS: 72/1243	NR
	CP: 64	CP: 83.4					CP: S 50 bid + Tio 18 qd	CP: 68/1242	
Ohar et al. (2014)	ICS: 63.1	ICS: 55	ICS: 38.5	ICS: 52	ICS: 28	6	ICS: SFC 250/50 bid	ICS: 13/314	NR
	CP: 62.7	CP: 54	CP: 41.2	CP: 55.3	CP: 28.3		CP: S 50 bid	CP: 10/325	
Pepin et al. (2014)	ICS: 66.7	ICS: 85	ICS: 45.6	ICS: 42.6	ICS: 27.1	3	ICS: FF/VI 100/25 qd	ICS: 3/127	NR
	CP: 67.7	CP: 86	CP: 47.4	CP: 44.6	CP: 27.2		CP: Tio 18 qd	CP: 0/130	
Rossi et al. (2014)	ICS: 66.8	ICS: 68.4	ICS: 62.4	ICS: 42	NR	6	ICS: SFC 500/50 bid	ICS: 2/288	NR
	CP: 65.3	CP: 69.6	CP: 64	CP: 41.4			CP: IND/GLY 110/50 qd	CP: 0/293	
Wedzicha et al. (2014)	ICS: 64.6	ICS: 69	ICS: 41.9	ICS: 43.1	ICS: 26.5	11	ICS: BDP/FM 100/6 bid	ICS: 23/601	NR
	CP: 63.9	CP: 69	CP: 41.6	CP: 42.7	CP: 26.5		CP: FM 6 bid	CP: 11/596	
Donohue et al. (2015)	ICS: 63.0	ICS: 72.5	ICS: 49.6	ICS: 38.3	ICS: 27	3	ICS: SFC 250/50 bid	ICS: 8/701	NR
	CP: 62.5	CP: 74	CP: 49.3	CP: 37.8	CP: 27.5		CP: UMEC/VI 62.5/ 25 qd	CP: 3/702	
Singh et al. (2015)	ICS: 61.4	ICS: 71	ICS: 51.1	ICS: 37.7	NR	3	ICS: SFC 500/50 bid	ICS: 0/358	NR
	CP: 61.8	CP: 73	CP: 50.2	CP: 37.8			CP: UMEC/VI 62.5/ 25 qd	CP: 1/358	
Zheng et al. (2015)	ICS: 64.4	ICS: 91.3	ICS: 48.4	ICS: 38	NR	5.6	ICS: FF/VI 200/25 qd; FF/VI 100/25 qd; FF/VI 50/25 qd	ICS: 8/480	BMI <25
	CP: 64.7	CP: 90	CP: 48.6	CP: 43.3			CP: P	CP: 4/162	
Zhong et al. (2015)	ICS: 65.3	ICS: 89.7	ICS: 52	NR	NR	6	ICS: SFC 500/50 bid	ICS: 10/369	NR
	CP: 64.8	CP: 91.7	CP: 51.6				CP: IND/GLY 110/50 qd	CP: 3/372	
Beeh et al. (2016)	63.6	64.6	56.4	39.1	NR	1.5	ICS: SFC 50/500 bid; SFC 50/250 bid	ICS: 2/431	NR
							CP: Tio/Olo 5/5 qd; Tio/ Olo 2.5/5 qd	CP: 3/436	
Covelli et al. (2016)	ICS: 62.9	ICS: 62	≥30 and ≤70	ICS: 43.2	ICS: 28.4	3	ICS: FF/VI 100/25 qd	ICS: 3/310	NR
	CP: 62.3	CP: 67		CP: 45.6	CP: 28.6		CP: Tio 18 qd	CP: 0/313	
Lee et al. (2016)	ICS: 66.8	ICS: 97.2	ICS: 35.8	NR	ICS: 21.3	3	ICS: BUD/FM 320/9 bid + Tio 18 qd	ICS: 2/289	NR
	CP: 66.9	CP: 94.1	CP: 37		CP: 21.2		CP: Tio 18 qd	CP: 4/289	
Vestbo et al. (2016a)	ICS: 65.0	ICS: 25	ICS: 59.7	ICS: 41	ICS: 28	22	ICS: FF/VI 100/25 qd	ICS: 465/ 8297	NR
	CP: 65.1	CP: 25.5	CP: 59.7	CP: 41	CP: 28		CP: VI 25 qd; P	CP: 377/ 8271	
Vestbo et al. (2016b)	ICS: 67	ICS: 50	NR	NR	ICS: 28	12	ICS: FF/VI 100/25 qd	ICS: 94/1396	NR
	CP: 67	CP: 52			CP: 28		CP: P	CP: 83/1403	
Vogelmeier et al. (2016)	ICS: 63.5	ICS: 64.4	ICS: 53.2	ICS: 42.6	NR	6	ICS: SFC 50/500 bid	ICS: 9/466	NR
	CP: 63.3	CP: 65.7	CP: 53.3	CP: 41.6			CP: ACL/FM 400/12 bid	CP: 3/467	
Wedzicha et al. (2016)	ICS: 64.5	ICS: 74.8	ICS: 44.1	NR	NR	12	ICS: SFC 50/500 bid	ICS: 80/1680	NR
	CP: 64.6	CP: 77.3	CP: 44				CP: IND/GLY 110/50 qd	CP: 53/1678	
	ICS: 68.5	ICS: 77	≤70	ICS: 50.1	ICS: 24.5	6	ICS: FF/VI 100/25 qd	ICS: 2/141	NR

(Continued on following page)

TABLE 1 | (*Continued*) Detailed characteristics of the included randomized controlled trials.

Study	Mean Age, y	Male, %	Postbron-chodilator FEV_1 (% predicted)	Tobacco use, Pack-years	BMI	Duration, months	Interventions, μg	Pneumonia incidence	Serious pneumonia incidence
								Events/ Patients	Events/ Patients
Bhatt et al. (2017)	CP: 68.5	CP: 80.5		CP: 49.4	CP: 24.6		CP: VI 25 qd; P	CP: 3/303	
Ferguson et al. (2017)	ICS: 63.1	ICS: 58.6	ICS: 48.5	ICS: 39	NR	6	ICS: BUD/FM 320/9 bid	ICS: 3/605	ICS: 0/605
	CP: 63.9	CP: 56	CP: 48.9	CP: 40			CP: FM 9 bid	CP: 6/613	CP: 5/613
Papi et al. (2017)	ICS: 63.4	ICS: 72.6	ICS: 37.9	ICS: 47.4	NR	12	ICS: FP/FM 500/20; FP/FM 250/10	ICS: 40/1175	NR
	CP: 64	CP: 75.9	CP: 37.7	CP: 50			CP: FM 12 bid	CP: 11/590	
Siler et al. (2017)	ICS: 65.3	ICS: 75	ICS: 50.3	ICS: 43.7	NR	3	ICS: FF/VI 100/25 qd	ICS: 7/806	NR
	CP: 65.4	CP: 77	CP: 50.5	CP: 44.1			CP: VI 25 qd	CP: 7/814	
Vestbo et al. (2017)	ICS: 63	ICS: 75.5	ICS: 36.7	NR	ICS: 26.4	12	ICS: BDP/FM 100/12.5 bid + Tio 18 qd; BDP/FM 100/6 bid + Tio 18 qd	ICS:40/1614	ICS: 30/1614
	CP: 63.3	CP: 77	CP: 36.6		CP: 26.2		CP: Tio 18 qd	CP: 19/1076	CP: 14/1076
Betsuyaku et al. (2018)	ICS: 68.6	ICS: 94	ICS: 59.5	ICS: 60.8	NR	6	ICS: SFC 50/250 bid	ICS:6/204	ICS: 4/204
	CP: 68	CP: 96	CP: 57.8	CP: 54.5			CP: Tio 18 qd	CP: 6/201	CP: 2/201
Chapman et al. (2018)	ICS: 65.3	ICS: 69.4	ICS: 57	NR	ICS: 28.2	6	ICS: SFC 50/500 bid	ICS: 9/526	NR
	CP: 65.5	CP: 71.7	CP: 56.2		CP: 27.8		CP: IND/GLY 110/50 qd	CP: 6/527	
Ferguson et al. (2018a)	ICS: 64.3	ICS: 60.5	ICS: 52.9	ICS: 44.6	ICS: 28.3	6	ICS: BUD/FM 320/10 bid; BUD/FM 160/10 bid; BUD/FM 400/12 bid; BUD 320 bid	ICS: 16/1717	ICS: 12/1717
	CP: 64.1	CP: 59.5	CP: 52.6	CP: 44.9	CP: 28.4		CP: FM 10 bid	CP: 9/644	CP: 6/644
Ferguson et al. (2018b)	ICS: 65.3	ICS: 72.4	ICS: 50.3	ICS: 45	ICS: 26.2	6	ICS: BGF 320/18/9.6 bid; BFF 320/9.6 bid; BFF 400/12 bid	ICS: 22/1271	NR
	CP: 65.1	CP: 68.8	CP: 50.2	CP: 45	CP: 26.3		CP: GFF 18/9.6 bid	CP: 10/625	
Frith et al. (2018)	ICS: 65.1	ICS: 89.6	ICS: 51.7	ICS: 45.3	ICS: 24.6	3	ICS: SFC 50/500 bid	ICS: 1/250	NR
	CP: 65	CP: 88.7	CP: 51.3	CP: 44.3	CP: 24.5		CP: IND/GLY 110/50 qd	CP: 1/248	
Lipson et al. (2018)	ICS: 65.3	ICS: 66.6	ICS: 45.6	NR	ICS: 26.6	12	ICS: FF/UMEC/VI 100/62.5/25 qd; FF/VI 100/25 qd	ICS: 609/8285	ICS: 336/8285
	CP: 65.2	CP: 66	CP: 45.4		CP: 26.7		CP: UMEC/VI 62.5/25 qd	CP: 97/2070	CP: 54/2070
Papi et al. (2018)	ICS: 64.4	ICS: 72	ICS: <50	NR	ICS: 25.7	12	ICS: BDP/FM/GLY 87/5/9 bid	ICS: 28/764	ICS: 18/764
	CP: 64.5	CP: 72	CP: <50		CP: 26.6		CP: IND/GLY 85/43 qd	CP: 27/768	CP: 17/768
Huang et al. (2019)	ICS: 63.8	ICS: 87.6	NR	ICS: 33.4	NR	3	ICS: BUD/F 320/9 bid + I/T	ICS: 1/293	NR
	CP: 64.4	CP: 85.3		CP: 32.7			CP: I/T	CP: 0/289	
Ichinose et al. (2019)	ICS: 69.7	ICS: 95.7	ICS: 51.8	ICS: 51.8	ICS: 22.9	6	ICS: BGF 320/18/9.6 bid; BFF 320/9.6 bid; BFF 400/12 bid	ICS: 19/278	NR
	CP: 69	CP: 97.1	CP: 52.2	CP: 52	CP: 22.5		CP: GFF 18/9.6 bid	CP: 5/138	
Kerwin et al. (2019)	ICS: 63.3	ICS: 55	≥25 and <80	ICS: 45.8	ICS: 29	6	ICS: BGF 320/18/9.6 bid; BFF 320/9.6 bid	ICS: 2/282	ICS: 2/282
	CP: 62.4	CP: 50		CP: 50	CP: 29		CP: GFF 18/9.6 bid	CP: 4/174	CP: 4/174
Rabe et al. (2020)	ICS: 64.6	ICS: 60.1	ICS: 43.4	ICS: 47.3	NR	12	ICS: BGF 320/18/9.6 bid; BGF 160/18/9.6 bid; BFF 320/9.6 bid	ICS: 261/6404	NR
	CP: 64.8	CP: 58.7	CP: 43.5	CP: 48.4			CP: GFF 18/9.6 bid	CP: 48/2125	

RCT, randomized controlled trial; FEV_1, forced expiratory volume in the first second; BMI, body-mass index; ICSs, inhaled corticosteroids; CP, control or placebo; BUD, budesonide; NR, not reported; bid, twice daily; qd, once daily; FP, fluticasone propionate; S, salmeterol; SFC, fluticasone propionate/salmeterol; EOC, eosinophil counts; BUD/FM, budesonide/formoterol fumarate; FM, formoterol fumarate; MF, mometasone furoate; Tio, tiotropium/olodaterol; BDP, Beclomethasone dipropionate; FF/VI, fluticasone furoate/vilanterol; VI, vilanterol; UMEC/VI, umeclidinium/vilanterol; ACL/FM, aclidinium/formoterol; IND/GLY, indacaterol/glycopyrronium; FF/UMEC/VI, fluticasone furoate/umeclidinium/vilanterol; BDP/FM/GLY, beclomethasone/formoterol/glycopyrronium; I/T, ipratropium/theophylline; BGF, budesonide/glycopyrronium/formoterol; BFF, budesonide/formoterol; GFF, glycopyrrolate/formoterol.

et al., 2000; Calverley et al., 2003; Szafranski et al., 2003; Aaron et al., 2007; Calverley et al., 2007; Kardos et al., 2007; Calverley et al., 2008; Ferguson et al., 2008; Tashkin et al., 2008; Wedzicha et al., 2008; Anzueto et al., 2009; Rennard et al., 2009; Welte et al., 2009; Calverley et al., 2010; Dransfield et al., 2011; Doherty et al., 2012; Hanania et al., 2012; Jung et al.,

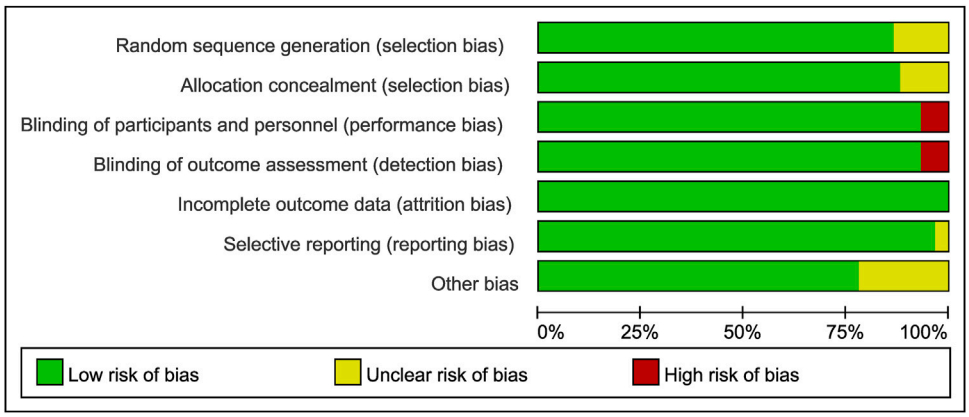

FIGURE 2 | Risk of bias graph.

2012; Sharafkhaneh et al., 2012; Tashkin et al., 2012a, Tashkin et al. 2012b; Dransfield et al., 2013; Fukuchi et al., 2013; Kerwin et al., 2013; Martinez et al., 2013; Vogelmeier et al., 2013; Magnussen et al., 2014; Ohar et al., 2014; Pepin et al., 2014; Rossi et al., 2014; Wedzicha et al., 2014; Donohue et al., 2015; Singh et al., 2015; Zheng et al., 2015; Zhong et al., 2015; Beeh et al., 2016; Covelli et al., 2016; Lee et al., 2016; Vestbo et al., 2016a; Vestbo et al., 2016b; Vogelmeier et al., 2016; Wedzicha et al., 2016; Bhatt et al., 2017; Ferguson et al., 2017; Papi et al., 2017; Siler et al., 2017; Vestbo et al., 2017; Betsuyaku et al., 2018; Chapman et al., 2018; Ferguson et al., 2018a; Ferguson et al., 2018b; Frith et al., 2018; Lipson et al., 2018; Papi et al., 2018; Huang et al., 2019; Ichinose et al., 2019; Kerwin et al., 2019; Rabe et al., 2020). These trials enrolled 103,477 patients, of whom 60,733 received ICSs treatment and 42,744 received non-ICSs treatment. The flowchart is shown in **Figure 1**. The studies included were published between 1999 and 2020, with sample size raging from 249 to 16,568 patients. All studies provided data on pneumonia, 14 of which provided data on serious pneumonia. Among the studies, 35 RCTs (67,109 patients) compared fluticasone and control, 17 RCTs (25,071 patients) compared budesonide and control, four RCTs (5,413 patients) compared mometasone and control, and four RCTs (5,884 patients) compared beclomethasone and control, respectively. No RCTs investigated triamcinolone or ciclesonide and the pneumonia risk in COPD patients. The detailed characteristics of the included RCTs are summarized in **Table 1**.

Assessment of Risk of Bias

All included studies were assessed using the Cochrane Collaboration risk of bias assessment tool. The results are presented in **Figures 2**, **3**. Thirty-five RCTs were assessed as being at low risk of bias for all aspects. Four had a high risk of bias for performance bias (blinding of participants and personnel) and detection bias (Blinding of outcome assessment). Twenty-two had an unclear risk for random sequence generation, selective reporting, allocation concealment, or other bias (**Figures 2**, **3**).

Various Types of ICSs and Pneumonia Risk

Compared with non-ICSs treatment, ICSs treatment significantly increased the pneumonia risk (Peto OR, 1.43; 95% CI, 1.34–1.53). Subgroup analysis based on types of ICSs showed that all types of ICSs increased the pneumonia risk ([fluticasone: Peto OR, 1.47; 95% CI, 1.36–1.59]; [budesonide: Peto OR, 1.24; 95% CI, 1.05–1.47]; [mometasone: Peto OR, 1.62; 95% CI, 1.05–2.49]; [beclomethasone: Peto OR, 1.43; 95% CI, 1.03–1.97]). Test for subgroup differences (I^2 = 16.4%) indicated that there was no significant difference in the pneumonia risk associated with different types of ICSs (**Table 2** and **Figure 4**).

Different Doses of ICSs and Pneumonia Risk

Of the included trials, 23 RCTs (54,287 patients), 26 RCTs (27,302 patients), and 27 RCTs (32,592 patients) assessed high-dose, medium-dose, and low-dose ICSs and pneumonia risk, respectively. Subgroup analysis showed that there was a dose-response relationship between ICSs treatment and pneumonia risk. Low-dose (Peto OR, 1.33; 95% CI, 1.22–1.45), medium-dose (Peto OR, 1.50; 95% CI, 1.28–1.76), and high-dose (Peto OR, 1.64; 95% CI, 1.45–1.85) ICSs all significantly increased the pneumonia risk. Test for subgroup differences (I^2 = 74%) indicated that there was a significant difference in the pneumonia risk associated with different doses of ICSs (**Table 2** and **Figure 5**).

Different Treatment Durations of ICSs and Pneumonia Risk

Of the included trials, 31 RCTs (26,408 patients), and 28 RCTs (76,826 patients) assessed short-term ICSs treatment and long-term ICSs treatment and pneumonia risk. Subgroup analysis showed that both short-term ICSs treatment (Peto OR, 1.30; 95% CI, 1.04–1.63) and long-term ICSs treatment (Peto OR, 1.44; 95% CI, 1.34–1.55) significantly increased the pneumonia risk. Test for subgroup differences (I^2 = 0%) indicated that there was no significant difference in the pneumonia risk associated with different treatment durations of ICSs (**Table 2** and **Figure 6**).

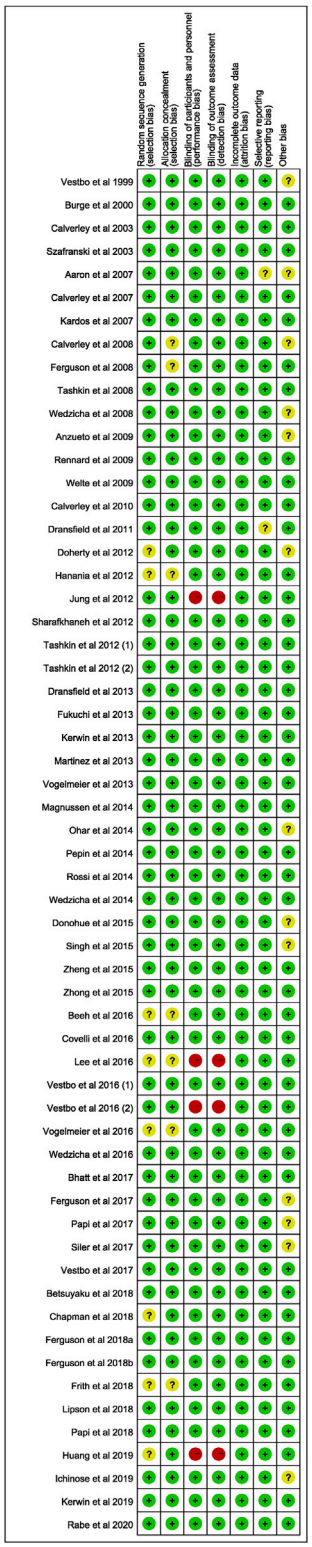

FIGURE 3 | Risk of bias summary.

ICSs Associated Pneumonia in COPD Patients With Different Severity

Eighteen RCTs (30,809 patients), 34 RCTs (65,773 patients) and two RCTs (1,148 patients) assessed ICSs associated pneumonia in moderate, severe, and very severe COPD patients, respectively. Subgroup analysis showed that the pneumonia risk was related with COPD severity. ICSs treatment significantly increased the pneumonia risk in all severity subgroups of COPD patients: ([Moderate COPD: Peto OR, 1.26; 95% CI, 1.11–1.43]; [Severe COPD: Peto OR, 1.54; 95% CI, 1.42–1.68]; [Very severe COPD: Peto OR, 2.52; 95% CI, 1.88–3.38]) (**Table 2** and **Figure 7**). Test for subgroup differences (I^2 = 90.1%) indicated that there was a significant difference in the pneumonia risk in patients with different severity.

ICSs Associated Pneumonia in COPD Patients With Different Age

Thirty-five RCTs (50,802 patients) and 19 RCTs (46,963 patients) assessed ICSs associated pneumonia in patients with different age. Subgroup analysis showed that ICSs treatment significantly increased the pneumonia risk in patients both age subgroups: ([<65 yr old: Peto OR, 1.43; 95% CI, 1.28–1.60]; [≥65 yr old: Peto OR, 1.41; 95% CI, 1.29–1.54]). Test for subgroup differences (I^2 = 0%) indicated that there was no significant difference in the pneumonia risk in patients with different age (**Table 2** and **Figure 8**).

ICSs Associated Pneumonia in COPD Patients With Different BMI

Eight RCTs (4,443 patients) and 23 RCTs (54,867 patients) assessed ICSs associated pneumonia in patients with different BMI. Subgroup analysis showed that ICSs treatment significantly increased the pneumonia risk in patients both BMI subgroups: ([<25: Peto OR, 1.47; 95% CI, 1.02–2.12]; [≥25: Peto OR, 1.43; 95% CI, 1.31–1.55]). Test for subgroup differences (I^2 = 0%) indicated that there was no significant difference in the pneumonia risk in patients with different BMI (**Table 2** and **Figure 9**).

Various Types of ICSs and Serious Pneumonia Risk

Of the included trials, 15 RCTs (29,008 patients) offered data on serious pneumonia associated with ICSs treatment. Compared with non-ICSs treatment, ICSs treatment significantly increased the serious pneumonia risk (Peto OR, 1.55; 95% CI, 1.31–1.84). Of the included RCTs, seven RCTs (17,091 patients) assessed fluticasone and serious pneumonia risk, six RCTs (7,695 patients) assessed budesonide and two RCTs (4,222 patients) assessed beclomethasone, respectively. Subgroup analysis showed that only fluticasone significantly increased the serious pneumonia

TABLE 2 | Summary of the pooled results.

Pooled results	No. of Patients	No. of Studies	Peto OR (95% CI)	Test for subgroup differences
Various types of ICSs and pneumonia risk				I^2 = 16.4%
All types of ICSs	103,477	59	1.43 (1.34–1.53)	
Fluticasone	67,109	35	1.47 (1.36–1.59)	
Budesonide	25,071	17	1.24 (1.05–1.47)	
Mometasone furoate	5,413	4	1.62 (1.05–2.49)	
Beclomethasone dipropionate	5,884	4	1.43 (1.03–1.97)	
Different doses of ICSs and pneumonia risk				I^2 = 74%
Low -dose	54,287	23	1.33 (1.22–1.45)	
Medium-dose	27,302	26	1.50 (1.28–1.76)	
High-dose	32,592	27	1.64 (1.45–1.85)	
Different treatment durations of ICSs and pneumonia risk				I^2 = 0%
≤6 mo	26,408	31	1.30 (1.04–1.63)	
>6 mo	76,826	28	1.44 (1.34–1.55)	
ICSs associated pneumonia in COPD patients with different severity				I^2 = 90.1%
Moderate COPD (GOLD stage II)	30,809	18	1.26 (1.11–1.43)	
Severe COPD (GOLD stage III)	65,773	34	1.54 (1.42–1.68)	
Very severe COPD (GOLD stage IV)	1148	2	2.52 (1.88–3.38)	
ICSs associated pneumonia in COPD patients with different age				I^2 = 0%
<65 yr	50,802	35	1.43 (1.28–1.60)	
≥65 yr	46,963	19	1.41 (1.29–1.54)	
ICSs associated pneumonia in COPD patients with different BMI				I^2 = 0%
<25	4,443	8	1.47 (1.02–2.12)	
≥25	54,867	23	1.43 (1.31–1.55)	
Various types of ICSs and serious pneumonia risk				I^2 = 61.9%
All types of ICSs	29,008	15	1.55 (1.31–1.84)	
Fluticasone	17,091	7	1.75 (1.44–2.14)	
Budesonide	7,695	6	1.06 (0.68–1.65)	
Beclomethasone dipropionate	4,222	2	1.24 (0.79–1.95)	
Sensitivity analysis after excluding RCTs with high risk of bias (various types of ICSs and pneumonia risk)				I^2 = 23.2%
All types of ICSs	99,063	55	1.45 (1.35–1.56)	
Fluticasone	63,855	33	1.50 (1.38–1.62)	
Budesonide	23,911	15	1.25 (1.06–1.48)	
Mometasone furoate	5,413	4	1.62 (1.05–2.49)	
Beclomethasone dipropionate	5,884	4	1.43 (1.03–1.97)	

ICSs, inhaled corticosteroids; Peto OR, Peto odds ratio; COPD, chronic obstructive pulmonary disease; GOLD, Global Initiative for Chronic Obstructive; BMI, body mass index.

risk (Peto OR, 1.75; 95% CI, 1.44–2.14) while budesonide (Peto OR, 1.06; 95% CI, 0.68–1.65) and beclomethasone (Peto OR, 1.24; 95% CI, 0.79–1.95) did not. Test for subgroup differences (I^2 = 61.9%) indicated that there was a significant difference in the serious pneumonia risk associated with different types of ICSs (**Table 2** and **Figure 10**).

Sensitivity Analysis

After excluding four RCTs (4,414 patients) with high risk of bias, the pooled results were similar in magnitude and direction to those (pooled results of association between various types of ICSs and pneumonia risk) obtained from all included RCTs (**Table 2**).

DISCUSSION

In this meta-analysis of 59 RCTs (including 103,477 patients), all types of ICSs, not only fluticasone, increased the pneumonia risk in COPD patients in a dose-dependent manner, and the risk was particularly evident in more severe COPD patients. Moreover, fluticasone increased the risk of serious pneumonia, while budesonide and beclomethasone did not. To our knowledge, this study was the first meta-analysis which revealed the pneumonia risk associated ICSs treatment was related with COPD severity. In addition, there was a dose-response relationship between the pneumonia risk and ICSs treatment.

At present, ICSs are widely used in the maintenance treatment of COPD patients. Since numerous COPD patients use ICSs every day, both its efficacy and safety should be considered. Although some studies have reported that fluticasone increases the pneumonia risk in COPD patients, whether other types of ICSs would increase the pneumonia risk in COPD patients remains controversial (Sin et al., 2009; Singh et al., 2009; Kew and Seniukovich, 2014; Festic et al., 2016; Yang et al., 2019; Zhang et al., 2020). In addition, it is still unclear whether different medication details and baseline characteristics (severity, age, and

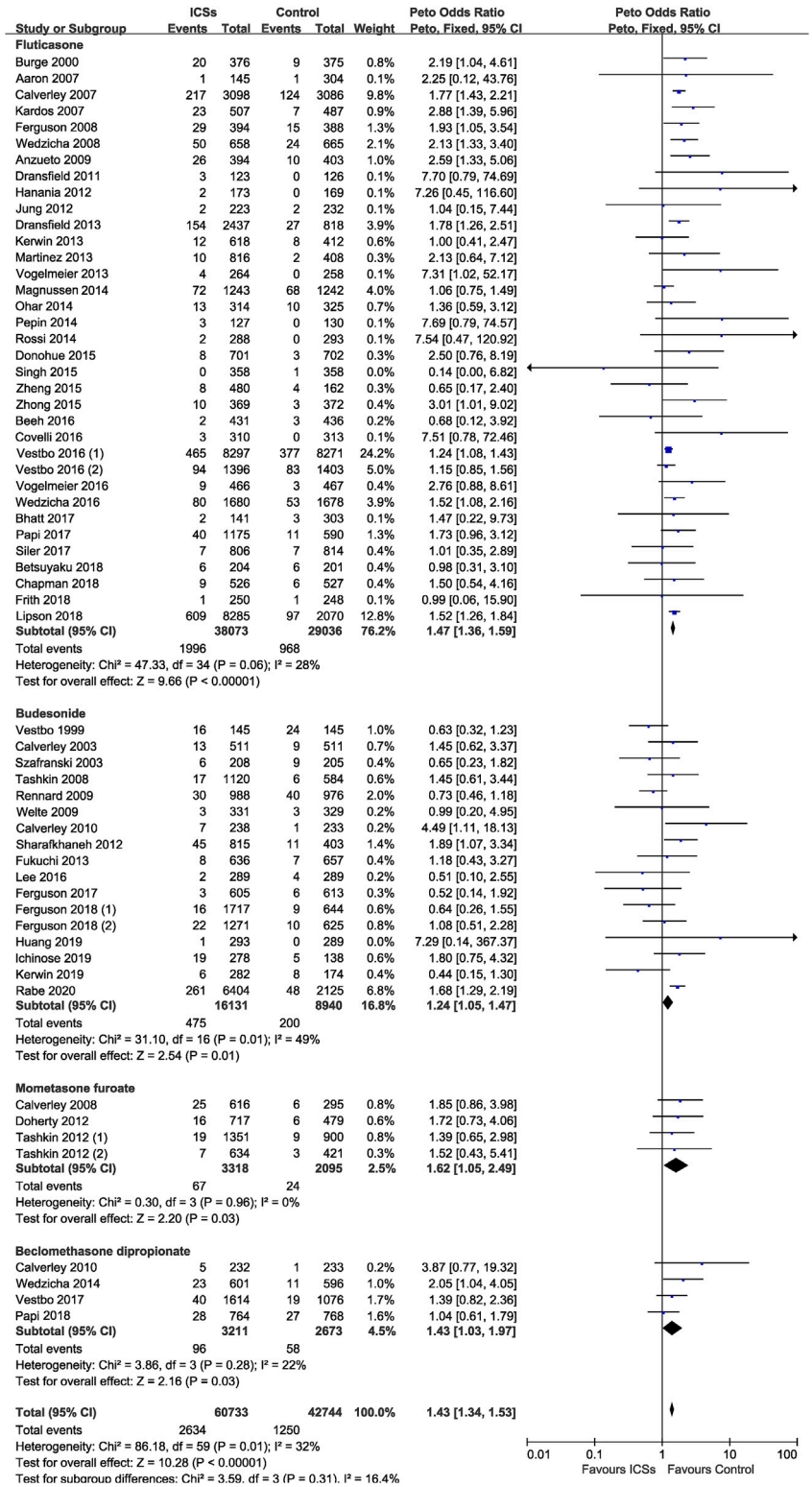

FIGURE 4 | Various types of inhaled corticosteroids and pneumonia risk.

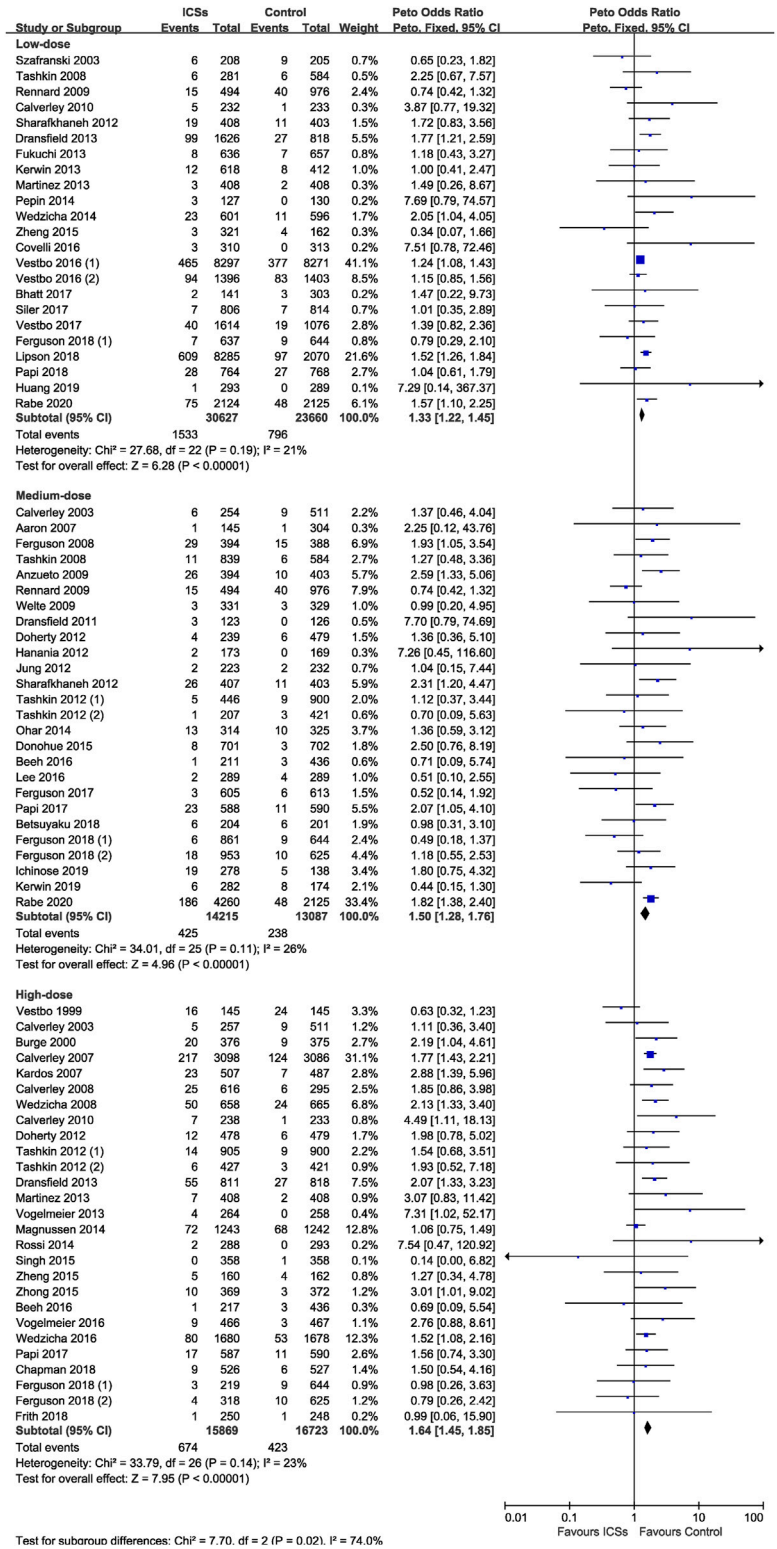

FIGURE 5 | Different doses of inhaled corticosteroids and pneumonia risk.

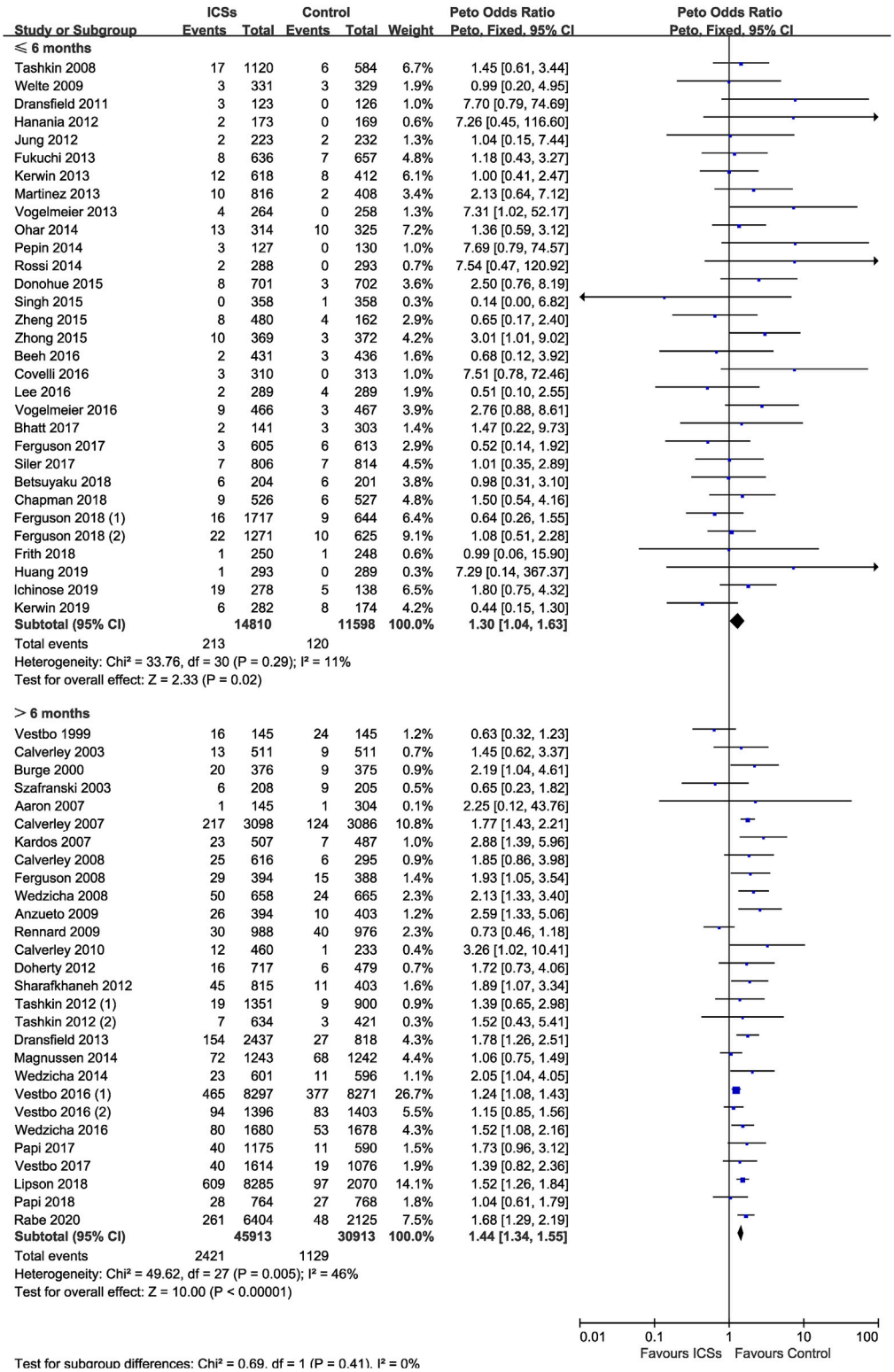

FIGURE 6 | Different treatment durations of inhaled corticosteroids and pneumonia risk.

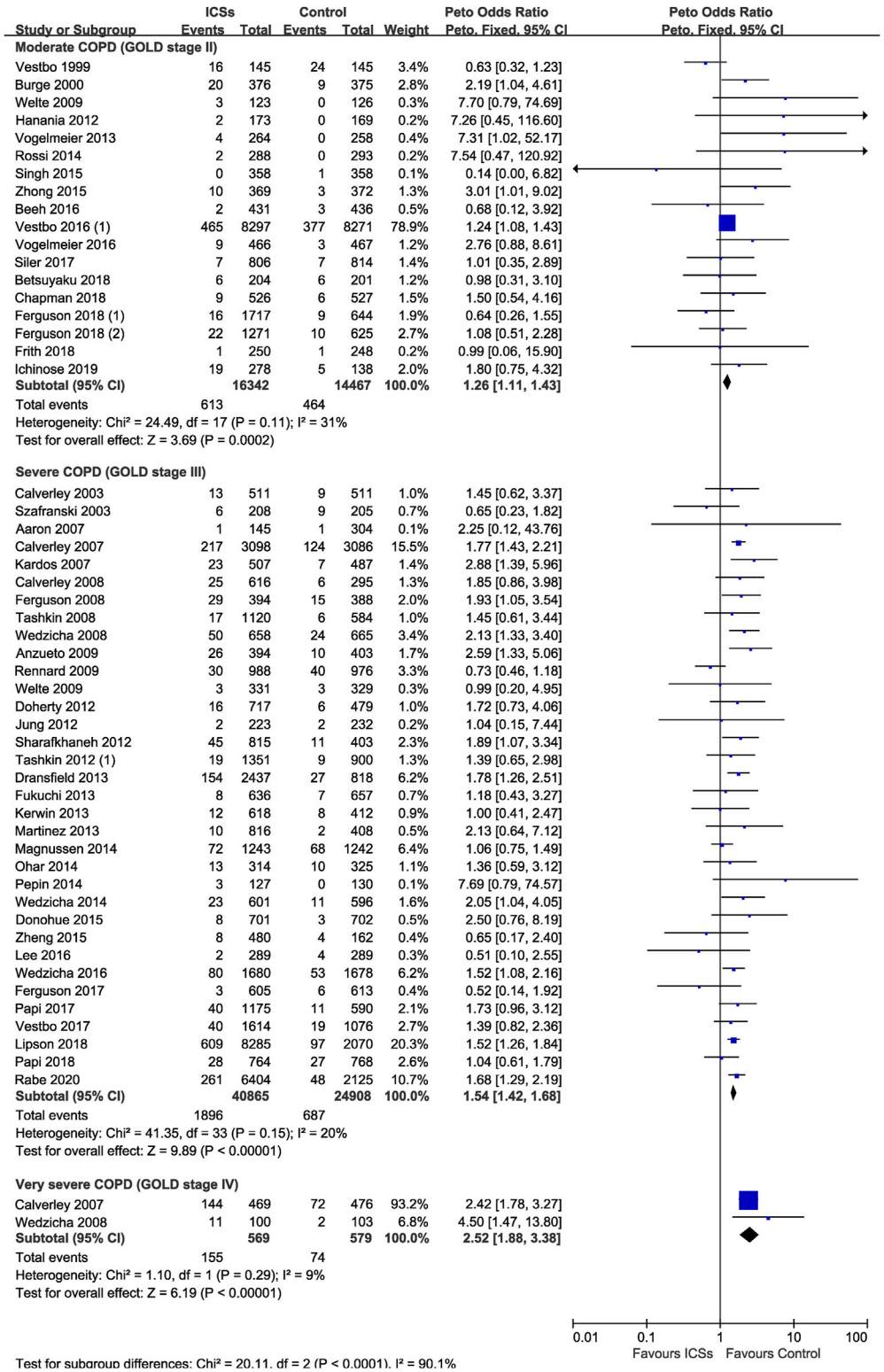

FIGURE 7 | Inhaled corticosteroids associated pneumonia in COPD patients with different severity.

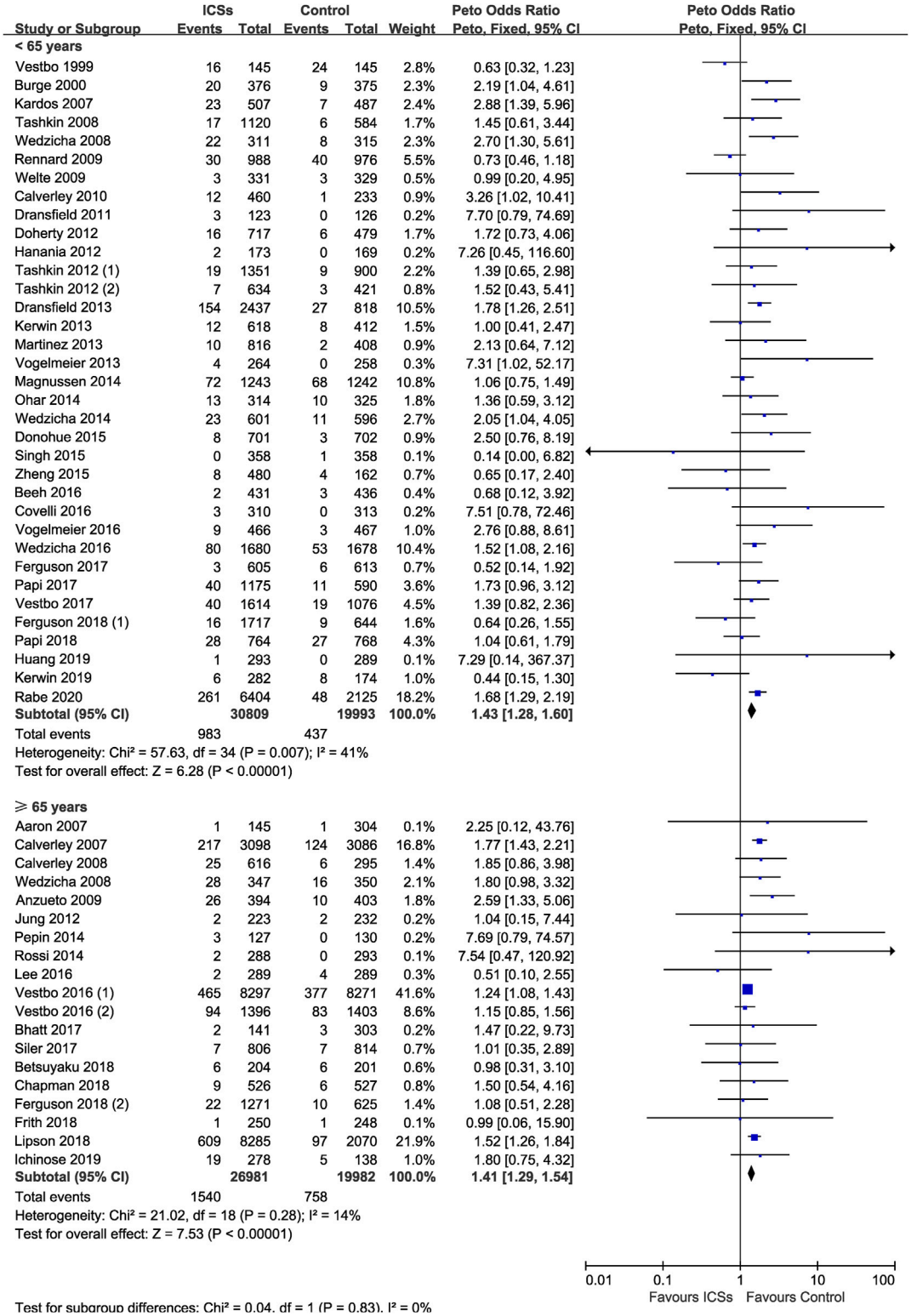

FIGURE 8 | Inhaled corticosteroids associated pneumonia in COPD patients with different age.

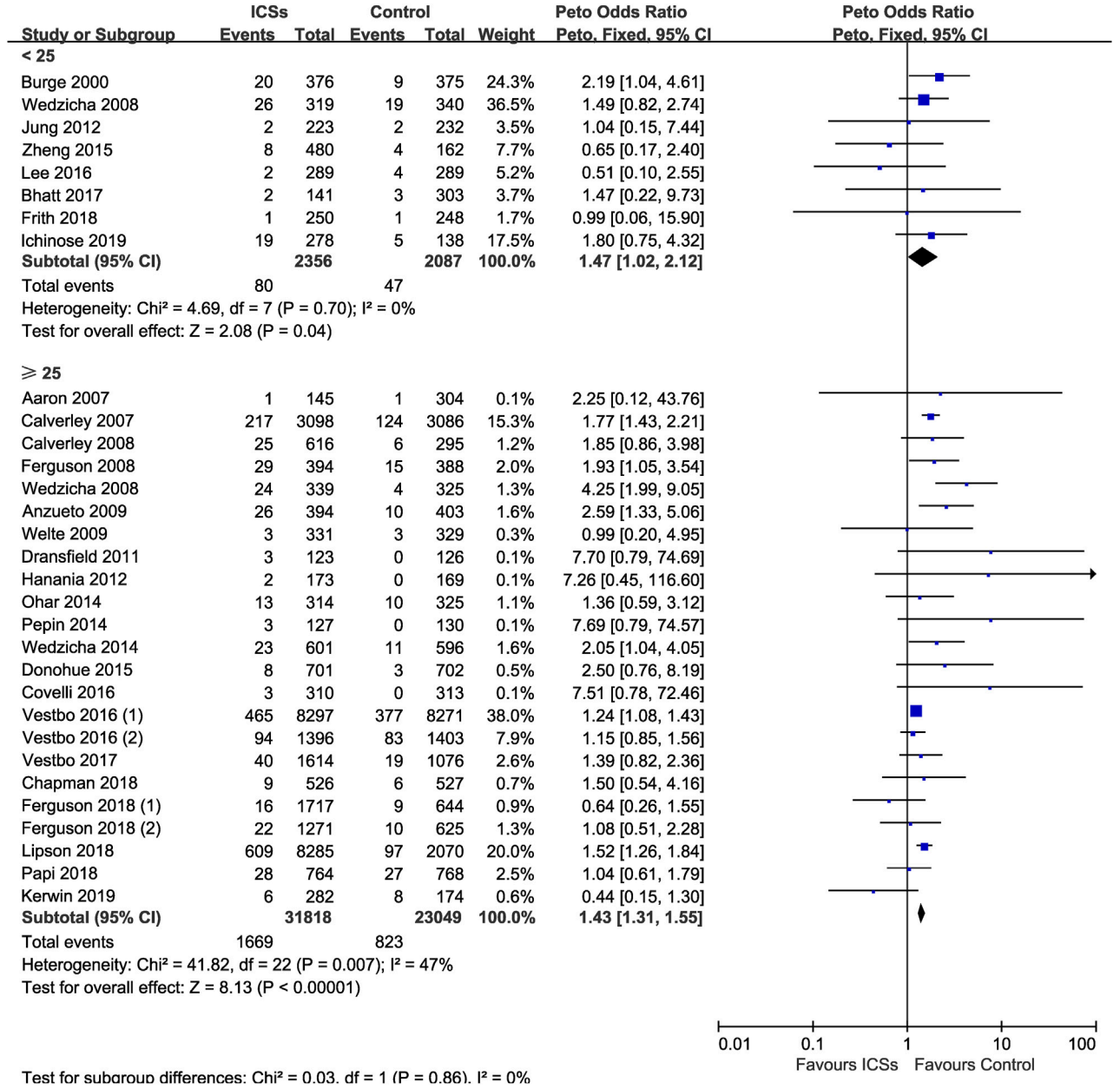

FIGURE 9 | Inhaled corticosteroids associated pneumonia in COPD patients with different body mass index.

body mass index) of patients would affect the incidence of pneumonia after ICSs treatment.

Our results first revealed that all types of ICSs significantly increased the pneumonia risk in COPD patients regardless of treatment duration. The dose-response relationship further confirmed the causality of ICSs treatment and increased pneumonia risk in COPD patients. Moreover, our results revealed that the pneumonia risk was related with COPD severity. However, age and BMI may not be the determinants of ICSs associated pneumonia. In addition, we found that COPD patients receiving different types of ICSs may have different risk of serious pneumonia. Only fluticasone increased the risk of serious pneumonia, while other types of ICSs did not. We speculated that this may be due to the different pharmacodynamics and pharmacokinetic characteristics of different types of ICSs. Previous studies reported that fluticasone could exhibit a longer retention in the airway mucosa and thus have a more prolonged suppression of local immunity of patients (Brattsand and Miller-Larsson, 2003; Dalby et al., 2009).

Compared With Other Studies

Several previous meta-analyses (Sin et al., 2009; Singh et al., 2009; Kew and Seniukovich, 2014; Festic et al., 2016; Yang et al., 2019;

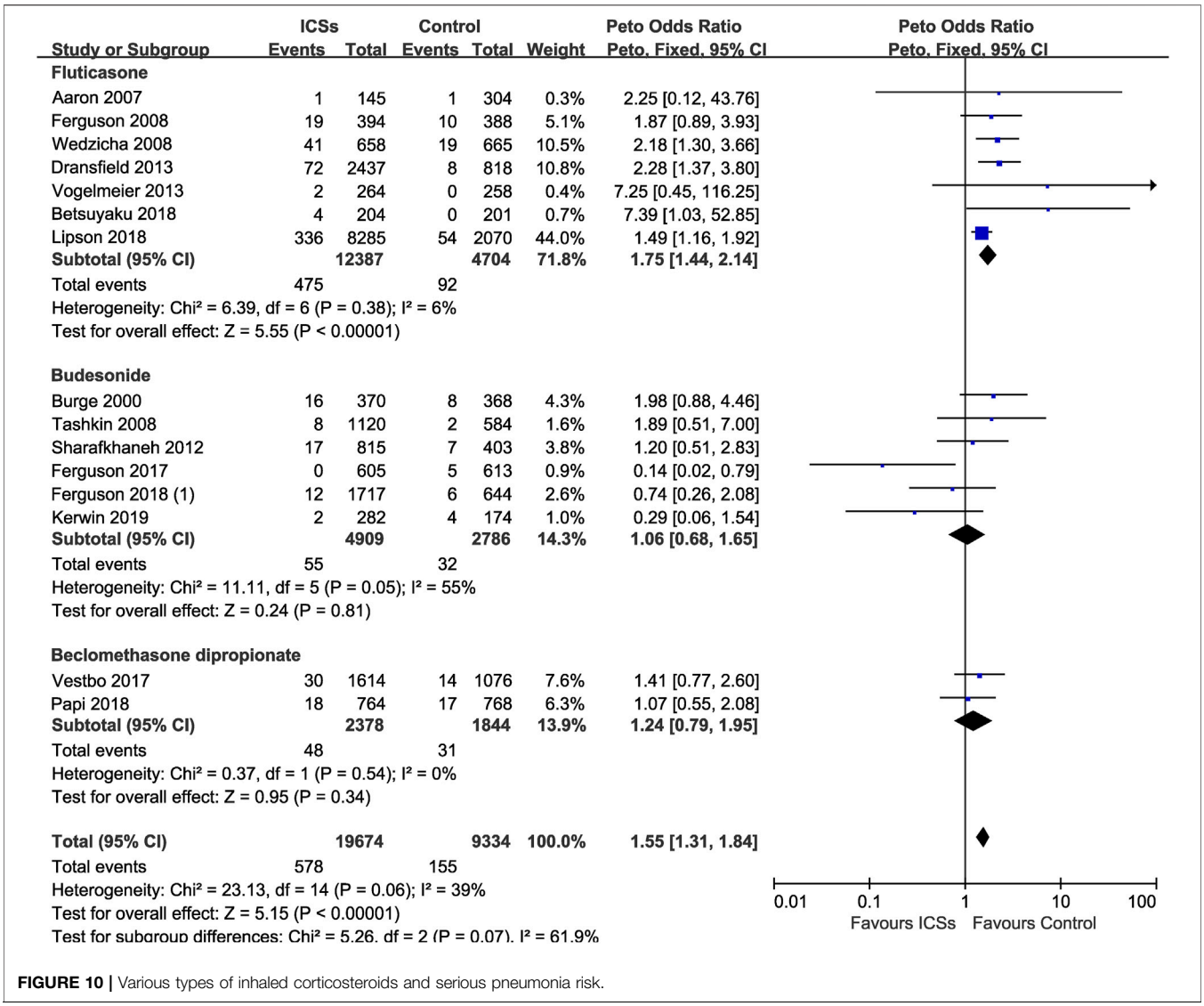

FIGURE 10 | Various types of inhaled corticosteroids and serious pneumonia risk.

Zhang et al., 2020) also assessed the pneumonia risk associated with ICSs treatment. However, there were major differences between our meta-analysis and the previous ones in terms of selected studies, statistical analyses, and outcomes. First, we included data of some recent large-scale RCTs (Bhatt et al., 2017; Papi et al., 2017; Siler et al., 2017; Vestbo et al., 2017; Betsuyaku et al., 2018; Chapman et al., 2018; Ferguson et al., 2018a; Ferguson et al., 2018b; Frith et al., 2018; Lipson et al., 2018; Papi et al., 2018; Ichinose et al., 2019; Kerwin et al., 2019; Rabe et al., 2020) which were published after some of the previous meta-analyses. In addition, varied search strategy may be an important reason for the difference in the number of RCTs included in different meta-analyses. We systematically searched four large databases for relevant RCTs, including PubMed, Embase, Cochrane Library, and Clinical Trials.gov. In particular, we systematically searched the online supplementary documents of relevant RCTs. Indeed, pneumonia risk was not the primary outcome in most RCTs, some researchers provided data on pneumonia risk in the online supplementary documents rather than in the text. Second, compared with the previous meta-analyses, we conducted more subgroup analyses based on the baseline demographic characteristics of the patients (severity, age and BMI) to clarify possible varied pneumonia risk in different patients receiving ICSs treatment. Third, our results indicated that all types of ICSs, not only fluticasone, increase the pneumonia risk in COPD patients in a dose-dependent manner, and the risk is particularly evident in more severe patients.

In 2009, Singh et al. (Singh et al., 2009) performed a meta-analysis (18 RCTs, 16,996 patients) and concluded that ICSs (fluticasone and budesonide) treatment significantly increased the pneumonia risk in COPD patients. However, their study failed to provide some important information on ICSs associated pneumonia due to a lack of subgroup analyses based on medication details of ICSs (including dose, type and treatment duration), and subgroup analyses based on the baseline

demographic characteristics of patients. In 2009, Sin et al. conducted a meta-analysis of budesonide and pneumonia risk (seven RCTs, 7,042 patients) and found that budesonide treatment for 12 mo did not increase the pneumonia risk in COPD patients. In 2014, a meta-analysis performed by Kew et al. (Kew and Seniukovich, 2014) (43 RCTs, 31,397 patients) suggested that both fluticasone and budesonide increased the serious pneumonia risk in COPD patients. However, that study did not further examine the association between other types of ICSs (momethasone and beclomethasone) and the pneumonia risk, nor conduct subgroup analyses based on the baseline demographic characteristics of patients. In 2016, another meta-analysis (29 RCTs, 33,472 patients) performed by Festic et al. (Festic et al., 2016) also revealed that ICSs increased the pneumonia risk in COPD patients. However, that study also limited by a smaller sample size and absent subgroup analyses. In addition, Yang et al. (Yang et al., 2019) conducted a meta-analysis (25 RCTs, 49,982 patients) and found ICSs significantly increased the pneumonia risk and serious pneumonia risk in COPD patients. However, their study also did not analyse the impact of baseline demographic characteristics of patients on the pneumonia risk. Moreover, in 2020, a meta-analysis (18 RCTs, 49,828 patients) performed by Zhang et al. (Zhang et al., 2020) also investigated the association between different types of ICSs and the pneumonia risk, and suggested that fluticasone increased the pneumonia risk while budesonide or beclomethasone did not. However, their results might be limited by the smaller sample size, since much fewer RCTs (especially RCTs on budesonide and beclomethasone) were included in their meta-analysis. In contrast, we searched more databases, used more search terms, and put less restrictions on literature search, which made more relevant RCTs were identified.

Limitations and Strengths

The major strength of our study was that we conducted a comprehensive literature search including all currently available RCTs, thus ensured the generalizability of the conclusions. Moreover, the multiple subgroup analyses based on the medication details (dose and treatment duration) and baseline of patients (severity, age and BMI of patients) enhanced the reliability of the conclusions, and also provided implications for the clinical practice. As far as we know, our study is the first meta-analysis which systematically assesses the association between various types of ICSs and the pneumonia risk based on baseline characteristics of patients.

This meta-analysis had several limitations. First, none of the included RCTs were specifically designed to monitor pneumonia event, therefore, there may be underreporting of pneumonia incidence. However, the underestimate of the pneumonia risk could not substantially impact the pooled results of this meta-analysis, since underreporting of pneumonia incidence might occur equally in ICSs treatment groups and non-ICSs treatment groups. Moreover, in the sensitivity analysis, after removing four non double-blind RCTs, the results were consistent with the previous pooled results. Second, the pooled results of momethasone (four RCTs, 5,413 patients) and beclomethasone (four RCTs, 5,884 patients) may weakened by the relatively small sample size. Third, some studies were excluded because of incomplete data or non-English literature, which may lead to inevitable selection bias.

CONCLUSIONS

ICSs treatment significantly increased the risk of pneumonia in COPD patients. There was a dose-response relationship between ICSs treatment and pneumonia risk. The pneumonia risk was related with COPD severity.

DATA AVAILABILITY STATEMENT

All datasets generated for this study are included in the article/ **Supplementary Material**.

AUTHOR CONTRIBUTIONS

HC and HY conceived and designed this study. HC and JS searched and selected studies. QH and YL extracted essential information. HC and MY assessed the risk of bias. HC and CM conducted the statistical analysis. HC wrote the original draft. All authors approved the final version to be published.

FUNDING

This study was supported by the Chengdu Science and Technology Project (No. 2015-HM0100621-SF).

ACKNOWLEDGMENTS

We would like to express our appreciation to all authors listed in these all primary studies which were included in the current meta-analysis.

SUPPLEMENTARY MATERIAL

The Supplementary Material for this article can be found online at: https://www.frontiersin.org/articles/10.3389/fphar.2021.691621/full#supplementary-material

REFERENCES

Aaron, S. D., Vandemheen, K. L., Fergusson, D., Maltais, F., Bourbeau, J., Goldstein, R., et al. (2007). Tiotropium in Combination with Placebo, Salmeterol, or Fluticasone-Salmeterol for Treatment of Chronic Obstructive Pulmonary Disease. *Ann. Intern. Med.* 146 (8), 545–555. doi:10.7326/0003-4819-146-8-200704170-00152

Anzueto, A., Ferguson, G. T., Feldman, G., Chinsky, K., Seibert, A., Emmett, A., et al. (2009). Effect of Fluticasone Propionate/salmeterol (250/50) on COPD Exacerbations and Impact on Patient Outcomes. *COPD: J. Chronic Obstructive Pulm. Dis.* 6 (5), 320–329. doi:10.1080/15412550903140881

Beeh, K. M., Derom, E., Echave-Sustaeta, J., Grönke, L., Hamilton, A., Zhai, D., et al. (2016). The Lung Function Profile of Once-Daily Tiotropium and Olodaterol Via Respimat® Is superior to that of Twice-Daily Salmeterol and Luticasone Propionate Via Accuhaler® (ENERGITO® Study). *Copd* 11, 193–205. doi:10.2147/copd.s95055

Betsuyaku, T., Kato, M., Fujimoto, K., Kobayashi, A., Hayamizu, T., Hitosugi, H., et al. (2018). A Randomized Trial of Symptom-Based Management in Japanese Patients with COPD. *Copd* 13, 2409–2423. doi:10.2147/copd.s152723

Bhatt, S., Dransfield, M., Cockcroft, J., Wang-Jairaj, J., Midwinter, D., Rubin, D., et al. (2017). A Randomized Trial of Once-Daily Fluticasone Furoate/vilanterol or Vilanterol Versus Placebo to Determine Effects on Arterial Stiffness in COPD. *Copd* 12, 351–365. doi:10.2147/copd.s117373

Bradburn, M. J., Deeks, J. J., Berlin, J. A., and Russell Localio, A. (2007). Much Ado about Nothing: a Comparison of the Performance of Meta-Analytical Methods with Rare Events. *Statist. Med.* 26, 53–77. doi:10.1002/sim.2528

Brattsand, R., and Miller-Larsson, A. (2003). The Role of Intracellular Esterification in Budesonide Once-Daily Dosing and Airway Selectivity. *Clin. Ther.* 25 (Suppl. C), C28–C41. doi:10.1016/s0149-2918(03)80304-1

Burge, P. S., Calverley, P. M., Jones, P. W., Spencer, S., Anderson, J. A., and Maslen, T. K. (2000). Randomised, Double Blind, Placebo Controlled Study of Fluticasone Propionate in Patients with Moderate to Severe Chronic Obstructive Pulmonary Disease: The ISOLDE Trial. *BMJ* 320 (7245), 1297–1303. doi:10.1136/bmj.320.7245.1297

Calverley, P. M. A., Anderson, J. A., Celli, B., Ferguson, G. T., Jenkins, C., Jones, P. W., et al. (2007). Salmeterol and Fluticasone Propionate and Survival in Chronic Obstructive Pulmonary Disease. *N. Engl. J. Med.* 356 (8), 775–789. doi:10.1056/nejmoa063070

Calverley, P. M. A., Kuna, P., Monsó, E., Costantini, M., Petruzzelli, S., Sergio, F., et al. (2010). Beclomethasone/formoterol in the Management of COPD: A Randomised Controlled Trial. *Respir. Med.* 104, 1858–1868. doi:10.1016/j.rmed.2010.09.008

Calverley, P. M., Boonsawat, W., Cseke, Z., Zhong, N., Peterson, S., and Olsson, H. (2003). Maintenance Therapy with Budesonide and Formoterol in Chronicobstructive Pulmonary Disease. *Eur. Respir. J.* 22 (6), 912–919. doi:10.1183/09031936.03.00027003

Calverley, P. M., Rennard, S., Nelson, H. S., Karpel, J. P., Abbate, E. H., Stryszak, P., et al. (2008). One-year Treatment with Mometasone Furoate in Chronic Obstructive Pulmonary Disease. *Respir. Res.* 9, 73. doi:10.1186/1465-9921-9-73

Chapman, K. R., Hurst, J. R., Frent, S.-M., Larbig, M., Fogel, R., Guerin, T., et al. (2018). Long-Term Triple Therapy De-escalation to Indacaterol/Glycopyrronium in Patients with Chronic Obstructive Pulmonary Disease (SUNSET): A Randomized, Double-Blind, Triple-Dummy Clinical Trial. *Am. J. Respir. Crit. Care Med.* 198 (3), 329–339. doi:10.1164/rccm.201803-0405oc

Covelli, H., Pek, B., Schenkenberger, I., Scott-Wilson, C., Emmett, A., and Crim, C. (2016). Efficacy and Safety of Fluticasone Furoate/vilanterol or Tiotropium in Subjects with COPD at Cardiovascular Risk. *Int. J. Chron. Obstruct Pulmon Dis.* 11, 1–12. doi:10.2147/COPD.S91407

Dalby, C., Polanowski, T., Larsson, T., Borgström, L., Edsbäcker, S., and Harrison, T. W. (2009). The Bioavailability and Airway Clearance of the Steroid Component of Budesonide/formoterol and Salmeterol/fluticasone after Inhaled Administration in Patients with COPD and Healthy Subjects: A Randomized Controlled Trial. *Respir. Res.* 10, 104. doi:10.1186/1465-9921-10-104

Doherty, D., Tashkin, D., Kerwin, E., Knorr, B. A., Shekar, T., Banerjee, S., et al. (2012). Effects of Mometasone Furoate/formoterol Fumarate Fixed-Dose Combination Formulation on Chronic Obstructive Pulmonary Disease (COPD): Results From a 52-week Phase III Trial in Subjects with Moderate-To-Very Severe COPD. *Copd* 7, 57–71. doi:10.2147/copd.s27320

Dong, Y.-H., Chang, C.-H., Wu, F.-L. L., Shen, L.-J., Calverley, P. M. A., Löfdahl, C.-G., et al. (2014). Use of Inhaled Corticosteroids in Patients with COPD and the Risk of TB and Influenza. *Chest* 145 (6), 1286–1297. doi:10.1378/chest.13-2137

Donohue, J. F., Worsley, S., Zhu, C.-Q., Hardaker, L., and Church, A. (2015). Improvements in Lung Function with Umeclidinium/vilanterol Versus Fluticasone Propionate/salmeterol in Patients with Moderate-To-Severe COPD and Infrequent Exacerbations. *Respir. Med.* 109 (7), 870–881. doi:10.1016/j.rmed.2015.04.018

Dransfield, M. T., Bourbeau, J., Jones, P. W., Hanania, N. A., Mahler, D. A., Vestbo, J., et al. (2013). Once-daily Inhaled Fluticasone Furoate and Vilanterol Versus Vilanterol Only for Prevention of Exacerbations of COPD: Two Replicate Double-Blind, Parallel-Group, Randomised Controlled Trials. *Lancet Respir. Med.* 1 (3), 210–223. doi:10.1016/s2213-2600(13)70040-7

Dransfield, M. T., Cockcroft, J. R., Townsend, R. R., Coxson, H. O., Sharma, S. S., Rubin, D. B., et al. (2011). Effect of Fluticasone Propionate/salmeterol on Arterial Stiffness in Patients with COPD. *Respir. Med.* 105 (9), 1322–1330. doi:10.1016/j.rmed.2011.05.016

Ferguson, G. T., Anzueto, A., Fei, R., Emmett, A., Knobil, K., and Kalberg, C. (2008). Effect of Fluticasone Propionate/salmeterol (250/50μg) or Salmeterol (50μg) on COPD Exacerbations. *Respir. Med.* 102 (8), 1099–1108. doi:10.1016/j.rmed.2008.04.019

Ferguson, G. T., Papi, A., Anzueto, A., Kerwin, E. M., Cappelletti, C., Duncan, E. A., et al. (2018a). Budesonide/formoterol MDI with Co-suspension Delivery Technology in COPD: The TELOS Study. *Eur. Respir. J.* 52 (3), 1801334. doi:10.1183/13993003.01334-2018

Ferguson, G. T., Rabe, K. F., Martinez, F. J., Fabbri, L. M., Wang, C., Ichinose, M., et al. (2018b). Triple Therapy with Budesonide/glycopyrrolate/formoterol Fumarate with Co-suspension Delivery Technology Versus Dual Therapies in Chronic Obstructive Pulmonary Disease (KRONOS): A Double-Blind, Parallel-Group, Multicentre, Phase 3 Randomised Controlled Trial. *Lancet Respir. Med.* 6 (10), 747–758. doi:10.1016/s2213-2600(18)30327-8

Ferguson, G. T., Tashkin, D. P., Skärby, T., Jorup, C., Sandin, K., Greenwood, M., et al. (2017). Effect of Budesonide/formoterol Pressurized Metered-Dose Inhaler on Exacerbations Versus Formoterol in Chronic Obstructive Pulmonary Disease: The 6-month, Randomized RISE (Revealing the Impact of Symbicort in Reducing Exacerbations in COPD) Study. *Respir. Med.* 132, 31–41. doi:10.1016/j.rmed.2017.09.002

Festic, E., Bansal, V., Gupta, E., and Scanlon, P. D. (2016). Association of Inhaled Corticosteroids with Incident Pneumonia and Mortality in COPD Patients; Systematic Review and Meta-Analysis. *COPD: J. Chronic Obstructive Pulm. Dis.* 13 (3), 312–326. doi:10.3109/15412555.2015.1081162

Frith, P. A., Ashmawi, S., Krishnamurthy, S., Gurgun, A., Hristoskova, S., Pilipovic, V., et al. (2018). Efficacy and Safety of the Direct Switch to Indacaterol/glycopyrronium From Salmeterol/fluticasone in Non-frequently Exacerbating COPD Patients: The FLASH Randomized Controlled Trial. *Respirology* 23 (12), 1152–1159. doi:10.1111/resp.13374

Fukuchi, Y., Samoro, R., Fassakhov, R., Taniguchi, H., Ekelund, J., Carlsson, L.-G., et al. (2013). Budesonide/formoterol Via Turbuhaler Versus Formoterol Via Turbuhaler in Patients with Moderate to Severe Chronic Obstructive Pulmonary Disease: Phase III Multinational Study Results. *Respirology* 18 (5), 866–873. doi:10.1111/resp.12090

GBD 2015 Chronic Respiratory Disease Collaborators (2017). Global, Regional, and National Deaths, Prevalence, Disability-Adjusted Life Years, and Years Lived With Disability for Chronic Obstructive Pulmonary Disease and Asthma, 1990-2015: A Systematic Analysis for the Global Burden of Disease Study 2015. *Lancet Respir. Med.* 5 (9), 691–706. doi:10.1016/S2213-2600(17)30293-X

Hanania, N. A., Crater, G. D., Morris, A. N., Emmett, A. H., O'Dell, D. M., and Niewoehner, D. E. (2012). Benefits of Adding Fluticasone Propionate/salmeterol to Tiotropium in Moderate to Severe COPD. *Respir. Med.* 106 (1), 91–101. doi:10.1016/j.rmed.2011.09.002

Higgins, J. P. T., Altman, D. G., Gotzsche, P. C., Jüni, P., Moher, D., Oxman, A. D., et al. (2011). The Cochrane Collaboration's Tool for Assessing Risk of Bias in Randomised Trials. *BMJ* 343, d5928. doi:10.1136/bmj.d5928

Higgins, J. P. T., Thompson, S. G., Deeks, J. J., and Altman, D. G. (2003). Measuring Inconsistency in Meta-Analyses. *BMJ* 327, 557–560. doi:10.1136/bmj.327.7414.557

Huang, K., Guo, Y., Kang, J., An, L., Zheng, Z., Ma, L., et al. (2019). The Efficacy of Adding Budesonide/formoterol to Ipratropium Plus Theophylline in Managing Severe Chronic Obstructive Pulmonary Disease: An Open-Label, Randomized Study in China. *Ther. Adv. Respir. Dis.* 13, 1753466619853500. doi:10.1177/1753466619853500

Ichinose, M., Fukushima, Y., Inoue, Y., Hataji, O., Ferguson, G. T., Rabe, K. F., et al. (2019). Long-Term Safety and Efficacy of Budesonide/Glycopyrrolate/Formoterol Fumarate Metered Dose Inhaler Formulated Using Co-suspension Delivery Technology in Japanese Patients with COPD. *Copd* 14, 2993–3002. doi:10.2147/copd.s220861

Janson, C., Johansson, G., Ställberg, B., Lisspers, K., Olsson, P., Keininger, D. L., et al. (2018). Identifying the Associated Risks of Pneumonia in COPD Patients: ARCTIC An Observational Study. *Respir. Res.* 19 (1), 172. doi:10.1186/s12931-018-0868-y

Jung, K. S., Park, H. Y., Park, S. Y., Kim, S. K., Kim, Y.-K., Shim, J.-J., et al. (2012). Comparison of Tiotropium Plus Fluticasone Propionate/salmeterol with Tiotropium in COPD: A Randomized Controlled Study. *Respir. Med.* 106 (3), 382–389. doi:10.1016/j.rmed.2011.09.004

Kardos, P., Wencker, M., Glaab, T., and Vogelmeier, C. (2007). Impact of Salmeterol/fluticasone Propionate Versus Salmeterol on Exacerbations in Severe Chronic Obstructive Pulmonary Disease. *Am. J. Respir. Crit. Care Med.* 175 (2), 144–149. doi:10.1164/rccm.200602-244oc

Kerwin, E. M., Ferguson, G. T., Mo, M., DeAngelis, K., and Dorinsky, P. (2019). Bone and Ocular Safety of Budesonide/glycopyrrolate/formoterol Fumarate Metered Dose Inhaler in COPD: A 52-week Randomized Study. *Respir. Res.* 20 (1), 167. doi:10.1186/s12931-019-1126-7

Kerwin, E. M., Scott-Wilson, C., Sanford, L., Rennard, S., Agusti, A., Barnes, N., et al. (2013). A Randomised Trial of Fluticasone Furoate/vilanterol (50/25 μg; 100/25 μg) on Lung Function in COPD. *Respir. Med.* 107 (4), 560–569. doi:10.1016/j.rmed.2012.12.014

Kew, K. M., and Seniukovich, A. (2014). Inhaled Steroids and Risk of Pneumonia for Chronic Obstructive Pulmonary Disease. *Cochrane Database Syst. Rev.* 3, CD010115. doi:10.1002/14651858.CD010115.pub2

Lee, S.-D., Xie, C.-m., Yunus, F., Itoh, Y., Ling, X., Yu, W.-c., et al. (2016). Efficacy and Tolerability of Budesonide/formoterol Added to Tiotropium Compared with Tiotropium Alone in Patients with Severe or Very Severe COPD: A Randomized, Multicentre Study in East Asia. *Respirology* 21 (1), 119–127. doi:10.1111/resp.12646

Lipson, D. A., Barnhart, F., Brealey, N., Brooks, J., Criner, G. J., Day, N. C., et al. (2018). Once-Daily Single-Inhaler Triple Versus Dual Therapy in Patients with COPD. *N. Engl. J. Med.* 378 (18), 1671–1680. doi:10.1056/nejmoa1713901

López-Campos, J. L., Soler-Cataluña, J. J., and Miravitlles, M. (2020). Global Strategy for the Diagnosis, Management, and Prevention of Chronic Obstructive Lung Disease 2019 Report: Future Challenges. *Archivos de Bronconeumología* 56, 65–67. doi:10.1016/j.arbres.2019.06.001

Magnussen, H., Disse, B., Rodriguez-Roisin, R., Kirsten, A., Watz, H., Tetzlaff, K., et al. (2014). Withdrawal of Inhaled Glucocorticoids and Exacerbations of COPD. *N. Engl. J. Med.* 371 (14), 1285–1294. doi:10.1056/nejmoa1407154

Martinez, F. J., Boscia, J., Feldman, G., Scott-Wilson, C., Kilbride, S., Fabbri, L., et al. (2013). Fluticasone Furoate/vilanterol (100/25; 200/25 μg) Improves Lung Function in COPD: A Randomised Trial. *Respir. Med.* 107 (4), 550–559. doi:10.1016/j.rmed.2012.12.016

Moher, D., Liberati, A., Tetzlaff, J., and Altman, D. G. (2009). PRISMA Group, Preferred Reporting Items for Systematic Reviews and Meta-Analyses: The PRISMA Statement. *Plos Med.* 6 (7), e1000097. doi:10.1371/journal.pmed.1000097

Morjaria, J. B., Rigby, A., and Morice, A. H. (2017). Inhaled Corticosteroid Use and the Risk of Pneumonia and COPD Exacerbations in the UPLIFT Study. *Lung* 195 (3), 281–288. doi:10.1007/s00408-017-9990-8

Ohar, J. A., Crater, G. D., Emmett, A., Ferro, T. J., Morris, A. N., Raphiou, I., et al. (2014). Fluticasone Propionate/salmeterol 250/50 μg Versus Salmeterol 50 μg After Chronic Obstructive Pulmonary Disease Exacerbation. *Respir. Res.* 15, 105. doi:10.1186/s12931-014-0105-2

Papi, A., Dokic, D., Tzimas, W., Mészáros, I., Olech-Cudzik, A., Koroknai, Z., et al. (2017). Fluticasone Propionate/formoterol for COPD Management: A Randomized Controlled Trial. *Copd* 12, 1961–1971. doi:10.2147/copd.s136527

Papi, A., Vestbo, J., Fabbri, L., Corradi, M., Prunier, H., Cohuet, G., et al. (2018). Extrafine Inhaled Triple Therapy Versus Dual Bronchodilator Therapy in Chronic Obstructive Pulmonary Disease (TRIBUTE): A Double-Blind, Parallel Group, Randomised Controlled Trial. *The Lancet* 391 (10125), 1076–1084. doi:10.1016/s0140-6736(18)30206-x

Pascoe, S., Locantore, N., Dransfield, M. T., Barnes, N. C., and Pavord, I. D. (2015). Blood Eosinophil Counts, Exacerbations, and Response to the Addition of Inhaled Fluticasone Furoate to Vilanterol in Patients with Chronic Obstructive Pulmonary Disease: A Secondary Analysis of Data From Two Parallel Randomised Controlled Trials. *Lancet Respir. Med.* 3 (6), 435–442. doi:10.1016/s2213-2600(15)00106-x

Pepin, J.-L., Cockcroft, J. R., Midwinter, D., Sharma, S., Rubin, D. B., and Andreas, S. (2014). Long-Acting Bronchodilators and Arterial Stiffness in Patients with COPD. *Chest* 146 (6), 1521–1530. doi:10.1378/chest.13-2859

Rabe, K. F., Martinez, F. J., Ferguson, G. T., Wang, C., Singh, D., Wedzicha, J. A., et al. (2020). Triple Inhaled Therapy at Two Glucocorticoid Doses in Moderate-To-Very-Severe COPD. *N. Engl. J. Med.* 383 (1), 35–48. doi:10.1056/nejmoa1916046

Rennard, S. I., Tashkin, D. P., McElhattan, J., Goldman, M., Ramachandran, S., Martin, U. J., et al. (2009). Efficacy and Tolerability of Budesonide/Formoterol in One Hydrofluoroalkane Pressurized Metered-Dose Inhaler in Patients with Chronic Obstructive Pulmonary Disease. *Drugs* 69 (5), 549–565. doi:10.2165/00003495-200969050-00004

Rossi, A., van der Molen, T., Olmo, R. d., Papi, A., Wehbe, L., Quinn, M., et al. (2014). INSTEAD: A Randomised Switch Trial of Indacaterol Versus Salmeterol/fluticasone in Moderate COPD. *Eur. Respir. J.* 44 (6), 1548–1556. doi:10.1183/09031936.00126814

Shamseer, L., Moher, D., Clarke, M., Ghersi, D., Liberati, A., Petticrew, M., et al. (2015). Preferred Reporting Items for Systematic Review and Meta-Analysis Protocols (PRISMA-P) 2015: Elaboration and Explanation. *BMJ* 349, g7647. doi:10.1136/bmj.g7647

Sharafkhaneh, A., Southard, J. G., Goldman, M., Uryniak, T., and Martin, U. J. (2012). Effect of Budesonide/formoterol pMDI on COPD Exacerbations: A Double-Blind, Randomized Study. *Respir. Med.* 106, 257–268. doi:10.1016/j.rmed.2011.07.020

Siler, T. M., Nagai, A., Scott-Wilson, C. A., Midwinter, D. A., and Crim, C. (2017). A Randomised, Phase III Trial of Once-Daily Fluticasone Furoate/vilanterol 100/25 μg Versus Once-Daily Vilanterol 25 μg to Evaluate the Contribution on Lung Function of Fluticasone Furoate in the Combination in Patients with COPD. *Respir. Med.* 123, 8–17. doi:10.1016/j.rmed.2016.12.001

Sin, D. D., Tashkin, D., Zhang, X., Radner, F., Sjöbring, U., Thorén, A., et al. (2009). Budesonide and the Risk of Pneumonia: A Meta-Analysis of Individual Patient Data. *The Lancet* 374 (9691), 712–719. doi:10.1016/S0140-6736(09)61250-2

Singh, D., Worsley, S., Zhu, C. Q., Hardaker, L., and Church, A. (2015). Umeclidinium/vilanterol Versus Fluticasone Propionate/salmeterol in COPD: A Randomised Trial. *BMC Pulm. Med.* 15, 91. doi:10.1186/s12890-015-0092-1

Singh, S., Amin, A. V., and Loke, Y. K. (2009). Long-term Use of Inhaled Corticosteroids and the Risk of Pneumonia in Chronic Obstructive Pulmonary Disease. *Arch. Intern. Med.* 169 (3), 219–229. doi:10.1001/archinternmed.2008.550

Sobieraj, D. M., Weeda, E. R., Nguyen, E., Coleman, C. I., White, C. M., Lazarus, S. C., et al. (2018). Association of Inhaled Corticosteroids and Long-Acting β-Agonists as Controller and Quick Relief Therapy with Exacerbations and Symptom Control in Persistent Asthma. *JAMA* 319 (14), 1485–1496. doi:10.1001/jama.2018.2769

Szafranski, W., Cukier, A., Ramirez, A., Menga, G., Sansores, R., Nahabedian, S., et al. (2003). Efficacy and Safety of Budesonide/formoterol in the Management of Chronic Obstructive Pulmonary Disease. *Eur. Respir. J.* 21 (1), 74–81. doi:10.1183/09031936.03.00031402

Tashkin, D. P., Doherty, D. E., Kerwin, E., Matiz-Bueno, C. E., Knorr, B., Shekar, T., et al. (2012a). Efficacy and Safety Characteristics of Mometasone Furoate/formoterol Fumarate Fixed-Dose Combination in Subjects with Moderate to Very Severe COPD: Findings From Pooled Analysis of Two Randomized, 52-

week Placebo-Controlled Trials. *Int. J. Chron. Obstruct Pulmon Dis.* 7, 73–86. doi:10.2147/COPD.S29444

Tashkin, D. P., Doherty, D. E., Kerwin, E., Matiz-Bueno, C. E., Knorr, B., Shekar, T., et al. (2012b). Efficacy and Safety of a Fixed-Dose Combination of Mometasone Furoate and Formoterol Fumarate in Subjects with Moderate to Very Severe COPD: Results From a 52-week Phase III Trial. *Int. J. Chron. Obstruct Pulmon Dis.* 7, 43–55. doi:10.2147/COPD.S27319

Tashkin, D. P., Rennard, S. I., Martin, P., Ramachandran, S., Martin, U. J., Silkoff, P. E., et al. (2008). Efficacy and Safety of Budesonide and Formoterol in One Pressurized Metered-Dose Inhaler in Patients with Moderate to Very Severe Chronic Obstructive Pulmonary Disease. *Drugs* 68 (14), 1975–2000. doi:10.2165/00003495-200868140-00004

Vestbo, J., Anderson, J. A., Brook, R. D., Calverley, P. M. A., Celli, B. R., Crim, C., et al. (2016a). Fluticasone Furoate and Vilanterol and Survival in Chronic Obstructive Pulmonary Disease with Heightened Cardiovascular Risk (SUMMIT): A Double-Blind Randomised Controlled Trial. *The Lancet* 387 (10030), 1817–1826. doi:10.1016/s0140-6736(16)30069-1

Vestbo, J., Leather, D., Diar Bakerly, N., New, J., Gibson, J. M., McCorkindale, S., et al. (2016b). Effectiveness of Fluticasone Furoate-Vilanterol for COPD in Clinical Practice. *N. Engl. J. Med.* 375 (13), 1253–1260. doi:10.1056/nejmoa1608033

Vestbo, J., Papi, A., Corradi, M., Blazhko, V., Montagna, I., Francisco, C., et al. (2017). Single Inhaler Extrafine Triple Therapy versus Long-Acting Muscarinic Antagonist Therapy for Chronic Obstructive Pulmonary Disease (TRINITY): a Double-Blind, Parallel Group, Randomised Controlled Trial. *The Lancet* 389 (10082), 1919–1929. doi:10.1016/s0140-6736(17)30188-5

Vestbo, J., Søorensen, T., Lange, P., Brix, A., Torre, P., and Viskum, K. (1999). Long-term Effect of Inhaled Budesonide in Mild and Moderate Chronic Obstructive Pulmonary Disease: A Randomised Controlled Trial. *The Lancet* 353 (9167), 1819–1823. doi:10.1016/s0140-6736(98)10019-3

Viniol, C., and Vogelmeier, C. F. (2018). Exacerbations of COPD. *Eur. Respir. Rev.* 27, 170103. doi:10.1183/16000617.0103-2017

Vogelmeier, C. F., Bateman, E. D., Pallante, J., Alagappan, V. K. T., D'Andrea, P., Chen, H., et al. (2013). Efficacy and Safety of Once-Daily QVA149 Compared with Twice-Daily Salmeterol-Fluticasone in Patients with Chronic Obstructive Pulmonary Disease (ILLUMINATE): A Randomised, Double-Blind, Parallel Group Study. *Lancet Respir. Med.* 1 (1), 51–60. doi:10.1016/s2213-2600(12)70052-8

Vogelmeier, C., Paggiaro, P. L., Dorca, J., Sliwinski, P., Mallet, M., Kirsten, A.-M., et al. (2016). Efficacy and Safety of Aclidinium/formoterol Versus Salmeterol/fluticasone: A Phase 3 COPD Study. *Eur. Respir. J.* 48 (4), 1030–1039. doi:10.1183/13993003.00216-2016

Wedzicha, J. A., Banerji, D., Chapman, K. R., Vestbo, J., Roche, N., Ayers, R. T., et al. (2016). Indacaterol-Glycopyrronium Versus Salmeterol-Fluticasone for COPD. *N. Engl. J. Med.* 374 (23), 2222–2234. doi:10.1056/nejmoa1516385

Wedzicha, J. A., Calverley, P. M. A., Seemungal, T. A., Hagan, G., Ansari, Z., Stockley, R. A., et al. (2008). The Prevention of Chronic Obstructive Pulmonary Disease Exacerbations by Salmeterol/fluticasone Propionate or Tiotropium Bromide. *Am. J. Respir. Crit. Care Med.* 177 (1), 19–26. doi:10.1164/rccm.200707-973oc

Wedzicha, J. A., Singh, D., Vestbo, J., Paggiaro, P. L., Jones, P. W., Bonnet-Gonod, F., et al. (2014). Extrafine Beclomethasone/formoterol in Severe COPD Patients with History of Exacerbations. *Respir. Med.* 108 (8), 1153–1162. doi:10.1016/j.rmed.2014.05.013

Welte, T., Miravitlles, M., Hernandez, P., Eriksson, G., Peterson, S., Polanowski, T., et al. (2009). Efficacy and Tolerability of Budesonide/formoterol Added to Tiotropium in Patients with Chronic Obstructive Pulmonary Disease. *Am. J. Respir. Crit. Care Med.* 180 (8), 741–750. doi:10.1164/rccm.200904-0492oc

Yang, M., Chen, H., Zhang, Y., Du, Y., Xu, Y., Jiang, P., et al. (2017). Long-term Use of Inhaled Corticosteroids and Risk of Upper Respiratory Tract Infection in Chronic Obstructive Pulmonary Disease: A Meta-Analysis. *Inhalation Toxicol.* 29 (5), 219–226. doi:10.1080/08958378.2017.1346006

Yang, M., Du, Y., Chen, H., Jiang, D., and Xu, Z. (2019). Inhaled Corticosteroids and Risk of Pneumonia in Patients with Chronic Obstructive Pulmonary Disease: A Meta-Analysis of Randomized Controlled Trials. *Int. Immunopharmacology* 77, 105950. doi:10.1016/j.intimp.2019.105950

Zhang, Q., Li, S., Zhou, W., Yang, X., Li, J., and Cao, J. (2020). Risk of Pneumonia with Different Inhaled Corticosteroids in COPD Patients: A Meta-Analysis. *COPD: J. Chronic Obstructive Pulm. Dis.* 17, 462–469. doi:10.1080/15412555.2020.1787369

Zheng, J., de Guia, T., Wang-Jairaj, J., Newlands, A. H., Wang, C., Crim, C., et al. (2015). Efficacy and Safety of Fluticasone Furoate/vilanterol (50/25 Mcg; 100/25 Mcg; 200/25 Mcg) in Asian Patients with Chronic Obstructive Pulmonary Disease: A Randomized Placebo-Controlled Trial. *Curr. Med. Res. Opin.* 31 (6), 1191–1200. doi:10.1185/03007995.2015.1036016

Zhong, N., Wang, C., Zhou, X., Zhang, N., Humphries, M., Wang, L., et al. (2015). LANTERN: A Randomized Study of QVA149 Versus Salmeterol/fluticasone Combination in Patients with COPD. *Int. J. Chron. Obstruct Pulmon Dis.* 10, 1015–1026. doi:10.2147/COPD.S84436

Conflict of Interest: The authors declare that the research was conducted in the absence of any commercial or financial relationships that could be construed as a potential conflict of interest.

frontiers in Pharmacology

REVIEW
published: 08 July 2021
doi: 10.3389/fphar.2021.671589

In situ Pulmonary Artery Thrombosis: A Previously Overlooked Disease

Yunshan Cao[1*†], *Chao Geng*[2†], *Yahong Li*[2] *and Yan Zhang*[2*]

[1]Department of Cardiology, Gansu Provincial Hospital, Lanzhou, China, [2]Tianjin Key Laboratory of Retinal Functions and Diseases, Tianjin Branch of National Clinical Research Center for Ocular Disease, Eye Institute and School of Optometry, Tianjin Medical University Eye Hospital, Tianjin, China

Pulmonary thromboembolism (PTE) is the third leading cause of death in cardiovascular diseases. PTE is believed to be caused by thrombi detached from deep veins of lower extremities. The thrombi travel with systemic circulation to the lung and block pulmonary arteries, leading to sudden disruption of hemodynamics and blood gas exchange. However, this concept has recently been challenged by accumulating evidence demonstrating that de novo thrombosis may be formed in pulmonary arteries without deep venous thrombosis. On the other hand, chronic thromboembolic pulmonary hypertension (CTEPH), a subtype of pulmonary hypertension, could have different pathogenesis than traditional PTE. Therefore, this article summarized and compared the risk factors, the common and specific pathogenic mechanisms underlying PTE, in situ pulmonary artery thrombosis, and CTEPH at molecular and cellular levels, and suggested the therapeutic strategies to these diseases, aiming to facilitate understanding of pathogenesis, differential diagnosis, and precision therapeutics of the three pulmonary artery thrombotic diseases.

Keywords: pulmonary thromboembolism, in situ pulmonary thrombosis, deep venous thrombosis, chronic thromboembolic pulmonary hypertension, risk factors, pathogenic mechanism

OPEN ACCESS

Edited by:
Yoshihiro Fukumoto, Kurume University, Japan

Reviewed by:
Nobuhiro Tanabe, Chiba University, Japan
Koichiro Sugimura, International University of Health and Welfare, Narita, Japan

***Correspondence:**
Yan Zhang
yanzhang04@tmu.edu.cn
Yunshan Cao
yunshancao@126.com

†These authors have contributed equally to this work and share first authorship.

Specialty section:
This article was submitted to Respiratory Pharmacology, a section of the journal Frontiers in Pharmacology

Received: *24 February 2021*
Accepted: *28 June 2021*
Published: *08 July 2021*

Citation:
Cao Y, Geng C, Li Y and Zhang Y (2021) In situ Pulmonary Artery Thrombosis: A Previously Overlooked Disease. Front. Pharmacol. 12:671589. doi: 10.3389/fphar.2021.671589

INTRODUCTION

Pulmonary thromboembolism (PTE) is the third common cardiovascular disease following myocardial infarction and ischemic stroke (Goldhaber and Bounameaux, 2012). PTE is caused by the thrombi that disrupt pulmonary circulation, leading to pulmonary hypertension (PH), right heart failure (Moorjani and Price, 2013; Agnelli and Becattini, 2015), and even death (Prabhu and Soukas, 2017). The thrombi were initially thought to originate from deep veins in lower extremities, pelvis or right heart, travel with systemic circulation to pulmonary vasculature, and suddenly or recurrently block pulmonary arteries. However, this concept has recently been challenged by the evidence demonstrating that *de novo* thrombosis may be formed in pulmonary arteries without deep vein thrombosis (DVT) in lower extremities.

THE ORIGIN OF "PULMONARY EMBOLISM"

More than a century ago, a German physician and scientist Rudolf Virchow proposed that blood clots in the leg could travel to the lung and cause pulmonary embolism (PE), because he discovered at autopsy that the emboli in the lung and the leg usually coexisted. He also performed an experiment showing that foreign bodies in deep veins can be found in pulmonary arteries (Virchow, 1856). Therefore, he coined the terms "PE" and "DVT" (Bagot and Arya, 2008). From then on, embolus from peripheral venous system, such as lower extremities and pelvis, has been deemed the predominant cause of pulmonary artery

obstruction. However, from the contemporary perspective, Dr. Virchow's proposal might be biased and excluded the possibility of *de novo* thrombosis in pulmonary vessels. Based on Virchow's proposal, PE and DVT are disparate manifestations of the same disease, both belonging to venous thromboembolism (VTE) (Sakuma et al., 2009). In addition, chronic thromboembolic pulmonary hypertension (CTEPH), the group IV in the WHO classification of PH, has been deemed as a chronic stage of PTE, and thus designated as post-PTE syndrome (Huisman et al., 2018; Mullin and Klinger, 2018). However, the conclusive evidence proving the causal relationship between DVT and PTE as well as that between PTE and CTEPH is lacking, and the origin of thrombi in CTEPH is controversial (Kantake et al., 2013; Huisman et al., 2018).

IN SITU PULMONARY THROMBOSIS: PULMONARY THROMBOEMBOLISM WITHOUT DEEP VEIN THROMBOSIS

In recent years, multiple lines of evidence have indicated the possibility of generating *de novo* thrombus in pulmonary arteries without DVT in lower extremities. For example, Benns et al. (2014) conducted a retrospective study of incipient PTE (within 72 h post admission) in post-traumatic patients, and found that 84.2% of the PTE patients had no DVT. Similarly, Paffrath et al. (2010) investigated 7,937 post-traumatic hospitalized patients, with only 146 of them developing VTE; furthermore, 37% of these VTE patients were not accompanied with DVT. In addition, among the 11,330 patients that had received post-traumatic services, 2,881 were monitored by duplex sonography, and the results demonstrated the greater prevalence of PTE without DVT than that of PTE with DVT (Van Gent et al., 2014). Velmahos et al. (2009) performed computed tomographic venography of the pelvic and lower extremity proximal veins and computed tomographic pulmonary angiography in post-traumatic patients, and they found that few PTE cases were accompanied with DVT. One possible explanation of these observations is the complete dislodgment of the deep vein thrombus and the subsequent obstruction of the main branch of pulmonary artery. Nevertheless, Van Gent et al. (2014) performed duplex sonography in 12 patients with PE and DVT, and found that 83% of these patients had residual clot in lower extremities. In addition, the autopsies revealed that 59% the patients with PE had a DVT at the time of death (Lindblad et al., 1991). Therefore, although we cannot exclude the possibility that the entire deep vein thrombus falls off and causes PTE, in the majority of cases, only a portion of the clot is dislodged to form thrombus in pulmonary artery. More interestingly, the alternative explanation may be that PTE and DVT are distinctive pathologies or occur simultaneously rather than one leading to another. This explanation has been supported by a considerable amount of literature (Knudson et al., 2011; Van Gent et al., 2014; Cha et al., 2015; Brown et al., 2018). Therefore, to distinguish from the PTE associated with DVT, we propose the term "*in situ* pulmonary artery thrombosis (*in situ* PAT)" to describe the pathology of *de novo* thrombosis in proximal (main, lobar, and segmental arteries), distal (segmental, mid-segmental, and sub-segmental arteries, down to small pulmonary arteries of 2–5 mm in diameter), and micro (microvasculature of 0.1–0.5 mm in diameter) pulmonary arteries (Burman et al., 2016; Madani et al., 2017).

THE RISK FACTORS OF PULMONARY THROMBOEMBOLISM ASSOCIATED WITH DEEP VEIN THROMBOSIS AND OF *IN SITU* PULMONARY ARTERY THROMBOSIS

It used to believe that PTE developed from DVT, and they belonged to the consecutive processes of venous thrombosis. However, Van Gent et al. (2017) assessed the risk factors of PTE and DVT in adult patients with traumatic injuries and suggested that PTE and DVT are clinically distinct events with independent risk factors and occur at different time post traumatic injuries. The PTE derived from DVT is associated with circulatory and anatomical susceptible characteristics in lower extremities; whereas the PTE concurring with DVT may be related to vascular dysfunctions caused by systemic disorders and stress, including genetic factor-related factor V Leiden mutation, endocrine dysregulation, obesity, and surgery (Huisman et al., 2018) (**Figure 1**).

On the other hand, lung trauma and congenital or acquired abnormalities in lung structures are considered high risk factors of *in situ* PAT (Van Gent et al., 2014; Fletcher-Sanfeliu et al., 2020) (**Figure 1**). Experimental studies have shown that chest trauma may induce focal inflammation and dysfunction in pulmonary vascular endothelial cells, eliciting *in situ* PAT (Knudson et al., 2011; Brakenridge et al., 2013) (**Figure 1**). For instance, in a mouse model of unilateral thoracic contusion, eccentric fibrin aggregates on and platelets adhere to the endothelial cells aligning inner surface of pulmonary arteries after chest trauma (Brown et al., 2018), initiating *in situ* PAT (Schutzman et al., 2018). Additionally, *in situ* PAT is associated with the aberrant pulmonary structures, such as pulmonary artery stump following pneumonectomy (Kim et al., 2005; Kwek and Wittram, 2005), compensatory dilation and sheer stress at the proximal pulmonary artery caused by congenital cardiovascular defects and the resulting PH (Celestin et al., 2015), and pulmonary tuberculosis-destoryed lungs (Cha et al., 2015), as well as with the systemic predisposing conditions, including Behcet's disease (Yilmaz and Cimen, 2010), Eisenmenger's syndrome (Silversides et al., 2003; Broberg et al., 2007), sickle cell disease (Mekontso Dessap et al., 2011), and other systemic diseases (Porembskaya et al., 2020) (**Figure 1**). In general, local factors in the lung or lower limbs may contribute to thrombosis in the corresponding organ; whereas systemic factors such as autoimmune diseases and inflammation could lead to both DVT and PAT (**Figure 1**).

THE RISK FACTORS OF CHRONIC THROMBOEMBOLIC PULMONARY HYPERTENSION

CTEPH is the mechanical obstruction of pulmonary vessels caused by thromboembolism, which leads to pulmonary

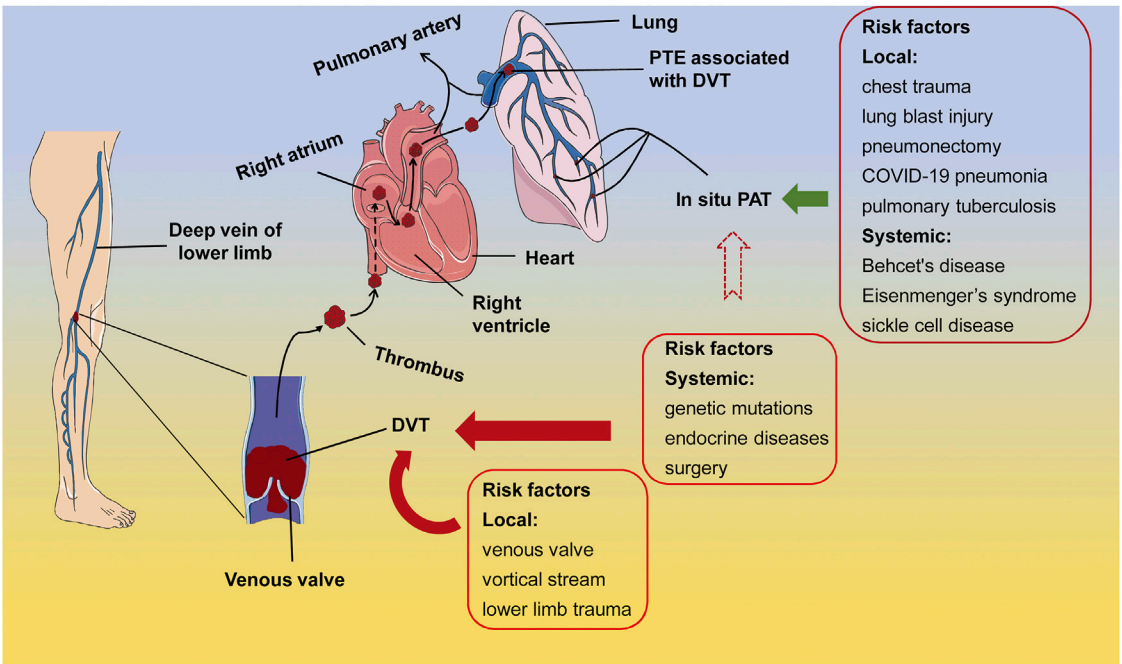

FIGURE 1 | The risk factors of PTE associated with DVT and *in situ* PAT. In the majority of cases, the systemic susceptible conditions, such as genetic mutations, endocrine disorders, and surgery, as well as the local conditions, such as anatomical and hemodynamic characteristics and trauma, elicit thrombus formation at the venous valves in lower extremities. After shedding from the venous valves, the thrombus travels through circulation to block either the main body or branches of pulmonary artery, leading to the PTE associated with DVT (arrows in dark red). On the other hand, pulmonary diseases, lung damage, and immunological, congenital, and hematological systemic diseases may cause *in situ* PAT (arrow in dark green). It is also possible that *in situ* PAT is formed under the susceptible systemic conditions of DVT, however, direct evidence is lacking (arrow in dark red dotted lines). PTE, pulmonary thromboembolism; DVT, deep vein thrombosis; *in situ* PAT, *in situ* pulmonary artery thrombosis.

vascular remodeling and progressive PH (Yandrapalli et al., 2018). The incidence of CTEPH after symptomatic PTE is reported between 0.1 and 9.1% (Lang and Madani, 2014). However, it is difficult to determine the actual CTEPH incidence, due to the absence or non-specificity of early symptoms and signs of this disease (Klok et al., 2018; Konstantinides et al., 2019). Moreover, a significant portion of CTEPH patients lack a history of acute PTE or DVT (Galie et al., 2015), thus *in situ* PAT has been considered as the cause of CTEPH in these cases (Egermayer and Peacock, 2000).

The initiating factors of CTEPH remain controversial, although several candidates have been proposed, including incomplete resolution and then organization of thrombi in pulmonary arteries following acute PTE, single and recurrent silent PTE derived from deep veins in lower extremities, and the thrombi formed at pulmonary arteries (Kantake et al., 2013; Huisman et al., 2018) (**Figure 2**). Therefore, the risk factors of CTEPH overlap with those of PTE, DVT, and *in situ* PAT. For the CTEPH patients with a history of acute or recurrent PTE, anatomical susceptible conditions in lower limbs, heamatological and endocrine disorders, and surgical interventions would be the risk factors of these patients; whereas tramatic injury and anatomical aberration in lung, and systemic diseases incurring inflammation, hypoxia, and abnormalities in pulmonary arteries subserve the risk factors for the CTEPH patients with no history of PTE and DVT. Moreover, ethnicity has been shown to play a role in determining CTEPH characteristics. Chausheva et al. (2019) compared the clinical parameters, hemodynamics, inflammatory factors, and thrombi of the CTEPH patients undergoing pulmonary endarterectomy in Austria and Japan, representing the people of European and Asian origins, respectively. The differences in the physiological parameters, including body size, lung vital capacity, cardiac output, and blood tests, are within expectation. Furthermore, the study revealed equipoise gender affliction, a prevalent history of PE, and a phenotype of metabolic syndrome in Austrian patients with CTEPH. Moreover, plasma levels of C-reactive protein and myeloperoxidase were significantly elevated in Austrian patients as compared to Japanese counterparts, implicating the proinflammatory pathogenesis of CTEPH in Australian patients. Consistent with these findings, the thrombi in Austrian patients occupied larger areas and exhibited a more inflammatory and fresh phenotype than Japanese patients (Chausheva et al., 2019). Additionally, abnormalities of fibrinogen (Morris et al., 2009), elevated factor VIII, antibodies to phospholipid, splenectomy, chronic inflammatory disease, ventriculoatrial shunt, hypothyroidism, and cancer (Bonderman et al., 2003; Jaïs et al., 2005; Kim and Lang, 2012) have been reported as risk factors of CTEPH (**Figure 2**).

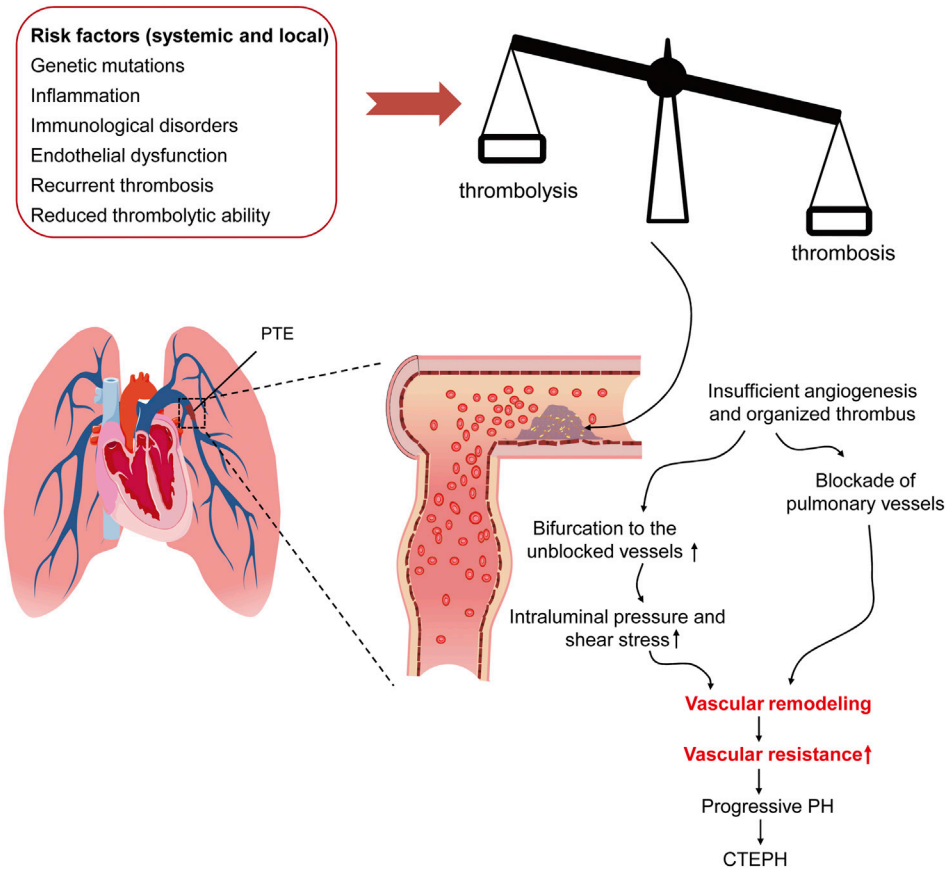

FIGURE 2 | The risk factors of and pathogenic mechanism underlying CTEPH. The pathological conditions, including genetic mutation, inflammation-associating endothelial dysfunction, recurrent thrombosis, and reduced thrombolytic activity, result in the imbalance between thrombosis and thrombolysis, which causes insolubility and organization of the thrombi in pulmonary arteries. As the thrombi block the pulmonary arteries, the pulmonary circulation is diverted to the unblocked ones, where intravascular pressure and shear stress is consequently elevated. Both the thrombus-mediated blockade of pulmonary arteries and the diverted blood-mediated elevation in mechanical stress lead to vascular remodeling, increased pulmonary vascular resistance, progressive PH. CTEPH, chronic thromboembolic pulmonary hypertension; PTE, pulmonary thromboembolism; PH, pulmonary hypertension.

Although CTEPH can present as acute attack, the majority of CTEPH patients manifest as chronic PH. For the CTEPH patients with a history of acute PE, a trigger, such as surgery, usually exist, and the clinical manefestations during the episode of acute PE include acute attack of shortness of breath and hypoxemia, sometimes the triad including chest pain, hemoptysis, and shortness of breath may be observed, and severe patients may have acute right heart failure (Klok et al., 2020). On the other hand, the CTEPH patients without PE present the similar clinical characterisctics as PH, such as exertional shortness of breath. It is of note, however, that when fresh thrombi in asymptomatic CTEPH generate salient symptoms and signs, CTEPH is often mistakenly diagnosed as acute PTE (Klok et al., 2018). Under such circumstance, the origin of thrombus, the presence of fresh intraluminal thrombus, the evidence of organic mural thrombus, the enlarged and hyperplastic right heart, and the formation of systemic collateral branches are of great significance for differential diagnosis between acute PTE and CTEPH.

COMMON PATHOGENIC MECHANISMS UNDERLYING THROMBOSIS

Vascular Endothelial Cell Injury

The vascular endothelial cells express anticoagulant and vasodilatory factors, thereby preventing blood coagulation and platelet adhesion as well as promoting vessel dilation and fibrinolysis (Gresele et al., 2010). Specifically, endothelial cells produce thrombomodulin and activate anti-coagulant protein C to maintain anti-coagulation. Moreover, endothelial cells express heparin sulfate and tissue factor pathway inhibitor (TFPI) to boost the activities of anti-thrombin III and fibrinolytic factors, respectively (Van Hinsbergh, 2012). Endothelial cells also generate nitric oxide, prostacyclin, and ectonucleotidase CD39, which can prevent platelet activation and inhibit coagulation (Furie and Furie, 2008). When the defense of vascular endothelial cells against thrombus is dismantled, thrombosis occurs.

On the other hand, the vascular endothelial cells can be activated by injuries, and the activated endothelial cells

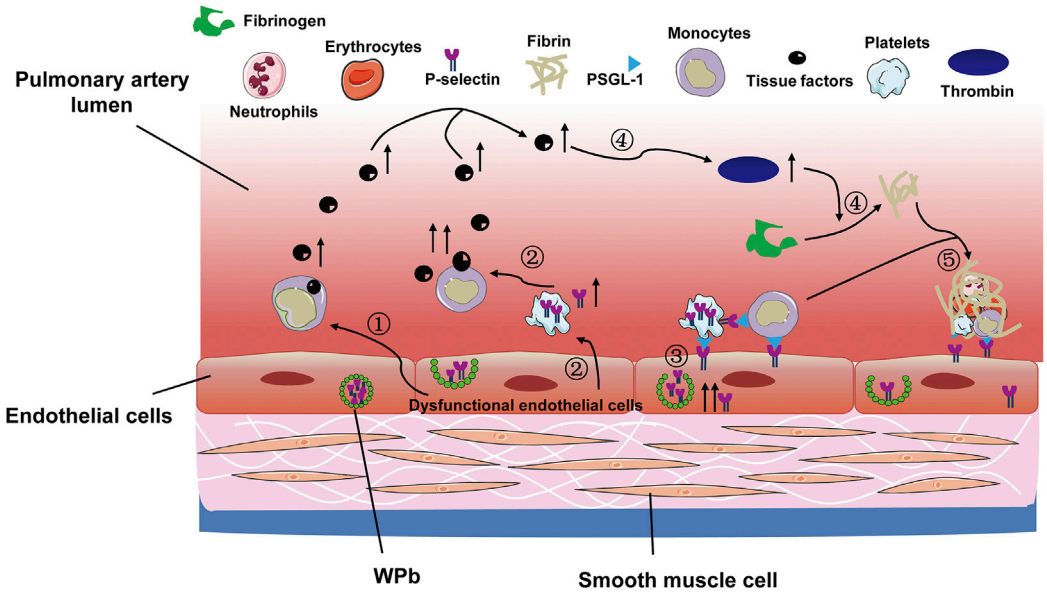

FIGURE 3 | The coagulation cascade activated following pulmonary vascular endothelial cell injury. The pulmonary vascular hypoxic and inflammatory scenario leads to the following events: 1) endothelial cell injury and upregulates TF expression on monocytes; 2) the injuried endothelial cells promote platelets to release P-selectin, which further increases TF production; 3) the endothelial cells per se release P-selectin, which adheres to platelets and leukocytes, facilitating their deposition onto the endothelia; 4) the increased production of TF enhances thrombin production, which promotes conversion of fibrinogen to fibrin; 5) the deposited leukocytes and platelets are entangled with fibrin, leading to *in situ* pulmonary thrombosis. TF, tissue factor; WPb, Weibel-Palade bodies; PSGL-1, P-selectin glycoprotein ligand 1.

stimulate leukocytes to express tissue factor (TF) and promote release of von Willebrand Factor and P-selectin in Weibel-Palade bodies (**Figure 3**). The released factors are rapidly transferred to the intraluminal surface and binds to P-selectin glycoprotein ligand 1 on platelets and leukocytes. Besides, the expression of P-selectin is also upregulated in platelet α granules (López and Chen, 2009; Schutzman et al., 2018; Schutzman et al., 2019). P-selectin could further upregulate TF expression in leukocytes, particularly in monocytes, thus forming a positive feedback regulatory loop (**Figure 3**). In addition, the endothelial injury renders the collagen and TF originally beneath endothelial cells exposed to blood circulation (Furie and Furie, 2008). Collagen triggers platelet accumulation and activation. The exposed subendothelial TF and the upregulated TF on leukocytes together mediate production of thrombin and catalyze conversion of fibrinogen to fibrin (Celi et al., 1994). The fibrin promotes deposition of monocytes and neutrophils, eventually leading to thrombosis (Yan et al., 2000) (**Figure 3**).

Hypercoagulable State

The balance between anticoagulants and procoagulants maintains homeostasis of blood flow (Aird, 2007). When the balance is tilted by congenital and/or acquired disorders, the reduction of anticoagulants and/or the elevation of procoagulants generates the hypercoagulable state. The congenital disorders include congenital deficiency in thromboplastin inhibitor, such as antithrombin, protein C, and protein S, prothrombin-induced protein C resistance (Crous-Bou et al., 2016), and factor V Leiden gene mutation (Martinelli et al., 1998).

The acquired disorders are comprised of age, cancer, pregnancy, oral contraceptives, hormone replacement therapy, and obesity. In specifics, during the process of senescence, vascular elastic fiber degenerates (Chattopadhyay et al., 2011); levels of vascular wall-associated anticoagulants decrease, and those of procoagulants increase (Lowe et al., 1997; Esmon, 2009).

Cancer cells induce the hypercoagulable state through activating host coagulation system, such as upregulating expression of haemostatic factors, pro-inflammatory factors, and adhesion molecules, as well as directly adhering to host cells (Soo Hoo, 2013; Falanga et al., 2017). Indeed, studies have shown that the activity of circulating microparticle-associated TF, which can induce coagulation and thrombosis, is augmented in the blood of the patients with malignancies (Tesselaar et al., 2007). In addition, cancer treatments with either cytotoxic drugs such as cisplatin (Seng et al., 2012) or targeted chemotherapies including monoclonal antibodies to epidermal growth factor receptor (Petrelli et al., 2012) and tyrosine kinase inhibitors of vascular endothelial growth factor receptor (Qi et al., 2014) have been reported to incur higher incidence of venous and arterial thrombotic events as compared to the treatment modalities not involving these cytotoxic or targeted drugs. The underlying mechanism could be due to the off-target effects of these drugs, for instance, the non-specific cytotoxicity of cisplatin to and the impact of growth factor deprivation exerted by the tyrosine kinase inhibitors on vascular endothelial cells. Alternatively, these drugs may decrease anticoagulants and increase procoagulants, hence tipping the balance towards coagulation. Finally, the anticancer drugs may directly or

indirectly activate platelets (Grover et al., 2021). All of these mechanisms may promote thrombosis under malignancies. There were also case reports showing that administration of immune checkpoint inhibitors, such as monoclonal antibodies to programmed cell death-1 or its ligand and to cytotoxic T lymphocyte-associated antigen 4, is associated with venous and arterial thrombosis (Boutros et al., 2018), however, the results of a systematic review demonstrated that the thrombotic events associated with the immune checkpoint inhibitors are relatively rare in the patients with advanced cancer (Solinas et al., 2020).

During pregnancy, the levels of coagulation factor V, VII, VIII, IX, X, XII, and von Willebrand Factor increase; while the level of anticoagulant protein S, plasma fibrinolytic activity, and acquired protein C resistance reduce (Brenner, 2004; Holmes and Wallace, 2005). What's more, pregnancy, oral contraceptives, and hormone replacement therapy trigger venous thrombosis through elevating estrogen levels and enhancing thrombin production (Ohashi et al., 2003).

In obese patients, the proinflammatory cytokines secreted by hypertrophic and hyperplastic adipocytes result in chronic low-grade inflammation, which in turn activates prothrombotic signals and upregulates plasminogen activator inhibitor 1, contributing to the occurrence of VTE (Samad et al., 1996; Vandanmagsar et al., 2011; Blokhin and Lentz, 2013).

Inflammation

At early stage of inflammation, the endothelial cells recruit inflammatory cells to the damaged or infected site for defense and repair (Gresele et al., 2010). The upregulated P-selectin on the endothelial cells binds to the P Selectin Glycoprotein Ligand 1 (PSGL-1) on the leukocytes, facilitating leukostasis and extravasation (Myers et al., 2003; Wakefield and Henke, 2005). Moreover, inflammation may also activate endothelial cells and promote their switch to the pre-thrombotic and anti-fibrinolytic phenotype. Then the activated endothelial cells upregulate the expression of adhesion molecules, facilitating their adhesion to monocytes and platelets (Van Hinsbergh, 2012). In addition, inflammation activates platelets to secrete modulators, including adenosine triphosphate, adenosine diphosphate (ADP), serotonin, cyclooxygenase, and thromboxane, thereby enhancing vasoconstriction and platelet aggregation (Shi and Morrell, 2011). What's more, the activated platelets bind to PSGL-1 and CD40 on the endothelial cells and leukocytes through the upregulated expression of P-selectin and the ligand of CD40, respectively, promoting the formation and deposition of platelet-leukocyte complex (Wakefield et al., 2008; Nurden, 2011). Finally, proinflammatory cytokines can stimulate monocytes to produce TF, which, as mentioned above, activates coagulation cascade (Aksu et al., 2012).

In addition, microparticles are small membranous vesicles containing bioactive molecules and participating in intercellular communications. Microparticles are released by different types of activated or apoptotic cells, including endothelial cells, platelets, and leukocytes (Yan et al., 2017; Zarà et al., 2019) The production of microparticles is increased under the conditions of inflammation, infection, and malignancy (Ardoin et al., 2007). The microparticles promote coagulation through three mechanisms. One is to directly activate coagulation cascade via expressing TF and phosphatidylserine. Another mechanism is that the endothelial cell-deriving microparticles carry P-selectin that can bind to PSGL-1 on monocytes and platelets, thereby facilitating the deposition of the latter two types of cells onto the vessel walls. Thirdly, the microparticles also express the biomarkers of leukocytes and platelets, which promotes cell-cell interaction and augments coagulation (Wakefield et al., 2008).

Hypoxia

Hypoxia is the stimulating factor of thrombosis. Under hypoxic conditions, hypoxia inducible factors (HIFs) accumulate in the nucleus and bind to the hypoxia-response element to drive the transcription of their target genes. Therefore, hypoxia-induced thrombosis can be controlled directly by HIFs and their target genes (Gupta et al., 2017; Gupta et al., 2019). For instance, HIFs promote thrombosis by downregulating expression of protein S and TFPI and upregulating expression of procoagulant tissue factor and plasminogen activator inhibitor 1 (PAI-1) (Ahn et al., 2010; Cui et al., 2017). On the other hand, hypoxia can boost the release of Weibel Palade bodies and upregulate P-selectin expression in endothelial cells (Pinsky et al., 1996), as well as stimulate platelet activity through prethrombotic response and increase the production of prethrombotic factor or reduce that of antithrombotic factor in an HIF-independent manner (Tyagi et al., 2014; Gupta et al., 2019).

SPECIFIC PATHOGENIC MECHANISMS FOR PULMONARY THROMBOEMBOLISM ASSOCIATED WITH DEEP VEIN THROMBOSIS

In addition to the common pathogenic mechanisms underlying thrombosis, local anatomical characteristics, traumatic, pharmacological, and infectious triggers, as well as biochemical imbalance also contribute to the specific pathogenesis of PTE, *in situ* PAT, and CTEPH.

The specific mechanism responsible for PTE derived from DVT begins with Virchow's triad: stagnation, plasma hypercoagulability, and endothelial injury at systemic level (Bagot and Arya, 2008). When the body is exposed to the systemic risk factors of thrombosis, the venous valve of the lower extremity become a major susceptible site to venous thrombosis due to its anatomical characteristic. Under normal circumstance, venous valves in the veins of lower extremities prevent blood reflux (Aird, 2007). As blood flows through venous valves, vortical stream behind the valve cusps attenuates blood stagnation in the valve pocket (Lurie et al., 2003). However, the blood in the valve pocket is more hypoxic and static than the main stream, hence generating a hypercoagulable microenvironment in the valve pocket (Aird, 2007). Especially in the patients with surgical anesthesia and long-term immobilization, reduced muscle activity slows venous blood flow and diminishes partial

oxygen pressure (Hamer et al., 1981; Soo Hoo, 2013), promoting blood stasis and thrombosis in the venous valve pocket. Finally, the thrombus develops in the deep veins of lower extremeties. Triggerred by surgical operations, drug adminstration, or patient activities, the clot falls off, travels with circulation, reaches right atrium and ventricle, blooks the main body or branches of pulmonary arteries, and ends up with PTE (Soo Hoo, 2013; Xiao et al., 2018).

SPECIFIC PATHOGENIC MECHANISMS FOR *IN SITU* PULMONARY ARTERY THROMBOSIS

The main pathogenesis for *in situ* PAT is deemed as pulmonary local factors including pulmonary vascular endothelial cell dysfunction, hypoxia, and inflammation (Bennett et al., 2009; López and Chen, 2009).

Chest contusion and blast injury destroy pulmonary alveolar capillaries and blood-air barrier, leading to exudation into pulmonary interstitia (Ganie et al., 2013). Besides, the patients with pulmonary trauma tend to have atelectasis, which impairs gas exchange and deteriorates hypoxia. Then the substantially reduced alveolar oxygen partial pressure induces hypoxic vasoconstriction (Van Gent et al., 2014). On the other hand, at the early stage of thoracic trauma, inflammatory cells infiltrate into the damaged lung tissue and release inflammatory mediators, such as Interleukin-8 (IL-8) and Interleukin-6 (IL-6), resulting in elevated levels of these inflammatory mediators in alveoli (Hoth et al., 2006). Subsequently, the pulmonary trauma-induced hypoxia and inflammation activate endothelial cells (Van Hinsbergh, 2012), platelets (Lowenberg et al., 2010), and monocytes (Levi et al., 2006), all of which coordinate to cause *in situ* PAT.

Coronavirus disease 2019 (COVID-19) is a highly contagious and potentially fatal disease that has caused a pandemic. The autopsy of the patients who died from COVID-19 showed diffusive alveolar damage and infiltration of inflammatory cells, which are non-specific however, as the patients who died from acute respiratory distress syndrome and infection of other respiratory viruses exhibited the similar pathology (Kamel et al., 2020). Nonetheless, the researchers did find three distinctive pathogloical features in the lungs infected with severe acute respiratory syndrome coronavirus 2 (SARS-CoV-2). First, the cytokines were dramatically induced (Mehta et al., 2020) and pulmonary vascular endothelial cells severely injured by the virus infection. Secondly, the microthrombi of different ages were present throughout pulmonary microvasculature, implicating their local pulmonary origin. Thirdly, angiogenesis was promoted by upregulated expression of angiogenic factors (Ackermann et al., 2020). Therefore, COVID-19 pathology suggests that *in situ* PAT may be induced by pulmonary vascular endothelial injuries and the locally-produced proinflammatory cytokine storm (Gabrielli et al., 2020; Mandal et al., 2021). The pathogenic mechanism underlying the thrombogenicity of COVID-19 has been proposed. After SARS-CoV-2 binds to angiotensin converting enzyme 2, the cell surface receptor of the virus on type II pneumocytes and pulmonary vascular endothelial cells, the expression of angiotensin II upregulated in compensation (Fraga-Silva et al., 2010), which may elicit cytokine storm from activated inflammatory cells and endothelial cells through dysregulation of the rennin-angiotensin-aldosterone system (Mandal et al., 2021). The cytokine storm, particularly the upregulated expression of IL-6, subsequently leads to the injuries of alveoli and pulmonary vascular endothelial cells, turning the phenotype of the endothelial cells into pro-inflammatory and pro-thrombotic (Schieffer et al., 2000; Li et al., 2020). The inflammation and hypoxaemia may further amplify the vascular endothelial response and augment thrombus formation (Gupta et al., 2019). It is notable that COVID-19 does involve multiple organs, the abovementioned pathogenic mechanism underlying COVID-19 thrombogenicity can be applied at systemic level.

SPECIFIC PATHOGENIC MECHANISMS FOR CHRONIC THROMBOEMBOLIC PULMONARY HYPERTENSION

CTEPH is a dual pulmonary vascular disease: obstruction of pulmonary arteries by unresolved thrombi and progressive remodeling of unobstructed vessels under increased pressure and shear stress (Simonneau et al., 2017; Yandrapalli et al., 2018) (**Figure 2**). The pathology of CTEPH corresponds to these two events. First, the organized thrombi comprised of collagens and fibrins entangled with debris of fibroblasts, lymphocytes, and macrophages attach to the arterial wall and form the lesion of "bands and webs". Small and insufficient neovessels in the organized clots try to "recalnal" the blocked vessels with systemic circulation. Second, the plexiform lesions, the histological hallmark of PH, can be observed in the unobstructed pulmonary arterioles, indicating intimal hyperplasia and vascular remodeling (Lang et al., 2016). Several factors, including fibrinolytic abnormality, inflammation, angiogenesis, vascular remodeling, and *in situ* PAT, have been considered causing the CTEPH pathology (Yan et al., 2019).

The primary pathogenic factor of CTEPH is continuous insoluble thrombus in pulmonary vessels. Fibrinolysis is the initial stage of thrombus breakdown, followed by an inflammatory response that recruits neutrophils to continue decomposition. In the meanwhile, monocytes and endothelial progenitor cells are also recruited to promote clot reorganization and angiogenesis (Medrek and Safdar, 2016). Studies have demonstrated impairment in fibrinolytic system and deficiency in fibrin in the patients with CTEPH (Yan et al., 2019). For instance, plasma levels of tissue plasminogen activators and PAI-1 were significantly increased in CTEPH patients as compared with age-matched controls, yet no difference in enzymatic activity was detected between the two cohorts (Olman et al., 1992). Similarly, Lang et al. (1994) showed that the expression of PAI-1 protein and transcript was drastically upregulated in the endothelial cells and smooth muscle cells in the highly organized

thrombus in comparison to the uninvolved areas in the pulmonary arteries of the CTEPH patients who had undergone pulmonary endarterectomy. In a recent study, Satoh et al. (2017) found that plasma level and pulmonary immunostaining intensity of thrombin-activatable fibrinolysis inhibitor were dramatically elevated in the patients with CTEPH as compared to the patients with lung cancer or pulmonary arterial hypertension. Furthermore, in a murine model of hypoxia-induced PH, ablation of the gene encoding TAFI ameliorated the phenotypes of PH, mitigated PAT, normalized plasma clot lysis time, and attenuated perivascular infiltration of macrophages and monocytes. Conversely, universal or liver-specific overexpression of TAFI exacerbated these parameters. These results implicate a crucial role of TAFI in the pathogenesis of CTEPH. Mechanistically, the plasma TAFI released from the liver binds to its binding partner thrombomodulin that is specifically upregulated in pulmonary artery endothelial cells. The TM-mediated enrichment and activation of TAFI specifically downregulate tight junction expression between the PAECs and lead to endothelial cell permeability, smooth muscle cell proliferation, and inflammatory cell infiltration. All of these events contribute to vascular remodeling and CTEPH (Satoh et al., 2017). Moreover, a genetic study has shown that the Thr312Ala mutation in the gene encoding fibrinogen protein may increase the risk of thrombosis and fibrinolytic resistance through altered homogenous cross linkage between fibrinogen α chains, thereby increasing the risk of CTEPH (Li et al., 2013).

In addition, transient inflammatory response is conducive to thrombolysis, however, the long-lasting one may exert the opposite effect. Studies have demonstrated that plasma levels of proinflammatory factors, including IL-6, IL-8, IL-10, interferon-γ, monocyte chemotactic protein-1, macrophage inflammatory protein-1α, and matrix metalloproteinase-9 were significantly elevated in CTEPH patients as compared with healthy controls (Zabini et al., 2014; Quarck et al., 2015).

Angiogenesis is crucial to recanalization and resolution of thrombus. The development of CTEPH may be associated with insufficient angiogenesis in thrombus (Alias et al., 2014). Quarck et al. (2015) proved that the plasma levels of vascular endothelial growth factor in CTEPH patients tended to be lower than healthy controls. Nonetheless, in the lung samples collected from CTEPH patients subjected to endarterectomy, the expression of angiostatic factors, such as platelet factor 4, collagen type I, and interferon-γ inducible 10 kD protein, was significantly upregulated as compared to those from healthy donors. Further, the angiostatic factors have been shown to disturb calcium homeostasis and induce endothelial cell dysfunction (Zabini et al., 2012). In addition, the high shear stress and pressure produced by redirected blood flow at unobstructed pulmonary vessels induce phenotypic changes and dysfunction of pulmonary vascular endothelial cells (Simonneau et al., 2017; Salibe-Filho et al., 2020). The endothelial cell dysfunction then stimulates secretion of inflammatory factors, such as fibroblast growth factor-2 and adhesion molecules, promoting proliferation of vascular smooth muscle cells and vascular remodeling (Mercier et al., 2017).

Finally, many CTEPH patients lack a history of acute PTE, and repeated embolization combined with ligation of pulmonary lobar artery failed to completely recapitulate CTEPH in animal models (Lang et al., 2013), thus for the cases of CTEPH without an acute PTE, it is possible that *in situ* PAT may initiate at the most susceptible site as a result of inflammation and imbalance between thrombosis and fibrinolysis, and then evolve to block the proximal and distal pulmonary arteries, leading to hypoperfusion and overflow of the blocked vessels and unblocked vessels, respectively. The unblocked vesels may be remodeled under excessive pressure and stress, eventually contributing to CTEPH (Egermayer and Peacock, 2000). However, this pathogenesis awaits further investigation and verification.

THERAPEUTIC STRATEGIES

Research has revealed that in addition to the common pathogenic mechanisms, differential molecular pathogenesis does exist for different types of thrombosis. Therefore, specific preventive interventions and therapeutic strategies should be provided based on the distinct risk factors and pathogenesis of different thrombotic diseases. Furthermore, the interventions and therapeutics should not only manage the acute presentation, but also mitigate long-term sequela and reduce recurrence.

Three therapeutic strategies are suggested. First, for the thrombotic patient with a specific trigger, the trigger should be removed for the optimal efficacy of the current treatment and long-term survival with minimized recurrence. For example, the patients under the condition of infection, systemic inflammation, or high altitude hypoxia should first receive systemic anti-inflammatory or oxygen therapy for trigger removal (Aksu et al., 2012), and anticoagulation or surgical therapies ensue.

Second, for the thrombotic patients without an obvious trigger or with an irremovable trigger, anticoagulation is a must. For instance, although balloon pulmonary angioplasty (BPA) is an effective interventional modality for the patients with CTEPH, especially for the CTEPH patients with thrombi in the distal pulmonary arteries, the oral anticoagulant drugs such as warfarin, should be maintained lifetime to prevent recurrence of CTEPH following BPA (Panahi et al., 2021).

Third, mechanistic studies have identified key molecules and cell types in the coagulation cascade, which may subserve the molecular and cellular targets to counteract thrombosis in the long run. Anticoagulant drugs can be developed by downregulating P-selectin or inhibiting the interaction between P-selectin and PSGL-1 in the thrombotic diseases where vascular endothelial cells are activated but not injured (Furie and Furie, 2008). Moreover, microparticles play an important role in promoting thrombosis under inflammatory and malignant conditions, therefore the agent targeting microparticles need to be developed and used in combination with anti-inflammatory and anticancer drugs. Additionally, antiplatelet medicines, such as aspirin targeting thromboxane synthesis and clopidogrel targeting ADP receptor, can be used in the diseases incurring platelet activation (Wu and Matijevic-Aleksic, 2005).

CONCLUSION

For a long time, the thrombi of PTE have been considered originated from deep veins of lower extremities, however, accumulating evidence reveals that pulmonary thrombi may be generated *in situ* following chest trauma, pulmonary diseases, and systemic inflammatory and immunological disorders. The currently known mechanism underlying *in situ* PAT originates from the local hypoxic and inflammatory milieu, which then induces pulmonary vascular endothelial cell dysfunctions following injury, diseases, and drug interventions and subsequently leads to imbalance between thrombosis and fibrinolysis. The thrombi of different sources, either deep veins in lower limbs or pulmonary vasculature *in situ*, if not resolved in lung in a timely manner, may cause CTEPH.

Collectively, we suggest that a new group of diseases involving PH, "pulmonary artery thrombotic diseases", be proposed. This group refers to all the thrombotic events that may occour in pulmonary artery, and currently can include three distinct diseases, PTE, *in situ* PAT, and CTEPH. The inter-relationship among the three diseases is complicated. PTE and *in situ* PAT can occur independently or coexist; either PTE or *in situ* PAT or both, if not appropriately managed in a timely manner, may progress to CTEPH.

AUTHOR CONTRIBUTIONS

YC and YZ conceived and designed the review, searched and sorted the literature. CG searched the literature and wrote the draft. YL searched the literature and drew the figures; YC, CG, and YZ made multiple revisions in the manuscript and figures as the research field evolved.

ACKNOWLEDGMENTS

The Training Program for Young and Middle-aged Backbone Talents in Colleges and Universities in Tianjin to YZ; The High-level Innovative Talent Program for Distinguished Scholar (YDYYRCXM-B2018-02 to YZ); The project from National Natural Science Foundation of China (81970827).

REFERENCES

Ackermann, M., Verleden, S. E., Kuehnel, M., Haverich, A., Welte, T., Laenger, F., et al. (2020). Pulmonary Vascular Endothelialitis, Thrombosis, and Angiogenesis in Covid-19. *N. Engl. J. Med.* 383, 120–128. doi:10.1056/NEJMoa2015432

Agnelli, G., and Becattini, C. (2015). Anticoagulant Treatment for Acute Pulmonary Embolism: a Pathophysiology-Based Clinical Approach. *Eur. Respir. J.* 45, 1142–1149. doi:10.1183/09031936.00164714

Ahn, Y. T., Chua, M. S., Whitlock, J. P., Jr., Shin, Y. C., Song, W. H., Kim, Y., et al. (2010). Rodent-specific Hypoxia Response Elements Enhance PAI-1 Expression through HIF-1 or HIF-2 in Mouse Hepatoma Cells. *Int. J. Oncol.* 37, 1627–1638. doi:10.3892/ijo_00000817

Aird, W. C. (2007). Vascular Bed-specific Thrombosis. *J. Thromb. Haemost.* 5 (Suppl. 1), 283–291. doi:10.1111/j.1538-7836.2007.02515.x

Aksu, K., Donmez, A., and Keser, G. (2012). Inflammation-induced Thrombosis: Mechanisms, Disease Associations and Management. *Curr. Pharm. Des.* 18, 1478–1493. doi:10.2174/138161212799504731

Alias, S., Redwan, B., Panzenböck, A., Winter, M. P., Schubert, U., Voswinckel, R., et al. (2014). Defective Angiogenesis Delays Thrombus Resolution. *Arterioscler. Thromb. Vasc. Biol.* 34, 810–819. doi:10.1161/atvbaha.113.302991

Ardoin, S. P., Shanahan, J. C., and Pisetsky, D. S. (2007). The Role of Microparticles in Inflammation and Thrombosis. *Scand. J. Immunol.* 66, 159–165. doi:10.1111/j.1365-3083.2007.01984.x

Bagot, C. N., and Arya, R. (2008). Virchow and His Triad: a Question of Attribution. *Br. J. Haematol.* 143, 180–190. doi:10.1111/j.1365-2141.2008.07323.x

Bennett, P., Silverman, S., Gill, P., and Lip, G. (2009). Peripheral Arterial Disease and Virchow's Triad. *Thromb. Haemost.* 101, 1032–1040. doi:10.1160/th08-08-0518

Benns, M., Reilly, P., and Kim, P. (2014). Early Pulmonary Embolism after Injury: a Different Clinical Entity? *Injury* 45, 241–244. doi:10.1016/j.injury.2013.02.026

Blokhin, I. O., and Lentz, S. R. (2013). Mechanisms of Thrombosis in Obesity. *Curr. Opin. Hematol.* 20, 437–444. doi:10.1097/MOH.0b013e3283634443

Bonderman, D., Turecek, P., Jakowitsch, J., Weltermann, A., Adlbrecht, C., Schneider, B., et al. (2003). High Prevalence of Elevated Clotting Factor VIII in Chronic Thromboembolic Pulmonary Hypertension. *Thromb. Haemost.* 90, 372–376. doi:10.1160/th03-02-0067

Boutros, C., Scoazec, J.-Y., Mateus, C., Routier, E., Roy, S., and Robert, C. (2018). Arterial Thrombosis and Anti-PD-1 Blockade. *Eur. J. Cancer* 91, 164–166. doi:10.1016/j.ejca.2017.11.018

Brakenridge, S. C., Henley, S. S., Kashner, T. M., Golden, R. M., Paik, D.-H., Phelan, H. A., et al. (2013). Comparing Clinical Predictors of Deep Venous Thrombosis versus Pulmonary Embolus after Severe Injury. *J. Trauma Acute Care Surg.* 74, 1231–1238. doi:10.1097/TA.0b013e31828cc9a0

Brenner, B. (2004). Haemostatic Changes in Pregnancy. *Thromb. Res.* 114, 409–414. doi:10.1016/j.thromres.2004.08.004

Broberg, C. S., Ujita, M., Prasad, S., Li, W., Rubens, M., Bax, B. E., et al. (2007). Pulmonary Arterial Thrombosis in Eisenmenger Syndrome Is Associated with Biventricular Dysfunction and Decreased Pulmonary Flow Velocity. *J. Am. Coll. Cardiol.* 50, 634–642. doi:10.1016/j.jacc.2007.04.056

Brown, I. E., Rigor, R. R., Schutzman, L. M., Khosravi, N., Chung, K., Becker, J. A., et al. (2018). Pulmonary Arterial Thrombosis in a Murine Model of Blunt Thoracic Trauma. *Shock* 50, 696–705. doi:10.1097/shk.0000000000001109

Burman, E. D., Keegan, J., and Kilner, P. J. (2016). Pulmonary Artery Diameters, Cross Sectional Areas and Area Changes Measured by Cine Cardiovascular Magnetic Resonance in Healthy Volunteers. *J. Cardiovasc. Magn. Reson.* 18, 12. doi:10.1186/s12968-016-0230-9

Celestin, C., Guillot, M., Ross-Ascuitto, N., and Ascuitto, R. (2015). Computational Fluid Dynamics Characterization of Blood Flow in central Aorta to Pulmonary Artery Connections: Importance of Shunt Angulation as a Determinant of Shear Stress-Induced Thrombosis. *Pediatr. Cardiol.* 36, 600–615. doi:10.1007/s00246-014-1055-7

Celi, A., Pellegrini, G., Lorenzet, R., De Blasi, A., Ready, N., Furie, B. C., et al. (1994). P-selectin Induces the Expression of Tissue Factor on Monocytes. *Proc. Natl. Acad. Sci.* 91, 8767–8771. doi:10.1073/pnas.91.19.8767

Cha, S.-I., Choi, K.-J., Shin, K.-M., Lim, J.-K., Yoo, S.-S., Lee, J., et al. (2015). Clinical Characteristics of *In-Situ* Pulmonary Artery Thrombosis in Korea. *Blood Coagul. Fibrinolysis* 26, 903–907. doi:10.1097/mbc.0000000000000343

Chattopadhyay, D., Al Samaraee, A., and Bhattacharya, V. (2011). An Update on the Management and Treatment of Deep Vein Thrombosis. *Cardiovasc. Hematol. Agents Med. Chem.* 9, 207–217. doi:10.2174/187152511798120921

Chausheva, S., Naito, A., Ogawa, A., Seidl, V., Winter, M.-P., Sharma, S., et al. (2019). Chronic Thromboembolic Pulmonary Hypertension in Austria and Japan. *J. Thorac. Cardiovasc. Surg.* 158, 604–614. doi:10.1016/j.jtcvs.2019.01.019

Crous-Bou, M., Harrington, L., and Kabrhel, C. (2016). Environmental and Genetic Risk Factors Associated with Venous Thromboembolism. *Semin. Thromb. Hemost.* 42, 808–820. doi:10.1055/s-0036-1592333

Cui, X. Y., Skretting, G., Tinholt, M., Stavik, B., Dahm, A. E. A., Sahlberg, K. K., et al. (2017). A Novel Hypoxia Response Element Regulates Oxygen-Related

Repression of Tissue Factor Pathway Inhibitor in the Breast Cancer Cell Line MCF-7. *Thromb. Res.* 157, 111–116. doi:10.1016/j.thromres.2017.07.013

Dessap, A. M., Deux, J.-F., Abidi, N., Lavenu-Bombled, C., Melica, G., Renaud, B., et al. (2011). Pulmonary Artery Thrombosis during Acute Chest Syndrome in Sickle Cell Disease. *Am. J. Respir. Crit. Care Med.* 184, 1022–1029. doi:10.1164/rccm.201105-0783OC

Egermayer, P., and Peacock, A. J. (2000). Is Pulmonary Embolism a Common Cause of Chronic Pulmonary Hypertension? Limitations of the Embolic Hypothesis. *Eur. Respir. J.* 15, 440–448. doi:10.1034/j.1399-3003.2000.15.03.x

Esmon, C. T. (2009). Basic Mechanisms and Pathogenesis of Venous Thrombosis. *Blood Rev.* 23, 225–229. doi:10.1016/j.blre.2009.07.002

Falanga, A., Russo, L., Milesi, V., and Vignoli, A. (2017). Mechanisms and Risk Factors of Thrombosis in Cancer. *Crit. Rev. Oncol. Hematol.* 18, 79–83. doi:10.1016/j.critrevonc.2017.08.003

Fletcher-Sanfeliu, D., Redón, J., García-Granero, Á., Frasson, M., Barreira, I., Martínez-León, J., et al. (2020). 'Pulmonary Thrombosis *In Situ*': Risk Factors, Clinic Characteristics and Long-Term Evolution. *Blood Coagul. Fibrinolysis* 31, 469–475. doi:10.1097/mbc.0000000000000949

Fraga-Silva, R. A., Sorg, B. S., Wankhede, M., Dedeugd, C., Jun, J. Y., Baker, M. B., et al. (2010). ACE2 Activation Promotes Antithrombotic Activity. *Mol. Med.* 16, 210–215. doi:10.2119/molmed.2009.00160

Furie, B., and Furie, B. C. (2008). Mechanisms of Thrombus Formation. *N. Engl. J. Med.* 359, 938–949. doi:10.1056/NEJMra0801082

Gabrielli, M., Lamendola, P., Esperide, A., Valletta, F., and Franceschi, F. (2020). COVID-19 and Thrombotic Complications: Pulmonary Thrombosis rather Than Embolism? *Thromb. Res.* 193, 98. doi:10.1016/j.thromres.2020.06.014

Galiè, N., Humbert, M., Vachiery, J.-L., Gibbs, S., Lang, I., Torbicki, A., et al. (2015). 2015 ESC/ERS Guidelines for the Diagnosis and Treatment of Pulmonary Hypertension. *Eur. Respir. J.* 46, 903–975. doi:10.1183/13993003.01032-2015

Ganie, F. A., Lone, H., Lone, G. N., Wani, M. L., Singh, S., Dar, A. M., et al. (2013). Lung Contusion: A Clinico-Pathological Entity with Unpredictable Clinical Course. *Bull. Emerg. Trauma* 1, 7–16. doi:10.4103/2320-8775.123208

Goldhaber, S. Z., and Bounameaux, H. (2012). Pulmonary Embolism and Deep Vein Thrombosis. *The Lancet* 379, 1835–1846. doi:10.1016/s0140-6736(11)61904-1

Gresele, P., Momi, S., and Migliacci, R. (2010). Endothelium, Venous Thromboembolism and Ischaemic Cardiovascular Events. *Thromb. Haemost.* 103, 56–61. doi:10.1160/th09-08-0562

Grover, S. P., Hisada, Y. M., Kasthuri, R. S., Reeves, B. N., and Mackman, N. (2021). Cancer Therapy-Associated Thrombosis. *Arterioscler. Thromb. Vasc. Biol.* 41, 1291–1305. doi:10.1161/atvbaha.120.314378

Gupta, N., Sahu, A., Prabhakar, A., Chatterjee, T., Tyagi, T., Kumari, B., et al. (2017). Activation of NLRP3 Inflammasome Complex Potentiates Venous Thrombosis in Response to Hypoxia. *Proc. Natl. Acad. Sci. USA* 114, 4763–4768. doi:10.1073/pnas.1620458114

Gupta, N., Zhao, Y.-Y., and Evans, C. E. (2019). The Stimulation of Thrombosis by Hypoxia. *Thromb. Res.* 181, 77–83. doi:10.1016/j.thromres.2019.07.013

Hamer, J. D., Malone, P. C., and Silver, I. A. (1981). The PO2 in Venous Valve Pockets: its Possible Bearing on Thrombogenesis. *Br. J. Surg.* 68, 166–170. doi:10.1002/bjs.1800680308

Holmes, V. A., and Wallace, J. M. W. (2005). Haemostasis in normal Pregnancy: a Balancing Act? *Biochem. Soc. Trans.* 33, 428–432. doi:10.1042/bst0330428

Hoth, J. J., Stitzel, J. D., Gayzik, F. S., Brownlee, N. A., Miller, P. R., Yoza, B. K., et al. (2006). The Pathogenesis of Pulmonary Contusion: an Open Chest Model in the Rat. *J. Trauma Inj. Infect. Crit. Care* 61, 32–45. doi:10.1097/01.ta.0000224141.69216.aa

Huisman, M. V., Barco, S., Cannegieter, S. C., Le Gal, G., Konstantinides, S. V., Reitsma, P. H., et al. (2018). Pulmonary Embolism. *Nat. Rev. Dis. Primers* 4, 18028. doi:10.1038/nrdp.2018.28

Jaïs, X., Ioos, V., Jardim, C., Sitbon, O., Parent, F., Hamid, A., et al. (2005). Splenectomy and Chronic Thromboembolic Pulmonary Hypertension. *Thorax* 60, 1031–1034. doi:10.1136/thx.2004.038083

Kamel, M. H., Yin, W., Zavaro, C., Francis, J. M., and Chitalia, V. C. (2020). Hyperthrombotic Milieu in COVID-19 Patients. *Cells* 9, 2392. doi:10.3390/cells9112392

Kantake, M., Tanabe, N., Sugiura, T., Shigeta, A., Yanagawa, N., Jujo, T., et al. (2013). Association of Deep Vein Thrombosis Type with Clinical Phenotype of Chronic Thromboembolic Pulmonary Hypertension. *Int. J. Cardiol.* 165, 474–477. doi:10.1016/j.ijcard.2011.08.851

Kim, N. H., and Lang, I. M. (2012). Risk Factors for Chronic Thromboembolic Pulmonary Hypertension. *Eur. Respir. Rev.* 21, 27–31. doi:10.1183/09059180.00009111

Kim, S. Y., Seo, J. B., Chae, E. J., Do, K.-H., Lee, J. S., Song, J.-W., et al. (2005). Filling Defect in a Pulmonary Arterial Stump on CT after Pneumonectomy: Radiologic and Clinical Significance. *Am. J. Roentgenol.* 185, 985–988. doi:10.2214/ajr.04.1515

Klok, F. A., Couturaud, F., Delcroix, M., and Humbert, M. (2020). Diagnosis of Chronic Thromboembolic Pulmonary Hypertension after Acute Pulmonary Embolism. *Eur. Respir. J.* 55, 2000189. doi:10.1183/13993003.00189-2020

Klok, F. A., Delcroix, M., and Bogaard, H. J. (2018). Chronic Thromboembolic Pulmonary Hypertension from the Perspective of Patients with Pulmonary Embolism. *J. Thromb. Haemost.* 16, 1040–1051. doi:10.1111/jth.14016

Knudson, M. M., Gomez, D., Haas, B., Cohen, M. J., and Nathens, A. B. (2011). Three Thousand Seven Hundred Thirty-Eight Posttraumatic Pulmonary Emboli. *Ann. Surg.* 254, 625–632. doi:10.1097/SLA.0b013e3182300209

Konstantinides, S. V., Meyer, G., Becattini, C., Bueno, H., Geersing, G.-J., Harjola, V.-P., et al. (2019). 2019 ESC Guidelines for the Diagnosis and Management of Acute Pulmonary Embolism Developed in Collaboration with the European Respiratory Society (ERS). *Eur. Respir. J.* 54, 1901647. doi:10.1183/13993003.01647-2019

Kwek, B. H., and Wittram, C. (2005). Postpneumonectomy Pulmonary Artery Stump Thrombosis: CT Features and Imaging Follow-Up. *Radiology* 237, 338–341. doi:10.1148/radiol.2371041686

Lang, I. M., Dorfmüller, P., and Noordegraaf, A. V. (2016). The Pathobiology of Chronic Thromboembolic Pulmonary Hypertension. *Ann. ATS* 13, S215–S221. doi:10.1513/AnnalsATS.201509-620AS

Lang, I. M., and Madani, M. (2014). Update on Chronic Thromboembolic Pulmonary Hypertension. *Circulation* 130, 508–518. doi:10.1161/circulationaha.114.009309

Lang, I. M., Marsh, J. J., Olman, M. A., Moser, K. M., Loskutoff, D. J., and Schleef, R. R. (1994). Expression of Type 1 Plasminogen Activator Inhibitor in Chronic Pulmonary Thromboemboli. *Circulation* 89, 2715–2721. doi:10.1161/01.cir.89.6.2715

Lang, I. M., Pesavento, R., Bonderman, D., and Yuan, J. X.-J. (2013). Risk Factors and Basic Mechanisms of Chronic Thromboembolic Pulmonary Hypertension: a Current Understanding. *Eur. Respir. J.* 41, 462–468. doi:10.1183/09031936.00049312

Levi, M., Van Der Poll, T., and Ten Cate, H. (2006). Tissue Factor in Infection and Severe Inflammation. *Semin. Thromb. Hemost.* 32, 033–039. doi:10.1055/s-2006-933338

Li, H., Liu, L., Zhang, D., Xu, J., Dai, H., Tang, N., et al. (2020). SARS-CoV-2 and Viral Sepsis: Observations and Hypotheses. *The Lancet* 395, 1517–1520. doi:10.1016/s0140-6736(20)30920-x

Li, J.-F., Lin, Y., Yang, Y.-H., Gan, H.-L., Liang, Y., Liu, J., et al. (2013). Fibrinogen Aα Thr312Ala Polymorphism Specifically Contributes to Chronic Thromboembolic Pulmonary Hypertension by Increasing Fibrin Resistance. *PLoS One* 8, e69635. doi:10.1371/journal.pone.0069635

Lindblad, B., Sternby, N. H., and Bergqvist, D. (1991). Incidence of Venous Thromboembolism Verified by Necropsy over 30 Years. *BMJ* 302, 709–711. doi:10.1136/bmj.302.6778.709

López, J. A., and Chen, J. (2009). Pathophysiology of Venous Thrombosis. *Thromb. Res.* 123, S30–S34. doi:10.1016/s0049-3848(09)70140-9

Lowe, G. D. O., Rumley, A., Woodward, M., Morrison, C. E., Philippou, H., Lane, D. A., et al. (1997). Epidemiology of Coagulation Factors, Inhibitors and Activation Markers: the Third Glasgow Monica Survey I. Illustrative Reference Ranges by Age, Sex and Hormone Use. *Br. J. Haematol.* 97, 775–784. doi:10.1046/j.1365-2141.1997.1222936.x

Löwenberg, E. C., Meijers, J. C., and Levi, M. (2010). Platelet-vessel wall Interaction in Health and Disease. *Neth. J. Med.* 68, 242–251.

Lurie, F., Kistner, R. L., Eklof, B., and Kessler, D. (2003). Mechanism of Venous Valve Closure and Role of the Valve in Circulation: a New Concept. *J. Vasc. Surg.* 38, 955–961. doi:10.1016/s074110.1016/s0741-5214(03)00711-0

Madani, M., Ogo, T., and Simonneau, G. (2017). The Changing Landscape of Chronic Thromboembolic Pulmonary Hypertension Management. *Eur. Respir. Rev.* 26, 170105. doi:10.1183/16000617.0105-2017

Mandal, A. K. J., Kho, J., Ioannou, A., Van Den Abbeele, K., and Missouris, C. G. (2021). Covid-19 and *In Situ* Pulmonary Artery Thrombosis. *Respir. Med.* 176, 106176. doi:10.1016/j.rmed.2020.106176

Martinelli, I., Mannucci, P. M., De Stefano, V., Taioli, E., Rossi, V., Crosti, F., et al. (1998). Different Risks of Thrombosis in Four Coagulation Defects Associated with Inherited Thrombophilia: a Study of 150 Families. *Blood* 92, 2353–2358. doi:10.1182/blood.v92.7.2353

Medrek, S., and Safdar, Z. (2016). Epidemiology and Pathophysiology of Chronic Thromboembolic Pulmonary Hypertension: Risk Factors and Mechanisms. *Methodist DeBakey Cardiovasc. J.* 12, 195–198. doi:10.14797/mdcj-12-4-195

Mehta, P., McAuley, D. F., Brown, M., Sanchez, E., Tattersall, R. S., Manson, J. J., et al. (2020). COVID-19: Consider Cytokine Storm Syndromes and Immunosuppression. *The Lancet* 395, 1033–1034. doi:10.1016/S0140-6736(20)30628-0

Mercier, O., Arthur Ataam, J., Langer, N. B., Dorfmüller, P., Lamrani, L., Lecerf, F., et al. (2017). Abnormal Pulmonary Endothelial Cells May Underlie the Enigmatic Pathogenesis of Chronic Thromboembolic Pulmonary Hypertension. *J. Heart Lung Transplant.* 36, 305–314. doi:10.1016/j.healun.2016.08.012

Moorjani, N., and Price, S. (2013). Massive Pulmonary Embolism. *Cardiol. Clin.* 31, 503–518. doi:10.1016/j.ccl.2013.07.005

Morris, T. A., Marsh, J. J., Chiles, P. G., Magaña, M. M., Liang, N.-C., Soler, X., et al. (2009). High Prevalence of Dysfibrinogenemia Among Patients with Chronic Thromboembolic Pulmonary Hypertension. *Blood* 114, 1929–1936. doi:10.1182/blood-2009-03-208264

Mullin, C. J., and Klinger, J. R. (2018). Chronic Thromboembolic Pulmonary Hypertension. *Heart Fail. Clin.* 14, 339–351. doi:10.1016/j.hfc.2018.02.009

Myers, D. D., Hawley, A. E., Farris, D. M., Wrobleski, S. K., Thanaporn, P., Schaub, R. G., et al. (2003). P-selectin and Leukocyte Microparticles Are Associated with Venous Thrombogenesis. *J. Vasc. Surg.* 38, 1075–1089. doi:10.1016/s0741-5214(03)01033-4

Nurden, A. (2011). Platelets, Inflammation and Tissue Regeneration. *Thromb. Haemost.* 105 (Suppl. 1), S13–S33. doi:10.1160/ths10-11-0720

Ohashi, R., Sugimura, M., and Kanayama, N. (2003). Estrogen Administration Enhances Thrombin Generation in Rats. *Thromb. Res.* 112, 325–328. doi:10.1016/j.thromres.2003.11.014

Olman, M. A., Marsh, J. J., Lang, I. M., Moser, K. M., Binder, B. R., and Schleef, R. R. (1992). Endogenous Fibrinolytic System in Chronic Large-Vessel Thromboembolic Pulmonary Hypertension. *Circulation* 86, 1241–1248. doi:10.1161/01.cir.86.4.1241

Paffrath, T., Wafaisade, A., Lefering, R., Simanski, C., Bouillon, B., Spanholtz, T., et al. (2010). Venous Thromboembolism after Severe Trauma: Incidence, Risk Factors and Outcome. *Injury* 41, 97–101. doi:10.1016/j.injury.2009.06.010

Panahi, L., Udeani, G., Horseman, M., Weston, J., Samuel, N., Joseph, M., et al. (2021). Review of Medical Therapies for the Management of Pulmonary Embolism. *Medicina* 57, 110. doi:10.3390/medicina57020110

Petrelli, F., Cabiddu, M., Borgonovo, K., and Barni, S. (2012). Risk of Venous and Arterial Thromboembolic Events Associated with Anti-EGFR Agents: a Meta-Analysis of Randomized Clinical Trials. *Ann. Oncol.* 23, 1672–1679. doi:10.1093/annonc/mdr592

Pinsky, D. J., Naka, Y., Liao, H., Oz, M. C., Wagner, D. D., Mayadas, T. N., et al. (1996). Hypoxia-induced Exocytosis of Endothelial Cell Weibel-Palade Bodies. A Mechanism for Rapid Neutrophil Recruitment after Cardiac Preservation. *J. Clin. Invest.* 97, 493–500. doi:10.1172/jci118440

Porembskaya, O., Toropova, Y., Tomson, V., Lobastov, K., Laberko, L., Kravchuk, V., et al. (2020). Pulmonary Artery Thrombosis: A Diagnosis that Strives for its Independence. *Int. J. Mol. Sci.* 21, 5086. doi:10.3390/ijms21145086

Prabhu, W., and Soukas, P. A. (2017). Pulmonary Embolism in 2017: Increasing Options for Increasing Incidence. *R. Med. J.* 100, 27–32.

Qi, W.-X., Shen, Z., Tang, L.-N., and Yao, Y. (2014). Risk of Arterial Thromboembolic Events with Vascular Endothelial Growth Factor Receptor Tyrosine Kinase Inhibitors: an Up-To-Date Meta-Analysis. *Crit. Rev. Oncol. Hematol.* 92, 71–82. doi:10.1016/j.critrevonc.2014.04.004

Quarck, R., Wynants, M., Verbeken, E., Meyns, B., and Delcroix, M. (2015). Contribution of Inflammation and Impaired Angiogenesis to the Pathobiology of Chronic Thromboembolic Pulmonary Hypertension. *Eur. Respir. J.* 46, 431–443. doi:10.1183/09031936.00009914

Sakuma, M., Nakamura, M., Yamada, N., Ota, S., Shirato, K., Nakano, T., et al. (2009). Venous Thromboembolism Deep Vein Thrombosis with Pulmonary Embolism, Deep Vein Thrombosis Alone, and Pulmonary Embolism Alone. *Circ. J.* 73, 305–309. doi:10.1253/circj.cj-08-0372

Salibe-Filho, W., Araujo, T. L. S., G. Melo, E., B. C. T. Coimbra, L., Lapa, M. S., Acencio, M. M. P., et al. (2020). Shear Stress-Exposed Pulmonary Artery Endothelial Cells Fail to Upregulate HSP70 in Chronic Thromboembolic Pulmonary Hypertension. *PLoS One* 15, e0242960. doi:10.1371/journal.pone.0242960

Samad, F., Yamamoto, K., and Loskutoff, D. J. (1996). Distribution and Regulation of Plasminogen Activator Inhibitor-1 in Murine Adipose Tissue *In Vivo*. Induction by Tumor Necrosis Factor-Alpha and Lipopolysaccharide. *J. Clin. Invest.* 97, 37–46. doi:10.1172/jci118404

Satoh, T., Satoh, K., Yaoita, N., Kikuchi, N., Omura, J., Kurosawa, R., et al. (2017). Activated TAFI Promotes the Development of Chronic Thromboembolic Pulmonary Hypertension. *Circ. Res.* 120, 1246–1262. doi:10.1161/circresaha.117.310640

Schieffer, B., Schieffer, E., Hilfiker-Kleiner, D., Hilfiker, A., Kovanen, P. T., Kaartinen, M., et al. (2000). Expression of Angiotensin II and Interleukin 6 in Human Coronary Atherosclerotic Plaques. *Circulation* 101, 1372–1378. doi:10.1161/01.cir.101.12.1372

Schutzman, L. M., Rigor, R. R., Khosravi, N., Chung, K., Galante, J. M., and Brown, I. E. (2018). P-selectin Expression Favors De Novo Pulmonary Arterial Thrombosis after blunt Thoracic Trauma. *Shock* 49, 116. doi:10.1097/SHK.0000000000001158

Schutzman, L. M., Rigor, R. R., Khosravi, N., Galante, J. M., and Brown, I. E. (2019). P-Selectin Is Critical for De Novo Pulmonary Arterial Thrombosis Following Blunt Thoracic Trauma. *J. Trauma Acute Care Surg.* 86, 583–591. doi:10.1097/ta.0000000000002166

Seng, S., Liu, Z., Chiu, S. K., Proverbs-Singh, T., Sonpavde, G., Choueiri, T. K., et al. (2012). Risk of Venous Thromboembolism in Patients with Cancer Treated with Cisplatin: a Systematic Review and Meta-Analysis. *J. Clin. Oncol.* 30, 4416–4426. doi:10.1200/jco.2012.42.4358

Shi, G., and Morrell, C. N. (2011). Platelets as Initiators and Mediators of Inflammation at the Vessel wall. *Thromb. Res.* 127, 387–390. doi:10.1016/j.thromres.2010.10.019

Silversides, C. K., Granton, J. T., Konen, E., Hart, M. A., Webb, G. D., and Therrien, J. (2003). Pulmonary Thrombosis in Adults with Eisenmenger Syndrome. *J. Am. Coll. Cardiol.* 42, 1982–1987. doi:10.1016/j.jacc.2003.07.022

Simonneau, G., Torbicki, A., Dorfmüller, P., and Kim, N. (2017). The Pathophysiology of Chronic Thromboembolic Pulmonary Hypertension. *Eur. Respir. Rev.* 26, 160112. doi:10.1183/16000617.0112-2016

Solinas, C., Saba, L., Sganzerla, P., and Petrelli, F. (2020). Venous and Arterial Thromboembolic Events with Immune Checkpoint Inhibitors: A Systematic Review. *Thromb. Res.* 196, 444–453. doi:10.1016/j.thromres.2020.09.038

Soo Hoo, G. W. (2013). Overview and Assessment of Risk Factors for Pulmonary Embolism. *Expert Rev. Respir. Med.* 7, 171–191. doi:10.1586/ers.13.7

Tesselaar, M. E. T., Romijn, F. P. H. T. M., Van Der Linden, I. K., Prins, F. A., Bertina, R. M., and Osanto, S. (2007). Microparticle-associated Tissue Factor Activity: a Link between Cancer and Thrombosis? *J. Thromb. Haemost.* 5, 520–527. doi:10.1111/j.1538-7836.2007.02369.x

Tyagi, T., Ahmad, S., Gupta, N., Sahu, A., Ahmad, Y., Nair, V., et al. (2014). Altered Expression of Platelet Proteins and Calpain Activity Mediate Hypoxia-Induced Prothrombotic Phenotype. *Blood* 123, 1250–1260. doi:10.1182/blood-2013-05-501924

Van Gent, J.-M., Calvo, R. Y., Zander, A. L., Olson, E. J., Sise, C. B., Sise, M. J., et al. (2017). Risk Factors for Deep Vein Thrombosis and Pulmonary Embolism after Traumatic Injury: A Competing Risks Analysis. *J. Trauma Acute Care Surg.* 83, 1154–1160. doi:10.1097/ta.0000000000001652

Van Gent, J.-M., Zander, A. L., Olson, E. J., Shackford, S. R., Dunne, C. E., Sise, C. B., et al. (2014). Pulmonary Embolism without Deep Venous Thrombosis. *J. Trauma acute Care Surg.* 76, 1270–1274. doi:10.1097/ta.0000000000000233

Van Hinsbergh, V. W. M. (2012). Endothelium-role in Regulation of Coagulation and Inflammation. *Semin. Immunopathol.* 34, 93–106. doi:10.1007/s00281-011-0285-5

Vandanmagsar, B., Youm, Y.-H., Ravussin, A., Galgani, J. E., Stadler, K., Mynatt, R. L., et al. (2011). The NLRP3 Inflammasome Instigates Obesity-Induced

Inflammation and Insulin Resistance. *Nat. Med.* 17, 179–188. doi:10.1038/nm.2279

Velmahos, G. C., Spaniolas, K., Tabbara, M., Abujudeh, H. H., De Moya, M., Gervasini, A., et al. (2009). Pulmonary Embolism and Deep Venous Thrombosis in Trauma. *Arch. Surg.* 144, 928–932. doi:10.1001/archsurg.2009.97

Virchow, R. (1856). Gesammelte Abhandlungen Zur Wissenschaftlichen Medizin. *Frankfurt Am: Taf.* 20, 1–1024.

Wakefield, T. W., and Henke, P. K. (2005). The Role of Inflammation in Early and Late Venous Thrombosis: Are There Clinical Implications? *Semin. Vasc. Surg.* 18, 118–129. doi:10.1053/j.semvascsurg.2005.05.003

Wakefield, T. W., Myers, D. D., and Henke, P. K. (2008). Mechanisms of Venous Thrombosis and Resolution. *Arterioscler. Thromb. Vasc. Biol.* 28, 387–391. doi:10.1161/atvbaha.108.162289

Wu, K. K., Matijevic-Aleksic, N., and Dahlback, B. (2005). Molecular Aspects of Thrombosis and Antithrombotic Drugs. *Crit. Rev. Clin. Lab. Sci.* 42, 249–277. doi:10.1080/10408360590951171

Xiao, S., Geng, X., Zhao, J., and Fu, L. (2018). Risk Factors for Potential Pulmonary Embolism in the Patients with Deep Venous Thrombosis: a Retrospective Study. *Eur. J. Trauma Emerg. Surg.* 46, 419–424. doi:10.1007/s00068-018-1039-z

Yan, C., Wang, X., Su, H., and Ying, K. (2017). Recent Progress in Research on the Pathogenesis of Pulmonary Thromboembolism: An Old Story with New Perspectives. *Biomed. Res. Int.* 2017, 1–10. doi:10.1155/2017/6516791

Yan, L., Li, X., Liu, Z., Zhao, Z., Luo, Q., Zhao, Q., et al. (2019). Research Progress on the Pathogenesis of CTEPH. *Heart Fail. Rev.* 24, 1031–1040. doi:10.1007/s10741-019-09802-4

Yan, S.-F., Pinsky, D. J., and Stern, D. M. (2000). A Pathway Leading to Hypoxia-Induced Vascular Fibrin Deposition. *Semin. Thromb. Hemost.* 26, 479–484. doi:10.1055/s-2000-13203

Yandrapalli, S., Tariq, S., Kumar, J., Aronow, W. S., Malekan, R., Frishman, W. H., et al. (2018). Chronic Thromboembolic Pulmonary Hypertension. *Cardiol. Rev.* 26, 62–72. doi:10.1097/crd.0000000000000164

Yilmaz, S., and Cimen, K. A. (2010). Pulmonary Artery Aneurysms in Behçet's Disease. *Rheumatol. Int.* 30, 1401–1403. doi:10.1007/s00296-009-1092-310.1007/s00296-009-1036-y

Zabini, D., Heinemann, A., Foris, V., Nagaraj, C., Nierlich, P., Bálint, Z., et al. (2014). Comprehensive Analysis of Inflammatory Markers in Chronic Thromboembolic Pulmonary Hypertension Patients. *Eur. Respir. J.* 44, 951–962. doi:10.1183/09031936.00145013

Zabini, D., Nagaraj, C., Stacher, E., Lang, I. M., Nierlich, P., Klepetko, W., et al. (2012). Angiostatic Factors in the Pulmonary Endarterectomy Material from Chronic Thromboembolic Pulmonary Hypertension Patients Cause Endothelial Dysfunction. *PLoS One* 7, e43793. doi:10.1371/journal.pone.0043793

Zarà, M., Guidetti, G. F., Camera, M., Canobbio, I., Amadio, P., Torti, M., et al. (2019). Biology and Role of Extracellular Vesicles (EVs) in the Pathogenesis of Thrombosis. *Int. J. Mol. Sci.* 20, 2840. doi:10.3390/ijms20112840

Conflict of Interest: The authors declare that the research was conducted in the absence of any commercial or financial relationships that could be construed as a potential conflict of interest.

frontiers in Pharmacology

ORIGINAL RESEARCH
published: 15 July 2021
doi: 10.3389/fphar.2021.696135

Naringin Ameliorates Monocrotaline-Induced Pulmonary Arterial Hypertension Through Endothelial-To-Mesenchymal Transition Inhibition

*Yonghui Wu†, Changhong Cai†, Yijia Xiang, Huan Zhao, Lingchun Lv and Chunlai Zeng**

Department of Cardiology, Lishui Hospital of Zhejiang University, The Fifth Affiliated Hospital of Wenzhou Medical University, Lishui Municipal Central Hospital, Lishui, China

OPEN ACCESS

Edited by:
Djuro Kosanovic, I.M. Sechenov First Moscow State Medical University, Russia

Reviewed by:
Argen Mamazhakypov, Max Planck Institute for Heart and Lung Research, Germany
Pouya Sarvari, Max Planck Institute for Heart and Lung Research, Germany
Prakash Chelladurai, Max Planck Institute for Heart and Lung Research, Germany

***Correspondence:**
Chunlai Zeng
lszengchunlai@mail.zju.edu.cn

†These authors have contributed equally to this work

Specialty section:
This article was submitted to Respiratory Pharmacology, a section of the journal Frontiers in Pharmacology

Received: *16 April 2021*
Accepted: *03 June 2021*
Published: *15 July 2021*

Citation:
Wu Y, Cai C, Xiang Y, Zhao H, Lv L and Zeng C (2021) Naringin Ameliorates Monocrotaline-Induced Pulmonary Arterial Hypertension Through Endothelial-To-Mesenchymal Transition Inhibition. Front. Pharmacol. 12:696135. doi: 10.3389/fphar.2021.696135

Pulmonary arterial hypertension (PAH) caused by enhanced arterial pressure increases vessel resistance in the lung. Endothelial-to-mesenchymal transition (EndMT) plays key roles in the vascular remodeling in PAH. Naringin, a protective gaseous mediator is commonly extracted from tomatoes and citrus fruits (such as grapefruits), and demonstrates anti-inflammation, anti-oxidant, anti-proliferation, and anti-tumor effects. Meanwhile, the association of Naringin and the process of EndMT is still unclear. In this study, monocrotaline (MCT) administration (60 mg/kg) was delivered for the induction of PAH in rats. Following this, Naringin (concentrations: 25, 50, and 100 mg/kg/day) was used for treatments. Human Umbilical Vein Endothelial Cells (HUVECs) were stimulated with Naringin and transforming growth factor β1 (TGFβ1, 10 ng/ml). As the result, Naringin was demonstrated to inhibit EndMT and alleviate PAH progression. In particular, in HUVECs, Naringin significantly suppressed the mesenchymal marker expression induced by TGFβ1 treatment, enhanced the endothelial marker expression, and inhibited the activation of ERK and NF-κB signaling pathways. To conclude, this study provided novel evidence suggesting the beneficial effects of Naringin in PAH through the inhibition of the ERK and NF-κB signaling pathways and the EndMT progression in pulmonary arteries.

Keywords: naringin, pulmonary arterial hypertension, endothelial-to-mesenchymal transition, monocrotaline, endothelial cell, rat

INTRODUCTION

Pulmonary arterial hypertension (PAH) is caused by continued enhanced pulmonary arterial pressure (PAP) and blockages formation in small and medium-sized pulmonary arterial (PAs), ultimately leading to right ventricular hypertrophy (RVH), functional failure, and untimely death (De Jesus Perez, 2016). A large number of studies have focused on the important role endothelial cell (EC) dysfunction played in the pathogenic mechanisms of PAH, meanwhile the pathogenesis of PAH is multi-factorial (Budhiraja et al., 2004). Injury of endothelial cells potentially lead to the loss of endothelial vasoactive mediator balancing, vasoconstriction, disorders in EC proliferations and small PAs loss (Sakao et al., 2009). Abnormal EC proliferations causes the plexiform lesion formation,

which is the characteristic of PAH (Derrett-Smith et al., 2013). For this reason, endothelial function improvement is potentially applicable for effective treatments of PAH.

Endothelial dysfunction causes changes in endothelial vasoactive mediators, vasoconstriction injury, endothelial cell proliferation/apoptosis imbalance and endothelium-mesenchymal transformation (EndMT), which contribute to the progression of PAH (Ranchoux et al., 2015). EndMT is featured by the loss of unique phenotype in endothelial cells, and subsequent gaining of the mesenchymal phenotypes, which are marked by the loss of connection and polarity between cells and the gaining of cellular motility and invasion (Good et al., 2015). This phenomenon is featured by the observation when ECs lost specific endothelial markers, including CD31, vascular endothelial cadherin (VE-cadherin), and Von Willebrand Factor (vWF), while progressively expressing mesenchymal markers, including fibronectin (FN), vimentin, and α-smooth muscle actin (α-SMA) (Frid et al., 2002). EndMT is reported to majorly contribute to the processes of both embryonic development and fibrotic lung disease pathogenesis (Leopold and Maron, 2016; Willis and Borok, 2007). EndMT has also been reported to play critical roles in pulmonary vascular remodeling in both patients and animals of PAH. For this reason, new therapeutic strategies targeting EndMT inhibition and endothelial function improvement are potentially applicable for the treatments of PAH.

Naringin, a flavanone -7- O–glycoside, naturally occurs in citrus fruits such as grapefruits (Burke et al., 2019). Previous studies suggest the beneficial effects of naringin supplements in preventing obesity, diabetes, and other metabolic syndromes (Alam et al., 2014). Naringin also has a variety of pharmacological properties, such as anti-oxidation, anti-inflammation, anti-mutagenesis, anticancer, antibacterial, and the lowering of cholesterol level (Wang et al., 2013). Recently, several reports have shown that naringin could inhibit inflammation in acute lung injury and carcinogenesis in mice (Kim et al., 2018; Zhang et al., 2018). Given these potentials of naringin, in this study, we mainly focused on the investigations of the effects of naringin in MCT-induced rat PAH *via* inhibitions of EndoMT and improvements of endothelial function.

MATERIALS AND METHODS

Animals

All Sprague-Dawley rats (230–250 g, 7 weeks-old, male) were commercially purchased from the experimental animal center of Zhejiang Province. All rats were caged under a standard environment (20–26°C, 45–55% humidity, 12 h light/dark cycle, standard diet). All procedures for animal study were approved by the ethics review of animal use application of the Fifth affiliated Hospital of Wenzhou Medical University.

Animal Model and Experimental Design

Rats were divided into five experimental groups: 1) control (n = 6), 2) MCT group (n = 10), 3) low- Naringin group (n = 10; 25 mg/kg/d), 4) medium- Naringin group (n = 10; 50 mg/kg/d) and 5) high- Naringin group (n = 10; 100 mg/kg/d). The PAH rat model was set up by a single dose of subcutaneous MCT injection (60 mg/kg, Sigma-Aldrich, MO, United States). Aliquots of saline were injected in the control group. According to a previous study, naringin (25, 50, and 100 mg/kg/d; MedChem Express, NJ, United States) was intragastrically administered for 14 consecutive days from day 15–28 after MCT injection in the treatment groups (Cai et al., 2019). Each Rat was weighed every week for the adjustment of administered doses.

Hemodynamic Measurement

Right ventricle systolic pressure (RVSP) measurement was conducted as in a previous study (Wu et al., 2020). Briefly, pentobarbital sodium (60 mg/kg, Sigma-Aldrich, MO, United States) through intraperitoneal (i.p.) injection was performed for anesthetization of the rats. A venous catheter (BioPac Systems, Inc.) connected to a pressure transducer through a tube was placed in the right ventricle (RV) through the right external jugular vein.

Right Heart Hypertrophy Assessment

After RVSP measurement, the body weight (BW) of each rat was measured. For the measurement of RVH, pentobarbital sodium (150 mg/kg) injection was performed for the scarification of rats. Weights of both RV and left ventricle (LV) plus septum (S) were recorded. RVH were assessed using both RV/(LV + S) ratio and RV/BW ratio as gravimetric indexes.

Morphological Analysis

Lung tissues were harvested, embedded into paraffin, and cut into slices (4 μm). Hematoxylin and eosin (H&E) staining was used for the evaluation of pulmonary arteries morphology. Five slices of pulmonary arteries with diameter ranged from 50 to 150 μm were randomly picked and assessed under microscope (Nikon, Japan; magnification, ×400). Pulmonary artery wall thickness was assessed as follows: vascular wall thickness percentage (wt%) = wall thickness/outer diameter × 100%; the percentage of vascular wall area (WA%) = wall transection area/cross-sectional area × 100%.

Cell Culture and Treatment

HUVECs were commercially purchased and cultivated in endothelial cell medium (ScienCell) with 10% fetal bovine serum (Gibco, Carlsbad, CA) and 1% penicillin/streptomycin solution, and incubated at 5% CO2 under 37°C. Cells with passage time between 3 and 8 were subjected to the following study.

Endothelial-to-Mesenchymal Transition of Human Umbilical Vein Endothelial Cells *in vitro*

Cells cultured with an approximate 80% confluency were ready for experiments. In order to investigate the potential effect of naringin to EndMT, HUVECs was pretreated with serum starvation overnight, followed by the treatment of TGFβ1 (10 ng/ml, PeproTech, NJ, United States) and with or without naringin at different concentrations (10, 50, and 100 μM, MedChem Express, NJ, United States) treatment for different treatment times (0, 6, 12, 24, and 48 h). EndMT was revealed by the decrease in endothelial markers (CD31 and vWF) and increase in mesenchymal markers (α-SMA and fibronectin) using both immunoblot analysis and Immunohistochemistry.

Cell Proliferation Assay

The cell counting Kit-8 (CCK-8, Beyotime, Jiangsu, China) was used for the assay of cell proliferations. Cells were plated into 96-well plates (1 × 104 cells/well) and cultivated for 24 h. Cells were treated with TGFβ1 and with or without different concentrations of naringin for different treatment times. Aliquots of 10 μL CCK-8 solutions were used to suspend (2 h, 37°C) samples. Cell absorbencies were measured at 450 nm by spectrophotometer.

Cell Scratch Test

Cells were plated into 6-well plates and cultivated for 24 h. A single scratch in each well was drawn using a 200 μL pipette tip. Cell culture was washed with PBS and then incubated in culture medium with or without TGFβ1 and naringin. Images of scratches were recorded and assessed at different time points (0, 24, and 48 h) using Olympus inverted microscope.

Histological Analysis of Endothelial-to Mesenchymal Transition

In vivo, lung tissue samples were used for immunohistochemical and immunofluorescence staining. Lung slices were treated by dewaxing and rehydrating, blocked in 5% BSA, and incubated with α-SMA (A2547, 1:400 dilution; Sigma-Aldrich, MO, United States), vWF (ab6994, 1:200 dilution; Abcam, Cambridge, United Kingdom), and CD31 (ab24590, 1:500 dilution; Abcam, Cambridge, United Kingdom) primary antibodies (4°C, overnight) and secondary antibodies at room temperature (RT) for 30 min.

In vitro, HUVECs were plated on glass slides, washed with PBS, and fixed by 4% paraformaldehyde (30 min). The cells were treated with PBS containing 0.5%TritonX-100 for 20 min for permeabilizing. Primary antibodies α-SMA (A2547, 1:400 dilution) and CD31 (ab24590, 1:500 dilution) antibody was incubated with the glass slides (4°C, overnight). Glass slides were washed with PBS (three times) and subjected to secondary antibody incubation (1:50, Beyotime, China) for 30 min at RT. Images were captured under a microscope. Images of 3–5 visual fields were randomly selected and analyzed by ImageJ software.

Western Blot Analysis

Lung tissues and huvec cells were lyzed using radio-immunoprecipitation assay buffer (Beyotime, Shanghai, China). Samples were centrifuged at 13,000 rpm for 10 min (4°C). Supernatants were collected. Protein concentrations were evaluated by bicinchoninic acid protein assay (Beyotime). Samples were fractionated by sodium dodecyl sulfate-polyacrylamide gel electrophoresis (SDS-PAGE) and transferred to polyvinylidene fluoride (PVDF) membranes. The membranes were then blocked in 5% BSA and incubated at 4°C overnight with primary antibodies: TGFβ1 (sc146, 1:1,000 dilution, Santa cruz Biotechnology), α-SMA (A2547, 1:1,000 dilution, Sigma), FN (ab6328, 1:1,000 dilution, abcam), CD31 (ab24590, 1:1,000 dilution, abcam), vWF (ab6994, 1:1,000 dilution, abcam), Vimentin (ab20346, 1:1,000 dilution, abcam), VE-cadherin (ab205336, 1:1,000 dilution, abcam), Twist (ab175430, 1:1,000 dilution, abcam), Snail (ab216347, 1:1,000 dilution, abcam), *p*-ERK (9101S, 1:1,000 dilution, CST), ERK (9102S, 1:1,000 dilution, CST), p-NF-κB (ab86299, 1:1,000 dilution, abcam), NF-κB (8242S, 1:1,000 dilution, CST), GAPDH (5174S, 1:1,000 dilution, CST). Subsequently, the membranes were washed with Tris-buffered saline/Tween (TBST) three times and incubated with anti-rabbit IgG HRP-conjugated antibody (7074S, 1:1,000, 1:1,000 dilution, CST) or anti-mouse IgG HRP-conjugated antibody (7076S, 1:1,000, 1:1,000 dilution, CST) for 1 h at room temperature, and scanned using the IBright protein Western blotting imaging system (Thermo Fisher, United States).

Statistical Analysis

All results were expressed as mean ± SEM. One-way analysis of variance and Tukey's post-hoc test was performed by GraphPad Prism 7.0. Survival analysis was used to analyze the survival rate of rats (#, $^{*}p < 0.05$ and ##, $^{**}p < 0.01$).

RESULTS

Naringin May Improve Survival in Rats With Pulmonary Arterial Hypertension

After 28 days, the survival rate of rats in the control group was 100%, and the survival rate of rats after MCT injection was about 60%. High-dose naringin (100 mg/kg) may improve the survival rate of rats with pulmonary hypertension (80%), but there was no statistical significance between each group ($p > 0.05$; Supplemental Materials **Figure 1**).

Naringin Alleviated Monocrotaline-Induced Hemodynamic Changes and Right Ventricular Hypertrophy

In order to investigate the potential inhibitory effects of Naringin in the development of PAH, multiple indicators including RVSP, RV/LV + S, and RV/BW were assessed. As shown in **Figures 1A,B**, Administrations of MCT significantly enhanced RVSP (76.78 ± 4.20) compared to that in the control group (19.80 ± 0.64), while the increase of RVSP was markedly down-regulated by the administration of medium and high-dose of naringin (50 and 100 mg/kg) (medium: 63.90 ± 1.99; high: 54.56 ± 1.20). Meanwhile, as shown in **Figures 1C,D**, RV/LV + S, and RV/BW were significantly elevated after MCT administration (RV/LV + S: 0.61 ± 0.03; RV/BW: 1.10 ± 0.07), while two doses of naringin (50 and 100 mg/kg) treatments significantly recused these increases ((RV/LV + S) medium: 0.54 ± 0.01, high: 0.49 ± 0.01 (RV/BW) medium: 0.89 ± 0.02, high: 0.73 ± 0.02), thereby alleviating the right ventricular hypertrophy.

Naringin Attenuated Monocrotaline-Induced Pulmonary Arterial Remodeling

For the assessments of cardiac fibrosis, histological analysis was performed based on the results of H&E staining. Subsequently,

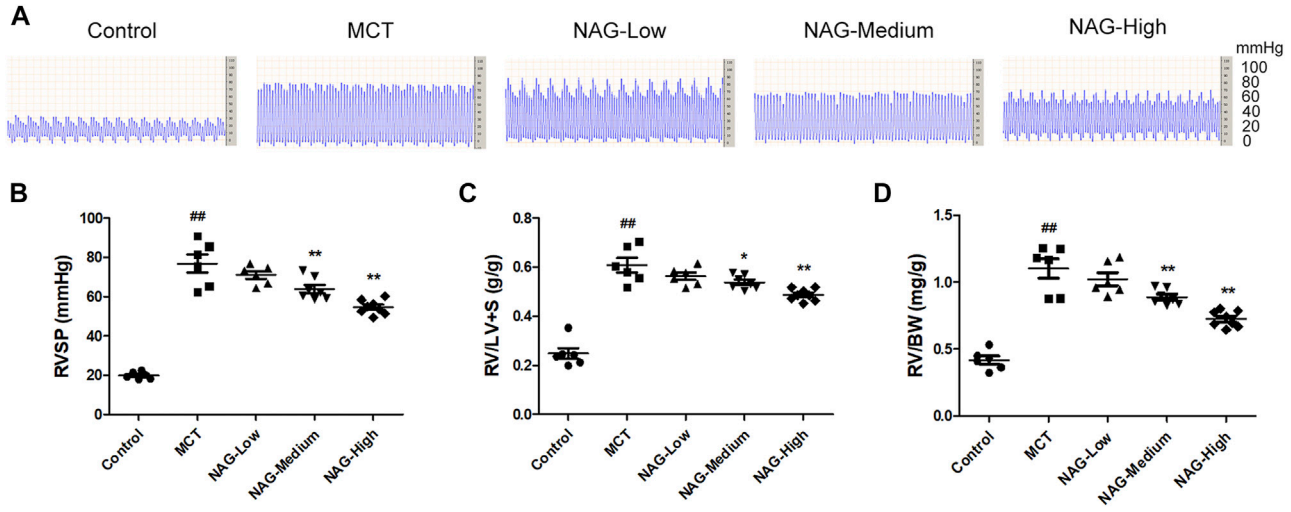

FIGURE 1 | Effects of naringin on hemodynamics and RVH in the MCT-induced PAH. **(A)** Representative images of RVSP waves. **(B)** RVSP, **(C)** RV/LV + S and **(D)** RV/BW ratio. n = 6–8. ##p < 0.01 vs. control; *p < 0.05, **p < 0.01 vs. MCT; n = 6–8. NAG, naringin.

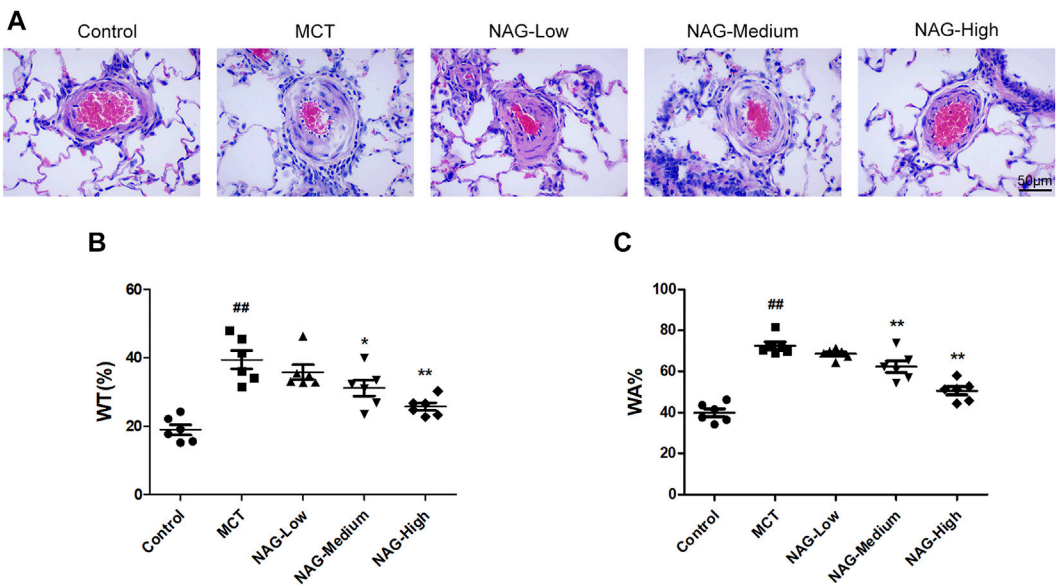

FIGURE 2 | Effects of naringin on pulmonary arterial remodeling in the PAH caused by MCT administration. **(A)** Representative histopathological images of rat PAs by H&E staining. Magnification, ×400; scale bars, 50 μm. Quantifications for **(B)** wt% and **(C)** WA%. ##p < 0.01 vs. control; *p < 0.05, **p < 0.01 vs. MCT. n = 6.

the thicknesses of pulmonary arterioles with 50–150 μm in diameter was measured. As a result, MCT administration induced significant enhancement of WT% (39.43 ± 2.44) and WA% (72.49 ± 1.76) of pulmonary arterioles. Meanwhile, both medium- (WT%: 31.16 ± 2.12; WA%: 62.35 ± 2.56) and high-dose (WT%: 25.72 ± 1.03; WA%: 50.55 ± 1.84) Naringin treatments rescued this MCT-promoted WT% and WA% increase. The results show that high-dose naringin can better improve MCT-induced PAH (**Figure 2**).

Naringin Suppressed Endothelial-to-MesenchymalTransition in Monocrotaline-Induced Pulmonary Arterial Hypertension

TGFβ1 expression changes during the development of PAH were determined by western blot. The result demonstrated that naringin rescued this up-regulation of TGFβ1 induced by MCT administration (**Figures 3A,B**). In previous studies, EndMT was

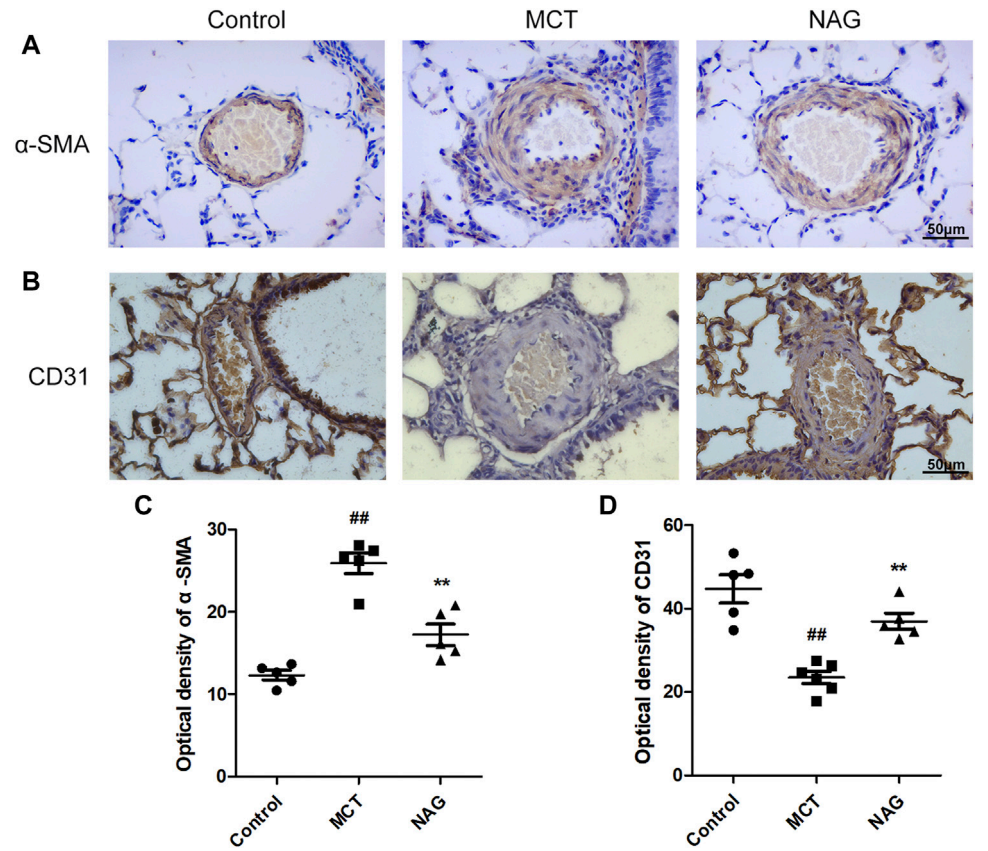

FIGURE 3 | Effects of naringin on expressions of α-SMA and CD31 in the MCT-induced PAH. The expressions of α-SMA **(A)** and CD31 **(B)** in lungs in immunohistochemistry staining. Quantifications of α-SMA optical density **(C)** and CD31 optical density **(D)**. Magnification ×400, scale bars = 50 μm ##$p < 0.01$ vs. control; **$p < 0.01$ vs. MCT. $n = 6$.

indicated as one of the major contributors to PAH pathogenesis. As shown in **Figure 3** and **Figure 4**, endothelial markers expressions (vWF, VE-cadherin and CD31) were downregulated, while mesenchymal markers (Vimentin, α-SMA and FN) and EndMT-related transcription factors (snail and twist) expressions were up-regulated in the lung samples collected from MCT-treated rats. Meanwhile, naringin treatments rescued these changes, which were further verified by western blot. The results from immunohistochemical staining were consistent with those from western blot, and we also obtained similar results by immunofluorescence staining (**Figure 5**), subsequently suggesting the protective effects of naringin in MCT-induced PAH through inhibiting EndMT.

Naringin Inhibited Transforming Growth Factor β1-Induced Human Umbilical Vein Endothelial Cells Proliferation and Migration

To explore the effect of naringin on HUVECs proliferation, TGFβ1 and different concentrations of naringin (10, 50, 100 μM) were used to treat HUVECs for different times (0, 12, 24, and 48 h). Subsequently, the HUVECs viability were determined using CCK-8. As is shown in **Figure 6A**, naringin could inhibit HUVECs viability in both a dose-dependent manner and time-dependent manner.

Cell migration was analyzed by cell scratch test. Wound closure levels were increased after TGFβ1 stimulation for 24 and 48 h (**Figure 6C**), whereas the TGFβ1-induced migration was inhibited by naringin, suggesting that the cell proliferation and migration were significantly inhibited after 48 h of TGFβ1 stimulation. Meanwhile naringin (100 μM) significantly inhibited the cell proliferation and migration (**Figure 6B**). Therefore, we chose the stimulation time and concentration of TGFβ1 and naringin for the following cell experiments.

Naringin Attenuated Transforming Growth Factor β1-Induced Endothelial-to-Mesenchymal Transition in Human Umbilical Vein Endothelial Cells

For the investigations of the effects of naringin on EndMT, TGFβ1 was used for the induction of EndMT in HUVECs. In

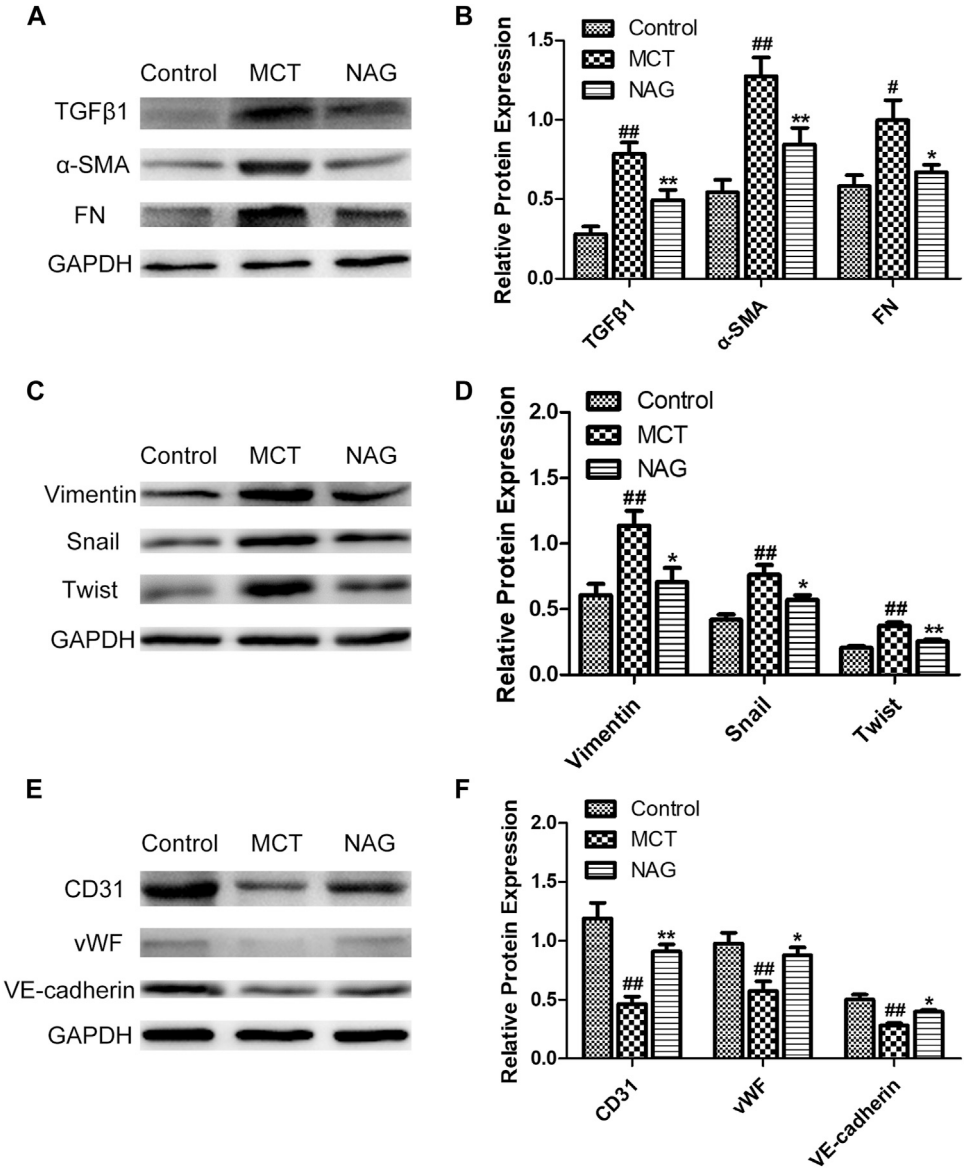

FIGURE 4 | Effects of naringin on expressions of TGFβ1, α-SMA, FN, Vimentin, Twist, Snail, CD31, vWF, and VE-cadherin in lung tissues in rats. Expressions of TGFβ1, α-SMA, FN **(A,B)**, Vimentin, Twist, Snail **(C,D)** and CD31, vWF, VE-cadherin **(E,F)**. #$p < 0.05$, ##$p < 0.01$ vs. control; *$p < 0.05$, **$p < 0.01$ vs. MCT. $n = 6$.

western blot, TGFβ1 treatments down-regulated the expressions of vWF, VE-cadherin, and CD31, while up-regulating the expressions of Vimentin, α-SMA, FN, snail, and twist, indicating that the process of EndMT was enhanced during this process (**Figures 7E–H**). These changes were validated by immunohistochemical staining, revealed by the observations that TGFβ1 significantly reduced the number of CD31 positive staining cells, while promoting the number of α-SMA positive cells (**Figures 7A–D**). However, naringin could markedly reverse TGFβ1-induced changes (**Figure 7**). These ffndings demonstrated that naringin attenuated TGFβ1-induced EndMT in HUVECs.

Naringin Modulated Extracellular Regulated Kinase and Nuclear Factor-κB Signaling Pathways Activation in Transforming Growth Factor β1-Induced Human Umbilical Vein Endothelial Cells

To further investigate molecular mechanisms underlying the observation that naringin recued the effects induced by TGFβ1 administration, the expressions of ERK and NF-κB signaling pathways were analyzed by western blot. Our results demonstrated that two signaling pathways were activated after TGFβ1 stimulation, while the activations were significantly blocked by naringin (**Figure 8**). All the clues above suggested

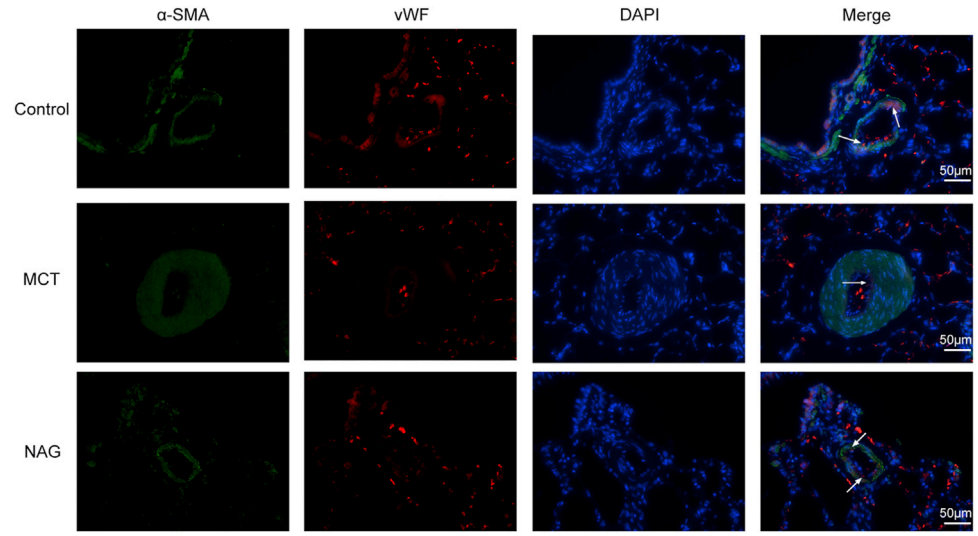

FIGURE 5 | Effects of naringin on EndMT of PAH in rats was demonstrated by immunofluorescence staining. Red fluorescence represents vWF, green fluorescence represents α-SMA and blue fluorescence indicates DAPI nuclei staining. The white arrows in the images indicate vWF-positive cells. Magnification ×400, scale bars = 50 μm.

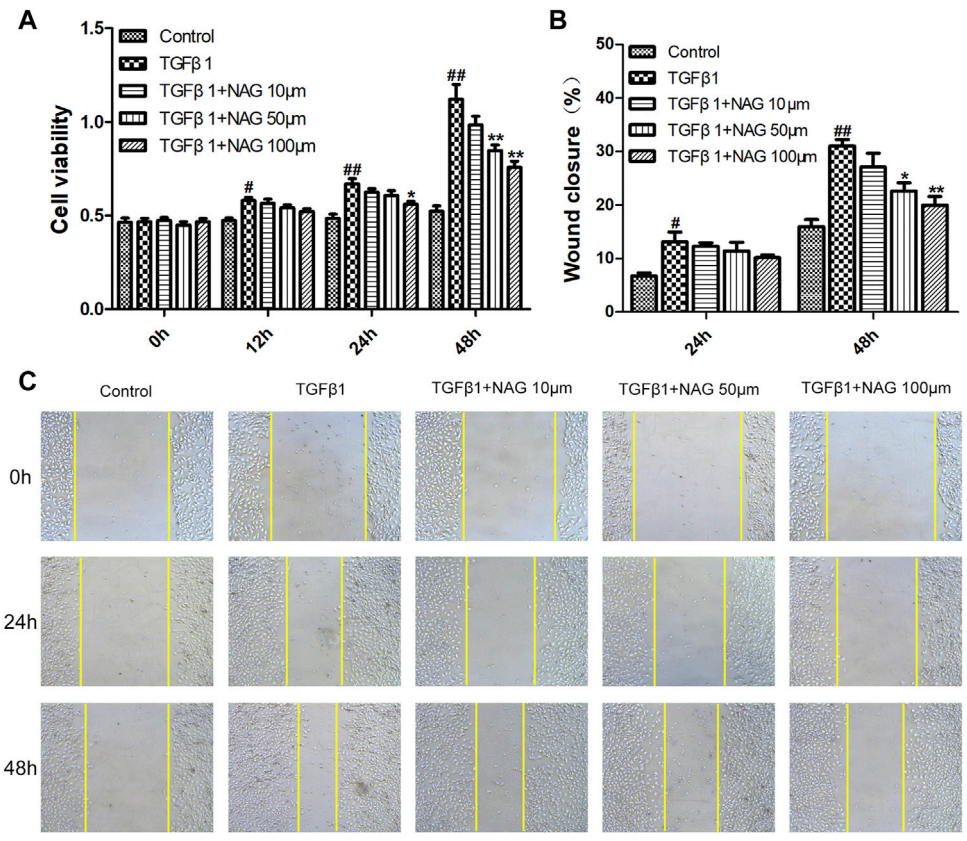

FIGURE 6 | Effects of naringin on proliferation and migration of HUVECs **(A)** Serum-starved HUVECs were incubated with TGF-β1 (10 ng/ml) and the absence or presence of naringin (10, 50 and 100 μmol/L) for 0, 12, 24, and 48 h **(B,C)** Serum-starved HUVECs were stimulated with TGF-β1 (10 ng/ml) and the absence or presence of naringin (10, 50 and 100 μmol/L) for 0, 24 and 48 h #$p < 0.05$, ##$p < 0.01$ vs. control; *$p < 0.05$, **$p < 0.01$ vs. TGFβ1. $n = 3$.

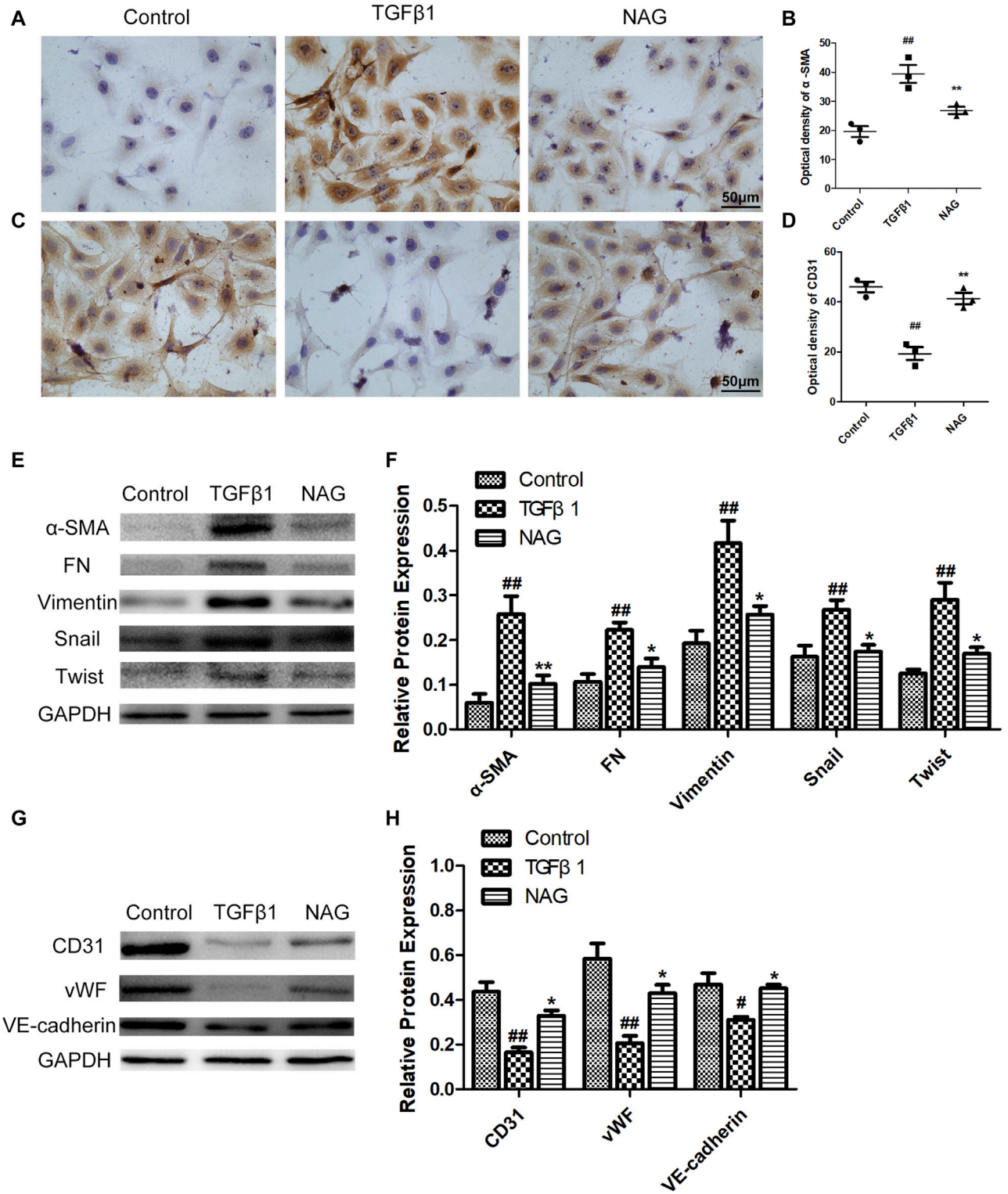

FIGURE 7 | Effects of naringin on expressions of α-SMA, FN, Vimentin, Twist, Snail, CD31, vWF, and VE-cadherin in TGFβ1-induced HUVECs. Serum-starved HUVECs were stimulated with TGF-β1 (10 ng/ml) and with or without naringin (100 μmol/L) for 48 h. The expressions of α-SMA **(A)** and CD31 **(C)** in HUVECs were analyzed by immunohistochemistry staining. Quantification of α-SMA optical density **(B)** and CD31 optical density **(D)** were calculated. The expressions of α-SMA, FN, Vimentin, Twist, Snail **(E,F)** and CD31, vWF, VE-cadherin **(G,H)** were analyzed with western blot. Magnification ×400, scale bars = 50 μm ##$p < 0.01$ vs. control; **$p < 0.01$ vs. TGFβ1. $n = 3$.

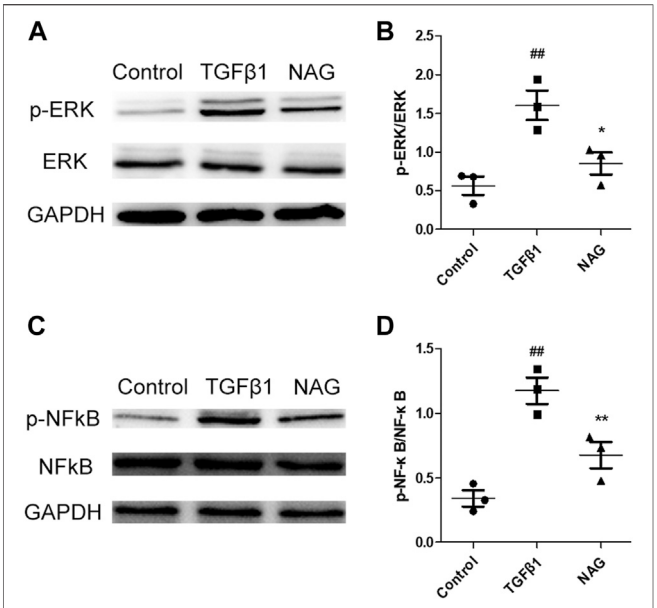

FIGURE 8 | Effects of naringin on ERK and NF-κB signals. Serum-starved HUVECs were stimulated with TGF-β1 (10 ng/ml) and the absence or presence of naringin (100 μmol/L) for 48 h. Expressions of *p*-ERK, ERK **(A,B)**, *p*-NFκB, and NFκB **(C,D)**. ##$p < 0.01$ vs. control; *$p < 0.05$, **$p < 0.01$ vs. MCT. $n = 3$.

that naringin regulated TGFβ1-induced EndMT *via* ERK and NF-κB signaling pathways.

DISCUSSION

In this study, we demonstrated the protective effects of naringin during the pathogenic progression of PAH in MCT-induced rat model. Naringin significantly attenuated symptoms of PAH, including pulmonary vascular remodeling and RVH. Also, our results demonstrated that naringin attenuated EndMT in PAH rat model. Furthermore, in cultured HUVECs, we also found the inhibitory role naringin played in TGFβ1-induced EndMT.

In previous studies, several animal models were widely used for novel pharmacotherapy preclinical studies of PAH. Animal models are commonly established through MCT lung injury, pulmonary hypertension caused by chronic hypoxia, and vascular endothelial growth factor receptor (VEGF-R) blockade using the tyrosine kinase inhibitor SU5416 (SU5416 plus chronic hypoxia model, SuHx model). Those different types of animal model have been intensively studied as they are able to mimic the vascular symptoms in PAH patients with severe conditions (de Raaf et al., 2014). In this study, we demonstrate decrease in survival, significant elevations in RVSP, pulmonary vascular remodeling, and RVH in PAH rat models caused by MCT administration, which are consistent with previous studies. Naringin is a flavanone glycoside synthesized from the flavanone naringenin and the disaccharide neohesperidose. Previous studies have demonstrated the potential protective effects of Naringin on diseases including osteoporosis, atherosclerosis, hypertension, and alcoholic hepatic steatosis (Zhao et al., 2020; Akintunde et al., 2020; Zhou et al., 2019). However, the efficacies of Naringin to the pathogenesis of PAH is still unknown. Here in this study, we demonstrated that naringin can improve survival and alleviate the symptoms of PAH caused by MCT administration, including diminished pulmonary vascular remodeling and RVH. Accumulating evidence has indicated that cardiac function is damaged by pulmonary interstitial fibrosis, contributing to the formation of pulmonary hypertension and causing RV failure (Andersen et al., 2019). Naringin attenuates damages in vascular endothelial caused by Oxidized low-density lipoprotein (ox-LDL) and alleviates paraquat-induced acute lung injury in mice through the suppression of collagen synthesis (Zhao et al., 2020; Chen et al., 2013). Naringenin, a conversion of naringin, can increase the protective effect of L-arginine against monocinine induced pulmonary hypertension in rats (Ahmed et al., 2014), therefore potentially participating in the protective effects of naringin on PAH. Some studies have shown that TGFβ1 can promote the proliferation and migration of endothelial cells (Wu et al., 2017; Jiang et al., 2018), while other literature has shown that TGFβ1 can reduce the proliferation and migration of endothelial cells (Baird and Durkin., 1986; Frater-Schroder et al., 1986). Thus, TGFβ1 is a special growth factor that may have two sides. Importantly, in our study, naringin is found to suppress the proliferation and migration of HUVECs induced by TGFβ1. Collectively, naringin significantly inhibited pulmonary injury and vascular endothelial injuries, therefore can be used as novel therapy for the clinical treatments of PAH.

EndMT contributes to the pathogenesis of abnormal pulmonary vascular remodeling and tissue fibrosis in PAH. As reported, some ECs are able to express both endothelial and mesenchymal phenotypes in PAH model caused by MCT administration (Good et al., 2015). EndMT is featured by the gaining of mesenchymal phenotypes and the decrease of endothelial cell markers in the endothelium (Suzuki et al., 2018). In pulmonary hypertension, EndMT causes matrix-generating fibroblasts and contributes to the progression of extracellular matrix productions and collagen depositions, and subsequently causes the pulmonary vascular remodeling (Xiong, 2015). Naringin are found to produce protective effects against End MT in atherosclerosis (Zhao et al., 2020). Here in this study, our data indicated significantly decreased endothelial markers, increased mesenchymal markers, and EndMT-related transcription factors in the lung tissue of an MCT-induced rat model of PAH. Most importantly, naringin treatments are able to rescue such alterations in PAH through the inhibition of EndMT. Our findings are further validated *in vitro* in the studies of HUVECs. Remarkably, TGFβ1-induced increase of mesenchymal markers (Vimentin, α-SMA and FN) and EndMT-related transcription factors (snail and twist), decrease of the endothelial markers expressions (vWF, VE-cadherin and CD31) in HUVECs are inhibited by naringin treatments. Collectively, both *in vivo* and *in vitro* studies demonstrate that naringin is able to delay the development of PAH through the inhibition of EndMT.

ERK and NF-κB signalling pathways have been reported as important factors in the maintenance of pulmonary vascular homeostasis (Cai et al., 2019; Wu et al., 2020). Increasing evidences have demonstrated the associations of ERK and NF-κB signalling pathways in the EndMT in PAH. Blockage of such pathways produces beneficial effects in PAH (Sabbineni et al., 2018; Zhang et al., 2019). In PAH patients, TGFβ1 induced EndMT vascular ECs are reported to associate with ERK and NF-κB signalling pathway activations, while activation inhibition of such signalling pathways partially recues the TGFβ1-induced EndMT in ECs (Shu et al., 2016; Zong et al., 2020). Naringin is reported to inhibit the process of osteoclastogenesis and bone resorptions through the inhibitory effects against ERK and NF-κB signalling pathway activations (Ang et al., 2011). Also, naringin is able to attenuate endothelial injuries and ox-LDL-induced EndMT (Zhao et al., 2020). In this study, consistent with previous reports, we find that TGFβ1 significantly increased the phosphorylation levels of ERK and NF-κB signalling pathway in HUVECs, which was partially reversed by naringin. Collectively, our results demonstrate that ERK and NF-κB signalling pathways are associated with the process of naringin inhibiting the TGFβ1-induced EndMT.

In conclusion, in this study, our data suggest that naringin can be used as a potential agent for the treatment of PAH, evidenced by the observation that naringin alleviates pulmonary vascular remodeling and RVH in MCT-induced PAH rats. This effect is potentially achieved through the improvement of EndMT via inhibiting ERK and NF-κB signalling pathways.

DATA AVAILABILITY STATEMENT

The raw data supporting the conclusion of this article will be made available by the authors, without undue reservation, to any qualified researcher.

ETHICS STATEMENT

The animal study was reviewed and approved by the ethics review of animal use application of the Fifth affiliated Hospital of Wenzhou Medical University.

AUTHOR CONTRIBUTIONS

YW, CC, and CZ designed the study. YW, CC, and YX performed the experiments and analyzed the data, and YW wrote the manuscript. YX and LL were responsible for data acquisition and provided technological assistance. HZ provided pathological assistance, and was involved in the data analysis and interpretation. CZ participated in critical revisions of the manuscript. All of the authors have read and approved the final manuscript.

REFERENCES

Ahmed, L. A., Obaid, A. A. Z., Zaki, H. F., Agha, A. M., Al Arqam, Z. O., Zaki, H. F., et al. (2014). Naringenin Adds to the Protective Effect of L-Arginine in Monocrotaline-Induced Pulmonary Hypertension in Rats: Favorable Modulation of Oxidative Stress, Inflammation and Nitric Oxide. *Eur. J. Pharm. Sci.* 62, 161–170. doi:10.1016/j.ejps.2014.05.011

Akintunde, J. K., Akintola, T. E., Hammed, M. O., Amoo, C. O., Adegoke, A. M., and Ajisafe, L. O. (2020). Naringin Protects against Bisphenol-A Induced Oculopathy as Implication of Cataract in Hypertensive Rat Model. *Biomed. Pharmacother.* 126, 110043. doi:10.1016/j.biopha.2020.110043

Alam, M. A., Subhan, N., Rahman, M. M., Uddin, S. J., Reza, H. M., and Sarker, S. D. (2014). Effect of Citrus Flavonoids, Naringin and Naringenin, on Metabolic Syndrome and Their Mechanisms of Action. *Adv. Nutr.* 5, 404–417. doi:10.3945/an.113.005603

Andersen, S., Nielsen-kudsk, J. E., Vonk Noordegraaf, A., and de Man, F. S. (2019). Right Ventricular Fibrosisfibrosis. *Circulation* 139, 269–285. doi:10.1161/circulationaha.118.035326

Ang, E. S. M., Yang, X., Chen, H., Liu, Q., Zheng, M. H., and Xu, J. (2011). Naringin Abrogates Osteoclastogenesis and Bone Resorption via the Inhibition of RANKL-Induced NF-Kb and ERK Activation. *FEBS Lett.* 585, 2755–2762. doi:10.1016/j.febslet.2011.07.046

Baird, A., and Durkin, T. (1986). Inhibition of Endothelial Cell Proliferation by Type Beta-Transforming Growth Factor: Interactions with Acidic and Basic Fibroblast Growth Factors. *Biochem. Biophys. Res. Commun.* 138, 1. doi:10.1016/0006-291x(86)90305-0

Budhiraja, R., Tuder, R. M., and Hassoun, P. M. (2004). Endothelial Dysfunction in Pulmonary Hypertension. *Circulation* 109, 159–165. doi:10.1161/01.cir.0000102381.57477.50

Burke, A. C., Sutherland, B. G., Telford, D. E., Morrow, M. R., Sawyez, C. G., Edwards, J. Y., et al. (2019). Naringenin Enhances the Regression of Atherosclerosis Induced by a Chow Diet in Ldlr Mice. *Atherosclerosis* 286, 60–70. doi:10.1016/j.atherosclerosis.2019.05.009

Cai, C., Xiang, Y., Wu, Y., Zhu, N., Zhao, H., Xu, J., et al. (2019). Formononetin Attenuates Monocrotaline induced P ulmonary Arterial Hypertension via Inhibiting Pulmonary Vascular Remodeling in Rats. *Mol. Med. Rep.* 20, 4984–4992. doi:10.3892/mmr.2019.10781

Chen, Y., Nie, Y.-c., Luo, Y.-l., Lin, F., Zheng, Y.-f., Cheng, G.-h., et al. (2013). Protective Effects of Naringin against Paraquat-Induced Acute Lung Injury and Pulmonary Fibrosis in Mice. *Food Chem. Toxicol.* 58, 133–140. doi:10.1016/j.fct.2013.04.024

De Jesus Perez, V. A. (2016). Molecular Pathogenesis and Current Pathology of Pulmonary Hypertension. *Heart Fail. Rev.* 21, 239–257. doi:10.1007/s10741-015-9519-2

de Raaf, M. A., Schalij, I., Gomez-arroyo, J., Rol, N., Happe, C., de Man, F. S., et al. (2014). SuHx Rat Model: Partly Reversible Pulmonary Hypertension and Progressive Intima Obstruction. *Eur. Respir. J.* 44, 160–168. doi:10.1183/09031936.00204813

Derrett-Smith, E. C., Dooley, A., Gilbane, A. J., Trinder, S. L., Khan, K., Baliga, R., et al. (2013). Endothelial Injury in a Transforming Growth Factor β-Dependent Mouse Model of Scleroderma Induces Pulmonary Arterial Hypertension. *Arthritis Rheum.* 65, 2928–2939. doi:10.1002/art.38078

Frater-Schroder, M., Muller, G., Birchmeier, W., and Bohlen, P. (1986). Transforming Growth Factor-Beta Inhibits Endothelial Cell Proliferation. *Biochem. Biophys. Res. Commun.* 137, 1. doi:10.1016/0006-291x(86)91209-x

Frid, M. G., Kale, V. A., and Stenmark, K. R. (2002). Mature Vascular Endothelium Can Give Rise to Smooth Muscle Cells via Endothelial-Mesenchymal Transdifferentiationfferentiation: *In Vitro* Analysis. *Circ. Res.* 90, 1189–1196. doi:10.1161/01.res.0000021432.70309.28

Good, R. B., Gilbane, A. J., Trinder, S. L., Denton, C. P., Coghlan, G., Abraham, D. J., et al. (2015). Endothelial to Mesenchymal Transition Contributes to Endothelial Dysfunction in Pulmonary Arterial Hypertension. *Am. J. Pathol.* 185, 1850–1858. doi:10.1016/j.ajpath.2015.03.019

Jiang, Y., Zhou, X., Hu, R., and Dai, A. (2018). TGF-β1-induced SMAD2/3/4 Activation Promotes RELM-β Transcription to Modulate the Endothelium-Mesenchymal Transition in Human Endothelial Cells. *Int. J. Biochem. Cel Biol.* 105, 52–60. doi:10.1016/j.biocel.2018.08.005

Kim, J. K., Park, J. H., Ku, H. J., Kim, S. H., Lim, Y. J., Park, J. W., et al. (2018). Naringin Protects Acrolein-Induced Pulmonary Injuries through Modulating Apoptotic Signaling and Inflammation Signaling Pathways in Mice. *J. Nutr. Biochem.* 59, 10–16. doi:10.1016/j.jnutbio.2018.05.012

Leopold, J. A., and Maron, B. A. (2016). Molecular Mechanisms of Pulmonary Vascular Remodeling in Pulmonary Arterial Hypertension. *Int. J. Mol. Sci.* 17, 761. doi:10.3390/ijms17050761

Ranchoux, B., Antigny, F., Rucker-martin, C., Hautefort, A., Péchoux, C., Bogaard, H. J., et al. (2015). Endothelial-to-Mesenchymal Transition in Pulmonary Hypertension. *Circulation* 131, 1006–1018. doi:10.1161/circulationaha.114.008750

Sabbineni, H., Verma, A., and Somanath, P. R. (2018). Isoform-specific Effects of Transforming Growth Factor β on Endothelial-To-Mesenchymal Transition. *J. Cel Physiol* 233, 8418–8428. doi:10.1002/jcp.26801

Sakao, S., Tatsumi, K., and Voelkel, N. F. (2009). Endothelial Cells and Pulmonary Arterial Hypertension: Apoptosis, Proliferation, Interaction and Transdifferentiation. *Respir. Res.* 10, 95. doi:10.1186/1465-9921-10-95

Shu, Y., Liu, Y., Li, X., Cao, L., Yuan, X., Li, W., et al. (2016). Aspirin-Triggered Resolvin D1 Inhibits TGF-B1-Induced EndMT through Increasing the Expression of Smad7 and Is Closely Related to Oxidative Stress. *Biomolecules Ther.* 24, 132–139. doi:10.4062/biomolther.2015.088

Suzuki, T., Carrier, E. J., Talati, M. H., Rathinasabapathy, A., Chen, X., Nishimura, R., et al. (2018). Isolation and Characterization of Endothelial-To-Mesenchymal Transition Cells in Pulmonary Arterial Hypertension. *Am. J. Physiology-Lung Cell Mol. Physiol.* 314, L118–L126. doi:10.1152/ajplung.00296.2017

Wang, D.-M., Yang, Y.-J., Zhang, L., Zhang, X., Guan, F.-F., and Zhang, L.-F. (2013). Naringin Enhances CaMKII Activity and Improves Long-Term Memory in a Mouse Model of Alzheimer's Disease. *Int. J. Mol. Sci.* 14, 5576–5586. doi:10.3390/ijms14035576

Willis, B. C., and Borok, Z. (2007). TGF-β-induced EMT: Mechanisms and Implications for Fibrotic Lung Diseasefibrotic Lung Disease. *Am. J. Physiology-Lung Cell Mol. Physiol.* 293, L525–L534. doi:10.1152/ajplung.00163.2007

Wu, Q. Q., Xiao, Y., Jiang, X. H., Yuan, Y., Yang, Z., Chang, W., et al. (2017). Evodiamine Attenuates TGF-Beta1-Induced Fibroblast Activation and Endothelial to Mesenchymal Transition. *Mol. Cel Biochem* 430, 1–2. doi:10.1007/s11010-017-2956-6

Wu, Y., Cai, C., Yang, L., Xiang, Y., Zhao, H., and Zeng, C. (2020). Inhibitory Effects of Formononetin on the Monocrotaline induced Pulmonary Arterial Hypertension in Rats. *Mol. Med. Rep.* 21, 1192–1200. doi:10.3892/mmr.2020.10911

Xiong, J. (2015). To Be EndMT or Not to Be, that Is the Question in Pulmonary Hypertension. *Protein Cell* 6, 547–550. doi:10.1007/s13238-015-0183-z

Zhang, H., Lin, Y., Ma, Y., Zhang, J., Wang, C., and Zhang, H. (2019). Protective Effect of Hydrogen Sulfide on Monocrotaline induced Pulmonary Arterial Hypertension via Inhibition of the Endothelial Mesenchymal Transition. *Int. J. Mol. Med.* 44, 2091–2102. doi:10.3892/ijmm.2019.4359

Zhang, Y.-S., Wang, F., Cui, S.-X., and Qu, X.-J. (2018). Natural Dietary Compound Naringin Prevents Azoxymethane/dextran Sodium Sulfate-Induced Chronic Colorectal Inflammation and Carcinogenesis in Mice. *Cancer Biol. Ther.* 19, 735–744. doi:10.1080/15384047.2018.1453971

Zhao, H., Liu, M., Liu, H., Suo, R., and Lu, C. (2020). Naringin Protects Endothelial Cells from Apoptosis and Inflammation by Regulating the Hippo-YAP Pathwayflammation by Regulating the Hippo-YAP Pathway. *Biosci. Rep.* 40, BSR20193431. doi:10.1042/bsr20193431

Zhou, C., Lai, Y., Huang, P., Xie, L., Lin, H., Zhou, Z., et al. (2019). Naringin Attenuates Alcoholic Liver Injury by Reducing Lipid Accumulation and Oxidative Stress. *Life Sci.* 216, 305–312. doi:10.1016/j.lfs.2018.07.031

Zong, J., Jiang, J., Shi, P., Liu, J., Wang, W., Li, B., et al. (2020). Fatty Acid Extracts Facilitate Cutaneous Wound Healing through Activating AKT, ERK, and TGF-β/Smad3 Signaling and Promoting Angiogenesis. *Am. J. Transl Res.* 12, 478–492.

Conflict of Interest: The authors declare that the research was conducted in the absence of any commercial or financial relationships that could be construed as a potential conflict of interest.

frontiers in Pharmacology

MINI REVIEW
published: 26 July 2021
doi: 10.3389/fphar.2021.724405

Association Between SGLT2is and Cardiovascular and Respiratory Diseases: A Meta-Analysis of Large Trials

Dao-Gen Yin[1], *Mei Qiu*[2]* *and Xue-Yan Duan*[1]*

[1]Center of Community Health Service Management, Shenzhen Longhua District Central Hospital, Shenzhen, China, [2]Department of General Medicine, Shenzhen Longhua District Central Hospital, Shenzhen, China

The association between sodium-glucose cotransporter 2 inhibitors (SGLT2is) and various cardiovascular and respiratory diseases is unestablished. This meta-analysis aimed to explore whether use of SGLT2is is significantly associated with the occurrences of 80 types of cardiovascular diseases and 55 types of respiratory diseases. Large randomized trials of SGLT2is were included in analysis. Meta-analysis was conducted to synthesize risk ratio (RR) and 95% confidence interval (CI). Nine large trials were included in analysis. Compared to placebo, SGLT2is were associated with the reduced risks of 9 types of cardiovascular diseases (e.g., atrial fibrillation [RR 0.78, 95% CI 0.67-0.91], bradycardia [RR 0.60, 95% CI 0.40-0.89], and hypertensive emergency [RR 0.29, 95% CI 0.12-0.72]) and 11 types of respiratory diseases (e.g., chronic obstructive pulmonary disease [RR 0.77, 95% CI 0.61-0.97], asthma [RR 0.57, 95% CI 0.35-0.95], and sleep apnoea syndrome [RR 0.36, 95% CI 0.15-0.87]). The results of random-effects meta-analysis were similar with those of fixed-effects meta-analysis. No heterogeneity or only little heterogeneity was found in most meta-analyses. No publication bias was observed in most of the meta-analyses conducted in this study. SGLT2is were not significantly associated with the other 115 cardiovascular and respiratory diseases. SGLT2is are associated with the reduced risks of 9 types of cardiovascular diseases (e.g., atrial fibrillation, bradycardia, and hypertensive emergency) and 11 types of respiratory diseases (e.g., chronic obstructive pulmonary disease, asthma, and sleep apnoea syndrome). This proposes the potential of SGLT2is to be used for prevention of these cardiovascular and respiratory diseases.

Keywords: SGLT2is, atrial fibrillation, bradycardia, hypertensive emergency, chronic obstructive pulmonary disease, asthma, sleep apnoea syndrome

Abbreviations: CI, confidence interval; CENTRAL, cochrane central register of controlled trials; PRISMA, preferred reporting items for systematic reviews and meta-analyses; RR, risk ratio; SAEs, serious adverse events; SGLT2is, sodium-glucose cotransporter 2 inhibitors.

OPEN ACCESS

Edited by:
Xiao-Jian Wang,
Fuwai Hospital (CAS) and Peking Union Medical College, China

Reviewed by:
Atsushi Tanaka,
Saga University, Japan
Yongyi Bai,
Chinese PLA General Hospital, China

***Correspondence:**
Mei Qiu
13798214835@sina.cn
Xue-Yan Duan
2872763957@qq.com

Specialty section:
This article was submitted to Respiratory Pharmacology, a section of the journal Frontiers in Pharmacology

Received: *13 June 2021*
Accepted: *15 July 2021*
Published: *26 July 2021*

Citation:
Yin D-G, Qiu M and Duan X-Y (2021) Association Between SGLT2is and Cardiovascular and Respiratory Diseases: A Meta-Analysis of Large Trials. Front. Pharmacol. 12:724405. doi: 10.3389/fphar.2021.724405

INTRODUCTION

Sodium-glucose cotransporter 2 inhibitors (SGLT2is) have been confirmed, by large cardiovascular outcome trials, to have the obvious efficacy in reducing arteriosclerotic cardiovascular events and heart failure events. However, the impact of this drug class on other cardiovascular diseases such as arrhythmia, hypertensive emergency, and varicose vein is not established. Meanwhile, relevant animal studies (Park et al., 2019; Chowdhury et al., 2020; Lin et al., 2020) have revealed the protective effects of SGLT2is against some respiratory diseases, whereas these benefits of SGLT2is have not been confirmed by large clinical trials.

Although there are no large randomized trials which have aimed to assess the impact of SGLT2is on the occurrences of various cardiovascular and respiratory diseases, those trials focusing on the cardiorenal endpoints with SGLT2is reported in detail the occurrences of various serious adverse events (SAEs), which included the occurrences of various cardiovascular and respiratory diseases. These data of SAEs make it possible to evaluate the association between use of SGLT2is and the occurrences of various cardiovascular and respiratory diseases.

However, due to the low incidences of most SAEs in cardiorenal outcome trials of SGLT2is, individual trials are not powered to draw a definitive conclusion on whether use of SGLT2is significantly affects the incidences of various cardiovascular and respiratory SAEs. Thus, we intended to, based on the SAEs data from the large cardiorenal outcome trials of SGLT2is, conduct a meta-analysis to explore whether use of SGLT2is is significantly associated with the occurrences of various cardiovascular and respiratory diseases.

METHODS

This study is reported according to the Preferred Reporting Items for Systematic Reviews and Meta-Analyses (PRISMA) statement (Moher et al., 2009). We searched Embase, Cochrane Central Register of Controlled Trials (CENTRAL), and PubMed, to obtain relevant studies published before April 7th, 2021. The search terms included but were not limited to "SGLT2 inhibitors," "Empagliflozin," "Dapagliflozin," "Canagliflozin," "Ertugliflozin", and "Trial." In this meta-analysis we included those large randomized trials that compared any SGLT2i with placebo. We excluded those trials assessing sotagliflozin because it also inhibits SGLT1 besides SGLT2, and excluded those trials in which there was at least one study group with less than one thousand participants for fear of small-study effects. Different doses of SGLT2is were not separately considered in this study. Included trials were evaluated for quality according to the Cochrane risk of bias assessment tool (Higgins et al., 2011). SAEs of interest for this study consisted of 80 kinds of cardiovascular disorders (detailed in **Supplementary Table S1**) and 55 respiratory disorders (detailed in **Supplementary Table S2**). The data regarding various SAEs of interest were extracted from the ClinicalTrials.gov website or included articles. Two authors independently conducted study selection, quality assessment, and data extraction; and all the inconsistencies they encountered were solved by a third author's arbitration.

The numbers of patients developing SAEs of interest and those of all randomly assigned patients in each group were used to perform meta-analysis to derive pooled risk ratios (RRs) and 95% confidence intervals (CIs). We conducted meta-analysis respectively using the fixed-effects model with the inverse variance method and the random-effects model with the method of DerSimonian & Laird (DerSimonian and Kacker, 2007), to evaluate the robustness of meta-analysis results. The magnitude of heterogeneity across studies was reflected by I^2 statistic. We detected publication bias by drawing funnel plots and conducting Egger test (Egger et al., 1997). $p < 0.05$ denotes statistical significance. All statistical analyses were implemented in the Stata software (version 16.0).

RESULTS

After study selection (**Supplementary Figure S1 in Supplementary Appendix S1**), we finally included nine large trials (Zinman et al., 2015; Neal et al., 2017; McMurray et al., 2019; Perkovic et al., 2019; Wiviott et al., 2019; Cannon et al., 2020; Heerspink et al., 2020; Packer et al., 2020) for meta-analysis. Included trials consisted of six trials enrolling patients with type 2 diabetes (i.e., CREDENCE (Perkovic et al., 2019), CANVAS (Neal et al., 2017), CANVAS-R (Neal et al., 2017), DECLARE-TIMI 58 (Wiviott et al., 2019), EMPA-REG OUTCOME (Zinman et al., 2015), and VERTIS CV (Cannon et al., 2020)), two trials enrolling patients with heart failure (i.e., EMPEROR-Reduced (Packer et al., 2020), and DAPA-HF (McMurray et al., 2019)), and one trial enrolling patients with chronic kidney disease (i.e., DAPA-CKD (Heerspink et al., 2020)). Included trials involved a total of 33,124 participants taking SGLT2is and 26,568 participants taking placebo, and all the trials were with low risk of bias (**Supplementary Figure S2 in Supplementary Appendix S1**).

Compared to placebo, SGLT2is were associated with the reduced risks of atrial fibrillation (RR 0.78, 95% CI 0.67–0.91; $I^2 = 0$; $P_{effect} = 0.002$), bradycardia (RR 0.60, 95% CI 0.40–0.89; $I^2 = 0$; $P_{effect} = 0.012$), cardiac failure (RR 0.74, 95% CI 0.68–0.80; $I^2 = 0$; $P_{effect} < 0.001$), cardiac failure acute (RR 0.68, 95% CI 0.53–0.87; $I^2 = 0$; $P_{effect} = 0.002$), cardiac failure chronic (RR 0.72, 95% CI 0.55–0.95; $I^2 = 0$; $P_{effect} = 0.021$), cardiac failure congestive (RR 0.74, 95% CI 0.65–0.85; $I^2 = 0$; $P_{effect} < 0.001$), hypertension (RR 0.67, 95% CI 0.49–0.93; $I^2 = 20.9\%$; $P_{effect} = 0.015$), hypertensive emergency (RR 0.29, 95% CI 0.12–0.72; $I^2 = 0$; $P_{effect} = 0.007$), and varicose vein (RR 0.30, 95% CI 0.09–0.99; $I^2 = 0$; $P_{effect} = 0.048$) (**Figure 1**). SGLT2is were not significantly associated with the risks of 71 other cardiovascular diseases (**Supplementary Table S1**). The detailed results of meta-analysis of SGLT2is and 80 cardiovascular diseases are provided in **Supplementary Figures S3–S82 in Supplementary Appendix S1**), which suggested that the results of random-effects meta-analysis were similar with those of fixed-effects meta-analysis.

Compared to placebo, SGLT2is were associated with the reduced risks of acute pulmonary oedema (RR 0.52, 95% CI 0.32–0.86; $I^2 = 7.5\%$; $P_{effect} = 0.011$), asthma (RR 0.57, 95% CI 0.35–0.95; $I^2 = 0$; $P_{effect} = 0.030$), bronchitis (RR 0.65, 95% CI 0.47–0.90; $I^2 = 18.3\%$; $P_{effect} =$

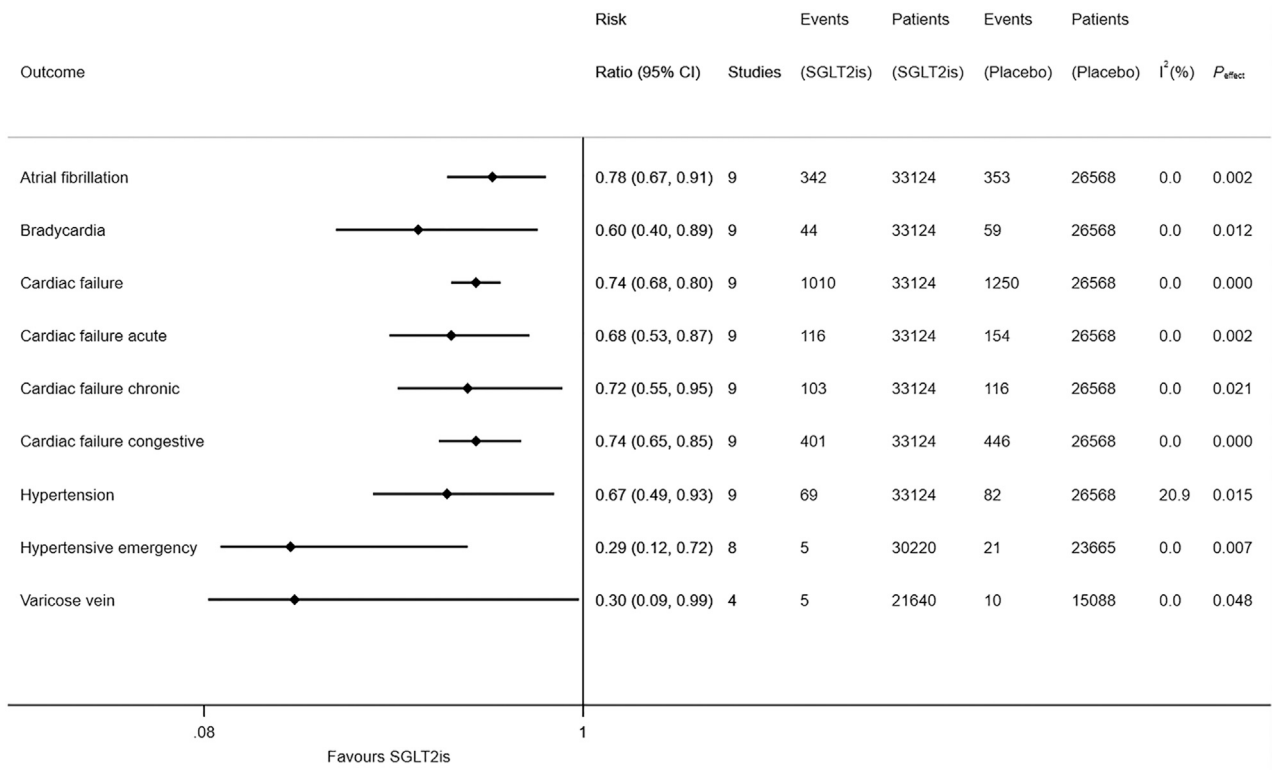

FIGURE 1 | Meta-analysis of SGLT2is and nine types of cardiovascular diseases.

0.009), chronic obstructive pulmonary disease (RR 0.77, 95% CI 0.61–0.97; $I^2 = 0$; $P_{effect} = 0.029$), non-small cell lung cancer (RR 0.27, 95% CI 0.07–0.99; $I^2 = 0$; $P_{effect} = 0.048$), pleural effusion (RR 0.56, 95% CI 0.34–0.92; $I^2 = 0$; $P_{effect} = 0.023$), pneumonia (RR 0.84, 95% CI 0.75–0.93; $I^2 = 0$; $P_{effect} = 0.001$), pulmonary mass (RR 0.36, 95% CI 0.13–0.97; $I^2 = 0$; $P_{effect} = 0.043$), pulmonary oedema (RR 0.40, 95% CI 0.25–0.65; $I^2 = 0$; $P_{effect} < 0.001$), respiratory tract infection (RR 0.42, 95% CI 0.23–0.75; $I^2 = 0$; $P_{effect} = 0.003$), and sleep apnoea syndrome (RR 0.36, 95% CI 0.15–0.87; $I^2 = 0$; $P_{effect} = 0.023$) (**Figure 2**). SGLT2is were not significantly associated with the risks of 44 other respiratory diseases (**Supplementary Table S2**). The detailed results of meta-analysis of SGLT2is and 55 respiratory diseases are provided in **Supplementary Figures S83–S137 in Supplementary Appendix S1**), which suggested that the results of random-effects meta-analysis were similar with those of fixed-effects meta-analysis.

The results of detection of publication bias are detailed in **Supplementary Figures S138–S272 in Supplementary Appendix S1**), suggesting that most of the meta-analyses conducted in this study had no publication bias since most of the *p* values from Egger test were greater than 0.05.

DISCUSSION

This is the first meta-analysis that assessed in detail the association between use of SGLT2is and the occurrence of various cardiovascular and respiratory diseases. Accordingly, it revealed that use of SGLT2is was associated with the reduced risks of nine types of cardiovascular diseases (i.e., atrial fibrillation, bradycardia, cardiac failure, cardiac failure acute, cardiac failure chronic, cardiac failure congestive, hypertension, hypertensive emergency, and varicose vein) and 11 types of respiratory diseases (i.e., acute pulmonary oedema, asthma, bronchitis, chronic obstructive pulmonary disease, non-small cell lung cancer, pleural effusion, pneumonia, pulmonary mass, pulmonary oedema, respiratory tract infection, and sleep apnoea syndrome).

Three previous meta-analyses (Li et al., 2021a; Li et al., 2021b; Zhou et al., 2021) identified SGLT2is with the reduced risk of atrial fibrillation, whereas they failed to explore the association between SGLT2is and bradycardia. Our meta-analysis further revealed the association between use of SGLT2is and a lower risk of bradycardia besides that of atrial fibrillation. Prior studies (Alqudsi et al., 2021; Hunter et al., 2021; Kario et al., 2021) showed the antihypertension effects of SGLT2is, while our meta-analysis further revealed SGLT2is with the lower incidences of hypertensive emergency and varicose vein besides hypertension. Another previous meta-analysis (Qiu et al., 2021) revealed the significant association between use of SGLT2is and the lower risks of three types of noninfectious respiratory disorders (i.e., asthma, acute pulmonary oedema, and sleep apnoea syndrome), whereas that meta-analysis (Qiu et al., 2021) failed to explore the association between SGLT2is and infectious respiratory diseases, and also failed to observe the significant association between SGLT2is and chronic obstructive pulmonary disease because it failed to incorporate

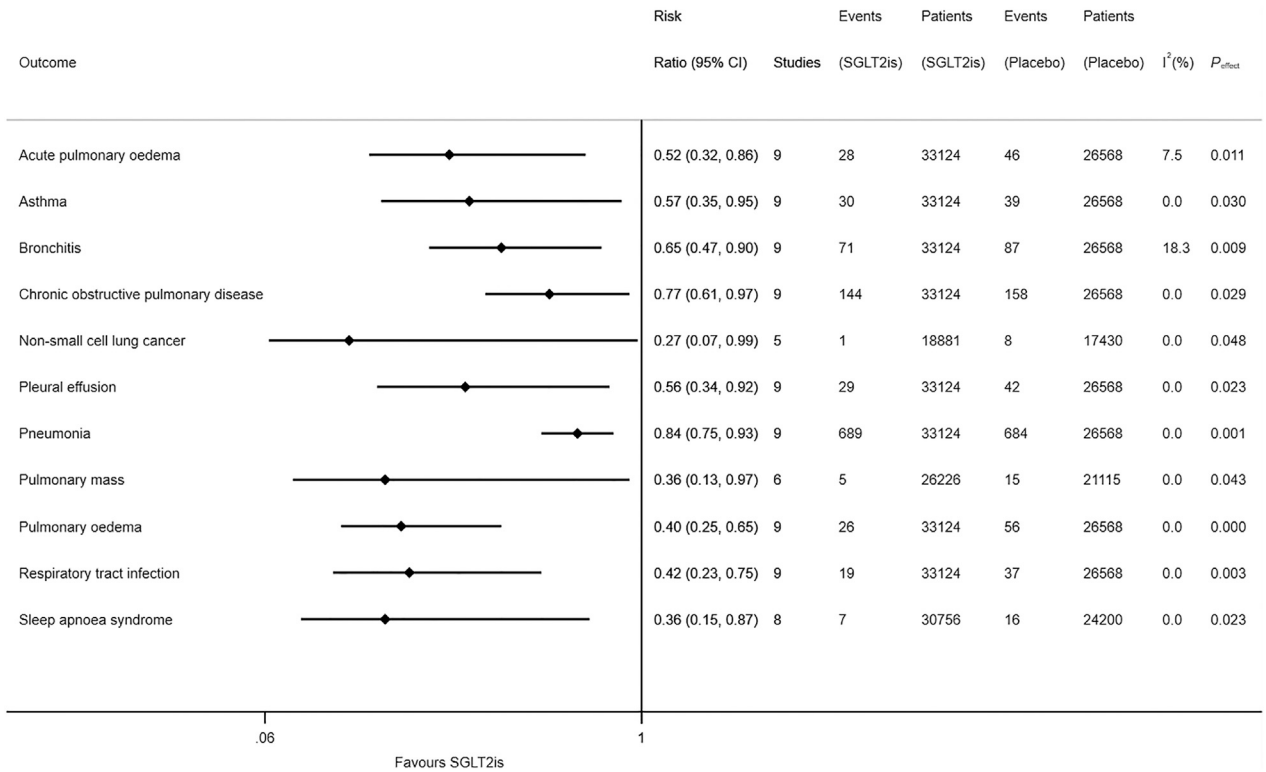

FIGURE 2 | Meta-analysis of SGLT2is and 11 types of respiratory diseases.

the data from the two trials of VERTIS CV (Cannon et al., 2020) and EMPEROR-Reduced (Packer et al., 2020), as was stated in the Limitations section of that article (Qiu et al., 2021). In contrast, our meta-analysis additionally revealed the significant association between use of SGLT2is and the lower occurrences of three types of infectious respiratory disorders (i.e., bronchitis, pneumonia, and respiratory tract infection) and four types of noninfectious respiratory disorders (i.e., chronic obstructive pulmonary disease, non-small cell lung cancer, pleural effusion, and pulmonary mass).

In this meta-analysis SGLT2is were observed with the reduced risks of cardiac failure, cardiac failure acute, cardiac failure chronic, cardiac failure congestive, acute pulmonary oedema, and pulmonary oedema; which is consistent with the benefits of SGLT2is on heart failure endpoints observed in two heart failure trials (McMurray et al., 2019; Packer et al., 2020). The mechanisms for the anti-heart failure activity of SGLT2is are to improve myocardial efficiency and mitochondrial function, and to reduce inflammation, oxidative stress, fibrosis, and sympathetic nervous system activation (Zelniker and Braunwald, 2020). In this meta-analysis SGLT2is were observed with the reduced risks of infectious respiratory disorders, which might be associated with the glucose-lowering efficacy of SGLT2is. However, the mechanisms for the reductions SGLT2is led to in the risks of noninfectious respiratory disorders are required to be further investigated.

The strengths of this study include that the original studies included were large trials with low risk of bias and that no heterogeneity or only little heterogeneity was found in most of the meta-analyses conducted in this study. Moreover, Egger test suggested that most meta-analyses conducted in this study were not with publication bias, and the similarity between random-effects results and fixed-effects results suggested the robustness of meta-analysis results. Conversely, the main limitation of this study was that SAEs of interest for this meta-analysis were not events of special interest in the included trials. Therefore, the association between use of SGLT2is and risk reductions of some cardiovascular and pulmonary diseases revealed in this study does not definitely represent for the causal relationship. Instead, the causal relationship needs to be further confirmed. Moreover, patients the included trials enrolled were not susceptible to most of the cardiovascular and respiratory diseases assessed in this meta-analysis, which led to the low occurrences of these diseases. Thus, prospective trials enrolling patients who are susceptible to cardiovascular and respiratory diseases are warranted to confirm the protective effects of SGLT2is against cardiopulmonary disorders and whether these effects are a class effect or drug-specific effects.

In conclusion, SGLT2is are associated with the reduced risks of nine types of cardiovascular diseases (e.g., atrial fibrillation, bradycardia, and hypertensive emergency) and 11 types of respiratory diseases (e.g., chronic obstructive pulmonary disease, asthma, and sleep apnoea syndrome). This proposes the potential of SGLT2is to be used for prevention of these cardiovascular and respiratory diseases. However, due to the low incidences of these diseases among included trials, these positive findings are needed to be confirmed by prospective trials enrolling susceptible individuals.

AUTHOR CONTRIBUTIONS

Design: MQ. Conduct/data collection: DY, MQ, and XD. Analysis: DY and XD. Writing manuscript: DY and MQ. Review: XD and MQ.

SUPPLEMENTARY MATERIAL

The Supplementary Material for this article can be found online at: https://www.frontiersin.org/articles/10.3389/fphar.2021.724405/full#supplementary-material

REFERENCES

Alqudsi, M., Velez, J. C. Q., and Navarrete, J. (2021). Medical management of resistant hypertension: the role of sodium-glucose cotransporter 2 inhibitors (SGLT2i). *CURR. OPIN. CARDIOL.* 36, 420–428. doi:10.1097/hco.0000000000000865

Cannon, C. P., Pratley, R., Dagogo-Jack, S., Mancuso, J., Huyck, S., Masiukiewicz, U., et al. (2020). Cardiovascular Outcomes with Ertugliflozin in Type 2 Diabetes. *N. Engl. J. Med.* 383, 1425–1435. doi:10.1056/nejmoa2004967

Chowdhury, B., Luu, A. Z., Luu, V. Z., Kabir, M. G., Pan, Y., Teoh, H., et al. (2020). The SGLT2 inhibitor empagliflozin reduces mortality and prevents progression in experimental pulmonary hypertension. *Biochem. Biophysical Res. Commun.* 524, 50–56. doi:10.1016/j.bbrc.2020.01.015

DerSimonian, R., and Kacker, R. (2007). Random-effects model for meta-analysis of clinical trials: an update. *Contemp. Clin. Trials* 28, 105–114. doi:10.1016/j.cct.2006.04.004

Egger, M., Smith, G. D., Schneider, M., and Minder, C. (1997). Bias in meta-analysis detected by a simple, graphical test. *BMJ* 315, 629–634. doi:10.1136/bmj.315.7109.629

Heerspink, H. J. L., Stefánsson, B. V., Correa-Rotter, R., Chertow, G. M., Greene, T., Hou, F.-F., et al. (2020). Dapagliflozin in Patients with Chronic Kidney Disease. *N. Engl. J. Med.* 383, 1436–1446. doi:10.1056/nejmoa2024816

Higgins, J. P. T., Altman, D. G., Gotzsche, P. C., Jüni, P., Moher, D., Oxman, A. D., et al. (2011). The Cochrane Collaboration's tool for assessing risk of bias in randomised trials. *BMJ* 343, d5928, 2011 . d5928. doi:10.1136/bmj.d5928

Hunter, P. G., Chapman, F. A., and Dhaun, N. (2021). Hypertension: Current trends and future perspectives. *Br. J. Clin. Pharmacol.* doi:10.1111/bcp.14825

Kario, K., Ferdinand, K. C., and Vongpatanasin, W. (2021). Are SGLT2 Inhibitors New Hypertension Drugs?. *CIRCULATION* 143, 1750–1753. doi:10.1161/circulationaha.121.053709

Li, D., Liu, Y., Hidru, T. H., Yang, X., Wang, Y., Chen, C., et al. (2021). Protective Effects of Sodium-Glucose Transporter 2 Inhibitors on Atrial Fibrillation and Atrial Flutter: A Systematic Review and Meta- Analysis of Randomized Placebo-Controlled Trials. *Front. Endocrinol. (Lausanne)* 12, 619586. doi:10.3389/fendo.2021.619586

Li, H. L., Lip, G. H., Feng, Q., Fei, Y., Tse, Y. K., Wu, M. Z., et al. (2021). Sodium-glucose cotransporter 2 inhibitors (SGLT2i) and cardiac arrhythmias: a systematic review and meta-analysis. *CARDIOVASC. DIABETOL.* 20, 100. doi:10.1186/s12933-021-01293-8

Lin, F., Song, C., Zeng, Y., Li, Y., Li, H., Liu, B., et al. (2020). Canagliflozin alleviates LPS-induced acute lung injury by modulating alveolar macrophage polarization. *Int. Immunopharmacology* 88, 106969. doi:10.1016/j.intimp.2020.106969

McMurray, J. J. V., Solomon, S. D., Inzucchi, S. E., Køber, L., Kosiborod, M. N., Martinez, F. A., et al. (2019). Dapagliflozin in Patients with Heart Failure and Reduced Ejection Fraction. *N. Engl. J. Med.* 381, 1995–2008. doi:10.1056/NEJMoa1911303

Moher, D., Liberati, A., Tetzlaff, J., and Altman, D. G. (2009). Preferred reporting items for systematic reviews and meta-analyses: the PRISMA statement. *PLOS MED.* 6, e1000097. doi:10.1371/journal.pmed.1000097

Neal, B., Perkovic, V., Mahaffey, K. W., de Zeeuw, D., Fulcher, G., Erondu, N., et al. (2017). Canagliflozin and Cardiovascular and Renal Events in Type 2 Diabetes. *N. Engl. J. Med.* 377, 644–657. doi:10.1056/nejmoa1611925

Packer, M., Anker, S. D., Butler, J., Filippatos, G., Pocock, S. J., Carson, P., et al. (2020). Cardiovascular and Renal Outcomes with Empagliflozin in Heart Failure. *N. Engl. J. Med.* 383, 1413–1424. doi:10.1056/NEJMoa2022190

Park, H. J., Han, H., Oh, E. Y., Kim, S. R., Park, K. H., Lee, J. H., et al. (2019). Empagliflozin and Dulaglutide are Effective against Obesity-induced Airway Hyperresponsiveness and Fibrosis in A Murine Model. *Sci. Rep.* 9, 15601. doi:10.1038/s41598-019-51648-1

Perkovic, V., Jardine, M. J., Neal, B., Bompoint, S., Heerspink, H. J. L., Charytan, D. M., et al. (2019). Canagliflozin and Renal Outcomes in Type 2 Diabetes and Nephropathy. *N. Engl. J. Med.* 380, 2295–2306. doi:10.1056/nejmoa1811744

Qiu, M., Ding, L. L., Zhan, Z. L., and Liu, S. Y. (2021). Use of SGLT2 inhibitors and occurrence of noninfectious respiratory disorders: a meta-analysis of large randomized trials of SGLT2 inhibitors. *ENDOCRINE*. 73, 31–36. doi:10.37766/inplasy2021.1.0102

Wiviott, S. D., Raz, I., Bonaca, M. P., Mosenzon, O., Kato, E. T., Cahn, A., et al. (2019). Dapagliflozin and Cardiovascular Outcomes in Type 2 Diabetes. *N. Engl. J. Med.* 380, 347–357. doi:10.1056/nejmoa1812389

Zelniker, T. A., and Braunwald, E. (2020). Mechanisms of Cardiorenal Effects of Sodium-Glucose Cotransporter 2 Inhibitors. *J. Am. Coll. Cardiol.* 75, 422–434. doi:10.1016/j.jacc.2019.11.031

Zhou, Z., Jardine, M. J., Li, Q., Neuen, B. L., Cannon, C. P., de Zeeuw, D., et al. (2021). Effect of SGLT2 Inhibitors on Stroke and Atrial Fibrillation in Diabetic Kidney Disease: Results From the CREDENCE Trial and Meta-Analysis. *STROKE* 52, 1545–1556. doi:10.1161/STROKEAHA.120.031623

Zinman, B., Wanner, C., Lachin, J. M., Fitchett, D., Bluhmki, E., Hantel, S., et al. (2015). Empagliflozin, Cardiovascular Outcomes, and Mortality in Type 2 Diabetes. *N. Engl. J. Med.* 373, 2117–2128. doi:10.1056/nejmoa1504720

Conflict of Interest: The authors declare that the research was conducted in the absence of any commercial or financial relationships that could be construed as a potential conflict of interest.

Publisher's Note: All claims expressed in this article are solely those of the authors and do not necessarily represent those of their affiliated organizations, or those of the publisher, the editors and the reviewers. Any product that may be evaluated in this article, or claim that may be made by its manufacturer, is not guaranteed or endorsed by the publisher.

frontiers in Pharmacology

ORIGINAL RESEARCH
published: 01 October 2021
doi: 10.3389/fphar.2021.691405

Novel Pyrazolo[3,4-b] Pyridine Derivative (HLQ2g) Attenuates Hypoxic Pulmonary Hypertension via Restoring cGKI Expression and BMP Signaling Pathway

*Lijun Li[1†], Minghui Yin[1†], Liqing Hu[2†], Xiaoting Tian[3], Xiangrong He[1], Congke Zhao[1], Ying Li[4], Qianbin Li[2] and Xiaohui Li[1,5]**

[1]Department of Pharmacology, Xiangya School of Pharmaceutical Sciences, Central South University, Changsha, China, [2]Department of Medicinal Chemistry, Xiangya School of Pharmaceutical Sciences, Central South University, Changsha, China, [3]Department of Pharmacy, Henan Provincial People's Hospital, People's Hospital of Zhengzhou University, Zhengzhou, China, [4]Department of Health Management, The Third Xiangya Hospital of Central South University, Changsha, China, [5]Hunan Key Laboratory for Bioanalysis of Complex Matrix Samples, Changsha, China

Pulmonary hypertension (PH) is an extremely serious cardiopulmonary disease, finally leading to progressive right ventricular failure and death. Our previous studies have nominated HLQ2g, a pyrazolo[3,4-b] pyridine derivative stimulating soluble guanylate cyclase (sGC), as a new candidate for the treatment of PH, but the specific mechanism is still not clear. The PH model induced by hypoxia was established in rats. Right ventricular systolic pressure (RVSP) was assessed by jugular vein catheterization. RV weight was the index to evaluate RV hypertrophy. The protein levels of cGMP-dependent protein kinase type I (cGKI), bone morphogenetic protein receptor 2 (BMPR2), phosphorylated Smad1/5/8 (p-Smad1/5/8), and inhibitor of differention 1 (Id1) in pulmonary artery and human pulmonary artery smooth muscle cells (HPASMCs) were determined by western blotting. Cell proliferation and migration were evaluated. In the whole experiment, the first clinically available sGC stimulator Riociguat was used as the reference. In hypoxic PH rat model, elevated RVSP and RV hypertrophy were significantly reduced by HLQ2g treatment. Both Riociguat and HLQ2g attenuated vascular remodeling accompanied with up-regulated cGKI expression and BMP signaling pathway, which was characterized by elevated expression of BMPR2, p-Smad1/5/8, and Id1 in HPH rats. In addition, HLQ2g inhibited proliferation and migration of HPASMCs induced by hypoxia and platelet-derived growth factor (PDGF), restored BMPR2 signaling, which was recalled by Rp-8-Br-PET-cGMPS, the inhibitor of cGKI. In summary, the novel pyrazolo[3,4-b] pyridine derivative HLQ2g can alleviate HPH progression by up-regulating cGKI protein and BMP signaling pathway.

Keywords: pulmonary hypertension, hypoxia, cGKI, BMP signaling pathway, pulmonary artery smooth muscle cells

OPEN ACCESS

Edited by:
Heike Wulff,
University of California, Davis, United States

Reviewed by:
Haiyang Tang,
University of Arizona, United States
Wei Huang,
First Affiliated Hospital of Chongqing Medical University, China
Deming Gou,
Shenzhen University, China

****Correspondence:***
Xiaohui Li
xiaohuili@csu.edu.cn

[†]These authors have contributed equally to this work

Specialty section:
This article was submitted to Respiratory Pharmacology, a section of the journal Frontiers in Pharmacology

Received: *06 April 2021*
Accepted: *27 August 2021*
Published: *01 October 2021*

Citation:
Li L, Yin M, Hu L, Tian X, He X, Zhao C, Li Y, Li Q and Li X (2021) Novel Pyrazolo[3,4-b] Pyridine Derivative (HLQ2g) Attenuates Hypoxic Pulmonary Hypertension via Restoring cGKI Expression and BMP Signaling Pathway. Front. Pharmacol. 12:691405. doi: 10.3389/fphar.2021.691405

INTRODUCTION

Pulmonary hypertension (PH) refers to the resting mean pulmonary arterial pressure ≥20 mmHg as evaluated by right heart catheterization, which has always been an important clinical challenge due to its high mortality (Simonneau et al., 2019). PH patients have a median survival time of 5–7 years, which is featured by pulmonary vascular system remodeling, resulting in decreased pulmonary arterial compliance and elevated pulmonary vascular resistance (Thenappan et al., 2019). Continuous elevation of pulmonary artery pressure increases right ventricular (RV) afterload, which may consequently lead to right heart failure or even death if left untreated (McLaughlin et al., 2009). In the past few years, considerable clinical trials are commonly confined to controlling symptoms to prolong and improve the patient's life, but PH is still incurable (Spaczynska et al., 2020). Hence, finding new effective drugs remains an urgent issue for the treatment of PH.

Nitric oxide (NO) has been revealed as critical messenger molecule in PH for long history and currently commonly used clinical drugs including Sildenafil, Tadalafil, and Riociguat exhibit therapeutical effects mainly by targeting on NO pathway. It is well known that NO binds to soluble guanylate cyclase (sGC) and increases the formation of cyclic guanosine monophosphate (cGMP) (Friebe et al., 2020). cGMP-dependent protein kinase I (cGKI) is one of the primary mediators of NO/cGMP-triggered signal transduction which is crucial in the regulation of vascular tension (Yang et al., 2013). During the past decades, experimental studies have demonstrated that sGC stimulator bear considerable potential benefits, including preventing or even reversing left ventricular hypertrophy and fibrosis, and reducing ventricular afterload through systemic and pulmonary vasodilation (Armstrong et al., 2018). For example, Riociguat, the first clinically available sGC stimulator, has been approved for PH and non-operable or recurrent/persistent chronic thromboembolic PH (Leuchte et al., 2015). HLQ2g is a new compound from our group, which is modified from the structure of Riociguat, with pyrazolpyridine ring (anti-fibrosis functional group) and pyrimidine ring (stimulating sGC functional group) in its structure. Similar to Riociguat, HLQ2g can regulate sGC/cGMP signaling pathway in PH model (Hu et al., 2020), but the specific mechanism of HLQ2g in the PH treatment remains to be elucidated.

BMPR2 is a serine/threonine membrane receptor. After being activated by bone morphogenetic protein (BMP) ligand, BMPR2 transfers from the cell membrane into the cytoplasm, and activates the phosphorylation of Smad protein in the cytoplasm (mainly Smad1/5/8). Subsequently, the complex formed by phosphorylated Smad1/5/8 (p-Smad1/5/8) with Smad protein, enters the nucleus, and initiates the transcription of downstream genes such as Id protein (Evans et al., 2016). Since 2000, numerous studies have revealed the critical role of BMP signaling pathway in PH. These studies found that BMPR2 gene mutations exist in 70% of patients with hereditary PH and 10–40% of patients with idiopathic PH (Atkinson et al., 2002; Yang et al., 2005). Down-regulation of the BMP signaling pathway is considered to be a key pathological mechanism affecting pulmonary vascular remodeling. Animal experiments have further found that the therapeutic effects of existing PH therapeutic drugs (such as sildenafil, prostacyclin, etc.) are related to the up-regulation of the BMP signaling pathway (Yang et al., 2013). Moreover, FK506 and BMP9 can reverse the development of PH by activating the BMP signaling pathway in animal models (Spiekerkoetter et al., 2013; Long et al., 2015). More importantly, it has been reported that crosstalk between cGKI and BMP signaling pathway are important mechanism hallmarks in PH (Schwappacher et al., 2009).

Therefore, we hypothesized that the novel pyrazolo[3,4-b] pyridine derivative (HLQ2g) could elevate cGMP level by increasing sGC activity, and thus activate cGKI and ultimately up-regulate the BMP signaling pathway. This study aims to reveal the mechanism of HLQ2g in the treatment of PH *in vivo* and *in vitro* and investigate the involvement of cGKI and BMP signaling pathway.

MATERIALS AND METHODS

Animal Experiment

Hunan Normal University Experimental Animal Welfare Ethics Committee and Animal Management and Committee approved all animal experimental protocols. Male healthy Sprague Dawley rats (100–150 g) were from Hunan SJA experimental animal Co., Ltd. (No.: SYXK [Changsha] 2015-0017). All animals were reared in a controlled temperature (18°C–25°C) and humidity (50–60%), and 12-h light/dark cycle with free food and water. After 1 week of adaptive feeding, the rats were weighed, arbitrarily grouped, and numbered. Hypoxia-induced PH rat model was established and assigned into control, Hypoxia, Riociguat, and HLQ2g (CN 2019104923511) groups, with 10 rats in each group. The modeling time was 4 weeks. In the first week, rats in the Hypoxia, Riociguat, and HLQ2g groups were raised in a hypoxia box (oxygen concentration was set at 10%). From the third week, rats in the Riociguat and HLQ2g groups were given by gavage with the dosage of 10 mg/kg/d (Lang et al., 2012) (the solvent was sodium carboxymethyl cellulose, CMC-Na) for 2 weeks. There was no intervention in the control rats.

Hemodynamic Measurements and Morphologic Analyses

After PH modeling, rats were anesthetized by 1% pentobarbital sodium (i.p., 50 mg/kg). A polyethylene catheter was inserted through the right jugular vein to the right atrium to record the RV systolic pressure (RVSP). After that, lung tissue samples were collected. The RV, left ventricle, and interventricular septum (LV + S) were separated and weighed to calculate the mass ratio of RV/(LV + S). The tibia of the hind limbs of rats was removed and the distance was measured with a ruler to calculate the RV/tibial length. The right lower lung was removed and fixed in 4% paraformaldehyde solution, and then for subsequent vascular morphological analysis. The tissue sections were kept at 60°C for 2 h and then in xylene solution for 30 min. Then the sections were put into ethanol solution (100, 95, 70%) successively for 5 min

each time. Next, the samples were washed in phosphate-buffered saline (PBS, Procell, China), for 3 times, 5 min each time. Next, the sections were kept for 5 min in high pressure antigen repair and 20 min in hydrogen peroxide. Hematoxylin-Eosin (HE) staining was used to observe the morphology of blood vessels. Structure remodeling of pulmonary arterioles was observed under light microscope (Nikon, Japan). Pulmonary arterioles with 50–150 μm diameter were arbitrarily observed and analyzed by Image-Pro Plus 6.0. The ratio of media wall thickness (WT%) = (outside diameter-inside diameter)/(outside diameter) × 100.

Cell Culture

Human pulmonary artery smooth muscle cells (HPASMCs, ScienCell, United States) were cultured in high glucose DMEM (Gibco, United States) containing 20% fetal bovine serum (FBS, Biological Industries, Israel) and 1% penicillin/streptomycin (HyClone, United States) in an incubator (5% CO_2, 37°C). Cells at passage 3 to 10 were used for the experiment.

HTRF cGMP Assays

The cGMP accumulation assays in HPASMCs followed standard protocols. Homogeneous time-resolved fluorescence (HTRF) cGMP assay was performed according to the cGMP kits (Cisbio). HPASMCs were resuspended in PBS containing 1 mM PDE-5 inhibitor 3-isobutyl-1-methylxanthine (IBMX) and 0.2% BSA at 1×10^5 cells/ml with or without 10 μM sGC inhibitor 1H-[1,2,4]oxadiazolo [4,3-a] quinoxalin-1-one (ODQ), and allocated into 384-well plates (HTRF®) at 5 μl/well. Test compounds were solubilized to 100 mM in DMSO and serially diluted by the diluent of the cGMP kits to achieve a 2 × stock, which was diluted using 10-fold dilutions to produce a 6-point dose-response curve with a top concentration of 200 μM. Diluted compounds were then transferred to a triplicate set of assay plates (5 μl/well). After 1 hour incubation, 5 μl cGMP-d2 reagent diluted in lysis buffer was added to each well followed by 5 μl europium cryptate reagent. Next, the plates were mounted and incubated for 1 hour before reading on an HTRF® compatible reader (Bio Tek, United States).

Cell Counting Kit-8 Assay

HPASMCs were plated into 96-well plates until the final concentration was 3,000 cells/well. After cell adhesion, HPASMCs were cultured in serum-free medium containing stimulating factors, and allocated into control, platelet-derived growth factor (PDGF) (20 ng/ml), PDGF + Riociguat (1 μM), PDGF + HLQ2g (0.5 μM), PDGF + HLQ2g (1 μM), Hypoxia, Hypoxia + Riociguat (1 μM), Hypoxia + HLQ2g (0.5 μM), Hypoxia + HLQ2g (1 μM) and Hypoxia + HLQ2g (1 μM) + Rp-8-Br-PET-cGMPS (30 μM) groups. HPASMCs in the Hypoxia, Hypoxia + Riociguat (1 μM), Hypoxia + HLQ2g (0.5 μM), Hypoxia + HLQ2g (1 μM) and Hypoxia + HLQ2g (1 μM) + Rp-8-Br-PET-cGMPS (30 μM) groups cultured in hypoxia incubator (3% O_2, 5% CO_2, 37°C) for 24 h, while other groups of cells were cultured in normal incubators for 24 h. Then culture medium was replaced with fresh medium containing 10 μl CCK8 (Dojindo, Japan). After incubation at 37°C for 2 h, the optical density at 450 nm was read using a microplate reader (ThermoFisher, United States). Six replicates were used for each treatment.

5-Ethynyl-2′-Deoxyuridine Assay

HPASMCs were plated into 96-well plates until the final concentration was 5,000 cells/well. After cell adhesion, HPASMCs were cultured in serum-free medium containing stimulating factors, and allocated into control, platelet-derived growth factor (PDGF) (20 ng/ml), PDGF + Riociguat (1 μM), PDGF + HLQ2g (1 μM), Hypoxia, Hypoxia + Riociguat (1 μM) and Hypoxia + HLQ2g (1 μM) groups. HPASMCs in the Hypoxia, Hypoxia + Riociguat (1 μM) and Hypoxia + HLQ2g (1 μM) groups cultured in hypoxia incubator (3% O_2, 5% CO_2, 37°C) for 24 h, while other groups of cells were cultured in normal incubators for 24 h. Then culture medium was replaced with fresh medium containing 10 μM EdU (Beyotime, China). After incubation at 37°C for 3 h, the staining treatment was carried out. Three replicates were used for each treatment.

Scratch Test

Cell scratch test was used to detect HPASMCs migration. In short, a 6-well plate was labeled on the back with evenly distributed horizontal lines at 1 cm interval. Then 5×10^5 cells were plated in each well, and starved overnight until reaching 70–80% confluence. After that, three parallel lines were randomly scratched using a 1 ml pipette. HPASMCs were washed with PBS and cultured in serum-free medium (DMEM, Gibco, United States) containing Riociguat (1 μM) or HLQ2g (1 μM). Then, HPASMCs were cultured in hypoxia incubators (3% O_2, 5% CO_2, 37°C), and photographed at 0 and 24 h after culture. The densitometric quantification was conducted with Image J 1.43 (NIH, United States).

Transwell Assay

HPASMCs were seeded into Transwell chamber. The volume of serum-free medium was 200 μl, and the number of cells in each well was 5×10^4. Cells were assigned into control, Hypoxia, Hypoxia + HLQ2g (1 μM), and Hypoxia + HLQ2g (1 μM) + Rp-8-Br-PET-cGMPS (30 μM) groups. The cells were cultured in the incubator for 24 h and then wiped off with cotton swabs. Then the cells were washed with PBS three times, fixed 30 min with 4% paraformaldehyde, and stained for 15 min with 0.4% crystal violet. Finally, the crystal violet dye was removed. The number of cells passing through the polycarbonate membrane was observed and calculated under Nikon microscope.

Western Blot Analysis

The proteins were isolated from pulmonary arteries or HPASMCs using radio-immunoprecipitation assay buffer (containing 0.1% phenylmethylsulfonyl fluoride), and equal proteins (30 μg) were separated by electrophoresis and moved to polyvinylidene fluoride membranes. Then the membranes were blocked with 1% BSA for 1 h, followed by overnight incubation with primary antibodies against cGKI (CST, United States), BMPR2 (Proteintech, United States), p-Smad1/5/8 (CST, United States), Id1 (Proteintech, United States), PCNA (CST, United States), and β-actin (Proteintech, United States) at

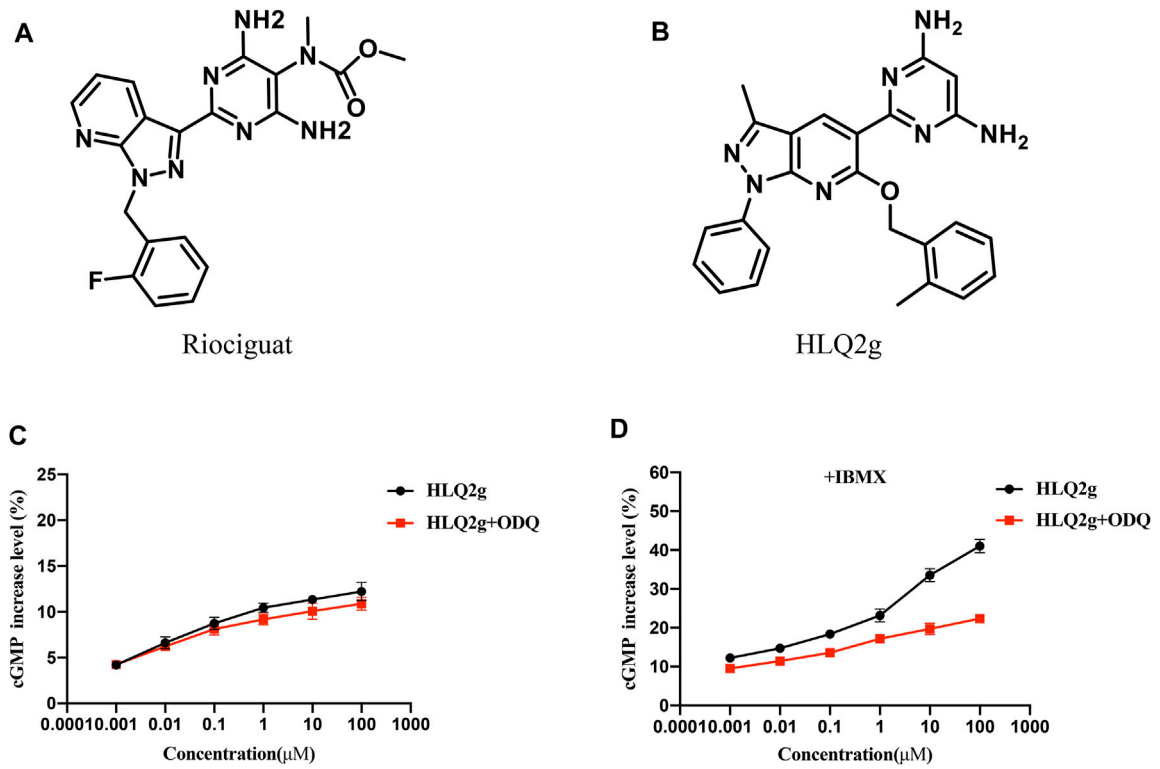

FIGURE 1 | HLQ2g can stimulate sGC and upregulate cGMP. **(A)**: The structure of Riociguat. **(B)**: The structure of HLQ2g. **(C)**: Dose-dependent curve of HLQ2g to elevate the cGMP levels in the absence or presence of 10 μM ODQ in HPASMCs without IBMX, values are the average of three independent experiments. **(D)**: Dose-dependent curve of HLQ2g to elevate the cGMP levels in the absence or presence of 10 μM ODQ in HPASMCs under condition of IBMX (10 μM), values are the average of three independent experiments.

4°C. After that, the membranes were probed with HRP-labeled secondary antibodies (Jackson, United States). The signals of bands were measured using Luminata Creseendo Western HRP Substrate (Millipore) through Molecular Imager ChemiDoc XRS System (Bio-Rad, United States). The protein levels were quantified using Image J 1.43.

Statistical Analysis

Statistical analysis was conducted by SPSS 18.0 (IBM Corp, United States). The results were described as mean ± standard deviation (SD) and analyzed using one-way analysis of variance (ANOVA) followed by Newman-Keuls test for multiple comparisons. $p < 0.05$ was considered significant.

RESULTS

HLQ2g Up-Regulated Intracellular cGMP Level by Stimulating sGC

sGC signal transduction is crucial for vascular tone modulation in PH pathogenesis. Pharmacological stimulation of sGC have intracellular effects by augmenting the formation of cGMP that can be degraded by phosphodiesterase 5 (PDE-5). To verify whether HLQ2g can activate sGC, we use HTRF cGMP assay to evaluate the effect of HLQ2g on cGMP generation in HPASMCs. Firstly, in the absence of IBMX (PDE-5 inhibitor), HLQ2g slightly enhanced intracellular cGMP levels (about 5% increase at 100 μM, **Figure 1C**). The presence or absence of ODQ (sGC inhibitor) had no significant difference on the levels of cGMP (**Figure 1C**). This is mainly due to the rapid cGMP degradation catalyzed by the intracellular PDE-5. Secondly, with the addition of IBMX, we investigated the influence of ODQ on cGMP formation in HPASMCs. Consequently, HLQ2g showed distinct ability to produce cGMP in a significant dose-dependent manner (**Figure 1D**). In addition, the elevated levels of cGMP were clearly reduced after adding ODQ compared with the groups without ODQ (**Figure 1D**). Taken together, these findings suggest that HLQ2g was effective in elevating the intracellular cGMP levels possibly through stimulating sGC.

HLQ2g Reduced RVSP and RV Hypertrophy and Improved Vascular Remodeling in Hypoxia-Induced PH Rat Model

To explore the role of HLQ2g *in vivo*, we established a PH rat model induced by hypoxia. Hypoxia significantly increased RVSP, and the administration of Riociguat and HLQ2g notably inhibited the increase of hypoxia-induced RVSP (**Figures 2A,B**). The RV hypertrophy index (RVHI) in the

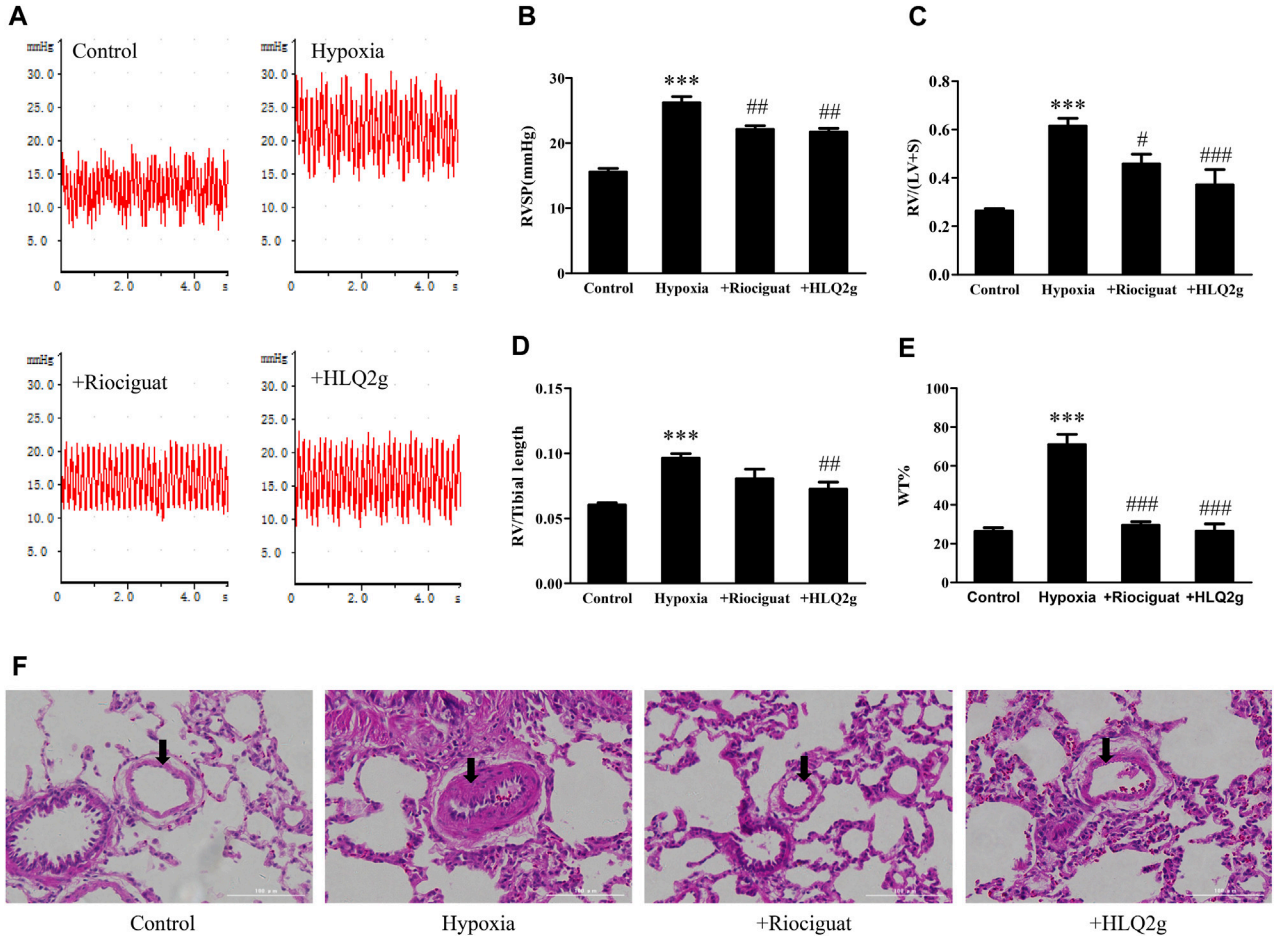

FIGURE 2 | Hemodynamics, right heart remodeling, pulmonary vascular remodeling in Hypoxia-induced PH rats. **(A)**: RVSP waveform; **(B)**: RVSP summary graph; **(C)**: RV/LV + S (**right** ventricle/**left** ventricle + interventricular septum) statistics; **(D)**: RV/Tibial length (**right** ventricle/tibial length) statistics; **(E)**: Statistical chart of HE staining (100 μm); (WT%) = (outside diameter-inside diameter)/(outside diameter) × 100. **(F)**: Representative image of HE staining. Control: the control rats; Hypoxia: Hypoxia-induced PH rats. Data are expressed as mean ± SD. n = 3–5. Vs. the control, ***$p < 0.001$; vs. the Hypoxia group, #$p < 0.05$, ##$p < 0.01$, ###$p < 0.001$.

hypoxia group was higher than that in the normal group; and the RVHI in the Riociguat group and HLQ2g group was lower than that in the hypoxia group (**Figures 2C,D**). HE staining indicated that compared with the normal group, the vascular remodeling index (WT%) in the hypoxia group was clearly increased; compared with the hypoxia group, the vascular remodeling index of Riociguat group and HLQ2g group was obviously decreased (**Figures 2E,F**). These results indicate that hypoxia can induce PH successfully, and HLQ2g can reduce RVSP and cardiac hypertrophy and improve vascular remodeling.

HLQ2g Up-Regulated cGKI Expression and Restored BMPR2 Signaling Pathway in Hypoxia-Induced PH Rat Model

To further explore the role of HLQ2g in the regulation of mechanism *in vivo*, we detected cGKI expression and BMPR2 signaling pathway in pulmonary artery of hypoxia-induced PH rat model. The down-regulation of cGKI, p-Smad1/5/8, and Id1 protein levels induced by hypoxia was significantly restored after HLQ2g administration (**Figures 3A–E**). These results suggest that HLQ2g could upregulate cGKI protein and BMPR2 signaling pathway in hypoxia-induced PH rat model.

HLQ2g Inhibited Proliferation and Migration of HPASMCs

Excessive proliferation and migration of HPASMCs play an important role in the vascular remodeling of PH. To detect the effect of HLQ2g on the proliferation of HPASMCs, HPASMCs were induced with hypoxia and incubated with HLQ2g for 24 h, and then the cell proliferation was measured. CCK8 and EdU results showed that hypoxia induced the proliferation of HPASMCs, while HLQ2g inhibited the proliferation of HPASMCs induced by hypoxia (**Figures 4A,C,I**). Similarly, HLQ2g inhibited the proliferation of

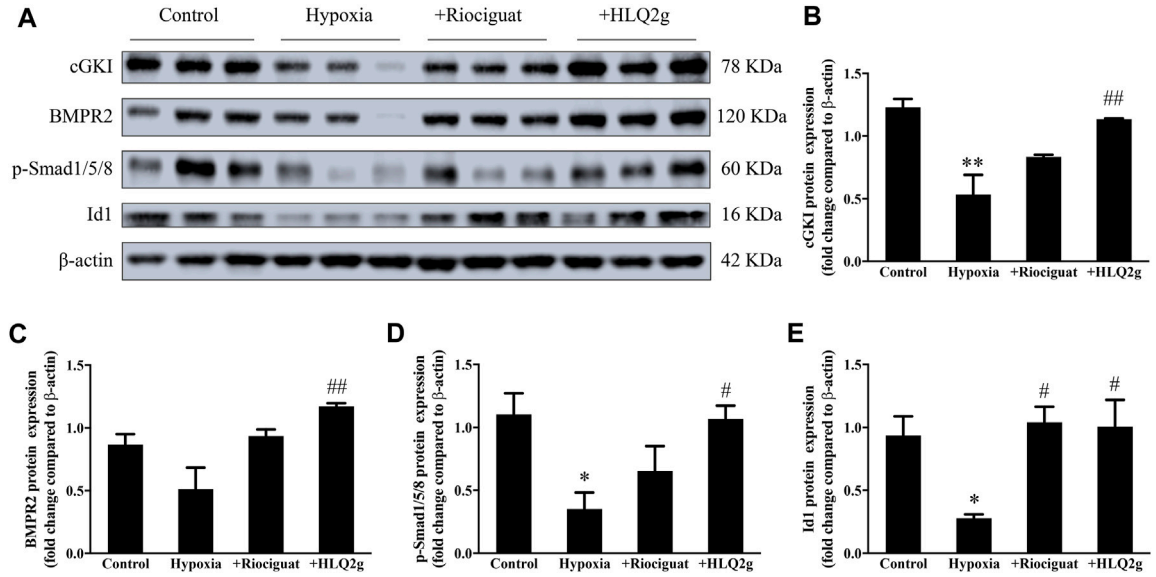

FIGURE 3 | In hypoxia-induced PH rat model, HLQ2g can regulate cGKI protein and BMPR2 pathway. **(A)**: The expression of cGKI, BMPR2, p-Smad1/5/8, and Id1 in pulmonary artery of rats; **(B–E)**: The quantitative analysis results of A. Control: the control rats; Hypoxia: Hypoxia-induced PH rats. Data are expressed as mean ± SD. $n = 3$. Vs. the control, $^{*}p < 0.05$, $^{**}p < 0.01$; vs. the Hypoxia group, $\#p < 0.05$, $\#\#p < 0.01$.

HPASMCs induced by PDGF (**Figures 4B,H,J**). We also examined the effect of HLQ2g on the proliferation of HPASMCs at protein level. The results revealed that PCNA protein was upregulated after hypoxia stimulation and downregulated after HLQ2g intervention (**Figures 4D,F**). We also used PDGF to stimulate HPASMCs, and the results were consistent with hypoxia (**Figures 4E,G**). These results suggest that HLQ2g could inhibit the proliferation of HPASMCs.

At the same time, we conducted scratch tests to detect the effect of HLQ2g on HPASMCs migration. Hypoxia induced PASMC migration, while HLQ2g inhibited the migration of PASMC induced by hypoxia (**Figures 5A,C**). The migration of HPASMCs induced by PDGFs was inhibited by HLQ2g (**Figures 5B,D**). These results suggest that HLQ2g could inhibit the proliferation and migration of HPASMCs induced by hypoxia and PDGF.

HLQ2g Up-Regulated cGKI Expression and Restored BMPR2 Signaling Pathway in HPASMCs

To further explore the role of HLQ2g in the regulation of mechanism *in vitro*, HPASMCs were induced with hypoxia and incubated with HLQ2g for 24 h, and then the intracellular protein levels were detected. Hypoxia significantly downregulated cGKI protein and the BMPR2 pathway, while HLQ2g intervention significantly inhibited the downregulation of cGKI, BMPR2, p-Smad1/5/8, and Id1 induced by hypoxia (**Figures 6A–E**). In short, HLQ2g could upregulate cGKI and BMPR2 pathway in HPASMCs.

cGKI Inhibition Abrogated the Effects of HLQ2g on BMP Signaling Pathway in HPASMCs

To confirm our hypothesis, HPASMCs were induced with hypoxia and incubated with both HLQ2g and Rp-8-Br-PET-cGMPS (a specific cGKI inhibitor), then cell proliferation and migration were detected, and the intracellular protein levels were detected. The results showed that adding Rp-8-Br-PET-cGMPS promoted cell proliferation and migration and down-regulated the BMPR2 pathway, compared with using HLQ2g alone (**Figures 7A–G**). These results suggest that Rp-8-Br-PET-cGMPS blocked the effects of HLQ2g, which was proved to up-regulate BMP signaling pathway by activating cGKI, thus inhibiting cell proliferation and migration.

DISCUSSION

In summary, the present study found that HLQ2g can reduce RVSP and inhibit the development of RV hypertrophy and pathological changes of pulmonary vascular remodeling in hypoxia-induced PH rat model. At the same time, HLQ2g restored the BMP pathway by up-regulating cGKI in PH. In addition, HLQ2g inhibited hypoxia and platelet-derived growth factor-induced proliferation and migration of HPASMCs which was abolished by cGKI inhibitor. In short, this study preliminarily revealed the therapeutic mechanism of the novel pyrazolo[3,4-b] pyridine derivative (HLQ2g), and also further proved the interaction between NO signaling and BMP signaling which gave us important clues in PH therapy.

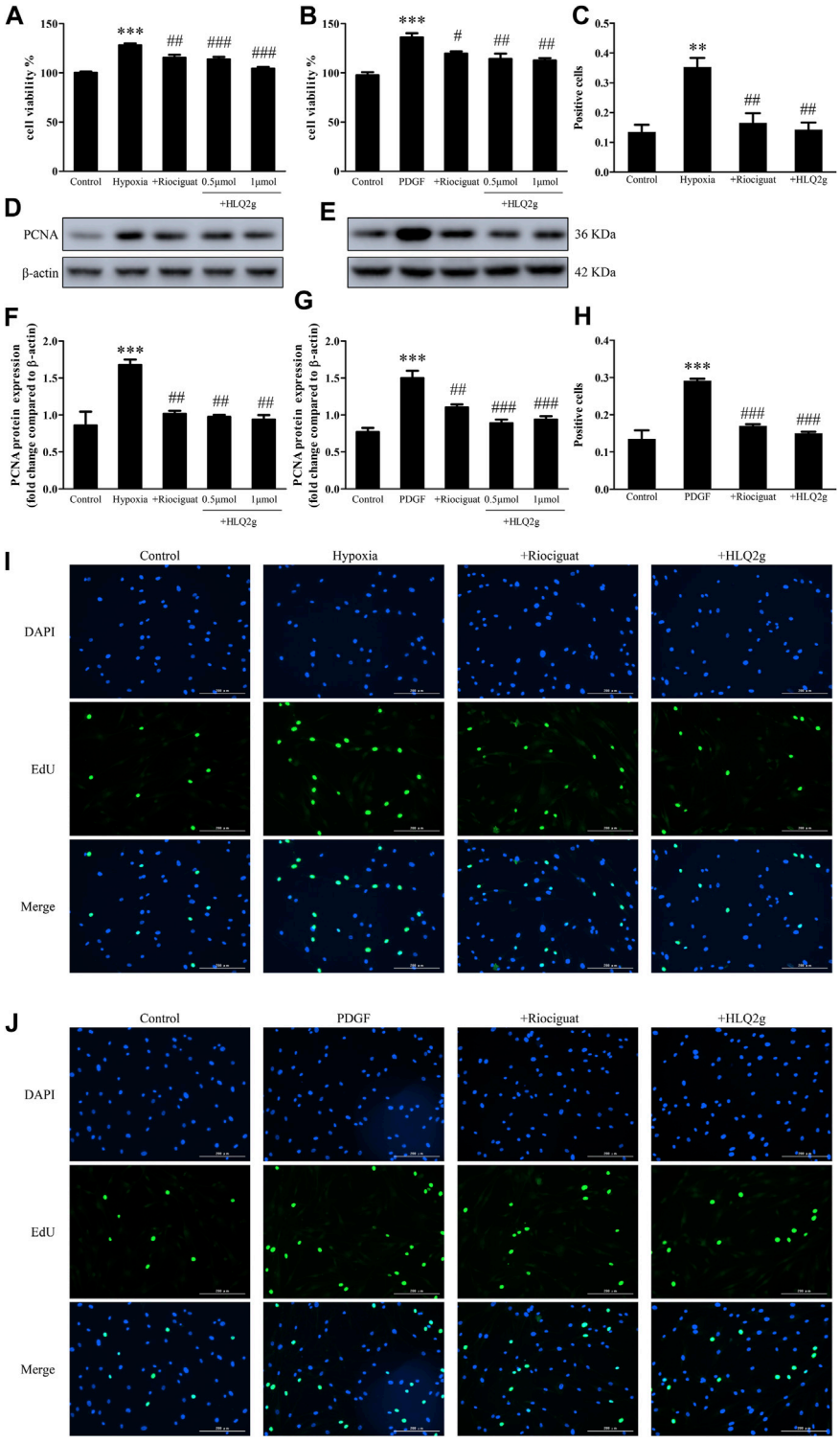

FIGURE 4 | HLQ2g can inhibit the proliferation of HPASMCs. **(A, B)**: CCK8 detected cell proliferation. **(C)**: Quantitative analysis of I. **(D)**: The expression of PCNA protein in HPASMCs stimulated by hypoxia. **(E)**: The expression of PCNA protein in HPASMCs induced by PDGF. **(F)**: Quantitative analysis of D. **(G)**: Quantitative analysis of E. **H**: Quantitative analysis of J. **(I, J)**: EdU detected cell proliferation. Riociguat (1 μM); HLQ2g (1 μM); **Vehicle**: 1% DMSO; **Control**: normal control group; **PDGF**: platelet-derived growth factor BB treatment group (20 ng/ml; 24 h). Data are expressed as mean ± SD, $n = 3–5$. Vs. the control, $^{**}p < 0.01$, $^{***}p < 0.001$; vs. the PDGF/Hypoxia group, $\#p < 0.05$, $\#\#p < 0.01$, $\#\#\#p < 0.001$.

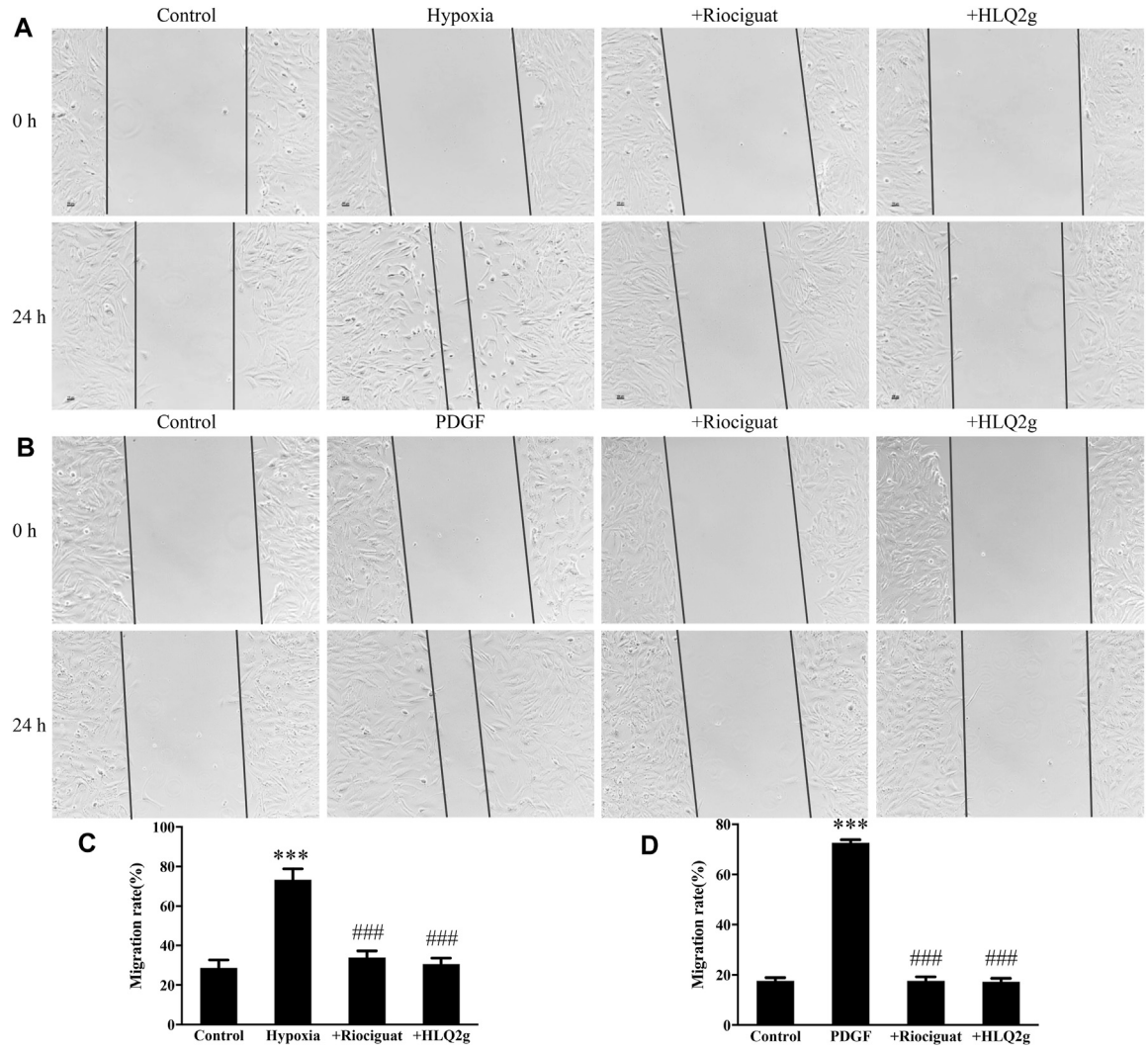

FIGURE 5 | HLQ2g can inhibit the migration of HPASMCs. **(A, B)**: Scratch test results (100 μm); **(C)**: Statistical analysis of A; **(D)**: Statistical analysis of B. Riociguat (1 μM); HLQ2g (1 μM). Data are expressed as mean ± SD, $n = 3$. Vs. the control, ***$p < 0.001$; vs. the PDGF/Hypoxia group, ###$p < 0.001$.

PH remains a serious clinical disease regardless of the availability to a variety of drugs interfering with endothelin, NO, and prostacyclin pathways in the past decades (Galie et al., 2019). NO/sGC/cGMP was accepted as a classic target pathway for the treatment of PH by modulating a variety of downstream targets including protein kinase, cyclic nucleotide-gated channel, and phosphodiesterase (Lundberg et al., 2015). Current medicines including sildenafil, tadalafil, and riociguat are commonly used in clinical mainly by increasing the cGMP level and causing pulmonary arteries relaxation. Different from other drugs which inhibit the degradation of cGMP, riociguat is the first approved sGC stimulator in 2013 to accelerate the production of cGMP. Since that time, exploring sGC stimulators and sGC activators have became hot spot in this fields, and some of them have been under clinical trials (Sandner et al., 2019). HLQ2g is a new compound modified from the structure of Riociguat by our group, which preserved the active fragment (pyrimidine and benzyl moieties) of riociguat to ensure its activity of activating sGC, which could achieve the vasodilation effect. In addition, the active fragment (pyrazolo[1,5-a] pyrimidine) of AMPK inhibitor was introduced in HLQ2g to increase the anti-proliferative activity. As a result, HLQ2g showed potential advantages with dual regulatory activities on vascular remodeling and vasodilation compared with riociguat. Previous study has revealed the comparable pharmacological effects of HLQ2g and Riociguat in PH treatment (Hu et al., 2020). This study further confirmed the cGMP elevation and therapeutical functions of HLQ2g *in vivo* and *in vitro* which defined the critical role of sGC/cGMP pathway in PH treatment again.

Firstly, we established a rat model of PH induced by hypoxia. It is well known that vasocontraction and vascular remodeling are considered as the primary pathological characteristic of PH

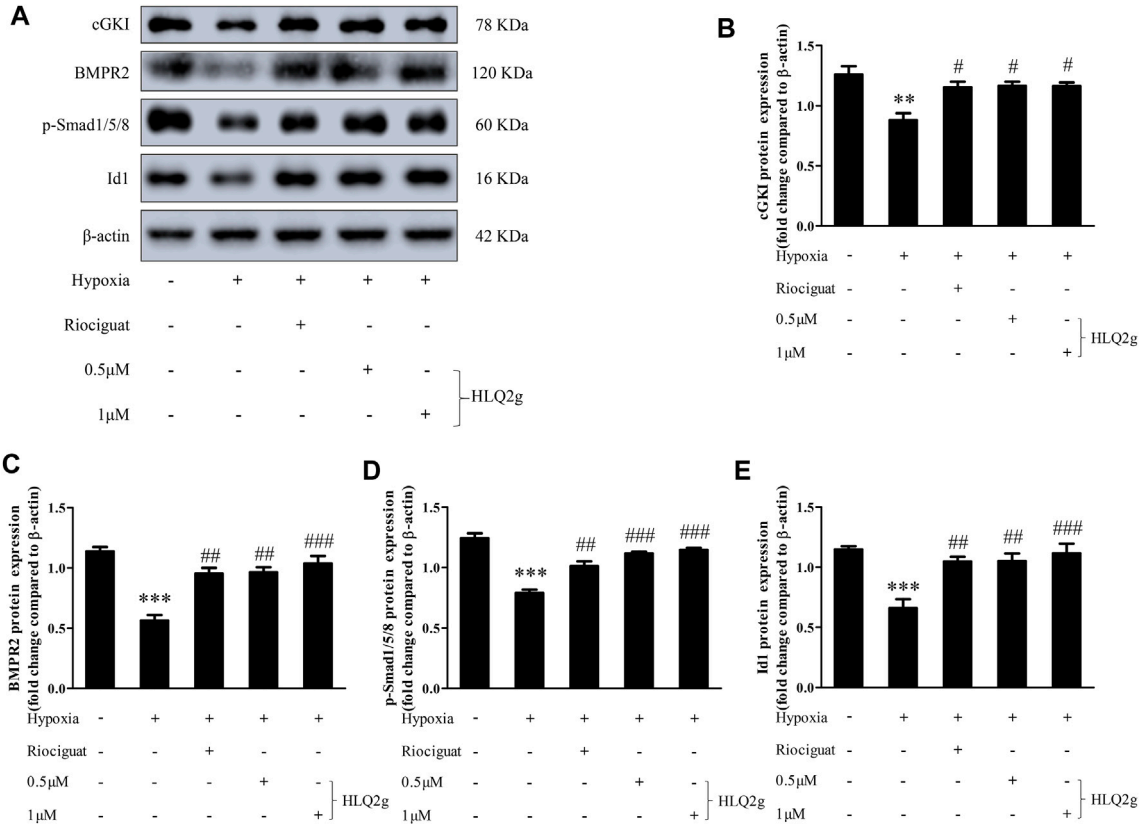

FIGURE 6 | HLQ2g can upregulate cGKI expression and BMP signaling pathway in Hypoxia-induced HPASMCs. **(A)**: The protein expression of cGKI, BMPR2, p-Smad1/5/8, and Id1 in HPASMCs determined by Western blot. Riociguat (1 μM). **(B–E)**: Quantitative analysis results of graph A. Data expressed as mean ± SD, $n = 3$. Vs. the control, $^{**}p < 0.01$, $^{***}p < 0.001$; vs. the Hypoxia group, $\#p < 0.05$, $\#\#p < 0.01$, $\#\#\#p < 0.001$.

(Humbert et al., 2004). Chronic hypoxia-induced right ventricular hypertrophy is mainly caused by mechanical stress of ventricular wall resulted from PH (Tual et al., 2006). Our data exhibited that RVSP, RVHI, and vascular remodeling index were significantly down-regulated in hypoxia-induced PH rats after the administration of HLQ2g. These solid proofs identified the therapeutic effects of HLQ2g in PH rat models. Furthermore, we conducted cell culture to explore the effects of HLQ2g *in vitro*. It is well accepted that the excessive proliferation and aberrant migration of PASMCs are critical abnormal phenotypes of PH, which largely contributes to the thickened pulmonary vascular wall and eventually lead to vascular occlusion (Li et al., 2016; Hu et al., 2020). HPASMCs were treated with hypoxia and incubated with HLQ2g for 24 h, and cellular proliferation and migration were investigated. These results revealed that HLQ2g inhibited the proliferation and migration of HPASMCs induced by hypoxia. Besides, PDGF was also used to induce proliferation and migration of HPASMCs as it is acknowledged as a mitogen to PASMCs and further facilitate pulmonary vascular remodeling (Li et al., 2018). Similarly, we found that HLQ2g inhibited the proliferation and migration of HPASMCs stimulated by PDGF. Taken together, these results indicate that HLQ2g can inhibit vascular remodeling and exert a considerable therapeutic effect on PH.

To explore the specific mechanism of HLQ2g, we turned our sight to the BMP signaling pathway. It is reported that mutations in BMPR2 result in the deficiency of the growth-inhibitory effects of BMPs in HPASMCs through a downregulated Smad1/5/8 phosphorylation and reduced transcription of Inhibitor of DNA binding protein 1, which is a primary target gene of BMP signaling (Machado et al., 2006). Dysfunction of BMP signaling is thought to be an important hallmark in various types of PH (Long et al., 2009). Notably, animal experiments have further found that the therapeutic effects of existing PH therapeutic drugs (such as sildenafil, prostacyclin, etc.) are related to the up-regulation of the BMP signaling pathway (Yang et al., 2013). Direct activation of BMPR2 and BMP signaling by BMP9 or FK506 have showed powerful effects on PH treatment in animal models and clinical transformation research is ongoing. Thus, the BMP signaling pathway has enormous potential to become next therapeutical target in PH. Here, this study showed that down-regulated protein expressions of BMPR2, p-Smad1/5/8, and Id1 protein were observed in rats and HPASMCs treated by hypoxia, while HLQ2g treatment notably restored the BMP signaling pathway. Up-regulated BMP signaling pathway is assumed to participate into the improvements of vascular remodeling and PH. Meanwhile these novel findings attracted

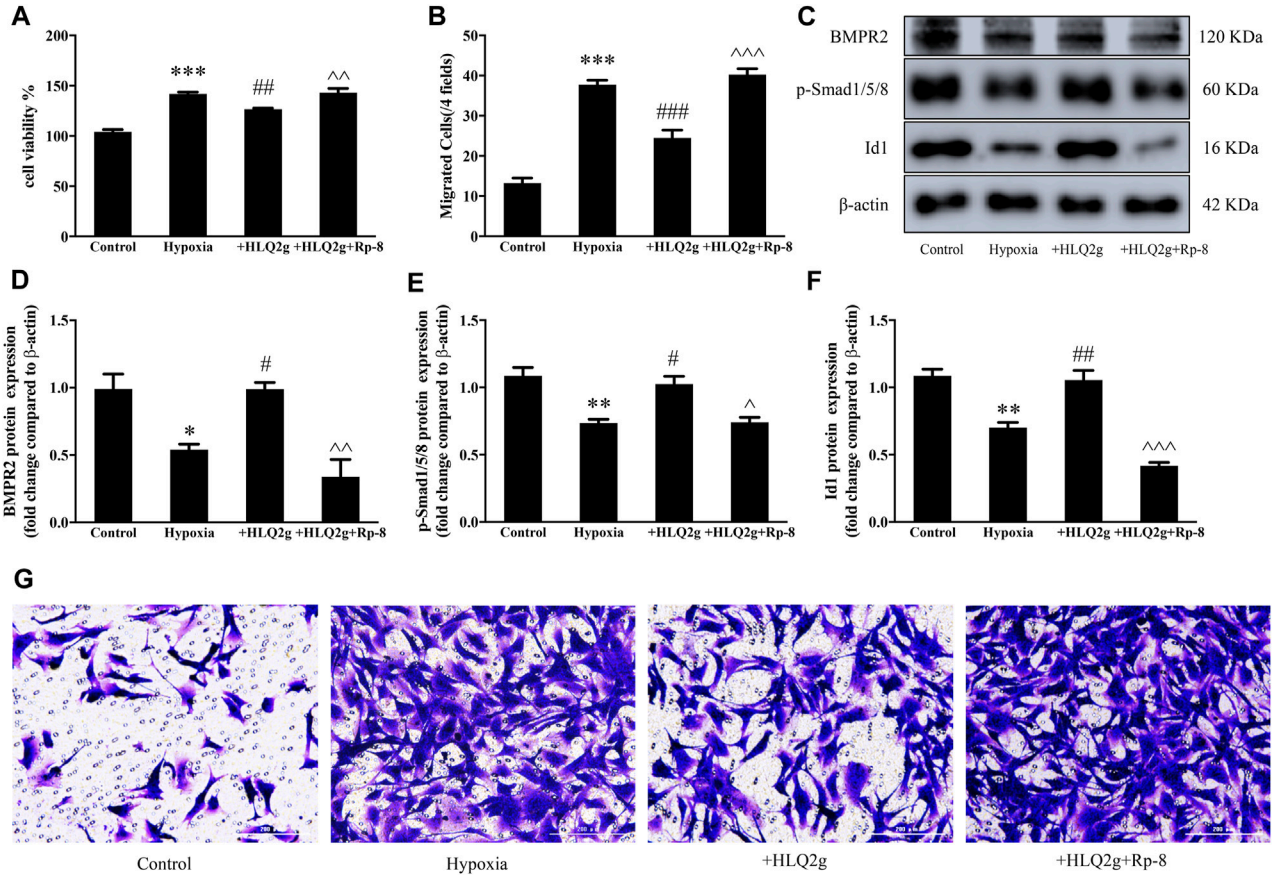

FIGURE 7 | Rp-8-Br-PET-cGMPS can block the effect of HLQ2g. **(A)**: CCK8 detected cell proliferation. **(B, G)**: Transwell test results (200 μm). **(C)**: The protein expression of BMPR2, p-Smad1/5/8, and Id1 in HPASMCs determined by Western blot. **(D–F)**: Quantitative analysis results of graph C. HLQ2g (1 μM); Rp-8: Rp-8-Br-PET-cGMPS (30 μM). Data expressed as mean ± SD, $n = 3–5$. Vs. the control, $^{*}p < 0.05$, $^{**}p < 0.01$, $^{***}p < 0.001$; vs. the Hypoxia group, $\#p < 0.05$, $\#\#p < 0.01$, $\#\#\#p < 0.001$; vs. the Hypoxia + HLQ2g group, $\hat{}p < 0.05$, $\hat{}p < 0.01$, $\hat{}p < 0.001$.

us to investigate the relationship between sGC activation and BMP signaling pathway.

As a key mediator of vasodilation, cGKI is mainly activated by cGMP. Interestingly, there is research reported that cGKI can regulate BMP receptor and Smads and enhance BMP signal transduction (Schwappacher et al., 2009). As a sGC stimulator and cGMP elevator, there is reason to image the role of cGKI in HLQ2g's biological function. Results from this study demonstrated that HLQ2g treatment notably renewed hypoxia-induced down-regulation of cGKI in rats and HPASMCs, confirming the up-regulation effects of HLQ2g on cGKI probably via elevated cGMP. Interestingly, when we interfered cGKI with Rp-8-Br-PET-cGMPS in HPASMCs, we found that the ability of HLQ2g to inhibit the proliferation and migration of HPASMCs and upregulate the BMP signaling pathway was significantly suppressed. It means that Rp-8-Br-PET-cGMPS blocks the effects of HLQ2g, which has been proved to restore BMP signaling pathway and inhibit vascular remodeling. The experimental results proved the direct interaction between sGC signaling and BMP signaling, and suggested that BMP/Smad/Id1 pathway is the key effector in hypoxic PH.

CONCLUSION

In conclusion, the results in this study demonstrated that HLQ2g inhibited the proliferation and migration of HPASMCs and alleviated the progression of PH by upregulating cGKI protein to activate the BMP signaling pathway. This study might shed lights on finding novel agents targeting on sGC and BMP signaling. Further study using *BMPR2* and *cGKI* knockout animal would be helpful to further prove the relationship between sGC signaling and BMPR2 signaling in PH. Furthermore, previous study suggested an anti-fibrosis effects of HLQ2g in PH which may partly attribute to inhibition of AMPK pathway. Actually, the unbalance of BMP and TGF-beta also play a key role in vascular fibrosis which worth further investigation. Importantly, we shall conduct more researches on the feasibility and safety of HLQ2g in the treatment of PH, and hope to push it into clinical trials.

DATA AVAILABILITY STATEMENT

The original contributions presented in the study are included in the article/Supplementary Material, further inquiries can be directed to the corresponding author.

ETHICS STATEMENT

The animal study was reviewed and approved by the Hunan Normal University Experimental Animal Welfare Ethics Committee and Animal Management and Committee.

AUTHOR CONTRIBUTIONS

LL, MY, and XL: Conceptualization, Methodology, Software; LH and XT: Data curation, Statistical analysis; XH and CZ: Visualization, Experimental studies; YL and QL: Article preparation, Reviewing and Editing, Validation; All authors read and approved the final article.

FUNDING

This work was supported by grants of the National Natural Science Foundation of China (No. 81773734 to XL, 81973324 to YL), Key R&D Programs of Hunan Province (2019SK2241 to XL), and was supported by Natural Science Foundation of Hunan Province (2018JJ2544 to XL), Hunan Young Talent grant (2020RC3063 to YL), Hunan Science Foundation (2020JJ5858 to YL) and the Wisdom Accumulation and Talent Cultivation Project of the Third XiangYa hosipital of Central South University (YX202002 to YL). We thank the support of Shandong Xinhua Pharmaceutical Co., Ltd.

REFERENCES

Armstrong, P. W., Roessig, L., Patel, M. J., Anstrom, K. J., Butler, J., Voors, A. A., et al. (2018). A Multicenter, Randomized, Double-Blind, Placebo-Controlled Trial of the Efficacy and Safety of the Oral Soluble Guanylate Cyclase Stimulator: The VICTORIA Trial. *JACC Heart Fail.* 6 (2), 96–104. doi:10.1016/j.jchf.2017.08.013

Atkinson, C., Stewart, S., Upton, P. D., Machado, R., Thomson, J. R., Trembath, R. C., et al. (2002). Primary Pulmonary Hypertension Is Associated with Reduced Pulmonary Vascular Expression of Type II Bone Morphogenetic Protein Receptor. *Circulation* 105 (14), 1672–1678. doi:10.1161/01.cir.0000012754.72951.3d

Evans, J. D., Girerd, B., Montani, D., Wang, X. J., Galiè, N., Austin, E. D., et al. (2016). BMPR2 Mutations and Survival in Pulmonary Arterial Hypertension: an Individual Participant Data Meta-Analysis. *Lancet Respir. Med.* 4 (2), 129–137. doi:10.1016/S2213-2600(15)00544-5

Friebe, A., Sandner, P., and Schmidtko, A. (2020). cGMP: a Unique 2nd Messenger Molecule - Recent Developments in cGMP Research and Development. *Naunyn Schmiedebergs Arch. Pharmacol.* 393 (2), 287–302. doi:10.1007/s00210-019-01779-z

Galiè, N., Channick, R. N., Frantz, R. P., Grünig, E., Jing, Z. C., Moiseeva, O., et al. (2019). Risk Stratification and Medical Therapy of Pulmonary Arterial Hypertension. *Eur. Respir. J.* 53 (1), 1801889. doi:10.1183/13993003.01889-2018

Hu, L., Li, L., Chang, Q., Fu, S., Qin, J., Chen, Z., et al. (2020). Discovery of Novel Pyrazolo[3,4-B] Pyridine Derivatives with Dual Activities of Vascular Remodeling Inhibition and Vasodilation for the Treatment of Pulmonary Arterial Hypertension. *J. Med. Chem.* 63 (19), 11215–11234. doi:10.1021/acs.jmedchem.0c01132

Humbert, M., Morrell, N. W., Archer, S. L., Stenmark, K. R., MacLean, M. R., Lang, I. M., et al. (2004). Cellular and Molecular Pathobiology of Pulmonary Arterial Hypertension. *J. Am. Coll. Cardiol.* 43 (12 Suppl. S), 13S–24S. doi:10.1016/j.jacc.2004.02.029

Lang, M., Kojonazarov, B., Tian, X., Kalymbetov, A., Weissmann, N., Grimminger, F., et al. (2012). The Soluble Guanylate Cyclase Stimulator Riociguat Ameliorates Pulmonary Hypertension Induced by Hypoxia and SU5416 in Rats. *PLoS One* 7 (8), e43433. doi:10.1371/journal.pone.0043433

Leuchte, H. H., Behr, J., Ewert, R., Ghofrani, H. A., Grünig, E., Halank, M., et al. (2015). Riociguat: Stimulator of Soluble Guanylate-Cyclase. New Mode of Action for the Treatment of Pulmonary Arterial and Non Operable Chronic Thromboembolic Pulmonary Hypertension. *Pneumologie* 69 (3), 135–143. doi:10.1055/s-0034-1391435

Li, F., Wang, J., Zhu, Y., Liu, L., Feng, W., Shi, W., et al. (2018). SphK1/S1P Mediates PDGF-Induced Pulmonary Arterial Smooth Muscle Cell Proliferation via miR-21/BMPRII/Id1 Signaling Pathway. *Cell Physiol. Biochem.* 51 (1), 487–500. doi:10.1159/000495243

Li, M. X., Jiang, D. Q., Wang, Y., Chen, Q. Z., Ma, Y. J., Yu, S. S., et al. (2016). Signal Mechanisms of Vascular Remodeling in the Development of Pulmonary Arterial Hypertension. *J. Cardiovasc. Pharmacol.* 67 (2), 182–190. doi:10.1097/FJC.0000000000000328

Long, L., Crosby, A., Yang, X., Southwood, M., Upton, P. D., Kim, D. K., et al. (2009). Altered Bone Morphogenetic Protein and Transforming Growth Factor-Beta Signaling in Rat Models of Pulmonary Hypertension: Potential for Activin Receptor-like Kinase-5 Inhibition in Prevention and Progression of Disease. *Circulation* 119 (4), 566–576. doi:10.1161/CIRCULATIONAHA.108.821504

Long, L., Ormiston, M. L., Yang, X., Southwood, M., Gräf, S., Machado, R. D., et al. (2015). Selective Enhancement of Endothelial BMPR-II with BMP9 Reverses Pulmonary Arterial Hypertension. *Nat. Med.* 21 (7), 777–785. doi:10.1038/nm.3877

Lundberg, J. O., Gladwin, M. T., and Weitzberg, E. (2015). Strategies to Increase Nitric Oxide Signalling in Cardiovascular Disease. *Nat. Rev. Drug Discov.* 14 (9), 623–641. doi:10.1038/nrd4623

Machado, R. D., Aldred, M. A., James, V., Harrison, R. E., Patel, B., Schwalbe, E. C., et al. (2006). Mutations of the TGF-Beta Type II Receptor BMPR2 in Pulmonary Arterial Hypertension. *Hum. Mutat.* 27 (2), 121–132. doi:10.1002/humu.20285

McLaughlin, V. V., Archer, S. L., Badesch, D. B., Barst, R. J., Farber, H. W., Lindner, J. R., et al. (2009). ACCF/AHA 2009 Expert Consensus Document on Pulmonary Hypertension: a Report of the American College of Cardiology Foundation Task Force on Expert Consensus Documents and the American Heart Association: Developed in Collaboration with the American College of Chest Physicians, American Thoracic Society, Inc., and the Pulmonary Hypertension Association. *Circulation* 119 (17), 2250–2294. doi:10.1161/CIRCULATIONAHA.109.192230

Sandner, P., Zimmer, D. P., Milne, G. T., Follmann, M., Hobbs, A., and Stasch, J.-P. (2019). Soluble Guanylate Cyclase Stimulators and Activators. *Handb Exp. Pharmacol.* 264, 355–394. doi:10.1007/164_2018_197

Schwappacher, R., Weiske, J., Heining, E., Ezerski, V., Marom, B., Henis, Y. I., et al. (2009). Novel Crosstalk to BMP Signalling: cGMP-dependent Kinase I Modulates BMP Receptor and Smad Activity. *EMBO J.* 28 (11), 1537–1550. doi:10.1038/emboj.2009.103

Simonneau, G., Montani, D., Celermajer, D. S., Denton, C. P., Gatzoulis, M. A., Krowka, M., et al. (2019). Haemodynamic Definitions and Updated Clinical Classification of Pulmonary Hypertension. *Eur. Respir. J.* 53 (1), 1801913. doi:10.1183/13993003.01913-2018

Spaczyńska, M., Rocha, S. F., and Oliver, E. (2020). Pharmacology of Pulmonary Arterial Hypertension: An Overview of Current and Emerging Therapies. *ACS Pharmacol. Transl. Sci.* 3 (4), 598–612. doi:10.1021/acsptsci.0c00048

Spiekerkoetter, E., Tian, X., Cai, J., Hopper, R. K., Sudheendra, D., Li, C. G., et al. (2013). FK506 Activates BMPR2, Rescues Endothelial Dysfunction, and Reverses Pulmonary Hypertension. *J. Clin. Invest.* 123 (8), 3600–3613. doi:10.1172/JCI65592

Thenappan, T., Khoruts, A., Chen, Y., and Weir, E. K. (2019). Can Intestinal Microbiota and Circulating Microbial Products Contribute to Pulmonary Arterial Hypertension? *Am. J. Physiol. Heart Circ. Physiol.* 317 (5), H1093–H1101. doi:10.1152/ajpheart.00416.2019

Tual, L., Morel, O. E., Favret, F., Fouillit, M., Guernier, C., Buvry, A., et al. (2006). Carvedilol Inhibits Right Ventricular Hypertrophy Induced by Chronic Hypobaric Hypoxia. *Pflugers Arch.* 452 (4), 371–379. doi:10.1007/s00424-006-0058-5

Yang, J., Li, X., Al-Lamki, R. S., Wu, C., Weiss, A., Berk, J., et al. (2013). Sildenafil Potentiates Bone Morphogenetic Protein Signaling in Pulmonary Arterial Smooth Muscle Cells and in Experimental Pulmonary Hypertension. *Arterioscler Thromb. Vasc. Biol.* 33 (1), 34–42. doi:10.1161/ATVBAHA.112.300121

Yang, X., Long, L., Southwood, M., Rudarakanchana, N., Upton, P. D., Jeffery, T. K., et al. (2005). Dysfunctional Smad Signaling Contributes to Abnormal Smooth Muscle Cell Proliferation in Familial Pulmonary Arterial Hypertension. *Circ. Res.* 96 (10), 1053–1063. doi:10.1161/01.RES.0000166926.54293.68

Conflict of Interest: The authors declare that this study received funding from Shandong Xinhua Pharmaceutical Co., Ltd. The funder was not involved in the study design, collection, analysis, interpretation of data, the writing of this article, or the decision to submit it for publication.

frontiers in Pharmacology

REVIEW
published: 19 October 2021
doi: 10.3389/fphar.2021.743945

The Function of microRNAs in Pulmonary Embolism: Review and Research Outlook

*Mingyao Luo[1], Mingyuan Du[2,3], Chang Shu[1,2,3], Sheng Liu[1], Jiehua Li[2,3], Lei Zhang[2,3] and Xin Li[*2,3]*

[1]State Key Laboratory of Cardiovascular Diseases, Center of Vascular Surgery, Fuwai Hospital, National Center for Cardiovascular Diseases, Chinese Academy of Medical Science and Peking Union Medical College, Beijing, China, [2]Department of Vascular Surgery, The Second Xiangya Hospital, Central South University, Changsha, China, [3]The Institute of Vascular Diseases, Central South University, Changsha, China

Pulmonary embolism (PE) is a common pathologic condition that frequently occurs in patients with deep venous thrombosis. Severe PE may critically suppress cardiopulmonary function, thereby threatening the life of patients. Chronic pulmonary hypertension caused by PE may lead to deterioration of respiratory dysfunction, resulting in complete disability. MicroRNAs (miRNAs) are a group of abundantly expressed non-coding RNAs that exert multiple functions in regulating the transcriptome *via* post-transcriptional targeting of mRNAs. Specifically, miRNAs bind to target mRNAs in a matching mechanism between the miRNA seed sequence and mRNA 3′ UTR, thus modulating the transcript stability or subsequent translation activity by RNA-induced silencing complex. Current studies have reported the function of miRNAs as biomarkers of PE, revealing their mechanism, function, and targetome in venous thrombophilia. This review summarizes the literature on miRNA functions and downstream mechanisms in PE. We conclude that various related miRNAs play important roles in PE and have great potential as treatment targets. For clinical application, we propose that miRNA biomarkers combined with traditional biomarkers or miRNA signatures generated from microchips may serve as a great predictive tool for PE occurrence and prognosis. Further, therapies targeting miRNAs or their upstream/downstream molecules need to be developed more quickly to keep up with the progress of routine treatments, such as anticoagulation, thrombolysis, or surgery.

Keywords: miRNA, biomarker, treatment target, pulmonary embolism, deep venous thrombosis, molecular regulation

OPEN ACCESS

Edited by:
Xiaohui Li,
Central South University, China

Reviewed by:
Benzhi Cai,
The Second Affiliated Hospital of Harbin Medical University, China
Antonio Molino,
University of Naples Federico II, Italy

****Correspondence:***
Xin Li
lixin1981@csu.edu.cn

Specialty section:
This article was submitted to Respiratory Pharmacology, a section of the journal Frontiers in Pharmacology

Received: *19 July 2021*
Accepted: *04 October 2021*
Published: *19 October 2021*

Citation:
Luo M, Du M, Shu C, Liu S, Li J, Zhang L and Li X (2021) The Function of microRNAs in Pulmonary Embolism: Review and Research Outlook. Front. Pharmacol. 12:743945. doi: 10.3389/fphar.2021.743945

INTRODUCTION

Pulmonary embolism (PE) is a common pathologic condition (Doherty, 2017). It is also the third-leading cause of cardiovascular death after cerebral stroke and heart attack (Essien et al., 2019). In particular, massive PE is a life-threatening event with a high mortality rate, and a total of 60,000–100,000 individuals die from PE annually in the United States (Centers for Disease Control and Prevention, 2015). Large pulmonary emboli often impair the hemodynamic condition, leading to high morbidity and mortality. PE is classified into acute PE (APE) and chronic PE (CPE), which may lead to thrombo-embolic pulmonary hypertension (CTEPH). Embolus originating from the lower extremities or pelvis may break apart and spread into the blood stream. A large embolus in the pulmonary circulation can also initiate a coagulation cascade in

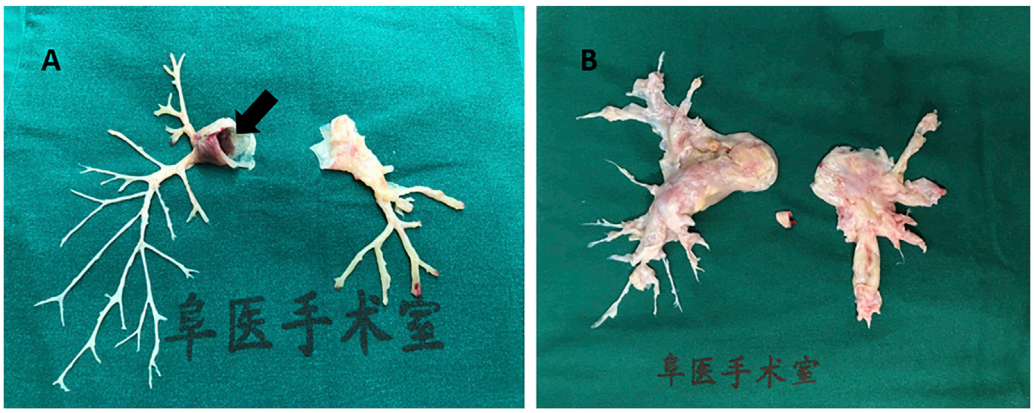

FIGURE 1 | Human pulmonary artery pathological specimen shows **(A)** inflammatory intima specimen accompanied with emboli in pulmonary artery main trunk (black arrow) taken from a patient of pulmonary vasculitis; **(B)** hyperplasia endothelial tissue from pulmonary endarterectomy operation in chronic thrombosis embolic pulmonary hypertension (CTEPH) patient.

pulmonary vessels. Recovery abscission of clot fragments can result in CTEPH (Piazza and Goldhaber, 2006). Although multidetector row computed tomography pulmonary angiography improved the understanding of PE as a clinical entity (Doherty, 2017) from 1998 to 2006, the detection rate of PE nearly doubled without any change in its mortality (Long, 2016). Further, although surgical embolectomy has been advocated to treat massive PE, the available medical centers that can perform this complicated surgery are few (Beckerman and Bolotin, 2017). Moreover, due to the compromise of respiration and hemodynamics, a large proportion of patients with acute massive PE do not qualify for surgery. **Figure 1** shows a massive embolus retrieved from the pulmonary artery and the chronic hyperplasia pulmonary artery endothelium *via* pulmonary endarterectomy. Deep venous thrombosis (DVT) is the major risk factor of PE. Lower limb extremity deep vein thrombosis is the most likely source of thrombus in PE. Of interest, Badireddy et al. reported that DVT accounts for one-third of all PE cases (Badireddy and Mudipalli, 2021). In recent years, accumulating efforts and attention have been directed to the pathophysiological mechanism of microRNAs (miRNAs), with the aim of developing novel therapies. Further, the novel emerging role of miRNAs as biomarkers contributes to the acceleration of research.

miRNAs are an abundantly expressed subgroup of non-coding RNAs that function as an important endogenous gene regulator, which acts in a post-transcriptional manner. miRNAs regulate the levels of mRNAs for translation by inducing mRNA degradation or translational repression (Bartel, 2004). Currently, approximately 1,000 miRNAs have already been identified, forming an extremely complex miRNA-mRNA regulatory network and strictly controlling nearly every physiological or pathological process. Each miRNA is capable of modulating a specific group of targets, a targetome, and each mRNA might be regulated by multiple miRNAs in a cell type-specific and context-dependent manner (Friedman et al., 2009; Garzon et al., 2009). As a consequence, many disease states are correlated with an abnormal profile of miRNA expression, including cardiovascular, cardiopulmonary, and coagulation conditions, which is quite relevant to PE pathogenesis. This review aimed to summarize the roles of miRNAs in PE as biomarkers and potential novel therapeutic targets and to explore their future research outlook and direction.

MIRNAS AS PE BIOMARKERS

Discovering novel biomarkers for prediction of fatal diseases is a hotspot in medical research. miRNAs have been identified as specific biomarkers, with great potential for clinical diagnosis, especially for diseases wherein protein-based biomarkers are lacking, for example, atrial fibrillation and APE. miRNA profile or signature has a very high sensitivity and specificity for some diseases (Schulte et al., 2017). Circulating miRNA expression is relatively stable in serum, plasma, and whole blood. Cheng et al. showed that these molecules circulate in the vascular system either by being encapsulated in micro-particles/exocrine bodies or binding to protein complexes to avoid degradation (Cheng et al., 2010). As an emerging group of novel non-invasive biomarkers, miRNAs have gradually attracted research attention, and literature has shown that they can be developed as an important biomarker for predicting PE in multiple pathologic events due to their high diagnostic potential (Deng et al., 2016).

miR-134 and miR-1233

Peng et al. reported that miR-134 and miR-1233 are upregulated 14.59 and 21.56 folds, respectively, in chronic obstructive pulmonary disease (COPD) patients with APE compared to levels in ordinary COPD patients. D-dimer is a classic biomarker for detecting and evaluating PE progression. Of interest, the areas under the curves (AUCs) for the correlation of miR-134 and miR-1233 with PE progression were 0.931 (95% confidence interval [CI] 0.863–0.999) and 0.884 (95% CI 0.79–0.978), respectively, which were higher than those of D-dimer (0.628) (95% CI 0.447–0.809) and Wells score (0.577)

(95% CI 0.389–0.765) (Peng et al., 2020). This study provided evidence that the levels of serum miR-1233 and miR-134 are significantly upregulated in COPD patients with APE complication. For miR-134, a meta-analysis also reported that its level was increased in APE patients compared to that in the control group (SMD = 2.84, z = 3.69, $p < 0.001$). The sensitivity, specificity, and diagnostic odds ratio were 0.86 (0.72–0.94), 0.75 (0.66–0.82), and 19 (7–51) respectively, which indicated its great potential as a PE biomarker (Liu et al., 2021). Among the variety of miRNA-related PE studies, research on miR-134 is the most extensive and reliable up to date (Xiao et al., 2011; Xiang et al., 2019). For miR-1233, it was reported to be the first miRNA biomarker for distinguishing APE from acute non-ST elevated myocardial infarction and healthy individuals (Kessler et al., 2016). Considering the confusing and overlapping clinical symptoms between APE and myocardial infarction, we consider these findings as exciting and meaningful evidences that contribute to the field.

miR-532-5p and miR-483-3p

miR-483-3p and miR-532-5p were found to correlate with PE, with sensitivity, specificity, and AUC of (1.00, 1.00, and 1.00) and (1.00, 1.00, and 1.00), respectively (Xiang et al., 2019). From the mechanistic point of view, miR-532-5p and miR-483-3p were found to share the same target, NFATC2IP gene, which is expressed in T-helper two cells and regulates the transcription of cytokine genes, including IL-3, 4, 5 and 13. In patients with PE, cytokines are abnormally expressed in peripheral circulating mononuclear cells. Moreover, the cellular immune response and pathways are impaired in PE, which is highly relevant to cytokine expression and implies the correlation between PE/venous thrombosis embolism and cellular immune dysfunction (Lv et al., 2013). Further, the target genes of these two miRNAs include molecules in the MAPK and PI3K-Akt signaling pathways, which are well-known to be involved in macrophage inflammatory, oxidative stress response (Zhang et al., 2015) as well as the apoptosis process of endothelial cells (Lou et al., 2016).

miR-221 and miR-27a/B

Liu et al. reported, in a cohort of 60 PE patients and 50 healthy volunteers, a significant increase in miR-221 level in the plasma from APE patients compared to that in healthy individuals. Correlation analysis showed a positive correlation between this miRNA and BNP (r = 0.842, $p < 0.05$), troponin I (r = 0.853; $p < 0.05$), and D-dimer (r = 0.838; $p < 0.05$) (Liu et al., 2018). Wang et al. also found that plasma miR-27a/b levels were significantly higher and showed positive correlation in APE patients compared to in the control group. Receiver operating characteristic (ROC) curve analyses showed that plasma miR-27a was superior to miR-27b with regard to the diagnosis of APE (AUC = 0.784, AUC = 0.707, respectively). Combining miR-27a or miR-27b with D-dimer significantly increased the diagnostic capacity for APE (Wang et al., 2018). Furthermore, miR-27a/b is related to the proliferation of pulmonary artery smooth muscle cells (PASMC). Endothelin-1 (ET-1) can stimulate miR-27a/b expression by activating the NF-κB pathway, which subsequently leads to a decrease in peroxisome proliferator-activated receptor γ and contributes to ET-1-induced PASMC proliferation. These processes may have a correlation with pulmonary vascular remodeling and pulmonary hypertension (Xie et al., 2017).

miR-338-5p

This miRNA has been proved to play a role in virus-associated cancers, such as esophageal squamous cell carcinoma, and neuropathies, such as Alzheimer's disease (Han et al., 2019; Qian et al., 2019). A recent publication by Zhang et al. reported that inhibition of miR-338-5p can increase the level of IL-6, which subsequently promotes the development and progression of DVT in a mouse study. In a cell model, it was shown that overexpression of miR-338-5p downregulated the expression of IL-6, while miR-338-5p inhibition upregulated IL-6 expression. An *in vivo* study found that mice treated with anti-IL-6 antibody or agomiR-338-5p delivery exhibited decreased expression of IL-6 and alleviation of DVT, whereas antagomiR-338-5p aggravated the progression of DVT (Zhang et al., 2020a).

miR-28-3p

Zhou et al. reported that among the twelve miRNAs they studied, miR-28-3p showed a significant increase in the plasma from PE patients. However, the increase in miR-28-3p level due to PE development was not significant compared to its level in the experimental dogs before inducing PE. The AUC of the ROC of plasma miR-28-3p was 0.792 (95% CI: 0.689–0.896). Moreover, pathway analysis revealed that the effect of miR-28-3p involves inositol phosphate metabolism and the phosphatidylinositol signaling system, which are highly relevant pathways to PE pathogenesis (Zhou et al., 2016).

The circulating miRNAs as biomarkers of PE introduced above may not be comprehensive, and there should be many other potential miRNAs for predicting PE (Suzuki et al., 2016). Using only one miRNA as a biomarker may have limitations. In the future, it is possible to use a group of miRNAs to achieve the ideal sensitivity and specificity for PE biomarker assays.

MIRNAS ARE POTENTIAL NOVEL THERAPEUTIC TARGETS FOR PE

Regarding APE treatment, one of the classic approaches is to inhibit the excessive proliferation and migration of PASMCs. Several miRNAs have been characterized and validated to regulate cell proliferation, apoptosis, and other related physiological processes. Therefore, finding miRNAs specific to these regulatory mechanisms may provide future therapeutic targets for PE or pulmonary artery hypertension induced by acute PE (APE-PAH).

miR-340-5p

A recent study on APE-PAH found that in APE-PAH patients, miR-340-5p was lowly expressed, whereas IL-1β and IL-6 were highly expressed. In a large sample cohort, linear regression was

found negatively correlated between miR-340-5p and IL-1β/IL-6. In cell culture, upon miR-340-5p overexpression, the levels of IL-1β and IL-6 were reduced, coupled with decreased proliferation and migration of PASMCs as well as ameliorated inflammatory response. As is well known, IL-1 has been characterized to significantly induce IL-6 expression (Tosato and Jones, 1990). In the dual-luciferase reporter assay regarding miR-340-5p, IL-1β and IL-6, both pro-inflammatory targets were confirmed to be downregulated by miR-340-5p directly, revealing a synergistic anti-inflammation effect of miR-340-5p. Therefore, miR-340-5p might be a promising therapeutic target as an anti-inflammatory agent (Ou et al., 2020).

miR-160b-5p

In an APE mouse model, Chen et al. demonstrated miR-106-5p as a novel regulator of PASMC proliferation and pulmonary vascular remodeling, and it performed its functions *via* targeting neuron-derived orphan receptor-1 (NOR1). Several literatures have reported NOR1 to regulate vascular cell migration and proliferation, and these important cellular processes are highly correlated with inflammation, growth factors, lipoproteins, and thrombin in vascular diseases (Martínez-González et al., 2003; Rius et al., 2004). Importantly, these findings highlight a novel therapeutic mechanism and improve the biological understanding of the complex network modulating APE progression (Chen et al., 2020).

miR-22-3p

Yang et al. reported that resveratrol successfully prevented PE-induced cardiac injury, possibly by modulating metastasis-associated lung carcinoma transcript 1 (MALAT1) expression through promoter regulation. MALAT1 was found to directly target miR-22-3p, as revealed by luciferase assay. Furthermore, miR-22-3p can bind complementarily to the 3′ UTR of NLR family pyrin domain containing 3 (NLRP3), leading to downregulation of NLRP3. In PE-associated cardiac injury, it was found that the levels of MALAT1, NLRP3, caspase-1, IL-1β, and IL-18 were significantly elevated, while miR-22-3p level was downregulated (Yang et al., 2019).

miR-21

A very recent study reported that curcumin can improve lung edema and outcomes of APE rats and that it decreased mPAP and RVSP levels, wet/dry weight ratio, thrombus size, and inflammatory markers in lung tissues. The possible mechanism is that curcumin modulated the miR-21-Sp1-PTEN axis, which reduced the NF-κB signaling pathway, thus suppressing lung injury and inflammation in APE (Liang et al., 2021).

miRNAs Correlated With Matrix Metalloproteinases and Venous Thrombophilia

As is known, pulmonary embolism is highly related to matrix metalloproteinases (MMPs) and venous thrombus (VT). miRNAs that modulate MMP biogenesis/degradation balance or VT pathophysiology have been demonstrated to indirectly modulate outcome of APE (Goldhaber and Bounameaux, 2012; Neto-Neves et al., 2013b).

Aberrant MMP activity has been demonstrated to be associated with APE-induced hemodynamic dysregulation. Neto-Neves et al. reported that MMPs were lowly expressed in healthy lung tissues and that the expression and activity of MMPs were augmented in lung injury (Neto-Neves et al., 2013a). Doxycycline, an inhibitor of MMP activity, was found to improve APE prognosis and protect against RV enlargement in a rat model, possibly *via* amelioration of APE-induced oxidative stress and inhibition of ventricular proteolytic activity (Cau et al., 2013). In addition, L-arginine also attenuated APE-induced pulmonary hypertension through other mechanisms, including the modulation of NO synthesis and downregulation of MMP-2 and MMP-9 activities (Souza-Costa et al., 2005). Therefore, specific miRNAs that are capable of modulating MMP expression also have potential treatment or prediction value in PE pathogenesis. Zhang et al. elucidated that miR-15a-5p expression was significantly increased in the lung tissue of PAH rats and that artificial overexpression of miR-15a-5p led to increased expression of MMP-2 (Zhang et al., 2020b). Some studies found that inhibition or degradation of the corresponding mRNA of MMP-12 could be a solution to treat pathological lung tissue remodeling (Garbacki et al., 2009).

VT is a complex pathologic condition with a highly heritable genetic component, which predisposes an individual to its development. VT often induces the occurrence of thrombosis or embolism, including PE, in multiple sites in both veins and arteries (Sun et al., 2021). There are four miRNAs (hsa-miR-126-3p, hsa-miR-885-5p, hsa-miR-194-5p, and hsa-miR-192-5p) that have been studied and proved to be correlated with VT. These showed significant correlations with intermediate phenotypes of VT. It was found that multiple miRNAs were correlated with several coagulation-related factors: miR-885-5p and miR-195-5p with the level of protein S and FVII; miR-192-5p with FVII and ADAMS13; and miR-126-3p with factor XI (Rodriguez-Rius et al., 2020). miR-494 has been shown to downregulate the expression of PROS1 and protein S in liver Huh cells (Tay et al., 2013). Further, factor X deficiency was found to be associated with aberrant expression of miR-24. In a cohort of 15 healthy adults and 36 severe trauma-induced coagulopathy patients, plasma miRNA screening showed that all coagulopathy patients had elevated levels of miR-24 and lower levels of factor X than did the healthy volunteers (Chen et al., 2017). It is believed that the expression pattern of miRNAs that target coagulation factors can result in thrombosis and coagulation-related diseases (Jankowska et al., 2020).

microRNA AND ITS RESEARCH OUTLOOK IN PE

With the popularization of sequencing and development of multiple human genetic projects, nearly 1,000 miRNAs have been identified, and the miRNA group has been predicted to

TABLE 1 | microRNAs' function and their characteristics from literature.

microRNA	Sensitivity	Specificity	AUC
microRNA-134	0.86	0.75	0.931
microRNA-1233	0.89	0.95	0.940
microRNA-532	1.00	1.00	1.000
microRNA-483-3p	1.00	1.00	1.000
microRNA-27a	0.78	0.83	0.784
microRNA-27b	0.65	0.78	0.707
microRNA-221	N.A	N.A	0.823
microRNA-28-3p	0.84	0.81	0.792
microRNA-22	0.63	0.79	0.750
let-7b	0.87	0.60	0.770

AUC, area under curve; N.A, not available.

regulate 30% of all human transcripts. Despite the accumulating literature and rapid progress in miRNA studies and research tools, only a small proportion of miRNAs have been well-characterized in dedicated cell types or diseases (Chang and Mendell, 2007). Nevertheless, they have been proved to have various functions that correlate with cancer, metabolic disease, neural system disease, and cardiovascular disease (Iorio and Croce, 2012; Vienberg et al., 2017; Wojciechowska et al., 2017; Juźwik et al., 2019; Hembrom et al., 2020). Microarrays are often used to find the correlations between miRNAs and diseases. A microarray study by Guo et al. revealed differential miRNA profile in CTEPH patients compared to that in healthy individuals, providing fundamental data for pathologic studies and biomarker screening for CTEPH. It was reported that a reduced level of let-7b might be involved in the pathogenesis of CTEPH by modulating ET-1 expression in pulmonary artery endothelial cells and PASMCs (Guo et al., 2014). In-silico studies have provided information on miRNAs that participate in the etiology of venous thrombosis, including their specific targetnetwork, and further investigation with a larger sample cohort is needed to explore and validate the mechanism and functional nature of miRNAs.

Further, as biomarkers for PE, miRNAs and their microchips may play more important roles in predicting PE or pre-judging PE prognosis. However, the existing biomarkers, such as D-dimer, are still necessary. Combining miRNAs and traditional biomarker molecules may increase their specificity and sensitivity. For example, studies have reported that accurate prediction of DVT can be achieved by comprehensive co-analysis of miR-96 and D-dimer level in patient plasma samples (Xie et al., 2016). Moreover, Jiang et al. reported that detection and co-analysis of miR-320a/b and D-dimer might further improve the accuracy of DVT diagnosis (Jiang et al., 2018). Because of the increasing number of miRNA research and complex network of PE biomarkers with their targets, **Table 1** has been provided to briefly display and visualize them.

In view of integrating miRNA observational study and functional analysis, there are still limitations and gap between miRNA as biomarker and miRNA as potential therapeutic method. Compared to biomarkers which correlate its expression with disease phenotype, miRNA therapeutics need further fundamental experiments to validate and decipher its underlying mechanism. As for current miRNA therapeutic clinical trials, the majority is focused on liver or circulation, by an approach of systemic injection (Zhang et al., 2021). A recent miRNA phase I study used MRX34, a liposomal miR-34a mimic to treat advanced solid tumors. The results showed a manageable toxicity level and improved clinical outcome (Hong et al., 2020). However, there is still long way to march in order of pushing miRNA from biomarker, animal study into reality treatment.

CONCLUSION

This review focused on the functions of miRNAs in PE. As the increasing number of miRNA and its functions being studied in PE, the predictive and therapeutic value of miRNA has been gradually improving. However, physicians do not see the importance of miRNAs in their clinical practice because they still use traditional biomarkers, such as D-dimer, and anti-coagulation agents or thrombolysis drugs. We need to break the barrier between scientific research and the clinical application of miRNAs in the future. The development of accurate and highly sensitive miRNA microchips that can predict APE or CTEPH using blood may be a future direction. We also expect that assays that combine miRNAs and traditional biomarkers of PE can be developed in the future. Further, because miRNAs function in gene expression, novel effective drugs, which can prevent or treat PE more efficiently than the current old and routine methods, such as anti-coagulation, thrombolysis, and surgery, are expected to be developed. So far, only literature on miRNAs exists, which cannot affect the diagnosis and treatment of diseases. We are thus eager to see more actual products that can be used in clinical practice in the near future.

AUTHOR CONTRIBUTIONS

ML and MD collect data and writing; CS and XL concept the paper and gain resources; SL, JL, and LZ collect data and gain the literatures.

FUNDING

This work was supported by the Hunan Provisional Nature Science Foundation (2020JJ 2054).

ACKNOWLEDGMENTS

Thanks for the teamwork and collaboration of State Key Laboratory of Cardiovascular Diseases, Center of Vascular Surgery, Fuwai Hospital, National Center for Cardiovascular Diseases, Chinese Academy of Medical Science and Peking Union Medical College and The Secondary Xiangya hospital, Central South University.

REFERENCES

Badireddy, M., and Mudipalli, V. R. (2021). "Deep Venous Thrombosis Prophylaxis," in *StatPearls [Internet]* (Treasure Island (FL): StatPearls Publishing).

Bartel, D. P. (2004). MicroRNAs: Genomics, Biogenesis, Mechanism, and Function. *Cell* 116, 281–297. doi:10.1016/s0092-8674(04)00045-5

Beckerman, Z., and Bolotin, G. (2017). Surgical Treatment of Acute Massive Pulmonary Embolism. *Adv. Exp. Med. Biol.* 906, 75–88. doi:10.1007/5584_2016_107

Cau, S. B., Barato, R. C., Celes, M. R., Muniz, J. J., Rossi, M. A., and Tanus-Santos, J. E. (2013). Doxycycline Prevents Acute Pulmonary Embolism-Induced Mortality and Right Ventricular Deformation in Rats. *Cardiovasc. Drugs Ther.* 27 (4), 259–267. doi:10.1007/s10557-013-6458-9

Centers for Disease Control and Prevention (2015). *Venous Thromboembolism (Blood Clots)*. Atlanta: CDC. Available at www.cdc.gov/ncbddd/dvt/data.html (Accessed May 2, 2017).

Chang, T. C., and Mendell, J. T. (2007). microRNAs in Vertebrate Physiology and Human Disease. *Annu. Rev. Genomics Hum. Genet.* 8, 215–239. doi:10.1146/annurev.genom.8.080706.092351

Chen, H., Ma, Q., Zhang, J., Meng, Y., Pan, L., and Tian, H. (2020). miR 106b 5p Modulates Acute Pulmonary Embolism via NOR1 in Pulmonary Artery Smooth Muscle Cells. *Int. J. Mol. Med.* 45 (5), 1525–1533. doi:10.3892/ijmm.2020.4532

Chen, L. J., Yang, L., Cheng, X., Xue, Y. K., and Chen, L. B. (2017). Overexpression of miR-24 Is Involved in the Formation of Hypocoagulation State after Severe Trauma by Inhibiting the Synthesis of Coagulation Factor X. *Dis. Markers* 2017, 3649693. doi:10.1155/2017/3649693

Cheng, Y., Tan, N., Yang, J., Liu, X., Cao, X., He, P., et al. (2010). A Translational Study of Circulating Cell-free microRNA-1 in Acute Myocardial Infarction. *Clin. Sci. (Lond)* 119, 87–95. doi:10.1042/CS20090645

Deng, H. Y., Li, G., Luo, J., Wang, Z. Q., Yang, X. Y., Lin, Y. D., et al. (2016). MicroRNAs Are Novel Non-invasive Diagnostic Biomarkers for Pulmonary Embolism: a Meta-Analysis. *J. Thorac. Dis.* 8 (12), 3580–3587. doi:10.21037/jtd.2016.12.98

Doherty, S. (2017). Pulmonary Embolism an Update. *Aust. Fam. Physician* 46 (11), 816–820.

Essien, E. O., Rali, P., and Mathai, S. C. (2019). Pulmonary Embolism. *Med. Clin. North. Am.* 103 (3), 549–564. doi:10.1016/j.mcna.2018.12.013

Friedman, R. C., Farh, K. K., Burge, C. B., and Bartel, D. P. (2009). Most Mammalian mRNAs Are Conserved Targets of microRNAs. *Genome Res.* 19, 92–105. doi:10.1101/gr.082701.108

Garbacki, N., Di Valentin, E., Piette, J., Cataldo, D., Crahay, C., and Colige, A. (2009). Matrix Metalloproteinase 12 Silencing: a Therapeutic Approach to Treat Pathological Lung Tissue Remodeling? *Pulm. Pharmacol. Ther.* 22 (4), 267–278. doi:10.1016/j.pupt.2009.03.001

Garzon, R., Calin, G. A., and Croce, C. M. (2009). MicroRNAs in Cancer. *Annu. Rev. Med.* 60, 167–179. doi:10.1146/annurev.med.59.053006.104707

Goldhaber, S. Z., and Bounameaux, H. (2012). Pulmonary Embolism and Deep Vein Thrombosis. *Lancet* 379 (9828), 1835–1846. doi:10.1016/S0140-6736(11)61904-1

Guo, L., Yang, Y., Liu, J., Wang, L., Li, J., Wang, Y., et al. (2014). Differentially Expressed Plasma microRNAs and the Potential Regulatory Function of Let-7b in Chronic Thromboembolic Pulmonary Hypertension. *PLoS One* 9 (6), e101055. doi:10.1371/journal.pone.0101055

Han, L., Cui, D., Li, B., Xu, W. W., Lam, A. K. Y., Chan, K. T., et al. (2019). MicroRNA-338-5p Reverses Chemoresistance and Inhibits Invasion of Esophageal Squamous Cell Carcinoma Cells by Targeting Id-1. *Cancer Sci.* 110 (12), 3677–3688. doi:10.1111/cas.14220

Hembrom, A. A., Srivastava, S., Garg, I., and Kumar, B. (2020). MicroRNAs in Venous Thrombo-Embolism. *Clin. Chim. Acta* 504, 66–72. doi:10.1016/j.cca.2020.01.034

Hong, D. S., Kang, Y. K., Borad, M., Sachdev, J., Ejadi, S., Lim, H. Y., et al. (2020). Phase 1 Study of MRX34, a Liposomal miR-34a Mimic, in Patients with Advanced Solid Tumours. *Br. J. Cancer* 122 (11), 1630–1637. doi:10.1038/s41416-020-0802-1

Iorio, M. V., and Croce, C. M. (2012). MicroRNA Dysregulation in Cancer: Diagnostics, Monitoring and Therapeutics. A Comprehensive Review. *EMBO Mol. Med.* 4 (3), 143–159. doi:10.1002/emmm.201100209

Jankowska, K. I., Sauna, Z. E., and Atreya, C. D. (2020). Role of microRNAs in Hemophilia and Thrombosis in Humans. *Int. J. Mol. Sci.* 21 (10), 3598. doi:10.3390/ijms21103598

Jiang, Z., Ma, J., Wang, Q., Wu, F., Ping, J., and Ming, L. (2018). Combination of Circulating miRNA-320a/b and D-Dimer Improves Diagnostic Accuracy in Deep Vein Thrombosis Patients. *Med. Sci. Monit.* 24, 2031–2037. doi:10.12659/msm.906596

Juźwik, C. A., S Drake, S., Zhang, Y., Paradis-Isler, N., Sylvester, A., Amar-Zifkin, A., et al. (2019). microRNA Dysregulation in Neurodegenerative Diseases: A Systematic Review. *Prog. Neurobiol.* 182, 101664. doi:10.1016/j.pneurobio.2019.101664

Kessler, T., Erdmann, J., Vilne, B., Bruse, P., Kurowski, V., Diemert, P., et al. (2016). Serum microRNA-1233 Is a Specific Biomarker for Diagnosing Acute Pulmonary Embolism. *J. Transl. Med.* 14 (1), 120. doi:10.1186/s12967-016-0886-9

Liang, D., Wen, Z., Han, W., Li, W., Pan, L., and Zhang, R. (2021). Curcumin Protects against Inflammation and Lung Injury in Rats with Acute Pulmonary Embolism with the Involvement of microRNA-21/PTEN/NF-κB axis. *Mol. Cel Biochem.* 476, 2823–2835. doi:10.1007/s11010-021-04127-z

Liu, T., Kang, J., and Liu, F. (2018). Plasma Levels of microRNA-221 (miR-221) Are Increased in Patients with Acute Pulmonary Embolism. *Med. Sci. Monit.* 24, 8621–8626. doi:10.12659/MSM.910893

Liu, Y., Xie, M., Gao, X., and Liu, R. (2021). Predictive Value of Circulating microRNA-134 Levels for Early Diagnosis of Acute Pulmonary Embolism: Meta-Analysis. *J. Cardiovasc. Trans. Res.* 14, 744–753. doi:10.1007/s12265-020-10087-4

Long, B. (2016). Controversies in Pulmonary Embolism Imaging and Treatment of Subsegmental Thromboembolic Disease. emDocs. Available at www.emdocs.net/controversies-in-pe-diagnosis-and-treatment (Accessed July 5, 2017).

Lou, X., Zhang, F., Dong, Z., Wang, B., and Zhao, X. (2016). Effects of PI3 - K/Akt and MAPKs Signal Pathway in Oxidative Stress Induced HUVECs Apoptosis. *Chin. J. Crit. Care Med.* 36, 78–82. doi:10.3969/j.issn.1002-1949.2016.01.018

Lv, W., Duan, Q., Wang, L., Gong, Z., Yang, F., and Song, Y. (2013). Gene Expression Levels of Cytokines in Peripheral Blood Mononuclear Cells from Patients with Pulmonary Embolism. *Mol. Med. Rep.* 7, 1245–1250. doi:10.3892/mmr.2013.1344

Martínez-González, J., Rius, J., Castelló, A., Cases-Langhoff, C., and Badimon, L. (2003). Neuron-derived Orphan Receptor-1 (NOR-1) Modulates Vascular Smooth Muscle Cell Proliferation. *Circ. Res.* 92, 96–103. doi:10.1161/01.es.0000050921.53008.47

Neto-Neves, E. M., Kiss, T., Muhl, D., and Tanus-Santos, J. E. (2013). Matrix Metalloproteinases as Drug Targets in Acute Pulmonary Embolism. *Curr. Drug Targets* 14 (3), 344–352. doi:10.2174/1389450111314030006

Neto-Neves, E. M., Kiss, T., Muhl, D., and Tanus-Santos, J. E. (2013). Matrix Metalloproteinases as Drug Targets in Acute Pulmonary Embolism. *Curr. Drug Targets* 14 (3), 344–352. doi:10.2174/1389450111314030006

Ou, M., Zhang, C., Chen, J., Zhao, S., Cui, S., and Tu, J. (2020). Overexpression of MicroRNA-340-5p Inhibits Pulmonary Arterial Hypertension Induced by APE by Downregulating IL-1β and IL-6. *Mol. Ther. Nucleic Acids* 21, 542–554. doi:10.1016/j.omtn.2020.05.022

Peng, L., Han, L., Li, X. N., Miao, Y. F., Xue, F., and Zhou, C. (2020). The Predictive Value of microRNA-134 and microRNA-1233 for the Early Diagnosis of Acute Exacerbation of Chronic Obstructive Pulmonary Disease with Acute Pulmonary Embolism. *Int. J. Chron. Obstruct Pulmon Dis.* 15, 2495–2503. doi:10.2147/COPD.S266021

Piazza, G., and Goldhaber, S. Z. (2006). Acute Pulmonary Embolism: Part I: Epidemiology and Diagnosis. *Circulation* 114 (2), e28–32. doi:10.1161/CIRCULATIONAHA.106.620872

Qian, Q., Zhang, J., He, F. P., Bao, W. X., Zheng, T. T., Zhou, D. M., et al. (2019). Down-regulated Expression of microRNA-338-5p Contributes to Neuropathology in Alzheimer's Disease. *FASEB J.* 33 (3), 4404–4417. doi:10.1096/fj.201801846R

Rius, J., Martínez-González, J., Crespo, J., and Badimon, L. (2004). Involvement of Neuron-Derived Orphan Receptor-1 (NOR-1) in LDL-Induced Mitogenic

Stimulus in Vascular Smooth Muscle Cells: Role of CREB. *Arterioscler Thromb. Vasc. Biol.* 24, 697–702. doi:10.1161/01.ATV.0000121570.00515.dc

Rodriguez-Rius, A., Lopez, S., Martinez-Perez, A., Souto, J. C., and Soria, J. M. (2020). Identification of a Plasma MicroRNA Profile Associated with Venous Thrombosis. *Arterioscler Thromb. Vasc. Biol.* 40 (5), 1392–1399. doi:10.1161/ATVBAHA.120.314092

Schulte, C., Karakas, M., and Zeller, T. (2017). microRNAs in Cardiovascular Disease - Clinical Application. *Clin. Chem. Lab. Med.* 55 (5), 687–704. doi:10.1515/cclm-2016-0576

Souza-Costa, D. C., Zerbini, T., Palei, A. C., Gerlach, R. F., and Tanus-Santos, J. E. (2005). L-arginine Attenuates Acute Pulmonary Embolism-Induced Increases in Lung Matrix Metalloproteinase-2 and Matrix Metalloproteinase-9. *Chest* 128 (5), 3705–3710. doi:10.1378/chest.128.5.3705

Sun, L., Li, X., Li, Q., Wang, L., Li, J., and Shu, C. (2021). Multiple Arterial and Venous Thromboembolism in a Male Patient with Hereditary Protein C Deficiency. *Medicine (Baltimore)* 100 (15), e25575. doi:10.1097/MD.0000000000025575

Suzuki, T., Lyon, A., Saggar, R., Heaney, L. M., Aizawa, K., Cittadini, A., et al. (2016). Editor's Choice-Biomarkers of Acute Cardiovascular and Pulmonary Diseases. *Eur. Heart J. Acute Cardiovasc. Care* 5 (5), 416–433. doi:10.1177/2048872616652309

Tay, J. W., Romeo, G., Hughes, Q. W., and Baker, R. I. (2013). Micro-ribonucleic Acid 494 Regulation of Protein S Expression. *J. Thromb. Haemost.* 11, 1547–1555. doi:10.1111/jth.12331

Tosato, G., and Jones, K. D. (1990). Interleukin-1 Induces Interleukin-6 Production in Peripheral Blood Monocytes. *Blood* 75 (6), 1305–1310. doi:10.1182/blood.v75.6.1305.bloodjournal7561305

Vienberg, S., Geiger, J., Madsen, S., and Dalgaard, L. T. (2017). MicroRNAs in Metabolism. *Acta Physiol. (Oxf)* 219 (2), 346–361. doi:10.1111/apha.12681

Wang, Q., Ma, J., Jiang, Z., Wu, F., Ping, J., and Ming, L. (2018). Diagnostic Value of Circulating microRNA-27a/b in Patients with Acute Pulmonary Embolism. *Int. Angiol.* 37 (1), 19–25. doi:10.23736/S0392-9590.17.03877-9

Wojciechowska, A., Braniewska, A., and Kozar-Kamińska, K. (2017). MicroRNA in Cardiovascular Biology and Disease. *Adv. Clin. Exp. Med.* 26 (5), 865–874. doi:10.17219/acem/62915

Xiang, Q., Zhang, H. X., Wang, Z., Liu, Z. Y., Xie, Q. F., Hu, K., et al. (2019). The Predictive Value of Circulating microRNAs for Venous Thromboembolism Diagnosis: A Systematic Review and Diagnostic Meta-Analysis. *Thromb. Res.* 181, 127–134. doi:10.1016/j.thromres.2019.07.024

Xiao, J., Jing, Z. C., Ellinor, P. T., Liang, D., Zhang, H., Liu, Y., et al. (2011). MicroRNA-134 as a Potential Plasma Biomarker for the Diagnosis of Acute Pulmonary Embolism. *J. Transl. Med.* 9, 159. doi:10.1186/1479-5876-9-159

Xie, X., Li, S., Zhu, Y., Liu, L., Pan, Y., Wang, J., et al. (2017). MicroRNA-27a/b Mediates Endothelin-1-Induced PPARγ Reduction and Proliferation of Pulmonary Artery Smooth Muscle Cells. *Cell Tissue Res* 369 (3), 527–539. doi:10.1007/s00441-017-2625-9

Xie, X., Liu, C., Lin, W., Zhan, B., Dong, C., Song, Z., et al. (2016). Deep Vein Thrombosis Is Accurately Predicted by Comprehensive Analysis of the Levels of microRNA-96 and Plasma D-Dimer. *Exp. Ther. Med.* 12 (3), 1896–1900. doi:10.3892/etm.2016.3546

Yang, K., Li, W., Duan, W., Jiang, Y., Huang, N., Li, Y., et al. (2019). Resveratrol Attenuates Pulmonary Embolism Associated Cardiac Injury by Suppressing Activation of the Inflammasome via the MALAT1 miR 22 3p Signaling Pathway. *Int. J. Mol. Med.* 44 (6), 2311–2320. doi:10.3892/ijmm.2019.4358

Zhang, S., Cheng, Z., Wang, Y., and Han, T. (2021). The Risks of miRNA Therapeutics: In a Drug Target Perspective. *Dddt* 15, 721–733. doi:10.2147/dddt.s288859

Zhang, W., Li, Y., Xi, X., Zhu, G., Wang, S., Liu, Y., et al. (2020). MicroRNA 15a 5p Induces Pulmonary Artery Smooth Muscle Cell Apoptosis in a Pulmonary Arterial Hypertension Model via the VEGF/p38/MMP2 Signaling Pathway. *Int. J. Mol. Med.* 45 (2), 461–474. doi:10.3892/ijmm.2019.4434

Zhang, Y., Zhang, Z., Wei, R., Miao, X., Sun, S., Liang, G., et al. (2020). IL (Interleukin)-6 Contributes to Deep Vein Thrombosis and Is Negatively Regulated by miR-338-5p. *Arterioscler Thromb. Vasc. Biol.* 40 (2), 323–334. doi:10.1161/ATVBAHA.119.313137

Zhang, Y., He, Y., Zong, Y., Guo, J., Sun, L., Ma, Y., et al. (2015). 17 Beta-Estradiol Attenuates Homocysteine-Induced Oxidative Stress and Inflammatory Response as Well as MAPKs cascade via Activating PI3-K/Akt Signal Transduction Pathway in Raw 264.7 Cells. *Acta Biochim. Biophys. Sin. (Shanghai)* 47, 65–72. doi:10.1093/abbs/gmu124

Zhou, X., Wen, W., Shan, X., Qian, J., Li, H., Jiang, T., et al. (2016). MiR-28-3p as a Potential Plasma Marker in Diagnosis of Pulmonary Embolism. *Thromb. Res.* 138, 91–95. doi:10.1016/j.thromres.2015.12.006

Conflict of Interest: The authors declare that the research was conducted in the absence of any commercial or financial relationships that could be construed as a potential conflict of interest.

The Handling Editor declared a shared parent affiliation with four of the authors MD, JL, LZ, XL at the time of the review

Publisher's Note: All claims expressed in this article are solely those of the authors and do not necessarily represent those of their affiliated organizations, or those of the publisher, the editors and the reviewers. Any product that may be evaluated in this article, or claim that may be made by its manufacturer, is not guaranteed or endorsed by the publisher.

frontiers in Pharmacology

CORRECTION
published: 05 January 2022
doi: 10.3389/fphar.2021.822059

Corrigendum: The Function of microRNAs in Pulmonary Embolism: Review and Research Outlook

Mingyao Luo[1], *Mingyuan Du*[2,3], *Chang Shu*[1,2,3], *Sheng Liu*[1], *Jiehua Li*[2,3], *Lei Zhang*[2,3] *and Xin Li*[2,3]*

[1]State Key Laboratory of Cardiovascular Diseases, Center of Vascular Surgery, Fuwai Hospital, National Center for Cardiovascular Diseases, Chinese Academy of Medical Science and Peking Union Medical College, Beijing, China, [2]Department of Vascular Surgery, The Second Xiangya Hospital, Central South University, Changsha, China, [3]The Institute of Vascular Diseases, Central South University, Changsha, China

OPEN ACCESS

Edited and reviewed by:
Xiaohui Li,
Central South University, China

***Correspondence:**
Xin Li
lixin1981@csu.edu.cn

Specialty section:
This article was submitted to Respiratory Pharmacology, a section of the journal Frontiers in Pharmacology

Received: 25 November 2021
Accepted: 07 December 2021
Published: 05 January 2022

Citation:
Luo M, Du M, Shu C, Liu S, Li J, Zhang L and Li X (2022) Corrigendum: The Function of microRNAs in Pulmonary Embolism: Review and Research Outlook. Front. Pharmacol. 12:822059. doi: 10.3389/fphar.2021.822059

Keywords: biomarker, deep venous thrombosis, miRNA, molecular regulation, pulmonary embolism, treatment target

A Corrigendum on

The Function of microRNAs in Pulmonary Embolism: Review and Research Outlook
by Luo, M., Du, M., Shu, C., Liu, S., Li, J., Zhang, L., and Li, X. (2021). Front. Pharmacol. 12:743945. doi: 10.3389/fphar.2021.743945

In the original article, there was a mistake in the caption for **Figure 1A** as published. The corrected sentence in the caption reads as follows: "**(A)** inflammatory intima specimen accompanied with emboli in pulmonary artery main trunk (black arrow) taken from a patient of pulmonary vasculitis." The corrected **Figure 1** appears below.

The authors apologize for this error and state that it does not change the scientific conclusions of the article in any way. The original article has been updated.

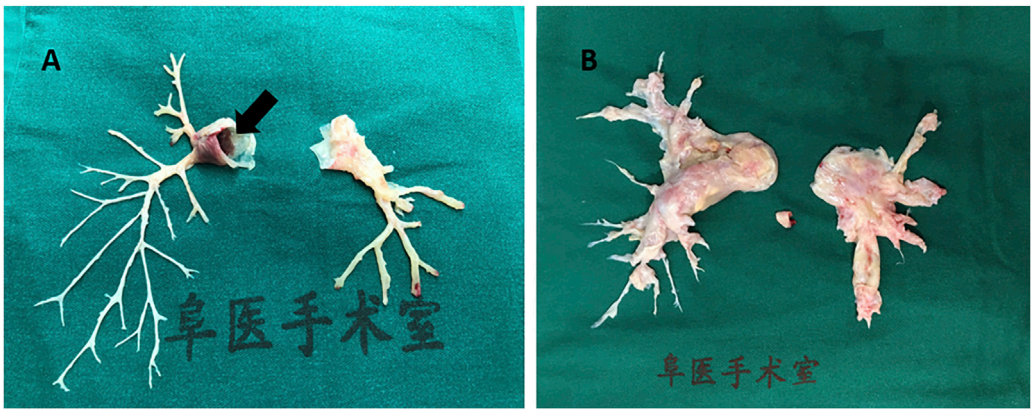

FIGURE 1 | Human pulmonary artery pathological specimen shows **(A)** inflammatory intima specimen accompanied with emboli in pulmonary artery main trunk (black arrow) taken from a patient of pulmonary vasculitis; **(B)** hyperplasia endothelial tissue from pulmonary endarterectomy operation in chronic thrombosis embolic pulmonary hypertension (CTEPH) patient.

frontiers in Pharmacology

ORIGINAL RESEARCH
published: 26 October 2021
doi: 10.3389/fphar.2021.755077

Magnolol Attenuates Right Ventricular Hypertrophy and Fibrosis in Hypoxia-Induced Pulmonary Arterial Hypertensive Rats Through Inhibition of the JAK2/STAT3 Signaling Pathway

Minyi Fu[1,2,3†], *Fangmei Luo*[4†], *Eli Wang*[1,5], *Yueping Jiang*[1,2,3], *Shao Liu*[1,2,3], *Jun Peng*[5,6] *and Bin Liu*[1,2,3*]

[1]Department of Pharmacy, Xiangya Hospital, Central South University, Changsha, China, [2]National Clinical Research Center for Geriatric Disorders, Xiangya Hospital, Institute for Rational and Safe Medication Practices, Central South University, Changsha, China, [3]The Hunan Institute of Pharmacy Practice and Clinical Research, Xiangya Hospital, Central South University, Changsha, China, [4]Department of Pharmacy, Hunan Children's Hospital, Changsha, China, [5]Department of Pharmacology, Xiangya School of Pharmaceutical Sciences, Central South University, Changsha, China, [6]Hunan Provincial Key Laboratory of Cardiovascular Research, Xiangya School of Pharmaceutical Sciences, Central South University, Changsha, China

Right ventricular (RV) remodeling is one of the essential pathological features in pulmonary arterial hypertension (PAH). RV hypertrophy or fibrosis are the leading causes of RV remodeling. Magnolol (6, 6′, 7, 12-tetramethoxy-2,2′-dimethyl-1-β-berbaman, C18H18O2) is a compound isolated from *Magnolia Officinalis*. It possesses multiple pharmacological activities, such as anti-oxidation and anti-inflammation. This study aims to evaluate the effects and underlying mechanisms of magnolol on RV remodeling in hypoxia-induced PAH. *In vivo*, male Sprague Dawley rats were exposed to 10% O_2 for 4 weeks to establish an RV remodeling model, which showed hypertrophic and fibrotic features (increases of Fulton index, cellular size, hypertrophic and fibrotic marker expression), accompanied by an elevation in phosphorylation levels of JAK2 and STAT3; these changes were attenuated by treating with magnolol. *In vitro*, the cultured H9c2 cells or cardiac fibroblasts were exposed to 3% O_2 for 48 h to induce hypertrophy or fibrosis, which showed hypertrophic (increases in cellular size as well as the expression of ANP and BNP) or fibrotic features (increases in the expression of collagen **I**, collagen **III**, and α-SMA). Administration of magnolol and TG-101348 or JSI-124 (both JAK2 selective inhibitors) could prevent myocardial hypertrophy and fibrosis, accompanied by the decrease in the phosphorylation level of JAK2 and STAT3. Based on these observations, we conclude that magnolol can attenuate RV hypertrophy and fibrosis in hypoxia-induced PAH rats through a mechanism involving inhibition of the JAK2/STAT3 signaling pathway. Magnolol may possess the potential clinical value for PAH therapy.

Keywords: magnolol, right ventricle remodeling, myocardial hypertrophy, myocardial fibrosis, JAK2, stat3

OPEN ACCESS

Edited by:
Xiaohui Li,
Central South University, China

Reviewed by:
Zongye Cai,
Zhejiang University, China
Benjamin Dunmore,
University of Cambridge, United Kingdom

****Correspondence:***
Bin Liu
liubin@csu.edu.cn

[†]These authors have contributed equally to this work and share first authorship

Specialty section:
This article was submitted to Respiratory Pharmacology, a section of the journal Frontiers in Pharmacology

Received: *07 August 2021*
Accepted: *11 October 2021*
Published: *26 October 2021*

Citation:
Fu M, Luo F, Wang E, Jiang Y, Liu S, Peng J and Liu B (2021) Magnolol Attenuates Right Ventricular Hypertrophy and Fibrosis in Hypoxia-Induced Pulmonary Arterial Hypertensive Rats Through Inhibition of the JAK2/STAT3 Signaling Pathway. Front. Pharmacol. 12:755077. doi: 10.3389/fphar.2021.755077

INTRODUCTION

Pulmonary arterial hypertension (PAH) is a malignant cardiopulmonary vascular disease characterized by a progressive increase in pulmonary vascular resistance and pulmonary arterial pressure, which eventually leads to right ventricular (RV) remodeling and even RV failure (Vonk-Noordegraaf et al., 2013; Zelt et al., 2019). In PAH, the continuous increase in RV afterload can initially lead to compensatory remodeling of the right ventricle. However, as the disease progresses, it will gradually develop into decompensated remodeling, manifesting as excessive myocardial hypertrophy and fibrosis (Vonk Noordegraaf et al., 2017; Andersen et al., 2019; de Man et al., 2019). A cohort study has verified that the 5-year survival rate for PAH patients with stable or improving RV function is significantly higher than that of patients with RV failure (van de Veerdonk et al., 2011), suggesting that RV failure is the leading cause for the death in PAH patients. Current clinical drug treatment strategies for RV failure aim to enhance RV contractility or reduce RV afterload (Cassady and Ramani, 2020). However, it cannot effectively reverse the process of RV remodeling and RV failure during PAH. Therefore, seeking drugs with the potential to target the RV remodeling during PAH is of great significance for delaying the progression of PAH and improving the survival rate of PAH patients.

Janus kinase (JAK)/signal transducer and activator of transcription (STAT) is a classic membrane-to-nucleus signaling pathway that can be activated by diverse cytokines, growth factors, and interferons (O'Shea et al., 2015). In mammals, there are 4 JAKs (JAK1, JAK2, JAK3, and TYK2) and 7 STATs (STAT1, STAT2, STAT3, STAT4, STAT5A, STAT5B, and STAT6) (Villarino et al., 2020). Recently studies showed that the JAK2/STAT3 pathway is involved in the development of PAH (Milara et al., 2018; Zhang et al., 2020; Yerabolu et al., 2021). Zhang et al. confirmed that hypoxia could stimulate the phosphorylation of JAK2, which in turn activates STAT3. The activated STAT3 enters the nucleus to regulate the gene expression of *CyclinA2*, which ultimately leads to the excessive proliferation of pulmonary artery smooth muscle cells and participates in vascular remodeling of PAH (Zhang et al., 2020). Furthermore, Ye et al. demonstrated that the JAK2/STAT3 pathway participates in myocardial hypertrophy and fibrosis induced by angiotensin II (AngII) by regulating the expression of downstream target genes (such as *Tgf-β*, *Col1a1*, and *Myh7*), and ultimately lead to cardiac remodeling (Ye et al., 2020). Based on these reports, we hypothesized that the JAK2/STAT3 pathway might be a valuable strategy to prevent the development of RV remodeling in PAH.

Magnolol, a compound isolated from *Magnolia Officinalis*, possesses multiple pharmacological activities such as anti-oxidation, anti-inflammation, and anti-tumor (Zhang et al., 2019; Lin et al., 2021). A recent study has found that magnolol can inhibit the proliferation and collagen synthesis of cardiac fibroblasts (Chen et al., 2021b). In another report, magnolol can inhibit the phosphorylation of STAT3 in a dose-dependent manner, but its regulatory effect on JAK2 remains unclear (Peng et al., 2021). By using the SwissTargetPrediction database, we found that JAK2 may be a potential target of magnolol. Based on these reports and our prediction, it is reasonable to speculate that magnolol can prevent the development of RV remodeling during PAH through mechanisms involving blocking the activation of the JAK2/STAT3 pathway.

The main purpose of this study is to explore the effect of magnolol on RV hypertrophy and fibrosis in hypoxia-induced PAH rats. Using a rat model of hypoxia-induced PAH, we first investigated the beneficial effect of magnolol on RV remodeling and its relevance to the JAK2/STAT3 pathway. To confirm the findings *in vivo*, we established hypoxia-induced cell hypertrophy and fibrosis models by using H9c2 cells and cardiac fibroblasts, respectively. Combining with TG-101348 and JSI-124, the specific inhibitor of JAK2, we confirmed that the inhibitory effect of magnolol on myocardial hypertrophy and fibrosis is related to the inhibition of the JAK2/STAT3 signaling pathway.

MATERIALS AND METHODS

Animal Experiments

Male SD rats (220 g) were randomly divided into five groups (n = 10 per group): the normoxia group, the hypoxia group, the hypoxia plus Magnolol (L) group (low dose, 10 mg/kg/d), the hypoxia plus Magnolol (H) group (high dose, 20 mg/kg/d), and the vehicle group. Rats in the normoxia group were kept in a normoxia environment for 4 weeks, while rats in the hypoxia group were kept in a hypoxic chamber (10% O_2). Magnolol (purity ≥98%) was purchased from Energy Chemical Company. The rats in the hypoxia plus magnolol groups were administered with magnolol at 10 or 20 mg/kg (i.p.) once a day for 4 weeks. The rats in the hypoxia plus vehicle group were given the same volume (0.1 ml/100 g per day) of vehicle (a mixture with 5% DMSO, 30% PEG 400, 5% Tween-80, and 60% normal saline) and then subjected to hypoxia. At the end of 4 weeks, the heart function was assessed by Doppler echocardiography. And then, the rats were anesthetized with sodium pentobarbital (30 mg/kg, i.p.). The RVSP was measured by the right heart catheterization method. The heart tissues were collected and dissected to calculate the Fulton index (RV/LV + IVS, RV/tibial length, or RV/body weight). Part of the RV samples was fixed with 4% paraformaldehyde for morphological analysis, while other samples were frozen at −80°C for molecular studies (measurements of ANP, BNP, α-SMA, and collagen I/III mRNA expression as well as p-JAK2/JAK2 and p-STAT3/STAT3 protein levels).

Cell Experiments

The rat heart-derived H9c2 cells were obtained from the Chinese Academy of Sciences (Shanghai, China). H9c2 cells were cultured in Dulbecco's Modified Eagle Medium (DMEM) containing 10% fetal bovine serum (FBS). The isolation and culture of cardiac fibroblasts from the heart tissues of neonatal male rats were performed as in previous studies (Jeppesen et al., 2011; Li et al., 2016; Li et al., 2020). Briefly, the heart tissues of neonatal rats were

harvested and cut into 1 mm^2 pieces with scissors, which were digested in an incubator at 37°C for 20 min with trypsin/EDTA (Gibco, USA) and collagenase II (Sigma Aldrich, USA). The supernatant was collected and centrifuged at 1,200 rpm for 8 min. Then the adherent cells were resuspended with DMEM containing 10% FBS and plated on the culture flask for 1.5 h. The identification of cardiac fibroblasts was performed by immunofluorescence staining (vimentin and α-SMA) as described in previous studies (Li et al., 2016; Li et al., 2020). Cells that are positive for vimentin and negative for α-SMA are cardiac fibroblasts. These cells were collected for subsequent experiments at the passage from 2 to 3.

To evaluate the effect of magnolol on hypoxia-induced myocardial hypertrophy and fibrosis, H9c2 or cardiac fibroblasts were divided into seven groups: 1) the control group, cells were cultured under normal conditions; 2) the hypoxia group, cells were cultured under hypoxic condition (3% O_2); 3) the hypoxia plus magnolol group (L), 10 μM of magnolol was added to the culture medium before the hypoxia treatment; 4) the hypoxia plus magnolol group (H), 20 μM of magnolol was added to the culture medium before the hypoxia treatment; 5) the hypoxia plus TG-101348 group, 1 μM of TG-101348 (a specific inhibitor of JAK2) was added to the culture medium before the hypoxia treatment; 6) the hypoxia plus JSI-124 group, 1 μM of JSI-124 (a specific inhibitor of JAK2) was added to the culture medium before the hypoxia treatment; and 7) the hypoxia plus vehicle group, an equal volume of vehicle (DMSO) was added to the culture medium before the hypoxia treatment. At the end of the experiments, the cells were collected for morphological and molecular analysis.

Echocardiographic Assessment

The echocardiographic assessment was conducted using a Vevo 2100 imaging system (Visual Sonics, Toronto, Canada) to evaluate the changes in RV function in rats. The RV wall thickness in the diastole and systole period was measured by short axis in motion mode. The differences in the ratio of pulmonary artery acceleration time to ejection time (PAAT/PAET) were calculated to evaluate the RV function in rats.

Morphological Observation

The staining with Hematoxylin-eosin (HE), Wheat germ agglutinin (WGA), Sirius red, Masson' trichrome (Masson), or Verhoeff elastic van Gieson (EVG) was performed to evaluate the morphological changes of the RV tissues. The procedures were conducted as described in our previous studies (Liu et al., 2014; Li et al., 2019a; Wang et al., 2019). Briefly, for HE staining, the paraffin sections were stained with HE staining solution (Servicebio, Wuhan, China) for 5 min. A minimum of 6 microscopic fields from each slide was randomly selected for observation under a microscope (Nikon, Tokyo, Japan). The cross-sectional width of RV tissue in each group was randomly measured to assess the degree of RV hypertrophy. 3 representative points per RV were chosen to measure the width, and the average value was used to represent the width for each RV to ensure the reliability of the results.

For WGA staining, the slices were deparaffinized and immersed in EDTA buffer for antigen retrieval. After washing 3 times with PBS, the slices were incubated with WGA staining solution (Servicebio, Wuhan, China) in the dark at 37°C for 30 min. DAPI staining solution was added to stain the nucleus for 5 min. The cross-sectional area and perimeter of 10 cells in the field of view were measured to obtain the average value. The Changes in the cross-sectional area and circumference of cardiomyocytes in the RV tissues were observed under a fluorescence microscope to assess the degree of myocardial hypertrophy.

For EVG staining, the paraffin sections of heart tissue were deparaffinized and stained with EVG staining solution (Servicebio, Wuhan, China) for 5 min, differentiated in 2% ferric chloride solution, and washed in running tap water. The formation of fibers in heart tissue was observed and analyzed under a microscope. The elastic fibers are purple-black, the collagen fibers are red, and the background is yellow.

For Sirius red or Masson staining, the slices were deparaffinized and stained with Sirius Red or Masson staining solution (Servicebio, Wuhan, China), the formation of collagen fibers in the interstitial or perivascular of RV tissue was observed under a microscope.

Immunofluorescence Staining

Morphological changes in H9c2 cells were observed by immunofluorescence staining as described in our previous studies (Li et al., 2019b). In brief, H9c2 cells were fixed with 4% paraformaldehyde for 20 min. After washing with PBS 3 times, the cells were permeabilized with 0.25% Triton-X-100 (Beyotime, Shanghai, China) and blocked with bovine serum albumin (Merck, Darmstadt, Germany) for 45 min. Then the cells were incubated with primary antibodies against α-SMA (Cell Signaling Technology, Massachusetts, USA) overnight at 4°C followed by incubation with the secondary antibody of Alexa Fluor 488-labeled Goat Anti-Mouse IgG (Beyotime, Shanghai, China). The cell morphological changes were observed under a fluorescence microscope, and the cross-sectional area of H9c2 cells was calculated to assess the degree of cell hypertrophy.

Tissue immunofluorescence staining was performed to evaluate the phosphorylation level of JAK2 in the RV tissue. After the treatment of deparaffinization, antigen retrieval, and blocking, RV tissue slices were incubated with primary antibodies against p-JAK2 (Abcam, Cambridge, MA, USA) overnight at 4°C followed by incubation with the secondary antibody of Cy3-labeled Goat Anti-Rabbit IgG (Beyotime, Shanghai, China). After washing with PBS 3 times, the cell nucleus was incubated with DAPI solution at room temperature for 5 min. The intensity of red fluorescence under a fluorescence microscope was observed to evaluate the level of p-JAK2 in RV tissues.

Real-Time PCR

Real-time PCR was performed to detect the mRNA level of ANP, BNP, collagen I, collagen III, and α-SMA. The real-time PCR primers for ANP, BNP, collagen I, collagen III, α-SMA, and GAPDH are displayed in **Table 1**. Briefly, total RNA was isolated and extracted from RV tissues, H9c2 cells, or cardiac

TABLE 1 | Primers for real-time PCR.

Gene	Forward primer	Reverse primer	Product size (bp)
ANP	aaccagagagtgagccgaga	gtggtctagcaggttcttgaaa	191
BNP	caatccacgatgcagaagctg	ggcgctgtcttgagacctaa	132
Collagen I	ccaactgaacgtgaccaaaaacca	gaaggtgctgggtagggaagtaggc	345
Collagen III	attctgccaccctgaactcaagagc	tccatgtaggcaatgctgtttttgc	342
α-SMA	ctattccttcgtgactact	atgctgttataggtggtt	255
GAPDH	tggcctccaaggagtaagaaac	ggcctctctcttgctctcagtatc	69

fibroblasts according to the RNAiso Plus kit instructions (TaKaRa Biomedical Technology, Beijing, China). 500 ng of RNA from each sample was subjected to reverse transcription reaction according to the PrimeScript™ RT Master Mix kit instructions (TaKaRa Biomedical Technology, Beijing, China). Then, a 20 μl real-time PCR reaction mixture containing 4 μl cDNA template, 10 μl PerfectStart™ Green qPCR SuperMix (Transgen Biotech, Beijing, China), 0.4 μl Passive Reference Dye, 4.8 μl Nuclease-free water, and 0.4 μl of each primer was amplified according to the following steps: an initial predenaturation at 94°C for 30 s, followed by 40 cycles of PCR reaction at 94°C for 5 s, annealing and extension at 60°C for 31 s. Gene expression was quantified using GAPDH as a loading control.

Western Blot Analysis

The procedures for sample preparation and Western blot were conducted as described in our previous studies (Liu et al., 2014; Li et al., 2019a; Wang et al., 2019). Briefly, the RV tissues, H9c2 cells, or cardiac fibroblasts were homogenized with ice-cool lysis buffer (20 mM Tris, pH 7.5, 150 mM NaCl, and 1% Triton-X-100) with a protease and phosphatase inhibitor cocktail (Beyotime, Shanghai, China). And then, the protein concentration was detected according to the BCA assay kit instructions (Beyotime, Shanghai, China). Samples containing 30–40 μg of protein were subjected to 8 or 10% SDS-PAGE gel, and then they were transferred to polyvinylidene fluoride (PVDF) blotting membranes (G.E. Healthcare, Germany). The PVDF membranes were incubated with primary antibodies against collagen I (Abcam, Cambridge, MA, USA), α-SMA (Cell Signaling Technology, Massachusetts, USA), p-JAK2 (Abcam, Cambridge, MA, USA), JAK2 (Beyotime, Shanghai, China), p-STAT3 (Signalway Antibody, Maryland, USA), STAT3 (Signalway Antibody, Maryland, USA), and α-tubulin (Santa Cruz, Texas, USA) followed by horseradish peroxidase (HRP) conjugated secondary antibody (Beyotime, Shanghai, China). The signals of Western blot bands were detected by BeyoECL Moon kit (Beyotime, Shanghai, China) through Molecular Imager ChemiDoc XRS System (Bio-Rad, Philadelphia, USA). Densitometric quantification was carried out by Image J (NIH, USA). The α-tubulin served as a loading control.

Prediction of Potential Targets of Magnolol

SwissTargetPrediction (http://www.swisstargetprediction.ch/) was used to predict the potential targets of magnolol as described in the previous study (Daina et al., 2019). The structural information of magnolol was obtained from the PubChem database (https://pubchem.ncbi.nlm.nih.gov), and then the target-related information was obtained by using SwissTargetPrediction Database. Finally, the interaction between magnolol and potential targets was analyzed and mapped by Cytoscape (Shannon et al., 2003).

Statistical Analysis

All quantitative data were presented as the means ± standard deviation (S.D.) and analyzed by using SPSS 20.0 software (SPSS, Chicago, United States). Dunnett's test or the Student-Newman Keuls test was used for multiple comparisons after one-way analysis of variance (ANOVA). A probability level of $p \leq 0.05$ was considered significant. ANOVA was used to compare the means among different groups.

RESULTS

Magnolol Prevented Hypoxia-Induced PAH and RV Remodeling

A rat model of PAH was established after continuous exposure to hypoxia (10% O_2) for 4 weeks. Compared with the control group, the right ventricular systolic pressure (RVSP) was significantly increased in the hypoxic group (**Figures 1A,B**); accompanied by the increases in the ratio of RV weight to left ventricle plus septum weight (RV/LV + IVS), RV weight to tibial length, and RV weight to body weight in the hypoxic group (**Figures 1C–E**), these phenomena were markedly attenuated by magnolol at both dosages (10 and 20 mg/kg). Interestingly, our study also found that magnolol can inhibit hypoxia-induced PAH vascular remodeling (**Supplementary Figures S1**), which is consistent with the results of Chang et al. (2018).

Magnolol Improved RV Function in the Hypoxic PAH Rats

Studies have shown that a sustained increase in pulmonary artery pressure can induce RV remodeling and eventually lead to right heart dysfunction and failure (Ciuclan et al., 2011). In this study, we found that the wall thickness of RV in the diastole and systole period was significantly increased in PAH rats (**Figures 2A–D**), accompanied by a decrease in the ratio of PAAT/PAET (**Figure 2E**); these phenomena were markedly attenuated by magnolol at both dosages (10 and 20 mg/kg). However, there was no significant difference in heart rate among all groups (**Figure 2F**).

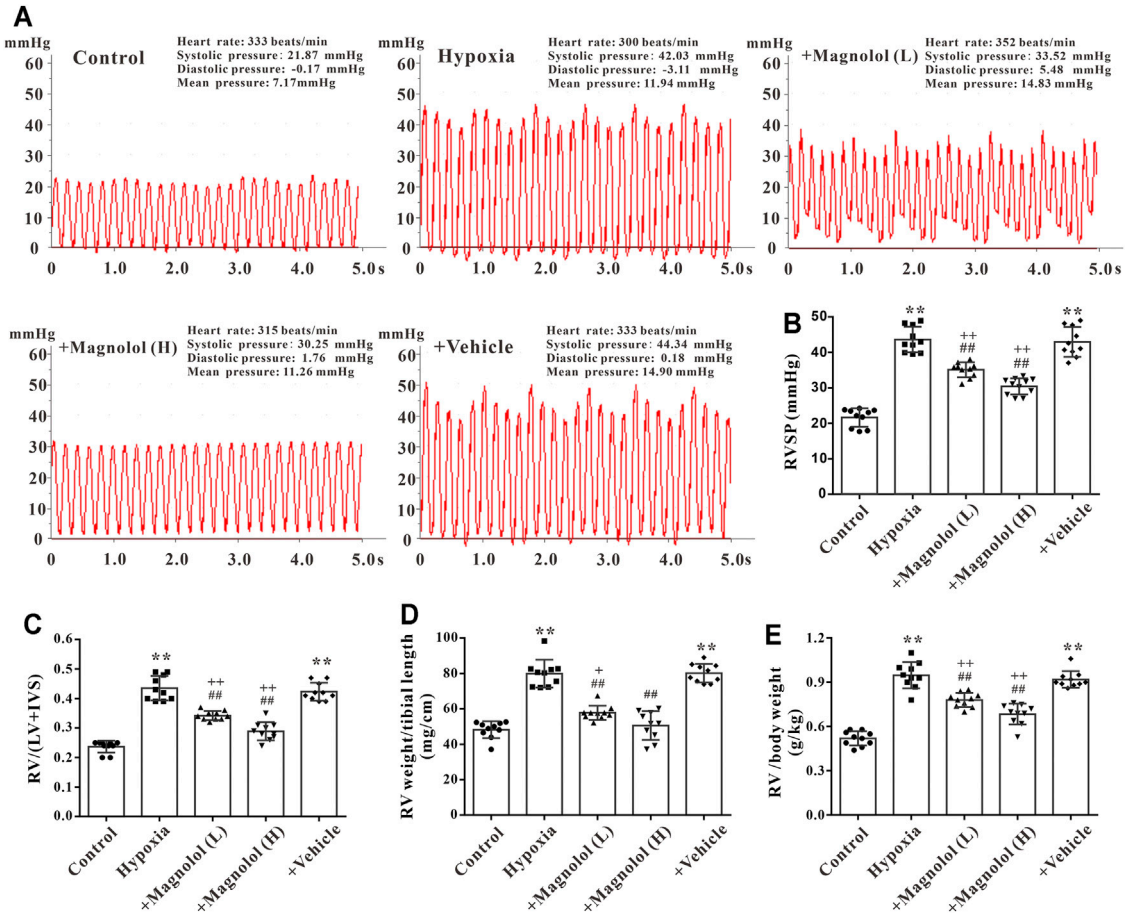

FIGURE 1 | Magnolol prevented hypoxia-induced PAH and RV remodeling. **(A)** Representative images for right ventricular systolic pressure (RVSP) were measured by the right heart catheterization method. **(B)** The value of RVSP in each group. **(C)** The ratio of RV weight to left ventricular (LV) plus interventricular septum (IVS). **(D)** The ratio of RV weight to tibial length. **(E)** The ratio of RV weight to body weight. All values are presented as mean ± S.D. (n = 10 per group). $^{**}p < 0.01$ vs. Control; $^{+}p < 0.05$, $^{++}p < 0.01$ vs. Control; $^{\#\#}p < 0.01$ vs. Vehicle.

Magnolol Attenuated RV Hypertrophy in the Hypoxic PAH Rats

Our previous study has shown that myocardial hypertrophy is one of the fundamental causes of RV remodeling in rats with hypoxia-induced PAH (Li et al., 2019b). Therefore, the effect of magnolol on RV hypertrophy in the hypoxic PAH rats was evaluated by HE and WGA staining. Compared with the control group, the cross-sectional area and perimeter of cardiomyocytes were significantly increased in the hypoxia group (**Figures 3A–E**). Besides, the mRNA levels of atrial natriuretic peptide (ANP) and brain natriuretic peptide (BNP), two biomarkers of cardiac hypertrophy, were significantly up-regulated in RV tissues of PAH rats (**Figures 3F,G**); these phenomena were reversed in the presence of magnolol.

Magnolol Attenuated RV Fibrosis in the Hypoxic PAH Rats

In addition to myocardial hypertrophy, myocardial fibrosis also plays a crucial role in the development of RV remodeling and failure. The formation of extracellular matrix (characterized by an excessive amount of collagen Ⅰ or Ⅲ) and the activation of myocardial fibroblasts into α-SMA are the main manifestations of myocardial fibrosis in PAH (Andersen et al., 2019). In this study, we observed that the collagen fibers in perivascular and interstitial RV tissue in hypoxia-induced PAH rats appeared to be increased, and those increased were inhibited by magnolol treatment (**Figures 4A–C**). To confirm these findings, we further found that the mRNA expression of collagen I, II, and a-SMA, as well as protein expression of collagen I and a-SMA, were significantly up-regulated in the RV tissue of

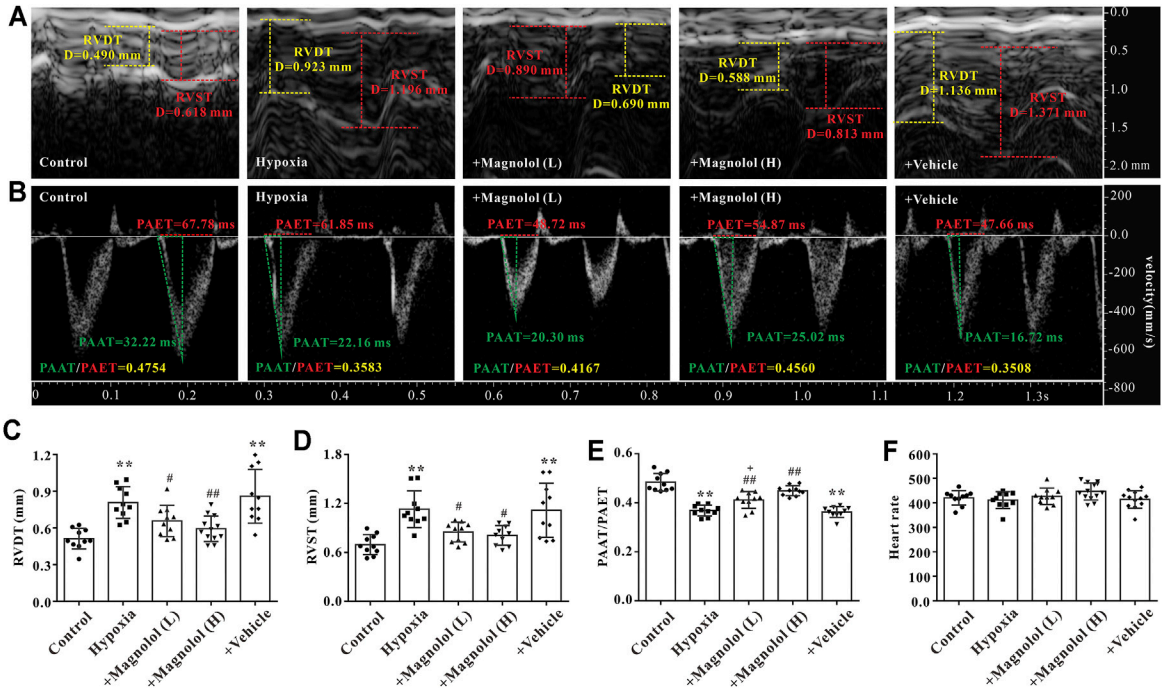

FIGURE 2 | Magnolol improved RV dysfunction in hypoxia-induced PAH rats. **(A)** Representative images of right ventricular wall thickness in diastole and systole period. **(B)** Representative images of pulsed Doppler from pulmonary artery flow tract recorded in parasternal long axis, the pulmonary artery acceleration time (PAAT, green horizontal line), the pulmonary artery ejection time (PAET, red horizontal line). **(C)** The value of right ventricular wall thickness during the diastole period (RVDT). **(D)** The value of right ventricular wall thickness during the systole period (RVST). **(E)** The ratio of PAAT/PAET. **(F)** Heart rate. All values are presented as mean ± S.D. (n = 10 per group). $^{**}p < 0.01$ vs. Control; $^{+}p < 0.05$ vs. Control; $^{\#}p < 0.05$, $^{\#\#}p < 0.01$ vs. Vehicle.

hypoxic-treated rats; these targets were markedly attenuated by magnolol treatment (**Figures 4D–I**).

Magnolol Blocked Hypoxia-Induced JAK2 and STAT3 Phosphorylation in RV Tissues

To further confirm the potential target of magnolol in inhibiting RV remodeling in hypoxia-induced PAH, we used the "SwisstargetPrediction" target prediction database. We found that JAK2 was the potential target of magnolol (**Figure 5A**). A number of studies have reported that the activation of JAK2 could promote STAT3 phosphorylation and thus participate in the process of myocardial remodeling induced by angiotensin II or $PM_{2.5}$ (Ye et al., 2020; Xing et al., 2021). Immunofluorescence staining showed that the level of p-JAK2 was increased in the RV tissues of hypoxia-induced PAH rats (**Figure 5B**), suggesting that the protective effect of magnolol on the RV remodeling in PAH rats is related to target JAK2. This phenomenon was further confirmed by western blotting, as phosphorylation levels of JAK2 and STAT3 in RV tissue were evidently elevated in hypoxia-induced PAH rats, which were blocked in the presence of magnolol (**Figures 5C,D**). However, there were no changes in total JAK2 and STAT3 levels in all groups.

Magnolol Attenuated Hypoxia-Induced H9c2 Cell Hypertrophy Through Inhibition of JAK2/STAT3 Signaling Pathway

As shown in **Figures 6A,B**, compared to the control group, the cross-sectional area of H9c2 was significantly increased in the hypoxia group, which was consistent with the results of our previous study (Li et al., 2019b). The hypoxia-induced H9c2 cell hypertrophy was inhibited by magnolol in a dose-dependent manner; TG-101348 or JSI-124 (JAK2 selective inhibitors) treatment showed a similar effect to magnolol, whereas the vehicle group had no such effect (**Figures 6A,B**). Consistent with the results *in vivo*, the mRNA expression of ANP and BNP in hypoxia-treated H9c2 cells were up-regulated; these increases were attenuated in the presence of magnolol, TG-101348, or JSI-124 (**Figures 6C,D**). The vehicle group had no such effects.

To further verify the potential mechanism of magnolol responsible for myocardial hypertrophy, the phosphorylation levels of JAK2 and STAT3 in hypoxia-treated H9c2 cells were observed. Consistent with the results *in vivo*, the phosphorylation levels of JAK2 and STAT3 in hypoxia-treated H9c2 were evidently elevated, which were attenuated in the presence of magnolol, TG-101348, or JSI-124 (**Figures 6E–G**). The vehicle group had no such effects. As shown in **Supplementary Figure S2**, under normoxic conditions, different doses of magnolol did not affect the phosphorylation levels of JAK2 and STAT3 in H9c2 cells.

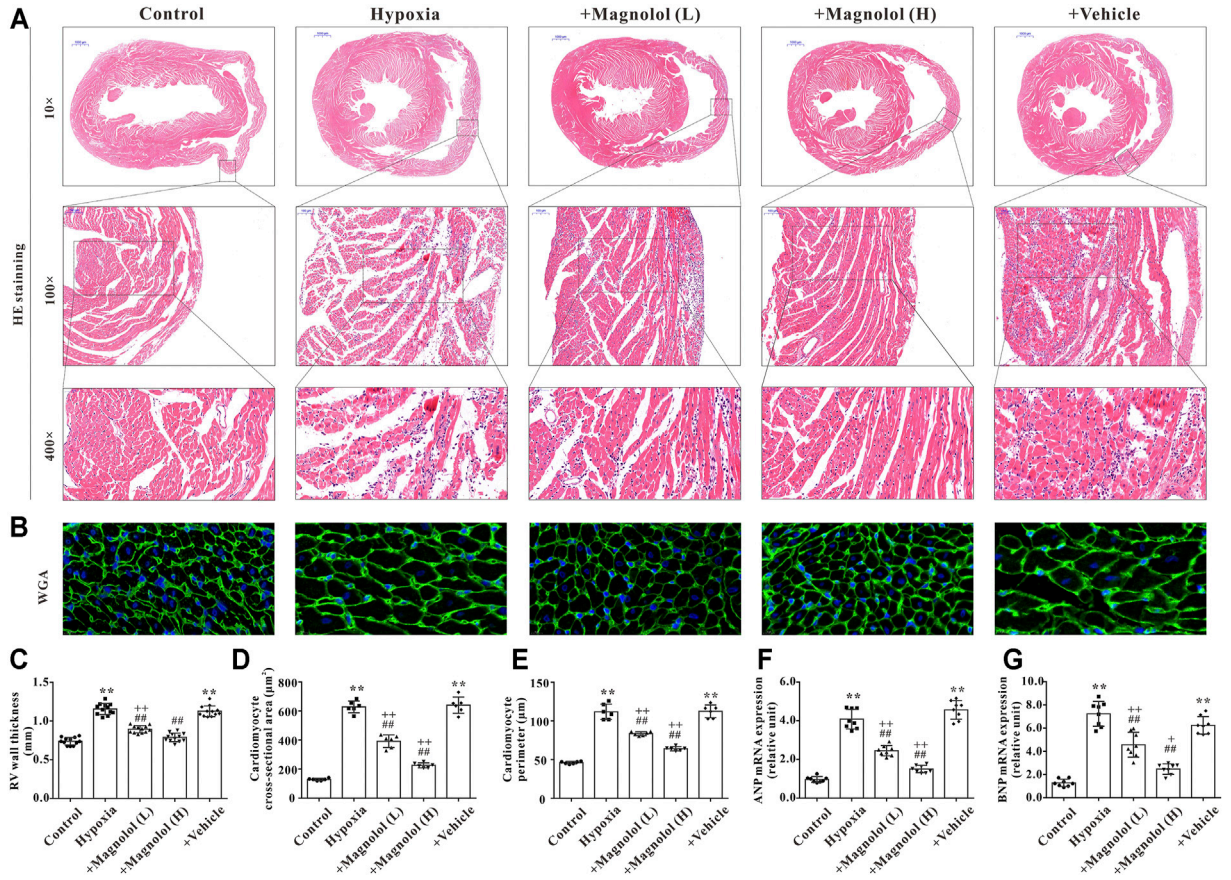

FIGURE 3 | Magnolol attenuated RV hypertrophy in hypoxia-induced PAH rats. **(A)** Representative images of HE staining for heart tissues. **(B)** Representative images of WGA staining for RV tissues. **(C)** The right ventricular wall thickness (calculated from HE staining). **(D)** The cross-sectional area of cardiomyocytes (calculated from WGA staining). **(E)** The perimeter of cardiomyocytes (calculated from WGA staining). **(F)** The mRNA levels of ANP in RV tissues. **(G)** The mRNA levels of BNP in RV tissues. $^{**}p < 0.01$ vs. Control; $^{+}p < 0.05$, $^{++}p < 0.01$ vs. Control; $^{\#\#}p < 0.01$ vs. Vehicle.

Magnolol Attenuated Hypoxia-Induced Fibrosis of Cardiac Fibroblasts Through Inhibition of the JAK2/STAT3 Signaling Pathway

Primary cardiac fibroblasts were cultured under hypoxic conditions for 24 h to establish an *in vitro* model of myocardial fibrosis. As shown in **Figure 7**, compared to the control group, the mRNA expressions of collagen Ⅰ, Ⅲ, and α-SMA, as well as the protein expressions of collagen Ⅰ and α-SMA in the hypoxia group were significantly up-regulated; these increases were attenuated by magnolol in a dose-dependent manner. Similarly, TG-101348 or JSI-124, the specific inhibitor of JAK2, could also mitigate the myocardial fibrosis induced by hypoxia, but the vehicle has no such effects (**Figures 7A–E**). Western blotting results showed that magnolol could inhibit the phosphorylation of JAK2 and STAT3 induced by hypoxia, similar to that of TG-101348 or JSI-124 did (**Figures 7D,F**). The vehicle had no such effects.

DISCUSSION

In this study, we explored the effects of magnolol on RV hypertrophy and fibrosis in hypoxia-induced PAH rats and the underlying mechanisms. The results from animal experiments demonstrated that administration of magnolol significantly prevented RV remodeling and dysfunction in PAH rats, accompanied by a decrease in the phosphorylation levels of JAK2 and STAT3. In hypoxia-treated H9c2 or cardiac fibroblasts, the cross-sectional area and mRNA levels of ANP/BNP in H9c2 were significantly increased, the expressions of collagen Ⅰ, Ⅲ, and α-SMA in cardiac fibroblasts were also elevated, concomitant with an increase of phosphorylation levels of JAK2 and STAT3; these phenomena were blocked in the presence of magnolol. To the best of our knowledge, this is the first study to provide evidence that magnolol prevents hypoxia-induced RV hypertrophy and fibrosis through inhibition of the JAK2/STAT3 pathway.

PAH is a progressive disease that can affect the normal function of pulmonary vessels and the heart (Vonk-

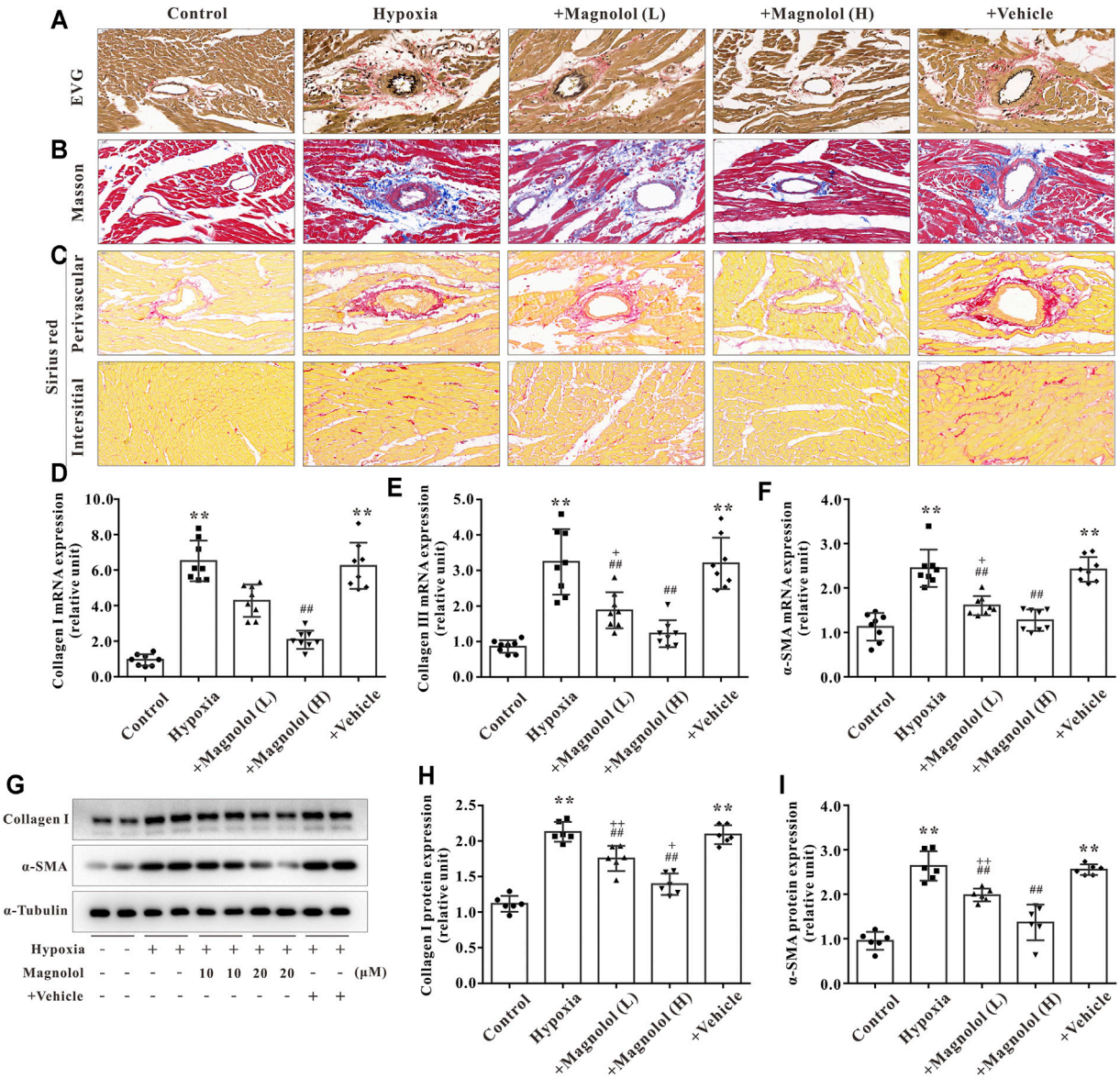

FIGURE 4 | Magnolol attenuated RV fibrosis in hypoxia-induced PAH rats. **(A)** Representative images of EVG staining for RV tissues. The collagen fibers are red, and the elastic fibers are purple-black. **(B)** Representative images of Masson staining for RV tissues. The collagen fibers are blue. **(C)** Representative images of Sirius red staining for RV tissues. The collagen fibers are red, and the background is yellow. **(D)** The mRNA levels of Collagen I in RV tissues. **(E)** The mRNA levels of Collagen III in RV tissues. **(F)** The mRNA levels of α-SMA in RV tissues. **(G)** Representative images of Western blot results for Collagen I, α-SMA, and α-tubulin. **(H, I)** The ratio of optical density between Collagen I or α-SMA and α-tubulin. All values are presented as mean ± S.D. (n = 6–10 per group). $^{**}p < 0.01$ vs Control; $^{+}p < 0.05$, $^{++}p < 0.01$ vs. Control; $^{\#\#}p < 0.01$ vs. Vehicle.

Noordegraaf et al., 2013; Frost et al., 2019). The continuous increase of pulmonary vascular resistance and pressure during PAH leads to an increase in RV afterload, which in turn induces RV remodeling. The constant expansion of the RV eventually causes right heart function damage and even right heart failure (Vonk Noordegraaf et al., 2017). In this paper, we observed a significant increase in the RVSP accompanied by an elevation in the index of RV/(LV + IVS), RV weight/tibial length, and RV weight/body weight in rats exposed to hypoxia for 4 weeks. In addition, our study also found that the RV function of rats was significantly impaired after 4 weeks of hypoxic treatment, manifesting as a significant increase in the wall thickness of the right ventricle during diastole and systole (RVDT and RVST), and a considerable reduction in the ratio of PAAT/PAET. These results indicate that the hypoxia-induced PAH rat model was successfully established.

It is well recognized that hypoxia-induced myocardial hypertrophy is the main pathological feature of RV remodeling in PAH (Zhu et al., 2017; Smith et al., 2020). Cardiac hypertrophy includes physiological and pathological

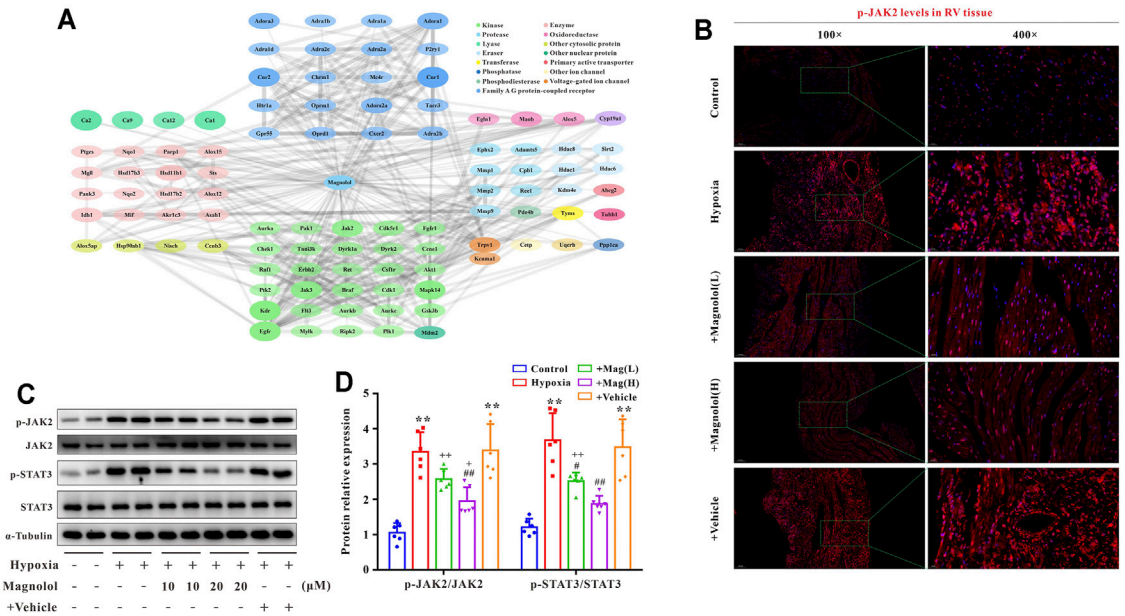

FIGURE 5 | Magnolol blocks hypoxia-induced JAK2 and STAT3 phosphorylation in RV tissues. **(A)** Results from "SwissTargetPrediction" target prediction database. **(B)** Representative images of immunofluorescence staining for p-JAK2 in each group. **(C)** Representative images of Western blot results for p-JAK2, JAK2, p-STAT3, STAT3, and α-tubulin. **(D)** The ratio of optical density between p-JAK2/JAK2 or p-STAT3/STAT3. All values are presented as mean ± S.D. (n = 6 per group).$^{**}p < 0.01$ vs. Control; $^{+}p < 0.05$, $^{++}p < 0.01$ vs. Control; $^{\#}p < 0.05$, $^{\#\#}p < 0.01$ vs. Vehicle.

hypertrophy, both manifest as the expansion of a single cardiomyocyte, but the characteristics of them are different (Nakamura and Sadoshima, 2018). Hypertrophy under physiological conditions is mainly characterized by an increase in the mass, length, and width of individual cardiomyocyte to increase myocardial contractility and maintain normal cardiac output. The above process is reversible and will not develop into heart failure. Different from physiological hypertrophy, cardiomyocytes gradually develop from the initial compensatory hypertrophy to decompensated hypertrophy under pathological conditions, which is mainly characterized by myocardial contractile dysfunction and heart failure. During this process, the expression of ANP and BNP, which is commonly regarded as a marker of heart failure, is significantly increased, accompanied by interstitial and perivascular fibrosis and myofibroblast activation (Nakamura and Sadoshima, 2018). In this study, by using HE and WGA staining, we found that the wall thickness of the RV, the cross-sectional area, and perimeter of individual cardiomyocyte significantly increased in rats exposed to hypoxia for 4 weeks, accompanied by an increase in the mRNA expressions of ANP and BNP in the RV tissue, confirmed the role of myocardial hypertrophy in RV remodeling in hypoxic PAH.

In addition to myocardial hypertrophy, myocardial fibrosis is also one of the critical factors leading to RV remodeling during PAH (Simpson and Hassoun, 2019; Tian et al., 2020). As mentioned above, the increase in RV afterload during PAH also leads to the activation of myofibroblasts, leading to myocardial fibrosis and an increase of extracellular matrix. In this study, we observed an elevation in the production of collagen fibers in interstitial and perivascular of RV, concomitant with a significant increase in the levels of myocardial fibrosis markers such as collagen Ⅰ, Ⅲ, and α-SMA, suggesting that myocardial fibrosis also plays a pivotal role in the process of RV remodeling.

Janus kinase 2 (JAK2) is an essential member of the non-receptor tyrosine kinase family, promoting the phosphorylation of signal transducer of activators of transcription 3 (STAT3). The activated STAT3 can enter the nucleus and participate in cell growth, differentiation, and apoptosis by regulating the expression of downstream target genes (Montero et al., 2021). Growing evidence has shown that JAK2/STAT3 pathway plays a vital role in the pathogenesis of PAH. Yerabolu et al. found that, compared with healthy individuals, the phosphorylation level of JAK2 in pulmonary artery smooth muscle cells derived from PAH patients was significantly increased. Using monocrotaline or hypoxia-induced PAH animal models, Yerabolu et al. demonstrated that ruxolitinib (JAK2 inhibitor) could inhibit PAH vascular remodeling and improve RV function (Yerabolu et al., 2021). Other studies reported that administration of JAK2 specific inhibitors, such as TG-101344 (also named Fedratinib) (Zhang et al., 2020) or JSI-124 (Milara et al., 2018), can delay the progression of PAH by inhibiting the activation of the JAK2/STAT3 pathway. Collectively, these studies have confirmed that the JAK2/STAT3 pathway plays a pivotal role in PAH vascular remodeling, but its role in RV remodeling has not been fully elucidated. The latest research found that the JAK2/STAT3 pathway participates in the process of AngⅡ-induced myocardial remodeling by promoting myocardial hypertrophy and fibrosis (Ye et al., 2020). In this study, we found that the phosphorylation levels of JAK2 and STAT3 were evidently

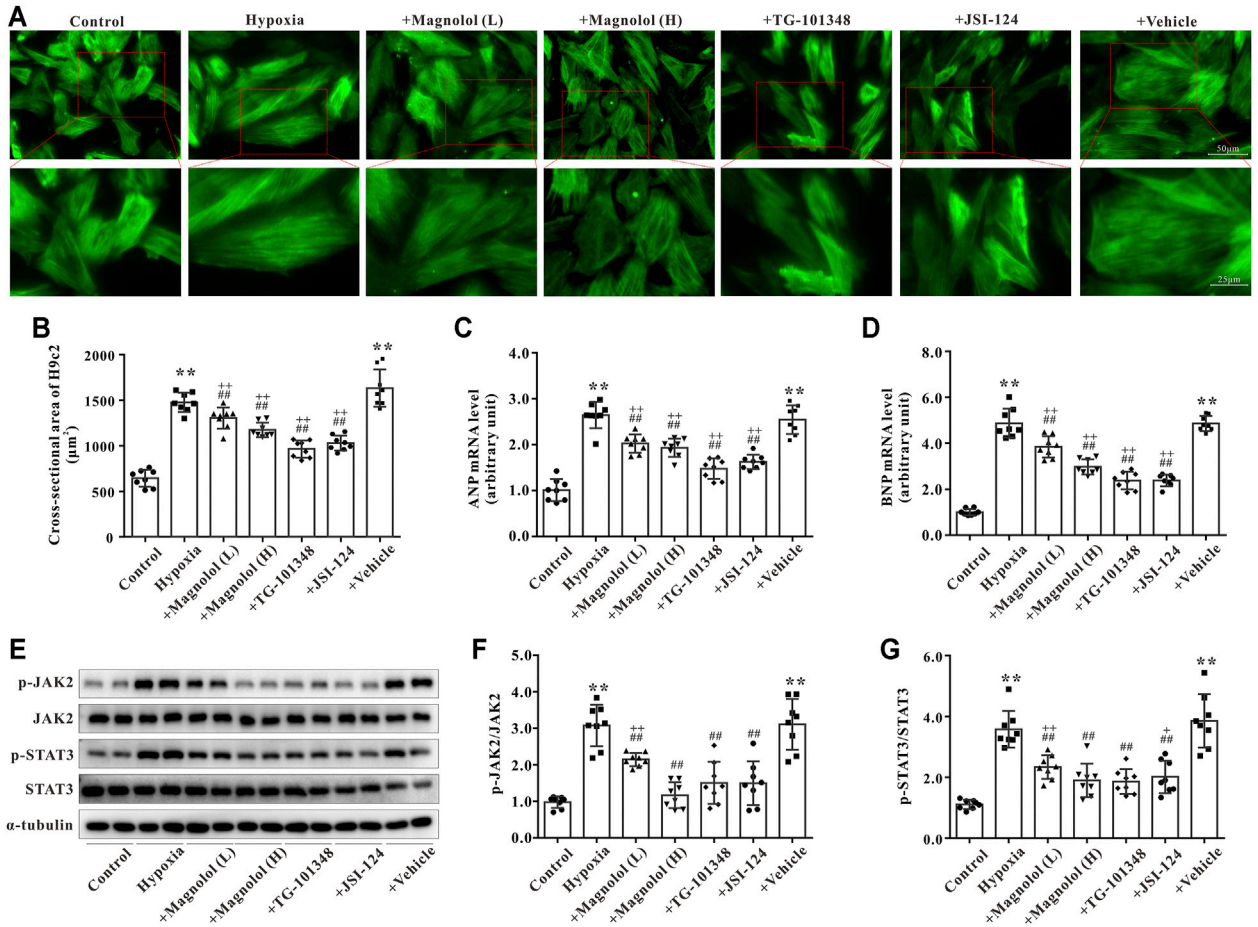

FIGURE 6 | Magnolol attenuated hypoxia-induced cardiac hypertrophy of H9c2 through inhibition of JAK2/STAT3 signaling pathway. **(A)** Representative images for H9c2 cell morphology under the fluorescence microscope. The cells were incubated with primary antibodies against α-SMA followed by incubation with the secondary antibody of Alexa Fluor 488-labeled Goat Anti-Mouse IgG (green fluorescence). **(B)** The cross-sectional area of H9c2 cells. **(C)** The mRNA levels of ANP in H9c2 cells. **(D)** The mRNA levels of BNP in H9c2 cells. **(E)** Representative images of Western blot results for p-JAK2, JAK2, p-STAT3, STAT3, and α-tubulin in H9c2 cells. **(F)** The ratio of optical density between p-JAK2 and JAK2. **(G)** The ratio of optical density between p-STAT3 and STAT3. All values are presented as mean ± S.D. (n = 8 per group). $^{**}p < 0.01$ vs. Control; $^{+}p < 0.05$, $^{++}p < 0.01$ vs. Control; $^{\#\#}p < 0.01$ vs. Vehicle.

elevated in the RV of hypoxic PAH rats, and the same results can be observed in hypoxia-treated H9c2 cells or cardiac fibroblasts. These results indicate that the JAK2/STAT3 pathway contributes to the process of hypoxia-induced cardiac hypertrophy and fibrosis. Therefore, the intervention of the JAK2/STAT3 pathway with specific drugs may provide a new strategy for preventing RV remodeling in PAH.

Magnolol is one of the foremost effective ingredients of traditional Chinese medicine *Magnolia Officinalis*, which has received widespread attention due to its anti-inflammatory (Zhou et al., 2019) and anti-tumor (Chen et al., 2021a) effects. A recent study reported that magnolol could ameliorate the vascular remodeling in monocrotaline-induced PAH rats (Chang et al., 2018). However, the impact of magnolol on RV remodeling in PAH remains unclear. In addition, Chen et al. confirmed that magnolol could inhibit cardiac fibroblasts' proliferation and collagen synthesis (Chen et al., 2021b). Expectedly, in the present study, we found that magnolol had a preventive effect on RV remodeling in hypoxia-induced PAH rats by inhibiting abnormal myocardial hypertrophy and excessive collagen fiber production. However, it is noteworthy that our current results can only prove that magnolol has a preventive effect on RV remodeling in PAH. Although magnolol may likely have a therapeutic effect on PAH, more studies are needed before drawing a firm conclusion.

To further confirm the possible mechanisms for magnolol against myocardial hypertrophy and fibrosis, the bioinformatics analysis was used to predict the potential targets for magnolol. Actually, nearly 100 potential targets have been identified (including kinases, oxidoreductases, and proteases). Among them, JAK2 and STAT3 have been attracted our attention because the JAK2/STAT3 pathway is closely related to myocardial hypertrophy and fibrosis (Ye et al., 2020). In addition, accumulating evidence indicates that magnolol has a regulatory effect on the activity of STAT3 (Chen et al., 2006; Peng et al., 2021). Based on the reports and bioinformatics prediction,

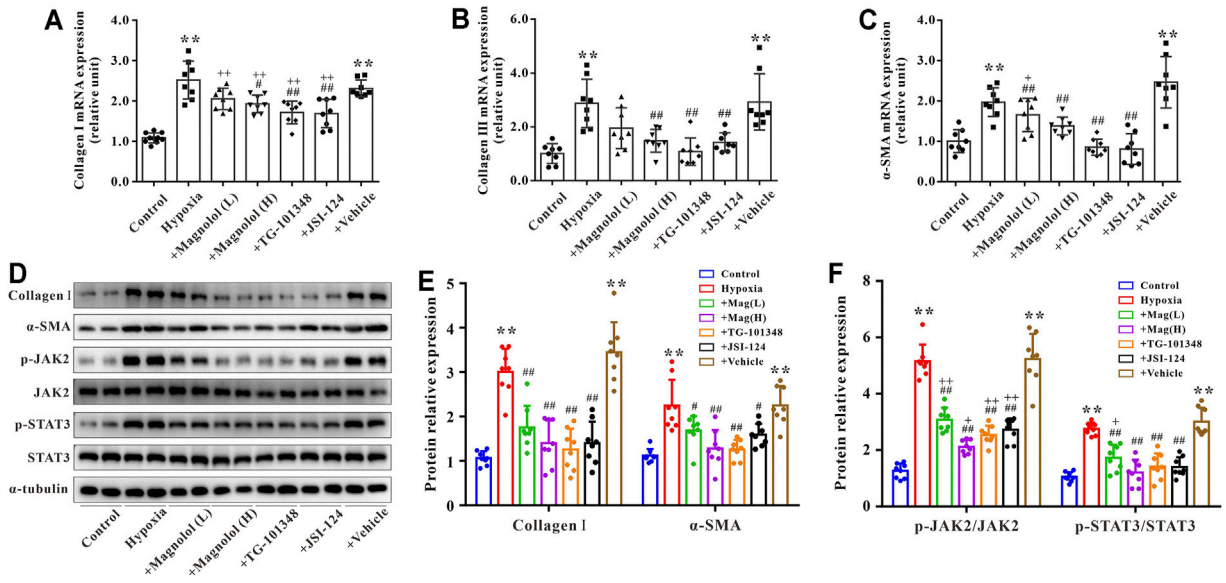

FIGURE 7 | Magnolol attenuated hypoxia-induced myocardial fibrosis of cardiac fibroblasts through inhibition of JAK2/STAT3 signaling pathway. **(A)** The mRNA levels of Collagen I in cardiac fibroblasts. **(B)** The mRNA levels of Collagen III in cardiac fibroblasts. **(C)** The mRNA levels of α-SMA in cardiac fibroblasts. **(D)** Representative images of Western blot results for Collagen I, α-SMA, p-JAK2, JAK2, p-STAT3, STAT3, and α-tubulin in cardiac fibroblasts. **(E)** The ratio of optical density between Collagen I or α-SMA and α-tubulin. **(F)** The ratio of optical density between p-JAK2/JAK2 or p-STAT3/STAT3. All values are presented as mean ± S.D. (n = 8–10 per group). $^{**}p < 0.01$ vs. Control; $^{+}p < 0.05$, $^{++}p < 0.01$ vs. Control; $^{\#}p < 0.05$, $^{\#\#}p < 0.01$ vs. Vehicle.

we hypothesize that magnolol prevents RV remodeling in hypoxia-induced PAH rats via suppressing the JAK2/STAT3 pathway. We thus examined the correlation between Magnolol and JAK2/STAT3 pathway. The results from the present study revealed that the levels of p-JAK2 and p-STAT3 in RV tissues were apparently elevated in the hypoxia-treated rats, which were reversed in the presence of magnolol. According to the results of bioinformatics analysis, the potential targets of magnolol also include kinases such as Raf1 or Akt1, which play an essential role in cardiac remodeling. Here, we could not rule out the role of Raf1 and/or Akt1 in the preventive effect of magnolol on RV remodeling.

To further confirm our findings *in vivo*, we performed cell experiments in H9c2 or primary cultured cardiac fibroblasts with Magnolol, TG-101348, and JSI-124. Here, TG-101348 or JSI-124 served as the positive control for JAK2 inhibitors, both of which have been proven to delay the development of PAH (Milara et al., 2018; Zhang et al., 2020). Consistent with the findings *in vivo*, H9c2 or cardiac fibroblasts displayed cell hypertrophy and fibrosis respectively under hypoxic conditions, accompanied by an elevation in p-JAK2 and p-STAT3 levels; these phenomena were attenuated in the presence of magnolol, TG-101348, or JSI-124.

There are two major limitations that need to be acknowledged and addressed regarding the present study. Firstly, as we mentioned above, pulmonary vascular remodeling is the most important pathological feature of PAH, which can induce an increase in RV afterload and ultimately lead to RV remodeling. Consistent with the results of Chang et al. (2018), we also found that magnolol has the effect of inhibiting pulmonary vascular remodeling. Although we have confirmed *in vitro* that magnolol has a protective effect on hypoxia-induced myocardial hypertrophy and fibrosis, we cannot rule out the beneficial effects of magnolol on RV remodeling and function are due to, at least in part, its indirect effect on inhibition of pulmonary vascular remodeling. Secondly, our existing results can only confirm that magnolol has a preventive effect on hypoxia-induced PAH right ventricular remodeling. Further studies are needed to verify the therapeutic effect of magnolol on RV hypertrophy and fibrosis.

CONCLUSION

In summary, the results presented here demonstrated for the first time that magnolol can prevent RV hypertrophy and fibrosis in hypoxia-induced PAH rats through a mechanism involving suppression of the JAK2/STAT3 pathway. Therefore, magnolol may have the potential to treat PAH.

DATA AVAILABILITY STATEMENT

The original contributions presented in the study are included in the article/**Supplementary Material**, further inquiries can be directed to the corresponding author.

ETHICS STATEMENT

The animal study was reviewed and approved by Central South University Veterinary Medicine Animal Care and Use Committee. Written informed consent was obtained from the owners for the participation of their animals in this study.

AUTHOR CONTRIBUTIONS

MF and FL participated in animal and cell experiments and were responsible for collecting and analyzing experimental data. MF wrote the first draft. EW was accountable for the construction of an animal model of hypoxia-induced PAH rats. BL, JP, YJ, and SL were responsible for the design of the experiments, coordination of the project, and preparation of the manuscript. All authors reviewed and approved the final version of the manuscript.

FUNDING

This work was supported by the National Natural Science Foundation of China (No. 81703516 to BL; No. 81872873 to JP), China Postdoctoral Science Foundation (No. 2021M693575 to BL), Natural Science Foundation of Hunan Province, China (No. 2019JJ50943 to BL), Scientific Research Project of Hunan Provincial Health Commission (No.C20180828 to BL), and Research Project of Hunan Children's Hospital (2019-50-B22 to FL).

SUPPLEMENTARY MATERIAL

The Supplementary Material for this article can be found online at: https://www.frontiersin.org/articles/10.3389/fphar.2021.755077/full#supplementary-material

Supplementary Figure S1 | Magnolol attenuated hypoxia-induced pulmonary vascular remodeling. **(A)** Representative images of HE staining for lung tissues. **(B)** The ratio of wall thickness to total vessel diameter. **(C)** The ratio of wall area to total vessel area. All values are presented as mean ± S.D. (n = 10 per group). $^{**}p < 0.01$ vs. Control; $^{+}p < 0.05$ vs. Control; $^{\#\#}p < 0.01$ vs. Vehicle.

Supplementary Figure S2 | Effect of magnolol on the phosphorylation of JAK2 and STAT3 in normal H9c2 cells. **(A)** Representative images of Western blot results for p-JAK2, JAK2, p-STAT3, STAT3, and α-tubulin in H9c2 cells. **(B–C)** The ratio of optical density between p-JAK2/JAK2 or p-STAT3/STAT3. n = 3 per group.

REFERENCES

Andersen, S., Nielsen-Kudsk, J. E., Vonk Noordegraaf, A., and de Man, F. S. (2019). Right Ventricular Fibrosis. *Circulation* 139 (2), 269–285. doi:10.1161/CIRCULATIONAHA.118.035326

Cassady, S. J., and Ramani, G. V. (2020). Right Heart Failure in Pulmonary Hypertension. *Cardiol. Clin.* 38 (2), 243–255. doi:10.1016/j.ccl.2020.02.001

Chang, H., Chang, C. Y., Lee, H. J., Chou, C. Y., and Chou, T. C. (2018). Magnolol Ameliorates Pneumonectomy and Monocrotaline-Induced Pulmonary Arterial Hypertension in Rats through Inhibition of Angiotensin II and Endothelin-1 Expression. *Phytomedicine* 51, 205–213. doi:10.1016/j.phymed.2018.10.001

Chen, C.-H., Hsu, F.-T., Chen, W.-L., and Chen, J.-H. (2021a). Induction of Apoptosis, Inhibition of MCL-1, and VEGF-A Expression Are Associated with the Anti-cancer Efficacy of Magnolol Combined with Regorafenib in Hepatocellular Carcinoma. *Cancers* 13 (9), 2066. doi:10.3390/cancers13092066

Chen, L., Wu, Y.-T., Gu, X.-Y., Xie, L.-P., Fan, H.-J., Tan, Z.-B., et al. (2021b). Magnolol, a Natural Aldehyde Dehydrogenase-2 Agonist, Inhibits the Proliferation and Collagen Synthesis of Cardiac Fibroblasts. *Bioorg. Med. Chem. Lett.* 43, 128045. doi:10.1016/j.bmcl.2021.128045

Chen, S. C., Chang, Y. L., Wang, D. L., and Cheng, J. J. (2006). Herbal Remedy Magnolol Suppresses IL-6-induced STAT3 Activation and Gene Expression in Endothelial Cells. *Br. J. Pharmacol.* 148 (2), 226–232. doi:10.1038/sj.bjp.0706647

Ciuclan, L., Bonneau, O., Hussey, M., Duggan, N., Holmes, A. M., Good, R., et al. (2011). A Novel Murine Model of Severe Pulmonary Arterial Hypertension. *Am. J. Respir. Crit. Care Med.* 184 (10), 1171–1182. doi:10.1164/rccm.201103-0412OC

Daina, A., Michielin, O., and Zoete, V. (2019). SwissTargetPrediction: Updated Data and New Features for Efficient Prediction of Protein Targets of Small Molecules. *Nucleic Acids Res.* 47 (W1), W357–W364. doi:10.1093/nar/gkz382

de Man, F. S., Handoko, M. L., and Vonk-Noordegraaf, A. (2019). The Unknown Pathophysiological Relevance of Right Ventricular Hypertrophy in Pulmonary Arterial Hypertension. *Eur. Respir. J.* 53 (4). doi:10.1183/13993003.00255-2019

Frost, A., Badesch, D., Gibbs, J. S. R., Gopalan, D., Khanna, D., Manes, A., et al. (2019). Diagnosis of Pulmonary Hypertension. *Eur. Respir. J.* 53 (1). doi:10.1183/13993003.01904-2018

Jeppesen, P. L., Christensen, G. L., Schneider, M., Nossent, A. Y., Jensen, H. B., Andersen, D. C., et al. (2011). Angiotensin II Type 1 Receptor Signalling Regulates microRNA Differentially in Cardiac Fibroblasts and Myocytes. *Br. J. Pharmacol.* 164 (2), 394–404. doi:10.1111/j.1476-5381.2011.01375.x

Li, T., Luo, X. J., Wang, E. L., Li, N. S., Zhang, X. J., Song, F. L., et al. (2019a). Magnesium Lithospermate B Prevents Phenotypic Transformation of Pulmonary Arteries in Rats with Hypoxic Pulmonary Hypertension through Suppression of NADPH Oxidase. *Eur. J. Pharmacol.* 847, 32–41. doi:10.1016/j.ejphar.2019.01.020

Li, T., Peng, J. J., Wang, E. L., Li, N. S., Song, F. L., Yang, J. F., et al. (2019b). Magnesium Lithospermate B Derived from Salvia Miltiorrhiza Ameliorates Right Ventricle Remodeling in Pulmonary Hypertensive Rats via Inhibition of NOX/VPO1 Pathway. *Planta Med.* 85 (9-10), 708–718. doi:10.1055/a-0863-4741

Li, W., Zhang, Z., Li, X., Cai, J., Li, D., Du, J., et al. (2020). CGRP Derived from Cardiac Fibroblasts Is an Endogenous Suppressor of Cardiac Fibrosis. *Cardiovasc. Res.* 116 (7), 1335–1348. doi:10.1093/cvr/cvz234

Li, W. Q., Li, X. H., Wu, Y. H., Du, J., Wang, A. P., Li, D., et al. (2016). Role of Eukaryotic Translation Initiation Factors 3a in Hypoxia-Induced Right Ventricular Remodeling of Rats. *Life Sci.* 144, 61–68. doi:10.1016/j.lfs.2015.11.020

Lin, Y., Li, Y., Zeng, Y., Tian, B., Qu, X., Yuan, Q., et al. (2021). Pharmacology, Toxicity, Bioavailability, and Formulation of Magnolol: An Update. *Front. Pharmacol.* 12, 632767. doi:10.3389/fphar.2021.632767

Liu, B., Luo, X. J., Yang, Z. B., Zhang, J. J., Li, T. B., Zhang, X. J., et al. (2014). Inhibition of NOX/VPO1 Pathway and Inflammatory Reaction by Trimethoxystilbene in Prevention of Cardiovascular Remodeling in Hypoxia-Induced Pulmonary Hypertensive Rats. *J. Cardiovasc. Pharmacol.* 63 (6), 567–576. doi:10.1097/FJC.0000000000000082

Milara, J., Ballester, B., Morell, A., Ortiz, J. L., Escrivá, J., Fernández, E., et al. (2018). JAK2 Mediates Lung Fibrosis, Pulmonary Vascular Remodelling and Hypertension in Idiopathic Pulmonary Fibrosis: an Experimental Study. *Thorax* 73 (6), 519–529. doi:10.1136/thoraxjnl-2017-210728

Montero, P., Milara, J., Roger, I., and Cortijo, J. (2021). Role of JAK/STAT in Interstitial Lung Diseases; Molecular and Cellular Mechanisms. *Int. J. Mol. Sci.* 22 (12). doi:10.3390/ijms22126211

Nakamura, M., and Sadoshima, J. (2018). Mechanisms of Physiological and Pathological Cardiac Hypertrophy. *Nat. Rev. Cardiol.* 15 (7), 387–407. doi:10.1038/s41569-018-0007-y

O'Shea, J. J., Schwartz, D. M., Villarino, A. V., Gadina, M., McInnes, I. B., and Laurence, A. (2015). The JAK-STAT Pathway: Impact on Human Disease and Therapeutic Intervention. *Annu. Rev. Med.* 66, 311–328. doi:10.1146/annurev-med-051113-024537

Peng, C.-Y., Yu, C.-C., Huang, C.-C., Liao, Y.-W., Hsieh, P.-L., Chu, P.-M., et al. (2021). Magnolol Inhibits Cancer Stemness and IL-6/Stat3 Signaling in Oral Carcinomas. *J. Formos. Med. Assoc.* doi:10.1016/j.jfma.2021.01.009

Shannon, P., Markiel, A., Ozier, O., Baliga, N. S., Wang, J. T., Ramage, D., et al. (2003). Cytoscape: a Software Environment for Integrated Models of Biomolecular Interaction Networks. *Genome Res.* 13 (11), 2498–2504. doi:10.1101/gr.1239303

Simpson, C. E., and Hassoun, P. M. (2019). Myocardial Fibrosis as a Potential Maladaptive Feature of Right Ventricle Remodeling in Pulmonary Hypertension. *Am. J. Respir. Crit. Care Med.* 200 (6), 662–663. doi:10.1164/rccm.201906-1154ED

Smith, K. A., Waypa, G. B., Dudley, V. J., Budinger, G. R. S., Abdala-Valencia, H., Bartom, E., et al. (2020). Role of Hypoxia-Inducible Factors in Regulating Right Ventricular Function and Remodeling during Chronic Hypoxia-Induced Pulmonary Hypertension. *Am. J. Respir. Cel Mol Biol* 63 (5), 652–664. doi:10.1165/rcmb.2020-0023OC

Tian, L., Wu, D., Dasgupta, A., Chen, K. H., Mewburn, J., Potus, F., et al. (2020). Epigenetic Metabolic Reprogramming of Right Ventricular Fibroblasts in Pulmonary Arterial Hypertension: A Pyruvate Dehydrogenase Kinase-dependent Shift in Mitochondrial Metabolism Promotes Right Ventricular Fibrosis. *Circ. Res.* 126 (12), 1723–1745. doi:10.1161/CIRCRESAHA.120.316443

van de Veerdonk, M. C., Kind, T., Marcus, J. T., Mauritz, G. J., Heymans, M. W., Bogaard, H. J., et al. (2011). Progressive Right Ventricular Dysfunction in Patients with Pulmonary Arterial Hypertension Responding to Therapy. *J. Am. Coll. Cardiol.* 58 (24), 2511–2519. doi:10.1016/j.jacc.2011.06.068

Villarino, A. V., Gadina, M., O'Shea, J. J., and Kanno, Y. (2020). SnapShot: Jak-STAT Signaling II. *Cell* 181 (7), 1696–e1. doi:10.1016/j.cell.2020.04.052

Vonk Noordegraaf, A., Westerhof, B. E., and Westerhof, N. (2017). The Relationship between the Right Ventricle and its Load in Pulmonary Hypertension. *J. Am. Coll. Cardiol.* 69 (2), 236–243. doi:10.1016/j.jacc.2016.10.047

Vonk-Noordegraaf, A., Haddad, F., Chin, K. M., Forfia, P. R., Kawut, S. M., Lumens, J., et al. (2013). Right Heart Adaptation to Pulmonary Arterial Hypertension: Physiology and Pathobiology. *J. Am. Coll. Cardiol.* 62 (25 Suppl), D22–D33. doi:10.1016/j.jacc.2013.10.027

Wang, E. L., Jia, M. M., Luo, F. M., Li, T., Peng, J. J., Luo, X. J., et al. (2019). Coordination between NADPH Oxidase and Vascular Peroxidase 1 Promotes Dysfunctions of Endothelial Progenitor Cells in Hypoxia-Induced Pulmonary Hypertensive Rats. *Eur. J. Pharmacol.* 857, 172459. doi:10.1016/j.ejphar.2019.172459

Xing, Q., Wu, M., Chen, R., Liang, G., Duan, H., Li, S., et al. (2021). Comparative Studies on Regional Variations in PM2.5 in the Induction of Myocardial Hypertrophy in Mice. *Sci. Total Environ.* 775, 145179. doi:10.1016/j.scitotenv.2021.145179

Ye, S., Luo, W., Khan, Z. A., Wu, G., Xuan, L., Shan, P., et al. (2020). Celastrol Attenuates Angiotensin II-Induced Cardiac Remodeling by Targeting STAT3. *Circ. Res.* 126 (8), 1007–1023. doi:10.1161/CIRCRESAHA.119.315861

Yerabolu, D., Weiss, A., Kojonazarov, B., Boehm, M., Schlueter, B. C., Ruppert, C., et al. (2021). Targeting Jak-Stat Signaling in Experimental Pulmonary Hypertension. *Am. J. Respir. Cel Mol Biol* 64 (1), 100–114. doi:10.1165/rcmb.2019-0431OC

Zelt, J. G. E., Chaudhary, K. R., Cadete, V. J., Mielniczuk, L. M., and Stewart, D. J. (2019). Medical Therapy for Heart Failure Associated with Pulmonary Hypertension. *Circ. Res.* 124 (11), 1551–1567. doi:10.1161/CIRCRESAHA.118.313650

Zhang, J., Chen, Z., Huang, X., Shi, W., Zhang, R., Chen, M., et al. (2019). Insights on the Multifunctional Activities of Magnolol. *Biomed. Res. Int.* 2019, 1847130. doi:10.1155/2019/1847130

Zhang, L., Wang, Y., Wu, G., Rao, L., Wei, Y., Yue, H., et al. (2020). Blockade of JAK2 Protects Mice against Hypoxia-Induced Pulmonary Arterial Hypertension by Repressing Pulmonary Arterial Smooth Muscle Cell Proliferation. *Cell Prolif* 53 (2), e12742. doi:10.1111/cpr.12742

Zhou, F., Jiang, Z., Yang, B., and Hu, Z. (2019). Magnolol Exhibits Anti-inflammatory and Neuroprotective Effects in a Rat Model of Intracerebral Haemorrhage. *Brain Behav. Immun.* 77, 161–167. doi:10.1016/j.bbi.2018.12.018

Zhu, T. T., Zhang, W. F., Luo, P., Qian, Z. X., Li, F., Zhang, Z., et al. (2017). LOX-1 Promotes Right Ventricular Hypertrophy in Hypoxia-Exposed Rats. *Life Sci.* 174, 35–42. doi:10.1016/j.lfs.2017.02.016

Conflict of Interest: The authors declare that the research was conducted in the absence of any commercial or financial relationships that could be construed as a potential conflict of interest.

Publisher's Note: All claims expressed in this article are solely those of the authors and do not necessarily represent those of their affiliated organizations, or those of the publisher, the editors and the reviewers. Any product that may be evaluated in this article, or claim that may be made by its manufacturer, is not guaranteed or endorsed by the publisher.

frontiers in Pharmacology

ORIGINAL RESEARCH
published: 26 October 2021
doi: 10.3389/fphar.2021.767982

Risk for Cardiovascular Disease and One-Year Mortality in Patients With Chronic Obstructive Pulmonary Disease and Obstructive Sleep Apnea Syndrome Overlap Syndrome

Manyun Tang[1†], *Yidan Wang*[1†], *Mengjie Wang*[1], *Rui Tong*[2] *and Tao Shi*[3*]

[1]*Department of Cardiovascular Medicine, The First Affiliated Hospital of Xi'an Jiaotong University, Xi'an, China,* [2]*Department of Geriatric Endocrinology, The First Affiliated Hospital of Xi'an Jiaotong University, Xi'an, China,* [3]*Department of Cardiovascular Surgery, The First Affiliated Hospital of Xi'an Jiaotong University, Xi'an, China*

OPEN ACCESS

Edited by:
Yunshan Cao,
Gansu Provincial Hospital, China

Reviewed by:
Jun-Jun Yeh,
Ditmanson Medical Foundation Chia-Yi Christian Hospital, Taiwan
Salvatore Fuschillo,
Fondazione Salvatore Maugeri (IRCCS), Italy

***Correspondence:**
Tao Shi
shitao068@xjtu.edu.cn

[†]*These authors contributed equally to this work and share first authorship*

Specialty section:
This article was submitted to Respiratory Pharmacology, a section of the journal Frontiers in Pharmacology

Received: *31 August 2021*
Accepted: *04 October 2021*
Published: *26 October 2021*

Citation:
Tang M, Wang Y, Wang M, Tong R and Shi T (2021) Risk for Cardiovascular Disease and One-Year Mortality in Patients With Chronic Obstructive Pulmonary Disease and Obstructive Sleep Apnea Syndrome Overlap Syndrome. Front. Pharmacol. 12:767982. doi: 10.3389/fphar.2021.767982

Background: Patients with chronic obstructive pulmonary disease (COPD) and obstructive sleep apnea (OSAS) overlap syndrome (OS) are thought to be at increased risk for cardiovascular diseases.

Objective: To evaluate the burden of cardiovascular diseases and long-term outcomes in patients with OS.

Methods: This was a retrospective cohort study. The prevalence of cardiovascular diseases and 1-year mortality were compared among patients diagnosed with OS (OS group), COPD alone (COPD group) and OSAS alone (OSAS group), and Cox proportional hazards models were used to assess independent risk factors for all-cause mortality.

Results: Overall, patients with OS were at higher risk for pulmonary hypertension (PH), heart failure and all-cause mortality than patients with COPD or OSAS (all $p < 0.05$). In multivariate Cox regression analysis, the Charlson comorbidity index (CCI) score [adjusted hazard ratio (aHR): 1.273 (1.050–1.543); $p = 0.014$], hypertension [aHR: 2.006 (1.005–4.004); $p = 0.048$], pulmonary thromboembolism (PTE) [aHR: 4.774 (1.335–17.079); $p = 0.016$] and heart failure [aHR: 3.067 (1.521–6.185); $p = 0.002$] were found to be independent risk factors for 1-year all-cause mortality.

Conclusion: Patients with OS had an increased risk for cardiovascular diseases and 1-year mortality. More efforts are needed to identify the causal relationship between OS and cardiovascular diseases, promoting risk stratification and the management of these patients.

Keywords: cardiopulmonary diseases, pulmonary hypertension, chronic obstructive pulmonary disease, obstructive sleep apnea syndrome, overlap syndrome, prognosis

INTRODUCTION

Chronic obstructive pulmonary disease (COPD) and obstructive sleep apnea syndrome (OSAS) are two common chronic diseases with increasing incidence worldwide and impose a heavy burden on the healthcare system (Lévy et al., 2015; Rabe and Watz, 2017). Moreover, both COPD and OSAS are considered to be risk factors for cardiovascular diseases (Tang et al., 2021). Common cardiovascular diseases associated with COPD and OSAS include hypertension, stroke, heart failure, atrial fibrillation, and coronary heart disease (CHD) (McNicholas et al., 2007; Macnee et al., 2008). The underlying mechanisms are multifactorial, including hypoxia, hypercapnia, systemic inflammation, oxidative stress, increased sympathetic nervous system activity, and endothelial dysfunction (Wolf et al., 2007; Macnee et al., 2008; Kohler and Stradling, 2010; Maclay and MacNee, 2013). COPD is a major risk factor for cardiovascular morbidity and mortality (Sin and Man, 2005), and evidence from a cohort study also suggests higher cardiovascular-related and all-cause mortality in patients with severe OSAS (Young et al., 2008).

Overlap syndrome (OS) is defined as coexisting COPD and OSAS in a single patient (Flenley, 1985). Studies have shown that patients with OS develop greater nocturnal oxygen desaturation and more severe hypercapnia, systemic inflammation, and endothelial dysfunction than patients with OSAS or COPD alone (Chaouat et al., 1995; McNicholas, 2017; Tang et al., 2021). All these findings suggest that patients with OS are at greater risk of cardiovascular diseases; however, there are few studies on cardiovascular morbidity and mortality in these patients, and the underlying risk factors are still unclear. Therefore, this study was conducted to evaluate the risk of cardiovascular diseases and 1-year mortality in OS patients and provide more real-world data on the burden of cardiovascular diseases in this cohort.

METHODS

Ethical Approval and Consent

This retrospective cohort study was performed in the Department of Cardiovascular Medicine and Respiratory Medicine of The First Affiliated Hospital of Xi'an Jiaotong University. The study was conducted in accordance with the Declaration of Helsinki and approved by the Ethics Committee of The First Affiliated Hospital of Xi'an Jiaotong University (No. XJTU1AF2020LSK-187). Written informed consents were obtained from the patients or their family members prior to the use of their anonymized clinical data.

Patients

Patients with a diagnosis of COPD or OSAS and discharged between July 2014 and July 2020 were initially searched in the Biobank of The First Affiliated Hospital of Xi'an Jiaotong University. All collected participants had to undergo screening. The exclusion criteria were: age <18 or >80 years old, loss to follow-up, lack of clinical data, previous upper airway surgery for OSAS, preexisting serious comorbidities or life expectancy less than 1 year, severe COPD with noninvasive or invasive respiratory ventilator use and unwillingness to participate in the study. Then, the consecutively enrolled patients were divided into three groups: (1) the OS group, (2) the COPD group, and (3) the OSAS group. OS was defined as coexisting COPD and OSAS in one patient. The two control groups were pair-matched with the OS group based on age and sex at a 1: 2 ratio.

Clinical Data Collection

This study was observational, reflected routine practice and did not interfere with medical management. Patients who met the criteria were consecutively enrolled, and their clinical data were collected from the Biobank of The First Affiliated Hospital of Xi'an Jiaotong University by designated investigators and recorded on dedicated electronic forms.

The patients' anonymous clinical data included baseline demographics [age, sex, body mass index (BMI)], medical history [hypertension, diabetes, hyperlipidemia, stroke, pulmonary thromboembolism (PTE) and smoking], laboratory examination (complete blood counts, biochemical tests, coagulation function, and arterial blood gas analysis), pulmonary function tests, full-night polysomnography and treatments [CPAP and medications (ACEIs/ARBs, β-blockers, antisterone, nifedipine, diuretic, and aspirin)]. The screening for the diagnosis of diseases was performed according to the International Classification of Diseases-10.

Outcomes and Follow-Up

We followed all enrolled patients from the index date to the end of 1 year. The primary endpoint was all-cause death, and survival status were obtained from outpatient records or telephone contact with the patients or their relatives. The secondary endpoint was the prevalence of four specific cardiovascular diseases, including pulmonary hypertension (PH), heart failure, arrhythmias, and CHD.

Statistical Analysis

Continuous variables were described as the mean and standard deviation (SD) and were tested for normal distribution by the Kolmogorov-Smirnov test. Analysis of variance with a post hoc test was used to compare continuous variables that satisfied normal distribution, and the Kruskal-Wallis test was used to compare continuous variables that did not satisfy normal distribution. Categorical variables were summarized as counts and percentages and compared by the chi-square test. As three comparisons of baseline characteristics and the incidence of cardiovascular events were performed, a p-value threshold of <0.017 was used for the descriptive analysis after applying Bonferroni correction. To evaluate the risk factors for all-cause mortality between OS, COPD, and OSAS patients during follow-up, univariate and multivariate Cox proportional hazards models were used to assess HR and 95% confidence interval (CI). The multivariable model was adjusted for covariates (BMI, the Charlson comorbidity index (CCI), hypoxemia, hypercapnia, respiratory failure, hypertension, diabetes, hyperlipidemia, stroke, PTE, heart failure, arrhythmia, and CHD).

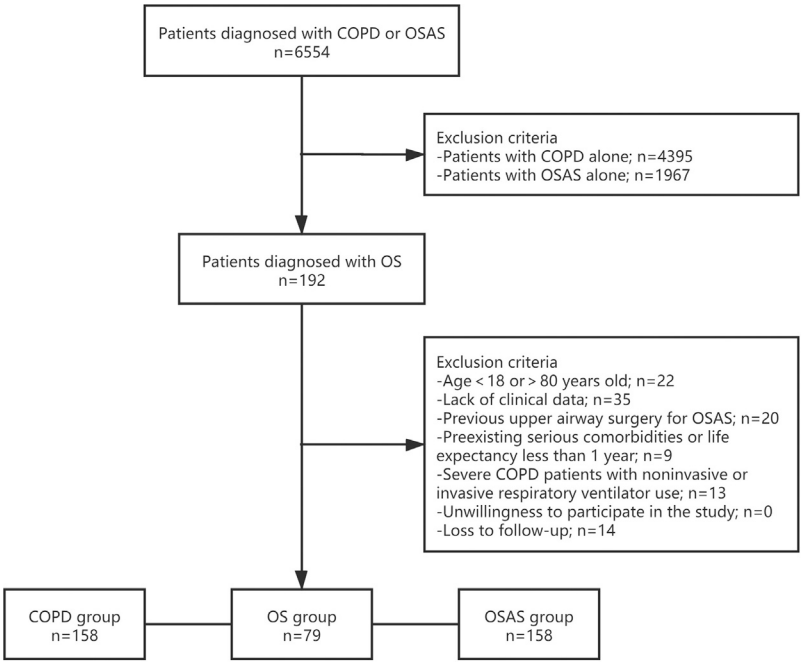

FIGURE 1 | Study Protocol. Flowchart of the selection process of the current study. OS, overlap syndrome; COPD, chronic obstructive pulmonary disease; OSAS, obstructive sleep apnea syndrome.

Furthermore, the 1-year mortality of the three groups was evaluated using the Kaplan-Meier method and compared by the use of log-rank tests. All data processing and statistical analyses were performed using the SPSS 26.0 statistical package, and a p-value < 0.05 was considered indicative of statistical significance.

RESULTS

Baseline Characteristics

Among the 6,554 patients initially collected from the biobank according to the diagnosis of COPD or OSAS, 4,587 had COPD, and 2,159 had OSAS. There were 192 patients suffering from COPD and OSAS overlap syndrome. Overall, 79 patients were enrolled in the OS group after screening (**Figure 1**). The rate of loss to follow-up was 7.3%. The clinical characteristics of the patients in the OS group, COPD group and OSAS group are described in **Table 1**.

The study population was predominantly male (69.6%), with an average age of 60.6 ± 9.5 years. Patients with OS had significantly lower blood oxygen pressure (PO_2) and arterial oxygen saturation (SaO_2) and higher BMI, partial pressure of carbon dioxide (PCO_2), and serum levels of B-type natriuretic peptide (BNP) than patients with COPD or OSAS alone (all $p < 0.001$). In the OS group, the serum levels of D-dimer, C-reactive protein (CRP), cardiac troponin T (cTnT), and lactate dehydrogenase (LDH) were higher than those in the OSAS group (all $p < 0.001$); and the serum levels of triglyceride and low-density lipoprotein (LDL) were higher than those in the COPD group (all $p < 0.001$).

Regarding medications, antisterone, nifedipine and diuretic were more commonly used in the OS group than in other two groups. There was a higher tendency to use angiotensin-converting enzyme inhibitors (ACEIs)/ angiotensin receptor blockers (ARBs), beta-blockers and aspirin in OS patients than in COPD patients (all $p < 0.001$); however, compared with OSAS patients, this tendency was significantly reduced.

Patients with OS had higher CCI scores ($p = 0.006$) and were more likely to concomitantly suffer PTE ($p = 0.006$), hypercapnia ($p < 0.001$), and respiratory failure ($p < 0.001$) than patients with COPD or OSAS alone. More patients had hypertension ($p < 0.001$) and diabetes mellitus ($p = 0.001$) in the OS group than in the COPD group.

Severity of COPD and OSAS of Patients in Three Groups

Table 2 shows the pulmonary function tests and GOLD classification of patients in OS and COPD group, respectively. No between-group difference in the GOLD classification was observed (all $p > 0.05$), FEVI% in COPD group was lower than that in OS group (40.8 ± 19.8 vs. 44.6 ± 19.4), though not statistically significant.

The baseline polysomnography data and treatment of patients in OS group and OSAS group were shown in **Table 3**. In the sleep testing study, the apnea-hypopnea index (AHI) was higher in

TABLE 1 | Baseline characteristics of all patients.

	All	OS group	COPD group	OSAS group	*p* Value	*p* Value OS and COPD	*p* Value OS and OSAS
	n = 395	*n* = 79	*n* = 158	*n* = 158			
Age (years)	60.6 ± 9.5	60.7 ± 9.6	60.6 ± 9.5	60.6 ± 9.6	0.993		
Male, n (%)	275 (69.6)	55 (69.6)	110 (69.6)	110 (69.6)	1.000		
BMI (kg/m^2)	25.0 ± 5.1	26.5 ± 2.3	24.4 ± 7.1	24.8 ± 3.4	<0.001	<0.001	<0.001
Smoker, n (%)	92 (23.3)	23 (29.1)	35 (22.2)	34 (21.5)	0.388		
Smoking index	717.6 ± 412.0	863.5 ± 487.8	622.6 ± 293.5	716.9 ± 442.2	0.130		
Laboratory data							
PO_2 (mmHg)	72.0 ± 15.3	60.2 ± 12.7	74.5 ± 16.2	75.4 ± 12.5	<0.001	<0.001	<0.001
PCO_2 (mmHg)	48.1 ± 11.2	57.1 ± 12.2	47.5 ± 10.7	44.1 ± 8.2	<0.001	<0.001	<0.001
SaO_2 (%)	91.2 ± 7.2	86.5 ± 9.4	92.8 ± 5.0	92.0 ± 6.9	<0.001	<0.001	<0.001
D-dimer (mg/L)	1.0 ± 1.9	1.3 ± 1.7	1.2 ± 2.2	0.8 ± 1.6	<0.001	0.497	<0.001
Fibrinogen (g/L)	3.5 ± 1.3	3.5 ± 1.3	3.8 ± 1.4	3.1 ± 0.9	<0.001	0.226	0.033
Hemoglobin (g/L)	144.3 ± 21.7	149.7 ± 25.9	142.4 ± 21.0	143.6 ± 19.7	0.053	0.051	0.118
CRP (mg/L)	9.8 ± 23.2	14.8 ± 30.3	11.2 ± 25.0	5.8 ± 15.3	<0.001	0.373	<0.001
Cholesterol (mmol/L)	4.0 ± 1.1	4.0 ± 1.4	4.0 ± 1.0	4.0 ± 1.2	0.459		
Triglyceride (mmol/L)	1.6 ± 1.0	1.7 ± 1.0	1.2 ± 0.3	1.8 ± 1.2	<0.001	<0.001	0.559
LDL (mmol/L)	2.2 ± 0.6	2.3 ± 0.7	2.0 ± 0.3	2.4 ± 0.8	<0.001	<0.001	0.440
BNP (pg/ml)	778.9 ± 2138.5	1181.8 ± 2286.2	937.7 ± 2729.5	418.6 ± 1091.8	<0.001	<0.001	<0.001
cTnT (ng/ml)	0.05 ± 0.24	0.03 ± 0.02	0.10 ± 0.38	0.02 ± 0.05	<0.001	0.700	0.001
CK (U/L)	101.8 ± 207.7	76.8 ± 105.4	91.7 ± 139.1	124.2 ± 286.9	<0.001	0.202	<0.001
CKMB (U/L)	16.1 ± 19.4	17.3 ± 17.6	14.7 ± 10.0	16.9 ± 26.2	0.764		
LDH (U/L)	245.2 ± 96.7	264.2 ± 80.5	261.5 ± 125.0	219.4 ± 59.1	<0.001	0.302	<0.001
Medications							
ACEI/ARB, n (%)	127 (32.2)	25 (31.6)	26 (16.5)	76 (48.1)	<0.001	0.007	0.016
Beta-blockers, n (%)	109 (27.6)	21 (26.6)	25 (15.8)	61 (38.6)	<0.001	<0.001	0.067
Antisterone, n (%)	90 (22.8)	26 (32.9)	40 (25.3)	24 (15.2)	0.006	0.029	0.002
Nifedipine, n (%)	87 (22.0)	26 (32.9)	24 (15.2)	37 (23.4)	0.007	0.002	0.019
Diuretic, n (%)	118 (29.9)	48 (60.8)	44 (27.8)	26 (16.5)	<0.001	<0.001	<0.001
Aspirin, n (%)	164 (41.5)	29 (36.7)	29 (18.4)	106 (67.1)	<0.001	<0.001	<0.001
Comorbidities							
CCI	3.0 ± 1.5	3.5 ± 1.5	2.9 ± 1.2	2.8 ± 1.6	0.006	0.009	0.005
Hypertension, n (%)	214 (54.2)	56 (70.9)	45 (28.5)	113 (71.5)	<0.001	<0.001	0.919
Diabetes, n (%)	112 (28.4)	30 (38.0)	29 (18.4)	53 (33.5)	0.001	0.001	0.500
Hyperlipidemia, n (%)	22 (5.6)	3 (3.8)	3 (1.9)	16 (10.1)	0.004	0.403	0.091
Stroke, n (%)	70 (17.7)	15 (19.0)	21 (13.3)	34 (21.5)	0.151	0.249	0.650
PTE, n (%)	5 (1.3)	4 (5.1)	1 (0.6)	0 (0)	0.006	0.014	0.012
Hypoxemia, n (%)	319 (80.8)	72 (91.1)	127 (80.4)	120 (75.9)	0.020	0.033	0.005
Hypercapnia, n (%)	96 (24.3)	55 (69.6)	33 (20.9)	8 (5.1)	<0.001	<0.001	<0.001
Respiratory failure, n (%)	56 (14.2)	29 (36.7)	17 (10.8)	10 (6.3)	<0.001	<0.001	<0.001

OS, overlap syndrome; COPD, chronic obstructive pulmonary disease; OSAS, obstructive sleep apnea syndrome; BMI, body mass index; PO2, oxygen partial pressure; PCO2, partial pressure of carbon dioxide; SaO2, oxygen saturation; CRP, C-reactive protein; LDL, low-density lipoprotein; BNP, B-type natriuretic peptide; cTnT, cardiac troponin T; CK, creatine kinase; CKMB, creatine kinase-MB; LDH, lactate dehydrogenase; ACEI, angiotensin-converting enzyme inhibitors; ARB, angiotensin receptor blockers; CCI, Charlson comorbidity index; PTE, pulmonary thromboembolism.

TABLE 2 | Pulmonary function tests and GOLD classification.

	All	OS group	COPD group	*p* Value
	n = 237	*n* = 79	*n* = 158	
FEV1/FVC ratio (%)	55.2 ± 15.7	58.7 ± 16.8	53.4 ± 14.9	0.015
FEV1% predicted	42.0 ± 19.7	44.6 ± 19.4	40.8 ± 19.8	0.109
Severity of COPD, n (%)				
GOLD 1	14 (5.9)	4 (5.1)	10 (6.3)	0.779
GOLD 2	67 (28.3)	27 (34.2)	40 (25.3)	0.153
GOLD 3	74 (31.2)	24 (30.4)	50 (31.6)	0.843
GOLD 4	82 (34.6)	24 (30.4)	58 (36.7)	0.334

FEV1, orced expiratory volume in 1 s; FVC, forced vital capacity; GOLD, Global Initiative for Chronic Obstructive Lung Disease; other abbreviations as in ***Table 1****.*

patients with OSAS than in those with OS (26.5 ± 16.6 vs. 25.1 ± 15.4; $p = 0.521$), there was no obvious difference in the distribution of severity of OSAS in two groups. However, patients in the OS group were more likely to receive CPAP therapy than those in the OSAS group (57.0 vs. 15.8%; $p < 0.001$).

Prevalence of Cardiovascular Events

Table 4 shows the incidence of five specific cardiovascular diseases—CHD, arrhythmias, heart failure, stroke and PH—in the OS group, COPD group and OSAS group. There was a significant increase in the incidence of heart failure (35.4 vs. 8.9% and 0.6%; $p < 0.001$) and PH (36.7 vs. 17.1% and 4.4%; $p < 0.001$) in the OS group compared with the COPD group or OSAS group. Patients with OS had a higher prevalence of CHD than patients with OSAS (30.4 vs. 9.5%; $p < 0.001$). The prevalence of stroke and arrhythmias did not differ significantly among the three groups, whereas more patients in the OS group had atrial fibrillation than those in the COPD group (13.9 vs. 4.4% and 6.8%; $p = 0.018$).

TABLE 3 | Baseline polysomnography data and treatment.

	All	OS group	OSAS group	*p* Value
	n = 237	*n* = 79	*n* = 158	
AHI	26.0 ± 16.2	25.1 ± 15.4	26.5 ± 16.6	0.521
Severity of OSAS, n (%)				
Mild	69 (29.1)	21 (26.6)	48 (30.4)	0.544
Moderate	81 (34.2)	35 (44.3)	46 (29.1)	0.020
Severe	87 (36.7)	23 (29.1)	64 (40.5)	0.086
CPAP, n (%)	70 (29.5)	45 (57.0)	25 (15.8)	<0.001

AHI = apnea–hypopnea index; CPAP = continuous positive airway pressure; other abbreviations as in ***Table 1****.*

Risk Factors for All-Cause Mortality

The primary outcome, all-cause death during the 1-year follow-up, occurred in 21.5% (17/79) of patients with OS, 7.0% (11/158) of patients with COPD and 10.1% (16/158) of patients with OSAS. The 1-year mortality was significantly higher in the OS group than in the other two groups (p = 0.003). The overall survival rate was lower in the OS group than in the COPD or OSAS group (**Figure 2**). In univariate Cox regression analysis, OS (HR: 2.892 [1.593–5.252], p < 0.001), the CCI score (HR: 1.277 [1.057–1.542], p = 0.011), hypercapnia (HR: 1.968 [1.077–3.597], p = 0.028), respiratory failure (HR: 2.370 [1.224–4.590], p = 0.010), hypertension (HR: 2.418 [1.249–4.683], p = 0.009), stroke (HR: 2.199 [1.169–4.134], p = 0.014), PTE (HR: 5.907 [1.828–19.083], p = 0.003), and heart failure (HR: 2.993 [1.516–5.907], p = 0.002) were associated with all-cause mortality during the 1-year follow-up. After adjusting for OS, BMI, the CCI score, smoking status, hypoxemia, hypercapnia, respiratory failure, diabetes, hyperlipidemia, stroke, PTE, PH, heart failure, arrhythmia, and CHD in multivariate Cox regression analysis, the CCI score (adjusted HR [aHR]: 1.273 [1.050–1.543]; p = 0.014), hypertension (aHR: 2.006 [1.005–4.004]; p = 0.048), PTE (aHR: 4.774 [1.335–17.079]; p = 0.016) and heart failure (aHR: 3.067 [1.521–6.185]; p = 0.002) were identified as independent predictors of all-cause mortality during the 1-year follow-up (**Table 5**).

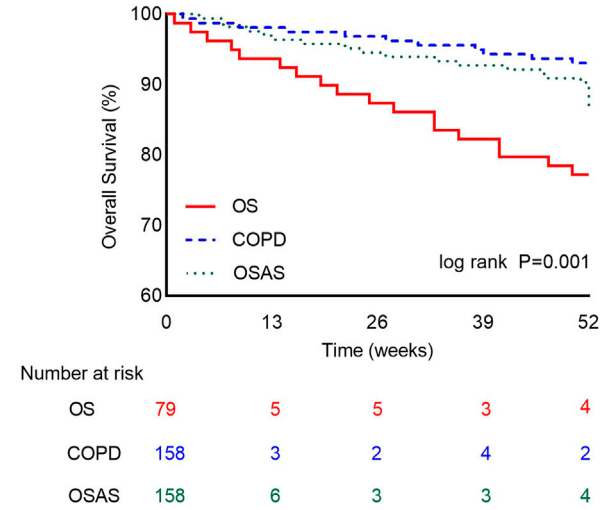

FIGURE 2 | The One-Year Kaplan-Meier Survival Curves. Survival rate between patients in the OS group (red line), COPD group (blue line), and OSAS group (green line). The difference is statistically significant. (Log-rank test = 14.128, p = 0.001).

DISCUSSION

In this study, OS was observed in 4.2% (192/4,587) of COPD patients and 8.9% (192/2,159) of OSAS patients. The prevalence of PH and heart failure was significantly higher in the OS group than in the COPD or OSAS group. Moreover, the OS group had a higher proportion of patients with CHD than the COPD group, suggesting a heavier cardiovascular burden in patients with OS. Moreover, patients with OS had a higher 1-year all-cause mortality than patients with COPD or OSAS alone. After adjusting for confounders, the rate of all-cause death was identified to be independently associated with the CCI score, hypertension, PTE and heart failure. To our knowledge, this is the first study to evaluate the burden of cardiovascular diseases and prognosis and search for risk factors among OS, COPD and OSAS populations.

TABLE 4 | Incidence of cardiovascular diseases in study patients.

	All	OS group	COPD group	OSAS group	*p* value	*p* value OS and COPD	*p* value OS and OSAS
	n = 395	*n* = 79	*n* = 158	*n* = 158			
CHD, n (%)	97 (24.6)	24 (30.4)	15 (9.5)	58 (36.7)	<0.001	<0.001	0.334
Arrhythmia, n (%)	58 (14.7)	18 (22.8)	19 (12.0)	21 (13.3)	0.072	0.031	0.063
Conduction block, n (%)	13 (3.3)	5 (6.3)	4 (2.5)	4 (2.5)	0.296	0.280	0.280
Ventricular arrhythmias, n (%)	9 (2.3)	2 (2.5)	4 (2.5)	9 (2.3)	1.000	1.000	1.000
Atrial arrhythmia, n (%)	36 (9.1)	11 (13.9)	11 (7.0)	14 (8.9)	0.212	0.082	0.232
AF, n (%)	27 (6.8)	11 (13.9)	7 (4.4)	9 (6.8)	0.018	0.009	0.032
Heart failure, n (%)	43 (10.9)	28 (35.4)	14 (8.9)	1 (0.6)	<0.001	<0.001	<0.001
Stroke, n (%)	70 (17.7)	15 (19.0)	21 (13.3)	34 (21.5)	0.151	0.249	0.650
PH, n (%)	64 (16.2)	29 (36.71)	28 (17.1)	7 (4.4)	<0.001	0.001	<0.001
Mild	33 (51.6)	14 (48.3)	15 (53.6)	4 (57.1)			
Moderate	20 (31.2)	11 (37.9)	7 (25.0)	2 (28.6)			
Severe	11 (17.2)	4 (13.8)	6 (21.4)	1 (14.3)			

CHD, coronary heart disease; AF, atrial fibrillation; PH, pulmonary hypertension; other abbreviations as in ***Table 1****.*

TABLE 5 | Results of univariate and multivariate Cox regression analysis.

Variables	Univariate analysis			Multivariate analysis		
	Curde HR	95%CI	*p* Value	Adjusted HR*	95%CI	*p* Value
OS	2.892	1.593–5.252	<0.001			
BMI	0.987	0.923–1.056	0.709			
CCI	1.277	1.057–1.542	0.011	1.273	1.050–1.543	0.014
smoker	0.697	0.324–1.496	0.354			
hyoxemia	1.132	0.527–2.430	0.751			
hypercapnia	1.968	1.077–3.597	0.028			
Respiratory failure	2.370	1.224–4.590	0.010			
hypertension	2.418	1.249–4.683	0.009	2.006	1.005–4.004	0.048
diabetes	1.215	0.628–2.353	0.563			
hyperlipidemia	1.434	0.445–4.628	0.546			
stroke	2.199	1.169–4.134	0.014			
PTE	5.907	1.828–19.083	0.003	4.774	1.335–17.079	0.016
PH	1.773	0.899–3.500	0.099			
heart failure	2.993	1.516–5.907	0.002	3.067	1.521–6.185	0.002
arrhythmia	1.752	0.905–3.393	0.096			
CHD	1.237	0.649–2.357	0.517			

Multivariable model adjusts forOS, BMI, CCI, smoker, hyoxemia, hypercapnia, respiratory failure, diabetes, hyperlipidemia, stroke, PTE, PH, heart failure, arrhythmia, and CHD. HR, hazard ratio; CI, confidence interval; other abbreviations as in* ***Tables 1**,* ***4****.*

The mechanisms that cause cardiovascular diseases in patients with COPD or OSAS are multifactorial, including hypoxia, systemic inflammation, oxidative stress, endothelial dysfunction and a hypercoagulable state (McNicholas et al., 2007; Wolf et al., 2007; Macnee et al., 2008; Kohler and Stradling, 2010; Maclay and MacNee, 2013; Cowie et al., 2021). As the severity of COPD or OSAS increases, cardiovascular diseases become more prevalent (Curkendall et al., 2006; Mills et al., 2008). In addition, in this study, there was a fact that patients with OS, of whom the FEV1% was higher and the AHI was lower than patients with COPD and OSAS, respectively, developed more severe oxygen desaturation and hypercapnia, suggesting a synergistic effect of COPD and OSA in one patient. This may, to some extent, explain why patients with OS are at greater risk of cardiovascular disease than patients with COPD or OSAS alone.

Hypoxemia has been identified as a risk factor for the development of cardiovascular disease in many studies because it can promote the release of reactive oxygen species, induce oxidative stress, and impair endothelial function (Bosc et al., 2010; Dewan et al., 2015). Nocturnal hypoxemia in OS patients has been confirmed by the results of sleep monitoring in many previous studies, and it usually manifests as decreased mean and the lowest SaO2 and increased sleep time with SaO2 < 90% (Chaouat et al., 1995; Shiina et al., 2012). Our study indicated that patients with OS had more severe hypoxia. In this study, we collected and further evaluated the patients' arterial blood gas analysis in three groups, finding that daytime hypoxemia, and hypercapnia were more common in OS patients. As clinical evidence has established that the majority of OSAS patients are eucapnic while conscious, the detection of daytime hypercapnia suggested a further impairment of the respiratory system in OSAS patients who had COPD. Moreover, evidence from cell culture studies, animal models, and controlled studies in humans has demonstrated that intermittent hypoxia can promote oxidative stress (Takabatake et al., 2000; Zhan et al., 2005; Mills et al., 2008; Pialoux et al., 2009), which is another risk factor for cardiovascular diseases. This more pronounced hypoxemia and hypercapnia might be one of the causes of increased cardiovascular morbidity and mortality.

Patients with COPD, OSAS, or OS always have an active status of systemic inflammation, which is a key factor that predisposes these individuals to cardiovascular diseases. C-reactive protein, an independent predictor of cardiovascular disease and an important serum marker of inflammation (Rutter et al., 2004), was significantly increased in the OS group, indicating an accelerated inflammatory process in this cohort. In addition, we found that patients in the OS group had a higher BMI. This finding was consistent with a previous study in that obesity can also induce systemic inflammation by upregulating the expression of systemic inflammatory mediators (Trayhurn and Wood, 2004).

In addition to hypoxia and inflammation, abnormal lipid metabolism also contributes to cardiovascular disease. An important interaction between hypoxia and lipids is assumed to exist in the development of atherosclerosis (Li et al., 1985). In an animal study, chronic intermittent hypoxia combined with a high-fat diet was found to promote the progression of atherosclerosis in male C57BL/6 mice, whereas hypoxia or a high-fat diet alone did not (Savransky et al., 2007). Evidence from a case-control study carried out by Barceló A also identified the abnormal lipid peroxidation in patients with sleep apnoea (Barceló et al., 2000). In our study, we found that abnormal lipid metabolism at baseline was more common in COPD patients who also had OSA and was characterized by higher serum levels of triglycerides and low-density lipoprotein (LDL). This may explain, to some extent, why OS patients had a higher incidence of coronary heart disease than COPD patients in our study.

COPD and OSAS have been reported to be correlated with hypertension, stroke, arrhythmia, heart failure and ischemic heart disease. Voulgaris et al. reported an increased risk for cardiovascular disease in OS patients by using the Framingham Risk Score (FRS) and Systematic COronary Risk Evaluation (SCORE) scoring models (Voulgaris et al., 2019), but specific changes in the incidence of each cardiovascular disease were not discussed. In this study, significantly higher incidence of heart failure and PH was observed in the OS group, and CHD was also more common in the OS group than in the COPD group. As in this study, most patients who had OSAS were diagnosed during the treatment of CHD, increasing the proportion of CHD in the OSAS population, so no significant difference in the prevalence of CHD was observed between the OS group and the OSAS group.

PH, a common complication of COPD, is the result of the remodeling of pulmonary arteries. Pulmonary vascular remodeling in COPD patients is considered to be caused by elevated pulmonary artery pressure due to a combination of hypoxia, inflammation, and impairment of endothelial function (Barberà and Blanco, 2009). There are also some studies exploring the relationship between OSAS and PH, confirming that the OSAS is associated with mild PH and this may be due to a combination of precapillary and postcapillary factors, such as pulmonary arteriolar remodeling, hyperreactivity to hypoxia, systemic inflammation and left atrial enlargement (Kessler et al., 1996; Sajkov and McEvoy, 2009). In this study, we found that in OS patients, those who had more severe hypoxia and systemic inflammation than patients with OSAS or COPD alone, the prevalence of PH increased significantly, suggesting that physicians should pay more attention to those COPD patients who already have OSAS or OSAS patients who have COPD.

During the 1-year follow-up, there were 17 (21.5%) all-cause deaths in the OS group, 11 (7.0%) all-cause deaths in the COPD group, and 16 (10.1%) all-cause deaths in the OSAS group, and a significantly higher mortality rate was found in the OS group. After adjusting for confounding factors, the CCI score, hypertension, PTE and heart failure were assumed to be independent risk factors for 1-year mortality in this population, suggesting a heavier burden of cardiovascular disease in this population. The causal relationship between OS and cardiovascular diseases is still unclear. This study provides an early recognition of the burden of cardiovascular disease in OS patients. We hope that it can promote timely aggressive management of these patients, including lifestyle changes and treatment targeting the CCI score, hypertension, PTE and heart failure, to improve these patients' long-term outcomes.

There are some limitations should be highlighted. First, this was a single-center study, and the study sample was small. Second, given the retrospective nature of the study, some clinical information, such as Holter and telemetry monitoring, was not available, which limited our assessment of recurrent arrhythmias. Third, as some patients with OSAS were diagnosed during treatment for CHD, this may have resulted in an overestimation of the actual risk of CHD in the OSAS group. Despite these limitations, this study may provide a basis for future research on the causal relationship between OS and cardiovascular diseases, promoting risk stratification and the management of these patients.

CONCLUSION

In conclusion, patients with OS had deteriorating baseline characteristics and a higher prevalence of cardiovascular diseases, including heart failure and PH, than patients with COPD or OSAS. Moreover, OS patients were found to be at a higher risk for all-cause death during the 1-year follow-up, which might be associated with the CCI score, hypertension, PH and heart failure. Clinicians should be aware that patients with OS have a heavier burden of cardiovascular diseases, and early identification and appropriate treatment are of great importance for the management of these patients.

DATA AVAILABILITY STATEMENT

The raw data supporting the conclusions of this article will be made available by the authors, without undue reservation.

ETHICS STATEMENT

The studies involving human participants were reviewed and approved by the Ethics Committee of The First Affiliated Hospital of Xi'an Jiaotong University (No. XJTU1AF2020LSK-187). The patients/participants provided their written informed consent to participate in this study.

AUTHOR CONTRIBUTIONS

MT: methodology, writing and original draft preparation; YW, MW, and RT: data curation and investigation; TS: supervision, reviewing and editing the article; all authors provided critical review of the article and approved the final draft for publication.

ACKNOWLEDGMENTS

We are grateful to the Biobank of The First Affiliated Hospital of Xi'an Jiaotong University for providing clinical data.

REFERENCES

Barberà, J. A., and Blanco, I. (2009). Pulmonary Hypertension in Patients with Chronic Obstructive Pulmonary Disease: Advances in Pathophysiology and Management. *Drugs* 69 (9), 1153–1171. doi:10.2165/00003495-200969090-00002

Barceló, A., Miralles, C., Barbé, F., Vila, M., Pons, S., and Agustí, A. G. (2000). Abnormal Lipid Peroxidation in Patients with Sleep Apnoea. *Eur. Respir. J.* 16 (4), 644–647. doi:10.1034/j.1399-3003.2000.16d13.x

Bosc, L. V., Resta, T., Walker, B., and Kanagy, N. L. (2010). Mechanisms of Intermittent Hypoxia Induced Hypertension. *J. Cel Mol Med* 14, 3–17. doi:10.1111/j.1582-4934.2009.00929.x

Chaouat, A., Weitzenblum, E., Krieger, J., Ifoundza, T., Oswald, M., and Kessler, R. (1995). Association of Chronic Obstructive Pulmonary Disease and Sleep Apnea Syndrome. *Am. J. Respir. Crit. Care Med.* 151 (1), 82–86. doi:10.1164/ajrccm.151.1.7812577

Cowie, M. R., Linz, D., Redline, S., Somers, V. K., and Simonds, A. K. (2021). Sleep Disordered Breathing and Cardiovascular Disease: JACC State-Of-The-Art Review. *J. Am. Coll. Cardiol.* 78 (6), 608–624. doi:10.1016/j.jacc.2021.05.048

Curkendall, S. M., DeLuise, C., Jones, J. K., Lanes, S., Stang, M. R., Goehring, E., et al. (2006). Cardiovascular Disease in Patients with Chronic Obstructive Pulmonary Disease, Saskatchewan Canada Cardiovascular Disease in COPD Patients. *Ann. Epidemiol.* 16 (1), 63–70. doi:10.1016/j.annepidem.2005.04.008

Dewan, N. A., Nieto, F. J., and Somers, V. K. (2015). Intermittent Hypoxemia and OSA: Implications for Comorbidities. *Chest* 147 (1), 266–274. doi:10.1378/chest.14-0500

Flenley, D. C. (1985). Sleep in Chronic Obstructive Lung Disease. *Clin. Chest Med.* 6 (4), 651–661. doi:10.1016/s0272-5231(21)00402-0

Kessler, R., Chaouat, A., Weitzenblum, E., Oswald, M., Ehrhart, M., Apprill, M., et al. (1996). Pulmonary Hypertension in the Obstructive Sleep Apnoea Syndrome: Prevalence, Causes and Therapeutic Consequences. *Eur. Respir. J.* 9 (4), 787–794. doi:10.1183/09031936.96.09040787

Kohler, M., and Stradling, J. R. (2010). Mechanisms of Vascular Damage in Obstructive Sleep Apnea. *Nat. Rev. Cardiol.* 7 (12), 677–685. doi:10.1038/nrcardio.2010.145

Lévy, P., Kohler, M., McNicholas, W. T., Barbé, F., McEvoy, R. D., Somers, V. K., et al. (2015). Obstructive Sleep Apnoea Syndrome. *Nat. Rev. Dis. Primers* 1, 15015. doi:10.1038/nrdp.2015.15

Li, J., Savransky, V., Nanayakkara, A., Smith, P. L., O'Donnell, C. P., and Polotsky, V. Y. (1985). Hyperlipidemia and Lipid Peroxidation Are Dependent on the Severity of Chronic Intermittent Hypoxia. *J. Appl. Physiol. (1985)* 102 (2), 557–563. doi:10.1152/japplphysiol.01081.2006

Maclay, J. D., and MacNee, W. (2013). Cardiovascular Disease in COPD: Mechanisms. *Chest* 143 (3), 798–807. doi:10.1378/chest.12-0938

Macnee, W., Maclay, J., and McAllister, D. (2008). Cardiovascular Injury and Repair in Chronic Obstructive Pulmonary Disease. *Proc. Am. Thorac. Soc.* 5 (8), 824–833. doi:10.1513/pats.200807-071TH

McNicholas, W. T., Bonsigore, M. R., and Bonsignore, M. R. (2007). Sleep Apnoea as an Independent Risk Factor for Cardiovascular Disease: Current Evidence, Basic Mechanisms and Research Priorities. *Eur. Respir. J.* 29 (1), 156–178. doi:10.1183/09031936.00027406

McNicholas, W. T. (2017). COPD-OSA Overlap Syndrome: Evolving Evidence Regarding Epidemiology, Clinical Consequences, and Management. *Chest* 152 (6), 1318–1326. doi:10.1016/j.chest.2017.04.160

Mills, N. L., Miller, J. J., Anand, A., Robinson, S. D., Frazer, G. A., Anderson, D., et al. (2008). Increased Arterial Stiffness in Patients with Chronic Obstructive Pulmonary Disease: a Mechanism for Increased Cardiovascular Risk. *Thorax* 63 (4), 306–311. doi:10.1136/thx.2007.083493

Pialoux, V., Hanly, P. J., Foster, G. E., Brugniaux, J. V., Beaudin, A. E., Hartmann, S. E., et al. (2009). Effects of Exposure to Intermittent Hypoxia on Oxidative Stress and Acute Hypoxic Ventilatory Response in Humans. *Am. J. Respir. Crit. Care Med.* 180 (10), 1002–1009. doi:10.1164/rccm.200905-0671OC

Rabe, K. F., and Watz, H. (2017). Chronic Obstructive Pulmonary Disease. *Lancet* 389 (10082), 1931–1940. doi:10.1016/S0140-6736(17)31222-9

Rutter, M. K., Meigs, J. B., Sullivan, L. M., D'Agostino, R. B., and Wilson, P. W. (2004). C-reactive Protein, the Metabolic Syndrome, and Prediction of Cardiovascular Events in the Framingham Offspring Study. *Circulation* 110 (4), 380–385. doi:10.1161/01.CIR.0000136581.59584.0E

Sajkov, D., and McEvoy, R. D. (2009). Obstructive Sleep Apnea and Pulmonary Hypertension. *Prog. Cardiovasc. Dis.* 51 (5), 363–370. doi:10.1016/j.pcad.2008.06.001

Savransky, V., Nanayakkara, A., Li, J., Bevans, S., Smith, P. L., Rodriguez, A., et al. (2007). Chronic Intermittent Hypoxia Induces Atherosclerosis. *Am. J. Respir. Crit. Care Med.* 175 (12), 1290–1297. doi:10.1164/rccm.200612-1771OC

Shiina, K., Tomiyama, H., Takata, Y., Yoshida, M., Kato, K., Nishihata, Y., et al. (2012). Overlap Syndrome: Additive Effects of COPD on the Cardiovascular Damages in Patients with OSA. *Respir. Med.* 106 (9), 1335–1341. doi:10.1016/j.rmed.2012.05.006

Sin, D. D., and Man, S. F. (2005). Chronic Obstructive Pulmonary Disease as a Risk Factor for Cardiovascular Morbidity and Mortality. *Proc. Am. Thorac. Soc.* 2 (1), 8–11. doi:10.1513/pats.200404-032MS

Takabatake, N., Nakamura, H., Abe, S., Inoue, S., Hino, T., Saito, H., et al. (2000). The Relationship between Chronic Hypoxemia and Activation of the Tumor Necrosis Factor-Alpha System in Patients with Chronic Obstructive Pulmonary Disease. *Am. J. Respir. Crit. Care Med.* 161, 1179–1184. doi:10.1164/ajrccm.161.4.9903022

Tang, M., Long, Y., Liu, S., Yue, X., and Shi, T. (2021). Prevalence of Cardiovascular Events and Their Risk Factors in Patients with Chronic Obstructive Pulmonary Disease and Obstructive Sleep Apnea Overlap Syndrome. *Front. Cardiovasc. Med.* 8, 694806. doi:10.3389/fcvm.2021.694806

Trayhurn, P., and Wood, I. S. (2004). Adipokines: Inflammation and the Pleiotropic Role of white Adipose Tissue. *Br. J. Nutr.* 92 (3), 347–355. doi:10.1079/bjn20041213

Voulgaris, A., Archontogeorgis, K., Papanas, N., Pilitsi, E., Nena, E., Xanthoudaki, M., et al. (2019). Increased Risk for Cardiovascular Disease in Patients with Obstructive Sleep Apnoea Syndrome-Chronic Obstructive Pulmonary Disease (Overlap Syndrome). *Clin. Respir. J.* 13 (11), 708–715. doi:10.1111/crj.13078

Wolf, J., Lewicka, J., and Narkiewicz, K. (2007). Obstructive Sleep Apnea: an Update on Mechanisms and Cardiovascular Consequences. *Nutr. Metab. Cardiovasc. Dis.* 17 (3), 233–240. doi:10.1016/j.numecd.2006.12.005

Young, T., Finn, L., Peppard, P. E., Szklo-Coxe, M., Austin, D., Nieto, F. J., et al. (2008). Sleep Disordered Breathing and Mortality: Eighteen-Year Follow-Up of the Wisconsin Sleep Cohort. *Sleep* 31 (8), 1071–1078. doi:10.5665/sleep/31.8.1071

Zhan, G., Serrano, F., Fenik, P., Hsu, R., Kong, L., Pratico, D., et al. (2005). NADPH Oxidase Mediates Hypersomnolence and Brain Oxidative Injury in a Murine Model of Sleep Apnea. *Am. J. Respir. Crit. Care Med.* 172 (7), 921–929. doi:10.1164/rccm.200504-581OC

Conflict of Interest: The authors declare that the research was conducted in the absence of any commercial or financial relationships that could be construed as a potential conflict of interest.

frontiers in Pharmacology

ORIGINAL RESEARCH
published: 02 November 2021
doi: 10.3389/fphar.2021.754268

Monoclonal Antibodies Targeting IL-5 or IL-5Rα in Eosinophilic Chronic Obstructive Pulmonary Disease: A Systematic Review and Meta-Analysis

Chuchu Zhang[1,2], *Yalei Wang*[1,2], *Meng Zhang*[1,2], *Xiaojie Su*[1,2], *Ting Lei*[1,2], *Haichuan Yu*[1,2] *and Jian Liu*[1]*

[1]Department of Intensive Care Unit, Lanzhou University First Affiliated Hospital, Lanzhou, China, [2]The First Clinical Medical College of Lanzhou University, Lanzhou University, Lanzhou, China

Background: Although the predominant airway inflammation in chronic obstructive pulmonary disease (COPD) is neutrophilic, approximately 20–40% of COPD patients present with eosinophilic airway inflammation. Compared with non-eosinophilic COPD patients, eosinophilic COPD patients are characterized by a greater number of total exacerbations and higher hospitalization rates. Furthermore, anti-interleukin-5 (IL-5) therapy, consisting of monoclonal antibodies (mAbs) targeting IL-5 or IL-5 receptor α (IL-5Rα), has been proven to be effective in severe eosinophilic asthma. This meta-analysis aimed to determine the efficacy and safety of anti-IL-5 therapy in eosinophilic COPD.

Methods: We searched the PubMed, Web of Science, Embase, and Cochrane Library databases from inception to August 2020 (updated in June 2021) to identify studies comparing anti-IL-5 therapy (including mepolizumab, benralizumab, and reslizumab) with placebo in eosinophilic COPD patients.

Results: Anti-IL-5 therapy was associated with a decrease in acute exacerbation rate (RR 0.89; 95% CI 0.84 to 0.95, I^2 = 0%) and the severe adverse events (RR 0.90; 95% CI 0.84 to 0.97, I^2 = 0%). However, no significant improvement was observed in pre-bronchodilator forced expiratory volume in 1 s (FEV_1) (WMD 0.01; 95% CI −0.01 to 0.03, I^2 = 25.9%), SGRQ score (WMD −1.17; 95% CI −2.05 to −0.29, I^2 = 0%), and hospital admission rate (RR 0.91; 95% CI 0.78 to 1.07, I^2 = 20.8%).

Conclusion: Anti-IL-5 therapy significantly reduced the annual acute exacerbation rate and severe adverse events in eosinophilic COPD patients. However, it did not improve lung function, quality of life, and hospitalization rate.

Keywords: eosinophils, monoclonal antibodies, anti-IL-5, COPD, meta-analysis

OPEN ACCESS

Edited by:
Djuro Kosanovic, I. M. Sechenov First Moscow State Medical University, Russia

Reviewed by:
Corrado Pelaia, University of Catanzaro, Italy
Srikanth Karnati, Julius Maximilian University of Würzburg, Germany
Deepak Khatry, Westat, United States

***Correspondence:**
Jian Liu
medecinliu@sina.com

Specialty section:
This article was submitted to Respiratory Pharmacology, a section of the journal Frontiers in Pharmacology

Received: *06 August 2021*
Accepted: *21 September 2021*
Published: *02 November 2021*

Citation:
Zhang C, Wang Y, Zhang M, Su X, Lei T, Yu H and Liu J (2021) Monoclonal Antibodies Targeting IL-5 or IL-5Rα in Eosinophilic Chronic Obstructive Pulmonary Disease: A Systematic Review and Meta-Analysis. Front. Pharmacol. 12:754268. doi: 10.3389/fphar.2021.754268

INTRODUCTION

Chronic obstructive pulmonary disease (COPD) is characterized by progressive and irreversible airflow limitation that is triggered by the response of the airways and the lungs to noxious particles or fumes (Dave and Arjun, 2021). It is a leading cause of chronic morbidity and mortality worldwide (Dave and Arjun, 2021). COPD is a heterogeneous disease with different underlying pathobiological

mechanisms (endotypes) and includes pulmonary and extra-pulmonary symptoms (phenotypes) (Han et al., 2010; Lange et al., 2016; Balkissoon, 2018; Dave and Arjun, 2021). Furthermore, as of May 2015, 99.9 million individuals suffering from COPD have been identified in China (Wang et al., 2018a). With continued exposure to COPD risk factors and an aging population, the prevalence of COPD is expected to increase over the next 40 years, and by 2060, more than 5.4 million may die from COPD and related conditions annually (Mathers and Loncar, 2006; Dave and Arjun, 2021).

Moreover, the exacerbation of COPD is associated with increased healthcare costs (Hilleman et al., 2000; Toy et al., 2010), progressive loss of lung function, subsequent cardiovascular events, and decline in quality of life (Dransfield et al., 2017; Kunisaki et al., 2018). Currently, Global Initiative for Chronic Obstructive Lung Disease (GOLD) guidelines have recommended triple inhaled therapy (inhaled glucocorticoids, long-acting β2-agonists, and long-acting muscarinic-receptor antagonists) as maintenance treatment for patients with frequent exacerbations, which was proven to decrease acute exacerbation rates in COPD patients (Calzetta et al., 2019; Dave and Arjun, 2021). Despite this, approximately 30–40% of patients continue to have moderate or severe exacerbations even after receiving triple inhaled therapy (Vestbo et al., 2017). Thus, it is essential to explore new treatment options for COPD patients with acute exacerbation.

Compared with non-eosinophilic COPD patients, eosinophilic COPD patients are associated with a higher number of total exacerbations and higher hospitalization rates (Couillard et al., 2017). Saha et al. have reported that 20–40% of COPD patients presented with airway eosinophilic inflammation (peripheral blood eosinophil count of 3% or more or >150 cells per cubic millimeter) (Dasgupta et al., 2013; Singh et al., 2014), although the predominant airway inflammation in COPD is neutrophilic (Hogg et al., 2004; Dasgupta et al., 2013). Interleukin-5 (IL-5) regulates the differentiation, proliferation, survival, and activation of eosinophils *via* the IL-5 receptor (Takatsu et al., 1994). Anti-IL-5 therapy includes monoclonal antibodies (mAbs) targeting IL-5 or IL-5R α (including mepolizumab, benralizumab, and reslizumab), which have been proven to be effective in severe eosinophilic asthma (Farne et al., 2017). Given the similarity between asthma and COPD in terms of eosinophilic airway inflammation, several randomized controlled trials (RCTs) have studied the efficacy and safety of anti-IL-5 treatment in eosinophilic COPD patients (Brightling et al., 2014; Dasgupta et al., 2017; Sciurba et al., 2018; Criner et al., 2019).

However, contrasting results on the efficacy of anti-IL-5 therapy to reduce annual exacerbation rates of eosinophilic COPD have been reported. Pavord et al. have found that treatment with mepolizumab was associated with a lower incidence of moderate and severe exacerbations than placebo (Sciurba et al., 2018). In contrast, Brightling et al. and Criner et al. have noted that benralizumab did not reduce the annual exacerbation rates compared with the placebo (Brightling et al., 2014; Criner et al., 2019). Takudzwa et al. have conducted a meta-analysis and demonstrated that mepolizumab decreased the exacerbation rate by 23% in COPD patients with eosinophil counts of 300 cells/μL or greater than controls. (Mkorombindo and Dransfield, 2019). The efficacy of anti-IL-5 therapy in eosinophilic COPD is therefore not consistent.

Although the meta-analysis on anti-IL-5 in COPD patients already existed (Donovan et al., 2020; Lan et al., 2020), study participants were not limited to eosinophilic COPD patients. To provide more accurate and stronger evidence for the efficacy of anti-IL-5 therapy in eosinophilic COPD patients, the current study differs in two ways from the previous meta-analysis (Dave and Arjun, 2021): we only included eosinophilic COPD patients (peripheral blood eosinophil count of 3% or more or >150 cells per cubic millimeter) (Balkissoon, 2018); we compared anti-IL-5 therapy in eosinophilic COPD and in asthma, which enabled a more robust assessment of the effect of anti-IL-5 therapy in eosinophilic COPD patients.

METHODS

This meta-analysis followed the guidelines of the Cochrane Handbook for Systematic Reviews of Interventions. Furthermore, we conducted this meta-analysis according to the Preferred Reporting Items for Systematic Reviews and Meta-analysis (PRISMA) guidelines (Moher et al., 2009). The protocol for this meta-analysis is available in PROSPERO (CRD42020156189) (Wang et al., 2018b; Ge et al., 2018).

Literature Search

We searched the PubMed, Web of Science, Embase, and Cochrane Library databases from inception to August 2020 (updated in June 2021) to identify studies comparing anti-IL-5 therapy (including mepolizumab, benralizumab, and reslizumab) with placebo in COPD patients. There was no language or population restriction. In addition, we searched the ClinicalTrials.gov database to identify completed studies. We used the following keywords to perform the search: monoclonal antibody (mepolizumab, benralizumab, and reslizumab) and chronic obstructive pulmonary disease. We have displayed the detailed search strategy in **Supplementary Material**.

Inclusion and Exclusion Criteria

Inclusion criteria were as follows:

1. RCTs included parallel group studies, had a controlled design, and compared anti-IL-5 therapies with placebo.
2. Studies were conducted in adult patients with eosinophilic COPD, defined as peripheral blood eosinophil count of 3% or more or >150 cells per cubic millimeter.
3. Intervention was restricted to anti-IL-5 therapy or placebo.
4. Study outcomes were required to be at least one of the following: annual exacerbations, hospital admission for acute exacerbation, improvement of pre-bronchodilator forced expiratory volume in 1 s (FEV_1), quality of life as assessed using the St. George's Respiratory Questionnaire (SGRQ) total score, and severe adverse events.

Exclusion criteria were as follows:

1. Studies including participants who suffered from clinically significant lung disease or asthma.
2. Conference abstracts, letters, comments, reviews, and meta-analyses.
3. Studies of animals or cells.

Study Selection and Data Extraction

Author CZ screened all titles and assessed full-text eligibility and then excluded studies that did not meet the inclusion and exclusion criteria. Author YW reassessed the selection results; all discrepancies were resolved by discussing them with a third author MZ. Two authors (XS and TL) independently extracted the following data from all included studies: lead author or study title, year of publication, location and duration, demographic characteristics of participants, drug and dose of anti-IL-5 therapy, annual exacerbations, hospital admission for acute exacerbation, change of pre-bronchodilator FEV_1 from baseline, SGRQ score, and severe adverse events. Disagreements were settled by cross-checking original papers and consensus was achieved. Author HY validated and sorted specific data in a tabular format. The primary outcome was annual exacerbations, as acute exacerbation is a major cause of hospitalization and poor prognosis in COPD. The secondary outcomes were hospital admission for acute exacerbation, pre-bronchodilator FEV_1, SGRQ score, and severe adverse events.

Assessment of Risk of Bias in Included Studies

Two authors (CZ and XS) independently evaluated the quality of the methodology of the eligible RCTs. They applied the Cochrane Collaboration tool following the Cochrane Handbook for Systematic Reviews of Interventions (Stovold et al., 2014). There were six perspectives used to assess the quality, including random sequence generation (selection bias), allocation concealment (selection bias), blinding (performance bias and detection bias), incomplete outcome data (attrition bias), selective outcome reporting (attrition bias), and other potential sources of bias. The criteria to grade the included studies were as follows: 1) low-quality trial: either randomization or allocation concealment was assessed to indicate a high risk of bias, regardless of other items; 2) high-quality trial: both randomization and allocation concealment were graded as low risk of bias, and all other items were assessed as low or unclear risk of bias; 3) moderate-quality trial: they did not meet the criteria for high or low risk. Any discrepancy was resolved by consulting an evidence-based medicine professor.

Statistical Analysis

Stata/SE 15.0 was used to perform data analysis. We pooled the rate ratio (RR) and 95% confidence interval (CI) to analyze the overall annual exacerbation rates. Dichotomous data, including hospital admission rate, severe adverse events, and all-cause mortality, were analyzed by calculating risk ratios (RR) and the corresponding 95% CI. Continuous data (pre-bronchodilator FEV_1 and SGRQ scores) were analyzed by calculating the weighted mean difference (WMD) or standardized mean difference (SMD) and 95% CI. We used P and I^2 statistics to measure heterogeneity among trials in each analysis. Fixed-effects models were used without important heterogeneity ($I^2 \leq 50\%$). Otherwise, random effects models were used. A funnel plot was generated for examining publication bias when there were >10 included trials (Lau et al., 2006; Stovold et al., 2014). A p-value <0.05 was considered statistically significant.

RESULTS

Eligible Studies and Risk of Bias

We obtained 1,227 articles from the four databases and five studies from the ClinicalTrials.gov database. After removing the duplicates, 1,048 articles remained. We excluded 1,015 articles after scanning the titles and abstracts. Finally, three articles, including five studies, were included in this meta-analysis after reading the full text (Criner et al., 2019; Sciurba et al., 2018; Brightling et al., 2014). The detailed selection process is shown in **Figure 1**, which was prepared based on the PRISMA guidelines (Moher et al., 1996). Three studies were rated as high quality based on the grade criteria, the six items of the Cochrane tool shown in **Supplementary Figures S1, S2**.

Description of Eligible Studies

All included studies were randomized, double-blinded, multicentered RCT, aiming to compare the clinical efficacy and safety of anti-IL-5 therapy with those of the placebo in adult patients with eosinophilic COPD. In the included five studies, the intervention was performed with benralizumab (10, 30, and 100 mg) targeting the IL-5 receptor α (20, 22) or mepolizumab (100 and 300 mg) targeting IL-5 (Brightling et al., 2014; Criner et al., 2019). Overall, there were 3902 COPD patients included in this meta-analysis. Current smoker status ranged from 25 to 42% among the study population and 58.0–70.7% of the patients were males. We have listed the detailed baseline characteristics in **Table1**.

Annual Rate of Acute Exacerbation

All included studies reported the annual rate of exacerbations. There were five RCTs (Brightling et al., 2014; Sciurba et al., 2018; Criner et al., 2019) that compared anti-IL-5 therapy with placebo, showing that anti-IL-5 therapy was associated with a lower risk of acute exacerbation rate of eosinophilic COPD patients (RR 0.89; 95% CI 0.84 to 0.95, $I^2 = 0\%$; **Figure 2**).

Secondary Outcomes

Mean change from baseline of pre-bronchodilator FEV_1 was used to assess lung function. Three RCTs reported an improvement in FEV_1. However, no significant difference between anti-IL-5 therapy and placebo with regard to pre-bronchodilator FEV_1 was observed (WMD 0.01; 95% CI −0.01 to 0.03, $I^2 = 25.9\%$; **Figure 3**) (Criner et al., 2019; Brightling et al., 2014). Improvement in quality of life was evaluated by the SGRQ total score, with a threshold of 4 units being considered

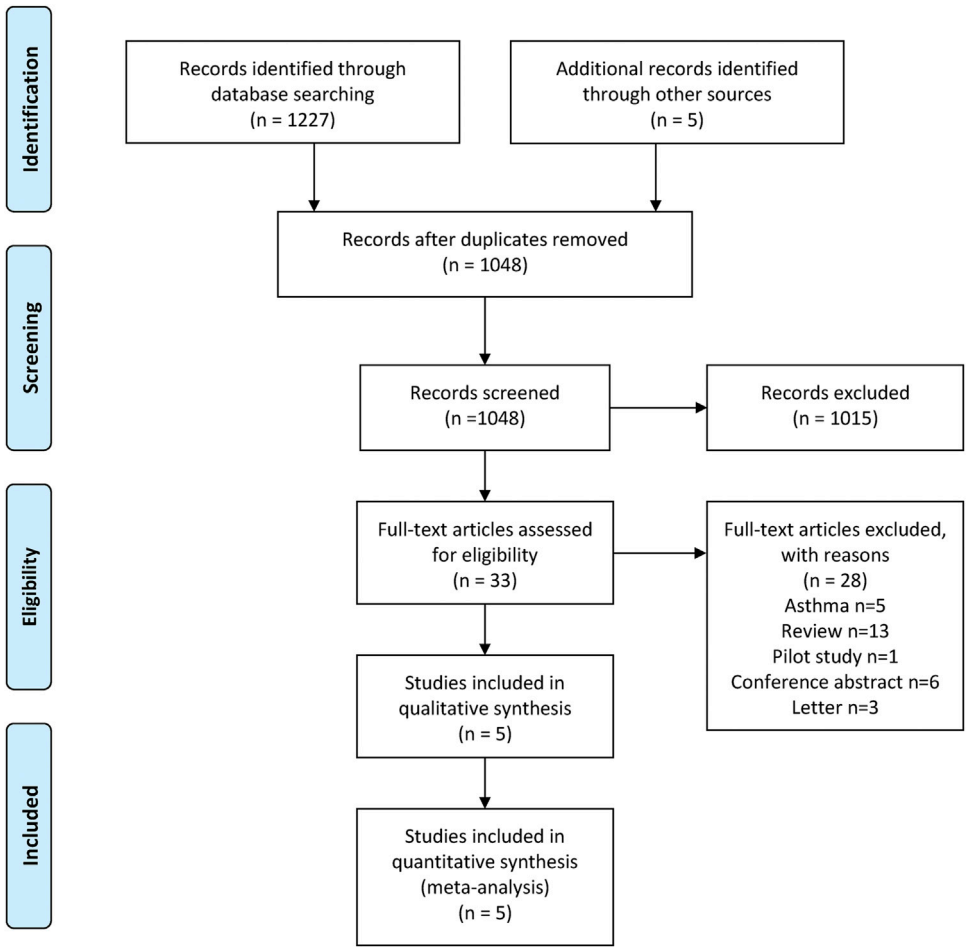

FIGURE 1 | Study selection process: PRISMA flow diagram identifying studies included in the meta-analysis. PRISMA, Preferred Reporting Items for Systematic Reviews and Meta-Analyses.

TABLE.1 | Characteristic of studies included in this meta-analysis.

Study	Year	N	Age	Male%	Smoker%	Baseline EOS	Intervention	Duration	Outcome
Brightling	2014	101	62.9 ± 8.2/64.6 ± 7.5	68.6/58.0	33/42	248.8 ± 193.4/229.2 ± 164.5	B 100 mg	56	①②③④⑤
GALATHEA	2019	1,120	65.6 ± 8.25	70.7	34.3	453.2 ± 280.25	a. B 100 mg b. B 30 mg	56	①②③④⑤
TERRANOVA	2019	1,545	65.2 ± 8.33	66.3	28.6	504.5 ± 393.08	a. B 100 mg b. B 30 mg c. B 10 mg	56	①②③④⑤
METREX	2017	462	66 ± 9/65 ± 9	62/63	25/28	260 ± 0.438/290 ± 0.558	M 100 mg	52	①③⑤
METREO	2017	674	65 ± 9/66 ± 9 65 ± 9/66 ± 9	59/69 70/69	25/28 32/28	300 ± 0.520/310 ± 0.515 310 ± 0.540/310 ± 0.515	a. M 100 mg b. M 300 mg	52	①③⑤

Outcome: ① annual rate of acute exacerbation; ② change from baseline of pre-bronchodilator FEV_1; ③ change from baseline of SGRQ total score; ④ hospital admission rate for acute exacerbation; ⑤ severe adverse events. B: benralizumab; M: mepolizumab.

clinically significant (Jones, 2005). Five RCTs reported changes in SGRQ total score. Anti-IL-5 was not associated with a significant improvement in the quality of life compared with placebo (WMD −1.17; 95% CI −2.05 to −0.29, I^2 = 0%; **Figure 4**) (Brightling et al., 2014; Sciurba et al., 2018; Criner et al., 2019). In addition, we assessed the hospital admission for acute exacerbation (Brightling et al., 2014; Criner et al., 2019). There was no significant difference in hospitalization rate between the anti-IL-5 therapy group and the placebo group (RR 0.91; 95% CI 0.78 to 1.07, I^2 = 20.8%; **Figure 5**). Regarding safety outcomes, the anti-IL-5 group

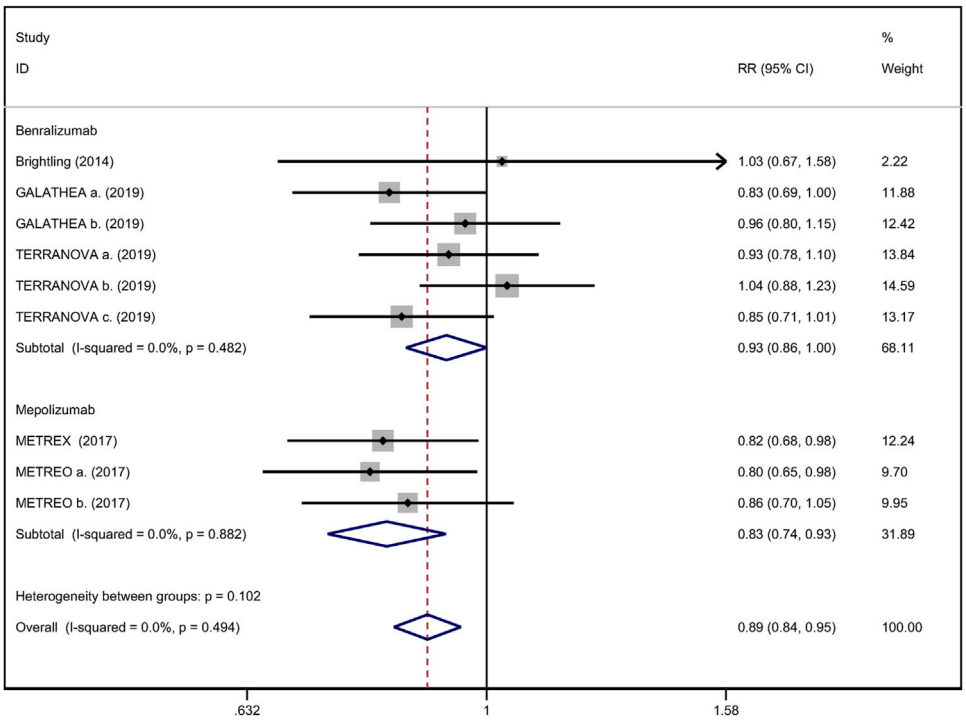

FIGURE 2 | Forest plot of annual acute exacerbation rates in eosinophilic COPD patients with anti-IL-5 therapy vs. placebo.

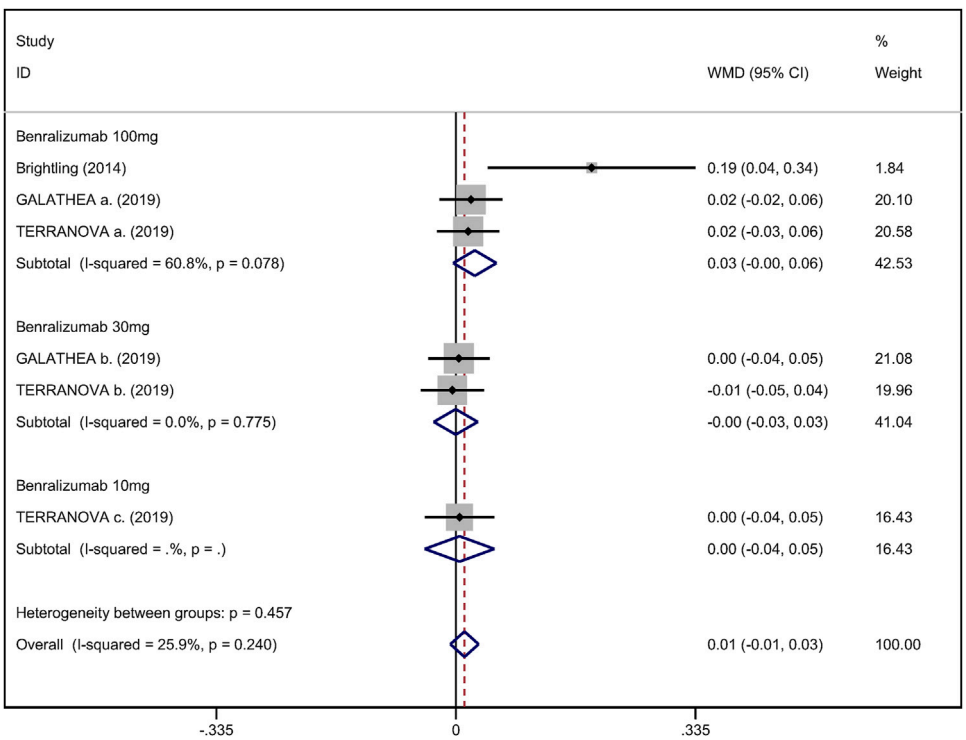

FIGURE 3 | Forest plot of pre-bronchodilator FEV_1 in eosinophilic COPD patients with anti-IL-5 therapy vs. placebo.

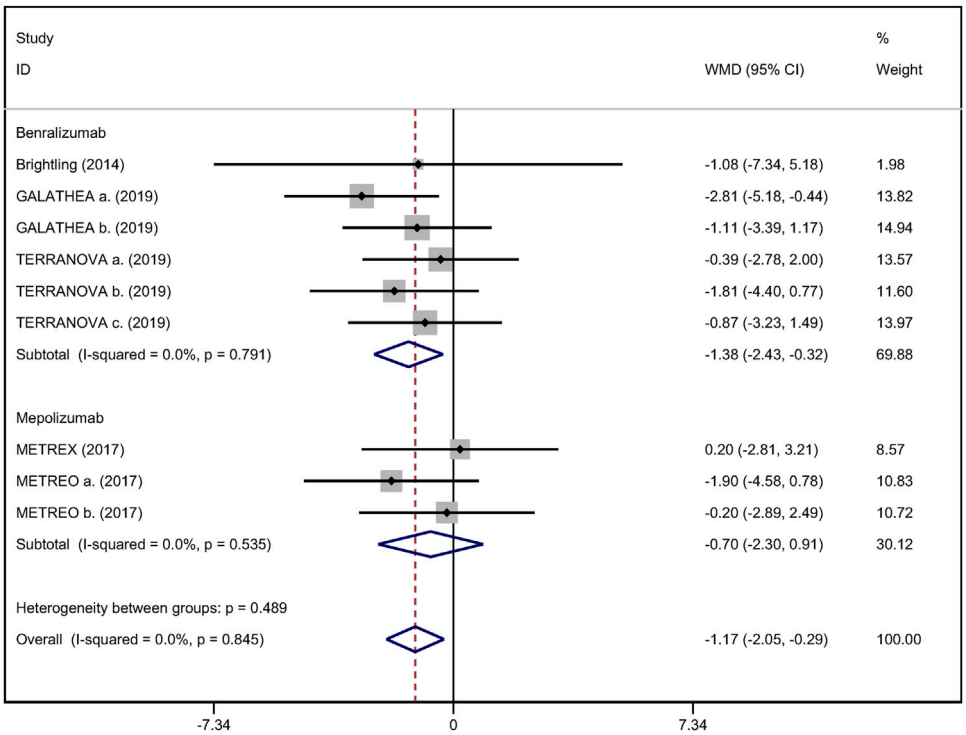

FIGURE 4 | Forest plot of SGRQ score in eosinophilic COPD patients with anti-IL-5 therapy vs. placebo.

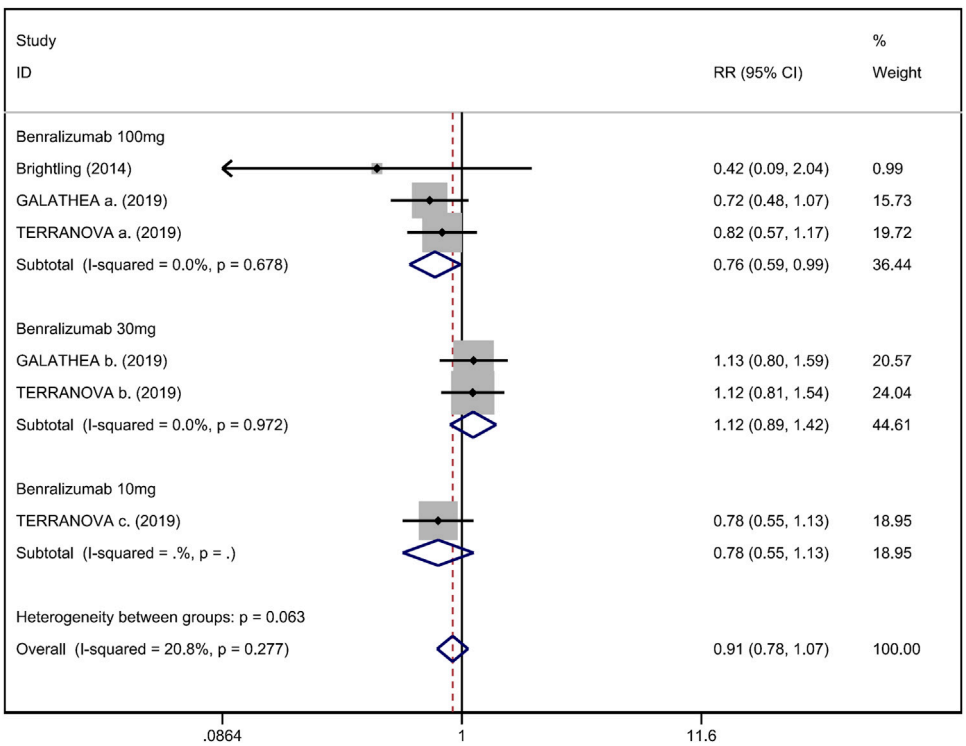

FIGURE 5 | Forest plot of hospital admission rate for acute exacerbation in eosinophilic COPD patients with anti-IL-5 therapy vs. placebo.

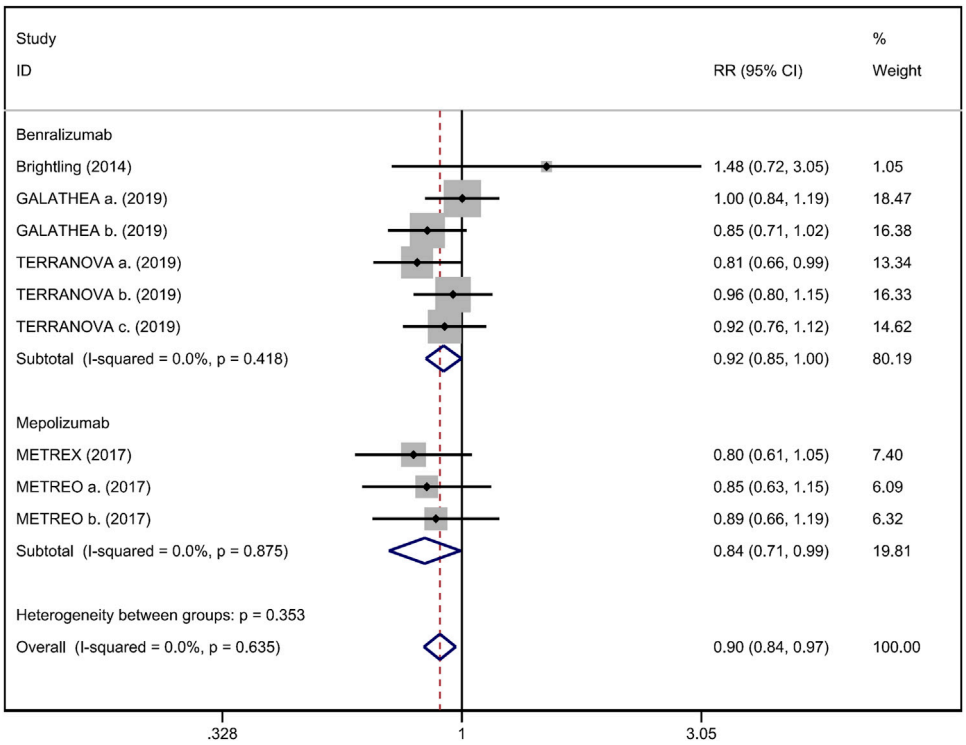

FIGURE 6 | Forest plot of severe adverse event in eosinophilic COPD patients with anti-IL-5 therapy vs. placebo.

TABLE 2 | Comparison of anti-IL-5 between eosinophilic COPD and asthma.

Outcome	Eosinophilic COPD		Asthma	
	Benralizumab	Mepolizumab	Benralizumab	Mepolizumab
Annual exacerbation rate	0.93 (0.86, 1.00)	0.83 (0.74, 0.93)	0.62 (0.55, 0.70)	0.45 (0.36, 0.55)
Pre-bronchodilator FEV_1	0.01 (−0.01, 0.03)	NA	0.10 (0.05, 0.14)	0.11 (0.06, 0.17)
Health-related quality of life				
SGRQ	−1.38 (−2.43, −0.32)	−0.70 (−2.30, 0.91)	NA	−7.40 (−9.50, −5.29)
ACQ	NA		−0.20 (−0.29, −0.11)	−0.42 (−0.56, −0.28)
AQLQ			0.23 (0.11, 0.35)	NA
Severe adverse events	0.92 (0.85, 1.00)	0.84 (0.71, 0.99)	0.81 (0.66, 1.01)	0.63 (0.41, 0.97)

ACQ, asthma control questionnaire; AQLQ, asthma quality of life questionnaire; SGRQ, St George's respiratory questionnaire.

demonstrated a significantly lower risk in the incidence of severe adverse events compared with the placebo group (RR 0.90; 95% CI 0.84 to 0.97, $I^2 = 0\%$; **Figure 6**) (Brightling et al., 2014; Sciurba et al., 2018; Criner et al., 2019).

Comparison With Anti-IL-5 Therapy in Asthma

To enrich our study, we compared the efficacy of anti-IL-5 therapy in eosinophilic COPD and asthma (Farne et al., 2017; He et al., 2018). The outcomes (including annual exacerbation rate, the pre-bronchodilator FEV_1, the health-related quality of life, and the severe adverse events) of anti-IL-5 therapy on eosinophilic COPD or asthma are listed in **Table 2**. Anti-IL-5 therapy was significantly more effective in reducing the annual exacerbation rate in asthma patients than in eosinophilic COPD patients. Similarly, anti-IL-5 therapy showed a more remarkable improvement of pre-bronchodilator FEV_1 in asthma patients than in eosinophilic COPD. Furthermore, mepolizumab led to a significant enhancement of health-related quality of life (by SGRQ score) in asthma but not in eosinophilic COPD. Finally, mepolizumab caused a more significant reduction of severe adverse events in asthma than in eosinophilic COPD.

DISCUSSION

In this meta-analysis, we assessed the efficacy and safety of anti-IL-5 therapy in eosinophilic COPD patients. Several key findings were obtained: anti-IL-5 therapy significantly reduced the annual

exacerbation rates without increasing the occurrence of severe adverse events (Brightling et al., 2014; Sciurba et al., 2018; Criner et al., 2019). However, the anti-IL-5 group did not show a significant improvement with regard to lung function, quality of life, and hospitalization (Brightling et al., 2014; Sciurba et al., 2018; Criner et al., 2019).

This meta-analysis demonstrated that anti-IL-5 therapy decreased the acute exacerbation rate in eosinophilic COPD patients. This result has physiological plausibility. IL-5 is a well-researched cytokine in eosinophilic inflammation, which is particularly vital for the differentiation, proliferation, and activation of eosinophils. It is released by the following 3 cells: $CD4^+$ Th2 lymphocytes, eosinophils, and innate lymphoid cells. Both eosinophils and basophils express the IL-5R (Bagnasco et al., 2017; Yousuf et al., 2019). Mepolizumab reduces eosinophil counts in the blood and tissues by avidly binding to IL-5, preventing IL-5 from binding to eosinophil surface receptors (Hart et al., 2001; Varricchi et al., 2016). Benralizumab enhances antibody-dependent cell-mediated cytotoxic effects by binding to IL-5Rα, in turn reducing sputum and blood eosinophil count (Busse et al., 2010; Laviolette et al., 2013).

Furthermore, similar results were reported in severe asthma patients. Pavord et al. (2012), Ortega et al. (2014), and Chupp et al. (2017) have reported that mepolizumab treatment was associated with lower rates of exacerbations and symptoms and with greater improvements in health-related quality of life compared with placebo among patients with severe eosinophilic asthma. Similarly, a meta-analysis by Farne et al. has revealed that anti-IL-5 reduced asthma exacerbations roughly by half (Farne et al., 2017). In addition, Cabon et al. have conducted an RCT and reported that mAbs targeting IL-5 significantly reduced blood and sputum eosinophil counts and attenuated bronchial submucosal eosinophils by approximately 50% in patients with eosinophilic asthma (Cabon et al., 2017).

However, no significant improvement in lung function, quality of life, and hospitalization rate was observed in the anti-IL-5 group. Anti-IL-5 therapy was associated with a mean difference of −0.01–0.03 L in pre-bronchodilator FEV_1 compared with placebo. A change of 0.1 L from baseline in FEV_1 has been described as a difference that patients can perceive (Donohue, 2005). The mean difference in SGRQ reduction between the anti-IL-5 and placebo groups was 0.29–2.05, while a threshold of 4 units is considered clinically significant (Jones, 2005). Likewise, other anti-inflammatory therapies for COPD, including macrolide antibiotics, have been reported to show similar results, i.e., significant reductions in exacerbation rate that were not associated with significant improvements in pre-bronchodilator FEV_1 or health-related quality of life (Herath et al., 2018). A major therapeutic goal in COPD patients is to prevent or reduce future exacerbations (Dave and Arjun, 2021). Therefore, anti-IL-5 therapy can be considered for use in eosinophilic COPD patients due to the decrease in acute exacerbation rate. Based on the GOLD guidelines, cornerstone treatments such as LAMA, LABA, and ICS greatly improve lung function and the quality of life (Dave and Arjun, 2021). Additionally, the anti-IL-5 group was associated with a lower risk of severe adverse events than the placebo group. This result was consistent with that noted in previous phase 3 trials of benralizumab for severe, uncontrolled eosinophilic asthma (Bleecker et al., 2016; FitzGerald et al., 2016).

There was heterogeneity in the SGRQ total score. We speculate that the main source of this heterogeneity was the subjectivity of the scorer's perception of the scale. In addition, a single scoring scale does not accurately reflect the true status of the quality of life. Heterogeneity also existed in the change from baseline of pre-bronchodilator FEV1. One possible reason might be that the measurement device or the professional level of the implementer may be different. Another reason may be that the education and cooperation level of COPD patients could influence lung function test results.

There are several limitations to this meta-analysis. First, among the RCTs admitted included in this meta-analysis, benralizumab failed to reduce the annual rate of acute exacerbation, whereas mepolizumab showed opposite results. The differences observed between benralizumab and mepolizumab might be due to the differences in sample sizes of the studies. In addition, owing to the limited original research, we could not perform subgroup analysis and the reliability of the conclusions inevitably decreased. Therefore, additional large RCTs assessing the efficacy of anti-IL-5 therapy (including benralizumab, mepolizumab, and reslizumab) in eosinophilic COPD patients are urgently needed. Second, although we conducted the comparison between anti-IL-5 therapy in eosinophilic COPD and in asthma, further RCTs that compare the anti-IL-5 therapy with ICS in eosinophilic COPD are needed, which may allow us to better determine the efficacy of anti-IL-5 therapy in eosinophilic COPD. Finally, all RCTs included in this meta-analysis were sponsored by a biopharmaceutical company.

CONCLUSION

In this meta-analysis, we found that anti-IL-5 therapy significantly reduced the annual acute exacerbation rate and severe adverse events among eosinophilic COPD patients. In contrast, anti-IL-5 therapy did not improve lung function, quality of life, or hospitalization rate.

DATA AVAILABILITY STATEMENT

The original contributions presented in the study are included in the article/**Supplementary Material**; further inquiries can be directed to the corresponding author.

ETHICS STATEMENT

Ethical review and approval were not required for the study on human participants in accordance with the local legislation and institutional requirements. Written informed consent for participation was not required for this study in accordance with the national legislation and the institutional requirements.

AUTHOR CONTRIBUTIONS

JL and CZ designed this systematic review. MZ and YW have been involved in the search strategy. CZ, MZ, and YW did the

collection and the analysis of the data. XS, TL, and HY interpreted the data. CZ wrote the systematic review and all the other authors revised the manuscript. JL provided general advice on the manuscript. All the authors read and approved the final manuscript.

FUNDING

This study was supported by the Science and Technology Projects of Gansu Province (Grant no. 18JR3RA344). The authors remain independent of any funding influence.

ACKNOWLEDGMENTS

The author gratefully acknowledges the support of the First Clinical Medical College of Lanzhou University, Lanzhou University First Affiliated Hospital, and all the authors who participated in this study.

SUPPLEMENTARY MATERIAL

The Supplementary Material for this article can be found online at: https://www.frontiersin.org/articles/10.3389/fphar.2021.754268/full#supplementary-material

REFERENCES

Bagnasco, D., Ferrando, M., Varricchi, G., Puggioni, F., Passalacqua, G., and Canonica, G. W. (2017). Anti-Interleukin 5 (IL-5) and IL-5Ra Biological Drugs: Efficacy, Safety, and Future Perspectives in Severe Eosinophilic Asthma. *Front. Med. (Lausanne)* 4, 135. doi:10.3389/fmed.2017.00135

Balkissoon, R. (2018). New Treatment Options for COPD: How Do We Decide Phenotypes, Endotypes or Treatable Traits? *Chronic Obstr Pulm. Dis.* 5 (1), 72–80.0128 doi:10.15326/jcopdf.5.1.201810.15326/jcopdf.5.1.2018.0128

Bleecker, E. R., FitzGerald, J. M., Chanez, P., Papi, A., Weinstein, S. F., Barker, P., et al. (2016). Efficacy and Safety of Benralizumab for Patients with Severe Asthma Uncontrolled with High-Dosage Inhaled Corticosteroids and Long-Acting β2-agonists (SIROCCO): a Randomised, Multicentre, Placebo-Controlled Phase 3 Trial. *Lancet* 388 (10056), 2115–2127. doi:10.1016/s0140-6736(16)31324-1

Brightling, C. E., Bleecker, E. R., Panettieri, R. A., ., Bafadhel, M., She, D., Ward, C. K., et al. (2014). Benralizumab for Chronic Obstructive Pulmonary Disease and Sputum Eosinophilia: a Randomised, Double-Blind, Placebo-Controlled, Phase 2a Study. *Lancet Respir. Med.* 2 (11), 891–901. doi:10.1016/s2213-2600(14)70187-0

Busse, W. W., Katial, R., Gossage, D., Sari, S., Wang, B., Kolbeck, R., et al. (2010). Safety Profile, Pharmacokinetics, and Biologic Activity of MEDI-563, an anti-IL-5 Receptor Alpha Antibody, in a Phase I Study of Subjects with Mild Asthma. *J. Allergy Clin. Immunol.* 125 (6), 1237–e2. doi:10.1016/j.jaci.2010.04.005

Cabon, Y., Molinari, N., Marin, G., Vachier, I., Gamez, A. S., Chanez, P., et al. (2017). Comparison of Anti-interleukin-5 Therapies in Patients with Severe Asthma: Global and Indirect Meta-Analyses of Randomized Placebo-Controlled Trials. *Clin. Exp. Allergy* 47 (1), 129–138. doi:10.1111/cea.12853

Calzetta, L., Cazzola, M., Matera, M. G., and Rogliani, P. (2019). Adding a LAMA to ICS/LABA Therapy: A Meta-Analysis of Triple Combination Therapy in COPD. *Chest* 155 (4), 758–770. doi:10.1016/j.chest.2018.12.016

Chupp, G. L., Bradford, E. S., Albers, F. C., Bratton, D. J., Wang-Jairaj, J., Nelsen, L. M., et al. (2017). Efficacy of Mepolizumab Add-On Therapy on Health-Related Quality of Life and Markers of Asthma Control in Severe Eosinophilic Asthma (MUSCA): a Randomised, Double-Blind, Placebo-Controlled, Parallel-Group, Multicentre, Phase 3b Trial. *Lancet Respir. Med.* 5 (5), 390–400. doi:10.1016/s2213-2600(17)30125-x

Couillard, S., Larivée, P., Courteau, J., and Vanasse, A. (2017). Eosinophils in COPD Exacerbations Are Associated with Increased Readmissions. *Chest* 151 (2), 366–373. doi:10.1016/j.chest.2016.10.003

Criner, G. J., Celli, B. R., Brightling, C. E., Agusti, A., Papi, A., Singh, D., et al. (2019). Benralizumab for the Prevention of COPD Exacerbations. *N. Engl. J. Med.* 381 (11), 1023–1034. doi:10.1056/NEJMoa1905248

Dasgupta, A., Kjarsgaard, M., Capaldi, D., Radford, K., Aleman, F., Boylan, C., et al. (2017). A Pilot Randomised Clinical Trial of Mepolizumab in COPD with Eosinophilic Bronchitis. *Eur. Respir. J.* 49 (3). doi:10.1183/13993003.02486-2016

Dasgupta, A., Neighbour, H., and Nair, P. (2013). Targeted Therapy of Bronchitis in Obstructive Airway Diseases. *Pharmacol. Ther.* 140 (3), 213–222. doi:10.1016/j.pharmthera.2013.07.001

Dave, S., and Arjun, R., (2021). Global Initiative for Chronic Obstructive Lung Disease (GOLD) [database on Internet]. *Glob. strategy Diagn. Manag. Prev. chronic obstructive Pulm. Dis.*.71(01): 9–14. Available at from: http://goldcopd.org. Accessed November 17, 2020. doi:10.1055/s-0042-121903

Donohue, J. F. (2005). Minimal Clinically Important Differences in COPD Lung Function. *Copd* 2 (1), 111–124. doi:10.1081/copd-200053377

Donovan, T., Milan, S. J., Wang, R., Banchoff, E., Bradley, P., and Crossingham, I. (2020). Anti-IL-5 Therapies for Chronic Obstructive Pulmonary Disease. *Cochrane database Syst. Rev.* Epub 2020/12/10. PubMed PMID: 33295032; PubMed Central PMCID: PMCPMC8106745 (respiratory medicine). EB: none known. PB: I work in a clinically relevant speciality (respiratory medicine). IC: I work in a clinically relevant speciality (respiratory medicine). I have been involved as a local investigator for a GSK-sponsored drug trial of inhaled nemiralisib for COPD, but did not directly receive funding for this, 12. 12. Cd013432. doi:10.1002/14651858.CD013432.pub2

Dransfield, M. T., Kunisaki, K. M., Strand, M. J., Anzueto, A., Bhatt, S. P., Bowler, R. P., et al. (2017). Acute Exacerbations and Lung Function Loss in Smokers with and without Chronic Obstructive Pulmonary Disease. *Am. J. Respir. Crit. Care Med.* 195 (3), 324–330. doi:10.1164/rccm.201605-1014OC

Farne, H. A., Wilson, A., Powell, C., Bax, L., and Milan, S. J. (2017). Anti-IL5 Therapies for Asthma. *Cochrane Database Syst. Rev.* 9 (9), Cd010834. doi:10.1002/14651858.CD010834.pub3

FitzGerald, J. M., Bleecker, E. R., Nair, P., Korn, S., Ohta, K., Lommatzsch, M., et al. (2016). Benralizumab, an Anti-interleukin-5 Receptor α Monoclonal Antibody, as Add-On Treatment for Patients with Severe, Uncontrolled, Eosinophilic Asthma (CALIMA): a Randomised, Double-Blind, Placebo-Controlled Phase 3 Trial. *Lancet* 388 (10056), 2128–2141. doi:10.1016/s0140-6736(16)31322-8

Ge, L., Tian, J. H., Li, Y. N., Pan, J. X., Li, G., Wei, D., et al. (2018). Association between Prospective Registration and Overall Reporting and Methodological Quality of Systematic Reviews: a Meta-Epidemiological Study. *J. Clin. Epidemiol.* 93, 45–55. doi:10.1016/j.jclinepi.2017.10.012

Han, M. K., Agusti, A., Calverley, P. M., Celli, B. R., Criner, G., Curtis, J. L., et al. (2010). Chronic Obstructive Pulmonary Disease Phenotypes: the Future of COPD. *Am. J. Respir. Crit. Care Med.* 182 (5), 598–604. doi:10.1164/rccm.200912-1843CC

Hart, T. K., Cook, R. M., Zia-Amirhosseini, P., Minthorn, E., Sellers, T. S., Maleeff, B. E., et al. (2001). Preclinical Efficacy and Safety of Mepolizumab (SB-240563), a Humanized Monoclonal Antibody to IL-5, in Cynomolgus Monkeys. *J. Allergy Clin. Immunol.* 108 (2), 250–257. doi:10.1067/mai.2001.116576

He, L. L., Zhang, L., Jiang, L., Xu, F., and Fei, D. S. (2018). Efficacy and Safety of Anti-interleukin-5 Therapy in Patients with Asthma: A Pairwise and Bayesian Network Meta-Analysis. *Int. Immunopharmacol* 64, 223–231. doi:10.1016/j.intimp.2018.08.031

Herath, S. C., Normansell, R., Maisey, S., and Poole, P. (2018). Prophylactic Antibiotic Therapy for Chronic Obstructive Pulmonary Disease (COPD), *Cochrane database Syst. Rev.*, 2018. 10. Cd009764. doi:10.1002/14651858.CD009764.pub3

Hilleman, D. E., Dewan, N., Malesker, M., and Friedman, M. (2000). Pharmacoeconomic Evaluation of COPD. *Chest* 118 (5), 1278–1285. doi:10.1378/chest.118.5.1278

Hogg, J. C., Chu, F., Utokaparch, S., Woods, R., Elliott, W. M., Buzatu, L., et al. (2004). The Nature of Small-Airway Obstruction in Chronic Obstructive

Pulmonary Disease. *N. Engl. J. Med.* 350 (26), 2645–2653. doi:10.1056/NEJMoa032158

Jones, P. W. (2005). St. George's Respiratory Questionnaire: MCID. *Copd* 2 (1), 75–79. doi:10.1081/copd-200050513

Kunisaki, K. M., Dransfield, M. T., Anderson, J. A., Brook, R. D., Calverley, P. M. A., Celli, B. R., et al. (2018). Exacerbations of Chronic Obstructive Pulmonary Disease and Cardiac Events. A Post Hoc Cohort Analysis from the SUMMIT Randomized Clinical Trial. *Am. J. Respir. Crit. Care Med.* 198 (1), 51–57. doi:10.1164/rccm.201711-2239OC

Lan, S.-H., Lai, C.-C., Chang, S.-P., Hsu, C.-C., Chen, C.-H., Wang, Y.-H., et al. (2020). Efficacy and Safety of Anti-interleukin-5 Therapy in Patients with Chronic Obstructive Pulmonary Disease: A Meta-Analysis of Randomized, Controlled Trials, *J. Microbiol. Immunol. Infect.*. S1684-1182(20). 30253-X. doi:10.1016/j.jmii.2020.11.001

Lange, P., Halpin, D. M., O'Donnell, D. E., and MacNee, W. (2016). Diagnosis, Assessment, and Phenotyping of COPD: beyond FEV_1. *Int. J. Chron. Obstruct Pulmon Dis.* 11 Spec Iss, 3–12. doi:10.2147/copd.S85976

Lau, J., Ioannidis, J. P., Terrin, N., Schmid, C. H., and Olkin, I. (2006). The Case of the Misleading Funnel Plot. *BMJ* 333 (7568), 597–600. doi:10.1136/bmj.333.7568.597

Laviolette, M., Gossage, D. L., Gauvreau, G., Leigh, R., Olivenstein, R., Katial, R., et al. (2013). Effects of Benralizumab on Airway Eosinophils in Asthmatic Patients with Sputum Eosinophilia. *J. Allergy Clin. Immunol.* 132 (5), 1086–e5. doi:10.1016/j.jaci.2013.05.020

Mathers, C. D., and Loncar, D. (2006). Projections of Global Mortality and burden of Disease from 2002 to 2030. *Plos Med.* 3 (11), e442. doi:10.1371/journal.pmed.0030442

Mkorombindo, T., and Dransfield, M. T. (2019). Mepolizumab in the Treatment of Eosinophilic Chronic Obstructive Pulmonary Disease. *Int. J. Chron. Obstruct Pulmon Dis.* 14, 1779–1787. doi:10.2147/copd.S162781

Moher, D., Jadad, A. R., and Tugwell, P. (1996). Assessing the Quality of Randomized Controlled Trials. Current Issues and Future Directions. *Int. J. Technol. Assess. Health Care* 12 (2), 195–208. doi:10.1017/s0266462300009570

Moher, D., Liberati, A., Tetzlaff, J., and Altman, D. G. (2009). Preferred Reporting Items for Systematic Reviews and Meta-Analyses: the PRISMA Statement. *BMJ* 339, b2535. doi:10.1136/bmj.b2535

Ortega, H. G., Liu, M. C., Pavord, I. D., Brusselle, G. G., FitzGerald, J. M., Chetta, A., et al. (2014). Mepolizumab Treatment in Patients with Severe Eosinophilic Asthma. *N. Engl. J. Med.* 371 (13), 1198–1207. doi:10.1056/NEJMoa1403290

Pavord, I. D., Korn, S., Howarth, P., Bleecker, E. R., Buhl, R., Keene, O. N., et al. (2012). Mepolizumab for Severe Eosinophilic Asthma (DREAM): a Multicentre, Double-Blind, Placebo-Controlled Trial. *Lancet* 380 (9842), 651–659. doi:10.1016/s0140-6736(12)60988-x

Sciurba, F. C., Bradford, E. S., and Pavord, I. D. (2018). Mepolizumab for Eosinophilic COPD. *N. Engl. J. Med.* 378 (7), 681–683. doi:10.1056/NEJMc1715454

Singh, D., Kolsum, U., Brightling, C. E., Locantore, N., Agusti, A., and Tal-Singer, R. (2014). Eosinophilic Inflammation in COPD: Prevalence and Clinical Characteristics. *Eur. Respir. J.* 44 (6), 1697–1700. doi:10.1183/09031936.00162414

Stovold, E., Beecher, D., Foxlee, R., and Noel-Storr, A. (2014). Study Flow Diagrams in Cochrane Systematic Review Updates: an Adapted PRISMA Flow Diagram. *Syst. Rev.* 3, 54. doi:10.1186/2046-4053-3-54

Takatsu, K., Takaki, S., and Hitoshi, Y. (1994). Interleukin-5 and its Receptor System: Implications in the Immune System and Inflammation. *Adv. Immunol.* 57, 145–190. doi:10.1016/s0065-2776(08)60673-2

Toy, E. L., Gallagher, K. F., Stanley, E. L., Swensen, A. R., and Duh, M. S. (2010). The Economic Impact of Exacerbations of Chronic Obstructive Pulmonary Disease and Exacerbation Definition: a Review. *Copd* 7 (3), 214–228. doi:10.3109/15412555.2010.481697

Varricchi, G., Bagnasco, D., Borriello, F., Heffler, E., and Canonica, G. W. (2016). Interleukin-5 Pathway Inhibition in the Treatment of Eosinophilic Respiratory Disorders: Evidence and Unmet Needs. *Curr. Opin. Allergy Clin. Immunol.* 16 (2), 186–200. doi:10.1097/aci.0000000000000251

Vestbo, J., Papi, A., Corradi, M., Blazhko, V., Montagna, I., Francisco, C., et al. (2017). Single Inhaler Extrafine Triple Therapy versus Long-Acting Muscarinic Antagonist Therapy for Chronic Obstructive Pulmonary Disease (TRINITY): a Double-Blind, Parallel Group, Randomised Controlled Trial. *Lancet* 389 (10082), 1919–1929. doi:10.1016/s0140-6736(17)30188-5

Wang, C., Xu, J., Yang, L., Xu, Y., Zhang, X., Bai, C., et al. (2018). Prevalence and Risk Factors of Chronic Obstructive Pulmonary Disease in China (The China Pulmonary Health [CPH] Study): a National Cross-Sectional Study. *Lancet* 391 (10131), 1706–1717. doi:10.1016/s0140-6736(18)30841-9

Wang, X., Chen, Y., Yao, L., Zhou, Q., Wu, Q., Estill, J., et al. (2018). Reporting of Declarations and Conflicts of Interest in WHO Guidelines Can Be Further Improved. *J. Clin. Epidemiol.* 98, 1–8. doi:10.1016/j.jclinepi.2017.12.021

Yousuf, A., Ibrahim, W., Greening, N. J., and Brightling, C. E. (2019). T2 Biologics for Chronic Obstructive Pulmonary Disease. *J. Allergy Clin. Immunol. Pract.* 7 (5), 1405–1416. doi:10.1016/j.jaip.2019.01.036

Conflict of Interest: The authors declare that the research was conducted in the absence of any commercial or financial relationships that could be construed as a potential conflict of interest.

Publisher's Note: All claims expressed in this article are solely those of the authors and do not necessarily represent those of their affiliated organizations, or those of the publisher, the editors and the reviewers. Any product that may be evaluated in this article, or claim that may be made by its manufacturer, is not guaranteed or endorsed by the publisher.

frontiers in Pharmacology

ORIGINAL RESEARCH
published: 11 November 2021
doi: 10.3389/fphar.2021.758763

Combination Therapy With Rapamycin and Low Dose Imatinib in Pulmonary Hypertension

Yinan Shi[1,2], Chenxin Gu[1], Tongtong Zhao[1], Yangfan Jia[1], Changlei Bao[1,3], Ang Luo[1], Qiang Guo[4], Ying Han[5], Jian Wang[3], Stephen M. Black[6,7], Ankit A. Desai[2] and Haiyang Tang[1,3]**

[1]College of Veterinary Medicine, Northwest A&F University, Yangling, China, [2]Department of Medicine, Krannert Institute of Cardiology, Indiana University, Indianapolis, IN, United States, [3]State Key Laboratory of Respiratory Disease, National Clinical Research Center for Respiratory Disease, Guangdong Key Laboratory of Vascular Disease, Guangzhou Institute of Respiratory Health, The First Affiliated Hospital of Guangzhou Medical University, Guangzhou, China, [4]Department of Critical Care Medicine, Suzhou Dushu Lake Hospital, The First Affiliated Hospital of Soochow University, Suzhou, China, [5]Department of Physiology, Nanjing Medical University, Nanjing, China, [6]Department of Cellular Biology and Pharmacology, Herbert Wertheim College of Medicine, Miami, FL, United States, [7]Department of Environmental Health Sciences, Center for Translational Science, Robert Stempel College of Public Health and Social Work, Florida International University, Port St. Lucie, FL, United States

Rationale: Enhanced proliferation and distal migration of human pulmonary arterial smooth muscle cells (hPASMCs) both contribute to the progressive increases in pulmonary vascular remodeling and resistance in pulmonary arterial hypertension (PAH). Our previous studies revealed that Rictor deletion, to disrupt mTOR Complex 2 (mTORC2), over longer periods result in a paradoxical rise in platelet-derived growth factor receptor (PDGFR) expression in PASMCs. Thus, the purpose of this study was to evaluate the role of combination therapy targeting both mTOR signaling with PDGFR inhibition to attenuate the development and progression of PAH.

Methods and Results: Immunoblotting analyses revealed that short-term exposure to rapamycin (6h) significantly reduced phosphorylation of p70S6K (mTORC1-specific) in hPASMCs but had no effect on the phosphorylation of AKT (p-AKT S473, considered mTORC2-specific). In contrast, longer rapamycin exposure (>24 h), resulted in differential AKT (T308) and AKT (S473) phosphorylation with increases in phosphorylation of AKT at T308 and decreased phosphorylation at S473. Phosphorylation of both PDGFRα and PDGFRβ was increased in hPASMCs after treatment with rapamycin for 48 and 72 h. Based on co-immunoprecipitation studies, longer exposure to rapamycin (24–72 h) significantly inhibited the binding of mTOR to Rictor, mechanistically suggesting mTORC2 inhibition by rapamycin. Combined exposure of rapamycin with the PDGFR inhibitor, imatinib significantly reduced the proliferation and migration of hPASMCs compared to either agent alone. Pre-clinical studies validated increased therapeutic efficacy of rapamycin combined with imatinib in attenuating PAH over either drug alone. Specifically, combination therapy further attenuated the development of monocrotaline (MCT)- or Hypoxia/Sugen-induced pulmonary hypertension (PH) in rats as demonstrated by further reductions in the Fulton index, right ventricular systolic pressure (RVSP), pulmonary vascular wall thickness and vessel muscularization, and decreased proliferating cell nuclear antigen (PCNA) staining in PASMCs.

OPEN ACCESS

Edited by:
Xiaohui Li,
Central South University, China

Reviewed by:
Wen-Qun Li,
Central South University, China
Antonio Molino,
University of Naples Federico II, Italy

***Correspondence:**
Ankit A. Desai
ankdesai@iu.edu
Haiyang Tang
tanghy2008@yahoo.com

Specialty section:
This article was submitted to Respiratory Pharmacology, a section of the journal Frontiers in Pharmacology

Received: 15 August 2021
Accepted: 25 October 2021
Published: 11 November 2021

Citation:
Shi Y, Gu C, Zhao T, Jia Y, Bao C, Luo A, Guo Q, Han Y, Wang J, Black SM, Desai AA and Tang H (2021) Combination Therapy With Rapamycin and Low Dose Imatinib in Pulmonary Hypertension. Front. Pharmacol. 12:758763. doi: 10.3389/fphar.2021.758763

Conclusion: Prolonged rapamycin treatment activates PDGFR signaling, in part, via mTORC2 inhibition. Combination therapy with rapamycin and imatinib may be a more effective strategy for the treatment of PAH.

Keywords: MTOR signaling, PDGFRs, PAH, PASMCs, rapamycin, imatinib

INTRODUCTION

Pulmonary arterial hypertension (PAH) is characterized by progressive increases in pulmonary vascular resistance (PVR) and pressure, which can lead to deterioration of right ventricular function (Voelkel et al., 2012; Humbert et al., 2019). The major factors contributing to the elevated PVR include sustained increases in pulmonary vascular contraction and obliterative pulmonary vascular remodeling (Rabinovitch, 2008; Archer et al., 2010; Schermuly et al., 2011). Similar to the pathways in cancer, hyperproliferation and enhanced migration of PASMCs are considered as major contributors to the vascular remodeling (Guignabert et al., 2013). Molecular mechanisms of PAH are complex and involve multiple signaling pathways including cell survival and proliferation, such as phosphoinositide 3-kinase (PI3K)/AKT/mammalian target of rapamycin (mTOR), platelet-derived growth factor (PDGF), and transforming growth factor (TGF)-β/bone morphogenetic protein (BMP) (Rabinovitch, 2008; Tang et al., 2018a; Rol et al., 2018).

mTOR is a key serine/threonine protein kinase that responds to a variety of extracellular stimuli including growth factors, insulin, nutrients (amino acids, glucose), and hypoxic stress (Lin et al., 2017). mTOR functions as the key component of two similar protein complexes: mTOR complex l (mTORC1) and mTORC2. mTORC1 regulates ribosomal S6 protein kinase (p70S6K) and eukaryotic promoter 4e binding protein 1 (4E-BP1), which both play important roles in protein translation and cell growth, respectively. mTORC2 controls cell growth, apoptosis, and regulates tumorigenesis through phosphorylation of AKT (Gulati et al., 2009; Jhanwar-Uniyal et al., 2017). The mTOR pathway is a major research focus for a

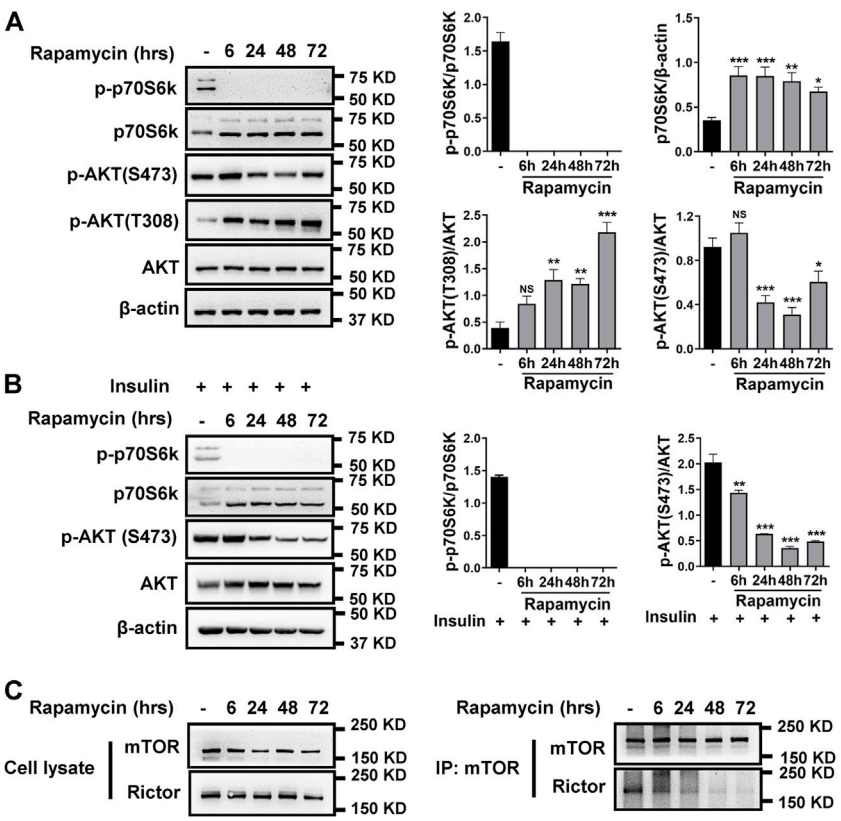

FIGURE 1 | Rapamycin inhibits mTORC1 and mTORC2. **(A)** hPASMCs were treated with 100 nM rapamycin for the indicated times and analyzed by immunoblotting for the proteins level of p-p70S6k, p70S6k, p-AKT (S473), p-AKT (T308), AKT. **(B)** immunoblotting analyses of p-p70S6k, p70S6k, p-AKT (S473), and AKT in hPASMCs, which were stimulated with 5 μg/ml insulin for 24h before treatment with 100 nM rapamycin. **(C)** hPASMCs were treated with 100 nM rapamycin for the indicated times, and then cell lysates were prepared for and immunoprecipitation (IP) with mTOR antibody. The elution from IP was analyzed by immunoblotting for the levels of mTOR and Rictor. Data are presented as the mean ± SE. One-way ANOVA was used for statistical analysis. NS means not significant. ***$p < 0.001$; **$p < 0.01$; *$p < 0.05$ versus control.

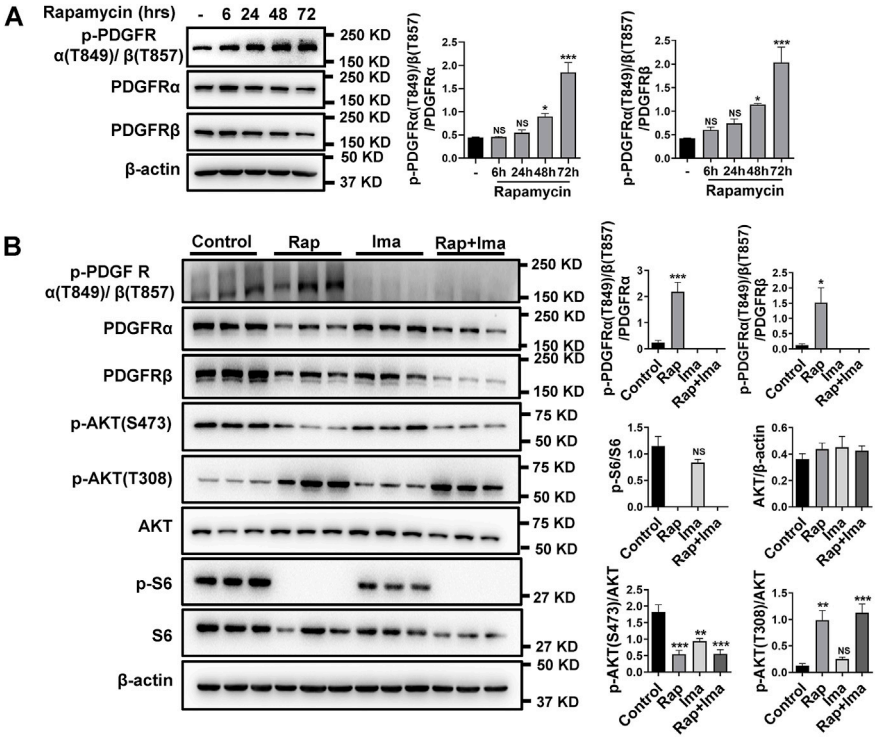

FIGURE 2 | Imatinib inhibits phosphorylation of PDGFRα/β induced by rapamycin in hPASMCs. **(A)** hPASMCs were treated with 100 nM rapamycin for the indicated times and analyzed by immunoblotting for the proteins level of p-PDGFRα/β, PDGFRα, PDGFRβ. **(B)** Immunoblotting analyses of p-PDGFRα/β, PDGFRα, PDGFRβ, p-AKT (S473), p-AKT (T308), p-S6 and S6 in hPASMCs treated with vehicle (Control), 100 nM rapamycin (Rap), 5 uM imatinib (Ima) and 100 nM rapamycin + 5 uM imatinib (Rap + Ima) for 48 h. Data are presented as the mean ± SE. One-way ANOVA was used for statistical analysis. NS means not significant. ***$p < 0.001$, **$p < 0.01$, *$p < 0.05$ versus control.

variety of diseases including an ongoing clinical trial with the mTOR inhibitor, rapamycin in PAH (Houssaini et al., 2013; Arriola Apelo and Lamming, 2016).

Prior studies have shown that mTORC1 inhibition with rapamycin attenuates pre-clinical PAH development (Houssaini et al., 2013; Goncharova et al., 2020). Furthermore, deletion of tuberous sclerosis complex ½ (TSC 1/2), which is an upstream inhibitor of mTORC1 signaling, also inhibits expression of PDGFRs in a rapamycin-sensitive manner (Zhang et al., 2007). In contrast to these data, smooth muscle cell-specific ablation of mTORC2 over prolonged periods results in spontaneous murine PAH, possibly due to unexpected increases in PDGFR expression (Tang et al., 2015; Tang et al., 2018a). Cumulatively, these findings raise concerns for a paradoxical increased risk in PDGFR activation with prolonged therapeutic use of rapamycin in PAH.

Receptor tyrosine kinase (RTK) signaling, including PDGF, mediates lung vascular remodeling in PAH (Perros et al., 2008a). RTK signaling activates several proliferative signaling cascades including PI3K, phospholipase Cγ (PLcγ), Ras-mitogen-activated protein kinase (Ras-MAPK) and Janus kinase (JAK) (Hubbard and Till, 2000). Imatinib, a tyrosine kinase inhibitor, decreases autophosphorylation of PDGFRs, resulting in the inhibition of PDGF signaling. Despite results of Phase II study demonstrating reasonable tolerability of imatinib in patients with PAH, severe adverse events, significant side effects, and a high discontinuation rate appeared in the Phase III trial, which clearly show that higher doses of imatinib are not suitable and limit the utility of imatinib in the treatment of PAH (Ghofrani et al., 2010; Frost et al., 2015). Moreover, additional studies further demonstrated that low dose imatinib did not attenuate the development of experiment PH, highlighting the importance of targeting other molecular pathways in PAH (Schermuly et al., 2005). While mTOR and PDGFR signaling pathways both independently hold potential for targeting as therapeutics in PAH, the effects of prolonged exposure to rapamycin on the activity of PDGFRs and PH development remain unknown. Thus, the aim of this study was to dissect mechanisms of short-term and prolonged rapamycin use on PDGFR signaling during PAH treatment and to investigate the therapeutic potential of combined therapy with rapamycin and the RTK inhibitor, imatinib.

MATERIALS AND METHODS

Animal Model and Experimental Design.

All animals in the studies were handled according to the National Institutes of Health guidelines and approved by the Institutional

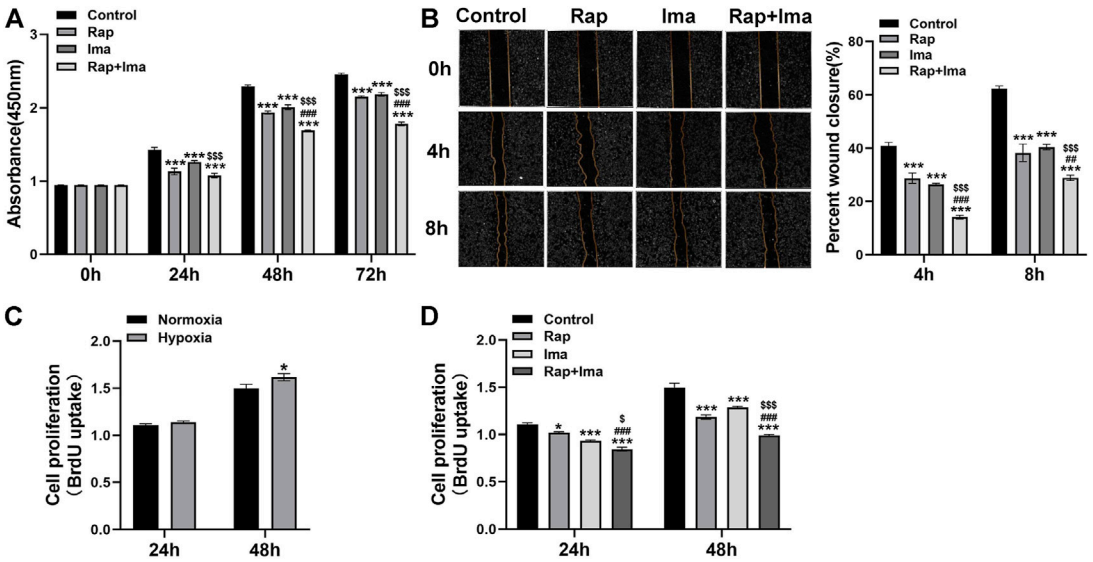

FIGURE 3 | Effects of rapamycin combined with imatinib on the viability, proliferation and migration of hPASMCs. **(A)** Cell viability was determined by measuring the absorbance at 0, 24, 48 and 72 h after different drug treatments. **(B)** A scratch was applied to cell monolayers, and migration of the cells towards the wound was recorded by photomicrographs at 0, 4, and 8h ($n = 3$); summarized data showing percent wound closure [(0h wound area–4h or 8h wound area)/0h wound area] * 100%. **(C)** BrdU assay was performed to determine hPASMCs proliferation under normoxia and hypoxia (3% 0_2) for 24 and 48 h. **(D)** BrdU assay was performed to determine hPASMCs proliferation at 24 and 48 h after different drug treatments. Data are presented as the mean ± SE. Two-way ANOVA was used for statistical analysis. $^{***}p < 0.001$; $^{**}p < 0.01$; $^{*}p < 0.05$ versus control; $^{\#\#\#}p < 0.001$, $^{\#\#}p < 0.01$, $^{\#}p < 0.05$ versus Rap; $^{\$\$\$}p < 0.001$, $^{\$\$}p < 0.01$, $^{\$}p < 0.05$ versus Ima.

Animal Care and Use Committee (IACUC) of Guangzhou Medical University. For the MCT model, male Sprague-Dawley (SD) rats (200–250 g) were studied after a single intraperitoneal monocrotaline (MCT) injection (50 mg/kg, #HY-N0750, MCE, United States). For the hypoxia-SU5416 model, SD rats (200–250 g) placed under hypoxic condition (FiO_2 10%) for 3 weeks after given single dose of SU5416 (20 mg/kg, #HY-10374, MCE, United States). They were transitioned to normoxia for 2 weeks. Rats were randomly assigned to four groups: rapamycin alone (2 mg/kg/d, #HY-10219, MCE, United States), imatinib alone (10 mg/kg/d, #S1026, Selleck, United States), rapamycin (2 mg/kg/d) combined with imatinib (10 mg/kg/d), or vehicle only. All drugs were given once daily by intraperitoneal injection for the last 2 weeks of each model. Terminal measurements were recorded. Right ventricular systolic pressure (RVSP) was measured as previously published (Tang et al., 2018b) with a pressure transducer catheter (Millar Instruments) and used as a surrogate for pulmonary arterial pressure. Hearts were excised and dissected to determine the ratio of the RV weight to the left ventricle (LV) and septum (S) weight ratio.

Cell Culture and Experiments

Human PASMCs (hPASMCs) were obtained from Sciencell (#3110) and Promocell (#399Z003.1). Cells were maintained in SMC medium (#1101, Sciencell, United States of America) with 2% fetal bovine serum and SMC growth supplement (#1152, Sciencell, United States). For migration assay, hPASMCs suspension was diluted to 2×10^5/ml. 70 ul of cell suspension was seeded into culture-inserts of 2-wells in 35 mm dish (#81176, IBIDI, Germany). After cell attachment, inserts were removed using sterilized forceps. Cells were cultured in serum-free medium containing rapamycin (100 nM), imatinib (5 μM) or vehicle and pictures recorded every 4 h. The number of cells migrating out of the wound edge was scored using Image J image analysis software. Cell viability was assessed by CCK8 kit (#96992, Sigma-Aldrich, United States). hPASMCs were seeded into 96-well plates at a density of 5,000 cells per well with six replicates per group. Cells were cultured in 2% serum-containing medium exposed to either rapamycin (100 nM), imatinib (5 μM), or vehicle. After addition of 10ul CCK8 per well, the plate was cultured for 4 h at 37°C. The absorbance value of each well was measured and collected at 450 nm. Cell proliferation assays were performed using BrdU incorporation kit (#QIA58, Merck Millipore, United States). hPASMCs were seeded into 96-well plates at a density of 5,000 cells per well with four replicates per group. Cells were cultured in 2% serum-containing medium exposed to either rapamycin (100 nM), imatinib (5 μM), or vehicle. BrdU assay was conducted according to the standard protocol of the manufacturer and BrdU uptake was measured in each well at dual wavelengths of 450–540 nm.

Western Blot and Co-Immunoprecipitation

Total cellular and isolated pulmonary arterial (PA) proteins were extracted using RIPA lysis buffer containing proteinase and phosphatase inhibitor. Western blotting was performed using the following antibodies: anti-mTOR (#2983), anti-Rictor (#5379) anti-phospho-PDGFRα/β (#3170), anti-PDGFRα (#3174), anti-PDGFRβ (#3169), anti-phospho-AKT (T308) (#13038), anti-phospho-AKT (S473) (#4060), anti-AKT (Pan) (#4691),

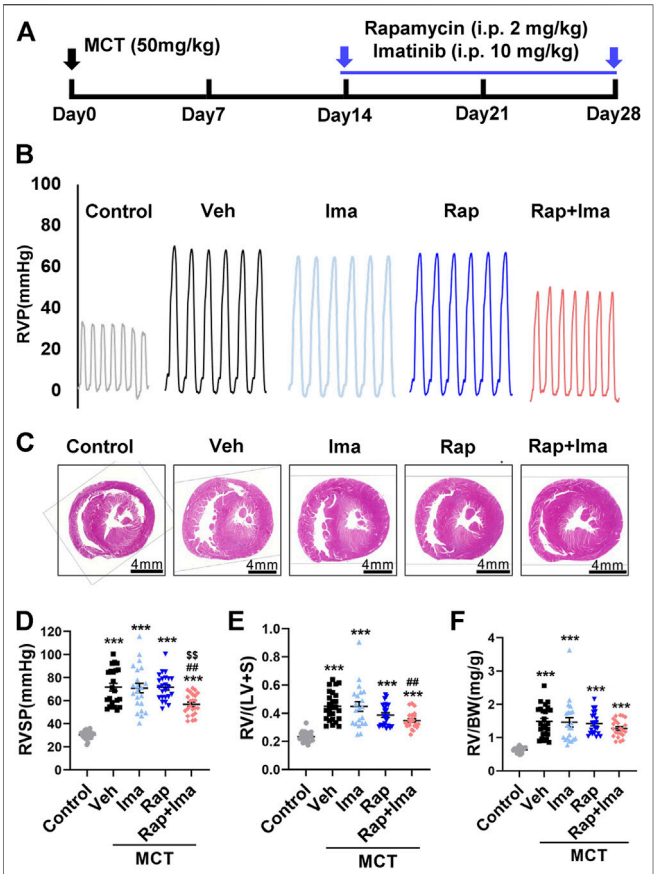

FIGURE 4 | Rapamycin combined with imatinib attenuates PH induced by MCT. **(A)** Schematic strategy for the MCT-induced PH rodent model and drugs administration. **(B)** Representative record of right ventricle pressure (RVP) in control and MCT rats treated with vehicle (Veh), imatinib (Ima), rapamycin (Rap), or combination of rapamycin and imatinib (Rap + Ima). **(C)** H&E staining of heart tissue in each group. **(D,E,F)** Summarized data showing RVSP, Fulton index ([RV/(LV + S)]) and the ratio of right ventricle weight to body weight (RV/BW) respectively. Data are presented as the mean ± SE. One-way ANOVA was used for statistical analysis. $^{***}p < 0.001$, $^{**}p < 0.01$, $^{*}p < 0.05$ versus control; $^{\#\#\#}p < 0.001$, $^{\#\#}p < 0.01$, $^{\#}p < 0.05$ versus MCT with vehicle; $^{\$\$\$}p < 0.001$, $^{\$\$}p < 0.01$, $^{\$}p < 0.05$ versus MCT with rapamycin.

anti-phospho-p70S6k (#9204), anti-p70S6k (9202), anti-phospho-S6 (#4858), and anti-S6 (#2317) (Cell Signaling Technology, United States). For Co-immunoprecipitation, cell protein was extracted in the non-deformed protein lysate. Non-specific proteins were removed by adding protein A/G-beads (#sc-2003, Santa Cruz Biotechnzazology, United States). An antibody targeting mTOR was incubated at room temperature to bind the antibody to the target antigen. The antigen-antibody complex was incubated overnight at 4°C and then, boiled for 5 mins. SDS-polyacrylamide gel electrophoresis was performed by adding the sample buffer on the protein (Sarbassov et al., 2006).

Immunofluorescence

For immunofluorescence staining, lung tissue sections were blocked in 2% BSA for 30 min and incubated overnight at 4°C with alpha-smooth muscle actin (α-SMA) and proliferating cell nuclear antigen (PCNA). After extensive washes with PBS for 30 min, lung tissue was incubated with Alexa 488 anti-rabbit secondary or Alexa 594 anti-mouse secondary antibodies at a 1:500 dilution for 1 h at room temperature. Nuclei were stained with DAPI (4, 6-diamidino-2-phenylindole).

Statistical Analysis

Data were presented as means ± standard error (SE) and analyzed by GraphPad Prism software. Statistical differences among multiple experimental groups were tested by one-way analysis of variance (ANOVA) and two-way ANOVA. $p < 0.05$ was considered as statistically significant.

RESULTS

Rapamycin Inhibits Both mTORC1 and mTORC2 in hPASMCs

While rapamycin is well-established as an mTORC1 inhibitor, its effects on mTORC2 has not been well studied. Thus, we initially investigated the effects of longer rapamycin exposure on mTORC2 in hPASMCs. As shown in **Figure 1A**, rapamycin treatment reduced phosphorylated p70S6k (p-p70S6k) and increased total p70S6k levels across all time points in hPASMCs, validating rapamycin-mediated inhibition of mTORC1. In contrast, phosphorylated AKT (p-AKT S473) levels were reduced only with longer exposures of rapamycin, suggesting reductions of mTORC2 activity with chronic exposure. Specifically, inhibition of mTORC1 by rapamycin can result in increased availability of free mTOR generating increases in mTORC2 activity (Hussain et al., 2013). To test this possibility, hPASMCs treated with insulin to activate mTORC2 and found that p-AKT S473 was not increased after treatment with rapamycin for 6 h (**Figure 1B**).

Rapamycin works through a gain-of-function mechanism in which it binds to the intracellular protein FKBP12 to generate a drug-receptor complex that binds to and inhibits mTORC1 (Annett et al., 2020). To determine whether rapamycin inhibits mTORC2 activity via a similar mechanism, we evaluated the effect of rapamycin on the interaction between Rictor and mTOR in hPASMCs using immunoprecipitation analysis. As shown in **Figure 1C**, rapamycin caused a time-dependent reduction in the binding between Rictor and mTOR. Expression levels of mTOR and Rictor remained unchanged in whole cell lysates.

Rapamycin Treatment Activates PDGFRα/β

Previously, we found elevated expression of PDGFRs in isolated pulmonary arteries (PA) from smooth muscle-specific Rictor knockout mice ($Rictor^{SM-/-}$) (Tang et al., 2018a). Base on rapamycin reducing mTORC2 activity, the effects of long-term rapamycin treatment on both phosphorylated and total PDGFRs was investigated. As shown in **Figure 2A**, phosphorylated PDGFR levels were increased in hPASMCs after treatment with rapamycin at 48 and 72 h. Impact of combination

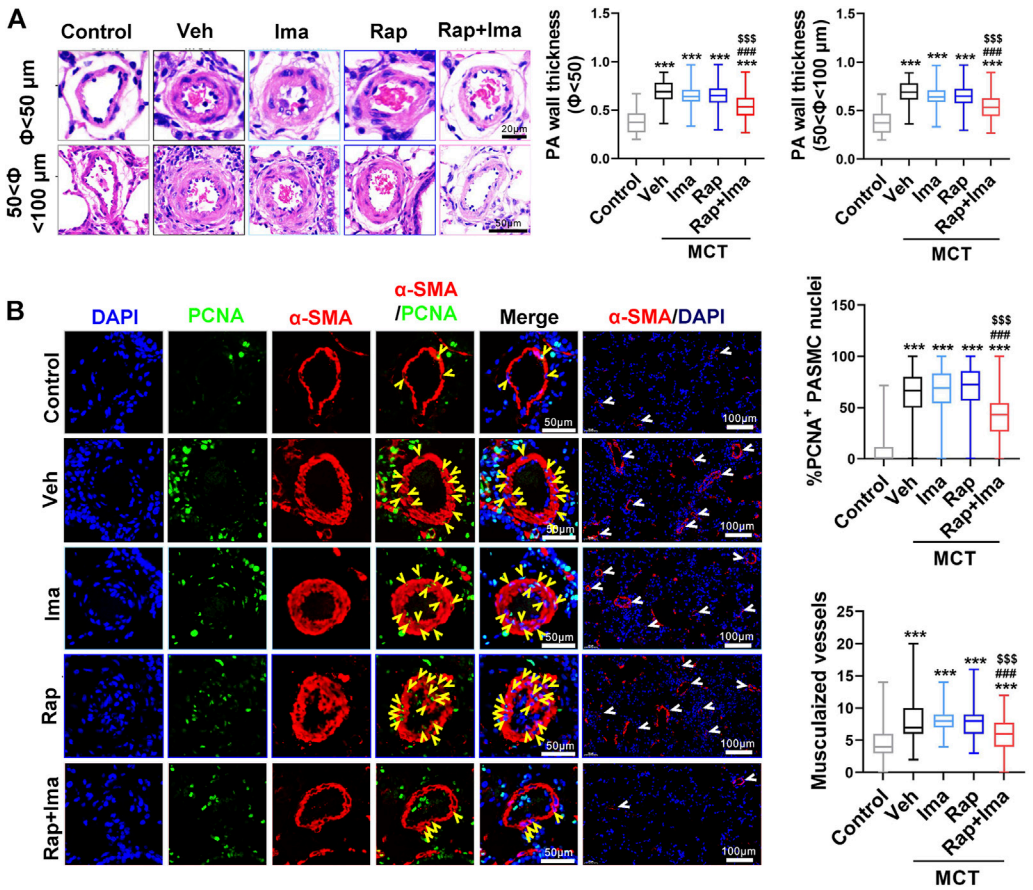

FIGURE 5 | Rapamycin combined with imatinib attenuates PASMC proliferation and remodeling induced by MCT. **(A)** H&E staining in lung tissue sections. Summarized data showing pulmonary artery media wall thickness. **(B)** Lung sections were stained α-SMA (red) and PCNA (green). Yellow arrowheads point at PCNA positive PASMCs and white arrowheads show the vessels. For each of the 5 groups, approximately 600 PASMC nuclei and 100 fields were analyzed. Summarized data showing PCNA positive cells and muscularization. Data are presented as the mean ± SE. One-way ANOVA was used for statistical analysis. $^{***}p < 0.001$, $^{**}p < 0.01$, $^{*}p < 0.05$ versus control; $^{\#\#\#}p < 0.001$, $^{\#\#}p < 0.01$, $^{\#}p < 0.05$ versus MCT with vehicle; $^{\$\$\$}p < 0.001$, $^{\$\$}p < 0.01$, $^{\$}p < 0.05$ versus MCT with rapamycin.

therapy on mTOR and PDGFR signaling pathways also was detected. Consistent with previous results, exposure to rapamycin alone significantly reduced p-S473AKT and increased phosphorylation of p-T308AKT (**Figure 2B**). In parallel, rapamycin increased p-PDGFRα (T849)/β (T857) in hPASMCs. Imatinib alone inhibited the phosphorylation of PDGFR. Imatinib use alone also mildly inhibited mTOR activation. Rapamycin combined with imatinib robustly inhibited the activation of mTORC1 and mTORC2 along with the phosphorylation of PDGFRα/β.

Rapamycin Combined With Imatinib Inhibits Viability, Proliferation and Migration of hPASMCs

Since hPASMCs proliferation and migration drives obliterative pulmonary arterial vascular remodeling in PAH, we investigated the impact of rapamycin and imatinib on each process. We first detected impact of rapamycin and imatinib on cell viability. Result showed that both rapamycin and imatinib alone significantly inhibited hPASMCs viability. Importantly, the inhibitory effects of rapamycin combined with imatinib was more significant than that of either drug alone (**Figure 3A**). Both drugs alone significantly inhibited the migration of hPASMCs using a cell scratch assay, while the inhibitory effect of the combined regimen was more potent than either drug alone (**Figure 3B**). To further confirm the inhibitory effects of rapamycin combined with imatinib on PASMCs proliferation, a BrdU assay was performed. As shown in **Figure 3C**, hypoxia induced hPASMCs proliferation at 48 h, validating our prior observations (Tang et al., 2015; Tang et al., 2016). Both rapamycin and imatinib alone significantly inhibited hPASMCs proliferation (**Figure 3D**) despite hypoxic exposure. The inhibitory effect of the combined regimen was more potent than either drug alone.

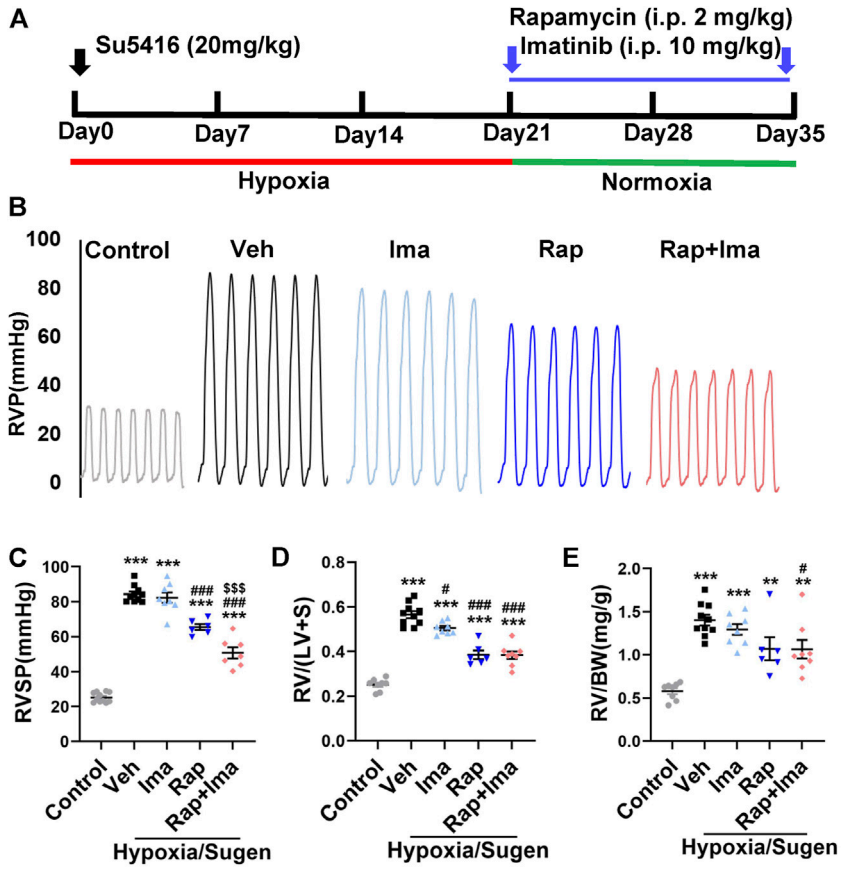

FIGURE 6 | Rapamycin combined with imatinib attenuates PH induced by Hypoxia/Sugen. **(A)** Schematic strategy for the Hypoxia/Sugen-induced PH rodent model and drugs administration. **(B)** Representative record of right ventricle pressure (RVP) in control and Hypoxia/Sugen treated with vehicle (Veh), imatinib (Ima), rapamycin (Rap) or combination of rapamycin and imatinib (Rap + Ima). **(C,D,E)** Summarized data showing RVSP, Fulton index [RV/(LV + S)] and the ratio of right ventricle weight to body weight (RV/BW) respectively. Data are presented as the mean ± SE. One-way ANOVA was used for statistical analysis. $^{***}p < 0.001$, $^{**}p < 0.01$, $^{*}p < 0.05$ versus control; $^{\#\#\#}p < 0.001$, $^{\#\#}p < 0.01$, $^{\#}p < 0.05$ versus Hypoxia/Sugen with vehicle; $^{\$\$\$}p < 0.001$, $^{\$\$}p < 0.01$, $^{\$}p < 0.05$ versus Hypoxia/Sugen with rapamycin.

Rapamycin Combined with Imatinib Attenuates PH in MCT and Hypoxia/Sugen Treated Rats

We evaluated combination therapy with rapamycin and imatinib in MCT and Hypoxia/Sugen rat models of PAH. Rats develop PH in both MCT and Hypoxia/Sugen treated (**Figures 4A, 6A**), as evidenced by significant increases in RVSP, [RV/(LV + S)] and RV/BW (**Figures 4B–F**, **6B–E**) compared to normal control animals. In the MCT model, as shown in **Figures 4B–F**, neither rapamycin or low dose imatinib (10 mg/kg) alone not attenuated the development of PH in MCT-rats with no significant reductions in RVSP, the Fulton index and RV/BW, compared to controls. However, combination therapy significantly decreased RVSP and Fulton index, but no effect on RV/BW. In the Hypoxia/Sugen rat model, as shown in **Figures 6B–E**, rapamycin exposure alone resulted in significant decreases in RVSP and the Fulton index but not RV/BW. Imatinib alone decreased the Fulton index but had no effect on RVSP and RV/BW. However, combination therapy resulted in significantly decreased RVSP, Fulton index and RV/BW, compared to controls.

We next evaluated the effects of combination therapy on the extensive vascular remodeling and muscularized vessels in both rat models. For the MCT rodent model (**Figures 5A,B**), H&E staining showed that rapamycin or imatinib alone had no significant effect on pulmonary vascular wall thickening or the number of muscularized vessels. However, combination therapy significantly inhibited the thickening of the vascular wall and the number of muscularized vessels. Moreover, rapamycin or imatinib alone had no effect on the percentage of proliferating cell nuclear antigen (PCNA)-positive PASMCs in the lung. The combination strategy significantly reduced the percentage of PCNA-positive PASMCs in small pulmonary arterioles. Similarly, in the Hypoxia/Sugen model (**Figures 7A,B**), imatinib alone had no significant effect on pulmonary vascular thickening or the number of muscularized vessel. Rapamycin alone significantly inhibited the thickening of pulmonary vascular

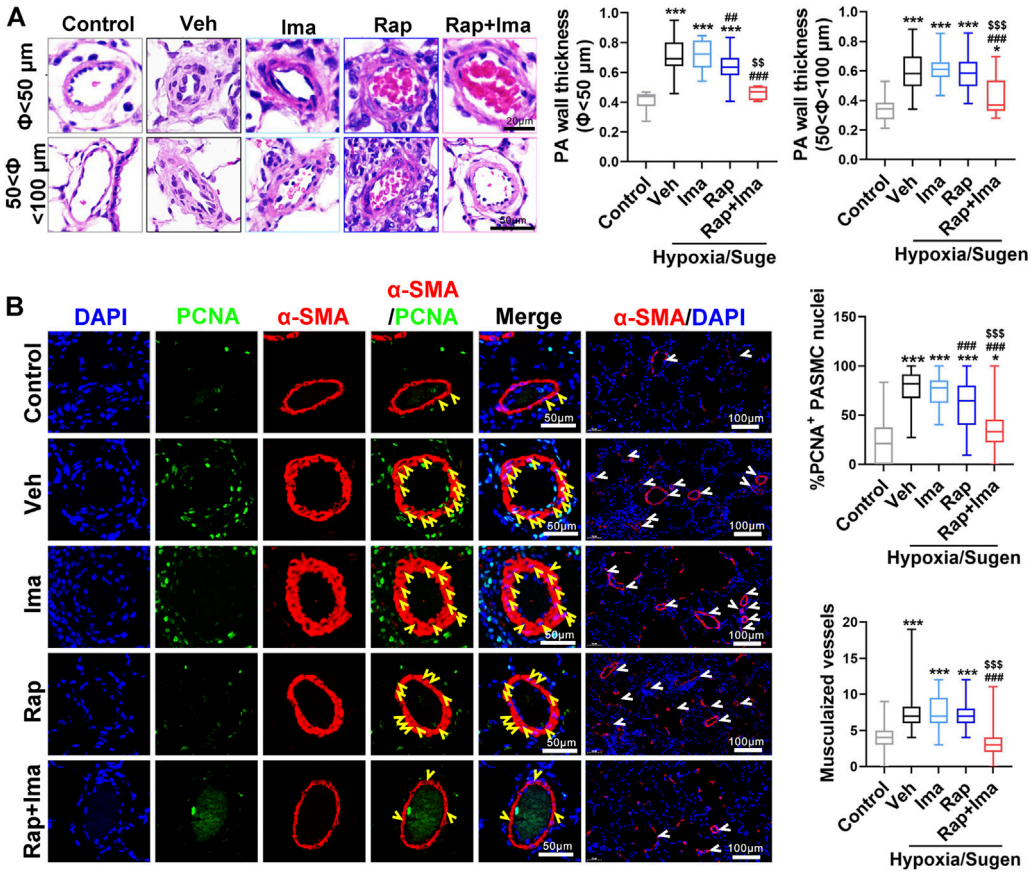

FIGURE 7 | Rapamycin combined with imatinib attenuates PASMC proliferation and remodeling induced by Hypoxia/Sugen. **(A)** H&E staining of lung tissue sections and summarized data showing pulmonary artery media wall thickness. **(B)** Lung sections were stained with α-SMA (red) and PCNA (green). Yellow arrowheads point at PCNA positive PASMCs and white arrowheads show the vessels. For each of the 5 groups, approximately 600 PASMC nuclei and 100 fields were analyzed. Summarized data showing PCNA positive cells and muscularization. Data are presented as the mean ± SE. One-way ANOVA was used for statistical analysis. NS means no significant. $^{***}p < 0.001$, $^{**}p < 0.01$, $^{*}p < 0.05$ versus control; $^{###}p < 0.001$, $^{##}p < 0.01$, $^{#}p < 0.05$ versus Hypoxia/Sugen with vehicle; $^{\$\$\$}p < 0.001$, $^{\$\$}p < 0.01$, $^{\$}p < 0.05$ versus Hypoxia/Sugen with rapamycin.

thickening with diameter less than 50 μm but had no effect on the number of muscularized vessels. Combination therapy of rapamycin with imatinib significantly inhibited both of vascular wall thickening and the number of muscularized vessels. Additionally, PCNA staining revealed significantly decreased cell proliferation within small pulmonary arterioles after combination strategy.

Rapamycin Combined With Imatinib Inhibits mTOR and PDGFR Signaling Pathway in Isolated Pulmonary Arteries

We evaluated the effects of combination therapy on mTOR and PDGFR signaling pathways in isolated PAs from rat lungs. As shown in **Figure 8A**, expression of p-PDGFR, p-S6 and pS473AKT was increased in PAs isolated from MCT-exposed rats. Confirming *in vitro* data, rapamycin inhibited the activity of both, mTORC1 and mTORC2. Imatinib alone inhibited the phosphorylation of PDGFR. Rapamycin combined with imatinib inhibited mTORC1, mTORC2 and PDGFR signaling mediators.

DISCUSSION

Both rapamycin and imatinib have been tested in clinical trials in patients with PAH (Ghofrani et al., 2005; Wessler et al., 2010). While the results of the latter have been unfavorable, the results of the trial testing rapamycin remain pending. On the surface, rapamycin and imatinib appear to inhibit two unrelated molecular targets including mTORC1 and PDGFR, respectively. Building upon our prior observations, our studies uncover a crossover between the two signaling cascades that could be leveraged to potentially develop a novel combination therapeutic strategy. Specifically, the current study confirms findings of a paradoxical and an unexpected rise in PDGFR activation with prolonged exposure to rapamycin *in vitro* and *in vivo*. While mTORC1 is a known target, our data suggest the PDGFR activation is due, in part, to additional inhibition of mTORC2 by rapamycin. Devising a strategy to address both seemingly related pathological cascades, the current study found greater attenuation of PH in two pre-clinical rat models when rapamycin and imatinib were combined compared to either drug alone.

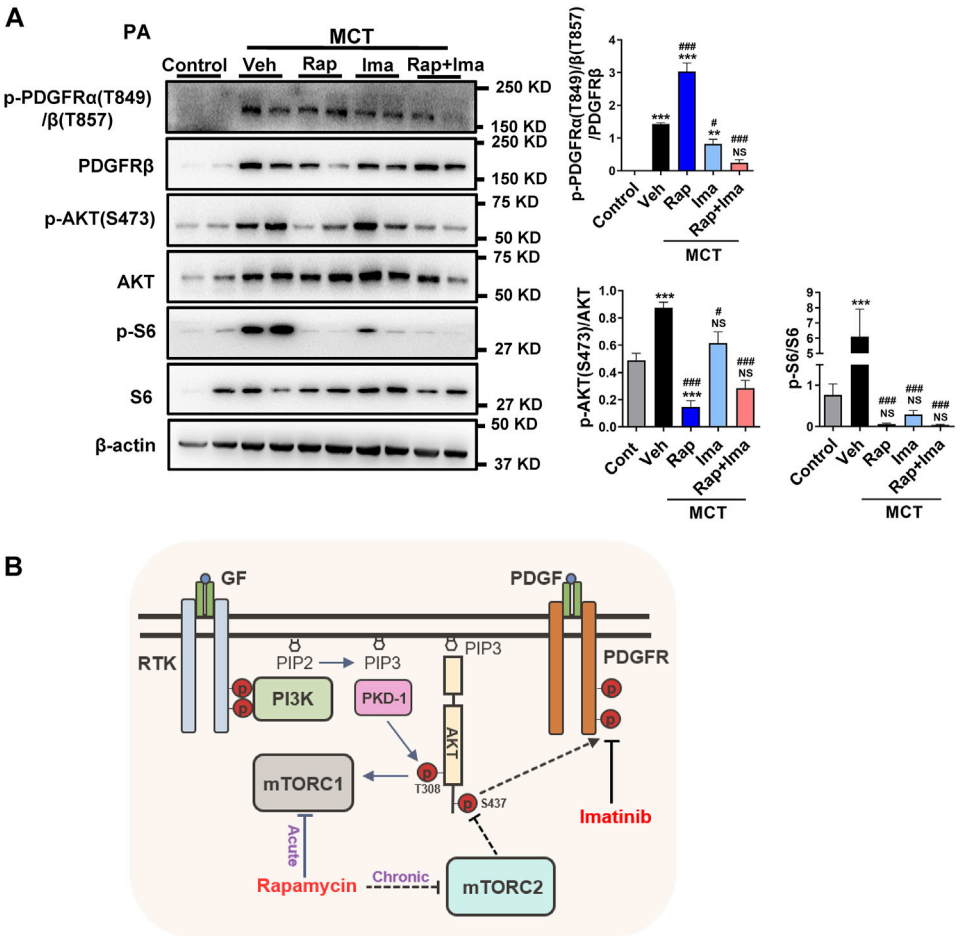

FIGURE 8 | Effects of rapamycin combined with imatinib on mTOR and PDGFR signaling pathways in pulmonary artery. **(A)** Pulmonary artery vessels of were isolated for protein extraction, and the expression of mTORC 1, mTORC 2 and PDGFR signaling pathway related proteins were detected by immunoblotting. Data are presented as the mean ± SE. One-way ANOVA followed by Graphpad prism was used for statistical analysis. NS means no significant. $^{***}p < 0.001$; $^{**}p < 0.01$; $^{*}p < 0.05$ versus control. $^{\#\#\#}p < 0.001$; $^{\#\#}p < 0.01$; $^{\#}p < 0.05$ versus MCT with vehicle. **(B)** The schematic representation of the findings of this study: rapamycin chronic treatment in hPASMCs induced the highly expression of phosphorylation of PDGFRs. Imatinib inhibits phosphorylation of PDGFRα/β induced by rapamycin. Abbreviations: GF, growth factors; RTK, receptor tyrosine kinase; PDGF, platelet derived growth factor; PDGFR, platelet derived growth factor receptor; PI3K, phosphoatidylinositol 3-kinase; PIP2, phosphatidylinositol-4,5-bisphosphate; PIP3, phosphatidylinositol-3,4,5-bisphosphate; mTORC1, mTOR complex 1; mTORC2, mTOR complex 2.

The PI3K/AKT/mTOR signaling pathway mediates PAH pathogenesis via its canonical role in cell survival and proliferation (Li et al., 2007; Tang et al., 2015). Rapamycin was approved by the US Food and Drug Administration as an immunosuppressant and has been proved to significantly inhibit mTORC1. However, the effect of rapamycin on mTORC2 is controversial (Sarbassov et al., 2004; Sarbassov et al., 2006; Schreiber et al., 2015). In fact, targeting this pathway for drug development requires a better understanding of the complexity of the cascade. Briefly, AKT is normally maintained in an inactive situation. However, AKT was activated by binding of phosphatidylinositol-3,4,5-bisphosphate (PIP3) generated by PI3K phosphorylated phosphatidylinositol-4,5-bisphosphate (PIP2), within biological membranes. Co-recruited Phosphoinositide-dependent protein kinase-1(PDK1) activates mTORC1 through the phosphorylation of AKT at Thr308 (Laplante and Sabatini, 2009; Hers et al., 2011), while mTORC2 phosphorylates AKT at Ser473 in a PI3 kinase-independent manner (Tsuchiya et al., 2014). Validating prior studies (Chung et al., 1992), we found that rapamycin inhibited mTORC1 with both short- and long-term exposure in hPSMCs. In addition, we observed a significant reduction in phosphorylated AKT (S473) with longer exposures of rapamycin, indicative of rapamycin-mediated mTORC2 inhibition. This observation was further supported by co-immunoprecipitation studies that demonstrated that rapamycin significantly inhibits the binding of Rictor to mTOR after 6 h, which is considered necessary to activate p-S473AKT.

Beyond reductions in p-S473AKT with longer exposures, rapamycin also inhibited p70S6k phosphorylation at 6 h, with a trend toward activation of p-S473AKT. A compensatory response by mTORC2 could explain this discrepant finding. Specifically, mTOR is a common component of the two complexes, and both mTORC1 and mTORC2 compete for mTOR binding (Hussain et al.,

2013). With shorter exposures, only mTORC1 is inhibited by rapamycin, resulting in increased availability of free mTOR that may result in a secondary increase of mTORC2 activity. Consistent with this idea, when insulin, which can activate mTORC2, was added into hPASMCs, we observed no change in p-S473AKT levels at 6 h.

Bolstering findings from our previous studies in *Rictor*$^{SM-/-}$ mice that demonstrated increased expression of PDGFRs with aging (Tang et al., 2018a), we found that sustained exposure to rapamycin increases PDGFR activation. PDGF is expressed in various cell types such as endothelial cells, smooth muscle cells and macrophages (Perros et al., 2008b). PDGF promotes cell proliferation, migration, and cell survival by activating two subtypes of receptors, PDGFRα and PDGFRβ (Heldin and Westermark, 1999). PDGF and PDGFR are significantly upregulated in lung tissues of PAH patients and experimental animal models of PAH. Given its pathological role in PAH, PDGFR signaling has been evaluated as a therapeutic target in PAH (Barst, 2005; Perros et al., 2008a; Grimminger and Schermuly, 2010). The current study further supports the notion of targeting PDGFR for therapeutic benefit in PAH. Rapamycin alone was able to mildly attenuate pre-clinical rodent PH with longer exposures, with its therapeutic effect potentially diminished by the reciprocal activation of PDGFR signaling. Moreover, the latter observation may have been mediated, in part, by the inhibition of mTORC2 with longer rapamycin exposures. To support this notion, we observed enhanced therapeutic attenuation of pre-clinical rodent PAH when we combined rapamycin with PDGFR inhibition using imatinib. Beyond robustly improving the hemodynamics and obliterative pulmonary vascular remodeling in two established rodent models, the combination therapy was able to inhibit the compensatory activation of p-PDGFRs induced by long-term treatment of rapamycin.

In summary, in contrast to mTORC1 inhibition with shorter duration, prolonged rapamycin treatment results in the inhibition of both mTORC1 and mTORC2. As illustrated in **Figure 8B**, long term exposure to rapamycin also results in activation of PDGFR signaling in PASMC, that is likely due to the mTORC2 inhibition. Combination therapy with rapamycin and imatinib was a more effective strategy that either drug alone in preventing PH development, alleviating both the pulmonary vascular remodeling, and improving right heart hemodynamics. These data highlight the need to further investigate the translatability of these findings in clinical trials of both drugs in PAH.

DATA AVAILABILITY STATEMENT

The original contributions presented in the study are included in the article/Supplementary Material, further inquiries can be directed to the corresponding authors.

ETHICS STATEMENT

The animal study was reviewed and approved by the Institutional Animal Care and Use Committee (IACUC) of Guangzhou Medical University.

AUTHOR CONTRIBUTIONS

YS, CG, TZ, YJ, CB, and AL performed the experiments. YS, HT, SB, and AD wrote the manuscript with input from QG, YH, and JW. All authors contributed to the article and approved the submitted version.

FUNDING

This work was funded by National Key Research and Development Program of China (2019YFE0119400), Natural Science Foundation of China (81970052, 81770059 and 82170057), Natural Science Basic Research Program of Shaanxi Province (2018JC-012), and National Institutes of Health grants (P01HL134610 and P01HL146369 to SB).

REFERENCES

Annett, S., Moore, G., and Robson, T. (2020). FK506 Binding Proteins and Inflammation Related Signalling Pathways; Basic Biology, Current Status and Future Prospects for Pharmacological Intervention. *Pharmacol. Ther.* 215, 107623. doi:10.1016/j.pharmthera.2020.107623

Archer, S. L., Weir, E. K., and Wilkins, M. R. (2010). Basic Science of Pulmonary Arterial Hypertension for Clinicians: New Concepts and Experimental Therapies. *Circulation* 121, 2045–2066. doi:10.1161/CIRCULATIONAHA.108.847707

Arriola Apelo, S. I., and Lamming, D. W. (2016). Rapamycin: An InhibiTOR of Aging Emerges from the Soil of Easter Island. *J. Gerontol. A. Biol. Sci. Med. Sci.* 71, 841–849. doi:10.1093/gerona/glw090

Barst, R. J. (2005). PDGF Signaling in Pulmonary Arterial Hypertension. *J. Clin. Invest.* 115, 2691–2694. doi:10.1172/JCI26593

Chung, J., Kuo, C. J., Crabtree, G. R., and Blenis, J. (1992). Rapamycin-FKBP Specifically Blocks Growth-dependent Activation of and Signaling by the 70 Kd S6 Protein Kinases. *Cell* 69, 1227–1236. doi:10.1016/0092-8674(92)90643-q

Frost, A. E., Barst, R. J., Hoeper, M. M., Chang, H. J., Frantz, R. P., Fukumoto, Y., et al. (2015). Long-term Safety and Efficacy of Imatinib in Pulmonary Arterial Hypertension. *J. Heart Lung Transpl.* 34, 1366–1375. doi:10.1016/j.healun.2015.05.025

Ghofrani, H. A., Morrell, N. W., Hoeper, M. M., Olschewski, H., Peacock, A. J., Barst, R. J., et al. (2010). Imatinib in Pulmonary Arterial Hypertension Patients with Inadequate Response to Established Therapy. *Am. J. Respir. Crit. Care Med.* 182, 1171–1177. doi:10.1164/rccm.201001-0123OC

Ghofrani, H. A., Seeger, W., and Grimminger, F. (2005). Imatinib for the Treatment of Pulmonary Arterial Hypertension. *N. Engl. J. Med.* 353, 1412–1413. doi:10.1056/NEJMc051946

Goncharova, E. A., Simon, M. A., and Yuan, J. X. (2020). mTORC1 in Pulmonary Arterial Hypertension. At the Crossroads between Vasoconstriction and Vascular Remodeling. *Am. J. Respir. Crit. Care Med.* 201, 1177–1179. doi:10.1164/rccm.202001-0087ED

Grimminger, F., and Schermuly, R. T. (2010). PDGF Receptor and its Antagonists: Role in Treatment of PAH. *Adv. Exp. Med. Biol.* 661, 435–446. doi:10.1007/978-1-60761-500-2_28

Guignabert, C., Tu, L., Le Hiress, M., Ricard, N., Sattler, C., Seferian, A., et al. (2013). Pathogenesis of Pulmonary Arterial Hypertension: Lessons

from Cancer. *Eur. Respir. Rev.* 22, 543–551. doi:10.1183/09059180.00007513

Gulati, N., Karsy, M., Albert, L., Murali, R., and Jhanwar-Uniyal, M. (2009). Involvement of mTORC1 and mTORC2 in Regulation of Glioblastoma Multiforme Growth and Motility. *Int. J. Oncol.* 35, 731–740. doi:10.3892/ijo_00000386

Heldin, C. H., and Westermark, B. (1999). Mechanism of Action and *In Vivo* Role of Platelet-Derived Growth Factor. *Physiol. Rev.* 79, 1283–1316. doi:10.1152/physrev.1999.79.4.1283

Hers, I., Vincent, E. E., and Tavaré, J. M. (2011). Akt Signalling in Health and Disease. *Cell Signal* 23, 1515–1527. doi:10.1016/j.cellsig.2011.05.004

Houssaini, A., Abid, S., Mouraret, N., Wan, F., Rideau, D., Saker, M., et al. (2013). Rapamycin Reverses Pulmonary Artery Smooth Muscle Cell Proliferation in Pulmonary Hypertension. *Am. J. Respir. Cel Mol Biol* 48, 568–577. doi:10.1165/rcmb.2012-0429OC

Hubbard, S. R., and Till, J. H. (2000). Protein Tyrosine Kinase Structure and Function. *Annu. Rev. Biochem.* 69, 373–398. doi:10.1146/annurev.biochem.69.1.373

Humbert, M., Guignabert, C., Bonnet, S., Dorfmüller, P., Klinger, J. R., Nicolls, M. R., et al. (2019). Pathology and Pathobiology of Pulmonary Hypertension: State of the Art and Research Perspectives. *Eur. Respir. J.* 53, 1801887. doi:10.1183/13993003.01887-2018

Hussain, S., Feldman, A. L., Das, C., Ziesmer, S. C., Ansell, S. M., and Galardy, P. J. (2013). Ubiquitin Hydrolase UCH-L1 Destabilizes mTOR Complex 1 by Antagonizing DDB1-CUL4-Mediated Ubiquitination of Raptor. *Mol. Cel Biol* 33, 1188–1197. doi:10.1128/MCB.01389-12

Jhanwar-Uniyal, M., Amin, A. G., Cooper, J. B., Das, K., Schmidt, M. H., and Murali, R. (2017). Discrete Signaling Mechanisms of mTORC1 and mTORC2: Connected yet Apart in Cellular and Molecular Aspects. *Adv. Biol. Regul.* 64, 39–48. doi:10.1016/j.jbior.2016.12.001

Laplante, M., and Sabatini, D. M. (2009). mTOR Signaling at a Glance. *J. Cel Sci* 122, 3589–3594. doi:10.1242/jcs.051011

Li, W., Petrimpol, M., Molle, K. D., Hall, M. N., Battegay, E. J., and Humar, R. (2007). Hypoxia-induced Endothelial Proliferation Requires Both mTORC1 and mTORC2. *Circ. Res.* 100, 79–87. doi:10.1161/01.RES.0000253094.03023.3f

Lin, J., Huo, X., and Liu, X. (2017). "mTOR Signaling Pathway": A Potential Target of Curcumin in the Treatment of Spinal Cord Injury. *Biomed. Res. Int.* 2017, 1634801. doi:10.1155/2017/1634801

Perros, F., Montani, D., Dorfmüller, P., Durand-Gasselin, I., Tcherakian, C., Le Pavec, J., et al. (2008). Platelet-derived Growth Factor Expression and Function in Idiopathic Pulmonary Arterial Hypertension. *Am. J. Respir. Crit. Care Med.* 178, 81–88. doi:10.1164/rccm.200707-1037OC

Perros, F., Montani, D., Dorfmüller, P., Durand-Gasselin, I., Tcherakian, C., Le Pavec, J., et al. (2008). Platelet-derived Growth Factor Expression and Function in Idiopathic Pulmonary Arterial Hypertension. *Am. J. Respir. Crit. Care Med.* 178, 81–88. doi:10.1164/rccm.200707-1037OC

Rabinovitch, M. (2008). Molecular Pathogenesis of Pulmonary Arterial Hypertension. *J. Clin. Invest.* 118, 2372–2379. doi:10.1172/JCI33452

Rol, N., Kurakula, K. B., Happé, C., Bogaard, H. J., and Goumans, M. J. (2018). TGF-β and BMPR2 Signaling in PAH: Two Black Sheep in One Family. *Int. J. Mol. Sci.* 19, 2585. doi:10.3390/ijms19092585

Sarbassov, D. D., Ali, S. M., Kim, D. H., Guertin, D. A., Latek, R. R., Erdjument-Bromage, H., et al. (2004). Rictor, a Novel Binding Partner of mTOR, Defines a Rapamycin-Insensitive and Raptor-independent Pathway that Regulates the Cytoskeleton. *Curr. Biol.* 14, 1296–1302. doi:10.1016/j.cub.2004.06.054

Sarbassov, D. D., Ali, S. M., Sengupta, S., Sheen, J. H., Hsu, P. P., Bagley, A. F., et al. (2006). Prolonged Rapamycin Treatment Inhibits mTORC2 Assembly and Akt/PKB. *Mol. Cel* 22, 159–168. doi:10.1016/j.molcel.2006.03.029

Schermuly, R. T., Dony, E., Ghofrani, H. A., Pullamsetti, S., Savai, R., Roth, M., et al. (2005). Reversal of Experimental Pulmonary Hypertension by PDGF Inhibition. *J. Clin. Invest.* 115, 2811–2821. doi:10.1172/JCI24838

Schermuly, R. T., Ghofrani, H. A., Wilkins, M. R., and Grimminger, F. (2011). Mechanisms of Disease: Pulmonary Arterial Hypertension. *Nat. Rev. Cardiol.* 8, 443–455. doi:10.1038/nrcardio.2011.87

Schreiber, K. H., Ortiz, D., Academia, E. C., Anies, A. C., Liao, C. Y., and Kennedy, B. K. (2015). Rapamycin-mediated mTORC2 Inhibition Is Determined by the Relative Expression of FK506-Binding Proteins. *Aging Cell* 14, 265–273. doi:10.1111/acel.12313

Tang, H., Babicheva, A., McDermott, K. M., Gu, Y., Ayon, R. J., Song, S., et al. (2018). Endothelial HIF-2α Contributes to Severe Pulmonary Hypertension Due to Endothelial-To-Mesenchymal Transition. *Am. J. Physiol. Lung Cel Mol Physiol* 314, L256–L275. doi:10.1152/ajplung.00096.2017

Tang, H., Chen, J., Fraidenburg, D. R., Song, S., Sysol, J. R., Drennan, A. R., et al. (2015). Deficiency of Akt1, but Not Akt2, Attenuates the Development of Pulmonary Hypertension. *Am. J. Physiol. Lung Cel Mol Physiol* 308, L208–L220. doi:10.1152/ajplung.00242.2014

Tang, H., Wu, K., Wang, J., Vinjamuri, S., Gu, Y., Song, S., et al. (2018). Pathogenic Role of mTORC1 and mTORC2 in Pulmonary Hypertension. *JACC Basic Transl Sci.* 3, 744–762. doi:10.1016/j.jacbts.2018.08.009

Tang, H., Yamamura, A., Yamamura, H., Song, S., Fraidenburg, D. R., Chen, J., et al. (2016). Pathogenic Role of Calcium-Sensing Receptors in the Development and Progression of Pulmonary Hypertension. *Am. J. Physiol. Lung Cel Mol Physiol* 310, L846–L859. doi:10.1152/ajplung.00050.2016

Tsuchiya, A., Kanno, T., and Nishizaki, T. (2014). PI3 Kinase Directly Phosphorylates Akt1/2 at Ser473/474 in the Insulin Signal Transduction Pathway. *J. Endocrinol.* 220, 49–59. doi:10.1530/JOE-13-0172

Voelkel, N. F., Gomez-Arroyo, J., Abbate, A., Bogaard, H. J., and Nicolls, M. R. (2012). Pathobiology of Pulmonary Arterial Hypertension and Right Ventricular Failure. *Eur. Respir. J.* 40, 1555–1565. doi:10.1183/09031936.00046612

Wessler, J. D., Steingart, R. M., Schwartz, G. K., Harvey, B. G., and Schaffer, W. (2010). Dramatic Improvement in Pulmonary Hypertension with Rapamycin. *Chest* 138, 991–993. doi:10.1378/chest.09-2435

Zhang, H., Bajraszewski, N., Wu, E., Wang, H., Moseman, A. P., Dabora, S. L., et al. (2007). PDGFRs Are Critical for PI3K/Akt Activation and Negatively Regulated by mTOR. *J. Clin. Invest.* 117, 730–738. doi:10.1172/JCI28984

Conflict of Interest: The authors declare that the research was conducted in the absence of any commercial or financial relationships that could be construed as a potential conflict of interest.

Publisher's Note: All claims expressed in this article are solely those of the authors and do not necessarily represent those of their affiliated organizations, or those of the publisher, the editors and the reviewers. Any product that may be evaluated in this article, or claim that may be made by its manufacturer, is not guaranteed or endorsed by the publisher.

frontiers in Pharmacology

REVIEW
published: 12 November 2021
doi: 10.3389/fphar.2021.767002

Therapy for Pulmonary Arterial Hypertension: Glance on Nitric Oxide Pathway

Abraham Tettey[1], *Yujie Jiang*[1], *Xiaohui Li*[1,3] *and Ying Li*[2,3]*

[1]Department of Pharmacology, School of Pharmaceutical Science, Central South University, Changsha, China, [2]Department of Health Management, The Third Xiangya Hospital, Central South University, Changsha, China, [3]Hunan Key Laboratory for Bioanalysis of Complex Matrix Samples, Changsha, China

Pulmonary arterial hypertension (PAH) is a severe disease with a resultant increase of the mean pulmonary arterial pressure, right ventricular hypertrophy and eventual death. Research in recent years has produced various therapeutic options for its clinical management but the high mortality even under treatment remains a big challenge attributed to the complex pathophysiology. Studies from clinical and non-clinical experiments have revealed that the nitric oxide (NO) pathway is one of the key pathways underlying the pathophysiology of PAH. Many of the essential drugs used in the management of PAH act on this pathway highlighting its significant role in PAH. Meanwhile, several novel compounds targeting on NO pathway exhibits great potential to become future therapy medications. Furthermore, the NO pathway is found to interact with other crucial pathways. Understanding such interactions could be helpful in the discovery of new drug that provide better clinical outcomes.

Keywords: nitric oxide, pulmonary arterial hypertension, phosphodiesterase 5 inhibitor, proliferation, crosstalk

OPEN ACCESS

Edited by:
Xiao-Jian Wang, Fuwai Hospital (CAS), and Peking Union Medical College, China

Reviewed by:
Rui Zhang, Tongji University, China
Weiping Xie, Nanjing Medical University, China

***Correspondence:**
Ying Li
lydia0312@csu.edu.cn

Specialty section:
This article was submitted to Respiratory Pharmacology, a section of the journal Frontiers in Pharmacology

Received: *30 August 2021*
Accepted: *25 October 2021*
Published: *12 November 2021*

Citation:
Tettey A, Jiang Y, Li X and Li Y (2021) Therapy for Pulmonary Arterial Hypertension: Glance on Nitric Oxide Pathway. Front. Pharmacol. 12:767002. doi: 10.3389/fphar.2021.767002

INTRODUCTION

Pulmonary arterial hypertension (PAH) is a fatal disease characterized by an increase in pulmonary arterial pressure with subsequent right ventricular failure and death (Rosenkranz, 2015). Generally, the major pathological changes of PAH are vasoconstriction and vascular remodelling of the small pulmonary arteries (Tuder et al., 2009) involving the thickening of the intima-media, smooth muscle cell proliferation, endothelial cell proliferative lesions formation, vascular inflammation and immune dysregulation (Tuder et al., 2007; Price et al., 2012; Humbert et al., 2019). There are different categories in PAH including idiopathic PAH, heritable PAH, drug or toxin-induced PAH and PAH associated with connective tissue disease, human immunodeficiency virus infection, portal hypertension, congenital heart disease and schistosomiasis (Galiè et al., 2016). Idiopathic PAH is the most common type of PAH in western countries with congenital heart disease-related PAH being the most prevalent in Asia (Humbert et al., 2006; Lim et al., 2019).

Currently approved PAH drugs such as prostacyclin analogues, endothelin receptor antagonists and phosphodiesterase-5 (PDE-5) inhibitors aim to control pulmonary vascular tone (Olsson and Hoeper, 2009). Enormous progress has been made in the therapeutic practice of PAH in the past decades but there is still a long way to go because none of these present drugs are curative. They reduce morbidity and only slightly improve survival with no effect on PAH mortality rate.

Many molecular pathways have been linked to the development and treatment of PAH.It has been revealed that the nitric oxide (NO) pathway plays a very essential and central role in regulating vascular tone in the pulmonary circulatory system by interacting with other crucial signaling pathways.

TABLE 1 | Classification of drugs used in treating PAH.

Class	Generic name	Dosing	Side-effects
Prostacyclin analogs	Epoprostenol	Continuous infusion	Abdominal pain, anxiety, arrhythmias, arthralgia, chest discomfort, diarrhea
	Treprostinil	Continuous IV or SC, inhalation, Oral	Infusion site reaction, pain, headache, nausea, diarrhoea, vasodilation, jaw pain, rash
	Iloprost	Inhalation	Chest discomfort, cough, diarrhea, dizziness, dyspnoea, hemorrhage, headache, hypotension, nausea
Prostacyclin IP receptor agonist	Selexipag	Oral	Abdominal pain, anemia, appetite decreased, arthralgia, diarrhea, flushing, headache
Endothelin Receptor Antagonists	Bosentan	Oral	Anemia, diarrhea, flushing, gastroesophageal reflux disease, headache, nasal congestion, palpitations
	Ambrisentan	Oral	Abdominal pain, anemia, asthenia, constipation, dizziness, epistaxis, flushing, headaches, hearing impairment
	Macitentan	Oral	Anaemia, headache, increased risk of infection, nasal congestion
PDE5 Inhibitors	Sildenafil	Oral, Intravenous	Dry mouth, flushing, gastrointestinal discomfort, hemorrhage, myalgia, headache
	Tadalafil	Oral	Flushing, gastrointestinal discomfort, headaches, myalgia, nasal congestion, pain
Soluble Guanylate Cyclase Stimulator	Riociguat	Oral	Anaemia, constipation, diarrhoea, dizziness, dysphagia, gastroenteritis, gastrointestinal discomfort

Phosphodiesterase-5 (PDE-5) inhibitors and soluble guanylate cyclase stimulators are the current drug classes acting on this pathway. Meanwhile, novel compounds targeting on NO pathway exhibits great potential in development of next generation therapy medications. This review seeks to summarize the research progress of PAH regarding to NO pathway, discuss the critical role of NO pathway in understanding the pathophysiology of PAH and new drug development.

CURRENT CLINICAL THERAPY IN PULMONARY ARTERIAL HYPERTENSION

Current PAH therapy focuses on three main pathways. These are the prostacyclin, nitric oxide, and endothelin pathways. Drugs acting on these pathways are summarized in **Table 1**.

Prostanoids

Prostacyclin or prostanoid is produced in the endothelium and it is a potent vasodilator in the pulmonary vasculature (Gryglewski, 2008). Prostacyclin activate the prostacyclin receptor which leads to an increase in cyclic adenosine monophosphate (cAMP) production and consequently, vasodilatation (Coleman et al., 1994). Activating the IP receptor also leads to antithrombotic and antiproliferative effects in the pulmonary vasculature (Wharton et al., 2000; Vane and Corin, 2003). Examples of prostacyclins used in PAH management include epoprostenol and treprostinil. Selexipag is a non-prostanoid IP receptor agonist. Epoprostenol is the only drug shown to improve mortality (Barst et al., 2009) and remains the drug of choice in severe cases (Galiè et al., 2016). It is administered by continuous infusion. The different prostanoids have different routes of administration with varying degrees of efficacy.

Endothelin-1 Receptor Blockers

Endothelin-1 is a potent vasoconstrictor produced by the endothelial cells and it facilitates pulmonary artery smooth muscle cell proliferation (Yanagisawa et al., 1988; Davie et al., 2002). Endothelin-1 binds to two main receptors namely endothelin receptor A (ET_A) and endothelin receptor B (ET_B). ET_A is predominant in vascular smooth muscle cells (VSMC) and facilitates contraction and proliferation of VSMCs in PAH (Rubin et al., 2011). ET_B is predominantly expressed in vascular endothelial cells where it enhances vasodilation via the production of prostacyclin and nitric oxide (NO) as well as clearance of ET-1 (Eguchi et al., 1993; Hirata et al., 1993; Seo et al., 1994). Interestingly, ET_B is also found in VSMCs where it possesses vasoconstrictive and proliferative properties (Seo et al., 1994). Endothelin-1 receptor blockers prevent endothelin-1 from binding to its receptors thereby abrogating its destructive effects in PAH. Endothelin-1 receptor blockers can be grouped as selective (eg., ambrisentan) and non-selective (eg., Bosentan and macitentan) depending on their endothelin-1 receptor binding properties (Correale et al., 2013). Bosentan is the first orally administered PAH drug, notably it causes abnormal liver function in some patients necessitating monthly liver function tests (Humbert et al., 2007). Ambrisentan and macitentan have lower chances of causing liver damage (Galiè et al., 2005a; Pulido et al., 2013).

Drugs Acting on the Nitric Oxide Pathway

Nitric oxide (NO) is produced by the endothelial cells and serves as a potent vasodilator of the pulmonary circulation through cyclic guanosine monophosphate (cGMP). Phosphodiesterase-5 (PDE5) inhibitors such as sildenafil and tadalafil and the soluble guanylate cyclase stimulator, riociguat act on this pathway. Further explanation of drugs acting on this pathway is in **section 4** of this review.

NITRIC OXIDE PATHWAY AND ITS IMPLICATION IN PULMONARY ARTERIAL HYPERTENSION

Nitric oxide (NO) is a biological molecule that regulates many physiological and pathological processes in the body. It was

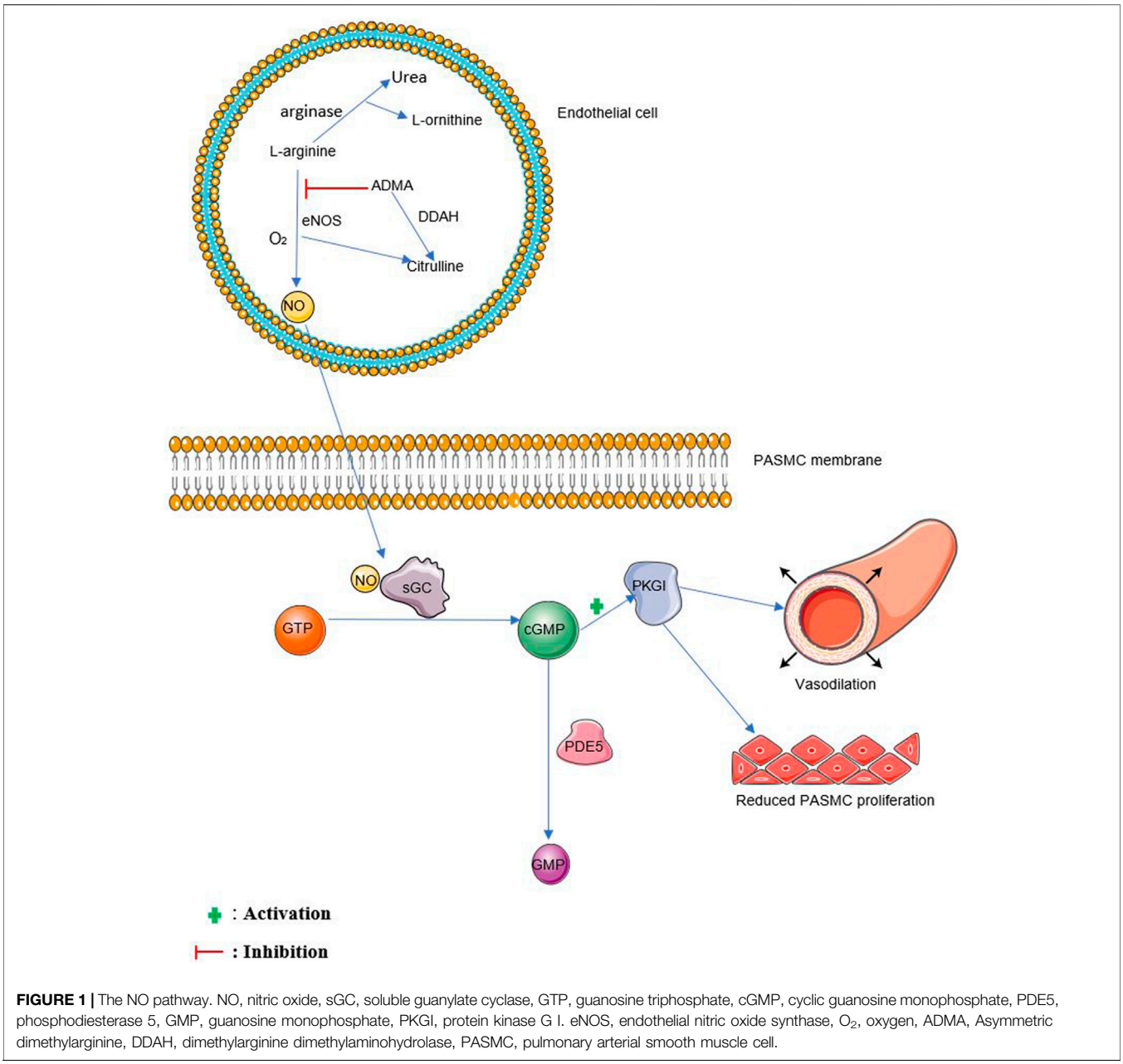

FIGURE 1 | The NO pathway. NO, nitric oxide, sGC, soluble guanylate cyclase, GTP, guanosine triphosphate, cGMP, cyclic guanosine monophosphate, PDE5, phosphodiesterase 5, GMP, guanosine monophosphate, PKGI, protein kinase G I. eNOS, endothelial nitric oxide synthase, O_2, oxygen, ADMA, Asymmetric dimethylarginine, DDAH, dimethylarginine dimethylaminohydrolase, PASMC, pulmonary arterial smooth muscle cell.

proposed that the release of a vasodilating factor by the endothelial cells as one of the mechanisms behind acetylcholine-induced vasodilation *in vivo* (Furchgott and Zarwodski, 1980). The identity of nitric oxide as the endothelial-derived relaxing factor was not known until 1987 when two different studies confirmed it (Ignarro et al., 1987; Palmer et al., 1987).

Nitric oxide is formed from the oxidation of L-arginine to form citrulline and NO in the presence of nitric oxide synthases (NOS) and molecular oxygen (Moncada and Higgs, 1993) as shown in **Figure 1**. Arginase competes with eNOS for L-arginine by converting L-arginine to urea and L-ornithine (Luiking et al., 2012). N^G, N^G-dimethyl-L-arginine (ADMA) is known to inhibit this process by competing with L-arginine for eNOS (Zakrzewicz and Eickelberg, 2009). N^G, N^G-dimethylarginine dimethylaminohydrolases (DDAH1 and DDAH2) are responsible for the degradation of ADMA (Tain and Hsu, 2017). Three isoforms of nitric oxide synthases have been described in mammals. These are neuronal NOS (nNOS, NOS1), inducible NOS (iNOS, NOS2), and endothelial NOS (eNOS, NOS3) (Nathan and Xie, 1994).

Endothelium-derived NO diffuses into vascular smooth muscle cells and stimulates soluble guanylate cyclase (sGC) to produce cGMP, further activating associated protein kinases such as protein kinase G I (PKGI) which causes vasorelaxation (Sausbier et al., 2000; Surks, 2007). cGMP is broken down mainly by phosphodiesterase 5 (PDE5) (Francis et al., 2000). See **Figure 1** for more details.

Conflicting levels of exhaled NO have been reported in PAH patients. Data from studies with patients suffering from idiopathic PAH and scleroderma-/drug-associated PAH indicated a reduction in exhaled NO as compared to healthy patients (Kharitonov et al., 1997; Kaneko et al., 1998; Archer et al., 2012). Other studies also found no significant change in exhaled NO levels in idiopathic PAH and scleroderma-associated PAH when compared to healthy subjects (Riley et al., 1997; Olivieri et al., 2006; Malekmohammad et al., 2019). There was no difference in exhaled NO after 3 months of treatment with endothelin receptor antagonists, guanylate cyclase stimulants, phosphodiesterase type 5 (PDE5) inhibitors and prostanoids in comparison with healthy subjects. However, other diagnostic markers such as 6MWD and N-terminal prohormone of brain natriuretic peptide (NT-proBNP) were significantly correlated to disease severity and treatment response (Malekmohammad et al., 2019). Confounding factors such as exhalation flow rate, measurement technique, the NO analyzer used, nasal NO contamination, age, height and smoking (Borrill et al., 2006; Dweik et al., 2012) makes exhaled NO an unreliable marker that needs standardization to be of diagnostic value in PAH.

The use of NO Plasma metabolites (NO_X) as a biomarker and prognostic indicator of PAH is being studied. A study found that patients (age range: 20–57 years) with IPAH had reduced levels of plasma NOx, which correlated inversely with mPAP and patient survival (Zhang et al., 2016). Contradictory studies found elevated levels of NOx in IPAH and congenital heart disease-associated PAH patients with age ranges of 31–77 and 5 days -12 years (Ikemoto et al., 2002; Malinovschi et al., 2011). The patients in the extreme age groups (age averages of 6 and 54 years) seem to show increased levels of NOx. The different results from the various studies could be attributed to the PAH type and ages of the patients studied (Zhang et al., 2016).

Reduced eNOS levels have been reported in PAH patients (Giaid and Saleh, 1995). Another study found an increased expression of eNOS in the plexiform lesions of PAH patients (Berger et al., 2012). The eNOS that is elevated in some PAH patients is likely to be in the uncoupled state causing it to produce more superoxides (NO scavengers) than NO (Klinger et al., 2013). eNOS uncoupling can occur as a result of a decrease in amounts of tetrahydrobiopterin (BH4), a cofactor for eNOS in NO synthesis. There are studies to confirm eNOS uncoupling in pulmonary hypertension models that are BH4-deficient (Khoo et al., 2005; Nandi et al., 2005).

Also, several studies have described elevated levels of ADMA in plasma and serum of IPAH and connective tissue disease (CTD)-associated pulmonary arterial hypertension patients (Kielstein et al., 2005; Fang et al., 2015; Liu et al., 2019). Monocotaline- and hypoxia-induced PAH rat model have been found to have increased ADMA levels with a corresponding decrease in DDAH levels (Millatt et al., 2003; Li et al., 2010). This makes ADMA/DDAH possible diagnostic indicators in PAH

NO signaling remains a very relevant pathway in understanding and treating PAH. Upregulation of NO signaling is crucial in the management of PAH.

CROSSTALK WITH NITRIC OXIDE

The nitric oxide pathway interacts with several other pathways reiterating its complex role in PAH. Nitric oxide interaction with some of these pathways is illustrated in **Figure 2**. The nitric oxide pathway has been shown to interact with the bone morphogenetic protein (BMP) pathway. Mutations in the bone morphogenetic protein receptor 2 (BMPR2) gene possess the strongest risk factor in the development of PAH, particularly heritable PAH (Machado et al., 2006). Bone Morphogenetic Protein Receptor II (BMPRII) and its ligands, BMP2 and BMP4 were found to be mediators of endothelial nitric oxide synthase activation (Gangopahyay et al., 2011). BMP2 and BMP4 activates eNOS by enhancing its phosphorylation by protein kinase A in pulmonary arterial endothelial cells (PAEC). Interestingly, knocking down BMPRII in PAEC reduced the ability of BMP2 and BMP4 to stimulate eNOS phosphorylation suggesting a crucial role of BMPRII in eNOS activation (Gangopahyay et al., 2011). Plasma nitric oxide metabolites have also been found to be markedly reduced in idiopathic pulmonary arterial hypertension patients with BMPR2 mutations (Zhang et al., 2016).Protein Kinase G I (PKGI) which is one of the downstream targets in the nitric oxide pathway has been found to crosstalk with the BMP pathway. PKGI contributes to the activation of BMP signaling by BMP4 in Human PASMCs (Yang et al., 2013). PKGI upregulates BMP signaling by phosphorylating the BMPRII receptor and smad proteins. Furthermore, PKGI binds to the phosphorylated smad proteins to form a complex and translocates into the nucleus where it upregulates the transcription of Id1 mRNA (Schwappacher et al., 2013). This then facilitates apoptosis and inhibits PASMC proliferation (Schwappacher et al., 2013; Yang et al., 2013).

The extracellular signal-regulated kinase 1/2 (ERK 1/2) pathway plays a significant role in the pathogenesis of PAH. Activation of the ERK pathway is known to be associated with increased proliferation and reduced apoptosis of PASMCs (Yang et al., 2008; Zhou et al., 2019). NO has been found to induce S-nitrosylation of ERK1/2 leading to reduced ERK phosphorylation and improved MCF-7 cell apoptosis (Feng et al., 2013). This crosstalk could be one of the ways with which NO inhibits proliferation and enhances apoptosis in PASMCs. S-nitrosylation of ERK1/2 by NO in PASMCs is yet to be explored.

The phosphatidylinositol 3-kinase/protein kinase B (PI3K/Akt) pathway is another major pathway that is implicated PAH. There have been contradictory reports on its role in PAH (Fang et al., 2016; Huang et al., 2017; Zheng et al., 2017). The PI3K/Akt pathway is known to phosphorylate eNOS and increase NO levels in many cell types including human pulmonary arterial endothelial cells (HPAECs) (Kim et al., 2008; Liang et al., 2009; Li et al., 2014). This helps to attenuate monocrotaline-induced pulmonary artery endothelial dysfunction and PAH in rats (Li et al., 2014; Zheng et al., 2017). Relaxation of rat pulmonary artery rings is enhanced through the activation of eNOS by the PI3K/Akt pathway (Zhang et al., 2010).

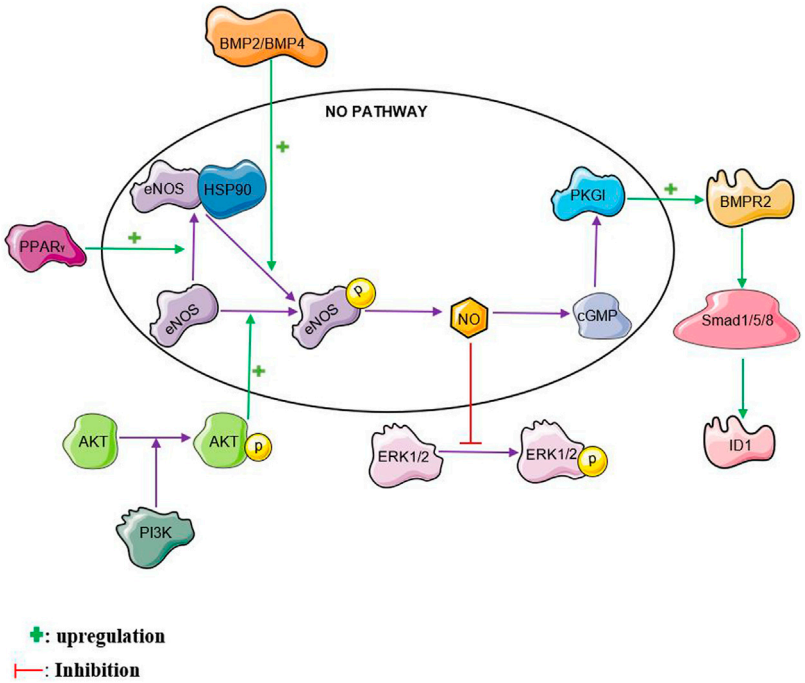

FIGURE 2 | NO crosstalk. NO, nitric oxide, BMPR2, bone morphogenetic protein receptor 2 $PPAR_{\gamma}$, peroxisome proliferator-activated receptor gamma ERK, extracellular signal-regulated kinase, PI3K, phosphatidylinositol 3-kinase, HSP90, heat shock protein 90, BMP2, bone morphogenetic protein 2, BMP4, bone morphogenetic protein 4, ID1, inhibitor of DNA binding 1

There is evidence that Peroxisome proliferator-activated receptor gamma (PPARγ) activity is reduced in PASMCs from idiopathic PAH patients (Falcetti et al., 2012). Activation of the Peroxisome proliferator-activated receptor gamma (PPARγ) pathway is known to reduce monocrotaline-and hypoxia-induced PAH in rats (Liu et al., 2012; Legchenko et al., 2018). Increased PPARγ expression has been found to enhance the phosphorylation and activation of eNOS in human pulmonary arterial endothelial cells (Li et al., 2014). Enhanced interaction between heat shock protein 90 and eNOS is one of the ways with which PPARγ facilitates eNOS phosphorylation. PPARγ agonists such as rosiglitazone, ciglitazone and pioglitazone have been found to stimulate eNOS activation through various mechanisms. Rosiglitazone was found to activate eNOS by stimulating heat shock protein (HSP)-90–eNOS interaction, with a subsequent eNOS phosphorylation at Ser^{1177} (Polikandriotis et al., 2005). Ciglitazone also caused a reduction in human umbilical vein endothelial cells (HUVEC) membrane NADPH-dependent superoxide anion generation leading to a decrease in endothelial superoxide anion generation and oxidative stress with a resulting increase in NO bioavailability (Hwang et al., 2005; Polikandriotis et al., 2005). Rho-kinase, a serine–threonine kinase is known to cause endothelial dysfunction by inactivating eNOS and reducing NO generation (Nohria et al., 2006). Pioglitazone enhances the dephosphorylation on tyrosine residues of the Vav protein, a group of guanosine nucleotide exchange factors (GEFs) involved in the activation of Rho Kinase. The deactivation of Rho Kinase leads to an increase in eNOS activation with a consequent increase in NO production (Wakino et al., 2004). The PPARγ agonist, telmisartan was found to increase the expression of DDAH II thereby enhancing the degradation of ADMA and increasing NO levels in human umbilical vein endothelial cells (Scalera et al., 2008).

CURRENT DRUGS ON NITRIC OXIDE PATHWAY IN PULMONARY ARTERIAL HYPERTENSION

There are two groups of drugs currently used in PAH that act on the nitric oxide pathway, the phosphodiesterase 5 inhibitors (sildenafil and tadalafil) and soluble guanylate cyclase inhibitors (riociguat).

Phosphodiesterase-5 Inhibitors

As the name suggests, PDE5 inhibitors inhibit the PDE5 enzyme responsible for the breakdown of cGMP. This increases the levels of cGMP which activates protein kinase G and consequently leads to vasodilation. PDE5 is very abundant in smooth muscle cells (Rybalkin et al., 2003). Sildenafil was the first PDE5 inhibitor accepted for the management of PAH.

The SUPER-1 trial found 20, 40 and 80 mg doses of sildenafil to increase 6MWD by 45, 46, and 50 m respectively after 12 weeks. These doses also reduced mPAP by 2.1, 2.6 and 4.7 mmHg respectively. The was no significant reduction in clinical worsening (as measured by death, hospitalization for pulmonary hypertension, initiation of prostacyclin and

initiation of bosentan) in the different sildenafil dose groups when compared to the placebo. Also, there were no significant dose-dependent changes in exercise capacity making the 20 mg dose the most appropriate for clinical use (Galiè et al., 2005b). A follow-up open-label trial by the SUPER-2 group found the improvement in 6MWD to be maintained after 1 year with a value of 51 m (Rubin et al., 2011). Sildenafil caused mild side effects such as headaches, flushing, and dyspepsia.

Contrary to the SUPER-1 study, the PACES-1 study found the combination of sildenafil with long-term intravenous epoprostenol therapy to improve clinical worsening as compared to intravenous epoprostenol alone after 16 weeks (Simonneau et al., 2008). The proportion of patients that needed a change in epoprostenol dose (an indicator of clinical worsening) was 0.195 in the epoprostenol-only group with a lower proportion (0.062) in the combination group. The sildenafil dose for this study was titrated up from 20 to 40 mg and 80 mg three times daily over 16 weeks depending on patient drug tolerability. An open-label extension study of the PACES-1 trial found the long-term combination of sildenafil and intravenous epoprostenol to be well tolerated with 33% of patients have a maintained or improved 6MWD after 3 years(Simonneau et al., 2014).

Administration of bosentan (125 mg twice daily) to patients on stable sildenafil therapy resulted in no significant difference between the two groups with regards to the primary endpoint (time to the first morbidity/mortality event) after 16 weeks in an event-driven trial. This may be due to limitations of the study such as enrollment of patients with many comorbidities and a high rate of patient dropout, to name but a few. Nonetheless, the addition of bosentan yielded an increase in 6MWD by 7.2 ± 66.0 m in the bosentan group with a reduction of 14.6 ± 80.4 m in the placebo group after 16 weeks. The mean difference in 6MWD between the two groups was 21.8 m. However, this was only a secondary and exploratory endpoint of the study (McLaughlin et al., 2015).

Conversely, a 12 weeks randomized controlled clinical trial found the administration of sildenafil (20 mg three times daily) to patients on stable bosentan therapy offers no significant benefit in terms of the 6MWD as compared to bosentan alone (Vizza et al., 2017). Limitations such as a possible ceiling effect in patients receiving effective bosentan therapy could be responsible for the insignificant difference between the groups.

In a 16 weeks double-blind, placebo-controlled study, 40 mg once daily administration of tadalafil was found to increase 6MWD by 44 m in the bosentan-naive group and by 23 m in patients on bosentan background therapy. These increments were statistically significant in comparison to the placebo group. Tadalafil also reduced the time to clinical worsening and the incidence of clinical worsening (68% relative risk reduction). The most common side-effects were headache, myalgia, and flushing (Galiè et al., 2009a). A 52 weeks extension study confirmed tadalafil to be well-tolerated with a sustained improvement in the 6MWD (Oudiz et al., 2012).

As compared to tadalafil and ambrisentan monotherapies, the combination of tadalafil and ambrisentan resulted in fewer occurrences of clinical failure as defined by the first occurrence of a composite endpoint of death, hospitalization for worsening pulmonary arterial hypertension, disease progression, or unsatisfactory long-term clinical response. Clinical failure occurred in only 18% of patients in the combination group with 34 and 28% occurrences in the ambrisentan only and tadalafil only groups respectively. Side-effects such as headache and nasal congestion occurred more in the combination group than in the monotherapy groups (Galiè et al., 2015a). Because of moderate quality evidence, the 2019 CHEST guideline weakly recommends the initial combination therapy with ambrisentan and tadalafil to improve 6MWD for treatment-naive PAH patients with WHO FC II and III. Also, the addition of tadalafil to improve 6MWD of stable or symptomatic PAH patients on background therapy with ambrisentan is weakly recommended because of low-quality evidence (Klinger et al., 2019).

Vardenafil is also a PDE5 inhibitor. A randomized, double-blind, placebo-controlled study found it to be well tolerated in patients with PAH and also increase 6-MWD by 69 m at a dose of 5 mg twice daily. It also reduced mean pulmonary arterial pressure by 5.3 mmHg at 12 weeks (Jing et al., 2011). Vardenafil was found to significantly decrease mean pulmonary arterial pressure when used for acute vasoreactivity testing in patients with PH (Sandqvist et al., 2015). Vardenafil is not yet approved for the treatment of PAH.

Soluble Guanylate Cyclase Stimulators

Soluble guanylate cyclase is activated by NO to convert guanosine triphosphate (GTP) to cGMP (Stasch et al., 2001). sGC stimulators directly activate soluble guanylate cyclase in smooth muscle cells. sGC stimulators also stabilize the complex formed between NO and sGC to enhance cGMP production (Stasch et al., 2011). Riociguat is the only approved sGC stimulator for treating PAH. It is approved to be used up to a maximum dose of 2.5 mg three times daily. Riociguat increases 6-MWD by a mean of 36 m as compared to placebo after 12 weeks. It also significantly decreases mPAP by 9 ± 11 mmHg from baseline. In the RESPITE trial, riociguat proved to be a viable alternative for patients with PAH not responding to PDE5 inhibitors because of reduced endogenous NO production (Hoeper et al., 2017a). The prospective randomized REPLACE trial further confirmed that patients irresponsive to PDE5 inhibitors are more likely to show clinical improvement upon switching to riociguat therapy (Hoeper et al., 2017b). This has made riociguat a crucial PAH treatment option. Some of its side effects include headache, syncope, and hypotension (Ghofrani et al., 2013a). There was sustained improvement in exercise capacity after 1 year as observed in a long-term extension trial (Rubin et al., 2011). Riociguat is also approved for treating inoperable chronic thromboembolic pulmonary hypertension (Ghofrani et al., 2013b). The combination of riociguat and PDE5 inhibitors is contraindicated due to increased hypotension (Galiè et al., 2015b).

Inhaled Nitric Oxide

Even though inhaled NO has the potential for use in treating PAH, it is mostly used in acute vasoreactivity testing during right heart catheterization. This is to identify acute responders likely to benefit from calcium-channel blockers (CCBs). Acute responders

are patients who show a decrease in mPAP of at least 10 mmHg to an absolute level below 40 mmHg with sustained or increased cardiac output (Badesch et al., 2009). These patients are rare with most of them having idiopathic PAH. Such patients have a very good prognosis with CCB use (Rich et al., 2010). Inhaled NO is only approved for the treatment of severe persistent pulmonary hypertension of the newborn (PPHN). There are not enough studies to support the safety and efficacy of the long-term ambulatory use of inhaled NO in PAH. Also, the lack of portable delivery systems and the need for continuous inhalation makes its daily ambulatory use impractical.

ONGOING PHARMACEUTICAL RESEARCH ON NITRIC OXIDE PATHWAY AND ITS IMPLICATION IN PULMONARY ARTERIAL HYPERTENSION

The NO pathway offers various molecular targets that can be exploited to help develop novel drugs to ameliorate the pathophysiological changes that occurs during PAH development. Some of the possible therapeutic targets offered by the NO pathway include arginase, ADMA, DDAH1, eNOS, PDE-5, cGMP, sGC and NO. This section highlights key drug molecules and target that focus mainly on the NO pathway and their implications in PAH.

L-arginine serves as a substrate not just for eNOS but arginase as well. This means an increase in arginase activity leads to a reduction in the availability of L-arginine to be converted to NO by eNOS (Pernow and Jung, 2013). Arginase metabolizes L-arginine to urea and L-ornithine (Luiking et al., 2012) as shown in **Figure 1**. Arginase exists in two isoforms namely arginase I and arginase II but arginase II has been found to be much more involved in the development of PAH in humans and animals (Jin et al., 2010; Cho et al., 2013). Deletion of arginase II in interleukin-13 overexpressing transgenic mice showed a significant decrease in medial wall thickness suggesting an important role of arginase II in PAH (Cho et al., 2013). PAH patients are known to have high arginase II activity compared to healthy controls with a consequent reduction in NO synthesis (Kao et al., 2015). A recent study found selective arginase II inhibitors L207-0525 and L327-0346 demonstrate a dose-dependent protective activity in monocrotaline-induced PAH rats. Furthermore, combining L207-0525 and L327-0346 with low dose (0.1 mg/kg) tadalafil produced a better protective effect in monocrotakine-induced PAH rats. Therefore, L207-0525 and L327-0346 are potential compounds needing further exploration for PAH treatment (Koklin and Danilenko, 2019).

Nitrates have shown promising signs in the amelioration of PAH in hypoxia- and monocrotaline-induced PAH animals. Both Intraperitoneal and nebulized sodium nitrite reduced pulmonary arterial pressure, right ventricular hypertrophy and vascular remodeling in MCT-induced PAH rats (Zuckerbraun et al., 2010; Pankey et al., 2012). Orally administered sodium nitrate have also shown protective effects in hypoxia-induced PAH mice (Baliga et al., 2012). However, a recent study found oral sodium nitrate does not substantially reduce established MCT-induced PAH in rats (Malikova et al., 2020). The different outcomes in the above studies could be attributed to the difference in disease severity in the PAH models as well as the routes and timing of drug administration (Malikova et al., 2020). Considering the poor response of certain patients to PDE5 inhibitors (PDE5i) due to reduced endogenous nitric oxide production, nitrates could serve as alternative sources of NO in such patients. Also, the impracticability of inhaled nitric oxide therapy further necessitates the need for alternate NO sources. More research has to be done to further explore the potential benefits of nitrates in PAH therapy especially in PDE5i-irresponsive patients.

Oxymatrine, an active alkaloid derived from the traditional Chinese herb *Sophora alopecuroides* was found to protect against hypoxia- and monocrotaline-induced PAH (Zhang et al., 2014). The mechanism behind the protective effect of Oxymatrine in monocrotaline-induced PAH is likely to be through the reduction of pulmonary ADMA levels even though it did not affect the level of DDAH1 (Dai et al., 2019).

Despite the fact that DDAH1 levels have been found to be reduced in hypoxia-induced PAH, it was uncertain how important of a role DDAH1 dysfunction plays in PAH. Recently, a study on a novel DDAH1 knockout ($DDAH1^{-/-}$) rat strain model found DDAH1 dysfunction to significantly worsen RVSP and RVHI in $DDAH1^{-/-}$ MCT model compared to the wild type MCT model (Wang et al., 2019). Although no *in vitro* experiment was carried out to target specific cells that are responsible for the progress of PAH, this study still shows how important DDAH1 dysfunction is in the development of PAH making it a possible PAH treatment target.

Apelin signaling is known to regulate endothelial NOS (eNOS) (Chandra et al., 2011). It has been discovered that the novel cyclic biased agonist of the apelin receptor, MM07 significantly reduces the elevation of right ventricular systolic pressure and hypertrophy induced by monocrotaline (Yang et al., 2019). They also found the elevation of eNOS and its mRNA as one of the mechanisms behind its protective effect in monocrotaline-induced PAH.

Udenafil, an oral phosphodiesterase-5 inhibitor approved for the treatment of erectile dysfunction has been found by a recent double-blind, placebo-controlled phase IIb clinical trial to improve 6-MWD in patients with PAH, especially those with a history of ERA therapy (Chang et al., 2019). The improvement in the 6-MWD with udenafil and ERA combination therapy group was found to be better than that of sildenafil and tadalafil in previous trials (Galiè et al., 2009a; Galiè et al., 2009b; Benza et al., 2018). Adverse side effects in the udenafil were also found to be mild and in the expected range (Chang et al., 2019).

TPN171, a new compound that inhibits PDE5 has been found to significantly reduce mPAP in a rat MCT-PAH model. Its efficacy was comparable to that of the sildenafil control group. It has a long half-life making once-daily dosing possible. The effective dose of TPN171 used in the animal experiment was 1 mg/kg which is lower than that of sildenafil (25 mg/kg). This property could make the occurrence of side-effects less likely if TPN171 is used in a clinical setting (Wang et al., 2019). TPN171 is currently in phase II clinical trial.

Evodiamine is a traditional Chinese medicine for the treatment of cancers (Dong et al., 2012). Evodiamine derivatives (S)-7e and (S)-7 days are newly discovered PDE5 inhibitors with very high selectivity (Zhang et al., 2020). Evodiamine derivative (S)-7 days significantly reduced mPAP and wall thickness in rat MCT-PAH model. Its efficacy is similar to that of sildenafil which was used as a positive control. Additionally, the study found a unique allosteric pocket of PDE5 using evodiamine derivative (S)-7e. Currently approved PDE5 inhibitors only bind to the substrate-binding pocket. This novel allosteric pocket regulates both enzymatic activity and pulmonary hemodynamic function of PDE5 thereby serving as a new therapeutic target for PAH treatment (Zhang et al., 2020).

A new study found PDE10 to be a novel therapeutic target for treating PAH. This study used a highly selective PDE10 inhibitor, 2b to explore the role of PDE10 in PAH. Compound 2b significantly reduced mPAP and RVHI in PAH rats making PDE10 a potential therapeutic target for PAH (Huang et al., 2019).

Studies have found natriuretic peptides to increase cGMP levels (Egom, 2015; Preston et al., 2016). Natriuretic peptides (NP) are inactivated by neprilysin. Natriuretic peptides are known to have antiproliferative effects on PASMCs and also attenuate the development of hypoxia-induced PH (Arjona at al., 1997; Zhao et al., 1999). Furthermore, the beneficial effect of sildenafil was found to be affected by natriuretic peptide activity in mice (Zhao et al., 2003). Also, the infusion of natriuretic peptides in the presence of sildenafil synergistically increased cGMP and reduced RVSP in hypoxia-induced PAH rats (Preston et al., 2016). A recent clinical trial demonstrated that the combination of a neprilysin inhibitor (racecadotril) with a PDE5 inhibitor (sildenafil or tadalafil) acutely increases NP and cGMP levels and improves pulmonary hemodynamics (Hobbs et al., 2019). This indicates that neprilysin inhibitors could have therapeutic use in PAH.

The mechanism of NO/cGMP-induced vasodilation is partly mediated by the activation of voltage-gated K^+ (K_v) channels (Cogolludo et al., 2001; Jackson, 2018). $K_v1.5$ is particularly known to contribute the most to K_v current in PASMCs. K_v7 channels have now been found to play a very significant role in generating K_v current in rat PASMCs (Mondéjar-Parreño et al., 2019). K_v7 channel activation is now thought to be imperative to the electrophysiological and relaxant effects of NO donors and riociguat (Mondéjar-Parreño et al., 2019). This makes activation of K_v7 channels a novel mechanism of action of vasodilators used in managing pulmonary arterial hypertension.

A new sGC stimulator, compound 13a (a pyrazolo [3,4-b] pyridine-3-yl pyrimidine derivative) has recently been found to exhibit similar *in vitro* vasorelaxation potential as riociguat on rat thoracic aorta rings and rat heart Langendorff preparation. Compound 13a also exhibited good oral bioavailability in male Beagle dogs which could make it a possible treatment candidate for PAH (Li et al., 2019). Compound 2 (a pyrazolo [3,4-b] pyridine derivative) is another novel sGC stimulator found to attenuate PAH (Hu et al., 2020). It reduced the migration of HPASMCs under hypoxic conditions significantly. Furthermore, it significantly improved RVSP, myocardial and vascular remodelling in hypoxia-induced PAH rats (Hu et al., 2020). We should notice that the PDE5 inhibitors block the breakdown of cGMP but these effects are dependent on NO availability and sGC activity. So the sGC stimulator or sGC activator may be effective in patients who have not sufficiently responded to a PDE5 inhibitor. Furthermore, sGC stimulator and sGC activator also show some difference, sGC stimulator acts on mature sGC and keep the activity of sGC, while sGC activator help to activate the damaged sGC.

CONCLUSION

Great strides have been made in PAH research in recent years but searching for new therapeutical agents remains a big challenge in this field. Current therapy only slows disease progression but does not cure the disease. So far the current clinical practice has strongly suggested that targeting the NO pathway is the strategy with the most potential. Critical molecules in the NO pathway such as DDAH1, PDE10 and cGKI show potential for becoming the next new therapeutic targets in PAH treatment. Compounds or derivatives from plant extracts also have very bright prospect. Furthermore, medicines harboring the ability to enhance NO signal and other key signaling pathways at the same time exhibit better hope to finally cure this thorny disease.

AUTHOR CONTRIBUTIONS

TT: Writing—Original Draft YJ: Writing—Original Draft XL: Conceptualization YL: Writing—Review&Editing

REFERENCES

Archer, S. L., Djaballah, K., Humbert, M., Weir, E. K., Fartoukh, M., Dall'ava-Santucci, J., et al. (2012). Nitric Oxide Deficiency in Fenfluramine- and Dexfenfluramine-Induced Pulmonary Hypertension. *Am. J. Respir. Crit. Care Med.* 158, 1061–1067. doi:10.1164/AJRCCM.158.4.9802113

Arjona, A. A., Hsu, C. A., Wrenn, D. S., and Hill, N. S. (1997). Effects of Natriuretic Peptides on Vascular Smooth-Muscle Cells Derived from Different Vascular Beds. *Gen. Pharmacol. Vasc. Syst.* 28, 387–392. doi:10.1016/S0306-3623(96)00275-3

Badesch, D. B., Champion, H. C., Gomez Sanchez, M. A., Hoeper, M. M., Loyd, J. E., Manes, A., et al. (2009). Diagnosis and Assessment of Pulmonary Arterial Hypertension. *J. Am. Coll. Cardiol.* 54, S55–S66. doi:10.1016/J.JACC.2009.04.011

Baliga, R. S., Milsom, A. B., Ghosh, S. M., Trinder, S. L., MacAllister, R. J., Ahluwalia, A., et al. (2012). Dietary Nitrate Ameliorates Pulmonary Hypertension. *Circulation* 125, 2922–2932. doi:10.1161/CIRCULATIONAHA.112.100586

Barst, R. J., Rubin, L. J., Long, W. A., McGoon, M. D., Rich, S., Badesch, D. B., et al. (2009). A Comparison of Continuous Intravenous Epoprostenol (Prostacyclin) with Conventional Therapy for Primary Pulmonary Hypertension. *N. Engl. J. Med.* 51, 993. doi:10.1056/NEJM199602013340504

Benza, R. L., Raina, A., Gupta, H., Murali, S., Burden, A., Zastrow, M. S., et al. (2018). Bosentan-Based, Treat-To-Target Therapy in Patients with Pulmonary

Arterial Hypertension: Results from the COMPASS-3 Study. *Pulm. Circ.* 8, 1–13. doi:10.1177/2045893217741480

Berger, R. M. F., Geiger, R., Hess, J., Bogers, A. J. J. C., and Mooi, W. J. (2012). Altered Arterial Expression Patterns of Inducible and Endothelial Nitric Oxide Synthase in Pulmonary Plexogenic Arteriopathy Caused by Congenital Heart Disease. *Am. J. Respir. Crit. Care Med.* 163, 1493–1499. doi:10.1164/AJRCCM.163.6.9908137

Borrill, Z., Clough, D., Truman, N., Morris, J., Langley, S., and Singh, D. (2006). A Comparison of Exhaled Nitric Oxide Measurements Performed Using Three Different Analysers. *Respir. Med.* 100, 1392–1396. doi:10.1016/J.RMED.2005.11.018

Chandra, S. M., Razavi, H., Kim, J., Agrawal, R., Kundu, R. K., Perez, V. de. J., et al. (2011). Disruption of the Apelin-APJ System Worsens Hypoxia-Induced Pulmonary Hypertension. *Arterioscler. Thromb. Vasc. Biol.* 31, 814–820. doi:10.1161/ATVBAHA.110.219980

Chang, H.-J., Song, S., Chang, S.-A., Kim, H.-K., Jung, H.-O., Choi, J.-H., et al. (2019). Efficacy and Safety of Udenafil for the Treatment of Pulmonary Arterial Hypertension: a Placebo-Controlled, Double-Blind, Phase IIb Clinical Trial. *Clin. Ther.* 41, 1499–1507. doi:10.1016/J.CLINTHERA.2019.05.006

Cho, W., Lee, C., Kang, M., Huang, Y., Giordano, F. J., Lee, P. J., et al. (2013). IL-13 Receptor α_2-arginase 2 Pathway Mediates IL-13-induced Pulmonary Hypertension. *Am. J. Physiol. Lung Cel. Mol. Physiol.* 304, L112–L124.

Cogolludo, A. L., Pérez-Vizcaíno, F., Zaragozá-Arnáez, F., Ibarra, M., López-López, G., López-Miranda, V., et al. (2001). Mechanisms Involved in SNP-Induced Relaxation and [Ca2+]I Reduction in Piglet Pulmonary and Systemic Arteries. *Br. J. Pharmacol.* 132, 959–967. doi:10.1038/SJ.BJP.0703894

Coleman, R. A., Smith, W. L., and Narumiya, S. (1994). International Union of Pharmacology Classification of Prostanoid Receptors: Properties, Distribution, and Structure of the Receptors and Their Subtypes. *Pharmacol. Rev.* 46.

Correale, M., Totaro, A., Lacedonia, D., Montrone, D., Di Biase, M., Foschino, M. P. B., et al. (2013). Novelty in Treatment of Pulmonary Fibrosis: Pulmonary Hypertension Drugs and Others. *Cardiovasc. Hematol. Agents Med. Chem.* 11, 169–178. doi:10.2174/18715257131100086

Dai, G., Li, B., Xu, Y., Zeng, Z., and Yang, H. (2019). Oxymatrine Prevents the Development of Monocrotaline-Induced Pulmonary Hypertension via Regulation of the NG, NG-Dimethyl-L-Arginine Metabolism Pathways in Rats. *Eur. J. Pharmacol.* 842, 338–344. doi:10.1016/J.EJPHAR.2018.11.007

Davie, N., Haleen, S., Upton, P., Polak, J., Yacoub, M., Morrell, N., et al. (2002). ET(A) and ET(B) Receptors Modulate the Proliferation of Human Pulmonary Artery Smooth Muscle Cells. *Am. J. Respir. Crit. Care Med.* 165, 398–405. doi:10.1164/AJRCCM.165.3.2104059

Dong, G., Wang, S., Miao, Z., Yao, J., Zhang, Y., Guo, Z., et al. (2012). New Tricks for an Old Natural Product: Discovery of Highly Potent Evodiamine Derivatives as Novel Antitumor Agents by Systemic Structure–Activity Relationship Analysis and Biological Evaluations. *J. Med. Chem.* 55, 7593–7613. doi:10.1021/JM300605M

Dweik, R. A., Boggs, P. B., Erzurum, S. C., Irvin, C. G., Leigh, M. W., Lundberg, J. O., et al. (2012). An Official ATS Clinical Practice Guideline: Interpretation of Exhaled Nitric Oxide Levels (FeNO) for Clinical Applications. *Am. J. Respir. Crit. Care Med.* 184, 602–615. doi:10.1164/RCCM.9120-11ST

Egom, E. E. (2015). BNP and Heart Failure: Preclinical and Clinical Trial Data. *J. Cardiovasc. Transl. Res.* 8, 149–157. doi:10.1007/s12265-015-9619-3

Eguchi, S., Hirata, Y., and Marumo, F. (1993). Endothelin Subtype B Receptors Are Coupled to Adenylate Cyclase via Inhibitory G Protein in Cultured Bovine Endothelial Cells. *J. Cardiovasc. Pharmacol.* 22. doi:10.1097/00005344-199322008-00043

Falcetti, E., Hall, S. M., Phillips, P. G., Patel, J., Morrell, N. W., Haworth, S. G., et al. (2012). Smooth Muscle Proliferation and Role of the Prostacyclin (IP) Receptor in Idiopathic Pulmonary Arterial Hypertension. *Am. J. Respir. Crit. Care Med.* 182, 1161–1170. doi:10.1164/RCCM.201001-0011OC

Fang, X., Chen, X., Zhong, G., Chen, Q., and Hu, C. (2016). Mitofusin 2 Downregulation Triggers Pulmonary Artery Smooth Muscle Cell Proliferation and Apoptosis Imbalance in Rats with Hypoxic Pulmonary Hypertension via the PI3K/Akt and Mitochondrial Apoptosis Pathways. *J. Cardiovasc. Pharmacol.* 67, 164–174. doi:10.1097/FJC.0000000000000333

Fang, Z., Huang, Y., Tang, L., Hu, X., Shen, X., Tang, J., et al. (2015). Asymmetric Dimethyl-L-Arginine Is a Biomarker for Disease Stage and Follow-Up of Pulmonary Hypertension Associated with Congenital Heart Disease. *Pediatr. Cardiol.* 36, 1062–1069. doi:10.1007/S00246-015-1127-3

Feng, X., Sun, T., Bei, Y., Ding, S., Zheng, W., Lu, Y., et al. (2013). S-nitrosylation of ERK Inhibits ERK Phosphorylation and Induces Apoptosis. *Sci. Rep.* 3, 1–6. doi:10.1038/srep01814

Francis, S. H., Turko, I. V., and Corbin, J. D. (2000). Cyclic Nucleotide Phosphodiesterases: Relating Structure and Function. *Prog. Nucleic Acid Res. Mol. Biol.* 65. doi:10.1016/s0079-6603(00)65001-8

Furchgott, R. F., and Zawadzki, J. V. (1980). The Obligatory Role of Endothelial Cells in the Relaxation of Arterial Smooth Muscle by Acetylcholine. *Nat* 288, 373–376. doi:10.1038/288373a0

Galié, N., Badesch, D., Oudiz, R., Simonneau, G., McGoon, M. D., Keogh, A. M., et al. (2005a). Ambrisentan Therapy for Pulmonary Arterial Hypertension. *J. Am. Coll. Cardiol.* 46, 529–535. doi:10.1016/J.JACC.2005.04.050

Galiè, N., Barberà, J. A., Frost, A. E., Ghofrani, H.-A., Hoeper, M. M., McLaughlin, V. V., et al. (2015a). Initial Use of Ambrisentan Plus Tadalafil in Pulmonary Arterial Hypertension. *N. Engl. J. Med.* 373, 834–844. doi:10.1056/NEJMOA1413687

Galiè, N., Ghofrani, H. A., Torbicki, A., Barst, R. J., Rubin, L. J., Badesch, D., et al. (2009b). Sildenafil Citrate Therapy for Pulmonary Arterial Hypertension. *N. Engl. J. Med.* 353, 2148–2157. doi:10.1056/NEJMOA050010

Galiè, N., Humbert, M., Vachiery, J.-L., Gibbs, S., Lang, I., Torbicki, A., et al. (2016). 2015 ESC/ERS Guidelines for the Diagnosis and Treatment of Pulmonary Hypertension. *Rev. Española Cardiol. (English Ed.* 69, 177. doi:10.1016/J.REC.2016.01.002

Galiè, N., Müller, K., Scalise, A.-V., and Grünig, E. (2015b). PATENT PLUS: A Blinded, Randomised and Extension Study of Riociguat Plus Sildenafil in Pulmonary Arterial Hypertension. *Eur. Respir. J.* 45, 1314–1322. doi:10.1183/09031936.00105914

Galiè, N., Brundage, B. H., Ghofrani, H. A., Oudiz, R. J., Simonneau, G., Safdar, Z., et al. (2009a). Tadalafil Therapy for Pulmonary Arterial Hypertension. *Circulation* 119, 2894–2903. doi:10.1161/CIRCULATIONAHA.108.839274

Gangopahyay, A., Oran, M., Bauer, E. M., Wertz, J. W., Comhair, S. A., Erzurum, S. C., et al. (2011). Bone Morphogenetic Protein Receptor II Is a Novel Mediator of Endothelial Nitric-Oxide Synthase Activation. *J. Biol. Chem.* 286. doi:10.1074/jbc.M111.274100

Ghofrani, H.-A., D'Armini, A. M., Grimminger, F., Hoeper, M. M., Jansa, P., Kim, N. H., et al. (2013a). Riociguat for the Treatment of Chronic Thromboembolic Pulmonary Hypertension. *N. Engl. J. Med.* 369, 319–329. doi:10.1056/NEJMOA1209657

Ghofrani, H.-A., Galiè, N., Grimminger, F., Grünig, E., Humbert, M., Jing, Z.-C., et al. (2013b). Riociguat for the Treatment of Pulmonary Arterial Hypertension. *N. Engl. J. Med.* 369, 330–340. doi:10.1056/NEJMOA1209655

Giaid, A., and Saleh, D. (1995). Reduced Expression of Endothelial Nitric Oxide Synthase in the Lungs of Patients with Pulmonary Hypertension. *N. Engl. J. Med.* 333, 214–221. doi:10.1056/NEJM199507273330403

Gryglewski, R. J. (2008). Prostacyclin Among Prostanoids. *Pharmacol. Rep.* 60, 3–11.

Hirata, Y., Emori, T., Eguchi, S., Kanno, K., Imai, T., Ohta, K., et al. (1993). Endothelin Receptor Subtype B Mediates Synthesis of Nitric Oxide by Cultured Bovine Endothelial Cells. *J. Clin. Invest.* 91, 1367–1373. doi:10.1172/JCI116338

Hobbs, A. J., Moyes, A. J., Baliga, R. S., Ghedia, D., Ochiel, R., Sylvestre, Y., et al. (2019). Neprilysin Inhibition for Pulmonary Arterial Hypertension: A Randomized, Double-Blind, Placebo-Controlled, Proof-Of-Concept Trial. *Br. J. Pharmacol.* 176, 1251–1267. doi:10.1111/BPH.14621

Hoeper, M. M., Ghofrani, H.-A., Benza, R. L., Corris, P. A., Gibbs, J., Klinger, J. R., et al. (2017b). REPLACE: A Prospective, Randomized Trial of Riociguat Replacing Phosphodiesterase 5 Inhibitor Therapy in Patients with Pulmonary Arterial Hypertension Who Are Not at Treatment Goal. *Eur. Respir. J.* 50, PA2417. doi:10.1183/1393003.CONGRESS-2017.PA2417

Hoeper, M. M., Simonneau, G., Corris, P. A., Ghofrani, H., Klinger, J. R., Langleben, D., et al. (2017a). RESPITE: Switching to Riociguat in Pulmonary Arterial Hypertension Patients with Inadequate Response to Phosphodiesterase-5 Inhibitors. *Eur. Respir. J.* 50. doi:10.1183/13993003.02425-2016

Hu, L., Li, L., Chang, Q., Fu, S., Qin, J., Chen, Z., et al. (2020). Discovery of Novel Pyrazolo[3,4-B] Pyridine Derivatives with Dual Activities of Vascular Remodeling Inhibition and Vasodilation for the Treatment of Pulmonary

Arterial Hypertension. *J. Med. Chem.* 63, 11215–11234. doi:10.1021/ACS.JMEDCHEM.0C01132

Huang, X., Wu, P., Huang, F., Xu, M., Chen, M., Huang, K., et al. (2017). Baicalin Attenuates Chronic Hypoxia-Induced Pulmonary Hypertension via Adenosine A2A Receptor-Induced SDF-1/CXCR4/PI3K/AKT Signaling. *J. Biomed. Sci.* 24, 1–14. doi:10.1186/S12929-017-0359-3

Huang, Y.-Y., Yu, Y.-F., Zhang, C., Chen, Y., Zhou, Q., Li, Z., et al. (2019). Validation of Phosphodiesterase-10 as a Novel Target for Pulmonary Arterial Hypertension via Highly Selective and Subnanomolar Inhibitors. *J. Med. Chem.* 62, 3707–3721. doi:10.1021/ACS.JMEDCHEM.9B00224

Humbert, M., Guignabert, C., Bonnet, S., Dorfmüller, P., Klinger, J. R., Nicolls, M. R., et al. (2019). Pathology and Pathobiology of Pulmonary Hypertension: State of the Art and Research Perspectives. *Eur. Respir. J.* 53. doi:10.1183/13993003.01887-2018

Humbert, M., Segal, E. S., Kiely, D. G., Carlsen, J., Schwierin, B., and Hoeper, M. M. (2007). Results of European Post-Marketing Surveillance of Bosentan in Pulmonary Hypertension. *Eur. Respir. J.* 30, 338–344. doi:10.1183/09031936.00138706

Humbert, M., Sitbon, O., Chaouat, A., Bertocchi, M., Habib, G., Gressin, V., et al. (2006). Pulmonary Arterial Hypertension in France: Results from a National Registry. *Am. J. Respir. Crit. Care Med.* 173, 1023–1030. doi:10.1164/rccm.200510-1668OC

Hwang, J., Kleinhenz, D. J., Lassègue, B., Griendling, K. K., Dikalov, S., Michael Hart, C., et al. (2005). Peroxisome Proliferator-Activated Receptor-Ligands Regulate Endothelial Membrane Superoxide Production. *Am. J. Physiol. Cel Physiol* 288, 899–905. doi:10.1152/ajpcell

Ignarro, L. J., Buga, G. M., Wood, K. S., Byrns, R. E., and Chaudhuri, G. (1987). Endothelium-Derived Relaxing Factor Produced and Released from Artery and Vein Is Nitric Oxide. *Proc. Natl. Acad. Sci.* 84, 9265–9269. doi:10.1073/PNAS.84.24.9265

Ikemoto, Y., Teraguchi, M., and Kobayashi, Y. (2002). Plasma Levels of Nitrate in Congenital Heart Disease: Comparison with Healthy Children. *Pediatr. Cardiol.* 23, 132–136. doi:10.1007/S00246-001-0036-9

Jackson, W. F. (2018). KV Channels and the Regulation of Vascular Smooth Muscle Tone. *Microcirculation* 25, e12421. doi:10.1111/MICC.12421

Jin, Y., Calvert, T. J., Chen, B., Chicoine, L. G., Joshi, M., Bauer, J. A., et al. (2010). Mice Deficient in *Mkp-1* Develop More Severe Pulmonary Hypertension and Greater Lung Protein Levels of Arginase in Response to Chronic Hypoxia. *Am. J. Physiol. Heart Circ. Physiol.* 298, H1518–H1528.

Jing, Z. C., Yu, Z. X., Shen, J. Y., Wu, B. X., Xu, K. F., Zhu, X. Y., et al. (2011). Vardenafil in Pulmonary Arterial Hypertension. *Am. J. Respir. Crit. Care Med.* 183, 1723–1729. doi:10.1164/RCCM.201101-0093OC

Kaneko, F. T., Arroliga, A. C., Dweik, R. A., Comhair, S. A., Laskowski, D., Oppedisano, R., et al. (1998). Biochemical Reaction Products of Nitric Oxide as Quantitative Markers of Primary Pulmonary Hypertension. *Am. J. Respir. Crit. Care Med.* 158, 917–923. doi:10.1164/ajrccm.158.3.9802066

Kao, C. C., Wedes, S. H., Hsu, J. W., Bohren, K. M., Comhair, S. A., Jahoor, F., et al. (2015). Arginine Metabolic Endotypes in Pulmonary Arterial Hypertension. *Pulm. Circ.* 5, 124–134. doi:10.1086/679720

Kharitonov, S. A., Cailes, J. B., Black, C. M., Bois, R. M. du., and Barnes, P. J. (1997). Decreased Nitric Oxide in the Exhaled Air of Patients with Systemic Sclerosis with Pulmonary Hypertension. *Thorax* 52, 1051–1055. doi:10.1136/THX.52.12.1051

Khoo, J. P., Zhao, L., Alp, N. J., Bendall, J. K., Nicoli, T., Rockett, K., et al. (2005). Pivotal Role for Endothelial Tetrahydrobiopterin in Pulmonary Hypertension. *Circulation* 111, 2126–2133. doi:10.1161/01.CIR.0000162470.26840.89

Kielstein, J. T., Bode-Böger, S. M., Hesse, G., Martens-Lobenhoffer, J., Takacs, A., Fliser, D., et al. (2005). Asymmetrical Dimethylarginine in Idiopathic Pulmonary Arterial Hypertension. *Arterioscler. Thromb. Vasc. Biol.* 25, 1414–1418. doi:10.1161/01.ATV.0000168414.06853.F0

Kim, K. H., Moriarty, K., and Bender, J. R. (2008). Vascular Cell Signaling by Membrane Estrogen Receptors. *Steroids* 73, 864–869. doi:10.1016/J.STEROIDS.2008.01.008

Klinger, J. R., Abman, S. H., and Gladwin, M. T. (2013). Nitric Oxide Deficiency and Endothelial Dysfunction in Pulmonary Arterial Hypertension. *Am. J. Respir. Crit. Care Med.* 188, 639–646. doi:10.1164/RCCM.201304-0686PP

Klinger, J. R., Elliott, C. G., Levine, D. J., Bossone, E., Duvall, L., Fagan, K., et al. (2019). Therapy for Pulmonary Arterial Hypertension in Adults: Update of the CHEST Guideline and Expert Panel Report. *Chest* 155, 565–586. doi:10.1016/J.CHEST.2018.11.030

Koklin, I. S., and Danilenko, L. M. (2019). Combined Use of Arginase II Inhibitors and Tadalafil for the Correction of Monocrotaline Pulmonary Hypertension. *Res. Results Pharmacol.* 5 (3), 79. doi:10.3897/RRPHARMACOLOGY.5.39522

Legchenko, E., Chouvarine, P., Borchert, P., Fernandez-Gonzalez, A., Snay, E., Meier, M., et al. (2018). PPARγ Agonist Pioglitazone Reverses Pulmonary Hypertension and Prevents Right Heart Failure via Fatty Acid Oxidation. *Sci. Transl. Med.* 10, 303. doi:10.1126/SCITRANSLMED.AAO0303

Li, H., Lu, W., Cai, W. W., Wang, P. J., Zhang, N., Yu, C. P., et al. (2014). Telmisartan Attenuates Monocrotaline-Induced Pulmonary Artery Endothelial Dysfunction through A PPAR Gamma-dependent PI3K/Akt/Enos Pathway. *Pulm. Pharmacol. Ther.* 28, 17–24. doi:10.1016/J.PUPT.2013.11.003

Li, L., Zhang, W., Lin, F., Lu, X., Chen, W., Li, X., et al. (2019). Synthesis and Biological Evaluation of Pyrazolo[3,4-B]Pyridine-3-Yl Pyrimidine Derivatives as sGC Stimulators for the Treatment of Pulmonary Hypertension. *Eur. J. Med. Chem.* 173, 107–116. doi:10.1016/J.EJMECH.2019.04.014

Li, X. H., Peng, J., Tan, N., Wu, W. H., Li, T. T., Shi, R. Z., et al. (2010). Involvement of Asymmetric Dimethylarginine and Rho Kinase in the Vascular Remodeling in Monocrotaline-Induced Pulmonary Hypertension. *Vascul. Pharmacol.* 53, 223–229. doi:10.1016/J.VPH.2010.09.002

Liang, C., Ren, Y., Tan, H., He, Z., Jiang, Q., Wu, J., et al. (2009). Rosiglitazone via Upregulation of Akt/Enos Pathways Attenuates Dysfunction of Endothelial Progenitor Cells, Induced by Advanced Glycation End Products. *Br. J. Pharmacol.* 158, 1865–1873. doi:10.1111/J.1476-5381.2009.00450.X

Lim, Y., Low, T.-T., Chan, S.-P., Teo, T. W., Jang, J.-H. J., Yip, N., et al. (2019). Pulmonary Arterial Hypertension in a Multi-Ethnic Asian Population: Characteristics, Survival and Mortality Predictors from a 14-Year Follow-Up Study. *Respirology* 24, 162–170. doi:10.1111/RESP.13392

Liu, J., Fu, Q., Jiang, L., Wang, Y., and Yang, Y. (20192019). Clinical Value of Asymmetrical Dimethylarginine Detection in Patients with Connective Tissue Disease-Associated Pulmonary Arterial Hypertension. *Cardiol. Res. Pract.* doi:10.1155/2019/3741909

Liu, Y., Tian, X. Y., Mao, G., Fang, X., Fung, M. L., Shyy, J. Y.-J., et al. (2012). Peroxisome Proliferator-Activated Receptor-γ Ameliorates Pulmonary Arterial Hypertension by Inhibiting 5-Hydroxytryptamine 2B Receptor. *Hypertension* 60, 1471–1478. doi:10.1161/HYPERTENSIONAHA.112.198887

Luiking, Y. C., Have, G. A. M. T., Wolfe, R. R., and Deutz, N. E. P. (2012). Arginine De Novo and Nitric Oxide Production in Disease States. *Am. J. Physiol. Endocrinol. Metab.* 303, 1177–1189. doi:10.1152/AJPENDO.00284.2012

Machado, R. D., Aldred, M. A., James, V., Harrison, R. E., Patel, B., Schwalbe, E. C., et al. (2006). Mutations of the TGF-B Type II Receptor BMPR2 in Pulmonary Arterial Hypertension. *Hum. Mutat.* 27, 121–132. doi:10.1002/HUMU.20285

Malekmohammad, M., Folkerts, G., Kashani, B. S., Naghan, P. A., Dastenae, Z. H., Khoundabi, B., et al. (20192020). Exhaled Nitric Oxide Is Not a Biomarker for Idiopathic Pulmonary Arterial Hypertension or for Treatment EfficacyEffects of Inorganic Nitrate in a Rat Model of Monocrotaline-Induced Pulmonary Arterial Hypertension. *BMC Pulm. Med.Basic Clin. Pharmacol. Toxicol.* 19126, 199–7109. doi:10.1186/s12890-019-0954-z10.1111/BCPT.13309

Malinovschi, A., Henrohn, D., Eriksson, A., Lundberg, J. O., Alving, K., and Wikström, G. (2011). Increased Plasma and Salivary Nitrite and Decreased Bronchial Contribution to Exhaled NO in Pulmonary Arterial Hypertension. *Eur. J. Clin. Invest.* 41, 889–897. doi:10.1111/J.1365-2362.2011.02488.X

McLaughlin, V., Channick, R. N., Ghofrani, H.-A., Lemarié, J.-C., Naeije, R., Packer, M., et al. (2015). Bosentan Added to Sildenafil Therapy in Patients with Pulmonary Arterial Hypertension. *Eur. Respir. J.* 46, 405–413. doi:10.1183/13993003.02044-2014

Millatt, L. J., Whitley, G. S., Li, D., Leiper, J. M., Siragy, H. M., Carey, R. M., et al. (2003). Evidence for Dysregulation of Dimethylarginine Dimethylaminohydrolase I in Chronic Hypoxia–Induced Pulmonary Hypertension. *Circulation* 108, 1493–1498. doi:10.1161/01.CIR.0000089087.25930.FF

Moncada, S., and Higgs, A. (1993). The L-Arginine-Nitric Oxide Pathway. *N. Engl. J. Med.* 329, 2002–2012. doi:10.1056/nejm199312303292706

Mondéjar-Parreño, G., Moral-Sanz, J., Barreira, B., Cruz, A. D. la., Gonzalez, T., Callejo, M., et al. (2019). Activation of Kv7 Channels as a Novel Mechanism for NO/Cgmp-Induced Pulmonary Vasodilation. *Br. J. Pharmacol.* 176, 2131–2145. doi:10.1111/BPH.14662

Nandi, M., Miller, A., Stidwill, R., Jacques, T. S., Lam, A. A. J., Haworth, S., et al. (2005). Pulmonary Hypertension in a GTP-Cyclohydrolase 1–Deficient Mouse. *Circulation* 111, 2086–2090. doi:10.1161/01.CIR.0000163268.32638.F4

Nathan, C., and Xie, Q. (1994). Nitric Oxide Synthases: Roles, Tolls, and Controls. *Cell* 78, 915–918. doi:10.1016/0092-8674(94)90266-6

Nohria, A., Grunert, M. E., Rikitake, Y., Noma, K., Prsic, A., Ganz, P., et al. (2006). Rho Kinase Inhibition Improves Endothelial Function in Human Subjects with Coronary Artery Disease. *Circ. Res.* 99. doi:10.1161/01.RES.0000251668.39526.c7

Olivieri, M., Talamini, G., Corradi, M., Perbellini, L., Mutti, A., Tantucci, C., et al. (2006). Reference Values for Exhaled Nitric Oxide (Reveno) Study. *Respir. Res.* 7, 1–6. doi:10.1186/1465-9921-7-94

Olsson, K. M., and Hoeper, M. M. (2009). Novel Approaches to the Pharmacotherapy of Pulmonary Arterial Hypertension. *Drug Discov. Today* 14, 284–290. doi:10.1016/J.DRUDIS.2008.12.003

Oudiz, R. J., Brundage, B. H., Gali, N., Ghofrani, H. A., Simonneau, G., Botros, F. T., et al. (2012). Tadalafil for the Treatment of Pulmonary Arterial Hypertension: A Double-Blind 52-Week Uncontrolled Extension Study. *J. Am. Coll. Cardiol.* 60, 768–774. doi:10.1016/J.JACC.2012.05.004

Palmer, R. M. J., Ferrige, A. G., and Moncada, S. (1987). Nitric Oxide Release Accounts for the Biological Activity of Endothelium-Derived Relaxing Factor. *Nature* 327, 524–526. doi:10.1038/327524a0

Pankey, E. A., Badejo, A. M., Casey, D. B., Lasker, G. F., Riehl, R. A., Murthy, S. N., et al. (2012). Effect of Chronic Sodium Nitrite Therapy on Monocrotaline-Induced Pulmonary Hypertension. *Nitric Oxide - Biol. Chem.* 27, 1–8. doi:10.1016/j.niox.2012.02.004

Pernow, J., and Jung, C. (2013). Arginase as a Potential Target in the Treatment of Cardiovascular Disease: Reversal of Arginine Steal? *Cardiovasc. Res.* 98, 334–343. doi:10.1093/CVR/CVT036

Polikandriotis, J. A., Mazzella, L. J., Rupnow, H. L., and Hart, C. M. (2005). Peroxisome Proliferator-Activated Receptor γ Ligands Stimulate Endothelial Nitric Oxide Production through Distinct Peroxisome Proliferator-Activated Receptor γ–Dependent Mechanisms. *Arterioscler. Thromb. Vasc. Biol.* 25, 1810–1816. doi:10.1161/01.ATV.0000177805.65864.D4

Preston, I. R., Hill, N. S., Gambardella, L. S., Warburton, R. R., and Klinger, J. R. (2016). Synergistic Effects of ANP and Sildenafil on cGMP Levels and Amelioration of Acute Hypoxic Pulmonary Hypertension. *Exp. Biol. Med.* 229, 920–925. doi:10.1177/153537020422900908

Price, L. C., Wort, S. J., Perros, F., Dorfmüller, P., Huertas, A., Montani, D., et al. (2012). Inflammation in Pulmonary Arterial Hypertension. *Chest* 141, 210–221. doi:10.1378/CHEST.11-0793

Pulido, T., Adzerikho, I., Channick, R. N., Delcroix, M., Galiè, N., Ghofrani, H.-A., et al. (2013). Macitentan and Morbidity and Mortality in Pulmonary Arterial Hypertension. *N. Engl. J. Med.* 369, 809–818. doi:10.1056/NEJMOA1213917

Rich, S., Kaufmann, E., and Levy, P. S. (2010). The Effect of High Doses of Calcium-Channel Blockers on Survival in Primary Pulmonary Hypertension. *N. Engl. J. Med.* 327, 76–81. doi:10.1056/NEJM199207093270203

Riley, M. S., Pórszósz, J., Miranda, J., Engelen, M. P. K. J., Wasserman, K., and Brundage, B. (1997). Exhaled Nitric Oxide during Exercise in Primary Pulmonary Hypertension and Pulmonary Fibrosis. *Chest* 111, 44–50. doi:10.1378/CHEST.111.1.44

Rosenkranz, S. (2015). Pulmonary Hypertension 2015: Current Definitions, Terminology, and Novel Treatment Options. *Clin. Res. Cardiol.* 104, 197–207. doi:10.1007/s00392-014-0765-4

Rubin, L. J., Badesch, D. B., Fleming, T. R., Galiè, N., Simonneau, G., Ghofrani, H. A., et al. (2011). Long-term Treatment with Sildenafil Citrate in Pulmonary Arterial Hypertension: The SUPER-2 Study. *Chest* 140, 1274–1283. doi:10.1378/CHEST.10-0969

Rybalkin, S. D., Yan, C., Bornfeldt, K. E., and Beavo, J. A. (2003). Cyclic GMP Phosphodiesterases and Regulation of Smooth Muscle Function. *Circ. Res.* 93, 280–291. doi:doi:10.1161/01.RES.0000087541.15600.2B

Sandqvist, A., Henrohn, D., Egeröd, H., Hedeland, M., Wernroth, L., Bondesson, U., et al. (2015). Acute Vasodilator Response to Vardenafil and Clinical Outcome in Patients with Pulmonary Hypertension. *Eur. J. Clin. Pharmacol.* 71, 1165–1173. doi:10.1007/s00228-015-1914-z

Sausbier, M., Schubert, R., Voigt, V., Hirneiss, C., Pfeifer, A., Korth, M., et al. (2000). Mechanisms of NO/cGMP-dependent Vasorelaxation. *Circ. Res.* 27, 825–830. doi:10.1161/01.res.87.9.825

Scalera, F., Martens-Lobenhoffer, J., Bukowska, A., Lendeckel, U., Ta'ger, M., and Bode-Bö'ger, S. M. (2008). Effect of Telmisartan on Nitric Oxide–Asymmetrical Dimethylarginine System. *Hypertension* 51, 696–703. doi:10.1161/HYPERTENSIONAHA.107.104570

Schwappacher, R., Kilic, A., Kojonazarov, B., Lang, M., Diep, T., Zhuang, S., et al. (2013). A Molecular Mechanism for Therapeutic Effects of cGMP-Elevating Agents in Pulmonary Arterial Hypertension. *J. Biol. Chem.* 288, 16557–16566. doi:10.1074/JBC.M113.458729

Seo, B., Oemar, B. S., Siebenmann, R., von Segesser, L., and Lüscher, T. F. (1994). Both ETA and ETB Receptors Mediate Contraction to Endothelin-1 in Human Blood Vessels. *Circulation* 89, 1203–1208. doi:10.1161/01.CIR.89.3.1203

Simonneau, G., Rubin, L. J., Galiè, N., Barst, R. J., Fleming, T. R., Frost, A. E., et al. (2008). Addition of Sildenafil to Long-Term Intravenous Epoprostenol Therapy in Patients with Pulmonary Arterial Hypertension: A Randomized Trial. *Ann. Intern. Med.* 149, 521–530. doi:10.7326/0003-4819-149-8-200810210-00004

Simonneau, G., Rubin, L. J., Galiè, N., Barst, R. J., Fleming, T. R., Frost, A., et al. (2014). Long-Term Sildenafil Added to Intravenous Epoprostenol in Patients with Pulmonary Arterial Hypertension. *J. Hear. Lung Transpl.* 33, 689–697. doi:10.1016/J.HEALUN.2014.02.019

Stasch, J.-P., Becker, E. M., Alonso-Alija, C., Apeler, H., Dembowsky, K., Feurer, A., et al. (2001). NO-independent Regulatory Site on Soluble Guanylate Cyclase. *Nat* 410, 212–215. doi:10.1038/35065611

Stasch, J.-P., Pacher, P., and Evgenov, O. V. (2011). Soluble Guanylate Cyclase as an Emerging Therapeutic Target in Cardiopulmonary Disease. *Circulation* 123, 2263–2273. doi:10.1161/CIRCULATIONAHA.110.981738

Surks, H. K. (2007). cGMP-dependent Protein Kinase I and Smooth Muscle Relaxation: a Tale of Two Isoforms. *Circ. Res.* 26, 1078–1080. doi:10.1161/CIRCRESAHA.107.165779

Tain, Y. L., and Hsu, C. N. (2017). Toxic Dimethylarginines: Asymmetric Dimethylarginine (ADMA) and Symmetric Dimethylarginine (SDMA). *Toxins (Basel).* 9, 92. doi:10.3390/toxins9030092

Tuder, R. M., Abman, S. H., Braun, T., Capron, F., Stevens, T., Thistlethwaite, P. A., et al. (2009). Development and Pathology of Pulmonary Hypertension. *J. Am. Coll. Cardiol.* 54, S3–S9. doi:10.1016/J.JACC.2009.04.009

Tuder, R. M., Marecki, J. C., Richter, A., Fijalkowska, I., and Flores, S. (2007). Pathology of Pulmonary Hypertension. *Clin. Chest Med.* 28, 23–42. doi:10.1016/J.CCM.2006.11.010

Vane, J., and Corin, R. E. (2003). Prostacyclin: A Vascular Mediator. *Eur. J. Vasc. Endovasc. Surg.* 26, 571–578. doi:10.1016/S1078-5884(03)00385-X

Vizza, C. D., Jansa, P., Teal, S., Dombi, T., and Zhou, D. (2017). Sildenafil Dosed Concomitantly with Bosentan for Adult Pulmonary Arterial Hypertension in a Randomized Controlled Trial. *BMC Cardiovasc. Disord.* 17, 1–13. doi:10.1186/S12872-017-0674-3

Wakino, S., Hayashi, K., Kanda, T., Tatematsu, S., Homma, K., Yoshioka, K., et al. (2004). Peroxisome Proliferator-Activated Receptor Ligands Inhibit Rho/Rho Kinase Pathway by Inducing Protein Tyrosine Phosphatase SHP-2. *Circ. Res.* 95. doi:10.1161/01.RES.0000142313.68389.92

Wang, D., Li, H., Weir, E. K., Xu, Y., Xu, D., and Chen, Y. (2019). Dimethylarginine Dimethylaminohydrolase 1 Deficiency Aggravates Monocrotaline-Induced Pulmonary Oxidative Stress, Pulmonary Arterial Hypertension and Right Heart Failure in Rats. *Int. J. Cardiol.* 295, 14–20. doi:10.1016/J.IJCARD.2019.07.078

Wang, Z., Jiang, X., Zhang, X., Tian, G., Yang, R., Wu, J., et al. (2019). Pharmacokinetics-Driven Optimization of 4(3H)-Pyrimidinones as Phosphodiesterase Type 5 Inhibitors Leading to TPN171, a Clinical Candidate for the Treatment of Pulmonary Arterial Hypertension. *J. Med. Chem.* 62, 4979–4990. doi:10.1021/ACS.JMEDCHEM.9B00123

Wharton, J., Davie, N., Upton, P. D., Yacoub, M. H., Polak, J. M., and Morrell, N. W. (2000). Prostacyclin Analogues Differentially Inhibit Growth of Distal and Proximal Human Pulmonary Artery Smooth Muscle Cells. *Circulation* 102, 3130–3136. doi:10.1161/01.CIR.102.25.3130

Yanagisawa, M., Kurihara, H., Kimura, S., Tomobe, Y., Kobayashi, M., Mitsui, Y., et al. (1988). A Novel Potent Vasoconstrictor Peptide Produced by Vascular Endothelial Cells. *Nature* 332, 411–415. doi:10.1038/332411a0

Yang, J., Davies, R. J., Southwood, M., Long, L., Yang, X., Sobolewski, A., et al. (2008). Mutations in Bone Morphogenetic Protein Type II Receptor Cause Dysregulation of Id Gene Expression in Pulmonary Artery Smooth Muscle Cells. *Circ. Res.* 102, 1212–1221. doi:10.1161/CIRCRESAHA.108.173567

Yang, J., Li, X., Al-Lamki, R. S., Wu, C., Weiss, A., Berk, J., et al. (2013). Sildenafil Potentiates Bone Morphogenetic Protein Signaling in Pulmonary Arterial Smooth Muscle Cells and in Experimental Pulmonary Hypertension. *Arterioscler. Thromb. Vasc. Biol.* 33, 34–42. doi:10.1161/ATVBAHA.112.300121

Yang, P., Read, C., Kuc, R. E., Nyimanu, D., Williams, T. L., Crosby, A., et al. (2019). A Novel Cyclic Biased Agonist of the Apelin Receptor, MM07, Is Disease Modifying in the Rat Monocrotaline Model of Pulmonary Arterial Hypertension. *Br. J. Pharmacol.* 176, 1206–1221. doi:10.1111/BPH.14603

Zakrzewicz, D., and Eickelberg, O. (2009). From Arginine Methylation to ADMA: A Novel Mechanism with Therapeutic Potential in Chronic Lung Diseases. *BMC Pulm. Med.* 9, 1–7. doi:10.1186/1471-2466-9-5

Zhang, B., Niu, W., Xu, D., Li, Y., Liu, M., Wang, Y., et al. (2014). Oxymatrine Prevents Hypoxia- and Monocrotaline-Induced Pulmonary Hypertension in Rats. *Free Radic. Biol. Med.* 69, 198–207. doi:10.1016/J.FREERADBIOMED.2014.01.013

Zhang, R., Wang, X.-J., Zhang, H.-D., Sun, X.-Q., Zhao, Q.-H., Wang, L., et al. (2016). Profiling Nitric Oxide Metabolites in Patients with Idiopathic Pulmonary Arterial Hypertension. *Eur. Respir. J.* 48, 1386–1395. doi:10.1183/13993003.00245-2016

Zhang, S., Liu, Y., Guo, S., Zhang, J., Chu, X., Jiang, C., et al. (2010). Vasoactive Intestinal Polypeptide Relaxes Isolated Rat Pulmonary Artery Rings through Two Distinct Mechanisms. *J. Physiol. Sci.* 60, 389–397. doi:10.1007/S12576-010-0107-X

Zhang, T., Lai, Z., Yuan, S., Huang, Y.-Y., Dong, G., Sheng, C., et al. (2020). Discovery of Evodiamine Derivatives as Highly Selective PDE5 Inhibitors Targeting a Unique Allosteric Pocket. *J. Med. Chem.* 63, 9828–9837. doi:10.1021/ACS.JMEDCHEM.0C00983

Zhao, L., Long, L., Morrell, N. W., and Wilkins, M. R. (1999). NPR-A–Deficient Mice Show Increased Susceptibility to Hypoxia-Induced Pulmonary Hypertension. *Circulation* 99, 605–607. doi:10.1161/01.CIR.99.5.605

Zhao, L., Mason, N. A., Strange, J. W., Walker, H., and Wilkins, M. R. (2003). Beneficial Effects of Phosphodiesterase 5 Inhibition in Pulmonary Hypertension Are Influenced by Natriuretic Peptide Activity. *Circulation* 107, 234–237. doi:10.1161/01.CIR.0000050653.10758.6B

Zheng, Z., Yu, S., Zhang, W., Peng, Y., Pu, M., Kang, T., et al. (2017). Genistein Attenuates Monocrotaline-Induced Pulmonary Arterial Hypertension in Rats by Activating PI3K/Akt/Enos Signaling. *Histol. Histopathol.* 32, 35–41. doi:10.14670/HH-11-768

Zhou, C., Chen, Y., Kang, W., Lv, H., Fang, Z., Yan, F., et al. (2019). Mir-455-3p-1 Represses FGF7 Expression to Inhibit Pulmonary Arterial Hypertension through Inhibiting the RAS/ERK Signaling Pathway. *J. Mol. Cel. Cardiol.* 130, 23–35. doi:10.1016/j.yjmcc.2019.03.002

Zuckerbraun, B. S., Shiva, S., Ifedigbo, E., Mathier, M. A., Mollen, K. P., Rao, J., et al. (2010). Nitrite Potently Inhibits Hypoxic and Inflammatory Pulmonary Arterial Hypertension and Smooth Muscle Proliferation via Xanthine Oxidoreductase-dependent Nitric Oxide Generation. *Circulation* 121, 98–109. doi:10.1161/CIRCULATIONAHA.109.891077

Conflict of Interest: The authors declare that the research was conducted in the absence of any commercial or financial relationships that could be construed as a potential conflict of interest.

Publisher's Note: All claims expressed in this article are solely those of the authors and do not necessarily represent those of their affiliated organizations, or those of the publisher, the editors, and the reviewers. Any product that may be evaluated in this article, or claim that may be made by its manufacturer, is not guaranteed or endorsed by the publisher.

frontiers in Pharmacology

ORIGINAL RESEARCH
published: 01 December 2021
doi: 10.3389/fphar.2021.773235

Upregulation of IRF9 Contributes to Pulmonary Artery Smooth Muscle Cell Proliferation During Pulmonary Arterial Hypertension

Yong-Jie Chen[1,2†], Yi Li[1†], Xian Guo[1], Bo Huo[1], Yue Chen[1], Yi He[1], Rui Xiao[3,4], Xue-Hai Zhu[1,5], Ding-Sheng Jiang[1,5]* and Xiang Wei[1,5]**

[1]Division of Cardiothoracic and Vascular Surgery, Sino-Swiss Heart-Lung Transplantation Institute, Tongji Hospital, Tongji Medical College, Huazhong University of Science and Technology, Wuhan, China, [2]Department of Cardiovascular Surgery, Union Hospital, Fujian Medical University, Fuzhou, China, [3]Department of Pathophysiology, School of Basic Medicine, Tongji Medical College, Huazhong University of Science and Technology, Wuhan, China, [4]Key Laboratory of Pulmonary Diseases of Ministry of Health, Tongji Medical College, Huazhong University of Science and Technology, Wuhan, China, [5]Key Laboratory of Organ Transplantation, Ministry of Education; NHC Key Laboratory of Organ Transplantation, Key Laboratory of Organ Transplantation, Chinese Academy of Medical Sciences, Wuhan, China

Abnormal proliferation of pulmonary artery smooth muscle cells (PASMCs) is a critical pathological feature in the pathogenesis of pulmonary arterial hypertension (PAH), but the regulatory mechanisms remain largely unknown. Herein, we demonstrated that interferon regulatory factor 9 (IRF9) accelerated PASMCs proliferation by regulating Prohibitin 1 (PHB1) expression and the AKT-GSK3β signaling pathway. Compared with control groups, the rats treated with chronic hypoxia (CH), monocrotaline (MCT) or sugen5416 combined with chronic hypoxia (SuHx), and mice challenged with CH had significantly thickened pulmonary arterioles and hyperproliferative PASMCs. More importantly, the protein level of IRF9 was found to be elevated in the thickened medial wall of the pulmonary arterioles in all of these PAH models. Notably, overexpression of IRF9 significantly promoted the proliferation of rat and human PASMCs, as evidenced by increased cell counts, EdU-positive cells and upregulated biomarkers of cell proliferation. In contrast, knockdown of IRF9 suppressed the proliferation of rat and human PASMCs. Mechanistically, IRF9 directly restrained PHB1 expression and interacted with AKT to inhibit the phosphorylation of AKT at thr308 site, which finally led to mitochondrial dysfunction and PASMC proliferation. Unsurprisingly, MK2206, a specific inhibitor of AKT, partially reversed the PASMC proliferation inhibited by IRF9 knockdown. Thus, our results suggested that elevation of IRF9 facilitates PASMC proliferation by regulating PHB1 expression and AKT signaling pathway to affect mitochondrial function during the development of PAH, which indicated that targeting IRF9 may serve as a novel strategy to delay the pathological progression of PAH.

Keywords: pulmonary arterial hypertension, pulmonary artery smooth muscle cell, interferon regulator factor 9, mitochondrial function, Akt, Phb1

OPEN ACCESS

Edited by:
Xiaohui Li,
Central South University, China

Reviewed by:
Yunping Mu,
Guangdong University of Technology, China
Bum-Yong Kang,
Emory University, United States
Paul Upton,
University of Cambridge, United Kingdom

***Correspondence:**
Xue-Hai Zhu
13072724207@163.com
Ding-Sheng Jiang
jds@hust.edu.cn
Xiang Wei
xiangwei@tjh.tjmu.edu.cn

[†]These authors have contributed equally to this work

Specialty section:
This article was submitted to Respiratory Pharmacology, a section of the journal Frontiers in Pharmacology

Received: *09 September 2021*
Accepted: *16 November 2021*
Published: *01 December 2021*

Citation:
Chen Y-J, Li Y, Guo X, Huo B, Chen Y, He Y, Xiao R, Zhu X-H, Jiang D-S and Wei X (2021) Upregulation of IRF9 Contributes to Pulmonary Artery Smooth Muscle Cell Proliferation During Pulmonary Arterial Hypertension. Front. Pharmacol. 12:773235. doi: 10.3389/fphar.2021.773235

INTRODUCTION

Pulmonary arterial hypertension (PAH) is a progressive and devastating lung disease that is precipitated by pulmonary arteriole remodeling, ultimately leading to pulmonary vascular resistance and right heart failure (RHF) (Leopold and Maron, 2016). The incidence of PAH ranges from 2.0 to 7.6 cases per million adults per year (Thenappan et al., 2018). Data from American National Institutes of Health (NIH) suggested that the median survival of patients is now 6 years compared with 2.8 years in the 1980s (Thenappan et al., 2010), and the one-year survival rate of PAH patients is 86%, compared with 65% in the 1990s (Rich et al., 1987; Benza et al., 2010). However, even with these recent advances in survival, available treatment approaches are still currently limited, and for the terminal stage of PAH, lung transplantation is the only choice. Therefore, it is urgent to develop a method of molecular targeting therapy that can reverse the pathogenesis of PAH.

PAH is a vasculopathy that is histopathologically characterized by excessive pulmonary vasoconstriction, abnormal arteriole remodeling and plexiform lesions (Schermuly et al., 2011). In these pathological processes, the cellular phenotype of pulmonary artery smooth muscle cells (PASMCs) changes from a quiescent state to a hyperproliferative state (Leopold and Maron, 2016), and the cancer-like phenotype and metabolic shift are closely aligned with the "Warburg effect" (Vander Heiden et al., 2009). In these cells, mitochondrial glucose oxidation is suppressed, whereas glycolysis is utilized as the major source of adenosine triphosphate production (J. Dai et al., 2018). The PI3K/AKT pathway is a main regulator of cell growth and glucose metabolism, the downregulation of which attenuates glucose uptake and utilization in mitochondria so that more biomass and carbon resources are maintained for the rapid biosynthesis that is essential for cell proliferation (Vander Heiden et al., 2009). Therefore, investigating the molecular mechanism of PASMC proliferation during PAH will provide novel insight into the development of medical therapies for PAH.

Growing evidences indicate that interferon therapy may trigger PAH (Al-Zahrani et al., 2003; Jochmann et al., 2005; Ledinek et al., 2009; Dhillon et al., 2010; Savale et al., 2014). Interferon beta (IFN-β) and interferon alpha (IFN-α) were listed among the substances with a possible risk of PAH induction in the guidelines of the European Society of Cardiology and the European Respiratory Society in 2015 (Galiè et al., 2015). The expression of interferons is regulated by interferon regulator factors (IRFs), and our previous results demonstrated that IRFs play critical roles in cardiovascular diseases (Jiang et al., 2013; Jiang et al., 2014a; Zhang et al., 2014a; Jiang et al., 2014b; Jiang et al., 2014c; Jiang et al., 2014d; Zhang et al., 2015). Moreover, we reported that IRF9 promotes VSMC proliferation and neointima formation induced by carotid wire injury (Zhang et al., 2014b). Although both neointima formation and PAH are related to the excessive proliferation of SMCs, the molecular mechanisms regulating neointima formation and PAH are quite different. Thus, it is very interesting to clarify the roles and mechanisms of IRF9 in PAH.

In the present study, we found that the expression level of IRF9 was elevated in the pulmonary arterioles of chronic hypoxia (CH)- induced rats or mice, and also in monocrotaline (MCT)- or sugen5416 combined with chronic hypoxia (SuHx)- induced rats. Overexpression of IRF9 promoted, while IRF9 knockdown inhibited the proliferation of rat PASMCs (RPASMCs) and human PASMCs (HPASMCs). IRF9 achieved these effects by suppressing the expression of PHB1 and AKT signaling pathway. Therefore, our findings reveal a new pathogenesis of PAH and provide a novel target for the treatment of PAH.

MATERIALS AND METHODS

Pulmonary Arterial Hypertension Models

In the present study, the chronic hypoxia-induced PAH animal models were established in male C57BL/6 mice (weighing 20–25 g) and male Sprague-Dawley rats (weighing 180–200 g) as our previous studies descripted (M. Dai et al., 2019; X. Zeng et al., 2017). In brief, for mice PAH models, they were housed in a chamber and exposed to mixed air with 10% O_2, 1% CO_2, and 89% N_2. At 1, 2, 3 or 4 weeks after hypoxia, the mice were sacrificed for the following detection. The control mice were raised in the chamber with air ventilation. The similar procedures were performed to generate the hypoxia-induced PAH model in rats. As for MCT- and SuHx-induced PAH models were generated as we previously reported in rats (Lu et al., 2015; Xiao et al., 2017). Rats were received once subcutaneous administration of MCT at 60 mg/kg per day, the standard dosage in rodent to produce the PAH model. In the SuHx-induced PAH model, rats were injected subcutaneously with 20 mg/ml sugen5416 (HY-10374, MCE; dissolved in 0.5% carboxymethylcellulose, 0.9% NaCl, 0.4% polysorbate, and 0.9% benzyl alcohol in deionized water) once a week and keep in normobaric hypoxia (10% O_2 concentration) for consecutive 3 weeks, after that, the rats were moved into normoxia condition for additional 2 weeks. As for rats in control groups, they were injected with saline intraperitoneally and housed in normoxia condition to the end of modeling. All experimental protocols for mice or rats in this study were approved by the Animal Experimental Ethics Committee of the Tongji Hospital, Tongji Medical College, Huazhong University of Science and Technology. The procedures followed the International Association for the Study of Pain guidelines for animal research and standard biosecurity and institutional safety procedures.

Echocardiography and Hemodynamic Measurements

Right heart function and heart structure are detected by echocardiography. M-mode images derived from the short axis of the right ventricle were recorded using a VisualSonics vevo 1100 imaging system with a 30-MHz probe. The right ventricle internal diameters were obtained from at least three beats and then averaged. After echocardiography experiments,

hemodynamic measurements were conducted as described in our previous study (J. Zhang et al., 2012; Zhu et al., 2016). Briefly, after modeling, rats and mice were intraperitoneally administered 3% mebubarbital, and a catheter was inserted in the trachea and connected to room air. A Millar Mikro-Tip catheter (SRP-671, AD Instruments) was set from the right jugular vein into the right heart to collect right ventricular pressure signal and other relative cardiac parameters. By the end of hemodynamic measurements, pre-warmed saline was injected into pulmonary circulation through the pulmonary artery catheter and drained from the left atrium to wash out the blood. Then the lungs and heart tissues were removed and fixed with formaldehyde solution (10%) for 3 days. The right ventricular hypertrophy was quantified by weighting the right ventricular free wall (RV) and the left ventricle (LV) together with the septum (S, LV + S).

Plasmid Construction

The promoter sequence of human PHB1 gene located between -1,540 and -525 was cloned into the pGL3-basic reporter vector. Full-length human IRF9 and AKT1 CDS sequences were amplified and cloned into the pHAGE-CMV expression vector. Primers of PHB1-promoter: forward 5′-TGCTAGCCC GGGCTCGAGCTCGTGTTCATGGATTGGTG-3′; reverse 5′-TACCGGAATGCCAAGCTTACCAACCGAGAGGAAGGA AT-3′; Primers of IRF9: forward 5′-CCGACGCGTGCCACC ATGGCATCAGGCAGG-3′; reverse 5′- CCGCTCGAGCAC CAGGGACAGAATG-3′; Primers of AKT1: forward 5′-CCG ACGCGTGCCACCATGAGCGACGTGGCT-3′; reverse 5′-CCGCTCGAGGGCCGTGCCGCTGGC-3′. Short hairpin RNAs target to human IRF9 and rattus IRF9 were inserted into PLKO.1 vector. The target sequences are as below: human-IRF9-shRNA#1: GCCATACTCCACAGAATCTTA; rattus-IRF9-shRNA#1: GCAGAACCCTACAAAGTATAT; rattus-IRF9-shRNA#2: GCAGGCCTTTGCCCGAAATTT.

Cells Culturing

The isolation and culturing of primary RPASMCs was described in our previous studies (Guo et al., 2019; Chen et al., 2020). Briefly, after anesthesia with 3% chloral hydrate, the pulmonary arteries of the rats were carefully separated from the lungs chilled in PBS solution. After carefully peeling off the adventitia and endarterium of the pulmonary arteries, pulmonary arteries tissue was cut into fragments less than 1 mm in length, placed in a culture flask, and dried for 30 min, after which 5 ml DMEM/F12 (SH30023.01; HyClone) supplemented with 10% fetal bovine serum (FBS; 1767839; Thermo Fisher Scientific) and 1% penicillin-streptomycin (15140-122; Thermo Fisher Scientific). The cells were digested with trypsin and transferred to Petri dishes from culture flasks after the cells were at an appropriate density (approximately 5–7 days) and passaged every two days.

The human pulmonary artery smooth muscle cells (HPASMCs) purchased from Lonza (Catalog #: CC-2581) were culturing in DMEM/F12 supplemented with 10% fetal bovine serum and 1% penicillin-streptomycin as our previous study (Zhu et al., 2021). After transfecting with indicated lentivirus, HPASMCs of hypoxia group were placed in a special cell incubator with 1% O_2 concentration (cells of normoxia group in incubator with 20% O_2 concentration) for 48 h. After that, the cells were immediately fixed or lysis for follow-up tests.

Drug Treatment and Lentivirus Infection

Cells were infected with Lenti-IRF9-Flag, Lenti-Flag, Lenti-PLKO.1, Lenti-shIRF9-1, or Lenti-shIRF9-2 as previously described (Li et al., 2018; Chen et al., 2020). RPASMCs which had infected with indicated lentivirus were seeded at a concentration of 1.2×10^5 in each 6 cm dish or 3×10^4 in each well of 12-well plates. After starvation for 12 h, the second passage of RPASMCs were treated with MK2206 (0.5 μM, S1078; Selleck) for 24 h, and dosing was repeated for another 24 h after renewing the medium. After total 48 h of treatment, RPASMCs were used for growth curve and EdU incorporation assays.

Immunohistochemistry Staining Analysis

Immunohistochemistry (IHC) staining was performed as described previously (Jiang et al., 2016; Yi et al., 2021). In brief, the paraffin slices were soaked in xylene, 100% ethanol, 95% ethanol and 70% ethanol successively for dewaxing and hydration. After that, the slides were put into EDTA buffer (pH 9.0, MVS-0099, MXB Biotechnologies) and maintained at 100°C for 20 min to retrieve the antigen. The slides were blocked with blocking buffer (5% bovine serum albumin, FA016-100G, Genview) for 30 min at 37°C after treatment with 3% hydrogen peroxide for 40 min. The IRF9 primary antibody (Proteintech, 14167-1-AP, at 1:500 dilution) was added to the slides for incubation overnight at 4°C after removing the blocking solution. The peroxidase-conjugated secondary antibody (Kit-9902, MXB Biotechnologies) was incubated for 30 min at 37°C. A DAB kit (DAB-0031, MXB Biotechnologies) was used to develop the color, and the sections were counterstained with hematoxylin. The slices were mounted with neutral resins (10004160, Sinopharm) after dehydration and observed under the microscope. The intensity of medial IRF9 staining was quantified relative to the area of the medial layer to evaluate the relative expression level of IRF9.

Western Blot Analysis and Antibodies Information

Western blot (WB) analyses were performed as previously described (Jiang et al., 2016; Jiang et al., 2017a; Jiang et al., 2017b; Guo et al., 2019). PASMCs infected with the indicated lentivirus were starved for 12 h before treating with a specific stimulus, such as hypoxia or pharmacological intervention. Total protein was extracted from PASMCs and HPASMCs by RIPA lysis buffer [900 μL RIPA, 20 μL PMSF, 10 μL protease and phosphatase inhibitor cocktail (Thermo Fisher, 78440), 10 μL EDTA solution (AM9260G, Thermo Fisher Scientific), 50 μL NaF, 10 μL Na_3VO_4]. The Pierce™ BCA Protein Assay Kit (23225, Thermo Fisher Scientific) was used to determine the protein concentration. Fifteen micrograms of denatured protein were loaded and separated by SDS-PAGE, and then transferred to a polyvinylidene fluoride (PVDF) membrane (IPVH00010, Millipore). The membrane was incubated with primary

antibodies against IRF9 (14167-1-AP; 1:1,000; rabbit; Proteintech), Flag (F1804; 1:1,000; mouse; Sigma), PCNA (GTX100539; 1:1,000; rabbit; Genetex), p-Histone H3 (sc-8656-R; 1:200; rabbit; Santa Cruz), β-Actin (#8457S; 1:1,000; rabbit; CST), p-p38 (#4511; 1:1,000; rabbit; CST), p38 (#8690; 1:1,000; rabbit; CST), P-ERK1/2 (#4370; 1:1,000; rabbit; CST), ERK1/2 (#4695; 1:1,000; rabbit; CST), DJ-1 (#11315; 1:1,000; rabbit; CST), GPX4 (ab125066; 1:1,000; rabbit; Abcam), PHB1 (#2426; 1:1,000; rabbit; CST), P-AKT^{Thr308} (#13038; 1:1,000; rabbit; CST), P-AKT^{Thr3473} (#4060; 1:1,000; rabbit; CST), AKT (#4685; 1:1,000; rabbit; CST), P-GSK3β (#12456; 1:1,000; rabbit, CST), GSK3β (#5558; 1:1,000; rabbit; CST) overnight at 4°C after blocked with 5% non-fat milk for 90 min at room temperature. Next day, the membrane was incubated with the peroxidase-conjugated secondary antibody (1:10000 dilution, 111-035-003, Jackson ImmunoResearch Laboratories) for 1 h at room temperature. The ChemiDocTM Touch Imaging System (Bio-Rad) was used to detect the protein signals and then analyzed by Image lab software (version 5.2.1, Bio-Rad).

EdU Incorporation Assay

A Cell-Light™ Edu Apollo567 *In Vitro* kit (C10310-1, RiboBio) was used to perform the EdU incorporation assay. After overexpressing and knocking down of IRF9, RPASMCs and HPASMCs were plated in 12-well plates at 3×10^4 cells per well and placed in cell incubators with indicated oxygen concentration (1% for hypoxia and 20% for normoxia) for 48 h. After incubating with 50 μM EdU medium (300 μL per well) for 2 h, the cells were fixed with 4% paraformaldehyde for 30 min and incubated with 2 mg/ml glycine to neutralize paraformaldehyde. After washing with PBS containing 0.5% Triton X-100 for 10 min, cells were incubated with 1× Apollo staining solution for 30 min. Finally, washing the cells with 0.5% Triton X-100 PBS solution again, and cells were incubated with 1× Hoechst 33342 for 30 min at room temperature. Fluorescence images of cells were collected under fluorescence microscope.

CCK-8 Assay

A cell counting kit-8 (CCK-8) assay (CK04, Dojindo, Kumamoto, Japan) was used to assess the proliferation capacity of RPASMCs and HPASMCs. RPASMCs and HPASMCs transfected with indicated lentivirus were treated with hypoxia or normoxia (1% or 20% O_2 concentration) for 48 h and then seeded in 96-well plates at a concentration of 8×10^3 cells per well. After washing with sterile PBS, cells were incubated with WST-8 [2-(2-methoxy-4-nitrophenyl)-3-(4-nitrophenyl)-5-(2,4-disulfophenyl)-2H-tetrazolium, monosodium salt] for 2 h. Then, the optical density value of absorbance at 450 nm was measured.

Real-Time PCR

Real-time PCR was performed as previously reported (Jiang et al., 2014d; Li et al., 2018). Briefly, total mRNA was isolated by using TRI Reagent® Solution (AM9738; ThermoFisher Scientific). Then, the mRNA was reversely transcribed into cDNA by using a transcriptor first strand cDNA synthesis kit (4896866001; Roche). The relative mRNA levels of target genes were detected by CFX connect™ real-time PCR detection system (Bio-Rad) using iQ™SYBR® green supermix (1708884; Bio-Rad) and quantified relative to 18S. Primers used in this study were IRF9 forward primer 5′-TGTAAGCCACTC AGACAGCG-3′ and IRF9 reverse primer 5′-TCCTCTTGAACG GTGGCTTC-3′, DJ-1 forward primer 5′-AGGTTACAGGGA TAGCCAAACA-3′ and DJ-1 reverse primer 5′-CAGGCTCTC AGTGTCAAGCA-3′, GPX4 forward primer 5′-GAACCTGGA CGCCAAAGTCCTA-3′ and GPX4 reverse primer 5′-TTGCTG GTCTGGGGAAGGTC-3′, PHB1 forward primer 5′-CAGAGC GAGCAGCAACATTC-3′ and PHB1 reverse primer 5′-TCT GGCTCTCTCTGCTTCCT-3′, 18S forward primer 5′-CTC AACACGGGAAACCTCAC-3′ and 18S reverse primer 5′-CGCTCCACCAACTAAGAACG-3′.

Luciferase Reporter Assay

HEK293T cells (3×10^4) were seeded in 48-well plates, and when the confluence reached 35%, empty vector or IRF9 overexpression vectors (0.15 μg per well), as well as IRF9 shRNA vectors (0.3 μg per well), were transiently transfected in combination with PHB1 promoter-PGL3 (0.05 μg per well) and TK (0.02 μg per well). After 48 h, cells were lysed, and firefly and Renilla luciferase activities were measured using a dual-luciferase reporter assay kit (E1910, Promega). We calculated relative luciferase activity as the ratio of firefly (PHB1 promoter-PGL3) to Renilla (TK) activity. The experiments were performed in sextuplicate wells.

Co-Immunoprecipitation Assays

Protein interactions between IRF9 and AKT were confirmed via co-immunoprecipitation (Co-IP), and western blotting was conducted with the indicated antibodies after Co-IP. Co-IP was performed in human pulmonary artery smooth muscle cells (HPASMCs) infected with Flag/IRF9-Flag lentivirus or untreated in three 10 cm dishes. Cells were lysed in 1 ml prelysis buffer (20 mM Tris-HCl, pH 7.4, 150 mM NaCl, 1 mM EDTA, 1% Triton X-100) with proteinase inhibitors (HY-K0010, MCE) per sample, and then sonicated (30% power output, 2 s, off 2 s, 15 times). The cell lysate was centrifuged at 12000 rpm at 4°C, for 15 min, and the supernatant was collected. Supernatant (100 μL) was reserved as input. For each immunoprecipitation, 850 μL supernatant was incubated with 1 μg of the indicated antibody and rotated at 4°C overnight. The next day, 35 μL magnetic beads (B23202, Biomake) were added to each sample and further incubated for 3 h in 4°C. Magnetic beads were collected after centrifugation, and the pellets was washing with washing buffer (0.5 M NaCl in prelysis buffer) 4 times. The coprecipitation product was eluted with 80 μL of 1× SDS loading buffer and denatured in 95°C for 15 min.

Mitochondrial Function Evaluation

JC-1 mitochondrial membrane potential assay kit (C2003S, Beyotime) was used to detect the mitochondrial membrane potential. The HPASMCs were transfected with indicated lentivirus and treated with indicated oxygen concentration stimulations as mentioned above were seeded into 24-wells plates. The cells were washed with PBS for once, and

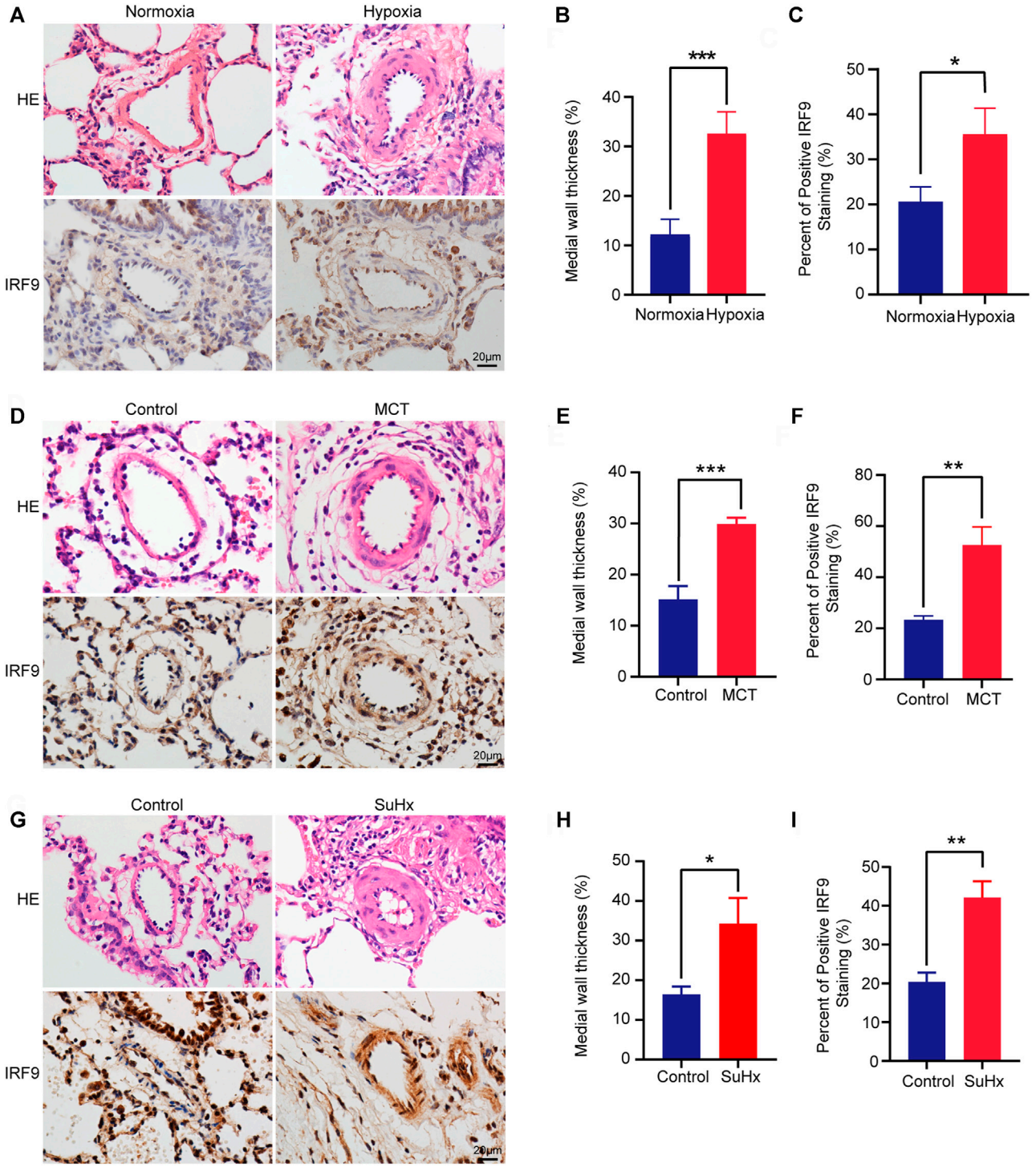

FIGURE 1 | IRF9 expression is upregulated in the thickened medial wall of the pulmonary artery in chronic hypoxia, MCT and SuHx rat PAH models. **(A)** The representative pulmonary arteriole with Haematoxylin and eosin (HE) staining (the upper panel) and immunohistochemical staining of IRF9 (the lower panel) in the lung sections of control group and chronic hypoxia-induced rat PAH model. Scale bar = 20 μm. **(B)** The statistics of medial wall thicknesses [inner diameter/(inner diameter + outside diameter)] of pulmonary arteriole in **(A)** (n = 3 rats per group). **(C)** According to the results of immunohistochemical staining, the intensity of medial IRF9 staining was quantified relative to the area of the medial layer (n = 3 rats per group). **(D–F)** The representative images of pulmonary arteriole with HE and IRF9 staining in MCT-induced rat PAH model **(D)**, quantification of medial wall thicknesses **(E)** and IRF9 expression level **(F)** (Scale bar = 20 μm, n = 3 rats per group). **(G–H)** In control and SuHx-induced rat PAH model, HE staining was used to show the remodeling of the pulmonary arterioles **(G)**, and the degree of thickening is quantified in **(H)**; the expression of IRF9 in the pulmonary arterioles was detected by immunohistochemical staining **(G)** and was quantified **(I)** Scale bar = 20 μm. (n = 3 rats per group). Values are means ± SD; ***p < 0.001, **p < 0.01, *p < 0.05.

incubated with 500 μL staining working buffer per well for 20 min, and the covering liquid was changed to DMEM/F12 after washing cells with staining buffer solution for twice, and the cell-fluorescence were observed by fluorescence microscope.

The mitochondrial permeability transition pore (mPTP) assay kit (C2009S, Beyotime) was used to detect opening of mPTP. After processing accordingly, HPASMCs were seed into 24-wells plates. The cells were incubated with 500 μL fluorescence quenching solution per well for 30 min, and then change the incubated liquid to pre-warmed DMEM/F12 for 30 min under light avoiding condition. The cell-fluorescence were observed under fluorescence microscope after washing with PBS for twice.

Statistical Analysis

The data were analyzed by SPSS (version 22.0.0, SPSS Inc., Chicago, IL, United States) or Prism (version 8.3.0, GraphPad software, LLC) and presented as the mean ± SD, A Two-tailed independent sample *t*-test was used to compare the difference between two groups. One-way or two-way ANOVA was used to compare the differences between three or more groups. $p < 0.05$ was considered statistically significant.

RESULTS

The Expression Level of IRF9 Is Upregulated in the Thickened Pulmonary Arterioles of PAH Rat and Mouse Models

To investigate the involvement of IRF9 in PAH, we generated a variety of PAH models of chronic hypoxia (CH)-induced rats or mice, and monocrotaline (MCT)-, sugen5416 combined with chronic hypoxia (SuHx)-induced rats. The results showed that right ventricle systolic pressure (RVSP), Fulton's mass index (RV/LV + S), right ventricular wall thickness at end-diastole (RVWd), right ventricular wall thickness at end-systole (RVWs), interventricular septal thickness at diastole (IVSd), and interventricular septal thickness at systole (IVSs) were increased in hypoxia-treated rats compared with normoxia-treated rats (**Supplementary Figures S1A–C**), while right ventricular inside diameter at end-diastole (RVIDd) and right ventricular inside diameter at end-systole (RVIDs) showed no significant difference between groups (**Supplementary Figure S1C**). Furthermore, HE staining revealed thickening of the medial layer of pulmonary arterioles in rats after exposure to hypoxia for 4 weeks (**Figures 1A,B**). These results indicated that severe PAH and RHF were induced by hypoxia in rats. Furthermore, a higher IRF9 expression level was observed in the pulmonary arteriole medial wall of hypoxia-treated rats than in normoxia-treated rats (**Figures 1A,C**). Moreover, in MCT- and SuHx-induced PAH rat models, the results of HE staining showed that obvious pulmonary arteriole remodeling was observed (**Figures 1D,E,G,H**). Consistent with hypoxia-induced PAH, IRF9 was increased in pulmonary arteriole of rats treated with MCT or SuHx compared with their counterparts (**Figures 1D,F,G,I**).

Consistently, in a mouse PAH model induced by chronic hypoxia treatment for 4 weeks, RVSP, Fulton's mass index, RVWs, and RVIDs were significantly increased compared with those of the normoxia mice, while comparable diameters of RVWd, RVIDd, IVSd and IVSs were observed between hypoxia- and normoxia-treated mice (**Supplementary Figures S1D–F**). HE staining revealed that the medial wall of pulmonary arterioles in hypoxia-treated mice was remarkably thickened (**Supplementary Figures S1G, H**). More importantly, by using immunohistochemical (IHC) staining, we found that IRF9 expression was increased in a time-dependent manner in the thickened pulmonary arteriole medial wall of mice exposed to hypoxia for 1, 2, 3 and 4 weeks compared with the mice in the normoxia group (**Supplementary Figures S1I, J**).

In addition, compared with normoxia group, the protein level of IRF9 was dramatically increased in HPASMCs treated with 1% oxygen for 6 and 24 h **(Supplementary Figures S2A, B)**.

Hence, our results demonstrated that the expression level of IRF9 was elevated in the thickened medial wall of pulmonary arterioles in multiple stimulations-induced *in vivo* and *in vitro* PAH models, which indicated that IRF9 may be involved in the process of pulmonary arteriole medial wall hyperplasia and PASMC proliferation during PAH formation.

Overexpression of IRF9 Promotes the Proliferation of RPASMCs

Since the expression level of IRF9 was increased in *in vivo* and *in vitro* models of PAH whose major pathological feature is PASMC proliferation, we were curious about whether overexpression of IRF9 induced the proliferation of PASMCs. Thus, to further investigate the function of IRF9 in regulating the proliferation of PASMCs, we constructed IRF9 overexpression plasmids that were transfected into primary RPASMCs via lentiviruses (**Figures 2A,B**). Compared with RPASMCs infected with Lenti-Flag (control), IRF9 overexpression obviously accelerated RPASMC growth after 48 and 72 h of culture under normal oxygen conditions (**Figure 2C**). In addition, the results of EdU incorporation assays and cell counting kit-8 (CCK-8) proliferation assays demonstrated that IRF9 overexpression obviously accelerated the proliferation of RPASMCs (**Figures 2D–F**). Furthermore, western blot analysis showed that the expression levels of proliferating cell nuclear antigen (PCNA) and phosphorylated histone H3 (p-Histone H3) which are the biomarkers of cell proliferation, were elevated in RPASMCs overexpressing IRF9 (**Figures 2G,H**). Together, these results suggested that increased IRF9 expression significantly promoted the RPASMC proliferation.

Knockdown of IRF9 Inhibits the Proliferation of RPASMCs

Next, we generated two different short hairpin RNA plasmids to knockdown IRF9 (shIRF9-1 and shIRF9-2) and tested the expression level of IRF9 in primary RPASMCs after infection with lentiviruses (**Figures 3A,B**). Compared with the control group (Lenti-PLKO.1), both Lenti-shIRF9-1 and Lenti-shIRF9-2 significantly suppressed the growth of RPASMCs, as evidenced by the growth curve (**Figure 3C**). The results of EdU incorporation

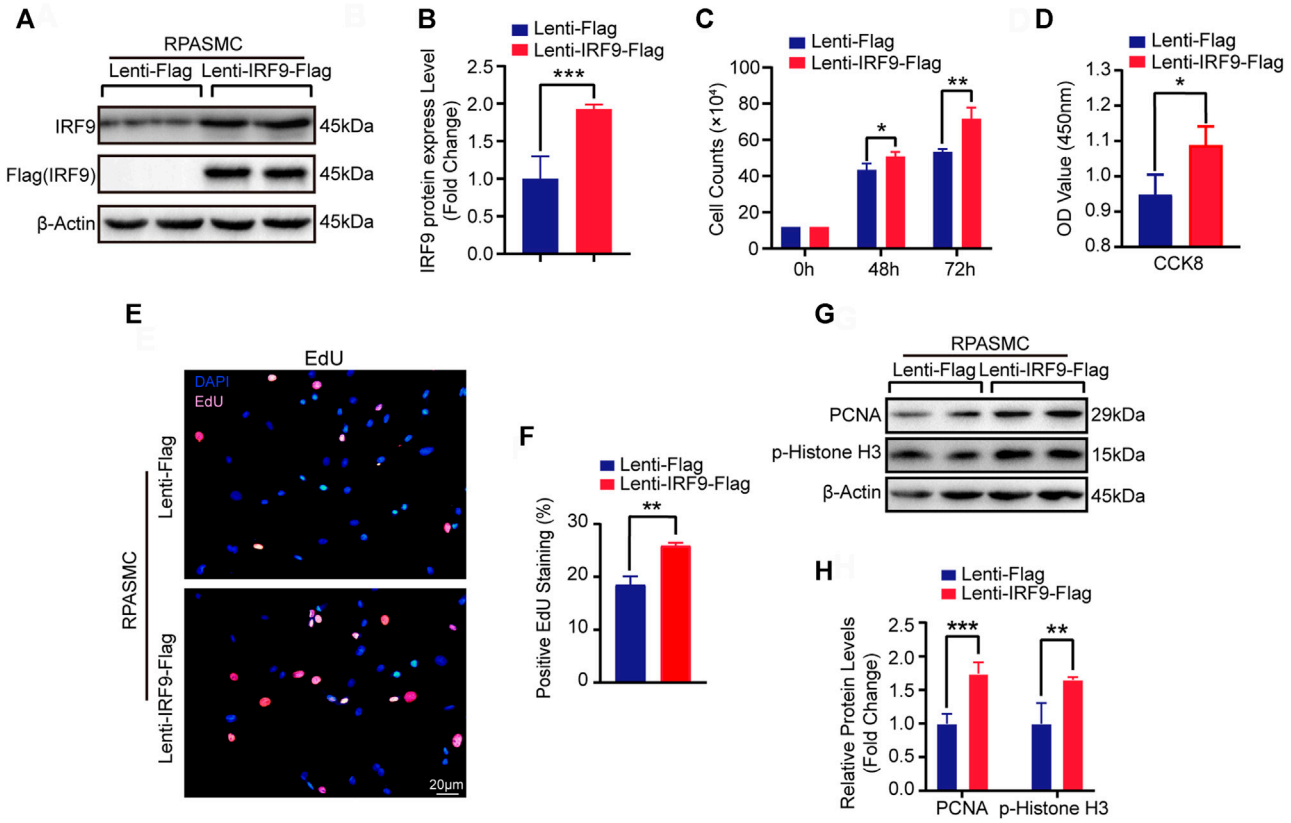

FIGURE 2 | IRF9 overexpression increased the proliferation of RPASMCs. **(A)** After overexpressing IRF9 (Lenti-IRF9-Flag) or not (Lenti-Flag) in RPASMCs, the expression level of IRF9 and the exogenous label protein Flag was determined using western blot ($n = 3$ independent experiments). **(B)** The expression levels of IRF9 were normalized to β-Actin and quantified ($n = 3$ independent experiments). **(C)** Cell numbers were counted at indicated time point after IRF9-overexpressing or not in RPASMCs under normoxia condition ($n = 3$ independent experiments). **(D)** CCK-8 assay was performed and the absorbance (OD value) at 450 nm was measured to shows the proliferation activity of Lenti-Flag and Lenti-IRF9-Flag RPASMCs under normoxia condition ($n = 3$ independent experiments). **(E)** EdU incorporation assay shows the ratio of cells incorporated EdU in Lenti-Flag and Lenti-IRF9-Flag RPASMCs under normoxia condition, in which nuclei were stained with DAPI (blue) and EdU merged with DAPI appears pink. Scale bar = 20 μm. **(F)** The positive EdU staining rates were quantified ($n = 3$ independent experiments). **(G)** The protein levels of proliferation biomarkers PCNA and p-Histone H3 were determined using western blot after overexpressing IRF9 or not in RPASMCs under normoxia condition. **(H)** The expression levels of PCNA and p-Histone H3 were quantified and normalized to β-Actin ($n = 3$ independent experiments). Values are means ± SD; $^{***}p < 0.001$, $^{**}p < 0.01$, $^{*}p < 0.05$.

assay and CCK-8 assay also supported the results that knockdown of IRF9 obviously restrained the proliferation of RPASMCs (**Figures 3D–F**). The expression levels of the proliferation biomarkers PCNA and p-Histone H3 were largely inhibited by IRF9 knockdown (**Figures 3G,H**). These results indicated that inhibition of IRF9 expression could be a novel strategy to retard RPASMC proliferation and alleviate PAH.

IRF9 Facilitates the Proliferation of Human PASMCs

In order to further explore the possibility of IRF9 affecting the occurrence of human PAH, we overexpressed or knocked down IRF9 in HPASMCs (**Figures 4A,B,I,J**). The results showed that compared with Lenti-Flag, IRF9 overexpression remarkably promoted the proliferation of HPASMCs, as evidenced by increased cell numbers (**Figure 4C** and **Supplementary Figure S2C**), cell viability (**Figure 4D** and **Supplementary Figure S2D**), EdU positive cells (**Figures 4E,F** and **Supplementary Figure S2E**), as well as higher protein levels of proliferation biomarkers, PCNA and p-Histone H3 (**Figures 4G,H** and **Supplementary Figure S2F**) under both normoxia and hypoxia conditions. In contrast, the results of cell counting, EdU incorporation assay, CCK8 assay and western blotting for PCNA and p-Histone H3 demonstrated that IRF9 knockdown suppressed the proliferation of HPASMCs treated with normoxia or hypoxia (**Figures 4K–P** and **Supplementary Figures S3A–D**). Therefore, our results suggested that IRF9 may contribute to human PAH by regulating PASMCs proliferation.

IRF9 Interacts With AKT to Affect PASMC Proliferation

Given that many signaling pathways are involved in PAH, such as the mitogen-activated protein kinase (MAPK) and AKT

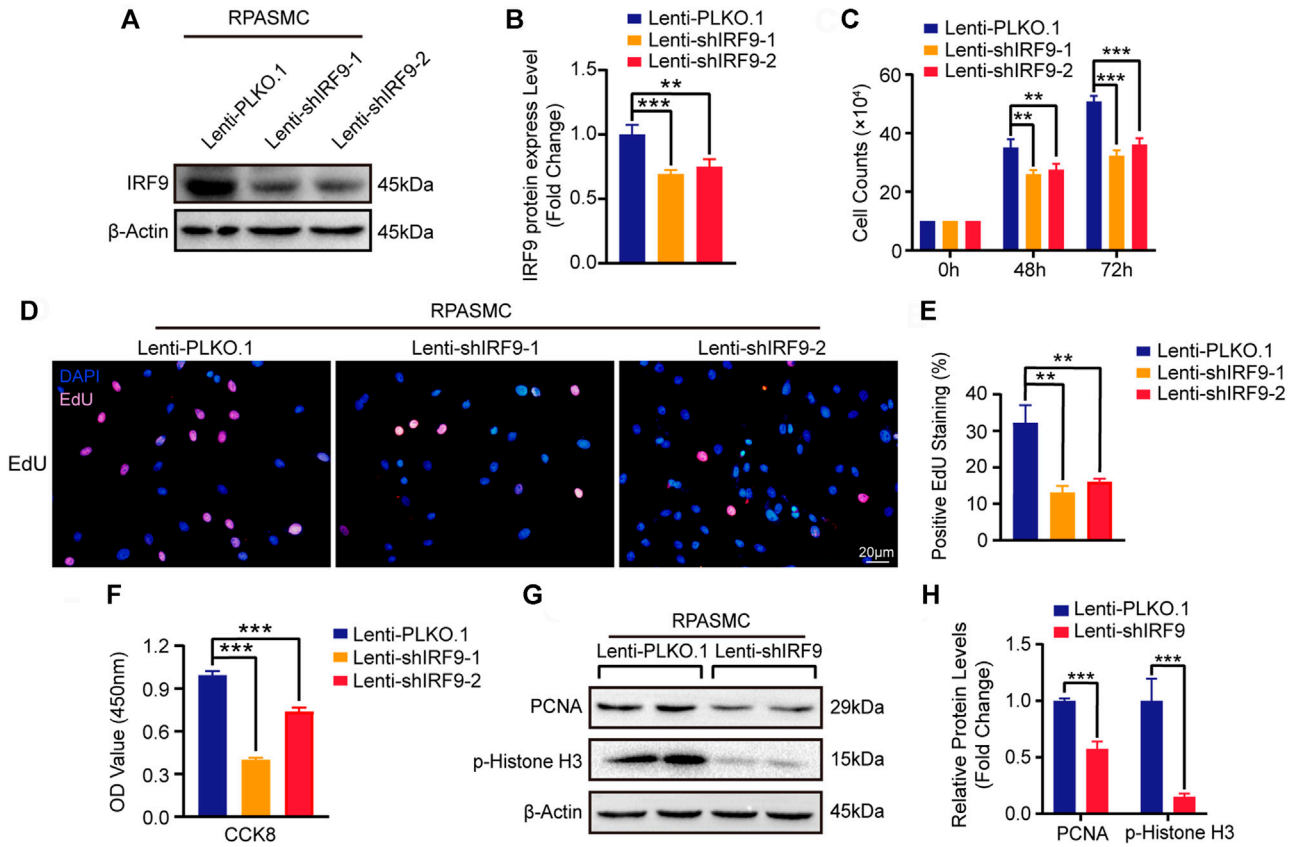

FIGURE 3 | IRF9 knockdown decreases the proliferation of RPASMCs. **(A)** The expression level of IRF9 was verified by western blot after knockdown IRF9 by infected indicated lentiviruses (Lenti-shIRF9-1, Lenti-shIRF9-2) or not (Lenti-PLKO.1) in RPASMCs under normoxia condition. **(B)** The protein level of IRF9 were normalized to β-Actin and quantified (n = 3 independent experiments). **(C)** Cell counting assay shows the count of RPASMCs with Lenti-PLKO.1 or Lenti-shIRF9-1/2 at time point culturing for 0, 48 and 72 h under normoxia condition (n = 3 independent experiments). **(D)** EdU incorporation assay shows the ratio of RPASMCs incorporated with EdU after infected with Lenti-shIRF9-1/2 or Lenti-PLKO.1 under normoxia condition, in which nuclei are stained with DAPI (blue) and incorporated EdU merged with DAPI are shown in pink. Scale bar, 20 μm. **(E)** The positive EdU staining rates were measured (n = 3 independent experiments). **(F)** CCK-8 assay shows the decrease of absorbance at 450 nm which indicate the attenuation of proliferation capacity in Lenti-shIRF9-1/2 RPASMCs comparing to Lenti-PLKO.1 under normoxia condition (n = 3 independent experiments). **(G)** The protein levels of proliferation biomarkers PCNA and p-Histone H3 were determined in IRF9-knockdown RPASMCs in normoxia condition. **(H)** The expression levels of PCNA and p-Histone H3 were normalized to β-Actin and quantified (n = 3 independent experiments). Values are means ± SD; ***p < 0.001, **p < 0.01.

signaling pathways (J. Dai et al., 2018; Y. Guo et al., 2020b), we wondered whether IRF9 could regulate these pathways to affect the proliferation of PASMCs. Thus, we first assessed the phosphorylation levels of ERK1/2 and p38 in RPASMCs, which are the key components of the MAPK signaling pathway. Our results showed that compared with the control group, neither IRF9 overexpression nor IRF9 knockdown affected the phosphorylation levels of either ERK1/2 or p38 in RPASMCs (**Supplementary Figure S4A**). However, IRF9 overexpression significantly inhibited the phosphorylation of AKT^{Thr308} but not AKT^{Ser473}, and its downstream GSK3β was also hypophosphorylated compared with cells infected with Lenti-Flag, and IRF9 knockdown accelerated the phosphorylation of AKT^{Thr308} and GSK3β in both RPASMCs and HPASMCs under normoxia condition (**Figures 5A,B**). Consistent with normoxia treatment, IRF9 inhibited the phosphorylation of AKT^{Thr308} and GSK3β under hypoxia treatment in HPASMCs (**Supplementary Figure S4B**). These results indicated that IRF9 inhibited the AKT-GSK3β signaling pathway in PASMCs under both normoxia and hypoxia conditions.

Next, co-immunoprecipitation (co-IP) was performed to investigate whether IRF9 interacted directly with AKT to regulate the AKT-GSK3β signaling pathway. Our results demonstrated that IRF9 interacted with AKT under both exogenous and endogenous conditions, and *vice versa* (**Figures 5C,D**). Furthermore, MK2206, an inhibitor of the AKT signaling pathway, obviously increased the cell number and EdU positive cells which were inhibited by IRF9 knockdown (**Figures 5E–G**). Thus, these results suggested that IRF9 interacted with AKT and then inhibited the phosphorylation of AKT^{Thr308} and GSK3β to promote the proliferation of PASMCs.

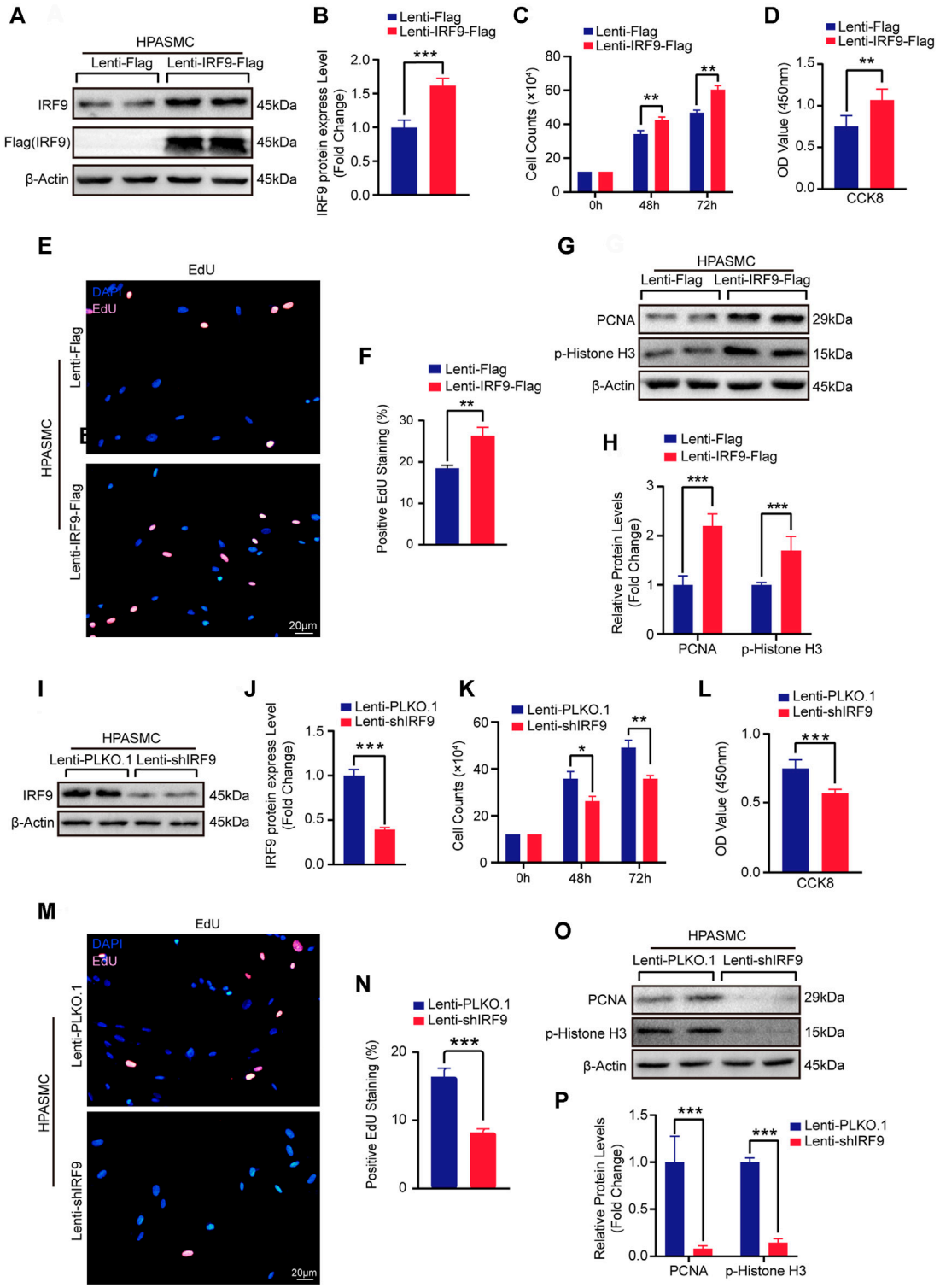

FIGURE 4 | Upregulation of IRF9 accelerate and downregulation attenuate the proliferation of HPASMCs. **(A,B,I and J)** The protein level of IRF9 in HPASMCs with IRF9 overexpression **(A)** or knockdown **(I)** were detected by using western blot (n = 3 independent experiments); the IRF9 protein level was quantified **(B,J)**. **(C,K)** The counts of cell number after HPAMSCs treated with Lenti-IRF9-Flag **(C)** or Lenti-shIRF9 **(K)** for indicated time under normoxia condition; Lenti-Flag and Lenti-PLKO.1 serve as control group (n = 3 independent experiments). **(D,L)** CCK-8 assay shows the absorbances at 450 nm of Lenti-Flag/Lenti-PLKO.1 and Lenti-IRF9-Flag/Lenti-shIRF9 HPASMCs under normoxia condition (n = 3 independent experiments). **(E,M)** EdU incorporation assay of HPASMCs infected with Lenti-Flag/Lenti-IRF9-Flag **(E)** or Lenti-PLKO.1/Lenti-shIRF9 (M) under normoxia condition, in which nuclei were stained with DAPI (blue) and EdU merged with DAPI appears pink. Scale bar,

(*Continued*)

FIGURE 4 | 20 μm. **(F,N)** The positive EdU staining rate was measured in HPASMCs after IRF9 overexpression **(F)** or knockdown (N) (n = 3 independent experiments). **(G,O)** Protein levels of PCNA and p-Histone H3 were determined by western blot after overexpressing (G) or knockdown **(O)** of IRF9 in HPASMCs under normoxia condition. **(H,P)** The expression levels were normalized to β-Actin and quantified (n = 3 independent experiments). β-Actin serves as loading control. Values are means ± SD; $^{***}p < 0.001$, $^{**}p < 0.01$, $^{*}p < 0.05$.

IRF9 Promotes the Proliferation of PASMCs by Downregulating PHB1 Expression

Given that AKT signaling pathway participates in regulating mitochondrial function during PAH development (Robey and Hay, 2009), we were curious about whether IRF9 plays a role in regulating mitochondrial function. Mitochondrial dysfunction contributes to the metabolic transformation of PASMCs from a quiescent state to a hyperproliferative state during PAH (Leopold and Maron, 2016; Vander Heiden et al., 2009; Marshall et al., 2018). Glutathione peroxidase 4 (GPX4) and DJ-1 are involved in the maintenance of mitochondrial reactive oxygen species (ROS) levels, since excessive ROS can damage mitochondria (Gao et al., 2019; J. Zeng et al., 2019). We found that compared with the control, the expression level of DJ-1 was inhibited by IRF9 overexpression but promoted by IRF9 knockdown in both RPASMCs and HPASMCs, and comparable levels of GPX4 were detected in both RPASMCs and HPASMCs with or without IRF9 overexpression or knockdown under normoxia condition (**Figures 6A,B**). Similar results were observed in HPASMCs treated with hypoxia **(Supplementary Figure S5A)**. As IRF9 is a transcript factor (Jiang et al., 2014c), we further detected the mRNA levels of DJ-1 and GPX4. The results showed that neither IRF9 overexpression nor knockdown affected the mRNA levels of GPX4 and DJ-1 (**Figures 6C,D**), which indicated that DJ-1 and GPX4 were not the direct targets regulated by IRF9.

Prohibitin 1 (PHB1) was reported to not only function as a chaperone protein that stabilizes mitochondrial respiratory enzymes and maintains mitochondrial integrity but also have anti-proliferative activity (S. D. Guo SD. et al., 2020; Cao et al., 2020). Thus, we assessed the expression level of PHB1 in RPASMCs and HPASMCs with overexpression or knockdown of IRF9. Our results showed that the protein level of PHB1 was significantly inhibited by IRF9 overexpression but elevated by IRF9 knockdown in both RPASMCs and HPASMCs under normoxia condition (**Figures 6A,B**), as well as in HPASMCs treated with hypoxia **(Supplementary Figure S5A)**. Unlike DJ-1 and GPX4, the mRNA level of PHB1 was obviously suppressed by overexpression of IRF9, but enhanced by IRF9 knockdown (**Figures 6C,D**). Moreover, the results of luciferase reporter gene harboring the promoter region of PHB1 demonstrated that IRF9 can inhibit the expression of PHB1 at transcriptional level (**Figures 6E,F**). Therefore, these results indicated that IRF9 can directly suppress the expression of PHB1.

Given that both AKT signaling pathway and PHB1 were regulators of mitochondrial function, we further evaluated the mitochondrial function by using JC-1 mitochondrial membrane potential assay kit and mitochondrial permeability transition pore (mPTP) assay kit in IRF9 knockdown and overexpressed HPASMCs. The normal cells have high level of mitochondrial membrane potential (MMP) (red fluorescence) and extremely low degree of mPTP opening (abundant green fluorescence). In our results, IRF9 overexpression results in a depolarization and decrease of MMP (green fluorescence) and abnormal opening (quench of green fluorescence) which indicated the damage of mitochondrial function (**Figures 6G,H** and **Supplementary Figures S5B, C**). On the contrary, IRF9 knockdown led to elevation of MMP and decrease of mPTP opening indicating a protecting affection to mitochondrial function under both normoxia and hypoxia condition (**Figures 6I,J** and **Supplementary Figures S2D, E**). Overall, our results demonstrated that IRF9 contributes to mitochondrial dysfunction by inhibiting PHB1 expression to promote the proliferation of PASMCs.

DISCUSSION

Pulmonary vascular remodeling is a common pathophysiological process that occurs in PAH, and the abnormal proliferation of PASMCs upon stimulation by endogenous and exogenous insults is of prime importance in this process (Leopold and Maron, 2016). However, the mechanisms underlying these PASMC responses remain poorly understood. In the present study, we revealed that the IRF9 expression level was elevated in the pulmonary arteriole medial wall of mice and rats exposed to multiple PAH inducers. The proliferation of PASMCs was promoted by overexpression of IRF9 and inhibited by knockdown of IRF9. Furthermore, we found that IRF9 not only directly suppressed PHB1 expression but also interacted with AKT to restrain the phosphorylation of AKT^{Thr308} and GSK3β to affect PASMC proliferation. Based on the results of our present study, we proposed an "IRF9-PHB1-AKT axis" that can be considered a therapeutic target for the prevention of pulmonary vascular remodeling and PAH.

In the search for ways to effectively prevent the progression of PAH, tremendous efforts have been made in recent decades to elucidate the pathogenesis and mechanism of pulmonary vascular remodeling. Remarkably, cases of interferon-induced PAH suggest a causal link between interferon (IFN) exposure and PAH (Al-Zahrani et al., 2003; Jochmann et al., 2005; Ledinek et al., 2009; Dhillon et al., 2010; Savale et al., 2014); subsequently, basic experiments validated the interaction between IFN and PH (Badiger et al., 2012; George et al., 2014). Furthermore, by knocking out the type I interferon receptor [interferon alpha receptor 1 $(IFNAR1)^{(-/-)}$] in mice, *Peter et al.* demonstrated that blocking the type I IFN signaling pathway attenuates the progression of vascular remodeling and right heart failure (George et al., 2014). As a member of the IFN regulator factor (IRF) family, IRF9 is a transcription factor that mediates the type

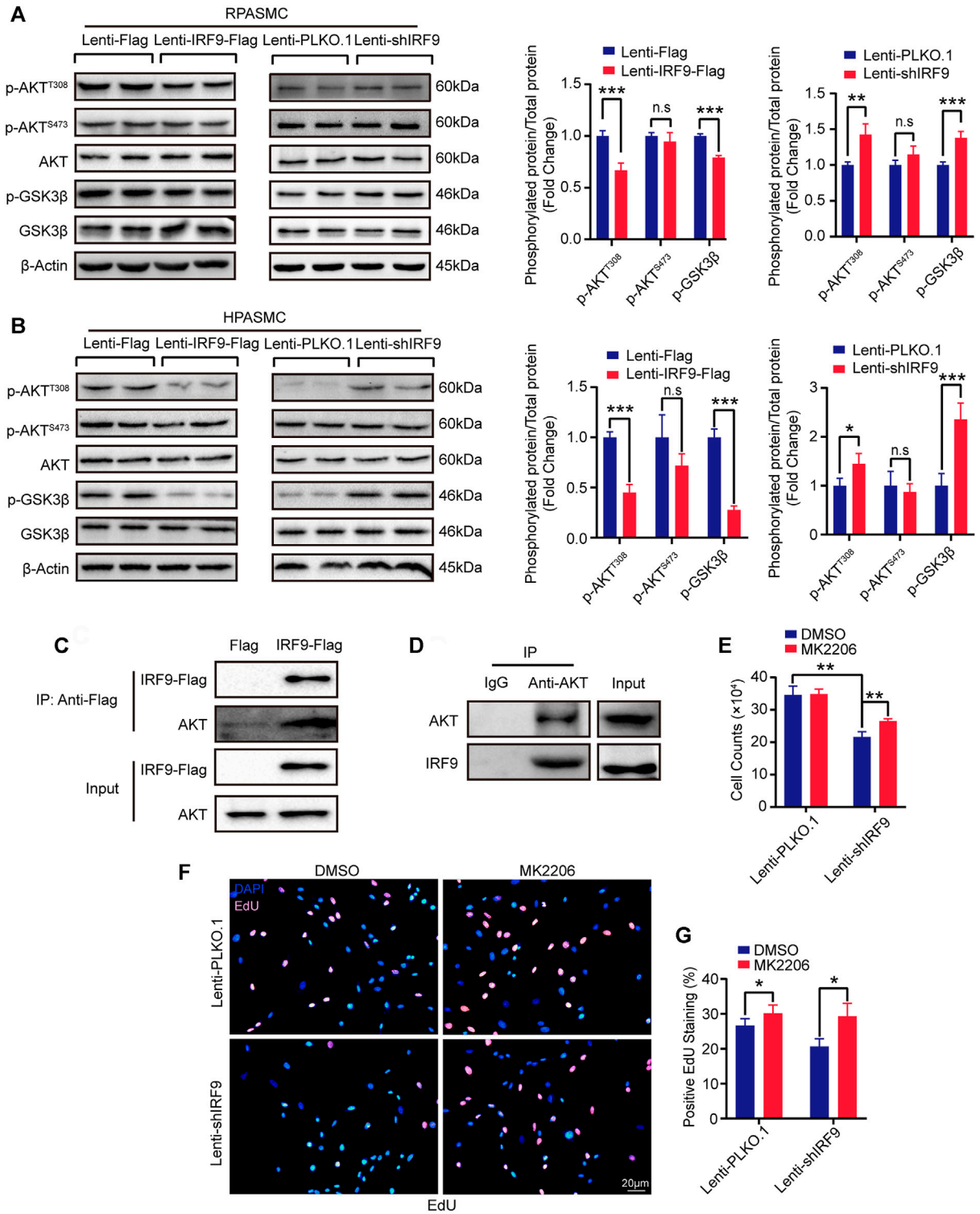

FIGURE 5 | IRF9 regulates PASMC proliferation through the AKT/GSK3β pathway. **(A,B)** Representative western blots **(left panel)** and quantification results **(right panel)** of p-AKT^{T308}, p-AKT^{S473}, AKT, p-GSK3β and GSK3β in IRF9-overexpressed (Lenti-IRF9-Flag) or knocked down (Lenti-shIRF9) RPASMCs **(A)** and HPASMCs **(B)** under normoxia condition. The relative levels of phosphorylated proteins were normalized by their total protein respectively (n = 3 independent experiments). β-Actin serves as loading control. **(C,D)** Co-immunoprecipitation results show that exogeneous IRF9 interacts with endogenous AKT **(C)** and that endogenous AKT interacts with endogenous IRF9 **(D)** in HPASMCs. **(E–G)** The cell counts **(E)**, EdU incorporation staining **(F)** and quantification **(G)** of RPASMCs with IRF9 knockdown (Lenti-shIRF9) or not (Lenti-PLKO.1) treated with MK2206 (AKT phosphorylation inhibitor, 0.5 μM, 48 h) or DMSO; the nuclei were stained with DAPI (blue) and incorporated EdU merged with DAPI appears pink **(F)** (n = 3 independent experiments). Values are means ± SD; ***p < 0.001, **p < 0.01, *p < 0.05, n.s indicates non significance.

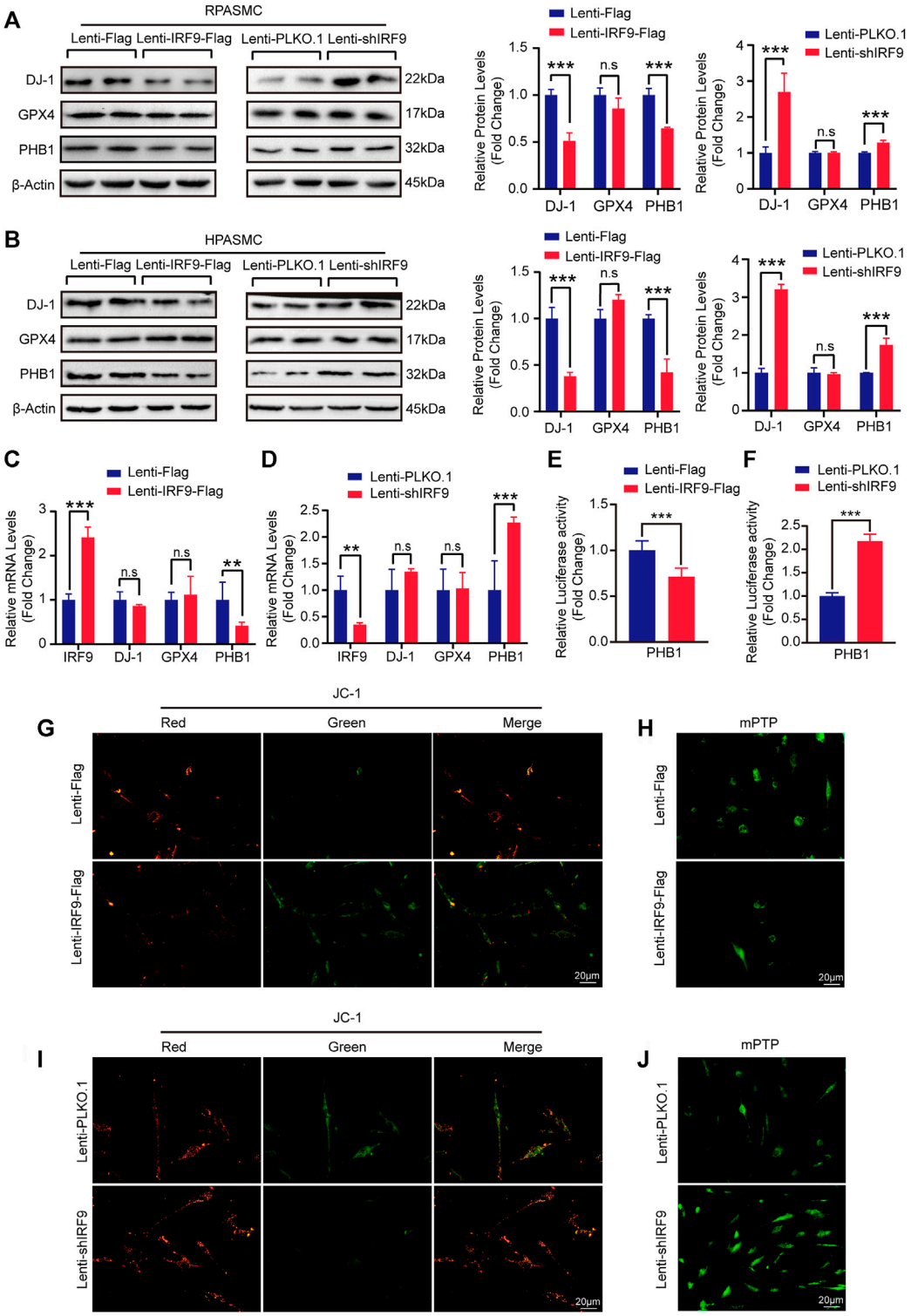

FIGURE 6 | IRF9 affects the mitochondrial function through regulating PHB1 expression. **(A,B)** The protein levels of DJ-1, GPX4 and PHB1 in IRF9-overexpressing (Lenti-IRF9-Flag), IRF9-knockdown (Lenti-shIRF9) and neither (Lenti-Flag/Lenti-PLKO.1) RPASMCs **(A)** and HPASMCs **(B)** were assessed by western blotting **(left panels)** under normoxia condition. Proteins levels were quantified and normalized to β-Actin **(right panels)** (n = 3 independent experiments). **(C,D)** The mRNA levels of IRF9, DJ-1, GPX4 and PHB1 in HPASMCs with IRF9 overexpression **(C)** or knockdown **(D)** were detected by RT-PCR (n = 3 independent experiments). **(E,F)** The luciferase activity controlled by PHB1 promoter was evaluated when IRF9 overexpression **(E)** or knockdown **(F)** (n = 6 independent experiments). **(G,I)** The representative images of mitochondrial membrane potential detected by using JC-1 kit in HPASMCs with IRF9 overexpression **(G)** or knockdown **(I)** under normoxia condition. Scale bar, 20 μm (n = 3 independent experiments). **(H, J)** The openness of mitochondrial permeability transition pore (mPTP) is detected by the mPTP kit in HPASMCs with IRF9 overexpression **(H)** or knockdown **(J)** under normoxia condition, Scale bar, 20 μm (n = 3 independent experiments). Values are means ± SD; $^{***}p < 0.001$, $^{**}p < 0.01$, n.s indicates non significance.

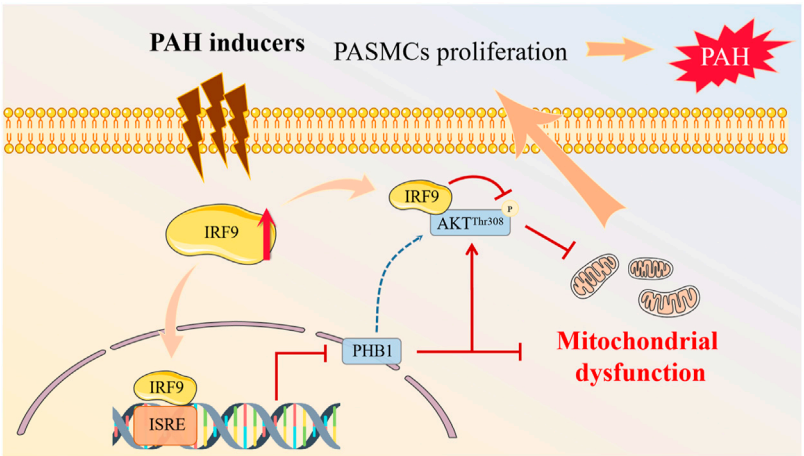

FIGURE 7 | Proposed mechanisms of IRF9 regulates proliferation of PASMCs in PAH. Multiple PAH inducers promote the expression of IRF9. On the one hand, increased IRF9 directly interacts with AKT to regulate the phosphorylation of AKT at T308 site, and on the other hand, IRF9 acts as a transcription factor to inhibit the expression of PHB1, which together leads to mitochondrial dysfunction in PASMCs, which in turn promotes PASMCs proliferation, and ultimately contributes to PAH development.

I IFN gene induction by activating distinct types of innate pattern-recognition receptors (Negishi et al., 2018) and usually plays pivotal roles in the immune response and inflammation (Jefferies, 2019). However, whether IRF9 regulates pulmonary vascular remodeling has never been investigated. In the current study, we explicitly determined that IRF9 expression levels were elevated in chronic hypoxia-, MCT- and SuHx-induced PAH rat models and hypoxia-induced mouse model. Although the related contribution of cells with different origins (for example, endothelial cells and adventitial fibroblasts) to pulmonary vascular remodeling remains to be determined (Schermuly et al., 2011), our results strongly suggested that IRF9 is predominantly involved in regulating arteriole medial smooth muscle layer thickening, and moreover, subsequent functional experiments by overexpressing and knocking down IRF9 in RPASMCs and HPASMCs substantiated that IRF9 is particularly important in PASMC proliferation. Similarly, our previous results also demonstrated that IRF9 facilitated the proliferation of carotid artery SMCs and injury-induced neointima formation, which further validated the results in this study (S. M. Zhang et al., 2014a). These results suggested that IRF9 is a hyperproliferative factor and that targeting IRF9 is a potential treatment for SMC proliferative diseases, such as PAH and coronary restenosis.

Similar to cancer cells, PASMCs in PAH exhibit a metabolic reprogramming referred to as the "Warburg effect", in which the metabolic shift from glucose oxidation toward uncoupled aerobic glycolysis, leads to a hyperproliferative state contributing to the progression of pulmonary vascular remodeling (Peng et al., 2016). As the center of energy metabolism, mitochondria are directly involved in the metabolic shift toward aerobic glycolysis under external stimuli such as hypoxia (Ryan et al., 2015). In addition, mitochondria are also oxygen sensors in lung circulation, altering the cytosolic redox state through the production of reactive oxygen species (ion channels and kinases), which regulate the effectors that mediate hypoxic pulmonary vasoconstriction (Weir et al., 2005). Hence, acquired mitochondrial abnormalities in PASMCs disrupt oxygen sensing and create a pseudo-hypoxic environment, inducing PASMC metabolic reprogramming and pulmonary vasoconstriction and vascular remodeling. As an oxidative stress sensor and as an antioxidant, DJ-1 exhibits the properties of molecular chaperone, protease, and transcriptional regulator that protects mitochondrial function from oxidative stress (Dolgacheva et al., 2019). Although we found that the protein level of DJ-1 was affected by IRF9 in PASMCs, neither IRF9 overexpression nor knockdown altered the mRNA level of DJ-1, which indicated that the protein stability of DJ-1 may indirectly regulated by IRF9.

In humans, PHB1, the N-terminus of which is necessary for mitochondrial localization, maintains the normal function of mitochondria and is implicated in the assembly and activity of the oxidative phosphorylation system (OXPHOS), mitochondrial biogenesis, and mitochondrial networks (Signorile et al., 2019). In the present study we found that IRF9 is the transcription factor regulating PHB1 expression in the process of PASMC proliferation. In cancer cells, depletion of PHB1 causes defects in proliferation (Cheng et al., 2020), but little is currently known about the regulation of PHB1 in pulmonary vascular remodeling and PAH. Here, we fill this knowledge gap by demonstrating that IRF9 negatively regulates PHB1 expression upon PASMC proliferation. Reduced PHB1 expression attenuates the protection of mitochondrial function and disturbs mitochondrial oxidative stress, the oxidative phosphorylation system and the glycolytic metabolic shift, leading to cancer-like hyperproliferation phenotype, ultimately resulting in pulmonary vascular remodeling and PAH.

AKT is considered to be the downstream target of PHB1 in regulating mitochondrial function (X. L. Zhang et al., 2019; Yang et al., 2005; Mishra et al., 2010). Studies on mitochondria regulating energy metabolism show that activation of AKT

increases the total cellular ATP content by content by 2-3-fold (Hahn-Windgassen et al., 2005), and oxygen consumption is elevated in cells expressing activated AKT, but reduced in AKT-deficient cells (Nogueira et al., 2008). In order to serve as original carbon materials for macromolecular synthesis, glucose cannot be committed to carbon catabolism for ATP production. For proliferative cells, a high ATP/ADP ratio is disadvantageous (Vander Heiden et al., 2009), and AKT deficiency induces a reduction in ATP/ADP, which suggests a cellular glucose metabolism shift from aerobic respiration to glycolysis, so that glucose is allowed to provide carbon, nitrogen, and free energy to generate biomass (Vander Heiden et al., 2009). Because of this, AKT is also known as the "Warburg kinase" (Robey and Hay, 2009). In the present study, our results reveal that on the one hand, IRF9 directly regulates the expression of PHB1 and also directly interacts with AKT to inhibit the phosphorylation of AKT at the Thr^{308} site but not at the Ser^{473} site; on the other hand, IRF9 overexpression results in mitochondrial dysfunction by increasing opening of mPTP and mitochondrial permeability. Given the important regulatory role of PHB1 and AKT in mitochondrial function, our results indicated that IRF9 may regulate mitochondrial function and energy metabolism to promote the proliferation of PASMCs in PAH via the IRF9- PHB1-AKT axis.

In summary, we demonstrate that the expression of IRF9 is elevated during PAH development. IRF9 gain-of-function reduces the expression of PHB1 and suppresses the activation of the AKT/GSK3β pathway to promote the proliferation of PASMCs. Our findings shed new light on the role of IRF9 in vascular pathology and implicate a newly identified "IRF9- PHB1-AKT axis" in the pathogenesis of PAH, which provides a new alternative target for the molecular therapy of PAH (**Figure 7**).

DATA AVAILABILITY STATEMENT

The original contributions presented in the study are included in the article/**Supplementary Materials**, further inquiries can be directed to the corresponding authors.

ETHICS STATEMENT

The animal study was reviewed and approved by Committee of Tongji Hospital for Animal Care and Use Tongji Hospital, Tongji Medical College, Huazhong University of Science and Technology.

AUTHOR CONTRIBUTIONS

Y-JC and YL carried out most of the experiments of this study. XG and BH performed the IP and luciferase report assay. XG constructed the plasmid and participated in the design of the study. YC and YH raised and bred the animals and sampled for testing. X-HZ, XW and D-SJ provided funding support. D-SJ conceived of the study, and participated in its design and coordination and helped to draft the manuscript. All authors read and approved the final manuscript.

FUNDING

This work was supported by grants from the National Natural Science Foundation of China (NO. 81670050).

ACKNOWLEDGMENTS

We thank the Integrated Innovative Team for Major Human Diseases Program of Tongji Medical College, HUST for technical assistance during the experiments.

SUPPLEMENTARY MATERIAL

The Supplementary Material for this article can be found online at: https://www.frontiersin.org/articles/10.3389/fphar.2021.773235/full#supplementary-material

REFERENCES

Al-Zahrani, H., Gupta, V., Minden, M. D., Messner, H. A., and Lipton, J. H. (2003). Vascular Events Associated with Alpha Interferon Therapy. *Leuk. Lymphoma* 44 (3), 471–475. doi:10.1080/1042819021000055066

Badiger, R., Mitchell, J. A., Gashaw, H., Galloway-Phillipps, N. A., Foser, S., Tatsch, F., et al. (2012). Effect of Different Interferonα2 Preparations on IP10 and ET-1 Release from Human Lung Cells. *PLoS One* 7 (10), e46779. doi:10.1371/journal.pone.0046779

Benza, R. L., Miller, D. P., Gomberg-Maitland, M., Frantz, R. P., Foreman, A. J., Coffey, C. S., et al. (2010). Predicting Survival in Pulmonary Arterial Hypertension: Insights from the Registry to Evaluate Early and Long-Term Pulmonary Arterial Hypertension Disease Management (REVEAL). *Circulation* 122 (2), 164–172. doi:10.1161/circulationaha.109.898122

Cao, Y. Y., Ba, H. X., Li, Y., Tang, S. Y., Luo, Z. Q., and Li, X. H. (2020). Regulatory Effects of Prohibitin 1 on Proliferation and Apoptosis of Pulmonary Arterial Smooth Muscle Cells in Monocrotaline-Induced PAH Rats. *Life Sci.* 250, 117548. doi:10.1016/j.lfs.2020.117548

Chen, T. Q., Hu, N., Huo, B., Masau, J. F., Yi, X., Zhong, X. X., et al. (2020). EHMT2/G9a Inhibits Aortic Smooth Muscle Cell Death by Suppressing Autophagy Activation. *Int. J. Biol. Sci.* 16 (7), 1252–1263. doi:10.7150/ijbs.38835

Cheng, W. J., Gu, M. J., Ye, F., Zhang, Y. D., Zhong, Q. P., Dong, H. F., et al. (2020). Prohibitin 1 (PHB1) Controls Growth and Development and Regulates Proliferation and Apoptosis in Schistosoma Japonicum. *Faseb j* 34 (8), 11030–11046. doi:10.1096/fj.201902787RRR

Dai, J., Zhou, Q., Chen, J., Rexius-Hall, M. L., Rehman, J., and Zhou, G. (2018). Alpha-enolase Regulates the Malignant Phenotype of Pulmonary Artery Smooth Muscle Cells via the AMPK-Akt Pathway. *Nat. Commun.* 9 (1), 3850. doi:10.1038/s41467-018-06376-x

Dai, M., Xiao, R., Cai, L., Ge, T., Zhu, L., and Hu, Q. (2019). HMGB1 Is Mechanistically Essential in the Development of Experimental Pulmonary Hypertension. *Am. J. Physiol. Cell Physiol* 316 (2), C175–c185. doi:10.1152/ajpcell.00148.2018

Dhillon, S., Kaker, A., Dosanjh, A., Japra, D., and Vanthiel, D. H. (2010). Irreversible Pulmonary Hypertension Associated with the Use of Interferon Alpha for Chronic Hepatitis C. *Dig. Dis. Sci.* 55 (6), 1785–1790. doi:10.1007/s10620-010-1220-7

Dolgacheva, L. P., Berezhnov, A. V., Fedotova, E. I., Zinchenko, V. P., and Abramov, A. Y. (2019). Role of DJ-1 in the Mechanism of Pathogenesis of

Parkinson's Disease. *J. Bioenerg. Biomembr* 51 (3), 175–188. doi:10.1007/s10863-019-09798-4

Galiè, N., Humbert, M., Vachiery, J. L., Gibbs, S., Lang, I., Torbicki, A., et al. (2015). 2015 ESC/ERS Guidelines for the Diagnosis and Treatment of Pulmonary Hypertension: The Joint Task Force for the Diagnosis and Treatment of Pulmonary Hypertension of the European Society of Cardiology (ESC) and the European Respiratory Society (ERS): Endorsed by: Association for European Paediatric and Congenital Cardiology (AEPC), International Society for Heart and Lung Transplantation (ISHLT). *Eur. Respir. J.* 46 (4), 903–975. doi:10.1183/13993003.01032-2015

Gao, M., Yi, J., Zhu, J., Minikes, A. M., Monian, P., Thompson, C. B., et al. (2019). Role of Mitochondria in Ferroptosis. *Mol. Cell* 73 (2), 354–e3. e353. doi:10.1016/j.molcel.2018.10.042

George, P. M., Oliver, E., Dorfmuller, P., Dubois, O. D., Reed, D. M., Kirkby, N. S., et al. (2014). Evidence for the Involvement of Type I Interferon in Pulmonary Arterial Hypertension. *Circ. Res.* 114 (4), 677–688. doi:10.1161/circresaha.114.302221

Guo, S. D., Yan, S. T., Li, W., Zhou, H., Yang, J. P., Yao, Y., et al. (2020a). HDAC6 Promotes Sepsis Development by Impairing PHB1-Mediated Mitochondrial Respiratory Chain Function. *Aging (Albany NY)* 12 (6), 5411–5422. doi:10.18632/aging.102964

Guo, X., Fang, Z. M., Wei, X., Huo, B., Yi, X., Cheng, C., et al. (2019). HDAC6 Is Associated with the Formation of Aortic Dissection in Human. *Mol. Med.* 25 (1), 10. doi:10.1186/s10020-019-0080-7

Guo, Y., Liu, X., Zhang, Y., Qiu, H., Ouyang, F., and He, Y. (2020b). 3-Bromopyruvate Ameliorates Pulmonary Arterial Hypertension by Improving Mitochondrial Metabolism. *Life Sci.* 256, 118009. doi:10.1016/j.lfs.2020.118009

Hahn-Windgassen, A., Nogueira, V., Chen, C. C., Skeen, J. E., Sonenberg, N., and Hay, N. (2005). Akt Activates the Mammalian Target of Rapamycin by Regulating Cellular ATP Level and AMPK Activity. *J. Biol. Chem.* 280 (37), 32081–32089. doi:10.1074/jbc.M502876200

Jefferies, C. A. (2019). Regulating IRFs in IFN Driven Disease. *Front. Immunol.* 10, 325. doi:10.3389/fimmu.2019.00325

Jiang, D. S., Bian, Z. Y., Zhang, Y., Zhang, S. M., Liu, Y., Zhang, R., et al. (2013). Role of Interferon Regulatory Factor 4 in the Regulation of Pathological Cardiac Hypertrophy. *Hypertension* 61 (6), 1193–1202. doi:10.1161/hypertensionaha.111.00614

Jiang, D. S., Li, L., Huang, L., Gong, J., Xia, H., Liu, X., et al. (2014a). Interferon Regulatory Factor 1 Is Required for Cardiac Remodeling in Response to Pressure Overload. *Hypertension* 64 (1), 77–86. doi:10.1161/hypertensionaha.114.03229

Jiang, D. S., Liu, Y., Zhou, H., Zhang, Y., Zhang, X. D., Zhang, X. F., et al. (2014b). Interferon Regulatory Factor 7 Functions as a Novel Negative Regulator of Pathological Cardiac Hypertrophy. *Hypertension* 63 (4), 713–722. doi:10.1161/hypertensionaha.113.02653

Jiang, D. S., Luo, Y. X., Zhang, R., Zhang, X. D., Chen, H. Z., Zhang, Y., et al. (2014c). Interferon Regulatory Factor 9 Protects against Cardiac Hypertrophy by Targeting Myocardin. *Hypertension* 63 (1), 119–127. doi:10.1161/hypertensionaha.113.02083

Jiang, D. S., Wei, X., Zhang, X. F., Liu, Y., Zhang, Y., Chen, K., et al. (2014d). IRF8 Suppresses Pathological Cardiac Remodelling by Inhibiting Calcineurin Signalling. *Nat. Commun.* 5, 3303. doi:10.1038/ncomms4303

Jiang, D. S., Yi, X., Huo, B., Liu, X. X., Li, R., Zhu, X. H., et al. (2016). The Potential Role of Lysosome-Associated Membrane Protein 3 (LAMP3) on Cardiac Remodelling. *Am. J. Transl Res.* 8 (1), 37–48.

Jiang, D. S., Yi, X., Li, R., Su, Y. S., Wang, J., Chen, M. L., et al. (2017a). The Histone Methyltransferase Mixed Lineage Leukemia (MLL) 3 May Play a Potential Role on Clinical Dilated Cardiomyopathy. *Mol. Med.* 23, 196–203. doi:10.2119/molmed.2017.00012

Jiang, D. S., Zeng, H. L., Li, R., Huo, B., Su, Y. S., Fang, J., et al. (2017b). Aberrant Epicardial Adipose Tissue Extracellular Matrix Remodeling in Patients with Severe Ischemic Cardiomyopathy: Insight from Comparative Quantitative Proteomics. *Sci. Rep.* 7, 43787. doi:10.1038/srep43787

Jochmann, N., Kiecker, F., Borges, A. C., Hofmann, M. A., Eddicks, S., Sterry, W., et al. (2005). Long-term Therapy of Interferon-Alpha Induced Pulmonary Arterial Hypertension with Different PDE-5 Inhibitors: a Case Report. *Cardiovasc. Ultrasound* 3, 26. doi:10.1186/1476-7120-3-26

Ledinek, A. H., Jazbec, S. S., Drinovec, I., and Rot, U. (2009). Pulmonary Arterial Hypertension Associated with Interferon Beta Treatment for Multiple Sclerosis: a Case Report. *Mult. Scler.* 15 (7), 885–886. doi:10.1177/1352458509104593

Leopold, J. A., and Maron, B. A. (2016). Molecular Mechanisms of Pulmonary Vascular Remodeling in Pulmonary Arterial Hypertension. *Int. J. Mol. Sci.* 17 (5), 1. doi:10.3390/ijms17050761

Li, R., Yi, X., Wei, X., Huo, B., Guo, X., Cheng, C., et al. (2018). EZH2 Inhibits Autophagic Cell Death of Aortic Vascular Smooth Muscle Cells to Affect Aortic Dissection. *Cell Death Dis* 9 (2), 180. doi:10.1038/s41419-017-0213-2

Lu, A., Zuo, C., He, Y., Chen, G., Piao, L., Zhang, J., et al. (2015). EP3 Receptor Deficiency Attenuates Pulmonary Hypertension through Suppression of Rho/TGF-B1 Signaling. *J. Clin. Invest.* 125 (3), 1228–1242. doi:10.1172/jci77656

Marshall, J. D., Bazan, I., Zhang, Y., Fares, W. H., and Lee, P. J. (2018). Mitochondrial Dysfunction and Pulmonary Hypertension: Cause, Effect, or Both. *Am. J. Physiol. Lung Cell Mol Physiol* 314 (5), L782–l796. doi:10.1152/ajplung.00331.2017

Mishra, S., Ande, S. R., and Nyomba, B. L. (2010). The Role of Prohibitin in Cell Signaling. *Febs j* 277 (19), 3937–3946. doi:10.1111/j.1742-4658.2010.07809.x

Negishi, H., Taniguchi, T., and Yanai, H. (2018). The Interferon (IFN) Class of Cytokines and the IFN Regulatory Factor (IRF) Transcription Factor Family. *Cold Spring Harb Perspect. Biol.* 10 (11), 1. doi:10.1101/cshperspect.a028423

Nogueira, V., Park, Y., Chen, C. C., Xu, P. Z., Chen, M. L., Tonic, I., et al. (2008). Akt Determines Replicative Senescence and Oxidative or Oncogenic Premature Senescence and Sensitizes Cells to Oxidative Apoptosis. *Cancer Cell* 14 (6), 458–470. doi:10.1016/j.ccr.2008.11.003

Peng, H., Xiao, Y., Deng, X., Luo, J., Hong, C., and Qin, X. (2016). The Warburg Effect: A New story in Pulmonary Arterial Hypertension. *Clin. Chim. Acta* 461, 53–58. doi:10.1016/j.cca.2016.07.017

Rich, S., Dantzker, D. R., Ayres, S. M., Bergofsky, E. H., Brundage, B. H., Detre, K. M., et al. (1987). Primary Pulmonary Hypertension. A National Prospective Study. *Ann. Intern. Med.* 107 (2), 216–223. doi:10.7326/0003-4819-107-2-216

Robey, R. B., and Hay, N. (2009). Is Akt the "Warburg Kinase"?Akt-Energy Metabolism Interactions and Oncogenesis. *Semin. Cancer Biol.* 19 (1), 25–31. doi:10.1016/j.semcancer.2008.11.010

Ryan, J., Dasgupta, A., Huston, J., Chen, K. H., and Archer, S. L. (2015). Mitochondrial Dynamics in Pulmonary Arterial Hypertension. *J. Mol. Med. (Berl)* 93 (3), 229–242. doi:10.1007/s00109-015-1263-5

Savale, L., Sattler, C., Günther, S., Montani, D., Chaumais, M. C., Perrin, S., et al. (2014). Pulmonary Arterial Hypertension in Patients Treated with Interferon. *Eur. Respir. J.* 44 (6), 1627–1634. doi:10.1183/09031936.00057914

Schermuly, R. T., Ghofrani, H. A., Wilkins, M. R., and Grimminger, F. (2011). Mechanisms of Disease: Pulmonary Arterial Hypertension. *Nat. Rev. Cardiol.* 8 (8), 443–455. doi:10.1038/nrcardio.2011.87

Signorile, A., Sgaramella, G., Bellomo, F., and De Rasmo, D. (2019). Prohibitins: A Critical Role in Mitochondrial Functions and Implication in Diseases. *Cells* 8 (1), 1. doi:10.3390/cells8010071

Thenappan, T., Ormiston, M. L., Ryan, J. J., and Archer, S. L. (2018). Pulmonary Arterial Hypertension: Pathogenesis and Clinical Management. *Bmj* 360, j5492. doi:10.1136/bmj.j5492

Thenappan, T., Shah, S. J., Rich, S., Tian, L., Archer, S. L., and Gomberg-Maitland, M. (2010). Survival in Pulmonary Arterial Hypertension: a Reappraisal of the NIH Risk Stratification Equation. *Eur. Respir. J.* 35 (5), 1079–1087. doi:10.1183/09031936.00072709

Vander Heiden, M. G., Cantley, L. C., and Thompson, C. B. (2009). Understanding the Warburg Effect: the Metabolic Requirements of Cell Proliferation. *Science* 324 (5930), 1029–1033. doi:10.1126/science.1160809

Weir, E. K., López-Barneo, J., Buckler, K. J., and Archer, S. L. (2005). Acute Oxygen-Sensing Mechanisms. *N. Engl. J. Med.* 353 (19), 2042–2055. doi:10.1056/NEJMra050002

Xiao, R., Su, Y., Feng, T., Sun, M., Liu, B., Zhang, J., et al. (2017). Monocrotaline Induces Endothelial Injury and Pulmonary Hypertension by Targeting the Extracellular Calcium-Sensing Receptor. *J. Am. Heart Assoc.* 6 (4), 1. doi:10.1161/jaha.116.004865

Yang, Y., Gehrke, S., Haque, M. E., Imai, Y., Kosek, J., Yang, L., et al. (2005). Inactivation of Drosophila DJ-1 Leads to Impairments of Oxidative Stress Response and Phosphatidylinositol 3-kinase/Akt Signaling. *Proc. Natl. Acad. Sci. U S A.* 102 (38), 13670–13675. doi:10.1073/pnas.0504610102

Yi, X., Zhou, Y., Chen, Y., Feng, X., Liu, C., Jiang, D. S., et al. (2021). The Expression Patterns and Roles of Lysyl Oxidases in Aortic Dissection. *Front. Cardiovasc. Med.* 8, 692856. doi:10.3389/fcvm.2021.692856

Zeng, J., Zhao, H., and Chen, B. (2019). DJ-1/PARK7 Inhibits High Glucose-Induced Oxidative Stress to Prevent Retinal Pericyte Apoptosis via the PI3K/AKT/mTOR Signaling Pathway. *Exp. Eye Res.* 189, 107830. doi:10.1016/j.exer.2019.107830

Zeng, X., Zhu, L., Xiao, R., Liu, B., Sun, M., Liu, F., et al. (2017). Hypoxia-Induced Mitogenic Factor Acts as a Nonclassical Ligand of Calcium-Sensing Receptor, Therapeutically Exploitable for Intermittent Hypoxia-Induced Pulmonary Hypertension. *Hypertension* 69 (5), 844–854. doi:10.1161/hypertensionaha.116.08743

Zhang, J., Zhou, J., Cai, L., Lu, Y., Wang, T., Zhu, L., et al. (2012). Extracellular Calcium-Sensing Receptor Is Critical in Hypoxic Pulmonary Vasoconstriction. *Antioxid. Redox Signal.* 17 (3), 471–484. doi:10.1089/ars.2011.4168

Zhang, S. M., Zhu, L. H., Chen, H. Z., Zhang, R., Zhang, P., Jiang, D. S., et al. (2014a). Interferon Regulatory Factor 9 Is Critical for Neointima Formation Following Vascular Injury. *Nat. Commun.* 5, 5160. doi:10.1038/ncomms6160

Zhang, S. M., Zhu, L. H., Li, Z. Z., Wang, P. X., Chen, H. Z., Guan, H. J., et al. (2014b). Interferon Regulatory Factor 3 Protects against Adverse Neo-Intima Formation. *Cardiovasc. Res.* 102 (3), 469–479. doi:10.1093/cvr/cvu052

Zhang, X. J., Jiang, D. S., and Li, H. (2015). The Interferon Regulatory Factors as Novel Potential Targets in the Treatment of Cardiovascular Diseases. *Br. J. Pharmacol.* 172 (23), 5457–5476. doi:10.1111/bph.12881

Zhang, X. L., Wang, Z. Z., Shao, Q. H., Zhang, Z., Li, L., Guo, Z. Y., et al. (2019). RNAi-Mediated Knockdown of DJ-1 Leads to Mitochondrial Dysfunction via Akt/GSK-3ß and JNK Signaling Pathways in Dopaminergic Neuron-like Cells. *Brain Res. Bull.* 146, 228–236. doi:10.1016/j.brainresbull.2019.01.007

Zhu, L., Liu, F., Hao, Q., Feng, T., Chen, Z., Luo, S., et al. (2021). Dietary Geranylgeranyl Pyrophosphate Counteracts the Benefits of Statin Therapy in Experimental Pulmonary Hypertension. *Circulation* 143 (18), 1775–1792. doi:10.1161/circulationaha.120.046542

Zhu, L., Zhang, J., Zhou, J., Lu, Y., Huang, S., Xiao, R., et al. (2016). Mitochondrial Transplantation Attenuates Hypoxic Pulmonary Hypertension. *Oncotarget* 7 (31), 48925–48940. doi:10.18632/oncotarget.10596

Conflict of Interest: The authors declare that the research was conducted in the absence of any commercial or financial relationships that could be construed as a potential conflict of interest.

Publisher's Note: All claims expressed in this article are solely those of the authors and do not necessarily represent those of their affiliated organizations or those of the publisher, the editors, and the reviewers. Any product that may be evaluated in this article, or claim that may be made by its manufacturer, is not guaranteed or endorsed by the publisher.

frontiers in Pharmacology

ORIGINAL RESEARCH
published: 01 December 2021
doi: 10.3389/fphar.2021.756131

Inhibition of Sirt2 Alleviates Fibroblasts Activation and Pulmonary Fibrosis *via* Smad2/3 Pathway

Hui Gong[1], *Chenyi Zheng*[1], *Xing Lyu*[2], *Lini Dong*[1], *Shengyu Tan*[1] *and Xiangyu Zhang*[1]*

[1]Department of Geriatrics, The Second Xiangya Hospital, Central South University, Changsha, China, [2]Laboratory of Clinical Medicine, The Second Xiangya Hospital, Central South University, Changsha, China

Idiopathic pulmonary fibrosis (IPF) is a fatal disease with unknown cause and limited treatment options. Its mechanism needs to be further explored. Sirtuin2 (Sirt2), a nicotinamide adenine dinucleotide (NAD)-dependent deacetylase, has been proved to be involved in the fibrosis and inflammation in the liver, kidney and heart. In this study, we aimed to evaluate the role of Sirt2 in pulmonary fibrosis. We found that Sirt2 expression was upregulated in transforming growth factor-β1 (TGF-β1) treated human embryonic lung fibroblasts. Sirt2 inhibitor AGK2 or the knockdown of Sirt2 expression by targeting small interfering RNA (siRNA) suppressed the fibrogenic gene α-SMA and Fibronectin expression in TGF-β1 treated fibroblasts and primary lung fibroblasts derived from patients with IPF. In addition, Sirt2 inhibition suppresses the phosphorylation of Smad2/3. Co-immunoprecipitation (Co-IP) showed that there is interaction between Sirt2 and Smad3 in the TGF-β1 treated lung fibroblasts. In bleomycin-induced pulmonary fibrosis in mice, AGK2 treatment significantly mitigated the degree of fibrosis and decreased the phosphorylation of Smad2/3. These data suggest that Sirt2 may participate in the development of IPF *via* regulating the Smad2/3 pathway. Inhibition of Sirt2 would provide a novel therapeutic strategy for this disease.

Keywords: Sirtuin2, pulmonary fibrosis, fibroblast activation, AGK2, Smad2/3

OPEN ACCESS

Edited by:
Xiaohui Li,
Central South University, China

Reviewed by:
Rajasekaran Subbiah,
ICMR-National Institute for Research in Environmental Health, India
Haiyang Tang,
University of Arizona, United States

***Correspondence:**
Xiangyu Zhang
xiangyuzhang@csu.edu.cn

Specialty section:
This article was submitted to Respiratory Pharmacology, a section of the journal Frontiers in Pharmacology

Received: *10 August 2021*
Accepted: *10 November 2021*
Published: *01 December 2021*

Citation:
Gong H, Zheng C, Lyu X, Dong L, Tan S and Zhang X (2021) Inhibition of Sirt2 Alleviates Fibroblasts Activation and Pulmonary Fibrosis via Smad2/3 Pathway. Front. Pharmacol. 12:756131. doi: 10.3389/fphar.2021.756131

INTRODUCTION

Idiopathic pulmonary fibrosis (IPF) is a devastating disease with increasing morbidity, and the median survival of the patients is only 3–5 years after diagnosis (Chanda et al., 2019). There is no effective treatment for this disease (Noble et al., 2012). The pathogenesis of IPF remains unclear. Aberrant activation and differentiation of fibroblasts to myofibroblasts plays a critical role in the development of this disease (Wynn and Ramalingam, 2012; Selman and Pardo, 2014; Meiners et al., 2015). Myofibroblast differentiation is induced by various cytokines and chemokines (Ballester et al., 2019), among these, transforming growth factor-β1 (TGF-β1) is a well-documented mediator (Meng et al., 2016; Morikawa et al., 2016). Myofibroblasts are characterized by the expression of α-smooth muscle actin (α-SMA), excessive accumulation of extracellular matrix (ECM) components including Fibronectin and collagen, which would form fibrotic scars and eventually lead to the loss of tissue function (Wynn, 2008). Understanding the molecular mechanisms of lung fibroblasts activation is important for developing new anti-fibrotic agents.

Accumulating evidence supports the role of epigenetic alterations including histone acetylation in the pathogenesis of IPF (O'Reilly, 2017; Wallner et al., 2020; Jones et al., 2019). Histone acetylation is regulated by histone deacetylases (HDACs) and histone acetylases (HATs) (Drazic et al., 2016).

Sirtuins are Class III HDACs that are nicotinamide adenine dinucleotide (NAD^+) dependent deacetylase (Imai and Guarente, 2014), including seven members (Sirtuin 1–7) (Gomes et al., 2019). The cytosol member Sirtuin 2 (Sirt2) is widely expressed in almost all mammalian organs. Previous studies suggest that Sirt2 is involved in inflammatory response and fibrosis progress in different organs, including kidney, heart and liver, however, its role is controversial (Ponnusamy et al., 2014; Arteaga et al., 2016; Tang et al., 2017). For instance, Sirt2 acts as a cardio-protective deacetylase in aging-related and angiotensin II (Ang II)-induced cardiac fibrosis and hypertrophy, and loss of Sirt2 promotes these pathological changes (Tang et al., 2017). While in hepatic and renal fibrosis, Sirt2 demonstrated the pro-fibrogenesis characteristics, blocking Sirt2 inhibited the activation of hepatic stellate cells and renal interstitial fibroblasts, and suppressed hepatic and renal fibrosis (Ponnusamy et al., 2014; He et al., 2018). It is noteworthy that a study involving triple antigen induced-allergic eosinophilic asthma has proved a stimulatory role of Sirt2 on the recruitment of eosinophils. This indicates a pro-inflammatory effect of Sirt2 in pulmonary microenvironment (Lee et al., 2019). The role of Sirt2 in pulmonary fibrosis remains elusive.

In the current study, we evaluated the role of Sirt2 in TGF-β1 induced lung fibroblasts activation and bleomycin induced pulmonary fibrosis in mice. Our findings indicated for the first time that the expression of Sirt2 is increased in TGF-β1- activated lung fibroblasts and fibrotic lung tissues of mice induced by bleomycin. Sirt2 inhibition suppressed the fibrogenic gene α-SMA and Fibronectin expression in TGF-β1 treated lung fibroblasts and primary lung fibroblasts derived from patients with IPF. In addition, Sirt2 inhibition suppresses the phosphorylation of Smad2/3. Co-immunoprecipitation demonstrated the interaction between Sirt2 and Smad3 in lung fibroblasts. In animal model, inhibition of Sirt2 alleviated pulmonary fibrosis and reduced the phosphorylation of Smad2/3 induced by bleomycin.

MATERIALS AND METHODS

Cell Culture and Treatment

The human embryonic lung fibroblasts (MRC-5) used in this study were purchased from the Chinese academy of sciences (Cat. no. GNHu41, Shanghai, China). Human primary IPF lung fibroblasts were purchased from The Global Bioresource Center (ATCC® CCL-134™, United States). In TGF-β1 concentration-dependent assay, when the MRC-5 reached 80% confluence, the growth medium was changed to serum free medium overnight; then the cells were treated with Recombinant human TGF-β1 (R&D Systems, Minneapolis, MN) at 0, 1, 2, 5, and 10 ng/ml for 24 h. In the time-dependent test, the cells were cultured for a period of 0, 3, 6, 12, 24, and 48 h at 2 ng/ml TGF-β1. In Sirt2 inhibition study, MRC-5 cells were treated with TGF-β1 at 2 ng/ml for 24 h, and then added 10 μM AGK2 (an inhibitor of Sirt2) (MCE, HY-100578) or vehicle control (dimethyl sulfoxide, a AGK2 solvent) for another 24 h in the presence of TGF-β1.

TABLE 1 | Primers used in the real-time RT-PCR.

Gene name	Sequence
Sirt2	F: 5′-TGCGGAACTTATTCTCCCAGA-3′
	R: 5′-GAGAGCGAAAGTCGGGGAT-3′
Fibronectin	F: 5′-TCGCTTTGACTTCACCACCAG-3′
	R: 5′-CCTCGCTCAGTTCGTACTCCAC-3′
α-SMA	F: 5′- CTATGAGGGCTATGCCTTGCC-3′
	R: 5′-GCTCAGCAGTAGTAACGAAGGA-3′
β-actin	F: 5′-CTGTCCCTGTATGCCTCTG-3′
	R: 5′-ATGTCACGCACGATTTCC-3′
GAPDH	F: 5′-CCCATGTTCGTCATGGGTGT-3′
	R: 5′-TGGTCATGAGTCCTTCCACGATA-3′

RNA Extraction and Real-Time RT-PCR

RNA was extracted with a RNeasy® Mini kit (Qiagen GmbH, Hilden, Germany), and converted into cDNA using a Revert Aid First stand cDNA synthesis Kit (Thermo Scientific, United States). Real-time PCR was performed using a SYBR Green/qPCR Master Mix kit according to the manufacturer's instructions (Thermo Scientific, United States). Real-time RT-PCR was performed in triplicate and normalized to GAPDH or β-actin with the $\Delta\Delta$Ct method. Primers are listed in **Table 1**.

Western Blot Analysis

Whole cell lysates were collected with RIPA Lysis Buffer containing protease and phosphatase inhibitor mixture. The total protein concentration of the lysates was quantified using a Micro BCA Protein Assay Kit (Thermo Scientific, United States). The same amount of protein was electrophoresed on 10% SDS-PAGEs and Western immunoblotting was performed according to the manufacturer's instructions. Immunoblots were imaged using an Amersham Biosciences 600 imager. Quantification of protein expression for all blots was performed using ImageJ software. Primary antibodies Sirt2 (1:1000; #9787), α-SMA (1:1000; #19245), Fibronectin (1:1000; #26836), phospho-Smad2 (1:1000; #3108), phospho-Smad3 (1:1000; #9520), Smad2/3 (1:1000; #8685), GAPDH (1:1000; #2118), β-actin (1:1000; #4970), and horseradish peroxidase-conjugated secondary antibody (1:5000; #7074) were all from Cell Signaling Technology.

Immunofluorescence Staining

MRC-5 cells were cultured on coverslips as described previously with or without 10 μM AGK2 in the presence of TGF-β1 for 24 h. The cells were fixed with 4% paraformaldehyde for 15 min at room temperature, permeabilized with 0.1% Triton X-100 for 10 min, blocked with 10% normal goat serum and incubated with anti-Fibronectin (1:400) or anti-α-SMA (1:400) followed by Alexa Fluor 558 goat anti-rabbit secondary antibody (1:1000). Fluorescence images were collected on a fluorescence microscope.

Small Interfering RNA Transfections

When MRC-5 cells and IPF lung fibroblasts grew to 70–80% confluence, the cells were transfected with negative control small interfering RNA (NC siRNA) or Sirt2 targeted siRNA (Sirt2 siRNA) (Santa Cruz Biotechnology, sc-40988, Inc. United States) using lipofectamine® 3000 (Invitrogen,

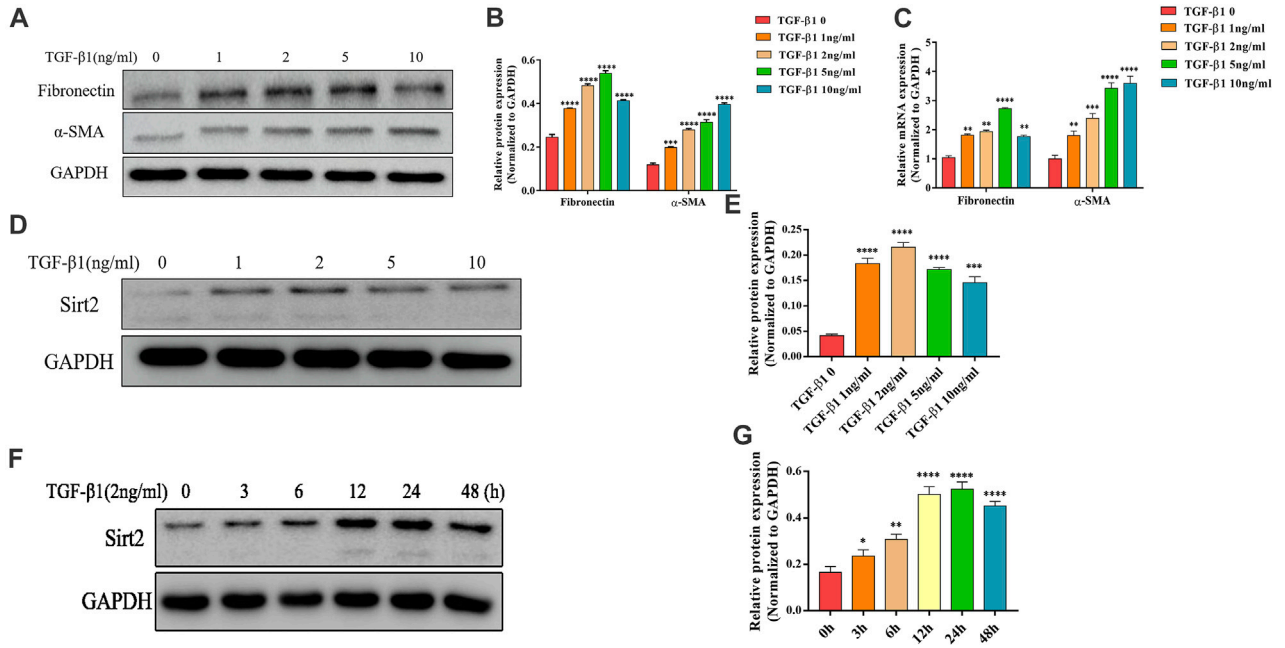

FIGURE 1 | Sirt2 expression is increased in TGF-β1 stimulated lung fibroblasts. **(A,D)** Expression of Fibronectin, α-SMA and Sirt2 proteins detected by Western blot in MRC-5 cells treated with 0 (control), 1, 2, 5, and 10 ng/ml TGF-β1 for 24 h **(B,E)** Densitometric analyses of the Western blot in **(A,D)**. **(C)** Expression of Fibronectin and α-SMA mRNA detected by real-time RT-PCR in MRC-5 cells treated with 0 (control), 1, 2, 5, and 10 ng/ml TGF-β1 for 24 h. **(F)** Expression of Sirt2 protein detected by Western blot in MRC-5 after 2 ng/ml TGF-β1 exposure for 0, 3, 6, 12, 24, and 48 h. **(G)** Densitometric analyses of the Western blot in **(F)**. GAPDH was used as a loading control. The bars indicated mean ± SD of three separate experiments. $^{*}p < 0.05$, $^{**}p < 0.01$, $^{***}p < 0.001$, $^{****}p < 0.0001$ compared to the control.

Carlsbad, CA, United States) according to manufacturer's instructions. After 24 h transfection, the medium was changed, and cells were incubated for another 24 h in the absence or presence of 2 ng/ml TGF-β1. The efficiency of transfection was evaluated by Sirt2 mRNA and protein expression using quantitative real-time RT-PCR and Western blot.

Co-Immunoprecipitation

Co-IP was carried out with IP/Co-IP Kit (88,804; Thermo Fisher Scientific, United States). Pierce protein A/G-Agarose beads were washed using 100 µl antibody binding and washing buffer to wash. Beads were collected and gently rotated with rabbit anti-Sirt2 (1:20, ab211033, Abcam) or rabbit IgG (1:20, ab6715, Abcam) antibodies for 10 min after supernatant was removed. Subsequently, incubate the antibody-beads complex with 400 µg total protein from hypotonic lysis buffer for 5 min. The supernatant was removed and the antibody-protein-beads complex was washed 3 times using washing buffer. The supernatant was removed again and the antibody-protein beads complex was gently resuspended with 100 µl elution buffer for 2 min. The sample was separated and subjected to Western blot analysis.

Experimental Mice Model of Pulmonary Fibrosis

Animal studies were approved by the Animal Ethics Committee of the Second Xiangya Hospital, Animal Center of Central South University (Approval No. 2021026). 6-8-week-old healthy C57BL/6 mice (male, 20–25 g) were randomly divided into three experimental groups: control group (n = 6, with saline treatment), bleomycin (BLM) group (n = 6, with BLM treatment), and BLM + AGK2 group (n = 6, with BLM/AGK2 co-treatment). A single dose of bleomycin sulfate at 1.5 U/kg body weight was conveyed *via* transtracheal injection. AGK2 in dimethyl sulfoxide solution was administered via daily intraperitoneal injection for successive 7 days at 50 mg/kg, starting at day 14 post-bleomycin injury. Mice were sacrificed on day 21 post bleomycin injury, and the lung tissues were prepared for Western blot and histology.

Histological Staining and Immunohistochemical Staining

Lung tissues were fixed with 4% paraformaldehyde for 24 h and underwent dehydration by alcohol of different concentration. Tissues were embedded into paraffin and placed at room temperature for 24 h, then cut into 5 µm sections. Haematoxylin-eosin (HE) staining kit (cat. no. C0109; Beyotime) and Masson staining kit (cat. no. C0215; Beyotime) were used to determine the degree of alveolitis and fibrosis withSzapiel's method (Szapiel et al., 1979). Images were captured under a microscope (BA210T; Motic). For IHC, the sections received antigen retrieval in citrate buffer at 95°C for 15 min, then blocked with 0.5% BSA-PBS containing 10% goat serum for 1h, and finally incubated with anti-Fibronectin (1:100; 66042-1-IG), anti-α-SMA (1:200; 55135-1-AP), or anti-Sirt2 (1:

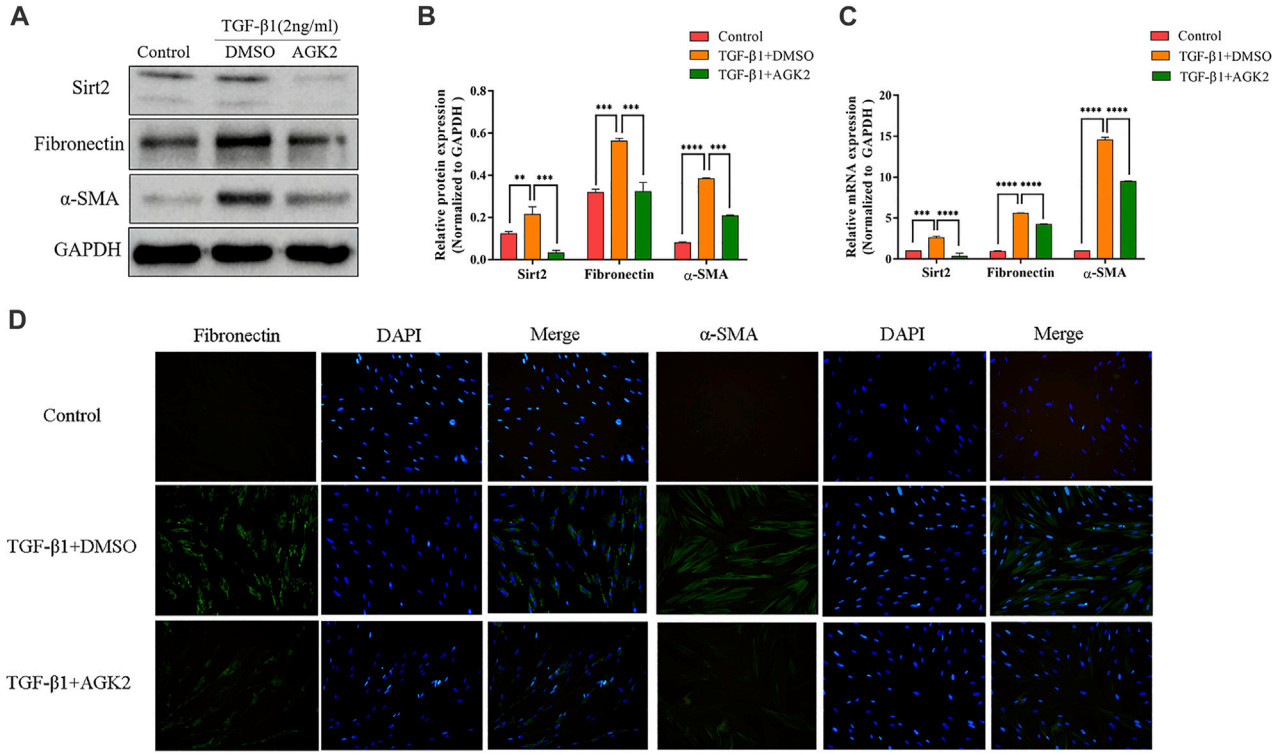

FIGURE 2 | AGK2 decreases fibrogenic gene expression in TGF-β1-induced lung fibroblasts activation. **(A,C)** Protein and mRNA expression of Sirt2, Fibronectin and α-SMA proteins by Western blot and real-time RT-PCR in MRC-5 cells treated with 2 ng/ml TGF-β1 for 24 h and then added 10 μM AGK2 or DMSO for another 24 h in the presence of TGF-β1. GAPDH was used as loading control. **(B)** Densitometric analyses of the Western blot in **(A)**. **(D)** Fibronectin and α-SMA was strongly expressed in response to TGF-β1, and AGK2 decreased the expression by immunofluorescence staining. Green means Fibronectin and α-SMA staining; Blue means DAPI. The bars indicated mean ± SD of three separate experiments. DMSO, dimethyl sulfoxide; $^{**}p < 0.01$, $^{***}p < 0.001$, $^{****}p < 0.0001$ compared to the TGF-β1+DMSO group.

100; 19655-1-AP) antibody overnight. The density of positive areas was measured using Image-Pro Plus 6.0 software.

Quantification and Statistical Analysis

GraphPad Prism version 7.0 software was used for graph preparation and data analysis. Densitometric analysis was performed by ImageJ software. All data were calculated as the means ± standard deviation (SD) based on at least three independent experiments. The significance of differences was analyzed using Student's t test or one-way ANOVA. A p-value of less than 0.05 was statistically significant.

RESULTS

Sirt2 Expression Is Increased in TGF-β1 Treated Lung Fibroblasts

Lung fibroblasts activation and differentiation is critical for the development of pulmonary fibrosis. Since TGF-β1 is a well-documented pro-fibrogenic cytokine in the progression of IPF, we used TGF-β1 as a fibroblast activator in this study. As shown in **Figures 1A–C**, after exposure to different concentrations of TGF-β1 (1, 2, 5 and 10 ng/ml for 24 h), the protein and mRNA expression of fibrogenic genes Fibronectin and α-SMA were increased significantly in MRC-5 cells. Next, in order to determine whether Sirt2 plays a role in pulmonary fibrosis, Sirt2 expression was examined in MRC-5 cells treated with the same concentration of TGF-β1 as described above (**Figures 1A–C**). As shown in **Figures 1D,E**, the protein expression of Sirt2 was elevated at different concentrations of TGF-β1 treatment, with a peak level at 2 ng/ml treatment. In order to determine the time course of TGF-β1 regulating Sirt2 expression, the cells were treated with 2 ng/ml TGF-β1 for different time periods and the results showed that Sirt2 expression was significantly increased at 3, 6, 12, 24, and 48 h, and the level peaked at 24 h after TGF-β1 stimulation (**Figures 1F,G**). The results suggested that Sirt2 may play a role in the process of lung fibroblasts activation.

AGK2 Attenuates TGF-β1-Induced Lung Fibroblasts Activation

To further examine the role of Sirt2 in lung fibroblasts activation, we used selective Sirt2 inhibitor AGK2 to inhibit its function in MRC-5 cells, and then analyzed the expression of Fibronectin and α-SMA. MRC-5 cells were treated with 10 μM AGK2 or vehicle control for 24 h in the presence of 2 ng/ml TGF-β1. The results showed that AGK2 significantly downregulated the increased

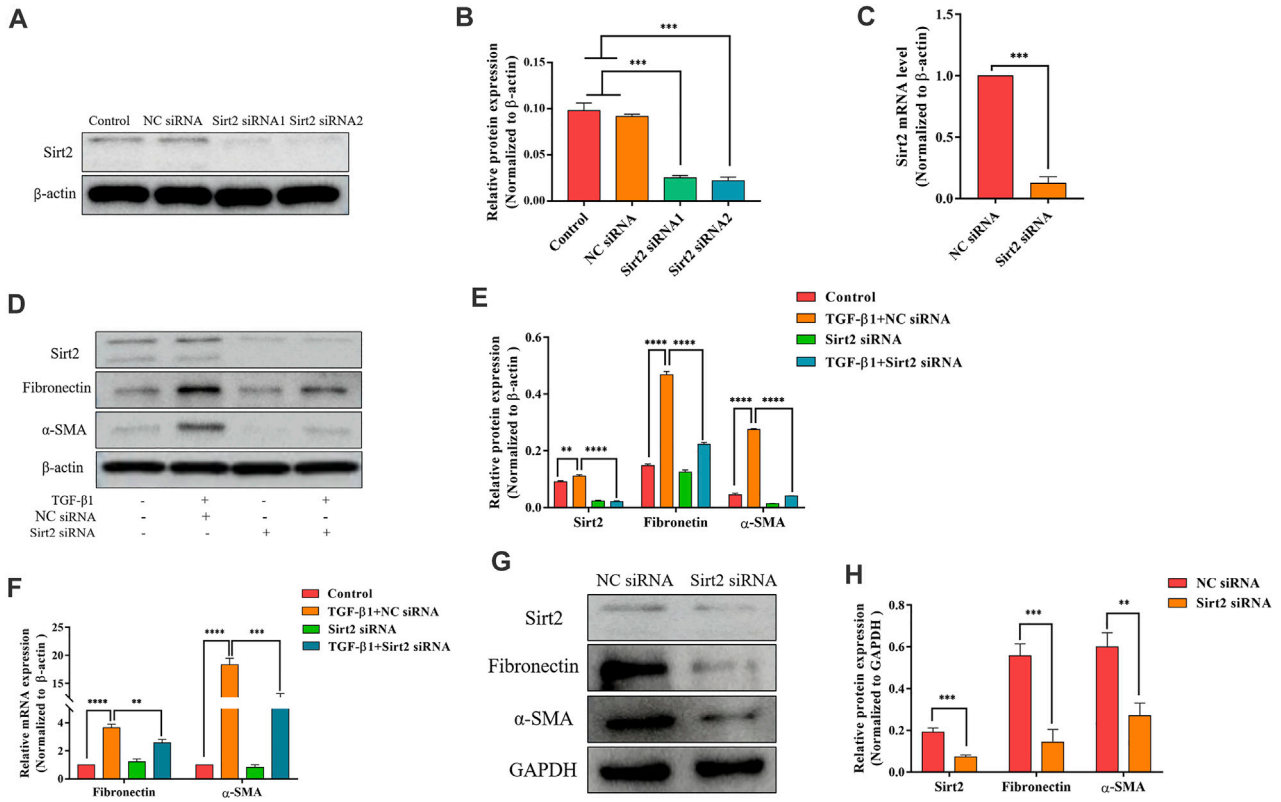

FIGURE 3 | Silencing Sirt2 inhibits fibrogenic gene expression in TGF-β1-treated lung fibroblasts and IPF lung fibroblasts. **(A,C)** MRC-5 cells were transfected with NC siRNA or Sirt2 siRNA for 24 h, Sirt2 siRNA successfully downregulated Sirt2 protein and mRNA expression detected by Western blot and real-time RT-PCR. **(B)** Densitometric analyses of the Western blot in **(A)**. **(D,F)** Protein and mRNA expression of Sirt2, Fibronectin, and α-SMA by Western blot and real-time RT-PCR in MRC-5 cells transfected with NC siRNA or Sirt2 siRNA for 24 h in the absence or presence of 2 ng/ml TGF-β1. **(E)** Densitometric analyses of the Western blot in **(D)**. **(G)** Expression of Sirt2, Fibronectin and α-SMA by Western blot in IPF lung fibroblasts treated with NC siRNA or Sirt2 siRNA for 24 h. **(H)** Densitometric analyses of the Western blot in **(G)**. GAPDH or β-actin was used as loading control. The bars indicated mean ± SD of three separate experiments. NC, negative control; siRNA, small interfering RNA. $^{**}p < 0.01$, $^{***}p < 0.001$, $^{****}p < 0.0001$.

protein and mRNA expression of Fibronectin and α-SMA induced by TGF-β1 (**Figures 2A–C**). Likewise, immunofluorescence staining further demonstrated that AGK2 treatment reversed the increased Fibronectin and α-SMA fluorescence intensity induced by TGF-β1 (**Figure 3D**). These data demonstrated that inhibiting Sirt2 can downregulate expression of Fibronectin and α-SMA at transcriptional and translational levels in TGF-β1-stimulated lung fibroblasts.

Sirt2 siRNA Attenuates Fibrogenic Gene Expression in TGF-β1-Treated Lung Fibroblasts and IPF Lung Fibroblasts

After analyzing the function of Sirt2 by the pharmacologic inhibitor AGK2, two kinds of siRNA targeting Sirt2 were used to further confirm the role of Sirt2 in fibroblast activation. First, the high knockdown efficiency of two Sirt2 siRNAs was verified by Western blot and real-time RT-PCR (**Figures 3A–C**). Considering these two Sirt2 siRNAs have the same silent efficiency in down-regulating Sirt2 protein expression, so we only used Sirt2 siRNA1 in the following Sirt2 knockdown experiments. Sirt2 siRNA or NC siRNA transfected MRC-5 cells were incubated with TGF-β1 for 24 h, and the results showed that silencing Sirt2 expression significantly attenuated the protein (**Figures 3D,E**) and mRNA expression (**Figure 3F**) of Fibronectin and α-SMA induced by TGF-β1 stimulation. Similarly, in primary lung fibroblasts derived from IPF patients, silencing Sirt2 expression with siRNA decreased the expression levels of Fibronectin and α-SMA protein (**Figures 3G,H**). Overall, these data suggest that interfering the expression of Sirt2 suppresses lung fibroblasts activation.

Inhibition of Sirt2 Alleviates the Increased Smad2/3 Phosphorylation Induced by TGF-β1

TGF-β1/Smad2/3 is a well-known signaling pathway involved in tissue fibrosis. Upon TGF-β1 stimulation, Smad2/3 are phosphorylated and the phosphorylated Smad2/3 combines with Smad4 to form heteromeric complexes, which translocate into the nucleus to modulate target gene transcription (Yan et al., 2016). Several studies showed that some Sirtuins, including Sirt1,

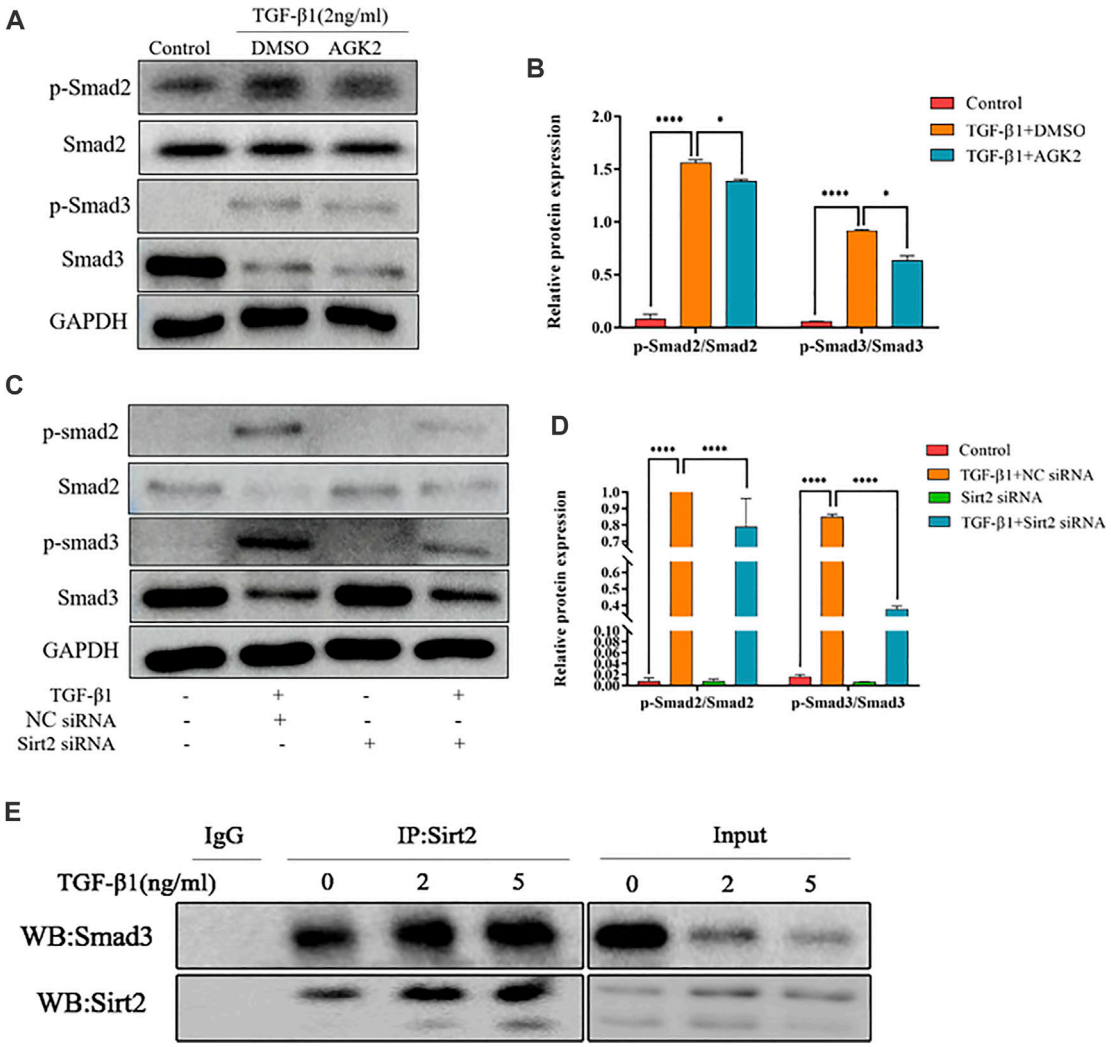

FIGURE 4 | Inhibiting Sirt2 activity and expression downregulates the increased Smad2/3 phosphorylation induced by TGF-β1. **(A)** Protein **e**xpression of p-Smad2/Smad2 and p-Smad3/Smad3 by Western blot in MRC-5 cells pretreated with 2 ng/ml TGF-β1 for 24 h and then 10 μM AGK2 or DMSO for 24 h in the presence of TGF-β1. **(B)** Densitometric analyses of the Western blot in **(A)**. **(C)** Protein expression of p-Smad2/Smad2 and p-Smad3/Smad3 by Western blot in MRC-5 cells transfected with NC siRNA or Sirt2 siRNA for 24 h in the absence or presence of 2 ng/ml TGF-β1. **(D)** Densitometric analyses of the Western blot in **(C)**. **(E)** MRC-5 cells were treated with TGF-β1 at 2 and 5 ng/ml for 24 h, and total protein was co-immunoprecipitated with anti-Sirt2 antibody or IgG and immunoblotted with Smad3 antibody. GAPDH was used as a loading control. The bars indicated mean ± SD of three separate experiments. NC, negative control; siRNA, small interfering RNA; DMSO, dimethyl sulfoxide. $^{*}p < 0.05$, $^{***}p < 0.001$.

Sirt3, Sirt6, and Sirt7, involved in the pathogenesis of fibrosis partially through TGF-β1/Smad2/3 signaling pathway (Sosulski et al., 2017; Wyman et al., 2017; Zhang et al., 2019). Therefore, we hypothesized that Sirt2 also modulates TGF-β1 induced lung fibroblasts activation through Smad2/3 pathway. Our results showed that phospho-Smad2 (p-Smad2) and phospho-Smad3 (p-Smad3) levels were significantly upregulated in response to TGF-β1 treatment compared with control (**Figures 4A–D**). AGK2 or Sirt2 siRNA treatment downregulated the increased phosphorylation of Smad2/3 induced by TGF-β1, decreased total Smad3 protein was also observed when Sirt2 was inhibited (**Figures 4A–D**). These indicated that Sirt2 promote the lung fibroblasts activation in a Smad2/3-dependent manner. Co-IP demonstrated directly that Sirt2 interacts with Smads in TGF-β1 treated MRC-5 (**Figure 4E**). Taken together, these results suggest that Sirt2 regulates fibroblasts activation through Smad2/3 signaling pathway in human embryonic lung fibroblasts.

AGK2 Alleviates Bleomycin-Induced Pulmonary Fibrosis in Mice

Mice model of bleomycin-induced pulmonary fibrosis was used to elucidate the protective effects of AGK2 treatment *in vivo*. Lung tissues were examined with HE and Masson staining. In HE staining, saline-treated lung tissue showed normal alveolar spaces and normal thickening of the alveolar septa; bleomycin

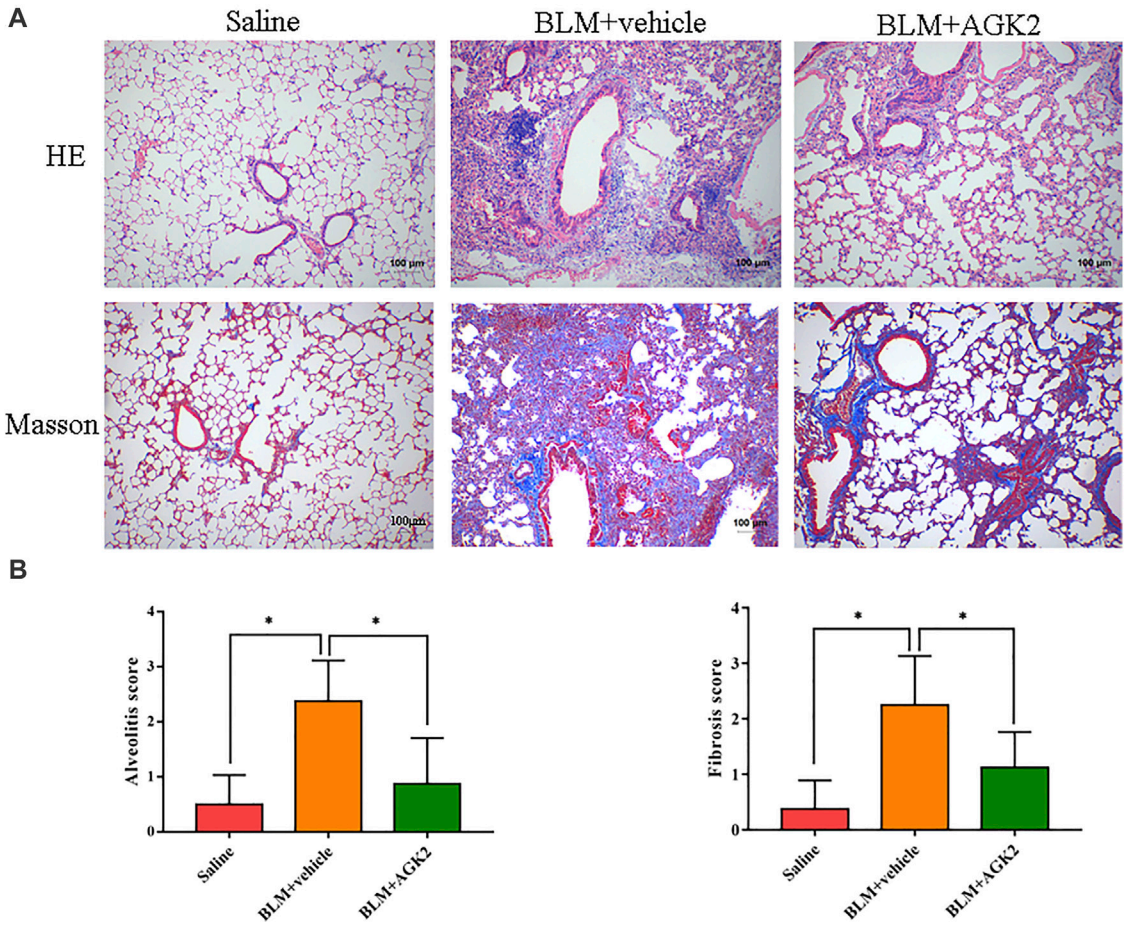

FIGURE 5 | AGK2 alleviates the degree of pulmonary fibrosis in bleomycin-induced pulmonary fibrosis in mice. **(A)** Representative images of HE and Masson staining of lung tissues. Magnification, ×100. **(B)** The quantitative results of alveolitis and fibrosis scoring. BLM, bleomycin. *p < 0.05.

stimulation induced obviously more interstitial infiltration by inflammatory cells than saline-treated control group, AGK2 administration apparently attenuated the degree of alveolitis (**Figure 5A** upper panel). In Masson staining, bleomycin stimulation induced a significant thickening of the alveolar septa with increased deposition of collagen in lung tissues compared with the control (**Figure 5A** lower panel). Quantitative analysis showed that the alveolitis and fibrosis scores induced by bleomycin were significantly reduced after AGK2 treatment (**Figure 5B**).

AGK2 Alleviates Bleomycin-Induced Pulmonary Fibrosis and Decreases the Expression of p-Smad2/3 *in vivo*

In mice model of bleomycin-induced pulmonary fibrosis, IHC was performed to further explore the effects of AGK2 on the expression of fibrosis-related proteins. As shown in **Figures 6A,B**, the staining of Fibronectin, α-SMA, and Sirt2 protein in the saline group was not remarkable, while the positive staining showed as dark brown was significantly increased after treating with bleomycin. Western blot showed similar results, which demonstrated the protein expression of Sirt2, Fibronectin and α-SMA were higher in the lung tissue of bleomycin-treated mice, but lower in those with AGK2 treatment, when compared to the saline control (**Figures 6C,D**). Furthermore, AGK2 treatment significantly decreased the levels of p-Smad2/Smad3 induced by bleomycin (**Figures 6E,F**). These results demonstrated that Sirt2 inhibitor can alleviated bleomycin-induced pulmonary fibrosis *in vivo* and inactivated Smad2/3 signaling pathway.

DISCUSSION

IPF is a progressively fatal disease and more effective therapeutic strategies are urgently needed. However, the underlying mechanism of the progress of IPF has not yet been fully elucidated. The chronic injuries or repetitive stimulation of lung epithelial cells lead to aberrantly activated fibroblast proliferation and excessive amount of ECM deposition may be a key process for this disease. Emerging evidence suggests that other Sirtuins are involved in the fibroblast activation and

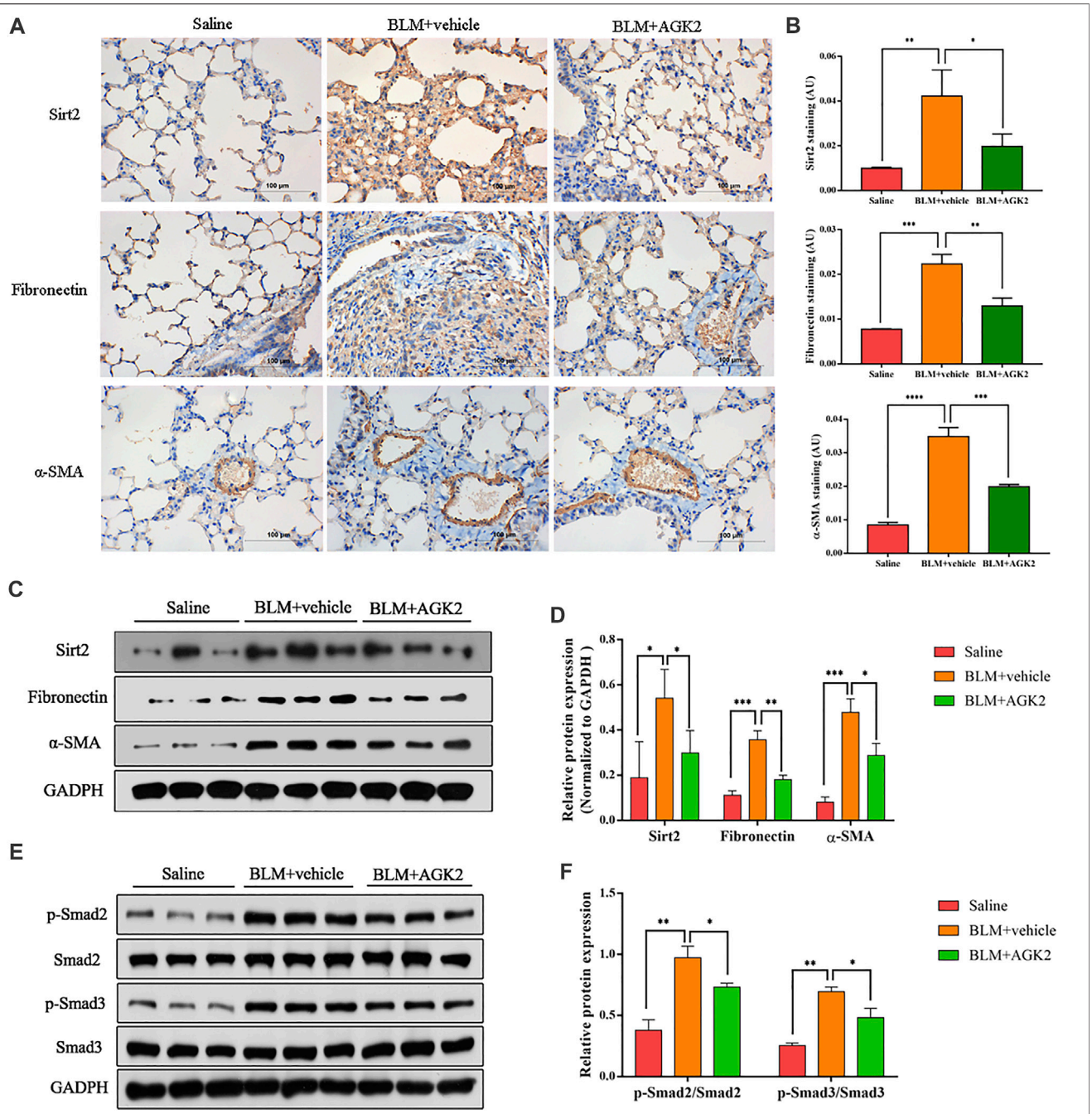

FIGURE 6 | AGK2 attenuated bleomycin-induced pulmonary fibrosis and decreased the expreesion of p-Smad2/3 *in vivo*. **(A)** Representative image of IHC staining of Sirt2 (top, brown), Fibronectin (middle, brown) and α-SMA (bottom, brown) (magnification: ×400). **(B)** Quantitative analysis of IHC in **(A)** with Image-Pro Plus 6.0 software. **(C,E)** Protein expression of Sirt2, Fibronectin, α-SMA, p-Smad2/Smad2 and p-Smad3/Smad3 of lung tissues by Western blot. **(D,F)** Densitometric analyses of the Western blot in **(C,E)**. BLM, bleomycin. $^{*}p < 0.05$, $^{**}p < 0.01$, $^{***}p < 0.001$, $^{****}p < 0.0001$.

progression of pulmonary fibrosis (Mazumder et al., 2020). For the first time, we demonstrate that the expression of Sirt2 is increased in lung fibroblasts stimulated with TGF-β1 *in vitro* and in the mice model of pulmonary fibrosis induced by bleomycin *in vivo*; inhibiting Sirt2 by the pharmacologic inhibitor or targeting small interfering RNA can inhibit fibrosis process by blocking Smad2/3 signaling pathway.

The occurrence and development of pulmonary fibrosis is complex. TGF-β1 is the most important primary driver and mediator in the process of pulmonary fibrosis through recruiting and activating fibroblasts, promoting epithelial-mesenchymal transition (EMT) and inducing ECM production (Hu et al., 2018). TGF-β1 regulates a complex networks of gene expression, including Smad and Sirtuins signaling pathway.

The mechanisms by which the Sirtuins contribute to the pathogenesis of fibrotic diseases are different in previous studies. Among these Sirtuins, Sirt1, Sirt3, Sirt6, and Sirt7 have been well studied in pulmonary fibrosis (Chun, 2015; Mazumder et al., 2020). Several studies have documented the regulatory function of Sirtuins on some classic fibrotic-related signaling pathway including TGF-β1/Smads. For instance, Sirt1 activation or overexpression can inhibit pulmonary fibrosis *in vitro* via inactivation of TGF-β1/Smad3 and mTOR signaling (Warburton et al., 2013; Chu et al., 2018). Sirt6 inhibits lung myofibroblasts differentiation by repressing NF-κB-dependent transcriptional activity and TGF-β1/Smad2 signaling pathway (Tian et al., 2017; Zhang et al., 2019).

Previous studies have demonstrated that Sirt2 is involved in the pathological process of tissue fibrosis. A pro-fibrotic function of Sirt2 has been documented in hepatic fibrosis. Genetic or pharmacological inhibition of Sirt2 significantly suppressed fibrogenic gene expression in hepatic stellate cells through ERK dephosphorylation and c-MYC degradation (Arteaga et al., 2016). In the study of hepatitis B virus (HBV) infection, Sirt2 overexpression was associated with Akt activation, which consequently downregulated glycogen synthase kinase 3β (GSK-3β) and increased β-catenin levels. These results indicate that Sirt2 inhibitor may control HBV infection and prevent the development of hepatic fibrosis (Piracha et al., 2018). In kidney fibrosis, AGK2 dose- and time-dependently inhibited the expression of fibrotic markers (Ponnusamy et al., 2014). Moreover, a stimulatory function of Sirt2 on eosinophil recruitment and inflammatory cytokines (TNF-α, IL-1β, IL-4 and IL-6) and mediators (myeloperoxidase, eosinophil peroxidase, and tumor growth factor-α) secretion in lung tissues was observed (Lee et al., 2019; Kim et al., 2020). However, the role of Sirt2 has not been explored in pulmonary fibrosis.

In this study, we showed that Sirt2 level was upregulated in TGF-β1 activated human lung fibroblasts and lung tissues of bleomycin-treated mice model, which suggested that Sirt2 may play a role in fibroblasts activation and pulmonary fibrogenesis. Downregulation of Sirt2 expression using pharmacologic inhibitor AGK2 and siRNAs alleviated TGF-β1 induced lung fibroblasts activation, as evidenced by reduced expression of α-SMA and Fibronectin. The anti-fibrotic effect of Sirt2 knockdown was also observed in IPF lung fibroblasts. Moreover, AGK2 treatment significantly mitigated the degree of pulmonary fibrosis in mice induced by bleomycin.

Smad2 and Smad3 are key mediators of TGF-β1-induced fibrogenesis and ECM production. TGF-β1 binds to its receptor and forms complexes with Smad2/3, then the phosphorylated Smad2/3 and its subsequent complex translocate to the nucleus, which are the key steps to modulate TGF-β1 dependent gene expression and fibrosis progress (Li et al., 2019; Zou et al., 2019; Nanri et al., 2020). Our results found that p-Smad2/3 expression was increased in activated lung fibroblasts induced by TGF-β1 and in lung tissues of bleomycin-induced pulmonary fibrosis. Sirt2 inhibitor AGK2 or Sirt2 siRNA can attenuated its expression. Co-IP further identify the interactions between Sirt2 and Smad3. Our results illustrated that Sirt2 possibly regulates Smad2/3 directly or indirectly and lead to higher phosphorylation of Smad2/3 in response to stimulators; Sirt2 may promote the activation of fibroblasts and the development of pulmonary fibrosis through Smad2/3 pathway. This result was similar to a previous study, which demonstrated that AGK2 reduced the level of collagen deposition in specific Smad signaling transfected cells (Kim et al., 2020).

In the present study, Sirt2 has been identified as an important factor in the process of pulmonary fibrosis, and inhibition of Sirt2 ameliorated the degree of fibrosis and decreased the phosphorylation of Smad2/3, which indicate that targeting Sirt2 would provide novel therapeutic candidate for preventing pulmonary fibrosis. However, the limitation of this study is that only small molecule inhibitor was used, and further studies with Sirt2-KO mice are needed to investigate the exact effects of Sirt2 on pulmonary fibrosis.

DATA AVAILABILITY STATEMENT

The original contributions presented in the study are included in the article/**Supplementary Material**, further inquiries can be directed to the corresponding author.

ETHICS STATEMENT

The animal study was reviewed and approved by The Second Xiangya Hospital, Central South University (No.2021026).

AUTHOR CONTRIBUTIONS

All authors listed have made a substantial, direct, and intellectual contribution to the work and approved it for publication.

FUNDING

This work is supported by grants from the National Natural Science Foundation of China (No. 81470256), the Foundation Research Funds for the Central Universities of Central South University (No. 2019zzts358), the Science and Technology Program Foundation of Changsha of China (No. kq2001040), the Science and Technology Department of Hunan Province (No. 2018SK52510), and National Natural Science Foundation of Hunan Province (No. 2020JJ5802). The corrsponding author XZ chairs theses two funds.

SUPPLEMENTARY MATERIAL

The Supplementary Material for this article can be found online at: https://www.frontiersin.org/articles/10.3389/fphar.2021.756131/full#supplementary-material

REFERENCES

Arteaga, M., Shang, N., Ding, X., Yong, S., Cotler, S. J., Denning, M. F., et al. (2016). Inhibition of SIRT2 Suppresses Hepatic Fibrosis. *Am. J. Physiol. Gastrointest. Liver Physiol.* 310 (11), G1155–G1168. doi:10.1152/ajpgi.00271.2015

Ballester, B., Milara, J., and Cortijo, J. (2019). Idiopathic Pulmonary Fibrosis and Lung Cancer: Mechanisms and Molecular Targets. *Int. J. Mol. Sci.* 20 (3), 593. doi:10.3390/ijms20030593

Chanda, D., Otoupalova, E., Smith, S. R., Volckaert, T., De Langhe, S. P., and Thannickal, V. J. (2019). Developmental Pathways in the Pathogenesis of Lung Fibrosis. *Mol. Aspects Med.* 65, 56–69. doi:10.1016/j.mam.2018.08.004

Chu, H., Jiang, S., Liu, Q., Ma, Y., Zhu, X., Liang, M., et al. (2018). Sirtuin1 Protects against Systemic Sclerosis-Related Pulmonary Fibrosis by Decreasing Proinflammatory and Profibrotic Processes. *Am. J. Respir. Cel Mol Biol* 58 (1), 28–39. doi:10.1165/rcmb.2016-0192OC

Chun, P. (2015). Erratum to: Role of Sirtuins in Chronic Obstructive Pulmonary Disease. *Arch. Pharm. Res.* 38 (1), 1–10. doi:10.1007/s12272-015-0555-1

Drazic, A., Myklebust, L. M., Ree, R., and Arnesen, T. (2016). The World of Protein Acetylation. *Biochim. Biophys. Acta* 1864 (10), 1372–1401. doi:10.1016/j.bbapap.2016.06.007

Gomes, P., Leal, H., Mendes, A. F., Reis, F., and Cavadas, C. (2019). Dichotomous Sirtuins: Implications for Drug Discovery in Neurodegenerative and Cardiometabolic Diseases. *Trends Pharmacol. Sci.* 40 (12), 1021–1039. doi:10.1016/j.tips.2019.09.003

He, F. F., You, R. Y., Ye, C., Lei, C. T., Tang, H., Su, H., et al. (2018). Inhibition of SIRT2 Alleviates Fibroblast Activation and Renal Tubulointerstitial Fibrosis via MDM2. *Cell Physiol Biochem* 46 (2), 451–460. doi:10.1159/000488613

Hu, H. H., Chen, D. Q., Wang, Y. N., Feng, Y. L., Cao, G., Vaziri, N. D., et al. (2018). New Insights into TGF-β/Smad Signaling in Tissue Fibrosis. *Chem. Biol. Interact* 292, 76–83. doi:10.1016/j.cbi.2018.07.008

Imai, S., and Guarente, L. (2014). NAD+ and Sirtuins in Aging and Disease. *Trends Cel Biol* 24 (8), 464–471. doi:10.1016/j.tcb.2014.04.002

Jones, D. L., Haak, A. J., Caporarello, N., Choi, K. M., Ye, Z., Yan, H., et al. (2019). Tgfβ-Induced Fibroblast Activation Requires Persistent and Targeted HDAC-Mediated Gene Repression. *J. Cel Sci* 132 (20), jcs233486. doi:10.1242/jcs.233486

Kim, Y. Y., Hur, G., Lee, S. W., Lee, S. J., Lee, S., Kim, S. H., et al. (2020). AGK2 Ameliorates Mast Cell-Mediated Allergic Airway Inflammation and Fibrosis by Inhibiting FcεRI/TGF-β Signaling Pathway. *Pharmacol. Res.* 159, 105027. doi:10.1016/j.phrs.2020.105027

Lee, Y. G., Reader, B. F., Herman, D., Streicher, A., Englert, J. A., Ziegler, M., et al. (2019). Sirtuin 2 Enhances Allergic Asthmatic Inflammation. *JCI Insight* 4 (4), e124710. doi:10.1172/jci.insight.124710

Li, N., Feng, F., Wu, K., Zhang, H., Zhang, W., and Wang, W. (2019). Inhibitory Effects of Astragaloside IV on Silica-Induced Pulmonary Fibrosis via Inactivating TGF-β1/Smad3 Signaling. *Biomed. Pharmacother.* 119, 109387. doi:10.1016/j.biopha.2019.109387

Mazumder, S., Barman, M., Bandyopadhyay, U., and Bindu, S. (2020). Sirtuins as Endogenous Regulators of Lung Fibrosis: A Current Perspective. *Life Sci.* 258, 118201. doi:10.1016/j.lfs.2020.118201

Meiners, S., Eickelberg, O., and Königshoff, M. (2015). Hallmarks of the Ageing Lung. *Eur. Respir. J.* 45 (3), 807–827. doi:10.1183/09031936.00186914

Meng, X. M., Nikolic-Paterson, D. J., and Lan, H. Y. (2016). TGF-β: the Master Regulator of Fibrosis. *Nat. Rev. Nephrol.* 12 (6), 325–338. doi:10.1038/nrneph.2016.48

Morikawa, M., Derynck, R., and Miyazono, K. (2016). TGF-beta and the TGF-Beta Family: Context-dependent Roles in Cell and Tissue Physiology. *Cold Spring Harb Perspect. Biol.* 8 (5). doi:10.1101/cshperspect.a021873

Nanri, Y., Nunomura, S., Terasaki, Y., Yoshihara, T., Hirano, Y., Yokosaki, Y., et al. (2020). Cross-Talk between Transforming Growth Factor-β and Periostin Can Be Targeted for Pulmonary Fibrosis. *Am. J. Respir. Cel Mol Biol* 62 (2), 204–216. doi:10.1165/rcmb.2019-0245OC

Noble, P. W., Barkauskas, C. E., and Jiang, D. (2012). Pulmonary Fibrosis: Patterns and Perpetrators. *J. Clin. Invest.* 122 (8), 2756–2762. doi:10.1172/JCI60323

O'Reilly, S. (2017). Epigenetics in Fibrosis. *Mol. Aspects Med.* 54, 89–102. doi:10.1016/j.mam.2016.10.001

Piracha, Z. Z., Kwon, H., Saeed, U., Kim, J., Jung, J., Chwae, Y. J., et al. (2018). Sirtuin 2 Isoform 1 Enhances Hepatitis B Virus RNA Transcription and DNA Synthesis through the AKT/GSK-3β/β-Catenin Signaling Pathway. *J. Virol.* 92 (21), e00955-18. doi:10.1128/JVI.00955-18

Ponnusamy, M., Zhou, X., Yan, Y., Tang, J., Tolbert, E., Zhao, T. C., et al. (2014). Blocking Sirtuin 1 and 2 Inhibits Renal Interstitial Fibroblast Activation and Attenuates Renal Interstitial Fibrosis in Obstructive Nephropathy. *J. Pharmacol. Exp. Ther.* 350 (2), 243–256. doi:10.1124/jpet.113.212076

Selman, M., and Pardo, A. (2014). Revealing the Pathogenic and Aging-Related Mechanisms of the Enigmatic Idiopathic Pulmonary Fibrosis. An Integral Model. *Am. J. Respir. Crit. Care Med.* 189 (10), 1161–1172. doi:10.1164/rccm.201312-2221PP

Sosulski, M. L., Gongora, R., Feghali-Bostwick, C., Lasky, J. A., and Sanchez, C. G. (2017). Sirtuin 3 Deregulation Promotes Pulmonary Fibrosis. *J. Gerontol. A. Biol. Sci. Med. Sci.* 72 (5), 595–602. doi:10.1093/gerona/glw151

Szapiel, S. V., Elson, N. A., Fulmer, J. D., Hunninghake, G. W., and Crystal, R. G. (1979). Bleomycin-induced Interstitial Pulmonary Disease in the Nude, Athymic Mouse. *Am. Rev. Respir. Dis.* 120 (4), 893–899. doi:10.1164/arrd.1979.120.4.893

Tang, X., Chen, X. F., Wang, N. Y., Wang, X. M., Liang, S. T., Zheng, W., et al. (2017). SIRT2 Acts as a Cardioprotective Deacetylase in Pathological Cardiac Hypertrophy. *Circulation* 136 (21), 2051–2067. doi:10.1161/CIRCULATIONAHA.117.028728

Tian, K., Chen, P., Liu, Z., Si, S., Zhang, Q., Mou, Y., et al. (2017). Sirtuin 6 Inhibits Epithelial to Mesenchymal Transition during Idiopathic Pulmonary Fibrosis via Inactivating TGF-β1/Smad3 Signaling. *Oncotarget* 8 (37), 61011–61024. doi:10.18632/oncotarget.17723

Wallner, M., Eaton, D. M., Berretta, R. M., Liesinger, L., Schittmayer, M., Gindlhuber, J., et al. (2020). HDAC Inhibition Improves Cardiopulmonary Function in a Feline Model of Diastolic Dysfunction. *Sci. Transl Med.* 12 (525), eaay7205. doi:10.1126/scitranslmed.aay7205

Warburton, D., Shi, W., and Xu, B. (2013). TGF-β-Smad3 Signaling in Emphysema and Pulmonary Fibrosis: an Epigenetic Aberration of normal Development? *Am. J. Physiol. Lung Cel Mol Physiol* 304 (2), L83–L85. doi:10.1152/ajplung.00258.2012

Wyman, A. E., Noor, Z., Fishelevich, R., Lockatell, V., Shah, N. G., Todd, N. W., et al. (2017). Sirtuin 7 Is Decreased in Pulmonary Fibrosis and Regulates the Fibrotic Phenotype of Lung Fibroblasts. *Am. J. Physiol. Lung Cel Mol Physiol* 312 (6), L945–L958. doi:10.1152/ajplung.00473.2016

Wynn, T. A. (2008). Cellular and Molecular Mechanisms of Fibrosis. *J. Pathol.* 214 (2), 199–210. doi:10.1002/path.2277

Wynn, T. A., and Ramalingam, T. R. (2012). Mechanisms of Fibrosis: Therapeutic Translation for Fibrotic Disease. *Nat. Med.* 18 (7), 1028–1040. doi:10.1038/nm.2807

Yan, X., Liao, H., Cheng, M., Shi, X., Lin, X., Feng, X.-H., et al. (2016). Smad7 Protein Interacts with Receptor-Regulated Smads (R-Smads) to Inhibit Transforming Growth Factor-β (TGF-β)/Smad Signaling. *J. Biol. Chem.* 291 (1), 382–392. doi:10.1074/jbc.m115.694281

Zhang, Q., Tu, W., Tian, K., Han, L., Wang, Q., Chen, P., et al. (2019). Sirtuin 6 Inhibits Myofibroblast Differentiation via Inactivating Transforming Growth Factor-β1/Smad2 and Nuclear Factor-Kb Signaling Pathways in Human Fetal Lung Fibroblasts. *J. Cel Biochem* 120 (1), 93–104. doi:10.1002/jcb.27128

Zou, G. L., Zuo, S., Lu, S., Hu, R. H., Lu, Y. Y., Yang, J., et al. (2019). Bone Morphogenetic Protein-7 Represses Hepatic Stellate Cell Activation and Liver Fibrosis via Regulation of TGF-β/Smad Signaling Pathway. *World J. Gastroenterol.* 25 (30), 4222–4234. doi:10.3748/wjg.v25.i30.4222

Conflict of Interest: The authors declare that the research was conducted in the absence of any commercial or financial relationships that could be construed as a potential conflict of interest.

The Handling Editor declared a shared parent affiliation with the authors at the time of the review.

frontiers in Pharmacology

ORIGINAL RESEARCH
published: 05 November 2021
doi: 10.3389/fphar.2021.753727

Identification of Hypoxia Induced Metabolism Associated Genes in Pulmonary Hypertension

Yang-Yang He[1], Xin-Mei Xie[1], Hong-Da Zhang[2], Jue Ye[2], Selin Gencer[3], Emiel P. C. van der Vorst[3,4,5,6,7], Yvonne Döring[3,4,8], Christian Weber[3,4,9,10], Xiao-Bin Pang[1], Zhi-Cheng Jing[11], Yi Yan[3,4†] and Zhi-Yan Han[2*†]*

[1]School of Pharmacy, Henan University, Kaifeng, China, [2]State Key Laboratory of Cardiovascular Disease and FuWai Hospital, Chinese Academy of Medical Sciences and Peking Union Medical College, Beijing, China, [3]Institute for Cardiovascular Prevention (IPEK), Ludwig-Maximilians-University Munich, Munich, Germany, [4]DZHK (German Centre for Cardiovascular Research), Partner Site Munich Heart Alliance, Munich, Germany, [5]Interdisciplinary Center for Clinical Research (IZKF), RWTH Aachen University, Aachen, Germany, [6]Institute for Molecular Cardiovascular Research (IMCAR), RWTH Aachen University, Aachen, Germany, [7]Department of Pathology, Cardiovascular Research Institute Maastricht (CARIM), Maastricht University Medical Centre, Maastricht, Netherlands, [8]Department of Angiology, Swiss Cardiovascular Center, Inselspital, Bern University Hospital, University of Bern, Bern, Switzerland, [9]Department of Biochemistry, Cardiovascular Research Institute Maastricht (CARIM), Maastricht University Medical Centre, Maastricht, Netherlands, [10]Munich Cluster for Systems Neurology (SyNergy), Munich, Germany, [11]State Key Laboratory of Complex, Severe, and Rare Diseases, Department of Cardiology, Peking Union Medical College Hospital, Chinese Academy of Medical Sciences and Peking Union Medical College, Beijing, China

OPEN ACCESS

Edited by:
Xiaohui Li,
Central South University, China

Reviewed by:
Zaixin Yu,
Central South University, China
Alexi Crosby,
University of Cambridge, United Kingdom
Ran Wang,
Anhui Medical University, China

***Correspondence:**
Yi Yan
yi.yan@med.uni-muenchen.de
Zhi-Yan Han
zhiyanhan2006@hotmail.com

†These authors have contributed equally to this work and share last authorship

Specialty section:
This article was submitted to Respiratory Pharmacology, a section of the journal Frontiers in Pharmacology

Received: 05 August 2021
Accepted: 11 October 2021
Published: 05 November 2021

Citation:
He Y-Y, Xie X-M, Zhang H-D, Ye J, Gencer S, van der Vorst EPC, Döring Y, Weber C, Pang X-B, Jing Z-C, Yan Y and Han Z-Y (2021) Identification of Hypoxia Induced Metabolism Associated Genes in Pulmonary Hypertension. Front. Pharmacol. 12:753727. doi: 10.3389/fphar.2021.753727

Objective: Pulmonary hypertension (PH) associated with hypoxia and lung disease (Group 3) is the second most common form of PH and associated with increased morbidity and mortality. This study was aimed to identify hypoxia induced metabolism associated genes (MAGs) for better understanding of hypoxic PH.

Methods: Rat pulmonary arterial smooth muscle cells (PASMCs) were isolated and cultured in normoxic or hypoxic condition for 24 h. Cells were harvested for liquid chromatography-mass spectrometry analysis. Functional annotation of distinguishing metabolites was performed using Metaboanalyst. Top 10 enriched metabolite sets were selected for the identification of metabolism associated genes (MAGs) with a relevance score >8 in Genecards. Transcriptomic data from lungs of hypoxic PH in mice/rats or of PH patients were accessed from Gene Expression Omnibus (GEO) database or open-access online platform. Connectivity Map analysis was performed to identify potential compounds to reverse the metabolism associated gene profile under hypoxia stress. The construction and module analysis of the protein-protein interaction (PPI) network was performed. Hub genes were then identified and used to generate LASSO model to determine its accuracy to predict occurrence of PH.

Results: A total of 36 altered metabolites and 1,259 unique MAGs were identified in rat PASMCs under hypoxia. 38 differentially expressed MAGs in mouse lungs of hypoxic PH

Abbreviations: ANOVA, Analysis of variance; CMap, Connectivity map; DEGs, Differentially expressed genes; GEO, Gene Expression Omnibus; FC, Fold change; LC/MS, Liquid chromatography-mass spectrometry; LASSO, Least absolute shrinkage and selection operator; MAGs, Metabolism associated genes; PLS-DA, Partial least squares discriminant analysis; PPI, Protein-protein interaction; PH, Pulmonary hypertension; PASMCs, Pulmonary arterial smooth muscle cells; PBS, Phosphate-buffered saline; ROC, Receiver operating characteristic; SuHx, Sugen 5416/hypoxia; SEM, Standard error of them mean; SphK1, Sphingosine kinases 1; UMAP, Uniform manifold approximation and projection; VIP, Variable important in projection.

were revealed, with enrichment in multi-pathways including regulation of glucose metabolic process, which might be reversed by drugs such as blebbistatin. 5 differentially expressed MAGs were displayed in SMCs of Sugen 5416/hypoxia induced PH rats at the single cell resolution. Furthermore, 6 hub genes (Cat, Ephx1, Gpx3, Gstm4, Gstm5, and Gsto1) out of 42 unique hypoxia induced MAGs were identified. Higher Cat, Ephx1 and lower Gsto1 were displayed in mouse lungs under hypoxia (all $p < 0.05$), in consistent with the alteration in lungs of PH patients. The hub gene-based LASSO model can predict the occurrence of PH (AUC = 0.90).

Conclusion: Our findings revealed six hypoxia-induced metabolism associated hub genes, and shed some light on the molecular mechanism and therapeutic targets in hypoxic PH.

Keywords: pulmonary hypertension, hypoxia, metabolism associated genes, metabolomics, transcriptomics

BACKGROUND

Pulmonary hypertension (PH) is a heterogenous disorder and characterized by high pulmonary artery pressure and elevated pulmonary vascular resistance that usually leads to right heart failure and even death (Hoeper et al., 2013). The pathogenesis of PH is driven or initiated by multiple factors including genetic mutations, epigenetic alterations, inflammation, altered metabolism, and environment insults such as hypoxia, drugs and toxins (de Jesus Perez, 2016). PH associated with hypoxia and lung disease (Group 3 PH) is the second most common form of PH and is associated with increased morbidity and mortality (Strange et al., 2012; McGettrick and Peacock, 2020). However, most of PAH-specific medications including endothelin receptor antagonists, phosphodiesterase type 5 inhibitors, and prostacyclin have not shown consistent benefit in the Group 3 PH (Harder and Waxman, 2020). Hence, the discovery of some targets for hypoxic PH would be of great value for those Group 3 population.

On one hand, hypoxic PH share a similar pathological changes with other type of PH including the accumulation of pulmonary artery adventitial fibroblasts and excessive deposition of extracellular matrix proteins, proliferation and migration of pulmonary arterial smooth muscle cells (PASMCs) and endothelial cell proliferation that promotes intimal thickening (Meyrick and Reid, 1980; Stenmark et al., 2006; Chen et al., 2009). Growing evidence indicates that the excessive proliferation, apoptosis resistance and a contractile-to-synthetic phenotype switch of PASMCs has emerged as essential mechanisms in the remodeling of the pulmonary vasculature associated with hypoxic PH. For example, our previous study demonstrated that overexpression of DNMT3B (encoding DNA methyltransferase 3B) mitigated the remodeling of hypoxic PH in mice, suggesting the protective role of DNMT3B on the pulmonary vascular remodeling via the modulation of PASMC proliferation/migration (Yan et al., 2020). In addition, the markedly increased CD146 expression in PASMCs under hypoxia and hypoxia-inducible transcription factor 1 alpha (HIF-1α) transcriptional program reinforce each other to enable PASMCs to adopt a more synthetic phenotype. Genetic ablation of CD146 in smooth muscle cells mitigates pulmonary vascular remodeling in chronic hypoxic mice (Luo et al., 2019). On the other hand, the activation of transcription factor HIF-1α under hypoxia stress induces the expression of glycolytic genes and actively suppressed mitochondrial oxidative phosphorylation by inducing pyruvate dehydrogenase kinase 1, which hampers pyruvate dehydrogenase from using pyruvate to fuel tricarboxylic acid cycle (Papandreou et al., 2006). The overall picture of metabolic shift and metabolite perturbations in PH have become clearer in recent years due to the application of metabolomics. The interventions of specific enzymes to restore the abnormal metabolism open a new avenue for the treatment of PH. For example, inhibitor of glucose-6-phosphate dehydrogenase, a rate-limiting enzyme in pentose phosphate pathway, was reported to modulate DNA methylation and alleviate pulmonary artery remodeling (Kitagawa et al., 2021). Sphingosine kinases 1 (SphK1) is determinant for the synthesis of sphingosine-1-phosphate, an critical mediator for cell proliferation, migration and angiogenesis. Deficiency and pharmacological inhibition of SphK1 mitigated the development of hypoxic PH *in vivo* and SphK1 deficiency inhibited PASMC proliferation *in vitro* (Chen et al., 2014).

Here, we sought to examine the metabolic profiles in PASMCs and metabolism associated genes in response to hypoxia. In combination of transcriptomics data sets from both PH rodent models and PH patients, we aimed to identify hypoxia induced metabolism associated hub genes, which might be prospective targets for the treatment of hypoxic PH.

METHODS

Rat PASMCs Isolation and Cell Culture

Rat PASMCs were isolated as previously described (Yan et al., 2020). Briefly, 6-week old Sprague-Dawley rat purchased from Charles River (Beijing, China) was sacrificed, which was approved by the Ethics and Animal Care and Use Committee of Henan University. The lungs were excised and rinsed with phosphate-buffered saline (PBS). The pulmonary arteries were isolated followed by removal of the adventitia under the microscope. Minced arteries were attached to bottom of Petri dish and then

immersed by Dulbecco's modified eagle medium/F12 containing 20% fetal bovine serum, 100 U/mL penicillin and 100 μg/ml streptomycin in a 37°C, 5% CO2 humidified incubator. Three days later, non-adherent cells were removed, and the adherent cells that had grown to 90% confluence were considered as passage 0 PASMCs. Passages 3 were used for the subsequent hypoxia experiments.

Hypoxia Experiment

Rat PASMCs at a density of 1×10^5/ml were seeded into 6-well plates and then placed in a 37°C, 5% CO2 humidified incubator. 24 h later cells were starved with Dulbecco's modified eagle medium/F12 containing 0.5% fetal bovine serum. Medium were refreshed and cells were then either cultured in normoxia condition (21% O_2) or hypoxia condition (1%O_2) in the incubator 24 h post-starvation. 24 h later cells under normaxia or hypoxia (n = 6 per group) were collected respectively. Cells were washed and centrifuged at 300 g at 4°C for 10 min and resuspend with 1 ml PBS. Cells were then counted with erythrocytometers and diluted to a final density of 1×10^5/ml with PBS. 1 ml cell suspension per sample was transferred to 1.5 ml clean tube and centrifugated at 300 g at 4°C for 5 min. Supernatants were discarded and cell pellets were stored at −80°C before further use. No repeated freezing and thawing occurred before sample processing to avoid potential degradation risks of metabolites.

Sample Preparation

1 ml of MeOH:ACN:H2O (2:2:1, v/v) solvent mixture was added into the cell samples. The cell mixtures were vortexed for 30 s followed by sonification at 4°C in the water bath for 10 min. The mixtures were transferred to liquid nitrogen for 1 min and thawed at room temperature followed by sonification at 4°C in the water bath for 10 min. After the repeat for 3 times, mixtures were put at −20°C for 1 h to facilitate protein precipitation. Mixtures were centrifuged at 13,000 rpm at 4°C for 15 min, supernatants were discarded, and pellets were vacuum dried and reconstituted with 100 μL of ACN:H2O (1:1, v/v). Mixtures were vortexed for 30 s and sonicated as previously stated followed by centrifugation at 13,000 rpm at 4°C for 15 min. Supernatants were stored at −80°C prior to Liquid chromatography-mass spectrometry (LC/MS) analysis.

Liquid Chromatography-Mass Spectrometry Analysis

Liquid chromatographic separation for processed cell samples was achieved on a ZORBAX Eclipse Plus C18 column (2.1 × 100 mm, 3.5 μm, Agilent, United States) maintained at 45°C, whereas mass spectrometry was performed on a Nexera X2 system (Shimadzu, Japan) coupled with a Triple TOF 5600 quadrupole-time-of-flight mass spectrometer (AB SCIEX, United States). The temperature of the sample chamber was maintained at 7°C. The gradient elution steps were shown in **Supplementary Table S1**. The injected sample volume was 10 μL for each run in the full loop injection mode, and the flow rate of the mobile phase was 0.5 ml/min. The mobile phase A was mainly composed of water and contains 0.1% formic acid. The mobile phase B was mainly composed of acetonitrile and contains 0.1% formic acid. Water (LC-MS grade) and acetonitrile (LC-MS grade) were purchased from Fisher Scientific. The purity of formic acid purchased from Acros was greater than 98%.

Data Availability and Process

In terms of metabolomics study, data preprocessing was performed before pattern recognition. The original data was processed by the instrument's own metabolomics processing software Progenesis QI (Waters Corporation, Milford, United States) for baseline filtering, peak identification, integration, retention time correction, peak alignment, and normalization. Finally, a data matrix of retention time, mass-to-charge ratio and peak intensity were obtained. The integrated data matrix was imported into the SIMCA-P+ (v 14.1) software package (Umetrics, Umeå, and Sweden), and partial least squares discriminant analysis (PLS-DA) was used to distinguish the overall difference in metabolic profile between groups. In PLS-DA analysis, variables with a variable weight value (Variable Important in Projection, VIP) > 1 were considered to be distinguishing among groups.

With regard to transcriptomic analysis, we accessed the data set GSE 1909 (Gharib et al., 2005) based on GPL1674 including mouse lung tissues during development of hypoxia-induced PH (days 1–21) and resolution of PH after return to normoxia (days 22–35). Mice were sampled during nine time-points and there were 4 replicates at each time-point. We selected samples at day 1, day 14, day 21, and day 35 after hypoxia for further analysis. Differential expression analysis was performed using the limma package in R (v3.6.3.). (Ritchie et al., 2015). p value <0.05 and fold change (FC) of gene expression >1.5 or <0.67 between two groups were considered to be differentially expressed genes (DEGs). To validate the hub gene in lung tissues from PH patients, we selected the datasets with a relative large sample size (lung tissues from control subjects >20, and lung tissues from PH patients >50) and two datasets GSE117261 (Stearman et al., 2019) consisting of 25 control subjects and 58 PH patients, and GSE24988 (Mura et al., 2012) including 22 controls and 62 PH patients were included for further analysis. Both were based on GPL6244. The ComBat function in the sva package was used to merge these two data sets and remove the batch effect (Leek et al., 2012). In addition, single cell RNA sequencing data from lung tissues of monocrotaline, Sugen 5416/hypxoixa (SuHx) or control rats were downloaded from an open-access online platform (http://mergeomics.research.idre.ucla.edu/PVDSingleCell/). (Hong et al., 2020)

Connectivity Map Analysis

The Connectivity Map (CMap) (https://portals.broadinstitute.org/cmap) is an open resource that connect genes, small molecules, and disease by virtue of common gene-expression signatures (Lamb et al., 2006). Drugs with Mean < −0.4 and $p < 0.05$ in CMap analysis were considered to be potential small molecular compounds that can reverse altered expression of user-defined gene list in cell lines.

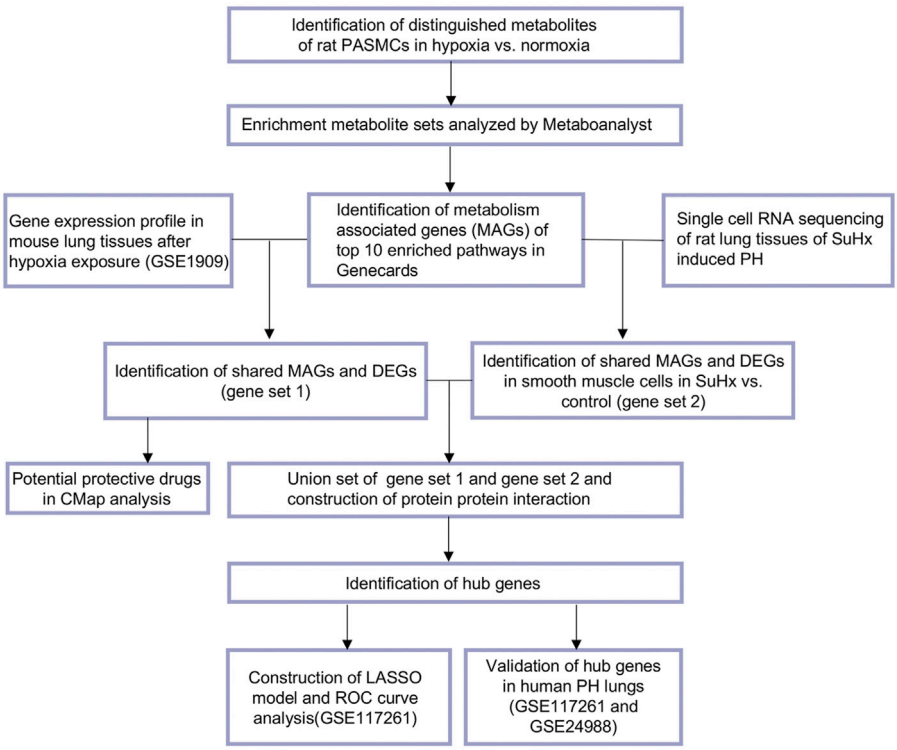

FIGURE 1 | Main analysis flowchart. Identification of distinguishing metabolites of rat pulmonary arterial smooth muscle cells (PASMCs) after hypoxia (1% O_2) exposure for 24 h versus PASMCs in normoxia condition. Enrichment metabolite sets were analyzed by Metaboanalyst (v 5.0). Top 10 enriched pathways were revealed, and 1,259 metabolism associated genes (MAGs) with a relevance score ≥8 of top 10 enriched pathways in Genecards were identified. Next the shared MAGs and differentially expressed genes (DEGs) in mouse lung tissues of hypoxia induced pulmonary hypertension (PH) were identified (gene set 1), and potential small molecular compounds (drugs) to reverse the altered expression of gene set 1 were revealed by Connectivity Map (CMap) analysis. Dataset of single cell RNA sequencing of rat lung tissues of Sugen 5416/hypoxia (SuHx) induced PH were obtained and shared genes of MAGs and DEGs in smooth muscle cells of SuHx versus control rats were listed in gene set 2. Gene set 1 and gene set 2 were combined and protein interaction were constructed and visualized. Hub gene were identified by cytoHubba or MCODE add-ins in Cytoscape. LASSO model was constructed with the expression profiles of hub genes and ROC curves generated to evaluate the ability of LASSO model to identify PH in dataset from GSE117261. Common hub genes were validated in human PH lung tissues versus controls in dataset from GSE117261 or combined datasets from GSE117261 and GSE24988.

Identification of Hub Genes and Network Interaction Visualization

Top 10 enriched metabolite pathways were identified by enrichment analysis of metabolite sets with online open-access platform Metaboanalyst (Chong et al., 2019) (v5.0, https://www.metaboanalyst.ca). Metabolism associated genes (MAGs) were acquired from Genecards (Safran et al., 2010) (https://www.genecards.org) database. The terms of top 10 enriched metabolite pathways were used as key word for analysis, and genes with relevance score >8 were regarded as MAGs. The intersection of MAGs and DEGs in mouse lung tissues of hypoxia induced PH was listed as gene set 1. The intersection of MAGs and DEGs in smooth muscle cells of SuHx versus control rats at single cell level was listed as gene set 2. The union set of these two gene sets were regarded as hypoxia induced metabolism associated genes. Protein protein interaction were analyzed and visualized by online tool STRING (v11.0, https://string-db.org). (Szklarczyk et al., 2019) Hub genes were identified by cytoHubba plugin with MCC algorithm or by MCODE plugin in Cytoscape (v 3.8.2) (Shannon et al., 2003).

Construction of LASSO Regression Model and Receiver Operating Characteristic Curve Analysis

To distinguish PH patients from control subjects, Least Absolute Shrinkage and Selection Operator (LASSO) regression model was constructed with the expression profiles of 6 metabolism associated hub genes by glmnet package in R. A model index for each sample was generated using the regression coefficients from the LASSO analysis to weight the expression value of the selected genes. GSE117261 data set were randomly assigned to training set (70%) and test set (30%). ROC curves were generated to evaluate the ability of LASSO model to identify PH by ROCR package.

Data Visualization and Statistics

The sample distribution of hypoxia exposed rat PASMCs (Hx) and control PASMCs (Nor), or mouse lung tissues under hypoxia at the indicated days were visualized in scatter plot with R package ggplot2. The distribution of data sets GSE117261 and GSE24988 before and after removal of batch effect was also visualized in scatter plot with ggplot2 package. Distinct

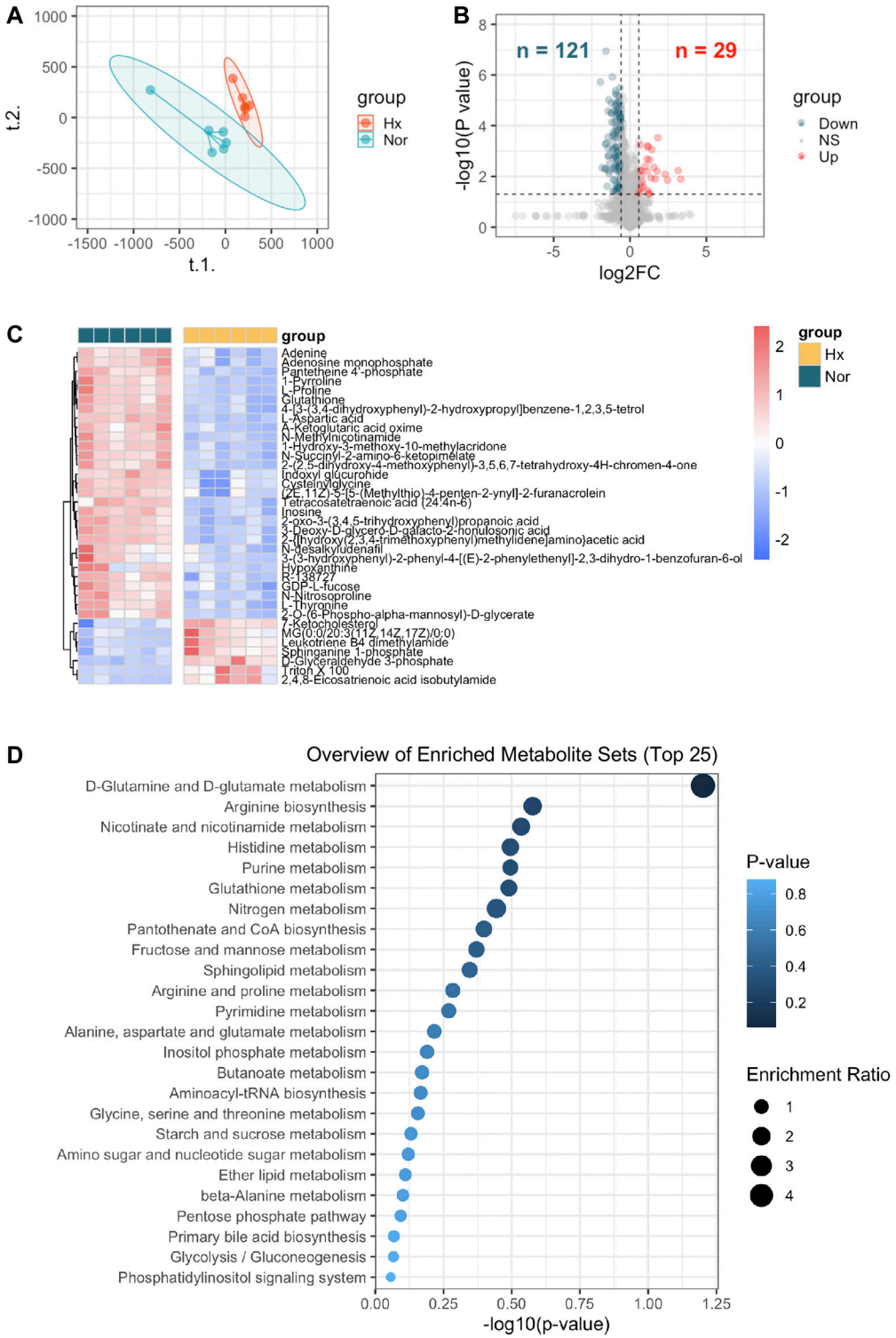

FIGURE 2 | Identification of metabolites distinguishing rat PASMCs under hypoxia from normoxic controls and enriched metabolite sets. **(A)** Partial least squares discriminant analysis (PLS-DA) demonstrated a well separated sample distribution of rat PASMCs under hypoxia (Hx) and control PASMCs (Nor) for 24 h and visualized in scatter plot (n = 6). **(B)** 29 upregulated metabolites (red dots) and 121 down-regulated metabolites (dark green) were identified and visualized in volcano plot (Fold change >1.5 or <0.67 and $p < 0.05$). **(C)** Expression of distinguishing metabolites in **(B)** with VIP score >1 were visualized in heatmap. **(D)** Top 25 enrichment metabolite sets of distinguishing metabolites were identified in Metaboanalyst (v 5.0).

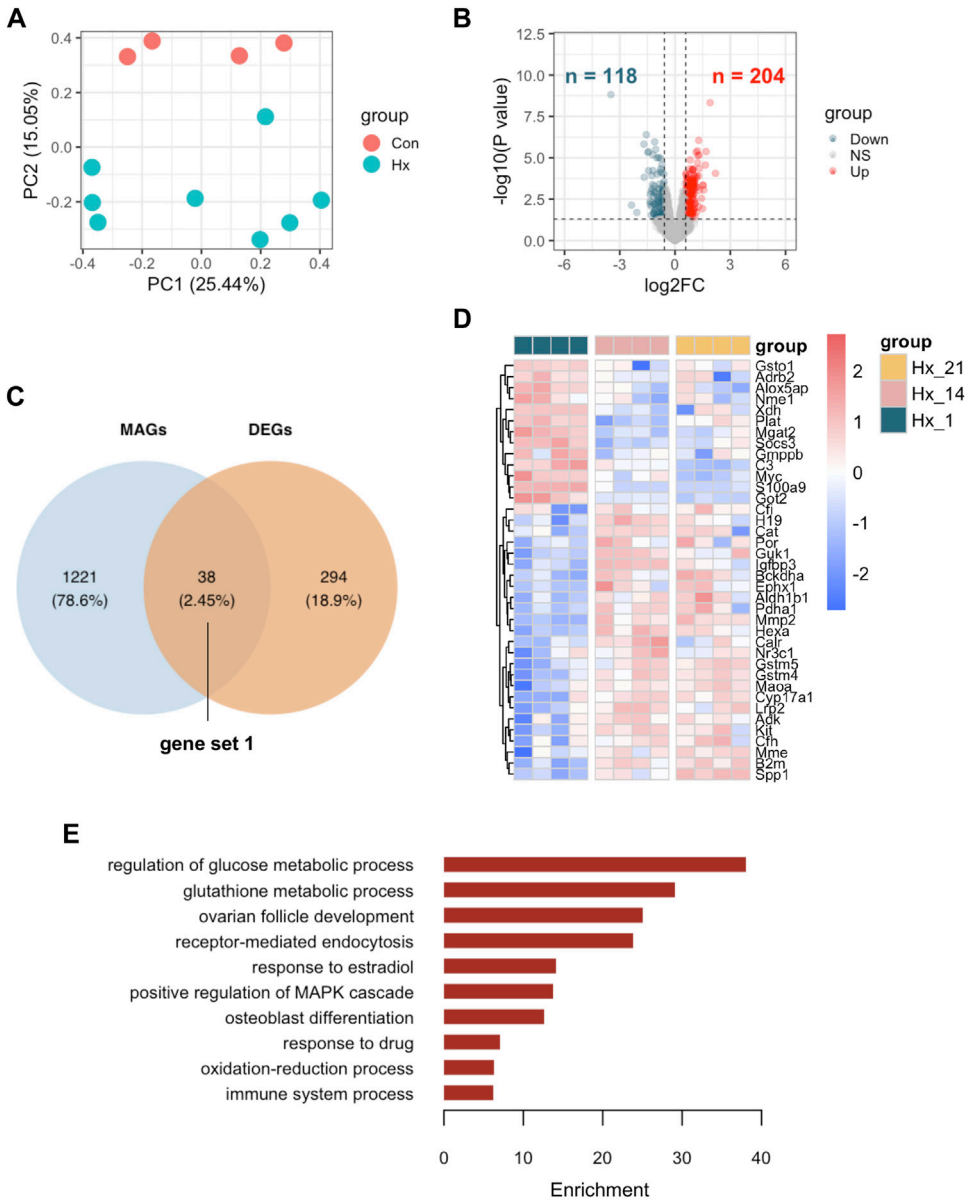

FIGURE 3 | Identification of metabolism associated DEGs in mouse lungs of hypoxia induced PH and enriched pathways. **(A)** Principal component analysis (PCA) demonstrated a well separated sample distribution of mouse lung tissues of hypoxia at day 14 and at day 21 (Hx) and those of hypoxia at day 1 (Con) from GSE 1909 (n = 4 per condition). **(B)** 204 upregulated genes (red dots) and 118 down-regulated metabolites (dark green) were identified and visualized in volcano plot (Fold change >1.5 or <0.67 and $p < 0.05$).**(C)** Overlap of metabolism associated genes (MAGs) and DEGs between Hx and Con were visualized in Venn diagram; 38 overlapped genes was listed as gene set 1. **(D)** Expression of 38 overlapped genes were visualized in heatmap at indicated time point after hypoxia; Hx_21: day 21 after hypoxia; Hx_14: day 14 after hypoxia; Hx_1: day 1 after hypoxia. **(E)** The enriched GO ontology (biological process) were identified by functional annotation tool DAVID and visualized in bar plot.

metabolites/genes between groups were visualized in volcano plot. Heatmap was generated to visualize the expression of all the distinct metabolites or indicated genes in each individual sample using pheatmap package in R. Venn diagram was generated to visualize the overlap of the indicated gene sets using R package VennDiagram. Pathway enrichment of indicated genes were analyzed in functional annotation bioinformatics tool DAVID (Huang et al., 2009) (v6.8, https://david.ncifcrf.gov/tools.jsp) and were then plotted with barplot function in R. Uniform manifold approximation and projection (UMAP) was generated based on Seurat_umap.coords data to visualize each clusters under different conditions. Hub gene network was visulized by Cytoscape.

Data are presented as the mean ± standard error of the mean (SEM). When two groups were compared, statistical differences were assessed with unpaired 2-tailed unpaired *t*-test if normally distributed. Otherwise, Mann-Whitney *U* test was utilized. Comparisons of more than three groups were performed by

analysis of variance (ANOVA) and Tukey's post-hoc test or Kruskal-Wallis test, as appropriate (GraphPad Prism 8). A two-sided p value of ≤0.05 was used to determine significant differences among groups.

RESULTS

Altered Metabolite Profiles in Rat PASMCs in Response to Hypoxia and Identification of Metabolism Associated Genes

According to flow chart as illustrated in **Figure 1**, the metabolite profiles in rat PASMCs under hypoxia stress and control PASMCs were explored. We found that distribution of hypoxia exposed rat PASMCs differed from control cells by PLS-DA analysis (**Figure 2A**). 29 up-regulated and 121 down-regulated metabolites were observed in hypoxia challenged PASMCs compared to control cells (FC > 1.5 or <0.67, $p < 0.05$) (**Figure 2B**). Among those only 36 metabolites were identified to have a VIP score >1 and their relative expressions among each individual sample were visualized in heatmap, of which 7 were upregulated and 29 were downregulated in response to hypoxia (**Figure 2C**). Next, we demonstrated that the metabolites distinguishing hypoxic and normoxic rat PASMCs were enriched in metabolite sets such as D-Glutamine and D-glutamate metabolism, arginine biosynthesis, nicotinate, and nicotinamide metabolism etc., and the top 25 enriched metabolite sets were display in **Figure 2D**.

We next selected top 10 metabolite sets to determine the MAGs potentially in response to hypoxia. A total of 1,259 unique MAGs with a relevance score >8 was identified from GeneCards website (**Supplementary Table S2**).

Identification of Differentially Expressed MAGs in Mouse Lungs of Hypoxia Induced PH and Potential Protective Drugs

To explore the differentially expressed MAGs in mouse lung tissues of hypoxia induced PH compared to control mice, we first scrutinize the DEGs in lung tissues of mice after hypoxia for 14 days or 21 days (Hx) compared to those after hypoxia for 1 day (Con) from GEO data set GSE 1909. Hx samples were well separate from Con samples (**Figure 3A**). In addition, 204 up-regulated and 118 down-regulated genes were displayed in Hx samples compared to Con samples (**Figure 3B**). The intersection of DEGs and MAGs is visualized in a Venn diagram (**Figure 3C**). The relative expression of 38 differentially expressed MAGs (gene set 1) in each individual lung tissue under hypoxia exposure at different time point were shown in heatmap, of which 25 were increased and 13 were decreased in Hx samples (**Figure 3D**). Next, the 38 MAGs were selected for functional analysis of GO ontology (biological process). It turned out that pathways including regulation of glucose metabolic process, glutathione metabolic process, receptor-mediated endocytosis, response to estradiol, positive regulation of MAPK cascade, etc. were enriched in response to chronic hypoxia exposure. In addition, CMap analysis were used to search for potential small molecular compounds to reverse altered expression of the 38 MAGs in gene set 1, and the top 10 most potential protective drugs including blebbistatin, corynanthine and butyl hydroxybenzoate were listed in **Table 1**.

Identification of Metabolism Associated Differentially Expressed Genes in Smooth Muscle Cells of Sugen 5416/Hypoxia Induced PH Rats and the Expressions in Mouse Hypoxic Lung Tissues

Due to the application of single cell RNA sequencing, we are allowed to examine the DEGs at a single cell resolution. Hence, we sought to further test the metabolism associated DEGs in smooth muscle cell from lung tissues of SuHx rats relative to control rats. As illustrated in **Figure 4A**, UMAP was generated based on Seurat_umap.coords data from an open-access online platform (http://mergeomics.research.idre.ucla.edu/PVDSingleCell/) and displayed the overlap of distinct clusters from control, monocrotaline or SuHx lungs. Overlap of 1,259 MAGs and 27 repoeted DEGs in smooth muscle cells (**Supplementary Table S3**) between SuHx and control rats were visualized in Venn diagram, with 5 overlapped genes (*Acox1*, *Gpx3*, *Mmp2*, *Taldo1,* and *Aldh6a1*) listed as gene set 2 (**Figure 4B**). We next examined the expression of 5 differentially expressed MAGs in lung tissues of hypoxia induced PH mice. All genes except *Aldh6a1* were detected in lung tissues from GSE1909 data set. *Mmp2* and *Gpx3* were significantly elevated in mouse lung tissues after hypoxia exposure for 21 days ($p < 0.05$), and had a tendancy towards elevation at day 14 post-hypoxia even though didn't reach any significance (**Figure 4C**).

Identification of Hypoxia Induced Metabolism Associated Hub Genes and the Expressions in Hypoxic Lung Tissues

We next combined the differentially expressed MAGs in mouse lungs of hypoxia induced PH (gene set 1) and differentially expressed MAGs in smooth muscle cells of lungs from SuHx rats (gene set 2). A total of 42 genes of both gene sets were then potentially regarded as hypoxia induced MAGs (**Figure 5A**). 61 Protein protein interactions among the 42 genes were analyzed and visualized by STRING (v11.0) (**Figure 5B**). To identify the hub genes of the protein protein network, cytoHubba plugin with MCC algorithm and MCODE plugin in Cytoscape were utilized, respectively. Ten hub genes were discovered by cytoHubba (**Figure 5C**) and six hub genes were identified by MCODE (**Figure 5D**). Of note, six genes including *Cat*, *Ephx1*, *Gpx3*, *Gstm4*, *Gstm5,* and *Gsto1* were identified as core hub genes as they were unveiled by both methods. We next investigated the expressions of six hub genes in mouse lung tissues from GSE1909 data set at indicated time point after hypoxia or recovery to normoxia after hypoxia exposure. *Cat* encoding catalase, *Ephx1* encoding epoxide hydrolase 1 and *Gstm4* encoding glutathione S-transferase, mu 4 were increased both at day 14 and day 21 after hypoxia stress compared to control group (all $p < 0.05$) and declined after 14 days recovery to normoxia, although the reduction is only significant in *Gstm4* ($p < 0.05$). A similar trend was also observed in *Gpx3* encoding glutathione peroxidase 3 and *Gstm5* encoding glutathione S-transferase mu 5. In contrast, *Gsto1* encoding glutathione S-transferase omega 1

TABLE 1 | List of 10 most significant small molecular compounds provided by CMap analysis to reverse altered expression of 38 differentially expressed MAGs of gene set 1 in cell lines.

CMap name	Mean	Enrichment	*p*	Percent non-null
blebbistatin	−0.658	−0.89	0.02388	100
corynanthine	−0.578	−0.933	0.0005	100
butyl hydroxybenzoate	−0.547	−0.847	0.00024	100
canadine	−0.545	−0.84	0.00117	100
ciclosporin	−0.476	−0.639	0.00638	66
flurbiprofen	−0.476	−0.666	0.00965	80
dyclonine	−0.445	−0.73	0.0107	75
ramifenazone	−0.445	−0.674	0.02528	75
ketorolac	−0.437	−0.746	0.00822	75
trimethylcolchicinic acid	−0.423	−0.653	0.03416	75

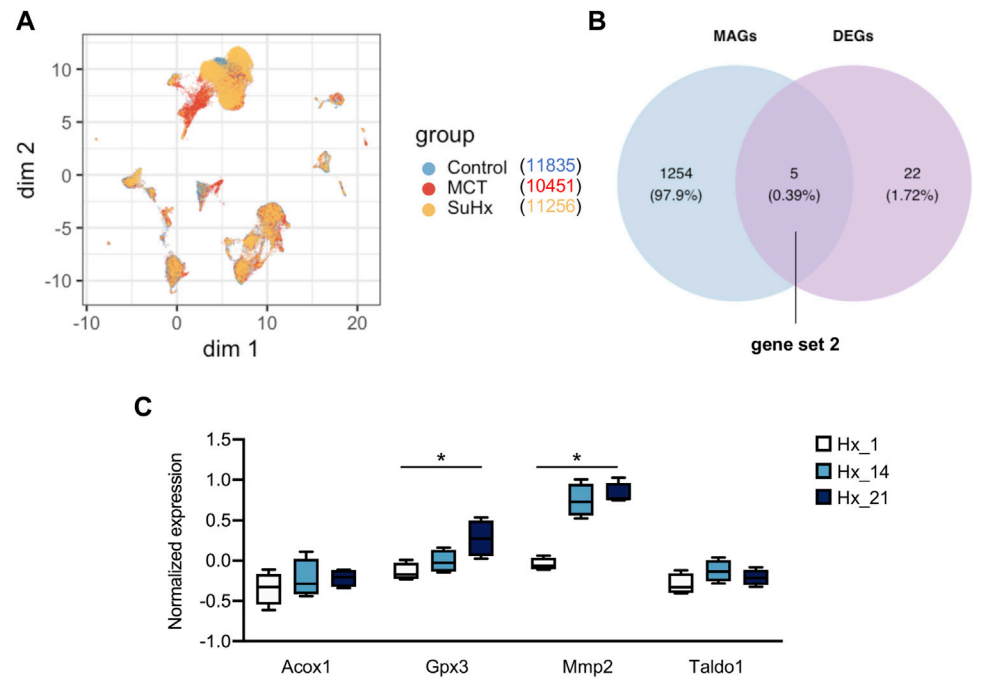

FIGURE 4 | Identification of metabolism associated DEGs in SMC of SuHx rats and expressions in mouse lungs. **(A)** Uniform manifold approximation and projection (UMAP) was generated based on Seurat_umap.coords data from an open-access online platform (http://mergeomics.research.idre.ucla.edu/PVDSingleCell/). **(B)** Overlap of metabolism associated genes (MAGs) and DEGs in smooth muscle cells between Sugen 5416/hypoxia induced PH (SuHx) and control rats were visualized in Venn diagram; 5 overlapped genes was listed as gene set 2. **(C)** Expression of 4 overlapped genes (Aldh6a1 was not detected in lung tissues from GSE1909 dataset) were visualized in box plot at indicated time point after hypoxia; Hx_1: day 1 after hypoxia, Hx_14: day 14 after hypoxia, Hx_21: day 21 after hypoxia. Data represent mean ± SEM. *$p < 0.05$, as analyzed by one-way ANOVA with Tukey's multiple comparisons or Kruskal-Wallis test respectively, as appropriate.

were declined at day 14 and day 21 after hypoxia stress and didn't alter after recovery to ambient atmosphere (**Figure 5E**).

Evaluation of Hypoxia Induced Metabolism Associated Hub Genes in Lung Tissues of Patients With Pulmonary Hypertension

As we revealed the six core hypoxia induced metabolism associated hub genes according to cellular metabolomics study and transcriptomics of lung tissues in rodent PH models, we next determined whether these hub genes altered in lung tissues of human PH lungs. To this end, we first examined the expression profile of hub genes in lung tissues of 58 patients with PH and 25 control subjects from GSE117261 data set. In line with the observation from mouse GSE1909 data set, *CAT*, *EPHX1* and *GSTM5* were higher and *GSTO1* was lower in PH patients compared to control subjects (all $p < 0.05$). While *GPX3* was lower in PH patients and *GSTM4* didn't differ PH from control subjects (**Figure 6A**). Next, we sought to construct LASSO model to examine whether the metabolism associated

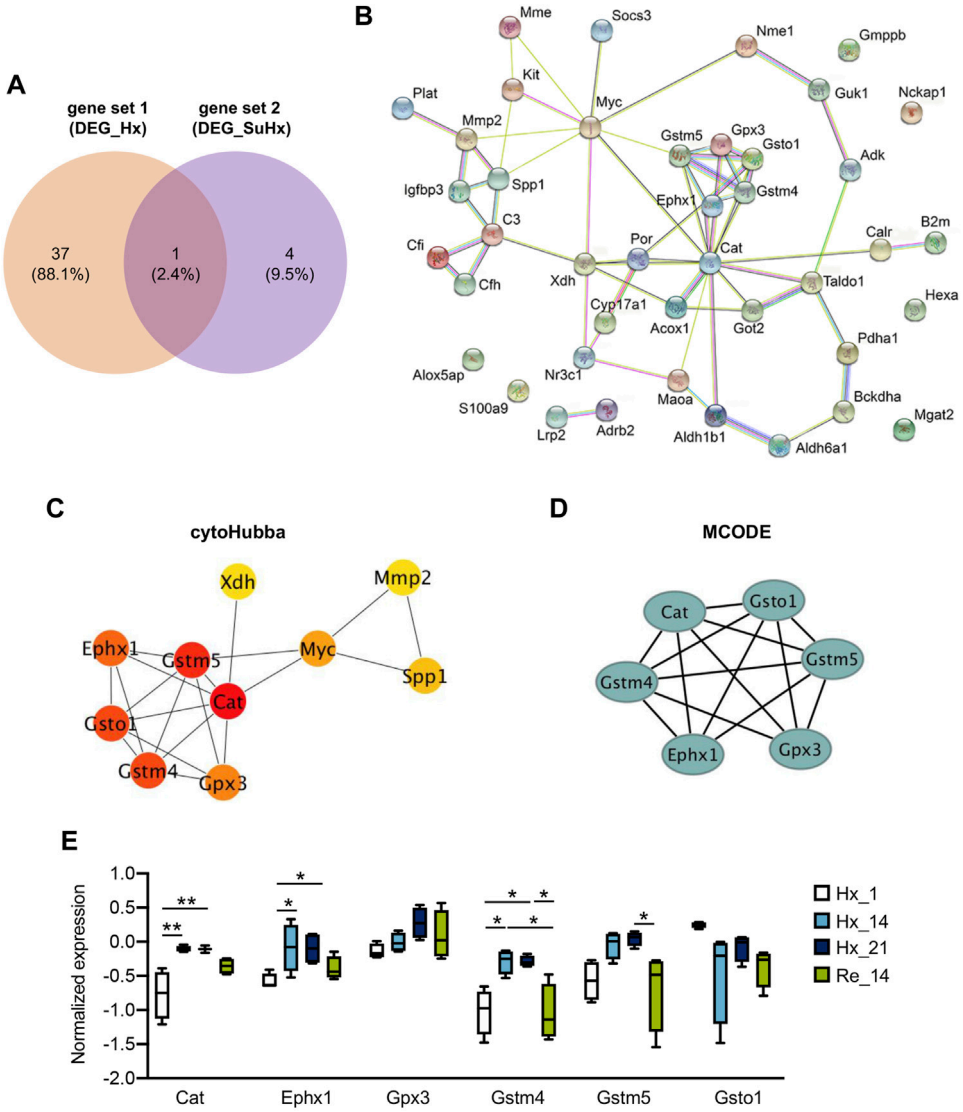

FIGURE 5 | Identification of hypoxia induced metabolism associated hub genes and the expressions in hypoxic lungs. **(A)** Overlap of gene set 1 and gene set 2 were visualized in Venn diagram; 42 genes in union set of both gene sets were regarded as hypoxia induced metabolism associated genes. **(B)** Protein protein interaction among the 42 genes were analyzed and visualized by online tool STRING (v11.0). **(C)** Identification of 10 hub genes by cytoHubba plugin with MCC algorithm in Cytoscape (v 3.8.2); each circle represents unique gene and the redder the color is, the higher the MCC score is. **(D)** Identification of 6 hub genes by MCODE plugin in Cytoscape (v 3.8.2); each circle represents unique gene. **(E)** Expression of 6 shared hub genes were visualized in box plot at indicated time point after hypoxia or recovery to normoxia; Hx_1: day 1 after hypoxia, Hx_14: day 14 after hypoxia, Hx_21: day 21 after hypoxia, Re_14: day 14 of normoxia recovery after 21 days of hypoxia exposure. Data represent mean ± SEM. $^{*}p < 0.05$, $^{**}p < 0.01$, as analyzed by one-way ANOVA with Tukey's multiple comparisons or Kruskal-Wallis test respectively, as appropriate.

hub genes could predict PH. 5 genes were identified with non-zero regression coefficients, and the value of lambda. min was 0.0132,974. The gene-based model index was generated as the following formula: index = *CAT*0.157* + *GSTM5*0.245* + *GPX3*(− 0.288)* + *GSTM4*(− 0.346)* + *GSTO1*(− 0.001)* + 2.641. ROC curve analysis indicated that area under the curve (AUC) of the 5-gene-based model was 0.90 in the training set from GSE117261 (**Figure 6B**) and 0.83 in the test set from GSE117261 (**Figure 6C**), suggesting the established LASSO model might be served as a predictor of PH.

To test the six hypoxia induced metabolism associated hub genes in a larger cohort, we then sought to combine two human PH cohorts (GSE117261 and GSE24988) consisting 120 PH patients and 47 control subjects. We noticed the robust batch effect between these two data sets and used ComBat function in the sva package to merge them and remove the batch effect (**Figure 6D**). Next, we explored the expression of six hub genes in lung tissues of the merged data sets from GSE117261 and GSE24988 after correction of batch effect. PH patients still exhibited higher *EPHX1* and *GSTM5* and lower *GSTO1* and *GPX3* in lung tissues compared to control subjects

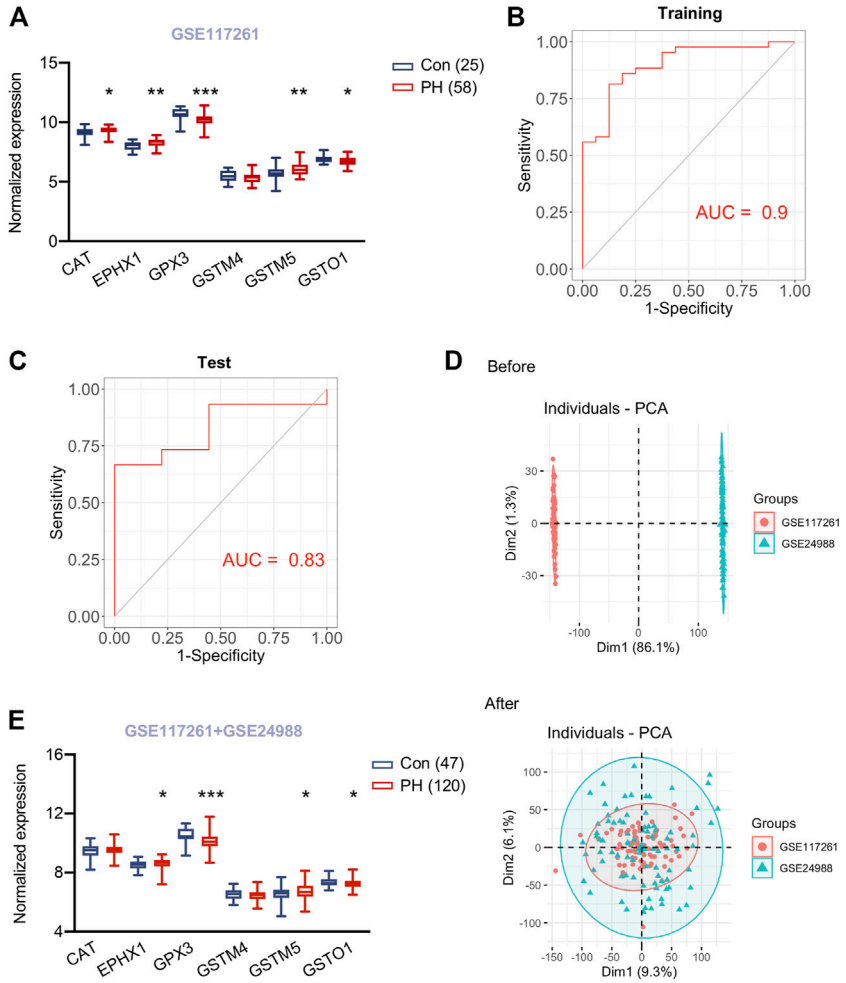

FIGURE 6 | Validation of hub genes in lungs of PH patients and a predicting model for PH. **(A)** Expression of six hypoxia induced metabolism associated hub genes in lung tissues of 58 patients with pulmonary hypertension (PH) and 25 control subjects from GSE117261. **(B)** ROC curve analysis of training set (GSE117261) using six hub genes. **(C)** ROC curve analysis of test set (GSE117261) using six hub genes. **(D)** PCA analysis demonstrated the distribution of data sets GSE117261 (red) and GSE24988 (green) before **(upper panel)** and after **(lower panel)** removal of batch effect. The distribution was visualized in scatter plot. **(E)** Expression of six hypoxia induced metabolism associated hub genes in lung tissues of 120 patients with pulmonary hypertension (PH) and 47 control subjects from GSE117261 and GSE24988 after correction of batch effect. Data represent mean ± SEM. $^{*}p < 0.05$, $^{**}p < 0.01$, $^{***}p < 0.001$ compared to corresponding control subjects, as analyzed by unpaired *t* test or Mann-Whitney *U* test respectively, as appropriate.

(all $p < 0.05$), *CAT* and *GSTM4* didn't differ from PH and control subjects (**Figure 6E**).

DISCUSSION

In the present study our metabolomics analysis at cellular level has identified altered metabolite profiles in rat PASMCs in response to hypoxia and MAGs based on enriched metabolite sets under hypoxia stress. In combination of the transcriptomics data from GEO database, we also figured out differentially expressed MAGs in mouse lungs of hypoxia induced PH. In addition, we identified metabolism associated DEGs in smooth muscle cells of Sugen 5416/hypoxia induced PH rats at a single cell resolution. Our findings highlight the critical function of metabolic adaptations in supporting PASMC proliferation and pulmonary vasculature remodeling under hypoxic condition. We also demonstrated six metabolism associated hub genes and confirmed the alteration of those hub gene expressions in lung tissues of PH patients relative to control subjects, thus providing some insight into the pathogenesis of pulmonary vascular remodeling in PH.

Metabolite perturbation is a very common feature in pulmonary hypertension. In 2014, higher levels of bile acid metabolites in PAH lung tissues were revealed via an untargeted metabolomics method (Zhao et al., 2014). A comprehensive metabolomics study in 2017 identified a distinguishing plasma metabolite pattern in a cohort of well-phenotyped PAH patients from both healthy and symptomatic disease control subjects without PAH, with some of the metabolites of prognostic value in PAH. Changes in the levels of metabolites over time were associated with survival (Rhodes et al., 2017). Circulating indoleamine 2,3-dioxygenase-dependent tryptophan metabolites, tricarboxylic acid intermediates, purine metabolites and arginine-

nitric oxide metabolites were revealed to be associated with hemodynamic indicators of right ventricular-pulmonary vascular function by targeted mass spectrometry (Lewis et al., 2016). Our previous study also showed higher plasma levels of spermine in two independent cohorts of idiopathic PAH patients by targeted metabolomic strategy and inhibition of spermine synthesis could inhibit PASMC proliferation *in vitro* and retard PH progression *in vivo* (He et al., 2020). All the findings implicate the disrupted metabolites could serve as potential biomarkers in PH and the correction of metabolism disturbance via modulation of related metabolism associated genes (eg. SMS encoding spermine synthase) might represent a novel therapeutic approach to treat PH.

It is increasingly recognized that the mitochondria, as the orchestrator of energy metabolism, in pulmonary vascular cells exhibit decreased oxidative phosphorylation and increased glycolysis, supporting the existence of the Warburg effect in PH (Cottrill and Chan, 2013; Dabral et al., 2019; Rhodes, 2020). Hypoxia is recognized as a contributor to pulmonary vascular remodeling and can induce local inflammation in pulmonary vasculature by release of growth factors with autocrine/paracrine effects on pulmonary arterial endothelial cells as well as PASMCs (Meuchel et al., 2011; Helan et al., 2014). Several studies have been focused on the imbalanced oxidative phosphorylation/glycolysis and metabolite maladaptation in hypoxic condition in PH. The expression of iron-sulfur scaffold protein BOLA3 (BolA Family Member 3) was reduced in endothelial cells of PH in a hypoxia-dependent manner. BOLA3 deficiency in endothelial cells were demonstrated to activate glycolysis and fatty acid oxidation and drive the production of reactive oxygen species governing proliferative and apoptosis-resistant phenotype of endothelial cells. Endothelial cell knockdown of BOLA3 dysregulate glycine metabolism and promote hemodynamic and histological manifestations of PH, which could be restored via overexpression of pulmonary vascular BOLA3 and glycine supplementation (Yu et al., 2019). Another study showed a metabolic reprogramming towards aerobic glycolysis in PH fibroblasts compared to control fibroblasts. Increased expression of C-terminal Binding Protein-1 (a transcriptional co-repressor that is activated by increased free-NADH secondary to glycolytic reprogramming) was revealed in the lungs of hypoxia-induced experimental PH and in idiopathic PAH patients to orchestrate a network of genes regulating cell proliferation and inflammation. The inhibition of this transcriptional factor was shown to correct the aberrant metabolic, hyper-proliferative and inflammatory phenotype of bovine and human PH fibroblasts and in hypoxic mice (Li et al., 2016). However, the metabolite disturbances in PASMCs under hypoxia stress and their metabolite associated genes in response to hypoxia *in vitro* and in the context of hypoxic pulmonary hypertension *in vivo* remains largely unexplored. Our findings of the metabolite associated genes could provide some novel metabolic targets for diagnostic and therapeutic development in this devastating disease.

In this study, we also identified a list of potential small molecular compounds that might reverse the metabolism associated genes under hypoxia stress. Blebbistatin, ranking the top in the list as a cell-permeable selective inhibitor of myosin II ATP activity, has been reported to reduce neointimal formation and luminal obstruction after vascular injury. It was also evident that blebbistatin had a dose-dependent inhibitory effect on DNA replication and cell proliferative responses to platelet-derived growth factor-BB, a critical trigger in PH progression (Huang et al., 2011). In addition, blebbistatin was shown to inhibit endothelial cell-derived microparticles and platelet-derived microparticles production, thus alleviating ischemia-reperfusion induced pulmonary vascular leakage and lung injury (Zhang et al., 2020). All the findings indicate that blebbistatin might modulate the pulmonary vasculature and open a new avenue for the treatment of PH.

A total of six metabolism associated hub genes (*Cat*, *Ephx1*, *Gpx3*, *Gstm4*, *Gstm5*, and *Gsto1*) were identified. An increase of catalase (hydrogen peroxide catalyser) encoded by *Cat* was demonstrated in both hypoxic mouse lung tissues as well as in lung tissues of PH patients in our study, which was in line with the increased catalase expression in hypoxia PASMCs in an AMPK- and FoxO1-dependent manner in another study (Awad et al., 2014). Additionally, catalase markedly inhibited relaxation mediated by endothelium-dependent hyperpolarization. The subsequent nitrosative stress may be potential triggers of the onset of PH (Tanaka et al., 2018). However, role of catalase in PH is controversial, it has been reported that chronic hypoxia induced reactive oxygen species production could be reversed by catalase (Song et al., 2021). Mice with mitochondrial targeted catalase overexpression attenuated hypoxia-induced PH and proliferative markers (Adesina et al., 2015). Therefore cell-specific *Cat* deletion would be of value to discern the role of catalase in the development of hypoxic PH. The soluble epoxide hydrolase (sEH) encoded by *Ephx2* metabolizes anti-inflammatory epoxyeicosatrienoic acids (EETs) to a less active dihydroxy derivatives. Inhibition of sEH attenuated monocrotaline induced PH in rats. As another key enzyme responsible for EETs hydrolysis *in vivo* (Edin et al., 2018), microsomal epoxide hydrolase (mEH) encoded by *Ephx1* remains to be fully elucidated. Study by Marowsky et al. identified the localization of mEH in brain vascular structure (endothelial and smooth muscle cells). mEH in their study was also reported to have a higher apparent affinity compared to sEH, suggesting that mEH might still contribute to EET turnover even with low substrate (EETs) concentrations (Marowsky et al., 2009). However, the role of *Ephx1* in pulmonary vascular remodeling was unexplored, and whether the two epoxide hydrolases have individual or distinct role in PH warrants further investigation. Recently, Gpx3 has been identified as a novel regulator of insulin receptor expression, and Gpx3 dysregulation would impact insulin receptor and lead to insulin resistance, a not uncommon feature in PAH patients (Pugh et al., 2013; Bradley and Bradley, 2014; Hauffe et al., 2020). In addition, Loss of glutathione peroxidase 3 encoded by *Gpx3* induces ROS and contributes to prostatic hyperplasia (Kim et al., 2020). Patients with systemic sclerosis-related PH displayed lower

serum levels of glutathione peroxidase 3 encoded by *Gpx3* (Sun et al., 2020), which was consistent with our observation of a reduction of *Gpx3* in lung tissues of PH patients transcriptionally. However, the role of Gpx3 is worth further scrutiny. *Gstm4* and *Gstm5* encode the proteins belonging to glutathione S-transferases, which are involved in limiting oxidative damage, a critical driver to the development of PH, to tissue (Strange et al., 2001). There is one study showing that glutathione S-transferase mu1 (GSTM1) was significantly decreased in the irreversible CHD-PAH patients, suggesting GSTM1 may be a potential biomarker and target in the irreversibility CHD-PAH (Huang et al., 2018). However, the antioxidant role of Gstm4 and Gstm5 in PH remains unknown. *Gsto1* encode glutathione transferase omega 1, which is a constitutively active deglutathionylating enzyme and required for the lipopolysaccharide-stimulated induction of NADPH oxidase 1 and the production of reactive oxygen species in macrophages (Menon et al., 2014). It also serves as a regulator of the nod-like receptor family, pyrin domain containing 3 (NLRP3) inflammasome via the modulation of NEK7 (Hughes et al., 2019). Of note, NLRP3 inflammasome and its regulated pro-inflammatory cytokines are identified to contribute to pathogenesis of PAH (Tang et al., 2015; Deng et al., 2019). Whether Gsto1 could modulate pulmonary vascular remodeling via NLRP3 or other biological activities remains to be elucidated. Our observation of the alteration of glutathione S-transferases in lung tissues of experimental PH as well as PH patients pinpoints the necessity to determine whether the distinct glutathione S-transferases has separating or overlapping functions in the development of PH, which might provide some insights for the treatment of various diseases triggered by oxidative stress.

There are some limitations in our study. First, in terms of dataset selection, not all datasets for PAH lung tissues were included in our study and our datasets were selected mainly based on sample size, which we considered as a very important factor for data mining. We were also unable to detect the transcriptional expression of hub genes in human lung tissues owing to the lack of transcriptomics studies from human PH due to hypoxia. However, the difference in expression of hub genes from lung tissues of PH patients compared to control subjects underlines their role in the common pathogenesis during the development of PH. Second, the differentially expressed MAGs are underrepresented given that the sample size of hypoxia induced PH mice is limited. Therefore, the lung tissue of hypoxic PH rodent models with larger sample size warranted further investigation and would add more value for the identification of MAGs. In addition, only one single cell RNA sequencing data from PH rodent models is available as of today, hence, hypoxic pulmonary arteries instead of whole lung tissues at the single cell resolution would provide more precise information in the alteration of PASMCs in response to hypoxia, which might aid in the discovery of mechanisms underlying hypoxic PH and thus lead to improved targeted therapies.

CONCLUSION

We identified a metabolic profile distinguishing hypoxia-treated from control PASMCs. The combination of the transcriptomics and metabolomics studies allow us to reveal six hypoxia-induced metabolism associated hub genes in response to hypoxia. This would shed some light on the molecular mechanism in hypoxic PH and provide potential therapeutic targets for PH.

DATA AVAILABILITY STATEMENT

The datasets presented in this study can be found in online repositories. The names of the repository/repositories and accession number(s) can be found in the article/**Supplementary Material**.

ETHICS STATEMENT

The animal study was reviewed and approved by the Ethics and Animal Care and Use Committee of Henan University.

AUTHOR CONTRIBUTIONS

Y-YH contributed to the study design, data interpretation, provided funding, and wrote the manuscript. X-MX contributed to data analysis and data interpretation. H-DZ provided funding and contributed to data interpretation. JY, SG, EvdV, YD, CW, and X-BP provided crucial intellectual support. Z-CJ provided crucial intellectual support and funding. YY conceived and supervised the study, performed the data analysis, contributed to data interpretation, and wrote the manuscript. Z-YH conceived and supervised the study, contributed to data interpretation, and wrote the manuscript.

FUNDING

This work was supported by the 13th Five-Year Plan—Precise Medicine—Key Research and Development Program—Clinical Cohort of Rare Disease (2016YFC0901500), Projects of National Natural Science Foundation of China (81630003, 82170058, 82000064), Beijing Natural Science Foundation (7181009), Science Foundation for Outstanding Young Scholars of Henan Province (212300410027), and Key Project of Ningxia Hui Autonomous Region (2019BFG02027).

ACKNOWLEDGMENTS

We thank J-W. Chen (University of Illinois at Chicago) for the professional editing of the paper.

SUPPLEMENTARY MATERIAL

The Supplementary Material for this article can be found online at: https://www.frontiersin.org/articles/10.3389/fphar.2021.753727/full#supplementary-material

REFERENCES

Adesina, S. E., Kang, B. Y., Bijli, K. M., Ma, J., Cheng, J., Murphy, T. C., et al. (2015). Targeting Mitochondrial Reactive Oxygen Species to Modulate Hypoxia-Induced Pulmonary Hypertension. *Free Radic. Biol. Med.* 87, 36–47. doi:10.1016/j.freeradbiomed.2015.05.042

Awad, H., Nolette, N., Hinton, M., and Dakshinamurti, S. (2014). AMPK and FoxO1 Regulate Catalase Expression in Hypoxic Pulmonary Arterial Smooth Muscle. *Pediatr. Pulmonol* 49, 885–897. doi:10.1002/ppul.22919

Bradley, E. A., and Bradley, D. (2014). Pulmonary Arterial Hypertension and Insulin Resistance. *J. Mol. Genet. Med.* 2, 15. doi:10.4172/1747-0862.S1-015

Chen, B., Calvert, A. E., Cui, H., and Nelin, L. D. (2009). Hypoxia Promotes Human Pulmonary Artery Smooth Muscle Cell Proliferation through Induction of Arginase. *Am. J. Physiol. Lung Cel Mol Physiol* 297, L1151–L1159. doi:10.1152/ajplung.00183.2009

Chen, J., Tang, H., Sysol, J. R., Moreno-Vinasco, L., Shioura, K. M., Chen, T., et al. (2014). The Sphingosine Kinase 1/sphingosine-1-Phosphate Pathway in Pulmonary Arterial Hypertension. *Am. J. Respir. Crit. Care Med.* 190, 1032–1043. doi:10.1164/rccm.201401-0121OC

Chong, J., Wishart, D. S., and Xia, J. (2019). Using MetaboAnalyst 4.0 for Comprehensive and Integrative Metabolomics Data Analysis. *Curr. Protoc. Bioinformatics* 68, e86. doi:10.1002/cpbi.86

Cottrill, K. A., and Chan, S. Y. (2013). Metabolic Dysfunction in Pulmonary Hypertension: the Expanding Relevance of the Warburg Effect. *Eur. J. Clin. Invest.* 43, 855–865. doi:10.1111/eci.12104

Dabral, S., Muecke, C., Valasarajan, C., Schmoranzer, M., Wietelmann, A., Semenza, G. L., et al. (2019). A RASSF1A-Hif1α Loop Drives Warburg Effect in Cancer and Pulmonary Hypertension. *Nat. Commun.* 10, 2130. doi:10.1038/s41467-019-10044-z

de Jesus Perez, V. A. (2016). Molecular Pathogenesis and Current Pathology of Pulmonary Hypertension. *Heart Fail. Rev.* 21, 239–257. doi:10.1007/s10741-015-9519-2

Deng, Y., Guo, S. L., Wei, B., Gao, X. C., Zhou, Y. C., and Li, J. Q. (2019). Activation of Nicotinic Acetylcholine α7 Receptor Attenuates Progression of Monocrotaline-Induced Pulmonary Hypertension in Rats by Downregulating the NLRP3 Inflammasome. *Front. Pharmacol.* 10, 128. doi:10.3389/fphar.2019.00128

Edin, M. L., Hamedani, B. G., Gruzdev, A., Graves, J. P., Lih, F. B., Arbes, S. J., 3rd, et al. (2018). Epoxide Hydrolase 1 (EPHX1) Hydrolyzes Epoxyeicosanoids and Impairs Cardiac Recovery after Ischemia. *J. Biol. Chem.* 293, 3281–3292. doi:10.1074/jbc.RA117.000298

Gharib, S. A., Luchtel, D. L., Madtes, D. K., and Glenny, R. W. (2005). Global Gene Annotation Analysis and Transcriptional Profiling Identify Key Biological Modules in Hypoxic Pulmonary Hypertension. *Physiol. Genomics* 22, 14–23. doi:10.1152/physiolgenomics.00265.2004

Harder, E. M., and Waxman, A. B. (2020). Clinical Trials in Group 3 Pulmonary Hypertension. *Curr. Opin. Pulm. Med.* 26, 391–396. doi:10.1097/MCP.0000000000000694

Hauffe, R., Stein, V., Chudoba, C., Flore, T., Rath, M., Ritter, K., et al. (2020). GPx3 Dysregulation Impacts Adipose Tissue Insulin Receptor Expression and Sensitivity. *JCI Insight* 5 (11), e136283. doi:10.1172/jci.insight.136283

He, Y. Y., Yan, Y., Jiang, X., Zhao, J. H., Wang, Z., Wu, T., et al. (2020). Spermine Promotes Pulmonary Vascular Remodelling and its Synthase Is a Therapeutic Target for Pulmonary Arterial Hypertension. *Eur. Respir. J.* 56. doi:10.1183/13993003.00522-2020

Helan, M., Aravamudan, B., Hartman, W. R., Thompson, M. A., Johnson, B. D., Pabelick, C. M., et al. (2014). BDNF Secretion by Human Pulmonary Artery Endothelial Cells in Response to Hypoxia. *J. Mol. Cel Cardiol* 68, 89–97. doi:10.1016/j.yjmcc.2014.01.006

Hoeper, M. M., Bogaard, H. J., Condliffe, R., Frantz, R., Khanna, D., Kurzyna, M., et al. (2013). Definitions and Diagnosis of Pulmonary Hypertension. *J. Am. Coll. Cardiol.* 62, D42–D50. doi:10.1016/j.jacc.2013.10.032

Hong, J., Arneson, D., Umar, S., Ruffenach, G., Cunningham, C. M., Ahn, I. S., et al. (2020). Single-cell Study of Two Rat Models of Pulmonary Arterial Hypertension Reveals Connections to Human Pathobiology and Drug Repositioning. *Am. J. Respir. Crit. Care Med.* 203 (8), 1006–1022. doi:10.1164/rccm.202006-2169OC

Huang, da. W., Sherman, B. T., and Lempicki, R. A. (2009). Bioinformatics Enrichment Tools: Paths toward the Comprehensive Functional Analysis of Large Gene Lists. *Nucleic Acids Res.* 37, 1–13. doi:10.1093/nar/gkn923

Huang, J., Zhang, J., Pathak, A., Li, J., and Stouffer, G. A. (2011). Perivascular Delivery of Blebbistatin Reduces Neointimal Hyperplasia after Carotid Injury in the Mouse. *J. Pharmacol. Exp. Ther.* 336, 116–126. doi:10.1124/jpet.110.174615

Huang, L., Li, L., Hu, E., Chen, G., Meng, X., Xiong, C., et al. (2018). Potential Biomarkers and Targets in Reversibility of Pulmonary Arterial Hypertension Secondary to Congenital Heart Disease: an Explorative Study. *Pulm. Circ.* 8, 2045893218755987. doi:10.1177/2045893218755987

Hughes, M. M., Hooftman, A., Angiari, S., Tummala, P., Zaslona, Z., Runtsch, M. C., et al. (2019). Glutathione Transferase Omega-1 Regulates NLRP3 Inflammasome Activation through NEK7 Deglutathionylation. *Cell Rep* 29, 151–e5. doi:10.1016/j.celrep.2019.08.072

Kim, U., Kim, C. Y., Lee, J. M., Ryu, B., Kim, J., Bang, J., et al. (2020). Loss of Glutathione Peroxidase 3 Induces ROS and Contributes to Prostatic Hyperplasia in Nkx3.1 Knockout Mice. *Andrology* 8, 1486–1493. doi:10.1111/andr.12828

Kitagawa, A., Jacob, C., Jordan, A., Waddell, I., McMurtry, I. F., and Gupte, S. A. (2021). Inhibition of Glucose-6-Phosphate Dehydrogenase Activity Attenuates Right Ventricle Pressure and Hypertrophy Elicited by VEGFR Inhibitor + Hypoxia. *J. Pharmacol. Exp. Ther.* 377, 284–292. doi:10.1124/jpet.120.000166

Lamb, J., Crawford, E. D., Peck, D., Modell, J. W., Blat, I. C., Wrobel, M. J., et al. (2006). The Connectivity Map: Using Gene-Expression Signatures to Connect Small Molecules, Genes, and Disease. *Science* 313, 1929–1935. doi:10.1126/science.1132939

Leek, J. T., Johnson, W. E., Parker, H. S., Jaffe, A. E., and Storey, J. D. (2012). The Sva Package for Removing Batch Effects and Other Unwanted Variation in High-Throughput Experiments. *Bioinformatics* 28, 882–883. doi:10.1093/bioinformatics/bts034

Lewis, G. D., Ngo, D., Hemnes, A. R., Farrell, L., Domos, C., Pappagianopoulos, P. P., et al. (2016). Metabolic Profiling of Right Ventricular-Pulmonary Vascular Function Reveals Circulating Biomarkers of Pulmonary Hypertension. *J. Am. Coll. Cardiol.* 67, 174–189. doi:10.1016/j.jacc.2015.10.072

Li, M., Riddle, S., Zhang, H., D'Alessandro, A., Flockton, A., Serkova, N. J., et al. (2016). Metabolic Reprogramming Regulates the Proliferative and Inflammatory Phenotype of Adventitial Fibroblasts in Pulmonary Hypertension through the Transcriptional Corepressor C-Terminal Binding Protein-1. *Circulation* 134, 1105–1121. doi:10.1161/CIRCULATIONAHA.116.023171

Luo, Y., Teng, X., Zhang, L., Chen, J., Liu, Z., Chen, X., et al. (2019). CD146-HIF-1α Hypoxic Reprogramming Drives Vascular Remodeling and Pulmonary Arterial Hypertension. *Nat. Commun.* 10, 3551. doi:10.1038/s41467-019-11500-6

Marowsky, A., Burgener, J., Falck, J. R., Fritschy, J. M., and Arand, M. (2009). Distribution of Soluble and Microsomal Epoxide Hydrolase in the Mouse Brain and its Contribution to Cerebral Epoxyeicosatrienoic Acid Metabolism. *Neuroscience* 163, 646–661. doi:10.1016/j.neuroscience.2009.06.033

McGettrick, M., and Peacock, A. (2020). Group 3 Pulmonary Hypertension: Challenges and Opportunities. *Glob. Cardiol. Sci. Pract.* 2020, e202006. doi:10.21542/gcsp.2020.6

Menon, D., Coll, R., O'Neill, L. A., and Board, P. G. (2014). Glutathione Transferase omega 1 Is Required for the Lipopolysaccharide-Stimulated Induction of NADPH Oxidase 1 and the Production of Reactive Oxygen Species in Macrophages. *Free Radic. Biol. Med.* 73, 318–327. doi:10.1016/j.freeradbiomed.2014.05.020

Meuchel, L. W., Thompson, M. A., Cassivi, S. D., Pabelick, C. M., and Prakash, Y. S. (2011). Neurotrophins Induce Nitric Oxide Generation in Human Pulmonary Artery Endothelial Cells. *Cardiovasc. Res.* 91, 668–676. doi:10.1093/cvr/cvr107

Meyrick, B., and Reid, L. (1980). Endothelial and Subintimal Changes in Rat Hilar Pulmonary Artery during Recovery from Hypoxia. A Quantitative Ultrastructural Study. *Lab. Invest.* 42, 603–615.

Mura, M., Anraku, M., Yun, Z., McRae, K., Liu, M., Waddell, T. K., et al. (2012). Gene Expression Profiling in the Lungs of Patients with Pulmonary Hypertension Associated with Pulmonary Fibrosis. *Chest* 141, 661–673. doi:10.1378/chest.11-0449

Papandreou, I., Cairns, R. A., Fontana, L., Lim, A. L., and Denko, N. C. (2006). HIF-1 Mediates Adaptation to Hypoxia by Actively Downregulating Mitochondrial Oxygen Consumption. *Cell Metab* 3, 187–197. doi:10.1016/j.cmet.2006.01.012

Pugh, M. E., Newman, J. H., Williams, D. B., Brittain, E., Robbins, I. M., and Hemnes, A. R. (2013). Hemodynamic Improvement of Pulmonary Arterial

Hypertension after Bariatric Surgery: Potential Role for Metabolic Regulation. *Diabetes Care* 36, e32–3. doi:10.2337/dc12-1650

Rhodes, C. J., Ghataorhe, P., Wharton, J., Rue-Albrecht, K. C., Hadinnapola, C., Watson, G., et al. (2017). Plasma Metabolomics Implicates Modified Transfer RNAs and Altered Bioenergetics in the Outcomes of Pulmonary Arterial Hypertension. *Circulation* 135, 460–475. doi:10.1161/CIRCULATIONAHA.116.024602

Rhodes, C. J. (2020). The Cancer Hypothesis of Pulmonary Arterial Hypertension: Are Polyamines the New Warburg. *Eur. Respir. J.* 56 (5), 2002350. doi:10.1183/13993003.02350-2020

Ritchie, M. E., Phipson, B., Wu, D., Hu, Y., Law, C. W., Shi, W., et al. (2015). Limma powers Differential Expression Analyses for RNA-Sequencing and Microarray Studies. *Nucleic Acids Res.* 43, e47. doi:10.1093/nar/gkv007

Safran, M., Dalah, I., Alexander, J., Rosen, N., Iny Stein, T., Shmoish, M., et al. (2010). GeneCards Version 3: The Human Gene Integrator. *Database(Oxford)* 2010, baq020. doi:10.1093/database/baq020

Shannon, P., Markiel, A., Ozier, O., Baliga, N. S., Wang, J. T., Ramage, D., et al. (2003). Cytoscape: a Software Environment for Integrated Models of Biomolecular Interaction Networks. *Genome Res.* 13, 2498–2504. doi:10.1101/gr.1239303

Song, J. L., Zheng, S. Y., He, R. L., Gui, L. X., Lin, M. J., and Sham, J. S. K. (2021). Serotonin and Chronic Hypoxic Pulmonary Hypertension Activate a NADPH Oxidase 4 and TRPM2 Dependent Pathway for Pulmonary Arterial Smooth Muscle Cell Proliferation and Migration. *Vascul Pharmacol.* 138, 106860. doi:10.1016/j.vph.2021.106860

Stearman, R. S., Bui, Q. M., Speyer, G., Handen, A., Cornelius, A. R., Graham, B. B., et al. (2019). Systems Analysis of the Human Pulmonary Arterial Hypertension Lung Transcriptome. *Am. J. Respir. Cel Mol Biol* 60, 637–649. doi:10.1165/rcmb.2018-0368OC

Stenmark, K. R., Davie, N., Frid, M., Gerasimovskaya, E., and Das, M. (2006). Role of the Adventitia in Pulmonary Vascular Remodeling. *Physiology (Bethesda)* 21, 134–145. doi:10.1152/physiol.00053.2005

Strange, G., Playford, D., Stewart, S., Deague, J. A., Nelson, H., Kent, A., et al. (2012). Pulmonary Hypertension: Prevalence and Mortality in the Armadale Echocardiography Cohort. *Heart* 98, 1805–1811. doi:10.1136/heartjnl-2012-301992

Strange, R. C., Spiteri, M. A., Ramachandran, S., and Fryer, A. A. (2001). Glutathione-S-transferase Family of Enzymes. *Mutat. Res.* 482, 21–26. doi:10.1016/s0027-5107(01)00206-8

Sun, Q., Hackler, J., Hilger, J., Gluschke, H., Muric, A., Simmons, S., et al. (2020). Selenium and Copper as Biomarkers for Pulmonary Arterial Hypertension in Systemic Sclerosis. *Nutrients* 12, 12. doi:10.3390/nu12061894

Szklarczyk, D., Gable, A. L., Lyon, D., Junge, A., Wyder, S., Huerta-Cepas, J., et al. (2019). STRING V11: Protein-Protein Association Networks with Increased Coverage, Supporting Functional Discovery in Genome-wide Experimental Datasets. *Nucleic Acids Res.* 47, D607–D613. doi:10.1093/nar/gky1131

Tanaka, S., Shiroto, T., Godo, S., Saito, H., Ikumi, Y., Ito, A., et al. (2018). Important Role of Endothelium-dependent Hyperpolarization in the Pulmonary Microcirculation in Male Mice: Implications for Hypoxia-Induced Pulmonary Hypertension. *Am. J. Physiol. Heart Circ. Physiol.* 314, H940–H953. doi:10.1152/ajpheart.00487.2017

Tang, B., Chen, G. X., Liang, M. Y., Yao, J. P., and Wu, Z. K. (2015). Ellagic Acid Prevents Monocrotaline-Induced Pulmonary Artery Hypertension via Inhibiting NLRP3 Inflammasome Activation in Rats. *Int. J. Cardiol.* 180, 134–141. doi:10.1016/j.ijcard.2014.11.161

Yan, Y., He, Y. Y., Jiang, X., Wang, Y., Chen, J. W., Zhao, J. H., et al. (2020). DNA Methyltransferase 3B Deficiency Unveils a New Pathological Mechanism of Pulmonary Hypertension. *Sci. Adv.* 6, eaba2470. doi:10.1126/sciadv.aba2470

Yu, Q., Tai, Y. Y., Tang, Y., Zhao, J., Negi, V., Culley, M. K., et al. (2019). BOLA (BolA Family Member 3) Deficiency Controls Endothelial Metabolism and Glycine Homeostasis in Pulmonary Hypertension. *Circulation* 139, 2238–2255. doi:10.1161/CIRCULATIONAHA.118.035889

Zhang, J., Zhu, Y., Wu, Y., Yan, Q. G., Peng, X. Y., Xiang, X. M., et al. (2020). Synergistic Effects of EMPs and PMPs on Pulmonary Vascular Leakage and Lung Injury after Ischemia/reperfusion. *Cell Commun Signal* 18, 184. doi:10.1186/s12964-020-00672-0

Zhao, Y. D., Yun, H. Z. H., Peng, J., Yin, L., Chu, L., Wu, L., et al. (2014). De Novo synthesize of Bile Acids in Pulmonary Arterial Hypertension Lung. *Metabolomics* 10, 1169–1175. doi:10.1007/s11306-014-0653-y

Conflict of Interest: The authors declare that the research was conducted in the absence of any commercial or financial relationships that could be construed as a potential conflict of interest.

Publisher's Note: All claims expressed in this article are solely those of the authors and do not necessarily represent those of their affiliated organizations, or those of the publisher, the editors and the reviewers. Any product that may be evaluated in this article, or claim that may be made by its manufacturer, is not guaranteed or endorsed by the publisher.

frontiers in Pharmacology

ORIGINAL RESEARCH
published: 20 December 2021
doi: 10.3389/fphar.2021.764046

Effect of Xuezhikang Therapy on Expression of Pulmonary Hypertension Related miR-638 in Patients With Low HDL-C Levels

Ruihua Cao[1†], Tao Sun[2†], Ruyi Xu[1], Jin Zheng[1], Hao Wang[1], Xiaona Wang[1], Yongyi Bai[1,3] and Ping Ye[1]**

[1]Department of Cardiology, The Second Medical Center and National Clinical Research Center for Geriatric Diseases, Chinese PLA General Hospital, Beijing, China, [2]Department of Cardiology, Huashan Hospital, Fudan University, Shanghai, China, [3]Beijing Key Laboratory of Precision Medicine for Chronic Heart Failure, Chinese PLA General Hospital, Beijing, China

OPEN ACCESS

Edited by:
Xiao-Jian Wang,
Chinese Academy of Medical Sciences and Peking Union Medical College, China

Reviewed by:
Fenling Fan,
The First Affiliated Hospital of Xi'an Jiaotong University, China
Yunshan Cao,
Gansu Provincial Hospital, China

***Correspondence:**
Yongyi Bai
baiyongyi301@sina.com
Ping Ye
yeping301@sina.com

†These authors have contributed equally to this work

Specialty section:
This article was submitted to Respiratory Pharmacology, a section of the journal Frontiers in Pharmacology

Received: 24 August 2021
Accepted: 23 November 2021
Published: 20 December 2021

Citation:
Cao R, Sun T, Xu R, Zheng J, Wang H, Wang X, Bai Y and Ye P (2021) Effect of Xuezhikang Therapy on Expression of Pulmonary Hypertension Related miR-638 in Patients With Low HDL-C Levels. Front. Pharmacol. 12:764046. doi: 10.3389/fphar.2021.764046

Objective: Low plasma level of high-density lipoprotein cholesterol (HDL-C) associated with poor outcomes in several cardiovascular diseases, including pulmonary arterial hypertension (PAH). Regulation of miR-638 have been proved to be associated with PAH. The aim of this study was to evaluate the expression of miR-638 after Xuezhikang (XZK) therapy in patients with low HDL-C.

Methods: Plasma levels of miR-638 were quantified by real-time polymerase chain reactions in 20 patients with PAH and 30 healthy controls. A total of 40 subjects with low HDL-C were assigned to receive an XZK therapy for 6 months. The miR-638 expression profiles were detected in PAH patients, XZK-treated subjects and lovastatin treated pulmonary arterial smooth muscle cells (PA-SMCs).

Results: The relative expression level of miR-638 in the plasma was lower in the PAH patients than that in the controls ($p < 0.001$). An increase of 11.2% from baseline in the HDL-C level was found after XZK therapy ($p < 0.001$). The relative expression of miR-638 was increased after XZK treatment ($p < 0.01$). The changes of miR-638 were inversely associated with baseline HDL-C levels. A significantly reduction in miR-638 expression were found in PDGF-BB-treated hPA-SMCs compared to the control cells, and the pre-treatment of the cells with lovastatin significantly re-gain the expression levels in miR-638.

Conclusion: In patients with low HDL-C levels, XZK therapy raised the expression of miR-638, suggesting that the potential therapeutic effect of XZK in PAH patients with low serum HDL-C levels deserves further exploration.

Keywords: Xuezhikang, therapy, pulmonary hypertension, miR-638, low HDL-C

INTRODUCTION

Pulmonary arterial hypertension (PAH) is a devastating and lethal cardio-pulmonary disease (Hoeper et al., 2016). Epidemiologic studies have demonstrated that low plasma level of high-density lipoprotein cholesterol (HDL-C) was associated with poor outcomes in pulmonary arterial hypertension (Rayner et al., 2010). However, clinical trials indicated that raising the levels of HDL-C

did not achieve the expected clinical benefit, which may be due to the change of particle size and the function of HDL-C (Keene et al., 2014; Probstfield et al., 2018). In view of the complex function of HDL, our understanding in the metabolic mechanisms of HDL is still incomplete.

MicroRNAs (miRNAs) are conserved small non-coding RNA molecules, as important posttranscriptional regulators of lipid metabolism, and important targets for therapeutic intervention (Poller et al., 2018; Sun et al., 2020). Circulating microRNAs (miRNAs) exist in body fluids in a stable, cell-free form, and are closely related to human diseases (Reddy et al., 2019). Several miRNAs have been demonstrated to regulate lipid metabolism, including miR-122, miR-370, miR-335, miR-378/378* and miR-33 (Rayner et al., 2010; Rayner et al., 2011a; Rayner et al., 2011b; Kim et al., 2017; Agbu and Carthew, 2021). Previous studies have demonstrated that MCT resulted in significant pulmonary vascular remodeling and down-regulation of miR-638; miR-638 mimics inhibited pulmonary arterial smooth muscle cells (PA-SMCs) proliferation and percentage of PCNA-positive cells *in vitro* (Luque et al., 2018; Liu et al., 2020; Mirhadi et al., 2021). The roles of miR-638 in lipid metabolism and expression profiles in patients with PAH are unclear.

Xuezhikang, an extract of cholestin, containing a combination of lovastatin, phytosterols and isoflavones. Each 1,200 mg XZK capsule contains about 10 mg lovastatin (Jia et al., 2016). It has the similar lipid-lowering effects with statins (Li et al., 2010). Our previous study demonstrated for the first time that plasma levels of miR-33a and miR-33b were significantly increased after XZK treatment, and the changes of miR-33a and miR-33b were inversely associated with the baseline levels of LDL-C (Cao et al., 2014). However, the potential mechanism of XZK in HDL-raising effect is still not completely clear. Furthermore, the effect of XZK therapy on the expression of miR-638 and whether there are "cross-talk" among pulmonary hypertension, miR-638 and HDL-C metabolism need further investigation.

In the present study, we aim to investigate relationship among the expression of miR-638, XZK treatment and pulmonary hypertension.

METHODS

Samples Obtained From Pulmonary Arterial Hypertension Patients

Blood samples were obtained from PAH patients and healthy controls for the PAH case-control study. Twenty patients with PAH were consecutively enrolled from January 2019 to December 2019 at the Chinese PLA General Hospital and Huashan Hospital. The clinical diagnosis of PAH was according to the 2015 ESC/ERS guidelines for the diagnosis and treatment of pulmonary hypertension (Galiè et al., 20152016). Thirty normal volunteers matched for age, gender and race were enrolled simultaneously. All blood samples were centrifuged at 3,000 ×g for 10 min at room temperature, and the obtained serum samples were stored at −80°C for RNA extraction.

TABLE 1 | Baseline characteristics of Xuezhikang study.

Characteristics	*N* = 40
Age (years)	58.7 ± 10.6
Male gender, *n* (%)	10 (25)
Hypertension *n* (%)	24 (60)
BMI(kg/m^2)	28.1 ± 4.8
SBP (mmHg)	138 ± 15
DBP (mmHg)	87 ± 9
TC (mmol/L)	5.54 ± 0.76
TG (mmol/L)	2.85 (2.16, 3.97)
HDL-C (mmol/L)	1.07 ± 0.13
LDL-C (mmol/L)	3.35 ± 0.72
Hcy (μmol/L)	14.6 ± 6.7

BMI, body mass index; SBP, systolic blood pressure; DBP, diastolic blood pressure; TC, total plasma cholesterol; HDL-C, high-density lipoprotein cholesterol; LDL-C, low-density lipoprotein cholesterol; Hcy, Homocysteine are given as mean ± standard deviation. Triglyceride (TG), values as median (quartile 1, quartile 3).

Subjects of Xuezhikang Study

From September 2010 to June 2011, patients were screened and enrolled from a community in the Pingguoyuan area of the Shijingshan district, Beijing, China. After signing informed written consent, 150 participants were tested for low plasma HDL-C levels. Eighteen subjects with bedridden status, severe systemic diseases or mental illness were excluded.

Clinical data collection and biomarker variable determination were obtained from the 132 subjects. Among them, 42 patients with low HDL-C levels <40 mg/dl (1.03 mmol/L) for men; <50 mg/dl (1.29 mmol/L) for women) were eligible for analysis (Galiè et al., 20152016). Patients who have taken any lipid-lowering medication within the past 4 weeks required to discontinue lipid-modifying drugs before registration, in order to obtain accurate baseline blood lipid values. All patients who were able to adapt during the study were assigned to take an XZK capsule, 600 mg twice daily (Beijing WBL Peking University Biotech Co., Ltd., Beijing, China) for 6 months.

The study was approved by the ethics committee of the Chinese PLA General Hospital, and each participant provided with written informed consent.

Laboratory Measurements

Blood samples were centrifuged immediately and stored at −80°C. Concentrations of fasting glucose, total cholesterol (TC), triglyceride (TG), HDL-C, LDL-C and creatinine were determined using the Roche enzymatic assays (Roche Diagnostics GmbH, Mannheim, Germany) on a Roche autoanalyser (Roche Diagnostics, Indianapolis, IN, United States).

Cell Culture Experiments

Human PA-SMCs (CP3110) and smooth muscle cell medium were purchased from ScienCell Research Laboratory (Calsbad, CA, United States). The hPA-SMCs were incubated in smooth muscle cell medium, which contained 20% fetal bovine serum and 1% penicillin and streptomycin and were cultured at 37°C with 5% CO_2 in humidified conditions.

The hPA-SMCs were seeded in Costar six 6-plate at a concentration of 2 × 10^5/well. After the cells were 80%

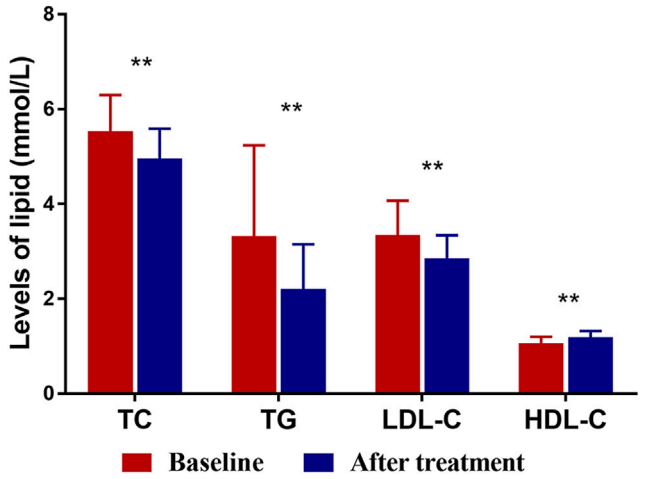

FIGURE 1 | The levels of TC, TG, LDL-C and HDL-C at baseline and after XZK treatment. After XZK treatment, the levels of TG, TC and LDL-C decreased significantly, while the levels of HDL-C increased significantly (**$p < 0.01$). Horizontal lines represent standard deviation.

confluent, they were then starved in an FCS-free medium for next 24 h, followed by pre-treated with lovastatin (Sigma, MO, United States, at a final concentration of 1 or 5 μM/L) or equal volume control (1% dimethylsulfoxide), and were exposed to PDGF-BB (Thermo Fisher, MA, United States) at a concentration of 20 ng/ml for next 48 h. At the endpoint, the cell supernatant was removed and cells were lysized with Trizol for total RNA isolation.

RNA Isolation and Real-Time Polymerase Chain Reaction

Total RNA from hPA-SMCs and plasma was isolated with the use of Trizol as previous described (Bai et al., 2021) and the extracted RNA was reverse transcribed in the presence of a poly-A polymerase with an oligo-dT adaptor. Real-time PCR was carried out with SYBR green detection using hsa-miR-638 and a universal adaptor reverse primer. Relative expression was evaluated by the comparative Ct (threshold cycle) method and normalized to the expression of U6 or U48 small RNA.

Statistical Analysis

Continuous variables are expressed as mean ± standard deviation (SD) or median; whereas dichotomous variables are expressed as numbers and percentages. Data that followed a normal distribution and met variance homogeneity were analyzed for statistical significance by unpaired Student's t test or ANOVA followed by Bonferroni's multiple comparison post hoc test. When the data did not meet the variance homogeneity, one-way ANOVA followed by Dunnett's multiple comparison post hoc test was used. The categorical variables were compared by chi-square test. Pearson correlation coefficients was used to analyzed the strength of the correlation between continuous variables. The analyses were performed using SPSS (version 17.0, Inc., Chicago, IL, United States). Statistical significance was set at $p < 0.05$, all reported p values are two-tailed.

RESULTS

Baseline Characteristics of Subjects of Xuezhikang Study

Of the 42 enrolled patients, two were lost after 6 months of follow-up. Finally, 40 subjects (mean age 58.7, 41–77 years, eight males) were eligible for analysis. The baseline demographic characteristics of the 40 patients who completed the trial are summarized in **Table 1**.

Effects of Xuezhikang Treatment on Lipid Profiles

Figure 1 and **Table 2** summarizes lipid profiles obtained in patients who completed the trial. The mean HDL-C level was 1.19 ± 0.13 mmol/L after XZK treatment, representing an increase of 11.2% from baseline ($p < 0.001$). The mean TG level after XZK treatment was 2.21 ± 0.94 mmol/L, a 22.5% reduction from baseline ($p < 0.001$). The mean LDL-C level was 2.86 ± 0.48 mmol/L after XZK treatment, representing a reduction of 14.6% from baseline ($p < 0.001$).

Effects of Xuezhikang Treatment on miR-638 Expression

Q-PCR analysis of plasma miRNAs showed that the relative expression of miR-638 increased after XZK treatment ($p = 0.008$) (**Figure 2**). The changes of miR-638 were negatively correlated with baseline HDL-C levels ($r = -0.350$, $p = 0.027$). Conversely, the changes of miR-638 correlated positively with baseline triglyceride (TG) levels ($r = 0.402$, $p = 0.01$) (**Figure 3**).

TABLE 2 | Changes of lipid profiles after Xuezhikang treatment.

Lipid profiles	Baseline	After treatment	Percent change (%)	*p* Value
TC (mmol/L)	5.54 ± 0.76	4.96 ± 0.63	−10.5	<0.001
TG (mmol/L)	3.32 ± 1.92	2.21 ± 0.94	−22.5	<0.001
LDL-C (mmol/L)	3.35 ± 0.72	2.86 ± 0.48	−14.6	<0.001
HDL-C (mmol/L)	1.07 ± 0.13	1.19 ± 0.13	11.2	<0.001
HDL-C/LDL-C ratio	0.33 ± 0.07	0.43 ± 0.07	30.3	<0.001

TC, total plasma cholesterol; HDL-C, high-density lipoprotein cholesterol; LDL-C, low-density lipoprotein cholesterol; TG, triglyceride.

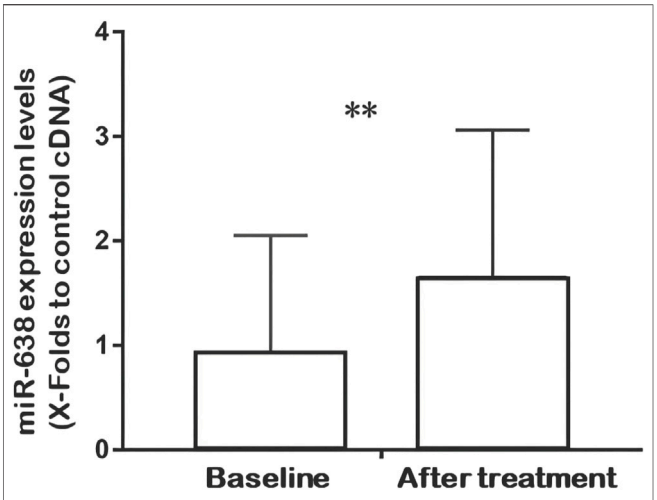

FIGURE 2 | Quantitative real-time fluorescence polymerase chain reaction (QRT-PCR) analysis of miR-638 expression at baseline and after XZK treatment. Relative expression of miR-638 was raised after XZK treatment. $^{**}p < 0.01$. Horizontal lines represent standard deviation.

Expression of miR-638 in Pulmonary Arterial Hypertension Patients and Lovastatin Treated PASMCs

The plasma miR-638 levels were significantly decreased in PAH patients (n = 20) compared with control individuals (n = 30) (**Figure 4A**). A similar pattern was found, as shown by the significantly reduction in miR-638 expression levels in PDGF-BB-treated hPA-SMCs compared to the control cells, and the pre-treatment of the cells with lovastatin significantly re-gain the expression levels in miR-638. When the cells were treated with lovastatin at a high concentration of 5 μM, the miR-638 expression level were reversed to near the normal levels (**Figure 4B**), indicating that the expression levels of miR-638 were negative correlation to PAH both *in vivo* and *in vitro*.

DISCUSSION

In this study, we demonstrated several valuable findings for the first time. Firstly, the expression levels of miR-638 were decreased in patients with PAH. Secondly, in patients with low-HDL-C levels, plasma levels of miR-638 were significantly increased after XZK treatment. Thirdly, lovastatin (one of the main ingredients of XZK) significantly re-gains the expression levels of miR-638 in PDGF-BB-treated hPA-SMCs.

Previous studies on miR-638 have focused on several types of cancers and pulmonary hypertension, the role of miR-638 in lipid metabolism has not been reported. In this study, we described the low expression of miR-638 in patients with low HDL-C for the first time. Recent studies have demonstrated that miR-638, which is highly expressed in human vascular smooth muscle cells (VSMCs), targets the orphan nuclear receptor NOR1 (a key regulator associated with proliferative vascular diseases) as a novel regulator to inhibit proliferation and migration (Li et al., 2013; Chen et al., 2019). These studies suggested that miR-638 may be a potential therapeutic target for the prevention and treatment of human vascular diseases, such as atherosclerosis and pulmonary hypertension (Luque et al., 2018; Mansueto et al., 2020; Zhang et al., 2020).

XZK is a traditional Chinese medicine with multiple cardioprotective effective, which contains isoflavones and lovastatin and unsaturated fatty acid. Studies have shown that the effect of XZK in reducing TC and LDL-C levels is equivalent to conventional doses statins, and increasing HDL-C levels (Xu et al., 2017; Jia et al., 2020). Our efficacy data were consistent with previous studies. In the present study, LDL-C decreased by 14.6%

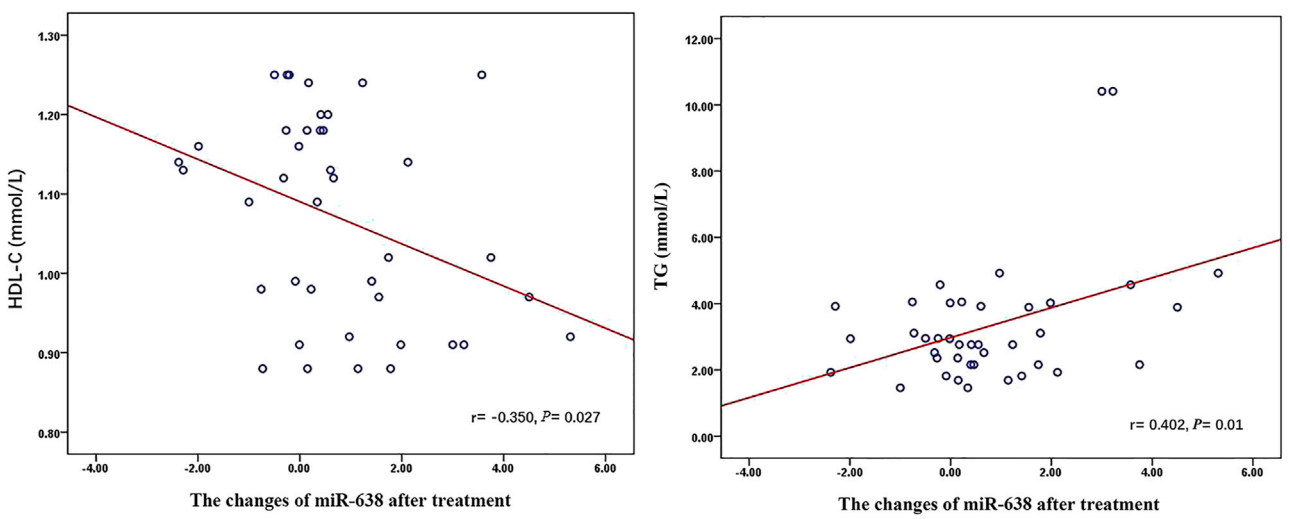

FIGURE 3 | The relationship between miR-638 and Lipid Profiles after XZK treatment. The changes of miR-638 were negatively correlated with baseline HDL-C levels (r = −0.350, p = 0.027). Conversely, the changes of miR-638 correlated positively with baseline triglyceride (TG) levels (r = 0.402, p = 0.01).

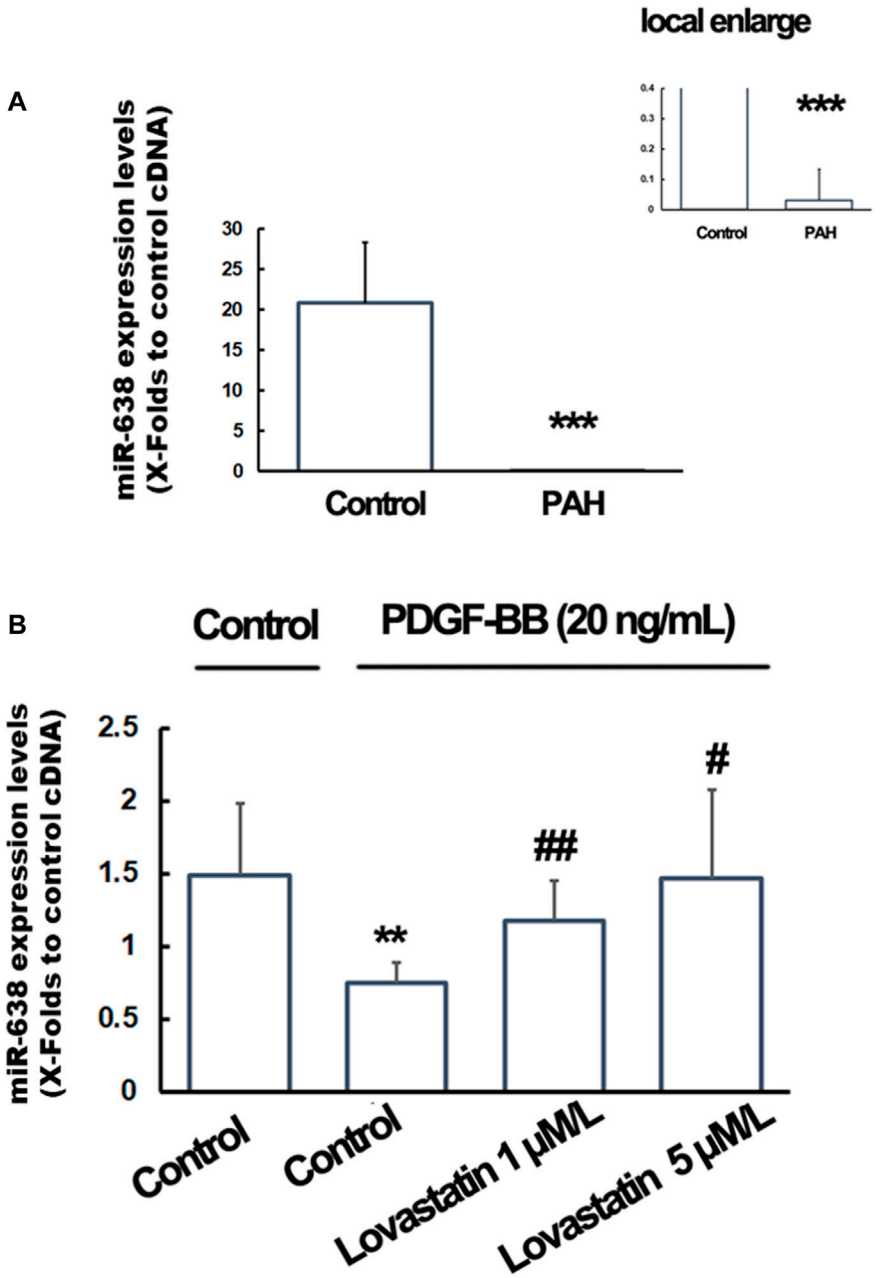

FIGURE 4 | Expression of miR-638 in PAH patients and lovastatin treated PASMCs. Total RNA from the plasma of PAH patients and hPA-SMCs were isolated with the use of Trizol and the expression levels of miR-168 were detected using qRT-PCR. **(A)**. The plasma miR-638 levels were significantly decreased in PAH patients (n = 20) compared with controls individuals (n = 30). Data was expressed as Mean ± SD. $^{*}p < 0.05$, $^{**}p < 0.01$, $^{***}p < 0.001$ vs the normal control. U48 were used as a control gene. **(B)**. The starved human PA-SMC were pre-treated with lovastatin at a final concentration of 0, 1or 5 μM/L, followed by incubated with PDGF-BB at a final concentration of 20 ng/ml. 1% DMSO were used as a solvent control. The U6 were used as a control gene. Data was expressed as Mean ± SD. $^{*}p < 0.05$, $^{**}p < 0.01$ vs. the normal control. $^{\#}p < 0.05$, $^{\#\#}p < 0.01$ vs. the PDGF-BB treated cells.

and HDL-C increased by 11.2% after treatment with XZK 1,200 mg daily for 6 months. In previous Chinese trials with XZK 1,200 mg daily, LDL-C decreased by approximately 17%, HDL-C concentration increased by 4.6% (Li et al., 2010). However, previous studies have not explored the epigenetic mechanism of XZK. We found that miR-638 changed after the treatment of XZK, which is synchronized and related to the changes of HDL-C, suggesting that XZK may have potential value in the treatment of pulmonary hypertension by regulating HDL-C metabolism and miR-638 expression. As recent reported (Wang et al., 2020), serum HDL-C is lower in PAH patients comparing with healthy people, suggesting that HDL-C would be

a potential biomarker for prediction and assessment of PAH. In the present study, the miR-638 raising effect of XZK were found negatively correlated with baseline HDL-C levels, indicating that XZK may have a potential therapeutic effect in PAH patients with low HDL-C.

Furthermore, *in vitro* experiments found that expression of miR-638 was increased in PDGF-BB-treated hPA-SMCs by lovastatin, one of the main ingredients of XZK, indicating that the miR-638-raising effect of XZK is at least partially related to lovastatin. However, the therapeutic effect of XZK cannot be explained by lovastatin alone. Besides lovastatin, XZK also contains other ingredients, including statin homologue, a variety of essential amino acids, unsaturated fatty acid, sterol, and small amounts of flavonoids. Whether XZK can be a potential drug for the treatment of pulmonary hypertension needs further *in vitro* and *in vivo* experiments and clinical investigations.

Although the mechanism of miR-638 in lipid metabolism and PAH is still unclear, previous studies have shown that circulating miR-638 may lead to the disorder of HDL-C metabolism by regulating the gene expression pathway related to oxidative stress response. The recent study has uncovered MAFB is a potential target of miR-638, ectopic expression of MAFB strongly induced the expression of ABCG1 and ABCA1, the key mediators of cholesterol efflux, and then affected lipid metabolism (Yang et al., 2015; Kim, 2017). Another recent study demonstrated that miR-638 induced apoptosis through regulating STARD10 signaling, the expression of miR-638 was inversely correlated with the expression of STARD10 mRNA (Zhao et al., 2017). Several previous studies have shown that apoptosis play a vital role in pulmonary arterial hypertension (Lv et al., 2021; Zimmer et al., 2021), indicating that the association of miR-638 with PAH may be partially related to STARD10, a target gene of miR-638.

Study Limitations

The present study had several limitations. First, since the primary purpose of XZK intervention study was only to observe the lipid-lowering effect of XZK, several parameters associated with pulmonary hypertension, such as the right heart and pulmonary artery pressure, were not measured. Future research should focus on higher-quality and more rigorous larger sample trials to validate the findings and hypothesis of this study. Second, whether there are "cross-talk" among pulmonary hypertension, miR-638 and HDL-C metabolism, and the mechanism in this cross-talk need be further revealed in subsequent studies.

CONCLUSION

In summary, the present study identified that, in patients with low HDL-C levels, XZK therapy raised the expression of miR-638, the changes of miR-638 were negatively correlated with baseline HDL-C levels. The potential therapeutic effect of XZK in PAH patients with low serum HDL-C levels deserves further exploration.

DATA AVAILABILITY STATEMENT

The raw data supporting the conclusion of this article will be made available by the authors, without undue reservation.

ETHICS STATEMENT

The studies involving human participants were reviewed and approved by the Ethics Committee of the Chinese PLA General Hospital. The patients/participants provided their written informed consent to participate in this study.

AUTHOR CONTRIBUTIONS

PY and YB designed the experiments. TS and JZ collected the clinical samples. TS, RC, RX, JZ, HW, and XW performed the experiments. YB analyzed the data. RC and YB prepared the manuscript. All authors have contributed to the study and approved the manuscript.

FUNDING

This research was supported by grants from the Project of the National Ministry of Industry and Information Technology (2020-0103-3-1), the Science Foundation of the PLA General Hospital (2019XXMBD-004) and the Nature Science Foundation of China (81100878).

ACKNOWLEDGMENTS

We would like to thank the Department of Laboratory Medicine of the PLA General Hospital. We are also grateful to all participants in the study.

REFERENCES

Agbu, P., and Carthew, R. W. (2021). MicroRNA-mediated Regulation of Glucose and Lipid Metabolism. *Nat. Rev. Mol. Cel Biol* 22 (6), 425–438. doi:10.1038/s41580-021-00354-w

Bai, Y., Wang, J., Chen, Y., Lv, T., Wang, X., Liu, C., et al. (2021). The miR-182/Myadm axis Regulates Hypoxia-Induced Pulmonary Hypertension by Balancing the BMP- and TGF-β-Signalling Pathways in an SMC/EC-crosstalk-associated Manner. *Basic Res. Cardiol.* 116 (1), 53. doi:10.1007/s00395-021-00892-6

Cao, R., Bai, Y., Sun, L., Zheng, J., Zu, M., Du, G., et al. (2014). Xuezhikang Therapy Increases miR-33 Expression in Patients with Low HDL-C Levels. *Dis. Markers* 2014, 781780. doi:10.1155/2014/781780

Chen, S., Chen, H., Yu, C., Lu, R., Song, T., Wang, X., et al. (2019). MiR-638 Repressed Vascular Smooth Muscle Cell Glycolysis by Targeting LDHA. *Open Med. (Wars)* 14, 663–672. doi:10.1515/med-2019-0077

Galiè, N., Humbert, M., and Vachiery, J. L. (20152016). ESC/ERS Guidelines for the Diagnosis and Treatment of Pulmonary Hypertension: The Joint Task Force for the Diagnosis and Treatment of Pulmonary Hypertension of the European Society of Cardiology (ESC) and the European Respiratory Society (ERS): Endorsed by: Association for European Paediatric and Congenital Cardiology (AEPC), International Society for Heart and Lung Transplantation (ISHLT). *Eur. Heart J.* 37 (1), 67–119.

Hoeper, M. M., Humbert, M., Souza, R., Idrees, M., Kawut, S. M., Sliwa-Hahnle, K., et al. (2016). A Global View of Pulmonary Hypertension. *Lancet Respir. Med.* 4 (4), 306–322. doi:10.1016/S2213-2600(15)00543-3

Jia, W., Li, Y., Wan, J., Cui, X., Lu, J., Liu, J., et al. (2020). Effects of Xuezhitong in Patients with Hypertriglyceridemia: a Multicentre, Randomized, Double-Blind, Double Simulation, Positive Drug and Placebo Parallel Control Study. *Cardiovasc. Drugs Ther.* 34 (4), 525–534. doi:10.1007/s10557-020-06965-3

Jia, Y. J., Zhang, Y., Liu, J., Guo, Y. L., Xu, R. X., and Li, J. J. (2016). Short- and Long-Term Effects of Xuezhikang, an Extract of Cholestin, on Serum Proprotein Convertase Subtilisin/kexin Type 9 Levels. *Chin. J. Integr. Med.* 22 (2), 96–100. doi:10.1007/s11655-014-1846-y

Keene, D., Price, C., Shun-Shin, M. J., and Francis, D. P. (2014). Effect on Cardiovascular Risk of High Density Lipoprotein Targeted Drug Treatments Niacin, Fibrates, and CETP Inhibitors: Meta-Analysis of Randomised Controlled Trials Including 117,411 Patients. *BMJ* 349, g4379. doi:10.1136/bmj.g4379

Kim, H. (2017). The Transcription Factor MafB Promotes Anti-inflammatory M2 Polarization and Cholesterol Efflux in Macrophages. *Sci. Rep.* 7 (1), 7591. doi:10.1038/s41598-017-07381-8

Kim, S. H., Kim, G. J., Umemura, T., Lee, S. G., and Cho, K. J. (2017). Aberrant Expression of Plasma microRNA-33a in an Atherosclerosis-Risk Group. *Mol. Biol. Rep.* 44 (1), 79–88. doi:10.1007/s11033-016-4082-z

Li, J. J., Lu, Z. L., Kou, W. R., Chen, Z., Wu, Y. F., Yu, X. H., et al. (2010). Impact of Xuezhikang on Coronary Events in Hypertensive Patients with Previous Myocardial Infarction from the China Coronary Secondary Prevention Study (CCSPS). *Ann. Med.* 42 (3), 231–240. doi:10.3109/07853891003652534

Li, P., Liu, Y., Yi, B., Wang, G., You, X., Zhao, X., et al. (2013). MicroRNA-638 Is Highly Expressed in Human Vascular Smooth Muscle Cells and Inhibits PDGF-BB-Induced Cell Proliferation and Migration through Targeting Orphan Nuclear Receptor NOR1. *Cardiovasc. Res.* 99 (1), 185–193. doi:10.1093/cvr/cvt082

Liu, Y. Y., Zhang, W. Y., Wang, C. G., Huang, J. A., Jiang, J. H., and Zeng, D. X. (2020). Resveratrol Prevented Experimental Pulmonary Vascular Remodeling via miR-638 Regulating NR4A3/cyclin D1 Pathway. *Microvasc. Res.* 130, 103988. doi:10.1016/j.mvr.2020.103988

Luque, A., Farwati, A., Krupinski, J., and Aran, J. M. (2018). Association between Low Levels of Serum miR-638 and Atherosclerotic Plaque Vulnerability in Patients with High-Grade Carotid Stenosis. *J. Neurosurg.* 131 (1), 72–79. doi:10.3171/2018.2.JNS171899

Lv, Y., Ma, P., Wang, J., Xu, Q., Fan, J., Yan, L., et al. (2021). Betaine Alleviates Right Ventricular Failure via Regulation of Rho A/ROCK Signaling Pathway in Rats with Pulmonary Arterial Hypertension. *Eur. J. Pharmacol.* 910, 174311. doi:10.1016/j.ejphar.2021.174311

Mansueto, G., Benincasa, G., Della Mura, N., Nicoletti, G. F., and Napoli, C. (2020). Epigenetic-sensitive Liquid Biomarkers and Personalised Therapy in Advanced Heart Failure: a Focus on Cell-free DNA and microRNAs. *J. Clin. Pathol.* 73 (9), 535–543. doi:10.1136/jclinpath-2019-206404

Mirhadi, E., Roufogalis, B. D., Banach, M., Barati, M., and Sahebkar, A. (2021). Resveratrol: Mechanistic and Therapeutic Perspectives in Pulmonary Arterial Hypertension. *Pharmacol. Res.* 163, 105287. doi:10.1016/j.phrs.2020.105287

Poller, W., Dimmeler, S., Heymans, S., Zeller, T., Haas, J., Karakas, M., et al. (2018). Non-coding RNAs in Cardiovascular Diseases: Diagnostic and Therapeutic Perspectives. *Eur. Heart J.* 39 (29), 2704–2716. doi:10.1093/eurheartj/ehx165

Probstfield, J. L., Boden, W. E., Anderson, T., Branch, K., Kashyap, M., Fleg, J. L., et al. (2018). Cardiovascular Outcomes during Extended Follow-Up of the AIM-HIGH Trial Cohort. *J. Clin. Lipidol.* 12 (6), 1413–1419. doi:10.1016/j.jacl.2018.07.007

Rayner, K. J., Esau, C. C., Hussain, F. N., McDaniel, A. L., Marshall, S. M., van Gils, J. M., et al. (2011). Inhibition of miR-33a/b in Non-human Primates Raises Plasma HDL and Lowers VLDL Triglyceride. *Nature* 478, 404–407. doi:10.1038/nature10486

Rayner, K. J., Sheedy, F. J., Esau, C. C., Hussain, F. N., Temel, R. E., Parathath, S., et al. (2011). Antagonism of miR-33 in Mice Promotes Reverse Cholesterol Transport and Regression of Atherosclerosis. *J. Clin. Invest.* 121, 2921–2931. doi:10.1172/JCI57275

Rayner, K. J., Suárez, Y., Dávalos, A., Parathath, S., Fitzgerald, M. L., Tamehiro, N., et al. (2010). MiR-33 Contributes to the Regulation of Cholesterol Homeostasis. *Science* 328, 1570–1573. doi:10.1126/science.1189862

Reddy, L. L., Shah, S. A., Ponde, C. K., Rajani, R. M., and Ashavaid, T. F. (2019). Circulating miRNA-33: a Potential Biomarker in Patients with Coronary Artery Disease. *Biomarkers* 24 (1), 36–42. doi:10.1080/1354750X.2018.1501760

Sun, L., Lin, P., Chen, Y., Yu, H., Ren, S., Wang, J., et al. (2020). miR-182-3p/Myadm Contribute to Pulmonary Arterial Hypertension Vascular Remodeling via a KLF4/p21-dependent Mechanism. *Theranostics* 10 (12), 5581–5599. doi:10.7150/thno.44687

Wang, G. F., Guan, L. H., Zhou, D. X., Chen, D. D., Zhang, X. C., and Ge, J. B. (2020). Serum High-Density Lipoprotein Cholesterol Is Significantly Associated with the Presence and Severity of Pulmonary Arterial Hypertension: A Retrospective Cross-Sectional Study. *Adv. Ther.* 37 (5), 2199–2209. doi:10.1007/s12325-020-01304-2

Xu, R. X., Zhang, Y., Guo, Y. L., Ma, C. Y., Yao, Y. H., Li, S., et al. (2017). Novel Findings in Relation to Multiple Anti-atherosclerotic Effects of XueZhiKang in Humans. *Chronic Dis. Transl Med.* 4 (2), 117–126. doi:10.1016/j.cdtm.2017.09.004

Yang, Q., Yin, R. X., Zhou, Y. J., Cao, X. L., Guo, T., and Chen, W. X. (2015). Association of Polymorphisms in the MAFB Gene and the Risk of Coronary Artery Disease and Ischemic Stroke: a Case-Control Study. *Lipids Health Dis.* 14, 79. doi:10.1186/s12944-015-0078-2

Zhang, X., Guan, M. X., Jiang, Q. H., Li, S., Zhang, H. Y., Wu, Z. G., et al. (2020). NEAT1 Knockdown Suppresses Endothelial Cell Proliferation and Induces Apoptosis by Regulating miR-638/AKT/mTOR Signaling in Atherosclerosis. *Oncol. Rep.* 44 (1), 115–125. doi:10.3892/or.2020.7605

Zhao, G., Li, Y., and Wang, T. (2017). Potentiation of Docetaxel Sensitivity by miR-638 via Regulation of STARD10 Pathway in Human Breast Cancer Cells. *Biochem. Biophys. Res. Commun.* 487 (2), 255–261. doi:10.1016/j.bbrc.2017.04.045

Zimmer, A., Teixeira, R. B., Constantin, R. L., Fernandes-Piedras, T. R. G., Campos-Carraro, C., Türck, P., et al. (2021). Thioredoxin System Activation Is Associated with the Progression of Experimental Pulmonary Arterial Hypertension. *Life Sci.* 284, 119917. doi:10.1016/j.lfs.2021.119917

Conflict of Interest: The authors declare that the research was conducted in the absence of any commercial or financial relationships that could be construed as a potential conflict of interest.

frontiers in Pharmacology

ORIGINAL RESEARCH
published: 24 December 2021
doi: 10.3389/fphar.2021.768513

Sanguinarine Reverses Pulmonary Vascular Remolding of Hypoxia-Induced PH *via* Survivin/HIF1α-Attenuating Kv Channels

Fenling Fan[1*†], *Yifan Zou*[2†], *Yousen Wang*[1], *Peng Zhang*[1], *Xiaoyu Wang*[1], *Anthony M. Dart*[3,4] *and Yuliang Zou*[5*]

[1]Department of Cardiovascular Medicine, The First Hospital of Xi'an Jiaotong University, Xi'an, China, [2]School of Economic and Finance, Xi'an Jiaotong University, Xi'an, China, [3]Baker Institute, Melbourne, VIC, Australia, [4]Department of Cardiovascular Medicine, The Alfred Hospital, Melbourne, VIC, Australia, [5]Department of Gynecology and Obstetrics, The First Hospital of Xi'an Jiaotong University, Xi'an, China

OPEN ACCESS

Edited by:
Xiao-Jian Wang,
Peking Union Medical College, China

Reviewed by:
Kuo Yang Wang,
Taichung Veterans General Hospital, Taiwan
Lan Sun,
Peking Union Medical College, China

***Correspondence:**
Fenling Fan
happyling@mail.xjtu.edu.cn
Yuliang Zou
zouyuliangfl@126.com

[†]These authors share first authorship

Specialty section:
This article was submitted to Respiratory Pharmacology, a section of the journal Frontiers in Pharmacology

Received: 31 August 2021
Accepted: 03 November 2021
Published: 24 December 2021

Citation:
Fan F, Zou Y, Wang Y, Zhang P, Wang X, Dart AM and Zou Y (2021) Sanguinarine Reverses Pulmonary Vascular Remolding of Hypoxia-Induced PH via Survivin/HIF1α-Attenuating Kv Channels. Front. Pharmacol. 12:768513. doi: 10.3389/fphar.2021.768513

Background: Similarities in the biology of pulmonary hypertension and cancer suggest that anticancer therapies, such as sanguinarine, may also be effective in treating pulmonary hypertension. This, along with underlying biochemical pathways, is investigated in this study.

Methods: Rats were subjected to 4-week hypoxia (or control) with or without sanguinarine treatment. In addition, pulmonary artery smooth muscle cells (PASMCs) were examined after 24–48 h hypoxia (with normoxic controls) and with or without sanguinirine. Pulmonary artery pressures and plasma survivin levels were measured *in vivo*. *Ex vivo* tissues were examined histologically with appropriate staining. mRNA and protein levels of survivin, HIF-1α, TGFb1, BMPR2, Smad3, P53, and Kv 1.2, 1.5, 2.1 were determined by real-time PCR and Western blot in PASMCs and distal PAs tissue. PASMC proliferation and changes of TGFb1 and pSmad3 induced by sanguinarine were studied using MTT and Western blot. Electrophysiology for Kv functions was measured by patch-clamp experiments.

Results: Four-week hypoxia resulted in an increase in serum survivin and HIF-1α, pulmonary artery pressures, and pulmonary vascular remodeling with hypertrophy. These changes were all decreased by treatment with sanguinarine. Hypoxia induced a rise of proliferation in PASMCs which was prevented by sanguinarine treatment. Hypoxic PASMCs had elevated TGFb1, pSmad3, BMPR2, and HIF1α. These increases were all ameliorated by sanguinarine treatment. Hypoxia treatment resulted in reduced expression and function of Kv 1.2, 1.5, 2.1 channels, and these changes were also modulated by sanguinarine.

Conclusion: Sanguinarine is effective in modulating hypoxic pulmonary vascular hypertrophy *via* the survivin pathway and Kv channels.

Keywords: hypoxia-induced pulmonary hypertension, pulmonary vascular remolding, cancer-like mechanism, sanguinarine, survivin, HIF1A, Kv channels

BACKGROUND

Pulmonary hypertension (PH) refers to a variety of conditions characterized by elevations in pulmonary arterial pressure. It is a life-threatening disease with about 1% incidence in adults (Nathan et al., 2019). The vascular pathology of PH is characterized by pulmonary vasoconstriction and abnormal ("pseudomalignant") inward remodeling processes, which may affect all vessel layers (intima, media, and adventitia). A prominent feature virtually in all PH entities is vascular smooth muscle cell (SMC) proliferation, causing medial hypertrophy of the intra-acinar muscular resistance vessels and muscularization of the normally nonmuscularized precapillary arterioles. Overall, these structural changes suggest a switch from "quiescent" toward "pro-proliferative," "apoptosis-resistant," and "pro-inflammatory" vascular cell phenotypes. It has become increasingly clear that PH can be viewed as a proliferative disease and has an incredible number of pathogenic mechanisms similar to cancer. The vast majority of cancer hallmarks during disease progression (except tissue invasion and metastasis) are also shared by pulmonary vascular cells in PH patients (Pullamsetti et al., 2020). Recent experimental and conceptual advances (Pullamsetti et al., 2020) in the cancer cell metabolism, evading immune destruction and inflammation by innate immune cells, provide the field of PH with the unique opportunity to target the metabolism and immune/inflammation axis.

There are several underlying causes and five categories are recognized. These are pulmonary arterial hypertension (PAH, Type 1), pulmonary hypertension due to left heart or lung/hypoxia diseases (Type 2 and Type 3, respectively), PH due to pulmonary arterial stenosis (Type 4), and PH due to miscellaneous cause (Type 5). The various types of PH differ widely with respect to their prevalence and treatment. Two most frequent causes of pulmonary hypertension are left heart diseases and hypoxic lung diseases. Global studies of chronic obstructive lung disease (COPD) stage IV showed that up to 90% have mPAP >20 mmHg, with most ranging between 20 and 35 mmHg. Approximately 1–5% of COPD patients have mPAP >35–40 mmHg at rest (Nathan et al., 2019). Whereas, the prognosis of fibrotic idiopathic pulmonary disease (IIP) with PH is even worse than that of idiopathic pulmonary arterial hypertension (IPAH) (Nathan et al., 2019). Unfortunately, none of the drugs licensed for treatment of PAH have proven any survival effect in patients with pulmonary hypertension due to left heart disease or lung/hypoxia disease. One possible important reason is that current therapies have focused on vasodilators, which fail to reverse vascular remodeling, a key outcome for most types of PH (Thenappan et al., 2018). Based on many points of overlap for most PH, including deregulated inflammation, sustained proliferation, and escape from apoptosis, vascular remolding of PH has emerged as cancer-like, as previously mentioned (Pullamsetti et al., 2020), providing a possibility that anticancer reagents would be a therapeutic perspective for targeting vascular remolding of PH (Thenappan et al., 2018).

Sanguinarine, a benzophenanthridine alkaloid derived primarily from the bloodroot plant, has antioxidant, anti-inflammatory, proapoptotic, and growth inhibitory effects on different tumor cells (Fu et al., 2018). Survivin has been believed to be the strongest inhibiting protein of apoptosis and is widely involved in various cancers (Li et al., 2019a; Tian et al., 2018). The transcription factor hypoxia inducible factor-1alpha (HIF-1α) mediates adaptive responses to oxidant stress, promotes inflammatory gene expression, and contributes to tumor proliferation (Tian et al., 2018; Luo et al., 2019; Cheng et al., 2019; Diez-Calzadilla et al., 2021). Together, both survivin and HIF-1α are involved in inflammation, oxidative stress, proliferation, and apoptosis imbalance which are all key pathways for pulmonary vascular remolding in PAH (Thenappan et al., 2018; Pullamsetti et al., 2020; Diez-Calzadilla et al., 2021). Furthermore, oxygen-sensitive voltage-dependent K^+ (Kv) channels regulate cell proliferation and apoptosis both in PH and tumors (Hasan and Jaggar, 2018; Haworth and Brackenbury, 2019). The similarity in disordered molecular pathways between cancer and pulmonary hypertension suggests the possibility that therapy which is successful in cancer may also be effective in pulmonary hypertension. Therefore, in this study, the plant-originating sanguinarine, a novel inhibitor of survivin, was investigated for reducing pulmonary vascular remolding. We hypothesized that the mechanism of reversing pulmonary vascular remodeling involved upregulation of Kv channels via survivin/HIF-1α in pulmonary artery smooth muscle cells (PASMCs). The mechanism would further illustrate the similarity of cancer and PAH. The results would add important data for revealing a new pathway of reversing pulmonary vascular remolding likely leading to a better long-term outcome.

MATERIALS AND METHODS

Animals

The experimental protocols in this study were approved by the Laboratory Animal Administration Committee at Xi'an Jiaotong University and performed according to the Guide for the Care and Use of Laboratory Animals, published by the US National Institutes of Health. Male Sprague–Dawley rats (weight 180–250 g, 6–8 weeks old) were purchased from the Laboratory Animal Center at Xi'an Jiaotong University (Xi'an, China). The rats were randomized into control and hypoxia groups (n = 28, respectively). Hypoxic rats were housed in a hypoxic (10% O_2) Plexiglas cabin for 8 h/day for 4 weeks (Luo et al., 2014), whilst controls were maintained under normoxic conditions. Half of the rats in each group were given 30 mg/kg/day of sanguinarine (Macklin Inc., Shanghai, China) by gavage (Control + Sang, Hypoxia + Sang, respectively). The remaining half of control and hypoxia groups were provided with an equal volume of 5 ml/kg/day of saline.

Hemodynamics Measurement

After 4 weeks, the rats were anesthetized with 100 g/L of chloral hydrate (3 ml/kg) intraperitoneally and placed on an operating table. Subsequently, a percutaneous jugular vein-catheter, through the right atrium and ventricular, was installed into

TABLE 1 | Primer sequences for the Real-time PCR in the study.

Primer	Forward/reverse (5′→3′)	Primer sequence	Product size(bp)
Kv1.5	Forward	CGGGTGTTCCGCATCTTC	169
	Reverse	TTCCCTGGTTGTCAGCCTCT	
Kv2.1	Forward	CCAAAAGTCTCCACGGGAGT	170
	Reverse	GCATTTCTCTTGAGCCCCAG	
Kv1.2	Forward	TGGGCACCCTCAAGACACCTAT	271
	Reverse	TAAGGGCACATTCACAGGTCGC	
HIF-1α	Forward	GAAACTTCTGGATGCTGGTG	167
	Reverse	CAAACTGAGTTAATCCCATG	
p53	Forward	CGAGCACTGCCCAACAACAC	224
	Reverse	TGGCGGGAGGTAGACTGACC	
Survivin	Forward	TCTCAAGGACCACCGCATCT	239
	Reverse	CGCACTTTCTCCGCAGTTTC	
TGFb1	Forward	GCAACAACGCAATCTATGAC	301
	Reverse	CCCTCTATTCCGTCTCCTT	
SMAD3	Forward	GGGCTTT GAGGC TGTCTA	224
	Reverse	CCCTTTACT CCCA GTGTCT	
GAPDH	Forward	CACTGTGCCCATCTACGAGG	155
	Reverse	TAATGTCACGCACGATTTCC	

the main pulmonary artery and then connected to a pre-corrected zero value pressure transducer of a multiple electroconductive physiological recorder (Shanghai Yuyan SciTech Instruments Ltd., China) to record the pulmonary artery pressure (including systolic, diastolic, and mean pressures, sPAP, dPAP, and mPAP) with the heart rate.

Assessment of Right Ventricle Hypertrophy and Pulmonary Artery Remodeling

After the rats were sacrificed, the heart, lung, and liver were immediately isolated and weighed. The right ventricle (RV) was dissected from the left ventricle and septum (LV + S), and the Fulton index [RV wet weight/(LV + S)] was calculated as an index of right ventricular hypertrophy (RVHI). Then, the right lower lobes of the lung tissues were collected and fixed with 4% paraformaldehyde, dehydrated, paraffin-embedded, cut into 10 μm sections, stained with hematoxylin and eosin (HE), and observed for pulmonary arteriole morphology under a light microscope (Olympus, Japan). 3 HE–stained lung tissue sections, each with at least three pulmonary arterioles, were randomly selected from every group for pulmonary arteriole measurement. Three views for each arteriole was observed, and the outer and inner circumference and wall thickness were calculated using Image-Pro Plus 6.0 software. The average values were used to assess vascular proliferation.

Enzyme-Linked Immunosorbent Assay

The content of survivin and HIF-1α in rat serum was determined by the ELISA method, using the Rat Survivin (Thermo Scientific, United States) and HIF1α (Abbkine, United States) ELISA kits following the manufacturer's instructions. In brief, 20 μL of each standard, control, and samples (serum) in duplicate was dispensed with new disposable tips into appropriate wells on a microplate coated with survivin and HIF1α antibodies. After that, each microplate well was filled with 200 μL enzyme conjugate, thoroughly mixed, and then incubated for 60 min at room temperature. After incubation, the solution in the wells was briskly shaken out and rinsed out four times with 350 μL diluted washing solution per well. Furthermore, 100 μL substrate solution was added to each well of the microplate, which was then re-incubated for 15–20 min at room temperature. After that, the enzymatic reaction was stopped by adding 100 μL stop solution to each well. Finally, absorbance was determined by using an ELISA reader (xMark™ Microplate Absorbance Spectrophotometer, Bio-Rad Laboratories Inc.) at 450 nm for quantification of protein abundances.

Preservation of Tissue Specimens

Second- to third-degree branches of the pulmonary artery were isolated from the lobes of the lungs, cleaned off blood in cold phosphate-buffered saline, dissected and removed the endothelium, frozen in liquid nitrogen, and stored at −80°C for subsequent mRNA or protein extraction.

Preparation and Treatment of Isolated Pulmonary Artery Myocytes

To functionally characterize Kv channels by whole-cell patch-clamp, PASMCs were freshly dissociated from intralobar pulmonary arteries of rats from control, Control + Sang, Hypoxia, and Hypoxia + Sang groups, as described previously (Fan et al., 2019). In brief, following initial PA equilibration in hypoxic iced low-Ca^{2+} Krebs solution, small pieces of muscle layers were stood for 20 min at room temperature prior to digestion with 4 mg/ml papain, 1.25 mg/ml BSA, and 2 mg/ml DTT in 2 ml hypoxic low-Ca^{2+} dissolution solution. Following threefold washing in low-Ca^{2+} solution, separated PASMCs were stored in hypoxic low-Ca^{2+} solution with 0.5% BSA at 4°C for use within 3–4 h.

PASMCs for the remaining cell experiments were isolated from normal adult SD rats and identified by immunohistochemical staining with α-SMC. Rat PASMCs were exposed to hypoxia (1% O_2, 5% CO_2, and rest N2) in the 1% (v/v) FCS and 1% (m/v)

TABLE 2 | Groups and *In vitro* indexes of study rats.

Parameter	Control	Control + Sang	Hypoxia	Hypoxia + Sang
Survival(%), (n/N)	100 (24/24)	100 (24/24)	75 (18/24)**	87.5 (21/24) ##
Body weight(g)				
Week 0	229.82 ± 5.82	231.46 ± 8.65	230.80 ± 7.31	229.96 ± 9.41
Week 4	391.9 ± 28.11	381.5 ± 50.02	310.4 ± 24.71*	347.8 ± 13.40 #
Pulmonary Pressure(mmHg)				
sPAP	16.19 ± 4.3	17.04 ± 4.6	23.65 ± 2.93***	22.64 ± 2.53#
mPAP	11.33 ± 2.11	10.33 ± 1.90	16.81 ± 2.04	14.48 ± 2.11 #
dPAP	8.48 ± 1.62	8.05 ± 1.54	13.47 ± 1.62	10.38 ± 1.64 #
Serum survivin (pg/ml)	248.16 ± 68.8	236.37 ± 63.2	639.32 ± 106.48***	314.66 ± 71.28 ###
Serum HIF1a (ng/L)	41.36 ± 6.74	38.69 ± 7.18	58.84 ± 8.32**	40.65 ± 5.87##
RVHI	0.275 ± 0.023	0.269 ± 0.030	0.385 ± 0.130***	0.283 ± 0.080 ###
Inner circumferencce (mm)	9.61 ± 2.30	9.22 ± 1.91	5.20 ± 1.62***	7.84 ± 2.38 #
Thickness (mm)	1.30 ± 0.42	1.25 ± 0.52	2.82 ± 0.64***	1.92 ± 0.44 #

*p < *0.05;* **p < *0.01* ; ***p < *0.001 Hypoxia vs. control.* #p < *0.05* ##p < *0.01* ; ###p < *0.001 Hypoxia + Sang vs. Hypoxia.*

penicillin and streptomycin M199 medium for the indicated period of time. All other measurements were performed under normoxic conditions, starting 30 min after termination of hypoxia.

For cells in the treatment groups, a series of doses of sanguinarine (0.05, 0.5, 5, and 50 μM; Macklin Inc., Shanghai, China) was separately added either in the hypoxia or normoxia medium for the indicated period. 1-10-100 nmol/L survivin selective inhibitor YM155 [YM155 (Sepantronium bromide) AbMole, United States.] was used as a positive control versus DMSO as a negative control. Cells were harvested at 24 h for 24-h MTT experiments, and the rest were collected at 48 h for 48-h MTT and RNA and protein extraction.

Immunofluorescence Staining

Isolated cells grown on glass slides were fixed with 4% formaldehyde in PBS for 30 min and incubated in blocking solution for 30 min (PBS containing 2% BSA-0.1% Triton X-100). Cells were incubated with primary antibodies against α-SMA, F-actin, collagen I, and collagen III for 1 h and incubated for 30 min at 37°C with secondary antibodies (Jackson ImmunoResearch). The cell nuclei were stained with 4′,6′-diamidino-2-phenylindole (DAPI; Sigma-Aldrich). Cells were observed with fluorescence microscopy (Olympus).

MTT

PASMC proliferation was determined by a MTT method. In brief, at the end of treatments, 20 mg of 5 mg/ml MTT solution was added to each well, and PASMCs were incubated for 24 and 48 h at 37°C. Then, the culture medium was removed, and 150 l DMSO was added to each well and incubated for 10 min to solubilize the formazan salt crystals. The formazan within cells was quantified at 490 nm using an enzyme-linked immunosorbent assay reader (Biotek, ELK 800, United States). Each group had six wells, and the average optical density value of those six wells was used as the result of each experiment.

Real-Time PCR

Total RNA was extracted using a TRIzol reagent (Invitrogen, United States), according to the manufacturer's instructions. The concentration and quality of isolated RNAs were determined using an ultraviolet spectrophotometer and by electrophoresis on agarose gel, respectively. The cDNA was synthesized using a Reverse Transcriptase kit (Takara, Japan). The specific primer sequences used for the real-time PCR (Rt-PCR) are presented in **Table 1**. The Rt-PCR was performed with the SYBR Premix Ex Taq (Takara, Japan) on the iQ5 Multicolor RT-PCR Detection System (Bio-Rad, CA, United States). The relative expression of genes was calculated from cycle thresholds (Ct) and normalized to β-actin using the $2^{-\Delta\Delta Ct}$ (Livak) method.

Western Blot

Total protein was extracted using RIPA buffer, and the concentration was quantified using a BCA Protein Assay Kit (Genshare Biological, China). Equal amounts of protein were loaded onto 10% SDS-PAGE gels for electrophoresis, transferred onto the PVDF membrane, blocked by 5% skim milk, and incubated with the primary antibody overnight at 4°C, including anti-survivin (1:500; Abcam, United States), anti-TGFb1(1:100; Abcam, United States), anti-pSmad3 (1:1,500; Abcam, United States), anti-BMPR2 (1:1,500; Abcam, United States), anti-HIF1α(1:500; Abcam, United States), anti-P53 (1:1,000; Abcam, United States), anti-Kv1.2 (1:400; Sigma, United States), anti-Kv1.5 (1:200; Abcam, United States), anti-Kv2.1 (1:500; Sigma), and anti-GAPDH (1:1,000; Epitomics, United States). The membrane was washed and incubated with HRP-conjugated goat anti-rabbit IgG (1:4,000; Abcam) at room temperature for 1 h. The blots were visualized using the chemiluminescence system and quantized by Quantity One.

Patch-Clamp Electrophysiology

Cells for patch-clamp experiments were performed under hypoxic or normoxic conditions as indicated. Drug interventions were as indicated in the "Results" section. The record of K+ current (IK) and EM in the PASMCs was performed using an Axopatch 200B patch-clamp amplifier and 3- to 5-M micropipettes. PASMCs were voltage-clamped at −70 mV, and currents were evoked by steps of 200-ms duration from −70 to +70 mV. Membrane currents were filtered at 5 kHz, digitized using a Digidata 1320A interface (Axon Instruments, Foster City, CA, United States), and analyzed using pCLAMP software.

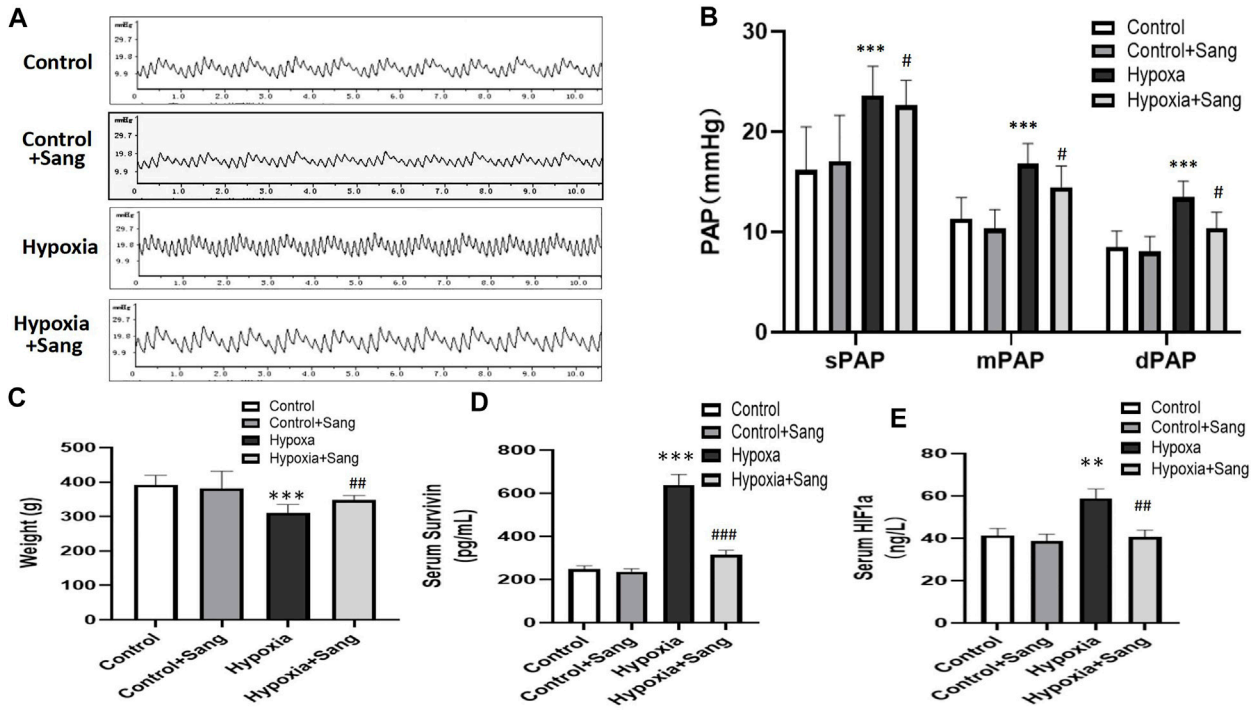

FIGURE 1 | Body weight, pulmonary artery pressures, and serum survivin and HIF1α of the rats: representative traces of pulmonary artery pressure (PAP) **(A)** and the value of systolic pressure (sPAP), mean pressure (mPAP), and diastolic pressure (dPAP) **(B)**, and body weight of the rats **(C)**. Survivin and HIF1α levels in serum **(D,E)** in control ($n = 12$), control treated with sanguinarine ($n = 12$) and untreated hypoxia PH rats ($n = 12$), and 28 days after sanguinarine treatment ($n = 12$). Survivin and HIF1α were measured by ELISA. Results are mean ± SEM. $^{**}p < 0.01$,$^{***}p < 0.001$ Hypoxia PH vs control group. $\#\#p < 0.01$ Hypoxia PH vs Hypoxia PH + Sanguinarine group.

Statistical Analysis

Values are given as mean ± SEM (standard error of the mean) or SD (standard deviation) or percentage (N). Calculations were performed using the GraphPad Prism software package (version 4.0.1; GraphPad Software, Inc., La Jolla, CA, United States). Statistical tests were two-sided, and data were tested for normality. Comparisons between two groups were assessed with a student "t" test. The "t" test was used with a Bonferroni correction for multiple comparisons too. The χ^2 test was used to evaluate the differences among groups with ordinal data. Dose–response was analyzed by a four-parameter logistic regression model. A p-value of less than 0.05 was considered significant.

RESULTS

Effects of Sanguinarine on Pulmonary Artery Pressures and Levels of Serum Survivin and HIF1α in Chronic Hypoxic Rats

There was no significant difference among the groups at baseline in body weight. After 4 weeks, weight gain was less in hypoxic that control rates. However, sanguinarine treatment significantly improved the nutritional status (**Table 2**; **Figure 1C**). Meanwhile along with increase of pulmonary artery pressure (PAP) (including systolic, diastolic, and mean pressures, sPAP, dPAP, and mPAP), in rats exposed to hypoxia, the levels of serum survivin and HIF1α were elevated, compared with those in the control animals. However, PAP and serum survivin and HIF1α remained at lower levels in hypoxic rats treated with sanguinarine than those in untreated hypoxic rats (**Table 2**; **Figures 1A,B,D,E**).

Effects of Sanguinarine on Remodeling of Pulmonary Arteries and Right Heart as Well as the Survival Rate in Chronically Hypoxic Rats

Histological examination showed that the right ventricles were enlarged, the lungs and livers looked edematous and congested, and pleural effusion and ascites were visible in rats subjected to hypoxia when rats were sacrificed after 4 weeks. All the aforementioned signs were significantly less after sanguinarine treatment (data not shown here). Furthermore, rats exposed to hypoxia showed hypertrophy of pulmonary arteries with a thicker medial smooth muscle layer and smaller inner lumen area. All these indices indicative of remodeling of the pulmonary arteries and right heart were reduced dramatically in the Sang + Hypoxia group (**Table 2**, **Figures 2A,B,C,D**). Sanguinarine also improved survival in rats exposed to hypoxia (**Figure 2E**).

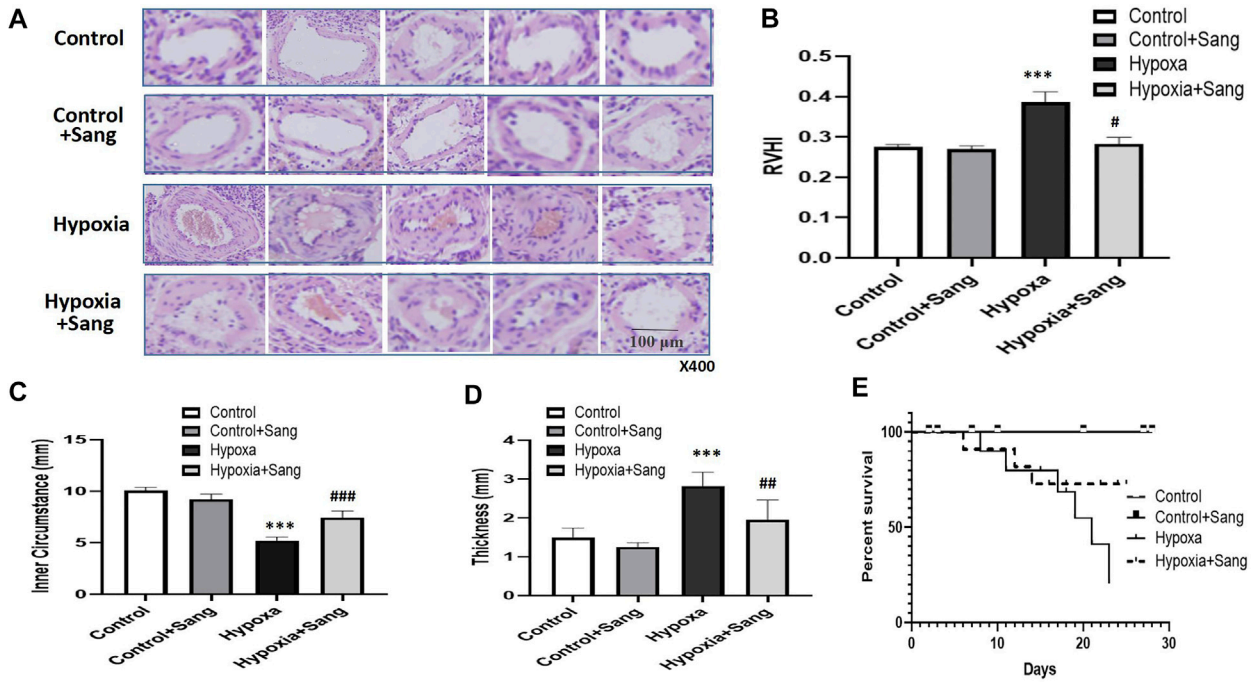

FIGURE 2 | Histology **(A)**, HE staining (under 400× magnification) of pulmonary arteries, and morphometric measures **(B–D)** in control rats (n = 12), control treated with Sanguinarine (n = 12) and hypoxia PH rats before (n = 12) and after (n = 12) 28 days of sanguinarine treatment. Survival rate curve are shown in figure 2E. RVHI was calculated as (RV weight/LV + S weight). Results are mean ± SEM. ***p < 0.001 Hypoxia PH vs control group. ##p < 0.01, ###p < 0.001, Hypoxia PH vs Hypoxia PH + Sanguinarine group.

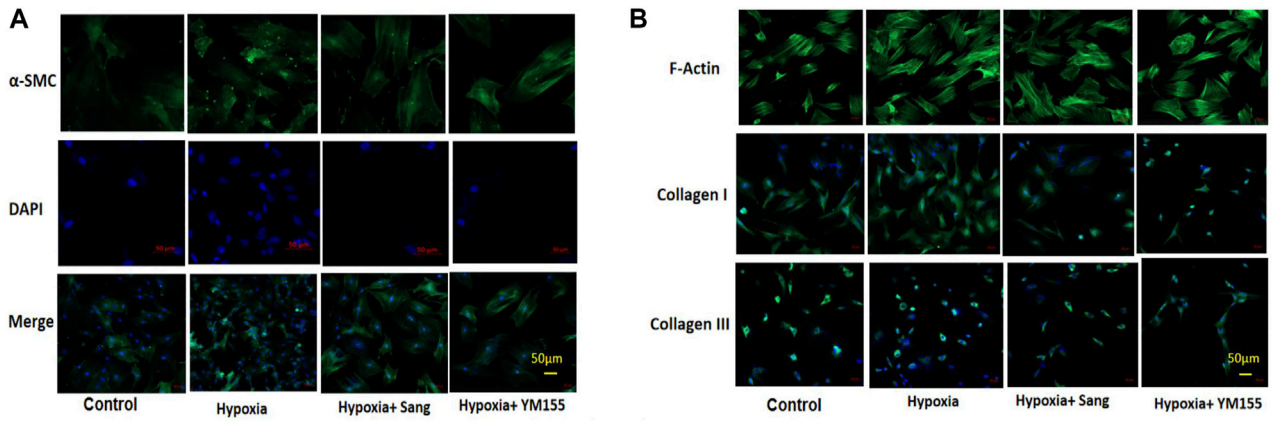

FIGURE 3 | Immunofluorescence staining of PASMC proliferation and fibrosis. α-SMC staining for PASMC, DAPI for nucleus, and merge for both cytoplasm and nucleus staining. **(A)** F-actin, collagen I, and collagen III represent the fibrosis in PASMCs **(B)**.

Effects of Sanguinarine on Proliferation and Fibrosis of Smooth Muscles of Pulmonary Arteries

In the cell experiments, the PASMCs and the proliferation were identified by immunofluorescence staining with α-SMC (**Figure 3**) and then determined with the MTT method (**Figure 4**). Both sanguinarine and survivin selective inhibitor YM155 significantly inhibited hypoxia-induced PASMC proliferation (**Figures 3A**, **4**), accompanied by decreases in SMC F-actin cytoskeleton, collagen I, and collagen III (**Figure3B**). These results are consistent with notion that sanguinarine prevents or inhibits pulmonary artery remodeling via the survivin pathway.

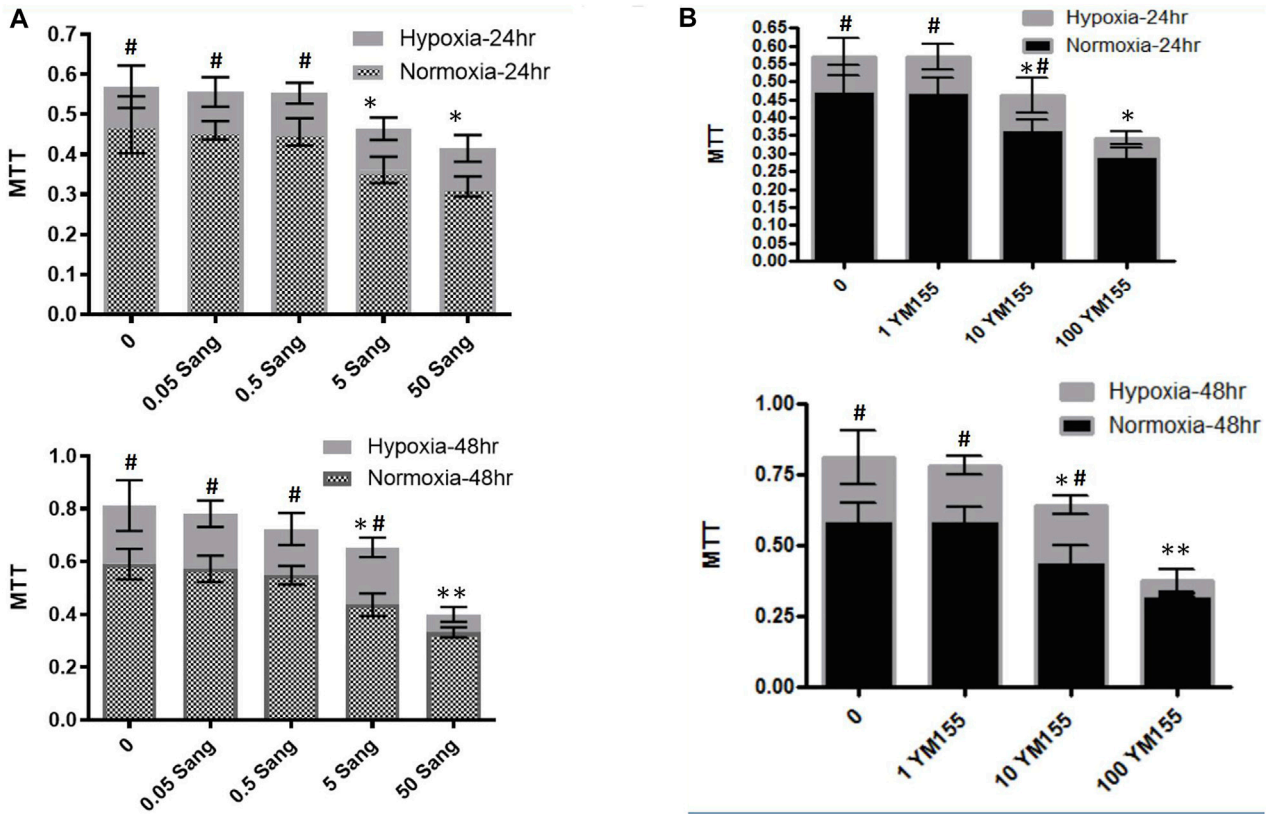

FIGURE 4 | MTT experiments in PASMCs for cell proliferation. MTT experiments for PASMC proliferation under treatment of different sanguinarine concentrations **(A)**. The cell numbers in the hypoxia group during sanguinarine treatment was presented with gray bar, while ones in the normoxia group during sanguinarine treatment were with combination of gray and small square **(A)**. Survivin selective inhibitor YM155 was used as a positive control. MTT experiments for PASMC proliferation under treatment of different YM155 concentrations **(B)**. The same style of symbols as in **(A)**. It means that cell numbers in the hypoxia group during YM155 treatment were presented with light gray bar, while ones in the normoxia group during YM155 treatment were with black bar **(B)**. $^{*}p < 0.05$,$^{**}p < 0.01$, Hypoxia PASMC with different doses of Ssnguinarine or YM155 vs control PASMC without treatment. $\#p < 0.05$,$\#\#p < 0.01$ Hypoxia PASMC vs normoxia PASMC.

Effects of Sanguinarine on HIF1α–Survivin/TGFb/Smad Pathways

HIF1α is one of the critical mediators in hypoxia-induced injury either by regulating proliferation and apoptosis, oxygen stress–related genes such as SMAD and survivin or interacting with other transcription factors such as p53. Thus, inhibiting the HIF1α pathway has been believed to be a potential therapy for cancer, as well as for hypoxia-induced diseases (Su et al., 2019; Gaber et al., 2021). Accordingly, in this study, we examined whether the inhibiting effects of sanguinarine on hypoxia-induced PASMC proliferation and fibrosis were mediated by the HIF1α/TGFβ/Smad pathway or/and by its feed-forward loop with survivin. The results showed that both serums HIF1α and survivin were significantly increased in rats after 4-week hypoxic exposure (**Figures 1D,E**, Hypoxia vs. Control, $P < 0.01$), but restored if rats were treated with sanguinarine during this period (Hypoxia + Sang v.s. Hypoxia, $P < 0.01$) (**Table 2**; **Figures 1D,E**). Furthermore, their gene expressions of mRNA and protein changed in the same ways with above serum levels of HIF1α and survivin (**Figures 5A,B**). Meanwhile, it was detected that both mRNA and protein expressions of TGFβ1 and pSmad3 were increased in a time-dependent manner in hypoxic PASMCs *in vivo* (**Figures 6A,B**). Additionally, TGFβ1 and pSmad3 gene expressions were dramatically decreased after sanguinarine intervention (**Figures 6C,D**) *in vitro* as well. These effects were similar with the positive control reagent, survivin selective inhibitor YM155 (**Figures 6C,D**). These results imply that HIF-1α/TGFβ/Smad and survivin are importantly involved in the hypoxia-induced PH mechanism so that sanguinarine being with the survivin inhibitor reversed hypoxic-related pulmonary remolding.

EFFECTS OF SANGUINARINE ON BMPR2/SMAD3/P53 PATHWAYS

Bone morphogenetic protein type 2 receptor (BMPR2)/BMP signaling is a typical molecular mechanism for not only primary but also hypoxic PH. It was proposed TGFβ, working partially via its downstream Smad, is critical in lung vascular remodeling (Takahashi et al., 2006; Liu et al., 2013). In this study, the changes of BMPR2, pSmad, and p53 were examined (pSmad results presented in result part 4) (**Figures 6B,D**). Hypoxia

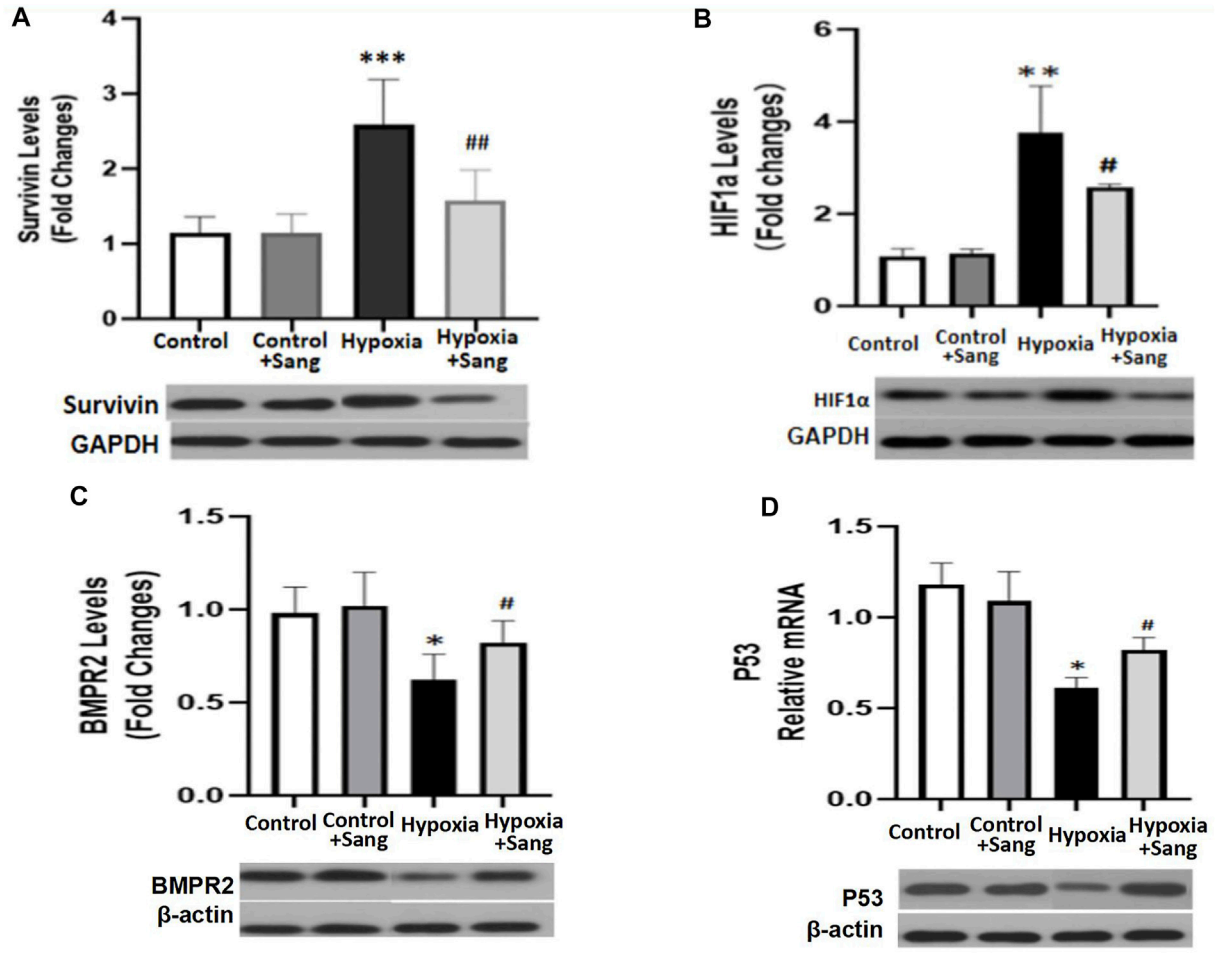

FIGURE 5 | mRNA and protein expressions of Survivin/HIF1α **(A,B)** and BMPR2/p53 **(C,D)** in distal PA tissue from different rat groups: control (n = 12) and hypoxia PH rats without (n = 24) and following (n = 12) sanguinarine treatment. The upper panel shows relative mRNA expression. The lower panel shows Western blots of protein expression. A different gel was used for each receptor, and the respective GAPDH band is shown for each. Gels were analyzed with a Biorad Universal Hood II Molecular Imager Gel System. Results are mean ± SEM. ***$p < 0.001$ **$p < 0.01$ *$p < 0.05$ Hypoxia PH vs control group. ##$p < 0.01$ #$p < 0.05$ Hypoxia PH vs Hypoxia PH + Sanguinarine group.

increased the mRNA and protein of BMPR2 and p53 (Hypoxia group vs. Control, $p < 0.05$), but these effects were reduced by sanguinarine treatment (Sang + Hypoxia group vs. Hypoxia group, $p < 0.05$) (**Figures 5C,D**). These results confirmed the important role of BMPR2/Smad3/p53 in hypoxia PH.

EFFECTS OF SANGUINARINE ON O_2-SENSITIVE KV CHANNELS

The occurrence of hypoxic vasoconstriction in the pulmonary circulation relates to the colocalization of an O_2 sensor and O_2-sensitive voltage-dependent potassium (Kv) channels in resistance pulmonary arteries. A reduction in Kv channels, in particular Kv1.2, Kv1.5, and Kv2.1, have been proven in the pathogenesis of hypoxia-induced pulmonary hypertension, leading to pulmonary vasoconstriction and vascular remodeling, while the upregulation of Kv channels is of therapeutic significance for pulmonary hypertension (Jackson et al., 2018). In the current study, in hypoxic rats, we observed a reduction in the slope of the current–voltage curve in Kv channels (**Figures 8A,B**, $p < 0.05$). However, the above reduction of IK was almost recovered completely by treating with sanguinarine (**Figures 7A,B**, $p < 0.05$), whereas when PASMCs were pre-treated by the Kv channel blocker 4-AP, all above interventions had much less effect on whole-cell voltage K+ current (**Figure 7C**).

Gene expressions of Kv1.2, Kv1.5, and Kv2.1 were also examined in PAs of experimental animals. The three Kv channels were down-expressed in the hypoxic group (**Figures 7D–F**, Control group vs. Hypoxia group, $P < 0.05$) but restored again when hypoxic rats were treated with sanguinarine (**Figures 7D–F**, Sang + Hypoxia group vs. Hypoxia group, $p < 0.05$). These results give another possibility that sanguinarine positively changed PA remolding by directly or indirectly (via survivin, Smad, Ca^{++}, etc.) restoring Kv channels.

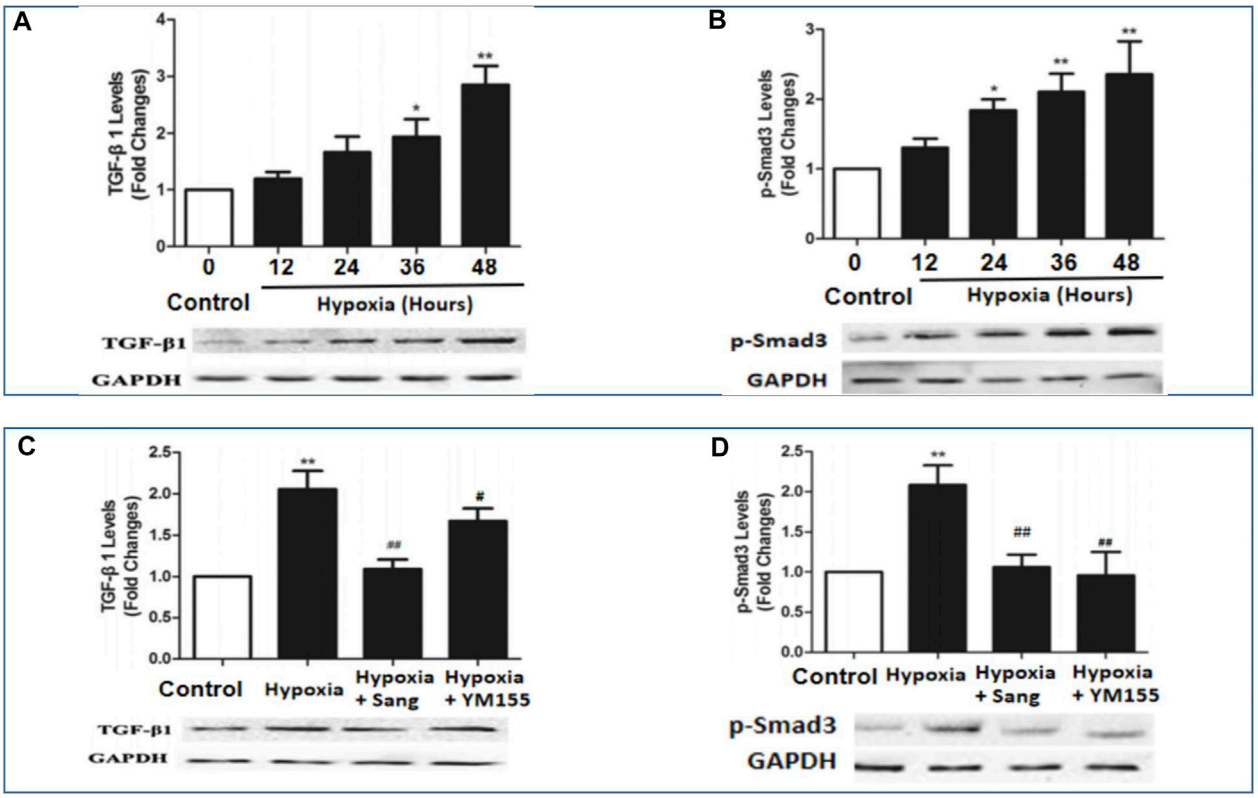

FIGURE 6 | mRNA and protein expressions of BMPR2 and pSmad3 in hypoxia-exposed PASMC **(A,B)** and PA from different rat groups **(C,D)** including control (n = 12) and hypoxia PH rats without (n = 12) and following (n = 12) sanguinarine treatment. Pulmonary artery tissues were obtained from the third and subsequent bifurcations. YM155 was used as a positive control. The upper bars show relative mRNA expression of PASMC under different hours of hypoxia exposure or PA tissue from different rat groups. The lower bands show Western blots of protein expression. A different gel was used for each receptor, and the respective GAPDH band is shown for each. Target gene bands compared with housekeeper GAPDH were analyzed with a Biorad Universal Hood II Molecular Imager Gel System. Results are mean ± SEM. *p < 0.05,**p < 0.01, Hypoxia PH vs control group. #p < 0.05,##p < 0.01 Hypoxia PH vs Hypoxia PH + Sanguinarine group or Hypoxia PH vs Hypoxia PH + YM155 group.

DISCUSSION

Pulmonary hypertension (PH) is a fatal disease, classified into five types according to clinical characteristics (as enumerated in the Introduction). However, irrespective of the clinical type, a consistent feature is pulmonary artery remodeling with features similar to those seen in cancer and resulting in increased pulmonary vascular resistance, pulmonary hypertension, right heart failure, and ultimately death. Regarding the mechanism of this cancer-like vascular remodeling, TGF-β/Smad3, BMPR2 pathways, and O_2-sensitive voltage-gated K + channels are believed to be the important pathways. Previous research has demonstrated that there are cross-talk and interaction between TGF-β/Smad3 and BMP/BMPR2 pathways, and all of them are regulated by apoptotic genes or transcription factors such as survivin,HIF1α, and p53 (Luo et al., 2014; Yang et al., 2020; Young et al., 2006). It has been noted that there is an interactive loop that leads to increased cancer-like stemness, proliferation, metastasis, chemo-resistance, angiogenesis, and immunosuppression, wherein it simultaneously mediates major oncogenic pathways from BMP/Smad to HIF1α and TGFb(Thomas and Wink, 2017). The role of survivin activating TGF-β1/Smad signaling has also been shown in a wide range of cellular processes such as growth, proliferation, differentiation, and apoptosis (Zhao et al., 2020; Park et al., 2019; Liu et al., 2015). We therefore examined these pathways, and the results showed most of them changed in the hypoxia group (**Figures 6**, **7**), consistent to cancer studies and other PH–related research studies (Li et al., 2019b). In the current study, genes and transcription factors related to both cancer and PH including survivin, HIF1α, and p53 were significantly changed in hypoxic rats (**Figures 5**, **6**). These findings confirmed that survivin/HIF1α modulated TGF-β/Smad3 and BMPR2, which is an important mechanism for hypoxia-induced PH as well.

Current treatments for pulmonary hypertension rely on vascular dilatation but do not deal with the underlying pathophysiology, namely pulmonary artery remodeling. The demonstration of the involvement of the survivin/HIF1α and related pathways provides a potential new therapeutic strategy. Sanguinarine (Sang) is a plant alkaloid

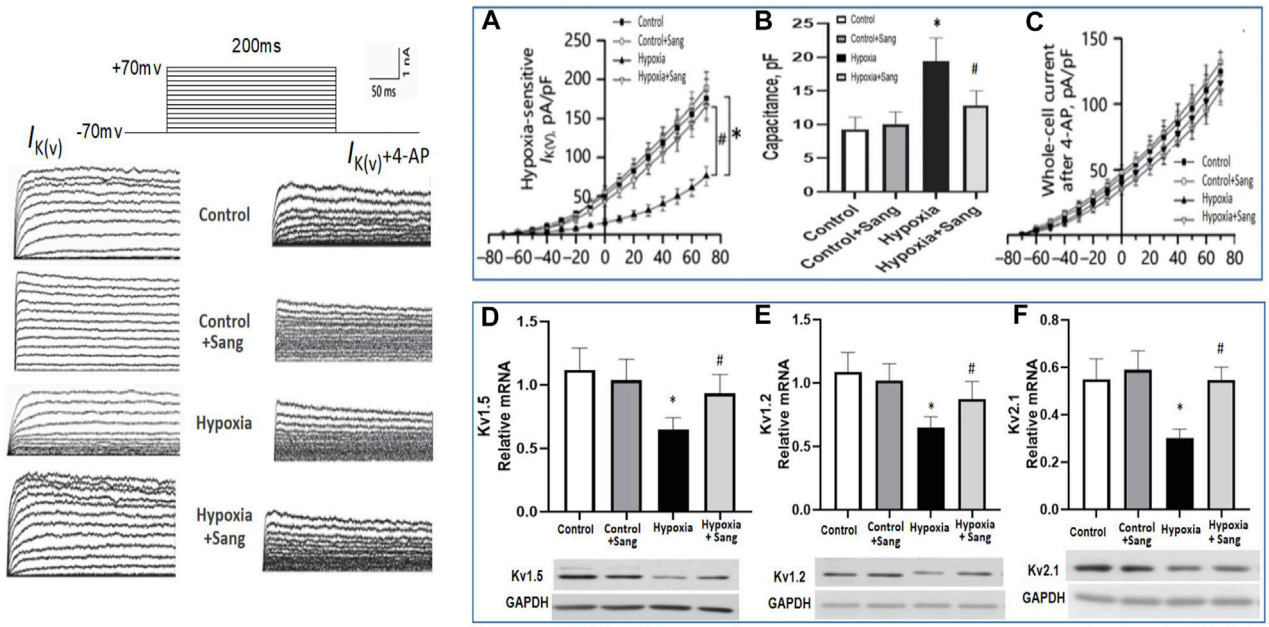

FIGURE 7 | Whole-cell K+ current (IK) and EM of PASMCs were measured by whole-cell patch-clamp in normoxia (control) and hypoxia setting with or without treatment as shown. **(A)**: In the absence of the Kv channel blocker 4-AP. **(B)**: Capacitance was measured in PASMC with different treatment as shown. **(C)**: In the existence of 4-AP. **(D–F)**: RT-PCR and Western blots of Kv channels in rats pulmonary arteries from different groups: control (n = 12) and hypoxia PH rats without (n = 12) and following (n = 12) sanguinarine treatment. The upper panel shows relative mRNA expression. The lower panel shows Western blots of protein expression. A different gel was used for each gene, and the respective GAPDH band is shown for each. Gels were analyzed with a Biorad Universal Hood II Molecular Imager Gel System. Results are mean ± SEM. *p < 0.05, Hypoxia PH vs control group. #p < 0.05 Hypoxia PH vs Hypoxia PH + Sanguinarine group.

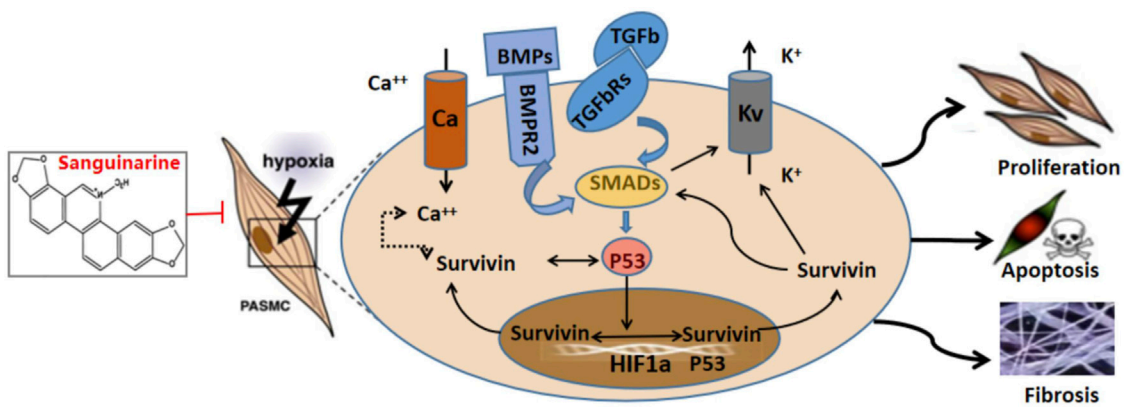

FIGURE 8 | Drawing for effects and the mechanisms of sanguinarine treatment in hypoxia-induced PH.

with the chemical structure of 13-methyl benzodioxole-1,3-dioxolo phenanthradinium. An important intermediate in its synthesis is protopine. Dihydrosanguinarine (DHSA) is formed by hydroxylation of protopine with NADPH, as a reduction cofactor, and molecular oxygen. It has diverse biological activities, including modulation of TGFb and HIF1α. It is also known to induce apoptosis, inflammation, and immunity as reviewed by Mackraj et al. (Cardiovasc Ther. 2008). These effects of sanguinarine were also involved in the development of pulmonary artery remodeling. So, it suggests that sanguinarine would be a potential new therapeutic approach for pulmonary artery remodeling from PH. Importantly, it is enhanced by the previous demonstration in animal and cell studies of a low level of toxicity as well (Wu et al., 2020). In accordance with them, the results from this study illustrated that sanguinarine was remarkably effective in suppressing abnormal proliferation and fibrosis of PASMCs from the exposure to hypoxia (**Figures 3**, **4**). Therefore,

sanguinarine significantly improved the PH- and RHF-related characters (elevated PAP, thickness of PA vessels, reduced artery lumen, hypertrophy of RH, etc.), inhibited PASMC proliferation, reduced right heart remolding, and increased the survival rate of rats suffering hypoxia PH. We further investigated the mechanism of anti-vascular remodeling effect of sanguinarine in hypoxic PH. Most of the changes noted previously in the hypoxia group including survivin/HIF1α, TGF-β/Smad3/P53 were restored significantly (**Figures 5**, **6**). The function and expressions of Kv channels were also restored (**Figure 7**).

Taken together, our findings presented that sanguinarine has a multi-function in suppressing the pathogenesis of PH. Sanguinarine alleviates pulmonary vascular remodeling and fibrosis during hypoxia-induced PH, suppresses the excessive proliferation, and induces apoptosis of PASMCs via inactivation of survivin/HIF1α and their interactions with TGF-β/Smad3/p53. Moreover, hypoxia-induced decrease in function and expression of Kv channels is repressed by sanguinarine, which could be directly or indirectly via survivin/HIF1α, while further study is needed on this (Table 8).

CONCLUSION

The study demonstrated that sanguinarine improving the hypoxia-induced characters and pulmonary vascular remodeling *via* survivin/HIF1α and by inhibiting their interactions with BMPR-TGFb/SMAD/p53 signals. It indicated that it is possible that sanguinarine could be a breakthrough anti-vascular remodeling agent for PH, possibly an ideal agent to use in combination with vasodilating agents.

DATA AVAILABILITY STATEMENT

The original contributions presented in the study are included in the article/Supplementary Material, further inquiries can be directed to the corresponding authors.

ETHICS STATEMENT

The animal study was reviewed and approved by the Laboratory Animal Administration Committee at Xi'an Jiaotong University. Written informed consent was obtained from the owners for the participation of their animals in this study.

AUTHOR CONTRIBUTIONS

FF contributed to study design, experiment control, analysis, and writing of the manuscript. YZ was the major contributor for the data collection and analysis. YW was the major contributor for molecular and patch-clamp experiments. PZ was the major contributor for molecular experiments. AD contributed in interpretation and analysis and writing of the manuscript. YZ contributed in study design, quality control, and decision for submission. All authors read and approved the final manuscript.

FUNDING

This study was supported by the Clinical Research Award of the First Affiliated Hospital of Xi'an Jiaotong University, China (No. XJTU1AF-CRF-2019-010), and Fundamental Project Plan in Shaanxi Province, China (No. 2020JM-364).

REFERENCES

Cheng, C. C., Chi, P. L., Shen, M. C., Shu, C. W., Wann, S. R., Liu, C. P., et al. (2019). Caffeic Acid Phenethyl Ester Rescues Pulmonary Arterial Hypertension through the Inhibition of AKT/ERK-Dependent PDGF/HIF-1α *In Vitro* and *In Vivo*. *Int. J. Mol. Sci.* 20 (6), 1468. doi:10.3390/ijms20061468

Diez-Calzadilla, N. A., Noguera Salvá, R., Soriano Sarrió, P., and Martínez-Jabaloyas, J. M. (2021). Genetic Profile and Immunohistochemical Study of clear Cell Renal Carcinoma: Pathological-Anatomical Correlation and Prognosis. *Cancer Treat. Res. Commun.* 27, 100374. doi:10.1016/j.ctarc.2021.100374

Fan, F., Tian, H., Geng, J., Deng, J., Liu, Y., Chen, C., et al. (2019). Mechanism of Beraprost Effects on Pulmonary Hypertension: Contribution of Cross-Binding to PGE2 Receptor 4 and Modulation of O2 Sensitive Voltage-Gated K+ Channels. *Front. Pharmacol.* 9, 1518. doi:10.3389/fphar.2018.01518

Fu, C., Guan, G., and Wang, H. (2018). The Anticancer Effect of Sanguinarine: A Review. *Curr. Pharm. Des.* 24 (24), 2760–2764. doi:10.2174/1381612824666180829100601

Gaber, G., El Achy, S., Khedr, G. A., Parimi, V., Helenowksi, I., Donnelly, E. D., et al. (2021). Impact of P53, HIF1a, Ki-67, CA-9, and GLUT1 Expression on Treatment Outcomes in Locally Advanced Cervical Cancer Patients Treated with Definitive Chemoradiation Therapy. *Am. J. Clin. Oncol.* 44 (2), 58–67. doi:10.1097/COC.0000000000000781

Hasan, R., and Jaggar, J. H. (2018). KV Channel Trafficking and Control of Vascular Tone. *Microcirculation* 25 (1). doi:10.1111/micc.12418

Haworth, A. S., and Brackenbury, W. J. (2019). Emerging Roles for Multifunctional Ion Channel Auxiliary Subunits in Cancer. *Cell Calcium* 80, 125–140. doi:10.1016/j.ceca.2019.04.005

Jackson, W. F. (2018). KV Channels and the Regulation of Vascular Smooth Muscle Tone. *Microcirculation* 25 (1). doi:10.1111/micc.12421

Li, G., Zhang, H., Zhao, L., Zhang, Y., Yan, D., Liu, Y., et al. (2019). The Expression of Survivin in Irreversible Pulmonary Arterial Hypertension Rats and its Value in Evaluating the Reversibility of Pulmonary Arterial Hypertension Secondary to Congenital Heart Disease. *Pulm. Circ.* 9 (3), 2045894019859480. doi:10.1177/2045894019859480

Li, Y., Ren, W., Wang, X., Yu, X., Cui, L., Li, X., et al. (2019). MicroRNA-150 Relieves Vascular Remodeling and Fibrosis in Hypoxia-Induced Pulmonary Hypertension. *Biomed. Pharmacother.* 109, 1740–1749. doi:10.1016/j.biopha.2018.11.058

Liu, N., Zhao, N., Chen, L., and Cai, N. (2015). Survivin Contributes to the Progression of Diabetic Retinopathy through HIF-1α Pathway. *Int. J. Clin. Exp. Pathol.* 8 (8), 9161–9167.

Liu, Y., Tian, H. Y., Yan, X. L., Fan, F. L., Wang, W. P., Han, J. L., et al. (2013). Serotonin Inhibits Apoptosis of Pulmonary Artery Smooth Muscle Cell by pERK1/2 and PDK through 5-HT1B Receptors and 5-HT Transporters. *Cardiovasc. Pathol.* 22, 451–457. doi:10.1016/j.carpath.2013.03.003

Luo, T., Cui, S., Bian, C., and Yu, X. (2014). Crosstalk between TGF-β/Smad3 and BMP/BMPR2 Signaling Pathways via miR-17-92 Cluster in Carotid Artery Restenosis. *Mol. Cell Biochem* 389 (1-2), 169–176. doi:10.1007/s11010-013-1938-6

Luo, Y., Teng, X., Zhang, L., Chen, J., Liu, Z., Chen, X., et al. (2019). CD146-HIF-1α Hypoxic Reprogramming Drives Vascular Remodeling and Pulmonary Arterial Hypertension. *Nat. Commun.* 10 (1), 3551. doi:10.1038/s41467-019-11500-6

Nathan, S. D., Barbera, J. A., Gaine, S. P., Harari, S., Martinez, F. J., Olschewski, H., et al. (2019). Pulmonary Hypertension in Chronic Lung Disease and Hypoxia. *Eur. Respir. J.* 53 (1), 1801914. doi:10.1183/13993003.01914-2018

Park, J. H., Kim, Y. H., Park, E. H., Lee, S. J., Kim, H., Kim, A., et al. (2019). Effects of Metformin and Phenformin on Apoptosis and Epithelial-Mesenchymal Transition in Chemoresistant Rectal Cancer. *Cancer Sci.* 110 (9), 2834–2845. doi:10.1111/cas.14124

Pullamsetti, S. S., Nayakanti, S., Chelladurai, P., Mamazhakypov, A., Mansouri, S., Savai, R., et al. (2020). Cancer and Pulmonary Hypertension: Learning Lessons and Real-Life Interplay. *Glob. Cardiol. Sci. Pract.* 2020 (1), e202010. doi:10.21542/gcsp.2020.10

Su, Q., Fan, M., Wang, J., Ullah, A., Ghauri, M. A., Dai, B., et al. (2019). Sanguinarine Inhibits Epithelial-Mesenchymal Transition via Targeting HIF-1α/tgf-β Feed-Forward Loop in Hepatocellular Carcinoma. *Cell Death Dis* 10 (12), 939. doi:10.1038/s41419-019-2173-1

Takahashi, H., Goto, N., Kojima, Y., Tsuda, Y., Morio, Y., Muramatsu, M., et al. (2006). Downregulation of Type II Bone Morphogenetic Protein Receptor in Hypoxic Pulmonary Hypertension. *Am. J. Physiol. Lung Cell Mol Physiol* 290 (3), L450–L458. doi:10.1152/ajplung.00206.2005

Thenappan, T., Ormiston, M. L., Ryan, J. J., and Archer, S. L. (2018). Pulmonary Arterial Hypertension: Pathogenesis and Clinical Management. *BMJ* 360, j5492. doi:10.1136/bmj.j5492

Thomas, D. D., and Wink, D. A. (2017). NOS2 as an Emergent Player in Progression of Cancer. *Antioxid. Redox Signal.* 26 (17), 963–965. doi:10.1089/ars.2016.6835

Tian, Q. G., Wu, Y. T., Liu, Y., Zhang, J., Song, Z. Q., Gao, W. F., et al. (2018). Expressions and Correlation Analysis of HIF-1α, Survivin and VEGF in Patients with Hepatocarcinoma. *Eur. Rev. Med. Pharmacol. Sci.* 22 (11), 3378–3385. doi:10.26355/eurrev_201806_15159

Wu, Y., Zhao, N. J., Cao, Y., Sun, Z., Wang, Q., Liu, Z. Y., et al. (2020). Sanguinarine Metabolism and Pharmacokinetics Study *In Vitro* and *In Vivo*. *J. Vet. Pharmacol. Ther.* 43 (2), 208–214. doi:10.1111/jvp.12835

Yang, C., Chen, X. C., Li, Z. H., Wu, H. L., Jing, K. P., Huang, X. R., et al. (2020). SMAD3 Promotes Autophagy Dysregulation by Triggering Lysosome Depletion in Tubular Epithelial Cells in Diabetic Nephropathy. *Autophagy*, 1–20. doi:10.1080/15548627.2020.1824694

Young, K. A., Ivester, C., West, J., Carr, M., and Rodman, D. M. (2006). BMP Signaling Controls PASMC KV Channel Expression *In Vitro* and *In Vivo*. *Am. J. Physiol. Lung Cell Mol Physiol* 290 (5), L841–L848. doi:10.1152/ajplung.00158.2005

Zhao, X., Yang, Y., Yu, H., Wu, W., Sun, Y., Pan, Y., et al. (2020). Polydatin Inhibits ZEB1-Invoked Epithelial-Mesenchymal Transition in Fructose-Induced Liver Fibrosis. *J. Cell Mol Med* 24 (22), 13208–13222. doi:10.1111/jcmm.15933

Conflict of Interest: The authors declare that the research was conducted in the absence of any commercial or financial relationships that could be construed as a potential conflict of interest.

Publisher's Note: All claims expressed in this article are solely those of the authors and do not necessarily represent those of their affiliated organizations, or those of the publisher, the editors, and the reviewers. Any product that may be evaluated in this article, or claim that may be made by its manufacturer, is not guaranteed or endorsed by the publisher.

frontiers in Pharmacology

ORIGINAL RESEARCH
published: 18 March 2022
doi: 10.3389/fphar.2022.743210

Text Mining-Based Drug Discovery for Connective Tissue Disease–Associated Pulmonary Arterial Hypertension

Jiang-Shan Tan[1†], *Song Hu*[1†], *Ting-Ting Guo*[1], *Lu Hua*[1*] and *Xiao-Jian Wang*[2*]

[1]*Key Laboratory of Pulmonary Vascular Medicine, State Key Laboratory of Cardiovascular Disease, Center for Respiratory and Pulmonary Vascular Diseases, National Clinical Research Center of Cardiovascular Diseases, National Center for Cardiovascular Diseases, Department of Cardiology, Fuwai Hospital, Chinese Academy of Medical Sciences and Peking Union Medical College, Beijing, China,* [2]*Key Laboratory of Pulmonary Vascular Medicine, State Key Laboratory of Cardiovascular Disease, Center for Respiratory and Pulmonary Vascular Diseases, National Center for Cardiovascular Diseases, Fuwai Hospital, Chinese Academy of Medical Sciences and Peking Union Medical College, Beijing, China*

Background: The current medical treatments for connective tissue disease–associated pulmonary arterial hypertension (CTD-PAH) do not show favorable efficiency for all patients, and identification of novel drugs is desired.

Methods: Text mining was performed to obtain CTD- and PAH-related gene sets, and the intersection of the two gene sets was analyzed for functional enrichment through DAVID. The protein–protein interaction network of the overlapping genes and the significant gene modules were determined using STRING. The enriched candidate genes were further analyzed by Drug Gene Interaction database to identify drugs with potential therapeutic effects on CTD-PAH.

Results: Based on text mining analysis, 179 genes related to CTD and PAH were identified. Through enrichment analysis of the genes, 20 genes representing six pathways were obtained. To further narrow the scope of potential existing drugs, we selected targeted drugs with a Query Score ≥5 and Interaction Score ≥1. Finally, 13 drugs targeting the six genes were selected as candidate drugs, which were divided into four drug–gene interaction types, and 12 of them had initial drug indications approved by the FDA. The potential gene targets of the drugs on this list are IL-6 (one drug) and IL-1β (two drugs), MMP9 (one drug), VEGFA (three drugs), TGFB1 (one drug), and EGFR (five drugs). These drugs might be used to treat CTD-PAH.

Conclusion: We identified 13 drugs targeting six genes that may have potential therapeutic effects on CTD-PAH.

Keywords: text mining, connective tissue disease, pulmonary arterial hypertension, drug discovery, drugs

OPEN ACCESS

Edited by:
Ekaterini Chatzaki, Democritus University of Thrace, Greece

Reviewed by:
Akylbek Sydykov, University of Giessen, Germany
Stylianos Orfanos, National and Kapodistrian University of Athens, Greece

***Correspondence:**
Lu Hua
ethannan@126.com
Xiao-Jian Wang
wang_xiaojian@vip.163.com

[†]*These authors have contributed equally to this work and share first authorship*

Specialty section:
This article was submitted to Respiratory Pharmacology, a section of the journal Frontiers in Pharmacology

Received: *17 July 2021*
Accepted: *24 February 2022*
Published: *18 March 2022*

Citation:
Tan J-S, Hu S, Guo T-T, Hua L and Wang X-J (2022) Text Mining-Based Drug Discovery for Connective Tissue Disease–Associated Pulmonary Arterial Hypertension. Front. Pharmacol. 13:743210. doi: 10.3389/fphar.2022.743210

INTRODUCTION

Pulmonary arterial hypertension (PAH) is a life-threatening complication of connective tissue disease (CTD) and has been described in patients with systemic sclerosis (SSc), systemic lupus erythematosus (SLE), mixed CTD (MCTD), primary Sjögren's syndrome, and rheumatoid arthritis (Sung and Chung, 2015). In Western countries, CTD-associated pulmonary arterial hypertension (CTD-PAH) was the second leading cause of PAH (25%), and almost 75% of CTD-PAH was SSc-related; the 3-year survival within this population was only 56% (Hachulla et al., 2009; Thakkar and Lau, 2016). Similarly, CTD-PAH was the third most common type of PAH (20%) in China (Jiang et al., 2012), and more than half of these cases were SLE-related (58.4%) (Zhao et al., 2017). The estimated 1-year and 3-years survival rates were 85.4 and 53.6%, respectively (Zhang et al., 2011). Recently, PAH-targeted drugs were used in patients with CTD-PAH, but the effect was unsatisfactory (Fisher et al., 2006; Zhang et al., 2011). Immunosuppressive therapy is an indispensable part of treatment for CTD-PAH as well (Kato et al., 2020). The administration of immunosuppressive agents, including systemic glucocorticoids and intravenous cyclophosphamide, may improve the clinical status of PAH patients who have SLE, MCTD, and Sjögren's syndrome; however, patients with SSc-PAH do not respond well to immunosuppressive therapy (Sanchez et al., 2006; Kato and Atsumi, 2018; Kato et al., 2020).

As mentioned above, an optimal regimen of treatment has not been established, and existing drugs do not show favorable efficiency for all CTD-PAH patients; therefore, novel drugs for this condition are needed. Drug discovery has long been a time- and capital-intensive process, and an unpredictable return on investment may result. Nevertheless, drug repurposing serves as a quicker, and a less costly method to expand indications for already approved drugs (Moosavinasab et al., 2016). A successful example is Pfizer's sildenafil, which was originally designed for the treatment of angina but then repositioned to treat erectile dysfunction in 1998 (Novac, 2013). Text mining is a feasible strategy to discover drugs with new treatment potential (Andronis et al., 2011). Based on the available literature and biomedical databases, combined with analytical tools, text mining aims to explore drugs with potential value for the treatment of targeted diseases among the currently available drugs. In this study, we discovered that some existing drugs may be used for CTD-PAH treatment by text mining.

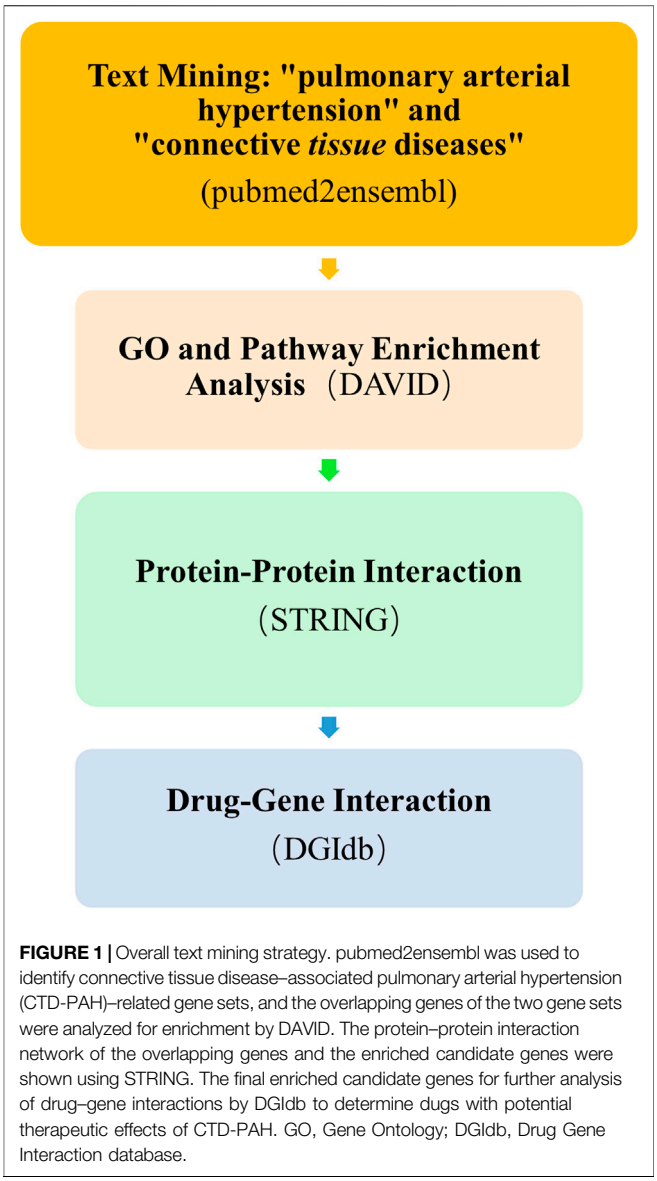

FIGURE 1 | Overall text mining strategy. pubmed2ensembl was used to identify connective tissue disease–associated pulmonary arterial hypertension (CTD-PAH)–related gene sets, and the overlapping genes of the two gene sets were analyzed for enrichment by DAVID. The protein–protein interaction network of the overlapping genes and the enriched candidate genes were shown using STRING. The final enriched candidate genes for further analysis of drug–gene interactions by DGIdb to determine dugs with potential therapeutic effects of CTD-PAH. GO, Gene Ontology; DGIdb, Drug Gene Interaction database.

MATERIALS AND METHODS

Text Mining

Text mining was performed to obtain disease–gene associations automatically based on a substantial number of biological studies, which was performed by querying the pubmed2ensembl database though http://pubmed2ensembl.ls.manchester.ac.uk/. The pubmed2ensembl is an extension of the BioMart system, which contains more than 2,000,000 articles in PubMed and almost 150,000 genes in Ensembl (Baran et al., 2011). With pubmed2ensembl, we can extract all of the associated genes using search strings from the available biological literature when we perform a query. In the present study, we performed two queries: one with the concept "pulmonary arterial hypertension" (PAH) and another with the concept "connective tissue diseases" (CTD). All unique genes were extracted from each result. Then, we conducted a genetic screen to identify intersecting genes that participate in both PAH and CTD.

Gene Ontology and Pathway Enrichment Analysis

The Gene Ontology (GO) analysis includes three main branches: cellular component (CC), molecular function

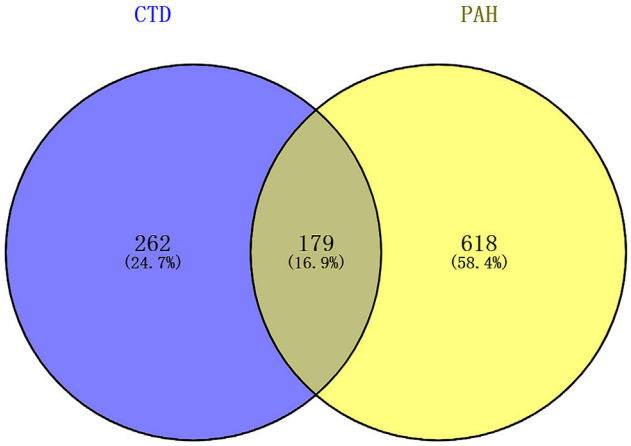

FIGURE 2 | The results of text mining. A total of 797 genes were related to PAH, 441 genes were related to CTD, and 179 genes overlapped between PAH and CTD. PAH, pulmonary arterial hypertension; CTD, connective tissue diseases.

(MF), and biological process (BP). The Kyoto Encyclopedia of Genes and Genomes (KEGG) (Kanehisa and Goto, 2000) is an open access and systematic analysis database from Japan that specializes in annotation and pathway enrichment analysis. The GO analysis and KEGG enrichment analysis of candidate overlapping genes were performed with DAVID (https://david.ncifcrf.gov/), an online gene functional annotation tool with visualization and gene attributes. A p value <0.05 was required for statistical significance as the threshold.

Protein Interaction and Module Analysis

We performed an analysis on the protein–protein interaction (PPI) network of the candidate overlapping genes using the web-based tool STRING (version 11.0, http://string-db.org/) (Szklarczyk et al., 2015). First, the overlapping genes were uploaded into the STRING website with a significance threshold of a minimum interaction score >0.9 (high confidence). Then, the TSV format file of PPI was downloaded, and further analysis was performed with Cytoscape software. STRING and the Molecular Complex Detection (MCODE) app were built in Cytoscape and used to classify the significant gene modules (clusters). The parameters in MCODE were set by default. Finally, the drug–gene interaction analysis was performed based on the genes in the gene modules.

Drug–Gene Interactions

The Drug Gene Interaction database (http://www.dgidb.org) was used for further analysis of drug–gene interactions based on the final list of genes, which could be used as potential therapeutic targets in a search for existing drugs (Wagner et al., 2016). Due to a large number of predicted drugs, we chose the targeted drugs with stringent criteria: Query Score ≥5 and Interaction Score ≥1. These candidate drugs targeting the genes/pathways relevant to PAH and CTD may represent potential treatments.

RESULTS

Results of Text Mining, GO, and Pathway Enrichment Analysis

The overall data mining strategy is described in **Figure 1**. From text mining searches, 797 genes were related to PAH, 441 genes

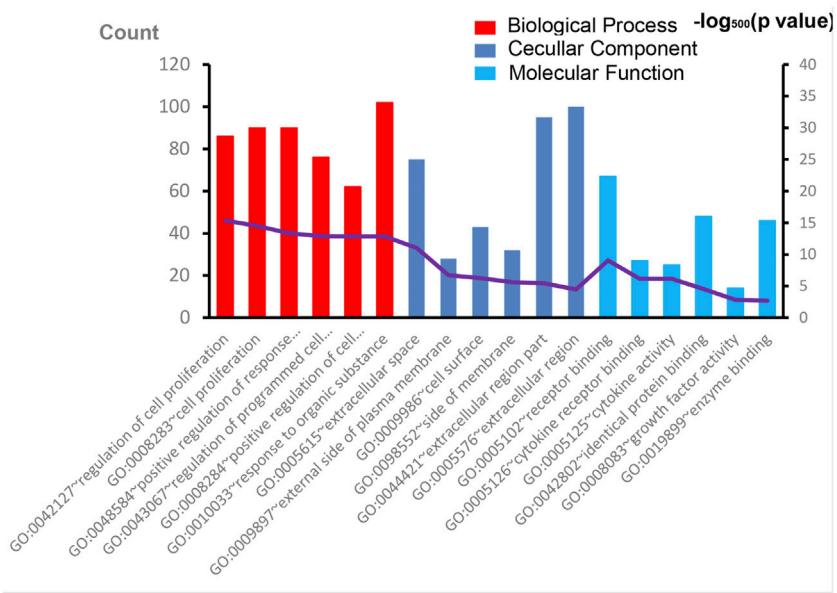

FIGURE 3 | The results of GO enrichment analysis. The top six significant enrichment terms of biological process, cellular component, and molecular function of overlapping genes are shown. GO, Gene Ontology.

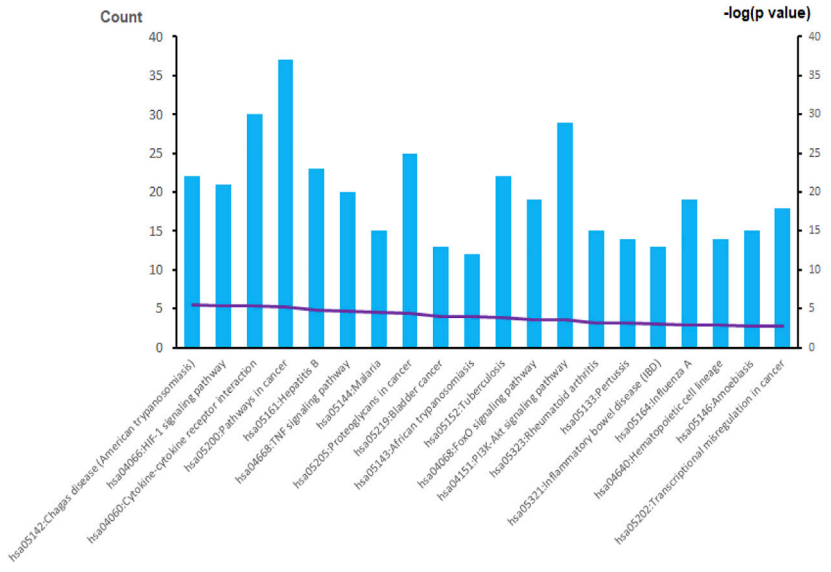

FIGURE 4 | The results of KEGG enrichment analysis. A total of 20 KEGG signaling pathways of overlapping genes are shown. KEGG, Kyoto Encyclopedia of Genes and Genomes.

were related to CTD, and 179 genes overlapped between PAH and CTD (**Figure 2**). The GO analysis was classified into three functional categories: BP, CC, and MF (in **Figure 3**, the top six significant enrichment terms for BP, CC, and MF and the top 20 KEGG signal pathways of the overlapping genes are shown). In the BP term, GO analysis showed that these common genes were mainly enriched in the regulation of response to organic substance, cell proliferation, and positive regulation of response to stimulus. In the CC term, these common genes were significantly enriched in the extracellular region, extracellular region part, and extracellular space. In the MF term, these common genes were mainly enriched in receptor binding, identical protein binding, and enzyme binding. Signaling pathway enrichment showed that these common genes were mainly involved in cancer, cytokine–cytokine receptor interaction, and the PI3K-Akt signaling pathway (**Figure 4**).

Protein Interaction and Module Analysis

We then uploaded the 179 genes to the STRING website to construct the PPI networks. After excluding 30 genes with low confidence (score <0.9), we identified 149 genes/nodes with score >0.9 (high confidence) and 1,205 edges in the construction of the PPI networks (**Figure 5A**). By using the MCODE application, we clustered two significant gene modules. Module 1 consisted of 25 genes/nodes and 180 edges (**Figure 5B**), while module 2 was made up of 20 genes/nodes and 104 edges (**Figure 5C**).

Drug–Gene Interaction and Functional Analysis of Potential Genes

To simplify our module and identify high-efficiency drugs to treat CTD-PAH, we chose module 2 for further analysis. The 20 genes in module 2 were selected for drug–gene interaction analysis. A total of 12 genes were targeted by 76 potential existing drugs, which were divided into 28 drug–gene interaction types, and all had initial drug indications (**Supplementary Table S1**). The potential gene targets of the drugs on this list are SERPINE1, IL6, IL1B, MMP9, MPO, VEGFA, VCAM1, ALB, ESR1, CREB1, TGFB1, and EGFR. Almost half of the drugs (36 of the 76) target estrogen receptor alpha (ESR1) and interact with estrogen receptor alpha in an inhibitory or antagonistic manner (**Supplementary Table S1**). To further narrow the scope of the potential existing drugs, we selected targeted drugs with Query Score ≥5 and Interaction Score ≥1 in the final results (**Table 1**). A total of six genes were targeted by 13 potential existing drugs, which were divided into four drug–gene interaction types, and 12 of them had initial drug indications approved by the FDA (**Table 1**). The potential gene targets of the drugs on this list are IL6 (one drug), IL1B (two drugs), MMP9 (one drug), VEGFA (three drugs), TGFB1 (one drug), and EGFR (five drugs).

DISCUSSION

CTD-PAH shares similar pathophysiological characteristics with other types of PAH, and dysfunction of multiple cells and molecular processes may contribute to vasoconstriction and inflammation of arterioles, which results in progressive increases in pulmonary vascular resistance and right ventricular afterload, heart failure, and even death (Thenappan et al., 2018b). Currently, all PAH-targeted drugs mainly target pulmonary vasoconstriction rather than vascular remodeling, which underlies the basic pathological characteristics of PAH. By performing text mining, we found six genes of interest and 13

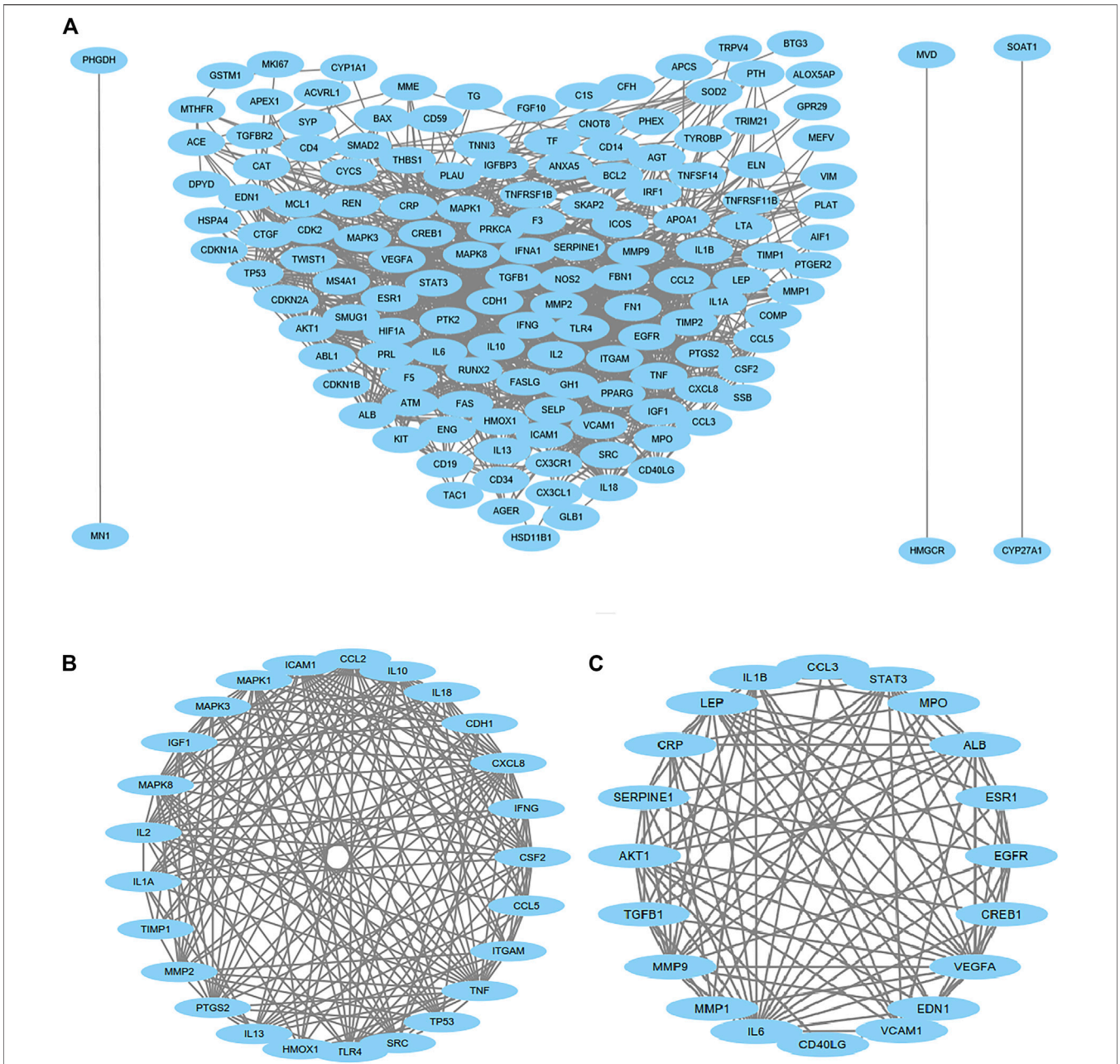

FIGURE 5 | Protein–protein interaction (PPI) network analysis. PPI of 149 genes/nodes with scores >0.9 (high confidence) and 1,205 edges are shown in **(A)**, and 30 genes have been excluded because of low confidence. For the most significant gene modules, two significant gene modules were clustered by using the MCODE application. Module 1 consisted of 25 genes/nodes and 180 edges **(B)**, and module 2 was made up of 20 genes/nodes and 104 edges **(C)**.

potential drugs for the treatment of CTD-PAH. Notably, the main drivers of vascular remodeling, including endothelial cells (ECs) or pulmonary artery smooth muscle cells (PASMCs), were implicated in the identified target gene–related signaling pathway.

Immunological disturbance and inflammatory mechanisms play a central role during the development of PAH in CTD (Dorfmüller et al., 2003). Elevated serum levels of some proinflammatory cytokines, such as interleukin (IL)-1 and IL-6, were reported in CTD-PAH patients (Dorfmüller et al., 2003). The downregulation of IL-1β and IL-6 expressions could inhibit the development of PAH by suppressing the proliferation and migration of PASMCs in rats (Ou et al., 2020). A study also demonstrated that the expression of IL-6 was increased in the lung, and IL-6 blockade by the monoclonal anti–IL-6 receptor antibody MR16-1 could ameliorate the pulmonary hypertension (PH) of pristane/hypoxia mice (a novel mouse model of PH reflecting the pathological features of CTD-PAH) (Mori et al.,

TABLE 1 | The available drugs that can target six candidate genes.

ID	Drug	Gene	Interaction types	Administration	Approved use by the FDA	Sources	Query score	Interaction score	PubMed ID
1	Siltuximab	IL6	Antagonist| antibody| inhibitor	Intravenous	Multicentric Castleman's disease	DrugBank| MyCancerGenome	21.78	8.61	88,23,310
2	Canakinumab	IL1B	Inhibitor| binder| antibody	Subcutaneous	Periodic fever syndromes; active Still's disease	DrugBank| MyCancerGenome	30.49	8.46	19,169,963
3	Rilonacept	IL1B	Binder|inhibitor	Subcutaneous	Cryopyrin-associated periodic syndrome; recurrent pericarditis	DrugBank| ChemblInteractions	7.26	2.01	23,319,019
4	Glucosamine*	MMP9	Antagonist	Oral	—	DrugBank	10.45	2.96	12,405,690
5	Ranibizumab	VEGFA	Inhibitor	Ophthalmic	Neovascular (wet) age-related macular degeneration; macular edema following retinal vein occlusion; diabetic macular edema; diabetic retinopathy; myopic choroidal neovascularization	DrugBank| TdgClinicalTrial	23.96	6.51	18,046,235
6	Pegaptanib Sodium	VEGFA	Antagonist	Ophthalmic	Neovascular (wet) age-related macular degeneration	TdgClinicalTrial| ChemblInteractions	8.71	2.37	23,953,100
7	Aflibercept	VEGFA	Antibody| binder|inhibitor	Ophthalmic	Neovascular (wet) age-related macular degeneration; macular edema following retinal vein occlusion; diabetic macular edema; Diabetic retinopathy	DrugBank| MyCancerGenome	6.97	1.89	22,813,448
8	Hyaluronidase	TGFB1	Inhibitor	Subcutaneous	As an adjuvant	DrugBank	21.78	7.1	9,435,505
9	Afatinib	EGFR	Inhibitor	Oral	Non–small-cell lung cancer	DrugBank|FDA	57.5	4.14	26,619,011
10	Osimertinib	EGFR	Inhibitor	Oral	Non–small-cell lung cancer	DrugBank|FDA	31.36	2.26	31,825,714
11	Dacomitinib	EGFR	Inhibitor	Oral	Non–small-cell lung cancer	DrugBankCKB|FDA	26.13	1.88	24,857,124
12	Necitumumab	EGFR	Antagonist| inhibitor| antibody	Intravenous	Non–small-cell lung cancer	TALC|DrugBank	17.42	1.26	20,197,484
13	Erlotinib	EGFR	Antagonist| inhibitor	Oral	Non–small-cell lung cancer; Pancreatic cancer	DrugBank|FDA	14.63	1.05	26,619,011

FDA, Food and Drug Administration.

**This drug has not yet been approved by the FDA (indicated use being investigated).*

2020). The IL-6 signaling pathway is a promising candidate in the treatment of CTD-PAH, and the use of tocilizumab, an anti-IL-6 receptor antibody was proven to result in clinical improvements in some cases of CTD-PAH (Arita et al., 2010; Furuya et al., 2010; Kadavath et al., 2014). Although siltuximab (targeting IL-6) seems to have a similar effect on CTD-PAH, the related evidence is limited. As for IL-1β blockade, whether it has a positive effect on CTD-PAH requires more evidence.

Pulmonary vascular remodeling is initiated by remodeling of the extracellular matrix resulting from the imbalance of proteolytic enzymes and their inhibitors (Thenappan et al., 2018a). Remodeling of the ECM of the pulmonary artery occurs in the early stage of PAH pathogenesis and even precedes the hemodynamic changes in pulmonary circulation (Thenappan et al., 2018a). As an important type of proteolytic enzyme, matrix metalloproteinase (MMP) shows an increase in activity associated with the proliferation and migration of PASMCs and intimal thickening during the development of PAH (Chelladurai et al., 2012). In the MMP family, the upregulation of gelatinases (MMP-2 and MMP-9) was identified in monocrotaline (MCT)–induced or hypoxia-induced mouse model of PH, and gelatinases were considered possible therapeutic targets for the treatment of PAH (George and D'Armiento, 2011; Liu et al., 2018). We found the possible use of glucosamine, an antagonist of MMP9, in CTD-PAH, but most studies have focused on its clinical use in patients with osteoarthritis thus far. Moreover, contraindications and drug interactions involving glucosamine use are uncommon (Dahmer and Schiller, 2008; Bruyère et al., 2016), therefore, the possible use of glucosamine should be explored.

The potential effect of epidermal growth factor receptor (EGFR)–mediated survival of PASMCs has led researchers to test the efficacy of selective targeting EGFR in the PH animal model (Merklinger et al., 2005). Dahal et al. (2010) found that erlotinib (one of the first generation EGFR tyrosine kinase inhibitors; it is also the drug we suggested in **Table 1**) showed therapeutic benefit in rats with MCT-induced PH, but it did not show therapeutic efficacy in chronic hypoxic mice model. The reason why partial therapeutic benefit was observed may be because different mechanisms were involved in these two commonly used animal models with respect to the involvement of EGF signaling. Most importantly, multiple growth factors,

TABLE 2 | Comprehensive recommendation of promising drugs for the treatment of CTD-PAH.

Gene targets	Reported in CTD animal model	Reported in PAH animal model	Proposed drugs by text-mining	Tested in clinical trials for CTD or PAH	Recommendation (candidate for therapy of CTD-PAH)	References (PubMed ID)
IL6	Yes	Yes	Siltuximab	No	High possibility	32,522,898
IL1B	Yes	Yes	Canakinumab; Rilonacept	No	High possibility	32,712,318
MMP9	Yes	Yes	Glucosamine	No	High possibility	21,063,214
VEGFA	Yes	Yes	Ranibizumab; Pegaptanib Sodium; Aflibercept	No	Uncertain (the drugs targeting VEGFA may induce PAH)	24,932,885
TGFB1	NO	Yes	Hyaluronidase	No	Less possibility (it could not be delivered to the lungs in its present formulation)	27,115,515
EGFR	Yes	Yes	Afatinib; Osimertinib; Dacomitinib; Necitumumab; Erlotinib	No	High possibility (but ineffective result of Erlotinib was reported in an animal model)	30,753,867

CTD, connective tissue disease; PAH, pulmonary arterial hypertension; CTD-PAH, connective tissue disease–associated pulmonary arterial hypertension.

including EGF, platelet-derived growth factor, and fibroblast growth factor, are all involved in PASMC proliferation in response to hypoxia. Therefore, no significant therapeutic efficacy was observed in chronic hypoxic mice. Notably, no significant alteration of EGFR expression in the lung tissues from patients with idiopathic PAH was also reported (Dahal et al., 2010). In Dahal's study, only patients with advanced-stage idiopathic PAH were enrolled. Therefore, as described in their study, the important role of EGF signaling in the early stage of PAH development could not be excluded. However, the second generation of EGFR tyrosine kinase inhibitors and a new pan-EGFR inhibitor, dacomitinib, showed a significant inhibitory effect on pulmonary vascular remodeling and attenuated pulmonary artery pressure and right ventricular hypertrophy in both MCT and hypoxia-induced mice model of PH (Yu et al., 2019). Other drugs that target EGFR in our list (necitumumab, afatinib, and osimertinib) have not yet been validated. The therapeutic effect of EGFR, a promising target, is required to be elucidated in the future.

Disturbed production of vasoactive, vasoconstrictive, and proliferative mediators from ECs may affect vascular tone and promote vascular remodeling (Zanatta et al., 2019). The vascular endothelial growth factor (VEGF) is the main angiogenic factor and is indispensable for the process of normal angiogenesis. The overexpression of VEGF is associated with proliferation of ECs in severe PAH (Sakao and Tatsumi, 2011). VEGF and its receptors showed increased expressions in animal models (hypoxia or MCT-induced PH), and elevated levels of plasma VEGF were also discovered in PAH patients (Voelkel and Gomez-Arroyo, 2014). However, many studies have revealed that combined with a second hit (high shear stress or chronic hypoxia), VEGF receptor blockade can drive the emergence of apoptosis-resistant ECs with the potential for hyperproliferation, and angio-obliterative PAH may form as a result (Sakao et al., 2009; Voelkel and Gomez-Arroyo, 2014). VEGFA is the most abundant isomer of VEGF in humans and is currently the main target of anti-VEGF treatment. It is unknown whether VEGF receptor antagonists would contribute to the development of PAH, but two patients developed PH were reported in patients who had ovarian cancer received bevacizumab (recombinant humanized monoclonal antibody against VEGF-A) (Garcia et al., 2008). Therefore, VEGF receptor antagonists may not be applicable in the treatment of PAH.

The predominant isoform of transforming growth factor β (TGFβ) in humans is TGFβ-1, and excessive TGFβ-1 signaling is a characteristic of PAH (Sturrock et al., 2006; Kajdaniuk et al., 2013; Calvier et al., 2019). By reducing the expression of PTEN and increasing the activation of PI3K/AKT, TGFβ-1 promotes the proliferation and decreases the apoptosis of PASMCs in lung tissue (Liu et al., 2016). Apoptosis-resistant PASMCs could promote progressive narrowing of the vascular lumen and excessive accumulation of ECM components, which reduced vascular compliance (Thenappan et al., 2018b). Selective trapping of the TGFβ-1 ligand has been demonstrated to improve hemodynamics, pulmonary vessel remodeling, and survival in mice model (Yung et al., 2016). Although hyaluronidase can target TGFβ-1, the indication is as an adjuvant to increase the absorption of other drugs in local use (**Table 1**). Moreover, hyaluronidase cannot be delivered to the lung by the venous system because the enzyme is rapidly inactivated following intravenous administration. Thus, hyaluronidase is not applicable in the clinical treatment of PAH, but a suitable formulation for delivery may be an alternative consideration.

The first limitation of this study is related to the databases we used. Not all the drug–gene interactions are fully clarified in the present databases. Therefore, the analysis may be more accurate as the databases are updated. Additionally, some candidate genes for targeting might have generalized effects that may not always be desirable. Thus, lack of experiments to validate the targets and drugs that we found is the other limitation of the present study. Experiments and clinical trials are required before these drugs are approved for clinical use.

As discussed above, some drugs that we found (**Table 2**) may have unfavorable effects depending on the current findings. For example, drugs that target VEGFA may induce PAH, erlotinib (target EGFR) was ineffective in animal model, and hyaluronidase (target TGFβ-1) could not be delivered to lung tissue in its present formulation. With the evolution and improvement of database and analytic tools, this method of data mining will promote drug discovery in CTD-PAH therapy.

In conclusion, 13 drugs targeting six genes that may have potential therapeutic effects on CTD-PAH were discovered, and none of them has been tested in clinical trials for PAH patients. Drug discovery by performing text mining and pathway analysis can help identify existing drugs that have the potential to treat CTD-PAH.

DATA AVAILABILITY STATEMENT

The original contributions presented in the study are included in the article/**Supplementary Material**, further inquiries can be directed to the corresponding authors.

AUTHOR CONTRIBUTIONS

J-ST, SH, LH, and X-JW designed the study. J-ST, SH, and T-TG performed the data analysis and wrote the manuscript. LH and X-JW revised the manuscript. All authors listed approved for the manuscript for publication.

FUNDING

The study was supported by grants from the Research Project of Clinical Toxicology from the Chinese Society of Toxicology (CST2020CT303), National Clinical Research Center for Cardiovascular Diseases, Fuwai Hospital, Chinese Academy of Medical Sciences (NCRC2020007), and National Natural Science Foundation of China (81870050).

SUPPLEMENTARY MATERIAL

The Supplementary Material for this article can be found online at: https://www.frontiersin.org/articles/10.3389/fphar.2022.743210/full#supplementary-material

REFERENCES

Andronis, C., Sharma, A., Virvilis, V., Deftereos, S., and Persidis, A. (2011). Literature Mining, Ontologies and Information Visualization for Drug Repurposing. *Brief Bioinform* 12 (4), 357–368. doi:10.1093/bib/bbr005

Arita, Y., Sakata, Y., Sudo, T., Maeda, T., Matsuoka, K., Tamai, K., et al. (2010). The Efficacy of Tocilizumab in a Patient with Pulmonary Arterial Hypertension Associated with Castleman's Disease. *Heart Vessels* 25 (5), 444–447. doi:10.1007/s00380-009-1215-5

Baran, J., Gerner, M., Haeussler, M., Nenadic, G., and Bergman, C. M. (2011). pubmed2ensembl: a Resource for Mining the Biological Literature on Genes. *PLoS One* 6 (9), e24716. doi:10.1371/journal.pone.0024716

Bruyère, O., Altman, R. D., and Reginster, J. Y. (2016). Efficacy and Safety of Glucosamine Sulfate in the Management of Osteoarthritis: Evidence from Real-Life Setting Trials and Surveys. *Semin. Arthritis Rheum.* 45 (4 Suppl. l), S12–S17. doi:10.1016/j.semarthrit.2015.11.011

Calvier, L., Chouvarine, P., Legchenko, E., Kokeny, G., Mozes, M. M., and Hansmann, G. (2019). Chronic TGF-β1 Signaling in Pulmonary Arterial Hypertension Induces Sustained Canonical Smad3 Pathways in Vascular Smooth Muscle Cells. *Am. J. Respir. Cel Mol. Biol.* 61 (1), 121–123. doi:10.1165/rcmb.2018-0275LE

Chelladurai, P., Seeger, W., and Pullamsetti, S. S. (2012). Matrix Metalloproteinases and Their Inhibitors in Pulmonary Hypertension. *Eur. Respir. J.* 40 (3), 766–782. doi:10.1183/09031936.00209911

Dahal, B. K., Cornitescu, T., Tretyn, A., Pullamsetti, S. S., Kosanovic, D., Dumitrascu, R., et al. (2010). Role of Epidermal Growth Factor Inhibition in Experimental Pulmonary Hypertension. *Am. J. Respir. Crit. Care Med.* 181 (2), 158–167. doi:10.1164/rccm.200811-1682OC

Dahmer, S., and Schiller, R. M. (2008). Glucosamine. *Am. Fam. Physician* 78 (4), 471–476.

Dorfmüller, P., Perros, F., Balabanian, K., and Humbert, M. (2003). Inflammation in Pulmonary Arterial Hypertension. *Eur. Respir. J.* 22 (2), 358–363. doi:10.1183/09031936.03.00038903

Fisher, M. R., Mathai, S. C., Champion, H. C., Girgis, R. E., Housten-Harris, T., Hummers, L., et al. (2006). Clinical Differences between Idiopathic and Scleroderma-Related Pulmonary Hypertension. *Arthritis Rheum.* 54 (9), 3043–3050. doi:10.1002/art.22069

Furuya, Y., Satoh, T., and Kuwana, M. (2010). Interleukin-6 as a Potential Therapeutic Target for Pulmonary Arterial Hypertension. *Int. J. Rheumatol.* 2010, 720305. doi:10.1155/2010/720305

Garcia, A. A., Hirte, H., Fleming, G., Yang, D., Tsao-Wei, D. D., Roman, L., et al. (2008). Phase II Clinical Trial of Bevacizumab and Low-Dose Metronomic Oral Cyclophosphamide in Recurrent Ovarian Cancer: a Trial of the California, Chicago, and Princess Margaret Hospital Phase II Consortia. *J. Clin. Oncol.* 26 (1), 76–82. doi:10.1200/JCO.2007.12.1939

George, J., and D'Armiento, J. (2011). Transgenic Expression of Human Matrix Metalloproteinase-9 Augments Monocrotaline-Induced Pulmonary Arterial Hypertension in Mice. *J. Hypertens.* 29 (2), 299–308. doi:10.1097/HJH.0b013e328340a0e4

Hachulla, E., Carpentier, P., Gressin, V., Diot, E., Allanore, Y., Sibilia, J., et al. (2009). Risk Factors for Death and the 3-year Survival of Patients with Systemic Sclerosis: the French ItinérAIR-Sclérodermie Study. *Rheumatology (Oxford)* 48 (3), 304–308. doi:10.1093/rheumatology/ken488

Jiang, X., Humbert, M., and Jing, Z.-C. (2012). Idiopathic Pulmonary Arterial Hypertension and its Prognosis in the Modern Management Era in Developed and Developing Countries. *Prog. Respir. Res.* 41, 85–93. doi:10.1159/000336068

Kadavath, S., Zapantis, E., Zolty, R., and Efthimiou, P. (2014). A Novel Therapeutic Approach in Pulmonary Arterial Hypertension as a Complication of Adult-Onset Still's Disease: Targeting IL-6. *Int. J. Rheum. Dis.* 17 (3), 336–340. doi:10.1111/1756-185X.12324

Kajdaniuk, D., Marek, B., Borgiel-Marek, H., and Kos-Kudła, B. (2013). Transforming Growth Factor β1 (TGFβ1) in Physiology and Pathology. *Endokrynol Pol.* 64 (5), 384–396. doi:10.5603/EP.2013.0022

Kanehisa, M., and Goto, S. (2000). KEGG: Kyoto Encyclopedia of Genes and Genomes. *Nucleic Acids Res.* 28 (1), 27–30. doi:10.1093/nar/28.1.27

Kato, M., and Atsumi, T. (2018). Pulmonary Arterial Hypertension Associated with Connective Tissue Diseases: A Review Focusing on Distinctive Clinical Aspects. *Eur. J. Clin. Invest.* 48 (2). doi:10.1111/eci.12876

Kato, M., Sugimoto, A., and Atsumi, T. (2020). Diagnostic and Prognostic Markers and Treatment of Connective Tissue Disease-Associated Pulmonary Arterial Hypertension: Current Recommendations and Recent Advances. *Expert Rev. Clin. Immunol.* 16 (10), 1–11. doi:10.1080/1744666X.2021.1825940

Liu, Y., Cao, Y., Sun, S., Zhu, J., Gao, S., Pang, J., et al. (2016). Transforming Growth Factor-Beta1 Upregulation Triggers Pulmonary Artery Smooth Muscle Cell Proliferation and Apoptosis Imbalance in Rats with Hypoxic Pulmonary

Hypertension via the PTEN/AKT Pathways. *Int. J. Biochem. Cel Biol.* 77 (Pt A), 141–154. doi:10.1016/j.biocel.2016.06.006

Liu, Y., Zhang, H., Yan, L., Du, W., Zhang, M., Chen, H., et al. (2018). MMP-2 and MMP-9 Contribute to the Angiogenic Effect Produced by Hypoxia/15-HETE in Pulmonary Endothelial Cells. *J. Mol. Cel Cardiol.* 121, 36–50. doi:10.1016/j.yjmcc.2018.06.006

Merklinger, S. L., Jones, P. L., Martinez, E. C., and Rabinovitch, M. (2005). Epidermal Growth Factor Receptor Blockade Mediates Smooth Muscle Cell Apoptosis and Improves Survival in Rats with Pulmonary Hypertension. *Circulation* 112 (3), 423–431. doi:10.1161/CIRCULATIONAHA.105.540542

Moosavinasab, S., Patterson, J., Strouse, R., Rastegar-Mojarad, M., Regan, K., Payne, P. R. O., et al. (2016). 'RE:fine Drugs': an Interactive Dashboard to Access Drug Repurposing Opportunities. *Database* 2016, baw083. doi:10.1093/database/baw083

Mori, H., Ishibashi, T., Inagaki, T., Okazawa, M., Masaki, T., Asano, R., et al. (2020). Pristane/Hypoxia (PriHx) Mouse as a Novel Model of Pulmonary Hypertension Reflecting Inflammation and Fibrosis. *Circ. J.* 84 (7), 1163–1172. doi:10.1253/circj.CJ-19-1102

Novac, N. (2013). Challenges and Opportunities of Drug Repositioning. *Trends Pharmacol. Sci.* 34 (5), 267–272. doi:10.1016/j.tips.2013.03.004

Ou, M., Zhang, C., Chen, J., Zhao, S., Cui, S., and Tu, J. (2020). Overexpression of MicroRNA-340-5p Inhibits Pulmonary Arterial Hypertension Induced by APE by Downregulating IL-1β and IL-6. *Mol. Ther. Nucleic Acids* 21, 542–554. doi:10.1016/j.omtn.2020.05.022

Sakao, S., and Tatsumi, K. (2011). Vascular Remodeling in Pulmonary Arterial Hypertension: Multiple Cancer-like Pathways and Possible Treatment Modalities. *Int. J. Cardiol.* 147 (1), 4–12. doi:10.1016/j.ijcard.2010.07.003

Sakao, S., Tatsumi, K., and Voelkel, N. F. (2009). Endothelial Cells and Pulmonary Arterial Hypertension: Apoptosis, Proliferation, Interaction and Transdifferentiation. *Respir. Res.* 10, 95. doi:10.1186/1465-9921-10-95

Sanchez, O., Sitbon, O., Jaïs, X., Simonneau, G., and Humbert, M. (2006). Immunosuppressive Therapy in Connective Tissue Diseases-Associated Pulmonary Arterial Hypertension. *Chest* 130 (1), 182–189. doi:10.1378/chest.130.1.182

Sturrock, A., Cahill, B., Norman, K., Huecksteadt, T. P., Hill, K., Sanders, K., et al. (2006). Transforming Growth Factor-Beta1 Induces Nox4 NAD(P)H Oxidase and Reactive Oxygen Species-dependent Proliferation in Human Pulmonary Artery Smooth Muscle Cells. *Am. J. Physiol. Lung Cel Mol. Physiol.* 290 (4), L661–L673. doi:10.1152/ajplung.00269.2005

Sung, Y. K., and Chung, L. (2015). Connective Tissue Disease-Associated Pulmonary Arterial Hypertension. *Rheum. Dis. Clin. North. Am.* 41 (2), 295–313. doi:10.1016/j.rdc.2015.01.003

Szklarczyk, D., Franceschini, A., Wyder, S., Forslund, K., Heller, D., Huerta-Cepas, J., et al. (2015). STRING V10: Protein-Protein Interaction Networks, Integrated over the Tree of Life. *Nucleic Acids Res.* 43 (Database issue), D447–D452. doi:10.1093/nar/gku1003

Thakkar, V., and Lau, E. M. (2016). Connective Tissue Disease-Related Pulmonary Arterial Hypertension. *Best Pract. Res. Clin. Rheumatol.* 30 (1), 22–38. doi:10.1016/j.berh.2016.03.004

Thenappan, T., Chan, S. Y., and Weir, E. K. (2018a). Role of Extracellular Matrix in the Pathogenesis of Pulmonary Arterial Hypertension. *Am. J. Physiol. Heart Circ. Physiol.* 315 (5), H1322–H1331. doi:10.1152/ajpheart.00136.2018

Thenappan, T., Ormiston, M. L., Ryan, J. J., and Archer, S. L. (2018b). Pulmonary Arterial Hypertension: Pathogenesis and Clinical Management. *BMJ* 360, j5492. doi:10.1136/bmj.j5492

Voelkel, N. F., and Gomez-Arroyo, J. (2014). The Role of Vascular Endothelial Growth Factor in Pulmonary Arterial Hypertension. The Angiogenesis Paradox. *Am. J. Respir. Cel Mol. Biol.* 51 (4), 474–484. doi:10.1165/rcmb.2014-0045TR

Wagner, A. H., Coffman, A. C., Ainscough, B. J., Spies, N. C., Skidmore, Z. L., Campbell, K. M., et al. (2016). DGIdb 2.0: Mining Clinically Relevant Drug-Gene Interactions. *Nucleic Acids Res.* 44 (D1), D1036–D1044. doi:10.1093/nar/gkv1165

Yu, X., Zhao, X., Zhang, J., Li, Y., Sheng, P., Ma, C., et al. (2019). Dacomitinib, a New Pan-EGFR Inhibitor, Is Effective in Attenuating Pulmonary Vascular Remodeling and Pulmonary Hypertension. *Eur. J. Pharmacol.* 850, 97–108. doi:10.1016/j.ejphar.2019.02.008

Yung, L. M., Nikolic, I., Paskin-Flerlage, S. D., Pearsall, R. S., Kumar, R., and Yu, P. B. (2016). A Selective Transforming Growth Factor-β Ligand Trap Attenuates Pulmonary Hypertension. *Am. J. Respir. Crit. Care Med.* 194 (9), 1140–1151. doi:10.1164/rccm.201510-1955OC

Zanatta, E., Polito, P., Famoso, G., Larosa, M., De Zorzi, E., Scarpieri, E., et al. (2019). Pulmonary Arterial Hypertension in Connective Tissue Disorders: Pathophysiology and Treatment. *Exp. Biol. Med. (Maywood)* 244 (2), 120–131. doi:10.1177/1535370218824101

Zhang, R., Dai, L. Z., Xie, W. P., Yu, Z. X., Wu, B. X., Pan, L., et al. (2011). Survival of Chinese Patients with Pulmonary Arterial Hypertension in the Modern Treatment Era. *Chest* 140 (2), 301–309. doi:10.1378/chest.10-2327

Zhao, J., Wang, Q., Liu, Y., Tian, Z., Guo, X., Wang, H., et al. (2017). Clinical Characteristics and Survival of Pulmonary Arterial Hypertension Associated with Three Major Connective Tissue Diseases: A Cohort Study in China. *Int. J. Cardiol.* 236, 432–437. doi:10.1016/j.ijcard.2017.01.097

Conflict of Interest: The authors declare that the research was conducted in the absence of any commercial or financial relationships that could be construed as a potential conflict of interest.

Publisher's Note: All claims expressed in this article are solely those of the authors and do not necessarily represent those of their affiliated organizations, or those of the publisher, the editors, and the reviewers. Any product that may be evaluated in this article, or claim that may be made by its manufacturer, is not guaranteed or endorsed by the publisher.

Advantages of publishing in Frontiers

OPEN ACCESS
Articles are free to read for greatest visibility and readership

FAST PUBLICATION
Around 90 days from submission to decision

HIGH QUALITY PEER-REVIEW
Rigorous, collaborative, and constructive peer-review

TRANSPARENT PEER-REVIEW
Editors and reviewers acknowledged by name on published articles

Frontiers
Avenue du Tribunal-Fédéral 34
1005 Lausanne | Switzerland

Visit us: www.frontiersin.org
Contact us: frontiersin.org/about/contact

REPRODUCIBILITY OF RESEARCH
Support open data and methods to enhance research reproducibility

DIGITAL PUBLISHING
Articles designed for optimal readership across devices

FOLLOW US
@frontiersin

IMPACT METRICS
Advanced article metrics track visibility across digital media

EXTENSIVE PROMOTION
Marketing and promotion of impactful research

LOOP RESEARCH NETWORK
Our network increases your article's readership